University of Alberta

Application of Transformational Roasting to the Treatment of Metallurgical Wastes

by

Preston Carl Holloway ©

A thesis submitted to the Faculty of Graduate Studies and Research in partial fulfillment
of the requirements for the degree of Doctor of Philosophy

in

Materials Engineering

Department of Chemical and Materials Engineering

Edmonton, Alberta

Fall 2006

Library and
Archives Canada

Published Heritage
Branch

395 Wellington Street
Ottawa ON K1A 0N4
Canada

Bibliothèque et
Archives Canada

Direction du
Patrimoine de l'édition

395, rue Wellington
Ottawa ON K1A 0N4
Canada

Your file Votre référence
ISBN: 978-0-494-23044-2
Our file Notre référence
ISBN: 978-0-494-23044-2

NOTICE:
The author has granted a non-exclusive license allowing Library and Archives Canada to reproduce, publish, archive, preserve, conserve, communicate to the public by telecommunication or on the Internet, loan, distribute and sell theses worldwide, for commercial or non-commercial purposes, in microform, paper, electronic and/or any other formats.

The author retains copyright ownership and moral rights in this thesis. Neither the thesis nor substantial extracts from it may be printed or otherwise reproduced without the author's permission.

AVIS:
L'auteur a accordé une licence non exclusive permettant à la Bibliothèque et Archives Canada de reproduire, publier, archiver, sauvegarder, conserver, transmettre au public par télécommunication ou par l'Internet, prêter, distribuer et vendre des thèses partout dans le monde, à des fins commerciales ou autres, sur support microforme, papier, électronique et/ou autres formats.

L'auteur conserve la propriété du droit d'auteur et des droits moraux qui protège cette thèse. Ni la thèse ni des extraits substantiels de celle-ci ne doivent être imprimés ou autrement reproduits sans son autorisation.

In compliance with the Canadian Privacy Act some supporting forms may have been removed from this thesis.

While these forms may be included in the document page count, their removal does not represent any loss of content from the thesis.

Conformément à la loi canadienne sur la protection de la vie privée, quelques formulaires secondaires ont été enlevés de cette thèse.

Bien que ces formulaires aient inclus dans la pagination, il n'y aura aucun contenu manquant.

Canada

Abstract

Transformational roasting involves the heating of a material along with specific additives to induce mineralogical changes in the starting material. By controlling the chemical composition, roasting atmosphere, temperature and time of reaction, the mineral transformations induced during roasting can be engineered to control the distribution of valuable or harmful metals and to produce new mineral assemblages that are more amenable to conventional methods of metals recovery or to environmentally safe disposal. However, to date, transformational roasting processes have only been applied to the recovery of a limited number of metals from a limited number of materials.

A generalized procedure for the application of transformational roasting techniques to the treatment of new materials was proposed that utilized a combination of thermodynamic analysis, scoping tests, Design of Experiments (DOE) testing, mineralogical studies, process optimization and analysis of the deportment of minor elements to identify promising roasting systems for further study. This procedure was developed, tested and refined through the application of these techniques to four different industrial metallurgical wastes, including oil sands fly ash from Suncor in northern Alberta, zinc ferrite residue from Doe Run Peru, electric arc furnace (EAF) dust from Altasteel's operations in Edmonton, Alberta, and copper-nickel-arsenic sulphide residue from Inco's refinery in Thompson, Manitoba.

A large number of potential reagents were identified and tested for the latter three materials and transformational roasting was effectively used to induce mineral transformations during the roasting of these wastes which increased the solubility of valuable elements, decreased the solubility of major impurities, produced a differential solubility between valuable and harmful elements or controlled the volatilization of harmful elements. Comprehensive studies of these mineralogical transformations and the solubility of the phases produced were accomplished by integrating common methods of mineralogical analysis, such as scanning electron microscopy and x-ray diffraction, with the results from specific roasting and leaching tests identified using Design of Experiments techniques.

Several promising reagent systems were identified for further study. These systems include roasting zinc ferrite residue with Na_2CO_3, $Na_2CO_3/MnCO_3$ or coal/$MnCO_3$, roasting EAF dust with Na_2CO_3, and roasting the copper residue with Na_2CO_3, $Ca(OH)_2$ or $Na_2CO_3/Ca(OH)_2$. Conceptual process flowsheets were also constructed for many of these promising reagent systems.

Acknowledgements

The author wishes to express his appreciation to Tina Barker for her continued excellence in and help with the scanning electron microscopy work for this project.

The author would also like to thank the following companies for supplying the materials used in this research: Suncor Inc. (oil sands fly ash), Doe Run Peru (zinc ferrite), Altasteel Ltd. (electric arc furnace dust) and Inco Ltd. (copper residue).

The author would like to thank the Natural Sciences and Engineering Research Council (NSERC) for providing funding in the form of a Canadian Graduate Scholarship (CGS), as well as the Alberta Ingenuity Fund for awarding me an Alberta Ingenuity Studentship and Alberta Learning for awarding me the Ralph Steinhauer Award of Distinction.

Finally, the author would also like to show his appreciation to several people who have been consulted on various aspects of the project: Diane Caird (Department of Earth and Atmospheric Sciences) and Heather Kaminsky, Patrick Kerr, and Shiraz Merali (Department of Chemical and Materials Engineering).

Many thanks to my supervisor Dr. Tom Etsell for his support and guidance throughout my Ph.D. and Master's research. His love for chemistry, extractive metallurgy and secondary recovery has been an inspiration and encouragement to me through my entire career so far as a metallurgist. I cannot imagine having a better supervisor for either degree and am very glad to count Dr. Etsell as an esteemed colleague and a friend.

TABLE OF CONTENTS

1.0 Introduction 1
2.0 Proof of Concept – Roasting of Oil Sands Fly Ash with Calcium and Potassium Reagents 5
  2.1 Literature Survey 5
  2.2 Feed Materials 6
  2.3 Experimental Procedure 6
  2.4 Roasting with Calcium Reagents 7
    2.4.1 Microstructure of Ash Roasted with Calcium Salts 11
  2.5 Roasting with Potassium Reagents 13
    2.5.1 Integration of KCl into Vanadium Recovery Flowsheet 16
  2.6 Conclusions 18
3.0 Procedure for Application of Induced Metamorphism to New Materials 21
  3.1 Generalized Procedure for the Application of Transformational Roasting. 21
    3.1.1 Literature Survey 22
    3.1.2 Thermodynamic Analysis 22
    3.1.3 Scoping Roast/Leach Tests 23
    3.1.4 Design of Experiments (DOE) Tests 23
    3.1.5 Mineralogical Studies 24
    3.1.6 Optimization 25
    3.1.7 Deportment of Minor Elements 25
  3.2 Selection of Feed Materials 25
    3.2.1 Feed Selection Criteria 26
    3.2.2 Selected Feeds 26
4.0 Application of the General Procedure to the Treatment of La Oroya Zinc Ferrite 27
  4.1 Feed Material 27
    4.1.1 History of Production of Zinc Ferrite at La Oroya 27
    4.1.2 Feed Sample 28
  4.2 Literature Survey 29
    4.2.1 Formation of Zinc Ferrite 29
    4.2.2 Treatment of Zinc Ferrite 30
      4.2.2.1 Waelz Process 30
      4.2.2.2 Roasting Processes 35
      4.2.2.3 Ausmelt Slag Fuming 36
      4.2.2.4 Hot Acid Leaching 37
    4.2.3 Conclusions 39
  4.3 Thermodynamic Analysis 41
    4.3.1 Potential Reaction Systems 42
      4.3.1.1 Zinc Replacement Reactions 42
      4.3.1.2 Reduction of $ZnFe_2O_4$ and Formation of Non-Zinc Ferrites 43
      4.3.1.3 Reaction with Metal Sulphates 45
      4.3.1.4 Reaction with Metal Chlorides 46
  4.4 Scoping Tests 47
    4.4.1 Roasting and Leaching Procedure 47
    4.4.2 Scoping Test Results 48

4.4.2.1 Zinc Replacement Reactions 48
4.4.2.2 Reactions for Reduction of $ZnFe_2O_4$ and Formation of Non-Zinc Ferrites 52
4.4.2.3 Reactions with Metal Chlorides 54
4.4.2.4 Reactions with Metal Sulphates 55
4.5 Design of Experiments (DOE) Tests 56
4.5.1 Multivariate Experimental Design 56
4.5.2 Results from Design of Experiment Studies and Mineralogical Analysis . 60
4.5.2.1 Roasting with Na_2CO_3 62
4.5.2.2 Reduction of $ZnFe_2O_4$ to Form Metal Ferrites 92
4.6 Deportment of Minor Elements 113
4.6.1 Roasting with Na_2CO_3 113
4.6.2 Roasting with Na_2CO_3 and $MnCO_3$ 115
4.6.3 Roasting with Coal 116
4.6.4 Roasting with Coal and $MnCO_3$ 117
4.7 Preliminary Evaluation of Potential Processing Options 118
4.7.1 Roasting with Na_2CO_3 and $MnCO_3$ 118
4.7.1.1 Na_2CO_3 Recovery and H_2SO_4 Regeneration 122
4.7.1.2 Potential for Iron and Manganese Recovery 129
4.7.1.3 Silver Recovery 131
4.7.2 Roasting with Coal and $MnCO_3$ (Modified Waelz Kiln Process) 131
4.7.2.1 Potential for Iron and Manganese Recovery 134
4.7.2.2 Silver Recovery 135
4.8 Conclusions 135
5.0 Application of the General Procedure to the Treatment of Altasteel Electric Arc Furnace (EAF) Dust 136
5.1 Feed Material 136
5.2 Literature Survey 139
5.2.1 Mineralogy and Formation of EAF Dust 139
5.2.2 World Production of EAF Dust and Concerns 139
5.2.3 Technologies for EAF Treatment 140
5.2.3.1 Pyrometallurgical Processes 140
5.2.3.2 Hydrometallurgical Processes 145
5.2.3.3 Hybrid Processes 147
5.2.3.4 Stabilization Processes 148
5.2.3.5 Recycling 149
5.2.4 Summary 149
5.3 Thermodynamic Analysis 150
5.4 Scoping Tests 150
5.5 Design of Experiment (DOE) Tests for Altasteel EAF Dust 152
5.5.1 Roasting with Na_2CO_3 154
5.5.1.1 Secondary Additions to Control Iron Dissolution 165
5.5.2 Reduction of EAF Dust to Form Metal Ferrites 188
5.5.2.1 Roasting with Coal 188
5.5.2.2 Roasting with Coal and $CaCO_3$ 198
5.6 Deportment of Minor Elements 207

5.6.1 Roasting with Na_2CO_3 207
5.6.2 Roasting with Coal 208
5.7 Preliminary Evaluation of Potential Processing Options 210
5.7.1 Roasting with Na_2CO_3 210
5.7.1.1 Iron and/or Manganese Recovery 212
5.7.2 Roasting with Coal (Waelz Kiln Processing) 213
5.8 Conclusions 215
6.0 Application of the General Procedure to the Treatment of Inco Copper Residue 216
6.1 Literature Survey 220
6.1.1 Lime Roasting of Copper Concentrates 220
6.1.2 Transformational Roasting of Gold Concentrates 223
6.1.2.1 Lime Roasting of Refractory Gold Concentrates 223
6.1.2.2 Sodium Carbonate/Sodium Hydroxide Roasting of Refractory Gold Ores 226
6.1.2.3 Roasting of Refractory Gold Ores with Iron Sulphates 228
6.1.3 Sodium Carbonate Roasting of Other Related Materials 228
6.1.3.1 Copper Electrolytic Slimes 228
6.1.3.2 Speiss 229
6.1.4 Conclusions 229
6.2 Thermodynamic Analysis 230
6.2.1 Roasting of As_2S_3 230
6.2.2 Roasting of Copper and Nickel Sulphides 232
6.3 Scoping Tests 233
6.3.1 Experimental Procedure 233
6.3.2 Results from Scoping Tests 235
6.3.2.1 Na_2CO_3 Roasting Tests 235
6.3.2.2 Screening of Secondary Reagents 238
6.4 Design of Experiment (DOE) Tests 240
6.4.1 Roasting with Na_2CO_3 242
6.4.1.1 Roasting of Inco Copper Residue (Feed #1) with Na_2CO_3 242
6.4.1.2 Roasting of Inco Copper Residue (Feed #2) with Na_2CO_3 254
6.4.2 Roasting of Inco Copper Residue (Feed #2) with $Ca(OH)_2$ 268
6.4.2.1 Roasting 268
6.4.2.2 Hot Water Leaching and Hot Acid Leaching 271
6.4.3 Roasting with Secondary Additives to Fix Arsenic 280
6.4.3.1 Roasting 280
6.4.3.2 Hot Water and Acid Leaching of Inco Copper Residue (Feed #2) Roasted with Na_2CO_3 and $FeSO_4 \cdot 7H_2O$ 284
6.5 Deportment of Minor Elements 297
6.6 Preliminary Evaluation of Potential Processing Options 299
6.6.1 Roasting and Leaching Unit Operations 299
6.6.2 Nickel Recovery from the Raffinate Bleed 301
6.6.2.1 Precipitation of Nickel Hydroxide from the Raffinate Bleed 302
6.6.2.2 Sulphide Precipitation of the Raffinate Bleed 304
6.6.2.3 Sodium Recovery and Arsenic Precipitation 307
6.6.2.4 Optimization of Arsenic Deportment and Flowsheet Implications 311

6.6.2.5 Process Evaluation 312
6.7 Conclusions 314
7.0 Evaluation of Transformational Roasting Techniques 315
7.1 Is the Procedure Proposed for the Application of Transformational Roasting Techniques to New Materials Effective? 315
7.2 Is Transformational Roasting a Realistic Option for Processing of Metallurgical Wastes? 318
8.0 Future Work 321
9.0 Conclusions 324

References 326

List of Tables

Table 1 Analysis of Decarbonized Suncor 1986 Fly Ash, wt% 6
Table 2 Summary of Mineral Phases Detected by X-ray Diffraction in Suncor Fly Ash Roasted with Calcium Reagents 9
Table 3 Chemical Analysis of La Oroya Zinc Ferrite Supplied by Doe Run Peru 28
Table 4 Chemical Analysis of La Oroya Zinc Ferrite Conducted at the University of Alberta 28
Table 5 Generalized Zinc Replacement Reactions 42
Table 6 Generalized Zinc Reduction/Ferrite Formation Reactions 44
Table 7 Generalized Chloridization Reactions 46
Table 8 Effect of Roasting Time on Zinc Extractions for Various Reagents 49
Table 9 Phases Identified in 7 h Roasted Samples with X-ray Diffraction 49
Table 10 Number of Trials for Various Factorial Designs and Number of Variables 57
Table 11 Generalized Experimental Design for a Rotatable 2^2 CCD Design 59
Table 12 Generalized Experimental Design for a Rotatable 2^3 CCD Design 59
Table 13 Experimental Conditions Used in Experimental Designs for Roasting Zinc Ferrite with Na_2CO_3 and Resulting Model Variance 60
Table 14 Experimental Conditions Used in Experimental Designs for Roasting Zinc Ferrite with Carbonaceous Reagents and Resulting Model Variance 61
Table 15 Phases Identified by X-ray Diffraction Analysis of Zinc Ferrite Roasted with Na_2CO_3 62
Table 16 Phases Identified by X-ray Diffraction Analysis of Zinc Ferrite Roasted with Na_2CO_3 and $CaCO_3$ at 950°C 68
Table 17 Phases Identified by X-ray Diffraction Analysis of Zinc Ferrite after Roasting with Na_2CO_3 and $CaCO_3$ and Leaching with 200 g/L H_2SO_4 72
Table 18 Phases Identified by X-ray Diffraction Analysis of Zinc Ferrite Roasted with Na_2CO_3 and $CaCO_3$ at 950°C 79
Table 19 Phases Identified by X-ray Diffraction Analysis of Zinc Ferrite Roasted with Na_2CO_3 and $CaCO_3$ at 950°C 86
Table 20 Phases Identified by X-ray Diffraction Analysis of Zinc Ferrite after Roasting with Na_2CO_3 and $CaCO_3$ and Leaching with 200 g/L H_2SO_4 88
Table 21 Phases Identified by XRD Analysis of Zinc Ferrite Roasted with Coal 94
Table 22 Phases Identified by X-ray Diffraction Analysis of Zinc Ferrite after Roasting with Coal and Leaching with 200 g/L H_2SO_4 95
Table 23 Phases Identified by XRD Analysis of Zinc Ferrite Roasted with Coal and 62% $CaCO_3$ 97
Table 24 Phases Identified by X-ray Diffraction Analysis of Zinc Ferrite after Roasting with Coal and 62% $CaCO_3$ and Leaching with 200 g/L H_2SO_4 103
Table 25 Phases Identified by XRD Analysis of Zinc Ferrite Roasted with Coal and 70.0% $MnCO_3$ 106

Table 26 Phases Identified by X-ray Diffraction Analysis of Zinc Ferrite after Roasting with Coal and 70.0% $MnCO_3$ and Leaching with 200 g/L H_2SO_4 110
Table 27 Deportment of Minor Elements in La Oroya Zinc Ferrite during Roasting with 80% Na_2CO_3 at 950°C 114
Table 28 Deportment of Minor Elements in La Oroya Zinc Ferrite during Roasting with 80% Na_2CO_3 and 33.25% $MnCO_3$ at 950°C 115
Table 29 Deportment of Minor Elements in La Oroya Zinc Ferrite during Roasting with 20% Coal at 1100°C 116
Table 30 Deportment of Minor Elements in La Oroya Zinc Ferrite during Roasting with 20% Coal and 70% $MnCO_3$ at 1100°C 118
Table 31 Chemical Reactions during the $Na_2CO_3/MnCO_3$ Roast Process 119
Table 32 Comparison of Leach Volumes and Zinc Concentrations for Various Ferrite Treatment Flowsheets 128
Table 32 Comparison of Thermodynamics of Waelz Kiln Reactions 131
Table 33 Typical Chemical Analysis of EAF Dust Supplied by Altasteel 136
Table 34 Chemical Analysis of As-Received Altasteel EAF Dust 136
Table 35 Operating or Developing Technologies for EAF Dust Treatment 141
Table 36 Dormant or Abandoned Technologies for EAF Dust Treatment 142
Table 37 Experimental Conditions Used in Experimental Designs for Roasting EAF Dust with Na_2CO_3 and Resulting Model Variance 153
Table 38 Experimental Conditions Used in Experimental Designs for Roasting EAF Dust with Carbonaceous Reagents and Resulting Model Variance 153
Table 39 Phases Identified by XRD Analysis of EAF Dust Roasted with Na_2CO_3 155
Table 40 Phases Identified by X-ray Diffraction Analysis of EAF Dust after Roasting with Na_2CO_3 and Leaching with 200 g/L H_2SO_4 159
Table 41 Deportment of Iron Minerals during Na_2CO_3 Roasting and H_2SO_4 Leaching of Altasteel EAF Dust 163
Table 42 Phases Identified by XRD Analysis of EAF Dust Roasted with Na_2CO_3 and 3.7% $CaCO_3$ 168
Table 43 Phases Identified by X-ray Diffraction Analysis of EAF Dust after Roasting with Na_2CO_3 and $CaCO_3$ and Leaching with 200 g/L H_2SO_4 172
Table 44 Deportment of Iron Mineral during Roasting of EAF Dust with Na_2CO_3 and $CaCO_3$ and Leaching with 200 g/L H_2SO_4 176
Table 45 Phases Identified by XRD Analysis of EAF Dust Roasted with Na_2CO_3 and $MnCO_3$ 180
Table 46 Phases Identified by X-ray Diffraction Analysis of EAF Dust after Roasting with Na_2CO_3 and $MnCO_3$ and Leaching with 200 g/L H_2SO_4 183
Table 47 Phases Identified by XRD Analysis of EAF Dust Roasted with Coal 189
Table 48 Estimated Distribution of Iron in Mineral Phases after Roasting of EAF Dust with Coal 191

Table 49 Phases Identified by X-ray Diffraction Analysis of EAF Dust after Roasting with Coal and Leaching with 200 g/L H_2SO_4 194
Table 50 Phases Identified by XRD Analysis of EAF Dust Roasted with Coal and 14.1% $CaCO_3$ 200
Table 51 Estimated Distribution of Iron in Mineral Phases after Roasting of EAF Dust with Coal and $CaCO_3$ 202
Table 52 Phases Identified by X-ray Diffraction Analysis of EAF Dust after Roasting with Coal and 14.1% $CaCO_3$ and Leaching with 200 g/L H_2SO_4 204
Table 53 Deportment of Minor Elements in Altasteel EAF Dust during Roasting with 40% Na_2CO_3 at 950°C 208
Table 54 Deportment of Minor Elements in Altasteel EAF Dust during Roasting with 16% Coal at 1000°C 209
Table 55 Analysis of INCO Copper Residue 216
Table 56 Phases Identified by XRD Analysis of Copper Residue Feed Samples 218
Table 57 Pyrite and Arsenopyrite Oxidation 223
Table 58 Lime Roasting Reactions for Pyrite and Arsenopyrite 224
Table 59 Elemental Deportment from Roasting and Leaching of Inco Copper Residue (Feed #1) with Na_2CO_3 and Various Secondary Additives 239
Table 60 Experimental Conditions Used in Experimental Designs for Roasting Inco Copper Residue with Na_2CO_3 and Resulting Model Variance 241
Table 61 Phases Identified by XRD Analysis of Copper Residue Roasted at 700°C with Na_2CO_3 243
Table 62 Phases Identified by XRD Analysis of Inco Copper Residue (Feed #1) Roasted with Na_2CO_3 and Leached with Hot Water 247
Table 63 Phases Identified by XRD Analysis of Inco Copper Residue (Feed #1) Roasted with Na_2CO_3 and Leached with 200 g/L H_2SO_4 at Room Temperature 251
Table 64 Phases Identified by XRD Analysis of Inco Copper Residue (Feed #2) Roasted with Na_2CO_3 255
Table 65 Phases Identified by XRD Analysis of Inco Copper Residue (Feed #2) Roasted with Na_2CO_3 and Leached with Hot Water 260
Table 66 Phases Identified by XRD Analysis of Inco Copper Residue (Feed #2) Roasted with Na_2CO_3 and Leached with 200 g/L H_2SO_4 at 95 to 97°C 264
Table 67 Phases Identified by XRD Analysis of Copper Residue (Feed #2) Roasted with $Ca(OH)_2$ 269
Table 68 Phases Identified by XRD Analysis of Copper Residue Roasted with $Ca(OH)_2$ and Leached with Hot Water 273
Table 69 Phases Identified by XRD Analysis of Copper Residue Roasted with $Ca(OH)_2$ and Leached with 300 g/L H_2SO_4 at 95 to 97°C 276
Table 70 Phases Identified by XRD Analysis of Copper Residue (Feed #2) Roasted with Na_2CO_3 and 22.6% $FeSO_4{\cdot}7H_2O$ 282

Table 71 Phases Identified by XRD Analysis of Copper Residue Roasted with Na_2CO_3 and 22.6% $FeSO_4 \cdot 7H_2O$ and Leached with Hot Water 291

Table 72 Phases Identified by XRD Analysis of Copper Residue Roasted with Na_2CO_3 and 22.6% $FeSO_4 \cdot 7H_2O$ and Leached with 200 g/L H_2SO_4 at 95 to 97°C 291

Table 73 Element Deportment from Roasting and Leaching of Inco Copper Residue (Feed #2) with 170% Na_2CO_3 at 450°C in Air and in Oxygen 297

Table 74 Deportment of Minor Elements in Inco Copper Residue (Sample #2) after Roasting with 170% Na_2CO_3 at 450°C in Air 298

Table 75 Deportment of Minor Elements in Inco Copper Residue (Sample #2) after Roasting with 170% Na_2CO_3 at 450°C in Oxygen 299

Table 76 Roasting and Leaching Reactions Expected during Na_2CO_3 Roasting 300

Table 77 Reactions during Nickel Hydroxide Precipitation of the Raffinate Bleed 303

Table 78 Reactions during Sulphide Precipitation of Raffinate Bleed 305

Table 79 Reactions during Sodium Recovery and Arsenic Precipitation 307

List of Figures

Figure 1 Effect of CaO and $Ca(OH)_2$ Addition and Temperature on Vanadium Extraction after Leaching with Hot Water (A)and 100 g/L Na_2CO_3 Solution (B) and on the Extent of $Ca(VO_3)_2$ Formation (C) 8

Figure 2 Effect of $CaCO_3$ and Gypsum Addition and Temperature on Vanadium Extraction after Leaching with Hot Water (A)and 100 g/L Na_2CO_3 Solution (B) and on the Extent of $Ca(VO_3)_2$ Formation (C) 8

Figure 3 Effect of Reagent Addition at 950°C - Leaching with 100 g/L H_2SO_4 10

Figure 4 SEM Micrographs of Roasted Suncor Ash: 10% CaO, 950°C, Water Leach (A,B), 10% CaO, 950°C, Na_2CO_3 Leach (C,D) and 10% $Ca(OH)_2$, 850°C, Na_2CO_3 Leach (E,F) 11

Figure 5 SEM Micrographs of Water Leached Roasted Suncor Fly Ash: 15% $CaCO_3$ at 950°C (A), 15% Gypsum at 950°C (B,C,D) 12

Figure 6 Effect of KCl and NaCl Addition and Temperature on Vanadium Extraction 13

Figure 7 Vanadium Extraction versus NaCl and KCl Addition (Mole Basis) 14

Figure 8 SEM Micrographs of Water Leached Suncor Fly Ash: 25% NaCl at 850°C (A), 25% KCl at 950°C (B,C) and 25% KCl at 850°C (D,E,F) 15

Figure 9 Effect of Roasting Time and Temperature on Vanadium Extraction 16

Figure 10 Solubility of Potassium and Vanadium in the KVO_3-KCl-H_2O System 17

Figure 11 Secondary Electron (SE) and Backscattered Electron (BSE) Images of La Oroya Zinc Ferrite Feed Sample 29

Figure 12 Potential Zinc Replacement Reactions (ΔG^o vs. Temperature) 43

Figure 13 Potential Zinc Reduction/Ferrite Formation Reactions (ΔG^o vs. Temperature) 44

Figure 14 Potential Sulphation Reactions (ΔG^o vs. Temperature) 45

Figure 15 Potential Chloridization Reactions (ΔG^o vs. Temperature) 46

Figure 16 Zinc Extractions for Ca, Mg and Mn Replacement Reactions 48

Figure 17 Zinc Extractions for Na Replacement Reactions 50

Figure 18 Iron Extractions for Na Replacement Reactions 51

Figure 19 Effect of Roasting with 60% Na_2CO_3-40% $CaCO_3$ Mixture on A) Zinc and B) Iron Extractions 52

Figure 20 Zinc Extractions for Roasting with Charcoal and Ferrite-Forming Reagents 53

Figure 21 Zn Extractions for Roasting with Various Types of Carbon at 1000°C with A) CaO (150% of Stoichiometric) and B) MgO (150% of Stoichiometric) 54

Figure 22 Zinc Extractions from Roasting with NaCl and $CaCl_2$ 55

Figure 23 Zinc Extractions from Roasting with $MgSO_4$ and $CaSO_4$ 55

Figure 24 Generation of a Circumscribed Central Composite Design for Two Factors (111) 57

Figure 25 Effect of Temperature and Na_2CO_3 Addition on A) Zinc Extraction and B) Iron Extraction from Roasted La Oroya Zinc Ferrite 62

Figure 26 X-ray Diffraction Patterns of Zinc Ferrite Roasted with Na_2CO_3 63

Figure 27 Secondary Electron (SE) and Backscattered Electron (BSE) Images of Zinc Ferrite Roasted at 950°C with 80% Na_2CO_3 (Sample E) 64

Figure 28 X-ray Diffraction Patterns of Zinc Ferrite Residue after Roasting with Na_2CO_3 and Leaching with 200 g/L H_2SO_4 65

Figure 29 Potential Reactions of Secondary Reagents with $NaFeO_2$ (ΔG^o vs. Temperature) 67

Figure 30 Effect of Na_2CO_3 and Temperature on Zn Extractions from La Oroya Zinc Ferrite Roasted with Various Amounts of $CaCO_3$ 68

Figure 31 Effect of Na_2CO_3 and $CaCO_3$ Additions on Zinc and Iron Extractions from La Oroya Zinc Ferrite Roasted at A) 750°C, B) 850°C and C) 950°C 69

Figure 32 X-ray Diffraction Patterns of Zinc Ferrite Roasted with Na_2CO_3 and $CaCO_3$ 70

Figure 33 Secondary Electron (SE) and Backscattered Electron (BSE) Images of Zinc Ferrite Roasted at 950°C with 80% Na_2CO_3 and 7.8% $CaCO_3$ (Sample C) 73

Figure 34 Secondary Electron (SE) and Backscattered Electron (BSE) Images of Zinc Ferrite Roasted at 950°C with 80% Na_2CO_3 and 29.5% $CaCO_3$ (Sample D) 73

Figure 35 X-ray Diffraction Patterns of Zinc Ferrite Residue after Roasting with Na_2CO_3 and $CaCO_3$ and Leaching with 200 g/L H_2SO_4 74

Figure 36 Secondary Electron (SE) and Backscattered Electron (BSE) Images of Zinc Ferrite Roasted at 950°C with 80% Na_2CO_3 and 7.8% $CaCO_3$ and Leached with 200 g/L H_2SO_4 (Sample C) 76

Figure 37 Secondary Electron (SE) and Backscattered Electron (BSE) Images of Zinc Ferrite Roasted at 950°C with 80% Na_2CO_3 and 29.5% $CaCO_3$ and Leached with 200 g/L H_2SO_4 (Sample D) 76

Figure 38 Effect of Na_2CO_3 and Temperature on Zn Extractions from La Oroya Zinc Ferrite Roasted with Various Amounts of $Mg(OH)_2$ 77

Figure 39 Effect of Na_2CO_3 and $Mg(OH)_2$ Additions on Zinc and Iron Extractions from La Oroya Zinc Ferrite Roasted at A) 750°C, B) 850°C and C) 950°C 78

Figure 40 X-ray Diffraction Patterns of Zinc Ferrite Roasted with Na_2CO_3 and $Mg(OH)_2$ 80

Figure 41 Secondary Electron (SE) and Backscattered Electron (BSE) Images of Zinc Ferrite Roasted at 950°C with 80% Na_2CO_3 and 4.5% $Mg(OH)_2$ (Sample C) 81

Figure 42 Secondary Electron (SE) and Backscattered Electron (BSE) Images of Zinc Ferrite Roasted at 950°C with 80% Na_2CO_3 and 17.1% $Mg(OH)_2$ (Sample D) 82

Figure 43 Secondary Electron (SE) and Backscattered Electron (BSE) Images of Zinc Ferrite Roasted at 950°C with 80% Na_2CO_3 and 4.5% $Mg(OH)_2$ after Leaching with 200 g/L H_2SO_4 (Sample C) 83

Figure 44 Effect of Na_2CO_3 and Temperature on Zn Extractions from La Oroya Zinc Ferrite Roasted with Various Amounts of $MnCO_3$ 84

Figure 45 Effect of Na_2CO_3 and $MnCO_3$ Additions on Zinc and Iron Extractions from La Oroya Zinc Ferrite Roasted at A) 750°C, B) 850°C and C) 950°C 85

Figure 46 XRD Patterns of Zinc Ferrite Roasted with Na_2CO_3 and $MnCO_3$ 87

Figure 47 Secondary Electron (SE) and Backscattered Electron (BSE) Images of Zinc Ferrite Roasted at 950°C with 80% Na_2CO_3 and 33.3% $MnCO_3$ (Sample D) 88

Figure 48 X-ray Diffraction Patterns of Zinc Ferrite Residue after Roasting with Na_2CO_3 and $MnCO_3$ and Leaching with 200 g/L H_2SO_4 89

Figure 49 Secondary Electron (SE) and Backscattered Electron (BSE) Images of Zinc Ferrite Roasted at 950°C with 80% Na_2CO_3 and 33.3% $MnCO_3$ after Leaching with 200 g/L H_2SO_4 (Sample D) 90

Figure 50 Effect of Carbon Black Addition and Temperature on Total Zinc and Iron Extractions from Roasted La Oroya Zinc Ferrite 92

Figure 51 Effect of Coal Addition and Temperature on Total Zinc and Iron Extractions from Roasted La Oroya Zinc Ferrite 93

Figure 52 Effect of Temperature and Carbon Black or Coal Addition on the Percentage of Zinc Removed as Fume during Roasting 93

Figure 53 XRD Patterns of Zinc Ferrite Roasted with Coal 94

Figure 54 X-ray Diffraction Patterns of Zinc Ferrite Residue after Roasting with Coal and Leaching with 200 g/L H_2SO_4 96

Figure 55 Effect of Coal Addition and Temperature on Zinc and Iron Extractions from La Oroya Zinc Ferrite Roasted with $CaCO_3$ Additions of A) 31.0%, B) 46.5% and C) 62.0% 98

Figure 56 Effect of Temperature and Coal Addition on the Percentage of Zinc Removed as Fume during Roasting for $CaCO_3$ additions of A) 31.0%, B) 46.5% and C) 62.0% 99

Figure 57 XRD Patterns of Zinc Ferrite Roasted with Coal and 62% $CaCO_3$ 100

Figure 58 Secondary Electron (SE) and Backscattered Electron (BSE) Images of Zinc Ferrite after Roasting at 1100°C with 12% Coal and 62% $CaCO_3$ (Sample C) 102

Figure 59 Secondary Electron (SE) and Backscattered Electron (BSE) Images of Zinc Ferrite after Roasting at 1100°C with 20% Coal and 62% $CaCO_3$ (Sample D) 102

Figure 60 X-ray Diffraction Patterns of Zinc Ferrite Residue after Roasting with Coal and $CaCO_3$ and Leaching with 200 g/L H_2SO_4 103

Figure 61 Secondary Electron (SE) and Backscattered Electron (BSE) Images of Zinc Ferrite after Roasting at 1100°C with 20% Coal and 62% $CaCO_3$ and Leaching with 200 g/L H_2SO_4 (Sample D) 104

Figure 62 Effect of Coal Addition and Temperature on Zinc and Iron Extractions from La Oroya Zinc Ferrite Roasted with $MnCO_3$ Additions of A) 35.0%, B) 52.5% and C) 70.0% 107
Figure 63 Effect of Temperature and Coal Addition on the Percentage of Zinc Removed as Fume during Roasting for $MnCO_3$ additions of A) 35.0%, B) 52.5% and C) 70.0% 108
Figure 64 XRD Patterns of Zinc Ferrite Roasted with Coal and 70.0% $MnCO_3$ 109
Figure 65 Secondary Electron (SE) and Backscattered Electron (BSE) Images of Zinc Ferrite after Roasting at 1100°C with 20% Coal and 70% $MnCO_3$ (Sample D) 110
Figure 66 X-ray Diffraction Patterns of Zinc Ferrite Residue after Roasting with Coal and $MnCO_3$ and Leaching with 200 g/L H_2SO_4 111
Figure 67 Secondary Electron (SE) and Backscattered Electron (BSE) Images of Zinc Ferrite after Roasting at 1100°C with 20% Coal and 70% $MnCO_3$ and Leaching with 200 g/L H_2SO_4 (Sample D) 112
Figure 68 Possible Flowsheet for $Na_2CO_3/MnCO_3$ Roasting and H_2SO_4 Leaching of La Oroya Zinc Ferrite Residue 120
Figure 69 Na_2CO_3 and H_2SO_4 Regeneration by Low Temperature Metathesis 123
Figure 70 Na_2CO_3 and H_2SO_4 Regeneration by Solvent Extraction or Ion Exchange 124
Figure 71 Modification of the $Na_2CO_3/MnCO_3$ Roasting Flowsheet to Incorporate Hot Water Leaching into the Process Flowsheet 127
Figure 72 Possible Process Flowsheet for Roasting with Coal and $MnCO_3$ and Leaching with Spent Electrolyte 133
Figure 73 X-ray Diffraction Pattern for Altasteel Electric Arc Furnace Dust 137
Figure 74 Secondary Electron (SE) and Backscattered Electron (BSE) Images of Altasteel Electric Arc Furnace Dust Feed Sample 138
Figure 75 Effect of Na_2CO_3 Addition on the Extraction of Cr, Zn and Fe from Altasteel EAF Dust 152
Figure 76 Effect of Temperature and Na_2CO_3 Addition on the A) Cr Extraction in Hot Water Leaching or B) Zn Extraction and C) Fe Extraction in Leaching with 200 g/L H_2SO_4 for Roasted Altasteel EAF Dust 154
Figure 77 XRD Patterns of EAF Dust Roasted with Na_2CO_3 156
Figure 78 Secondary Electron (SE) and Backscattered Electron (BSE) Images of EAF Dust after Roasting at 950°C with 40% Na_2CO_3 (Sample D) 157
Figure 79 Secondary Electron (SE) and Backscattered Electron (BSE) Images of EAF Dust after Roasting at 950°C with 80% Na_2CO_3 (Sample E) 158
Figure 80 Secondary Electron (SE) and Backscattered Electron (BSE) Images of EAF Dust after Roasting at 950°C with 80% Na_2CO_3 and Leaching with Hot Water (Sample E) 159
Figure 81 XRD Patterns of EAF Dust Residue after Roasting with Na_2CO_3 and Leaching with 200 g/L H_2SO_4 160

Figure 82 Secondary Electron (SE) and Backscattered Electron (BSE) Images of EAF Dust after Roasting at 950°C with 40% Na_2CO_3 and Leaching with 200 g/L H_2SO_4 (Sample D) 161
Figure 83 Secondary Electron (SE) and Backscattered Electron (BSE) Images of EAF Dust after Roasting at 950°C with 80% Na_2CO_3 and Leaching with 200 g/L H_2SO_4 (Sample E) 161
Figure 84 Reactions of $ZnFe_2O_4$ and Fe_3O_4 with Na_2CO_3 and $CaCO_3$ 164
Figure 85 Extrapolation of the Response Surface Models Describing the Effect of Temperature and Na_2CO_3 Addition on the A) Chromium Extraction in Hot Water Leaching or B) Zinc Extraction and C) Iron Extraction in Leaching with 200 g/L H_2SO_4 for Roasted Altasteel EAF Dust 166
Figure 86 Effect of Na_2CO_3 and Temperature on Chromium Hot Water Leach Extractions of Altasteel EAF Dust Roasted with A) 3.7% $CaCO_3$, B) 8.9% $CaCO_3$ and C) 14.1% $CaCO_3$ 167
Figure 87 Effect of Na_2CO_3 and Temperature on Zinc and Iron Extractions from Altasteel EAF Dust Roasted with A) 3.7% $CaCO_3$, B) 8.9% $CaCO_3$ and C) 14.1% $CaCO_3$ after Leaching with 200 g/L H_2SO_4 169
Figure 88 XRD Patterns of EAF Dust Residue after Roasting with Na_2CO_3 and $CaCO_3$ 170
Figure 89 Secondary Electron (SE) and Backscattered Electron (BSE) Images of EAF Dust after Roasting at 1000°C with 50% Na_2CO_3 and 3.7% $CaCO_3$ (Sample C) 171
Figure 90 XRD Patterns of EAF Dust Residue after Roasting with Na_2CO_3 and $CaCO_3$ and Leaching with 200 g/L H_2SO_4 173
Figure 91 Secondary Electron (SE) and Backscattered Electron (BSE) Images of EAF Dust after Roasting at 1000°C with 50% Na_2CO_3 and 3.7% $CaCO_3$ and Leaching with 200 g/L H_2SO_4 (Sample C) 174
Figure 92 Secondary Electron (SE) and Backscattered Electron (BSE) Images of EAF Dust after Roasting at 1000°C with 90% Na_2CO_3 and 3.7% $CaCO_3$ and Leaching with 200 g/L H_2SO_4 (Sample D) 175
Figure 93 Effect of Na_2CO_3 and Temperature on Chromium Extractions from Altasteel EAF Dust Roasted with A) 4.3% $MnCO_3$, B) 10.2% $MnCO_3$ and C) 16.3% $MnCO_3$ 178
Figure 94 Effect of Na_2CO_3 and Temperature on Zinc and Iron Extractions from Altasteel EAF Dust Roasted with A) 4.3% $MnCO_3$, B) 10.2% $MnCO_3$ and C) 16.3% $MnCO_3$ 179
Figure 95 XRD Patterns of EAF Dust Roasted with Na_2CO_3 and $MnCO_3$ 181
Figure 96 Secondary Electron (SE) and Backscattered Electron (BSE) Images of EAF Dust after Roasting at 1000°C with 50% Na_2CO_3 and 16.3% $MnCO_3$ (Sample C) 182
Figure 97 XRD Patterns of EAF Dust Residue after Roasting with Na_2CO_3 and $MnCO_3$ and Leaching with 200 g/L H_2SO_4 183

Figure 98 Secondary Electron (SE) and Backscattered Electron (BSE) Images of EAF Dust after Roasting at 1000°C with 50% Na_2CO_3 and 16.3%$MnCO_3$ and Leaching with 200 g/L H_2SO_4 (Sample C) 184
Figure 99 Comparison of Maximum Zinc Extractions and Zinc Extractions at 50% Na_2CO_3, from the Response Surface Models (RSM) with Maximum Extractions Calculated from the Change in Activity in a $(Zn,Mn)Fe_2O_4$ Solid Solution 187
Figure 100 Effect of Coal Addition and Temperature on the A) Zn Extraction and B) Fe Extractions after Leaching with 200 g/L H_2SO_4 and C) the Amount of Zinc Fumed during Roasting from the Roasted Altasteel EAF Dust 188
Figure 101 XRD Patterns of EAF Dust Roasted with Coal 190
Figure 102 Secondary Electron (SE) and Backscattered Electron (BSE) Images of EAF Dust after Roasting at 1000°C with 16% Coal (Sample C) 192
Figure 103 Secondary Electron (SE) and Backscattered Electron (BSE) Images of EAF Dust after Roasting at 1100°C with 20% Coal (Sample E) 193
Figure 104 XRD Patterns of EAF Dust Residue after Roasting with Coal and Leaching with 200 g/L H_2SO_4 195
Figure 105 Secondary Electron (SE) and Backscattered Electron (BSE) Images of EAF Dust after Roasting at 1000°C with 16% Coal and Leaching with 200 g/L H_2SO_4 (Sample C) 196
Figure 106 Effect of Coal Addition and Temperature on Zinc and Iron Extractions from Altasteel EAF Dust Roasted with $CaCO_3$ Additions of A) 3.7%, B) 8.9% and C) 14.1% 199
Figure 107 Effect of Coal Addition and Temperature on the Amount of Zinc Fumed from Altasteel EAF Dust Roasted with $CaCO_3$ Additions of A) 3.7%, B) 8.9% and C) 14.1% 200
Figure 108 XRD Patterns of EAF Dust Roasted with Coal and $CaCO_3$ 201
Figure 109 Secondary Electron (SE) and Backscattered Electron (BSE) Images of EAF Dust after Roasting at 1050°C with 18% Coal and 14.1% $CaCO_3$ (Sample D) 203
Figure 110 XRD Patterns of EAF Dust Residue after Roasting with Coal and $CaCO_3$ and Leaching with 200 g/L H_2SO_4 205
Figure 111 Secondary Electron (SE) and Backscattered Electron (BSE) Images of EAF Dust after Roasting at 1050°C with 18% Coal and 14.1% $CaCO_3$ and Leaching with 200 g/L H_2SO_4 (Sample D) 206
Figure 112 Possible Process Flowsheet for Na_2CO_3 Roasting of EAF Dust 210
Figure 113 Potential Process Flowsheet for Roasting of EAF Dust with Coal 214
Figure 114 Secondary Electron (SE) and Backscattered Electron (BSE) Images of As-Received Inco Copper Residue (Feed #1) 217
Figure 115 Secondary Electron (SE) and Backscattered Electron (BSE) Images of As-Received Inco Copper Residue (Feed #2) 217
Figure 116 XRD Patterns of Copper Residue Samples before and after Leaching with Hot Water 219

Figure 117 Potential Reactions for Roasting As_2S_3 (ΔG^o vs. Temperature) 231
Figure 118 Potential Reactions for Roasting Copper and Nickel Sulphides (ΔG^o vs. Temperature) 232
Figure 119 Setup for Tube Furnaces Used in Roasting Tests for A) Preliminary Scoping Tests and DOE Tests and B) All Other Roasting Tests (Not Drawn to Scale) 234
Figure 120 Deportment of Sulphur during Scoping Roasting and Leaching Tests on Inco Copper Residue (Feed #1) 236
Figure 121 Deportment of Arsenic during Scoping Roasting and Leaching Tests on Inco Copper Residue (Feed #1) 236
Figure 122 Deportment of Copper during Scoping Roasting and Leaching Tests on Inco Copper Residue (Feed #1) 237
Figure 123 Deportment of Nickel during Scoping Roasting and Leaching Tests on Inco Copper Residue (Feed #1) 237
Figure 124 Effect of Na_2CO_3 Addition and Temperature on Sulphur and Arsenic Emissions During Roasting of Inco Copper Residue (Feed #1) 242
Figure 125 XRD Patterns of Inco Copper Residue (Feed #1) after Roasting with Na_2CO_3 243
Figure 126 Secondary Electron (SE) and Backscattered Electron (BSE) Images of Inco Copper Residue (Feed #1) after Roasting at 550°C with 150% Na_2CO_3 (Sample B) 244
Figure 127 Effect of Na_2CO_3 Addition and Temperature on Sulphur Deportment from Inco Copper Residue (Feed #1) 245
Figure 128 Effect of Na_2CO_3 Addition and Temperature on Arsenic Deportment from Inco Copper Residue (Feed #1) 247
Figure 129 Effect of Na_2CO_3 Addition and Temperature on Copper and Nickel Extractions from Inco Copper Residue (Feed #1) 248
Figure 130 XRD Patterns of Inco Copper Residue (Feed #1) after Roasting with Na_2CO_3 and Leaching with Hot Water 249
Figure 131 XRD Patterns of Inco Copper Residue (Feed #1) after Roasting with Na_2CO_3 and Leaching with 200 g/L H_2SO_4 at Room Temperature 250
Figure 132 Secondary Electron (SE) and Backscattered Electron (BSE) Images of Inco Copper Residue (Feed #1) after Roasting at 550°C with 150% Na_2CO_3 and Leaching with Hot Water (Sample B) 253
Figure 133 Secondary Electron (SE) and Backscattered Electron (BSE) Images of Inco Copper Residue (Feed #1) after Roasting at 550°C with 150% Na_2CO_3 and Leaching with 200 g/L H_2SO_4 at Room Temperature (Sample B) 253
Figure 134 Effect of Na_2CO_3 Addition and Temperature on Sulphur and Arsenic Emissions During Roasting of Inco Copper Residue (Feed #2) 254
Figure 135 XRD Patterns of Inco Copper Residue (Feed #2) after Roasting with Na_2CO_3 256

Figure 136 Effect of Na_2CO_3 Addition and Temperature on Sulphur Deportment from Inco Copper Residue (Feed #2) 257
Figure 137 Effect of Na_2CO_3 Addition and Temperature on Arsenic Deportment from Inco Copper Residue (Feed #2) 259
Figure 138 Effect of Na_2CO_3 Addition and Temperature on Copper and Nickel Extractions from Inco Copper Residue (Feed #2) 261
Figure 139 XRD Patterns of Inco Copper Residue (Feed #2) after Roasting with Na_2CO_3 and Leaching with Hot Water 262
Figure 140 XRD Patterns of Inco Copper Residue (Feed #2) after Roasting with Na_2CO_3 and Leaching with 200 g/L H_2SO_4 at 95 to 97°C 263
Figure 141 Secondary Electron (SE) and Backscattered Electron (BSE) Images of Inco Copper Residue (Feed #2) after Roasting at 550°C with 150% Na_2CO_3 and Leaching with Hot Water (Sample B) 266
Figure 142 Secondary Electron (SE) and Backscattered Electron (BSE) Images of Inco Copper Residue (Feed #2) after Roasting at 550°C with 150% Na_2CO_3 and Leaching with 200 g/L H_2SO_4 at 95 to 97°C (Sample B) 266
Figure 143 Effect of $Ca(OH)_2$ Addition and Temperature on Sulphur and Arsenic Emissions During Roasting 268
Figure 144 XRD Patterns of Inco Copper Residue after Roasting with $Ca(OH)_2$ 270
Figure 145 Effect of $Ca(OH)_2$ Addition and Temperature on Sulphur Deportment 271
Figure 146 Effect of $Ca(OH)_2$ Addition and Temperature on Arsenic Deportment 272
Figure 147 Effect of $Ca(OH)_2$ Addition and Temperature on Copper and Nickel Extractions 274
Figure 148 XRD Patterns of Inco Copper Residue after Roasting with $Ca(OH)_2$ and Leaching with Hot Water 275
Figure 149 XRD Patterns of Inco Copper Residue after Roasting with $Ca(OH)_2$ and Leaching with 300 g/L H_2SO_4 at 95 to 97°C 276
Figure 150 Effect of Na_2CO_3 Addition and Temperature on Sulphur Emissions During Roasting with 22.6 and 45.2% $FeSO_4 \cdot 7H_2O$ 280
Figure 151 Effect of Na_2CO_3 Addition and Temperature on Arsenic Emissions During Roasting with 22.6 and 45.2% $FeSO_4 \cdot 7H_2O$ 281
Figure 152 XRD Patterns of Inco Copper Residue after Roasting with Na_2CO_3 and 22.6% $FeSO_4 \cdot 7H_2O$ 283
Figure 153 Effect of Na_2CO_3 Addition, Temperature and $FeSO_4 \cdot 7H_2O$ Additions on Sulphur Deportment 285
Figure 154 Effect of Na_2CO_3 Addition, Temperature and $FeSO_4 \cdot 7H_2O$ Additions on Arsenic Deportment 286
Figure 155 Effect of Na_2CO_3 Addition, Temperature and $FeSO_4 \cdot 7H_2O$ Additions on Copper Extractions 288
Figure 156 Effect of Na_2CO_3 Addition, Temperature and $FeSO_4 \cdot 7H_2O$ Additions on Nickel Extractions 290

Figure 157 XRD Patterns of Inco Copper Residue after Roasting with Na_2CO_3 and 22.6% $FeSO_4 \cdot 7H_2O$ and Leaching with Hot Water 292
Figure 158 XRD Patterns of Inco Copper Residue after Roasting with Na_2CO_3 and 22.6% $FeSO_4 \cdot 7H_2O$ and Leaching with 200 g/L H_2SO_4 at 95 to 97°C 293
Figure 159 Secondary Electron (SE) and Backscattered Electron (BSE) Images of Inco Copper Residue (Feed #2) after Roasting at 450°C with 150% Na_2CO_3 and 45.2% $FeSO_4 \cdot 7H_2O$ and Leaching with Hot Water (Sample Z) 296
Figure 160 Secondary Electron (SE) and Backscattered Electron (BSE) Images of Inco Copper Residue (Feed #2) after Roasting at 450°C with 150% Na_2CO_3 and 45.2% $FeSO_4 \cdot 7H_2O$ and Leaching with 200 g/L H_2SO_4 at 95 to 97°C (Sample Z) 296
Figure 161 Proposed Roasting and Leaching Flowsheet for Na_2CO_3 Roasting of the Inco Copper Residue 300
Figure 162 Proposed Flowsheet for the Precipitation of Nickel Hydroxide from the Raffinate Bleed from Na_2CO_3 Roasting of Inco Copper Residue 302
Figure 163 Proposed Flowsheet for Sulphide Precipitation of Copper, Arsenic and Nickel from the Raffinate Bleed from Na_2CO_3 Roasting of Inco Copper Residue 305
Figure 164 Proposed Flowsheet for Sodium Recovery and Arsenic Precipitation from the Barren Solutions from Na_2CO_3 Roasting of the Inco Copper Residue 308

1.0 Introduction

Metamorphism is a well known geological process where minerals in a rock undergo changes in the solid state by the combined effects of temperature, pressure, interactions with geothermal fluids and time. The forces involved in metamorphism are extremely powerful and can alter the mineralogy of rocks on a massive scale. However, although geological metamorphism is very common in nature, a combination of chemical and kinetic constraints, including the low concentrations of valuable metals and relatively low temperatures in the Earth's crust and the low mobility of reactants and products in the solid state, limit the location and frequency of instances where these processes work together to concentrate valuable metals into an economically viable ore body.

Similar principles can be observed in high temperature reactions in metallurgical systems as the minerals in these systems can undergo a series of mineralogical changes and chemical reactions in the solid state upon heating. However, since the reaction conditions in metallurgical systems, such as temperature, time and gas composition, can be more closely controlled than in geological metamorphism and since reagents can be added to selectively alter the chemical composition of a system, it is possible to engineer the mineral transformations during roasting to control the distribution of valuable, or harmful, metals and to produce new groups of minerals that are more amenable to conventional methods of metals recovery or to environmentally safe disposal. To distinguish this type of process from other types of roasting processes, the term *transformational,* or *metamorphic, roasting* will be used throughout the descriptions in this study.

To be of any economic interest, a transformational roasting process must produce mineral assemblages which give at least one of the following results:

a) an increased solubility of valuable elements upon leaching (i.e., to allow for metals recovery)
b) a decreased solubility of undesirable elements in ground water (i.e., to produce stable residues for disposal)

c) a differential solubility between elements (i.e., to allow for a selective separation of various elements using different leaching reagents)
d) a potential physical separation between minerals using conventional mineral processing techniques, such as froth flotation or magnetic or electrostatic separation, or
e) a decrease in the emission of volatile elements (i.e., to control the release of harmful elements during roasting)

With proper selection of conditions, it may also be possible to tailor this type of process to produce residues with compositions and mineral assemblages that would make them potentially valuable for use in the manufacturing, construction or high tech industries.

An example of a process that uses these principles is the process developed at the University of Alberta for the recovery of vanadium from oil sands fly ash (1-3). Oil sands fly ash is formed during the combustion of oil sands bitumen, with V and Ni from the burned bitumen combining with minerals that are entrained in the bitumen, such as clays and sand, to form an ash consisting primarily of poorly crystalline cenospheres (2). The ash routinely contains from 3.6 to 6.2% V_2O_5 (carbon-free basis), which is two to five times higher than the highest grade vanadium concentrates processed in the world today. Initially, the ash contains less than 10% water soluble vanadium and is not amenable to being processed directly by leaching due to its high aluminum and silicon content. In the process developed at the U of A, the oil sands fly ash is roasted at 850 to 900°C with NaCl. During roasting, the ash reacts with the NaCl to form water soluble vanadium compounds, making between 75 and 85% of the vanadium in the ash readily recoverable by leaching with hot water (2). Sodium chloride also reacts with the aluminosilicate matrix of the ash to transform the roasted ash from a glassy, poorly crystalline material to a crystalline assemblage containing albite ($NaAlSi_3O_8$), hauyne ($Na_4Ca_2Al_6Si_6O_{24}SO_4$), pseudobrookite ($Fe_2TiO_5$) and hematite ($Fe_2O_3$) as its major phases (2). As a result, the residue remaining after hot water leaching to remove vanadium and also molybdenum is environmentally benign and, thus, readily disposable. With fine grinding and removal of iron and titanium using wet high intensity magnetic separation, this residue could even be potentially saleable as a substitute for feldspar or nepheline syenite products that are used as additives in glassmaking (3). Thus, in this case, transformational roasting was able, not only to improve the recovery of vanadium and molybdenum from this waste material, but to produce a much more stable, and potentially valuable, waste in the process.

Metallurgically, there are a number of commercial processes that already employ these principles in either metals recovery or control of waste products, including soda roasting of vanadium and chromium ores and molybdenum wastes (4-6), caustic fusion of zircon (7), alkali digestion of lithium ores (8) and lime roasting of auriferous arsenopyrite ores (9). However, to date, this type of roasting has only been limited to the recovery of a small number of metals from an even narrower range of materials.

Thus, the major focus of this research is to try to develop a generalized procedure which can be used to apply these high temperature mineral transformation techniques to recover more metals from a wider range of feed materials. In particular, this study will focus on the transformational roasting of metallurgical wastes. These types of materials include metal sulphides, oxides, silicates or sulphates, in the form of slags, dusts and leach residues. These materials often contain significant metals values, but their complexity, or high levels of impurities, often makes them difficult to treat using the conventional routes employed in existing smelters or processing plants. However, these materials often represent low cost or "zero" cost feeds as their disposal generally is an economic liability to the companies that produce them. The use of actual industrial wastes, rather than materials synthesized in the laboratory, also allows the deportment, and interference, of impurities during transformational roasting to be studied.

Three stages of research were used to accomplish this objective. First, a familiar material and reaction system (i.e., vanadium recovery from oil sands fly ash) was selected and this material was roasted with previously untested reagents to test the fundamental premise of this research. Second, a generalized procedure for applying these techniques to other metallurgical systems was proposed. Third, this procedure was tested on three materials to evaluate and refine the procedure and identify interesting reaction systems for each material tested for future study. Zinc ferrite residue from Peru, electric arc furnace dust from Edmonton, Alberta and copper residue from Thompson, Manitoba were selected as the three materials for the third stage of the research.

2.0 Proof of Concept – Roasting of Oil Sands Fly Ash with Calcium and Potassium Reagents

The roasting of oil sands fly ash with potassium and calcium reagents to recover vanadium was selected as a starting point to try to extend the understanding of transformational roasting processes and to investigate the feasibility of this research approach. This system was chosen as the oil sands fly ash represents a well understood, familiar system with an established test procedure and tested equipment and, thus, there is significant process knowledge and expertise and a well-defined range of applicable process conditions from which to work. Calcium and potassium compounds were chosen as potential roasting reagents, based on their potential both to form soluble potassium or calcium vanadate compounds and to react with the aluminosilicate matrix of the ash to form crystalline potassium or calcium aluminosilicates.

Thus, the major focus of this proof of concept study is to determine whether soluble vanadium compounds and crystalline aluminosilicates can be formed from the ash using atypical (i.e., Ca or K) reagents as predicted from the understanding of the Na-fly ash system. If successful, the observations made throughout this study could then be used to help modify the procedures and techniques for application to transformational roasting in other reagent-mineral systems. As well, since a process flowsheet for vanadium recovery by roasting with NaCl has already been developed (3), the effectiveness of calcium and potassium reagents, relative to NaCl, can also be evaluated and the potential use of K- or Ca- reagents in commercial vanadium recovery can be discussed.

2.1 Literature Survey

Roasting oil sands fly ash with calcium reagents for vanadium recovery has only been documented once in the literature in previous research by the author (1). Ash was roasted at 850°C with a range of CaO additions and, although water extractions were low, vanadium extractions of 50 to 70% were possible by leaching with 100 g/L Na_2CO_3 solution.

Improved vanadium solubility has also been reported from ash formed by coking oil sands bitumen in the presence of various calcium reagents (10,11), but the differences in thermal history between this material and the Suncor fly ash do not allow them to be compared directly.

Roasting of oil sands fly ash with potassium reagents is not reported in published literature and, hence, is entirely novel.

2.2 Feed Materials

A typical Suncor ash sample was chosen as the feed material for this study. The ash was decarbonized at 500°C in a muffle furnace before performing roasting tests. A chemical analysis of this ash sample is included in Table I.

Table 1 Analysis of Decarbonized Suncor 1986 Fly Ash, wt%

V	Al	Ca	Fe	Mo	Ni	Si	Ti	L.O.I.
2.81	13.1	1.18	5.65	0.18	1.01	26.4	1.46	26.7

Before roasting, less than 1% of the vanadium in this ash sample was water soluble. (Roasting with no additives at 850°C gave a water leach extraction of less than 20%.)

Reagent grade KCl, CaO and $Ca(OH)_2$ were used in the roasting tests. Limestone ($CaCO_3$) for testing was obtained from Graymont Western Canada (>95% purity) while gypsum for testing was produced by hydrating construction grade plaster of paris.

2.3 Experimental Procedure

Similar test procedures to those used for the roasting of oil sands fly ash with NaCl were used (1). The ash, after decarbonization at 500°C, was combined with the respective additive, mixed in a mortar and pestle and placed in porcelain crucibles. The crucibles were then inserted into a muffle furnace preheated to the desired temperature and allowed to react for the required time. The samples were then removed from the furnace, air cooled, ground in a mortar and pestle and leached in water at 95 to 97°C for 1 h. Filter cakes were washed three times with distilled water, with the volume of the combined filtrate and wash solution measured and a sample taken for analysis. The filter cake was dried overnight at 95 to 100°C and the weight of the solids recorded. Selected samples of roasted, water-leached ash were also leached in 100 g/L Na_2CO_3 and 100 g/L H_2SO_4 solutions at 95 to 97°C for 1 h, with the samples filtered and washed following the procedure outlined above.

Solution and solids samples were analyzed using a single-element Perkin-Elmer 4000 atomic absorption (AA) spectrometer. Solids were digested using lithium metaborate fusion prior to analysis. Potassium concentrations were measured using a Buck Scientific PFP-7 flame photometer.

2.4 Roasting with Calcium Reagents

Suncor fly ash was roasted with varying amounts of CaO, $Ca(OH)_2$, $CaCO_3$ and gypsum ($CaSO_4 \cdot 2H_2O$) at 750, 850 and 950°C. The results from these tests are shown in Figures 1 and 2.

Figures 1A and 2A show that the water leaching extractions from the ash roasted with calcium compounds are quite low (0 to 44%). The low water leach extractions are largely a result of the relatively low solubility of calcium vanadates in water when compared to sodium vanadates. Calcium metavanadate ($Ca(VO_3)_2$ has a solubility of 1 to 5.5 g/L V while other calcium vanadates, such as calcium pyrovanadate ($Ca_2V_2O_7$) or orthovanadate ($Ca_3V_2O_8$), have much lower solubilities (<0.5 g/L V) (4). Thus, particularly at higher calcium additions, there could be a significant portion of the calcium vanadates formed that is not recoverable by water leaching.

To compensate for this decrease in solubility, the ash samples were then leached with 100 g/L Na_2CO_3 to dissolve more of the remaining water insoluble calcium vanadates (Fig 1B and 2B). Based on this differential solubility, the leaching extractions from these two leaching reagents were then used to give an estimate of the distribution between the types of calcium vanadate that are formed during roasting (Figures 1C and 2C). The phases detected using x-ray diffraction are also summarized in Table 2.

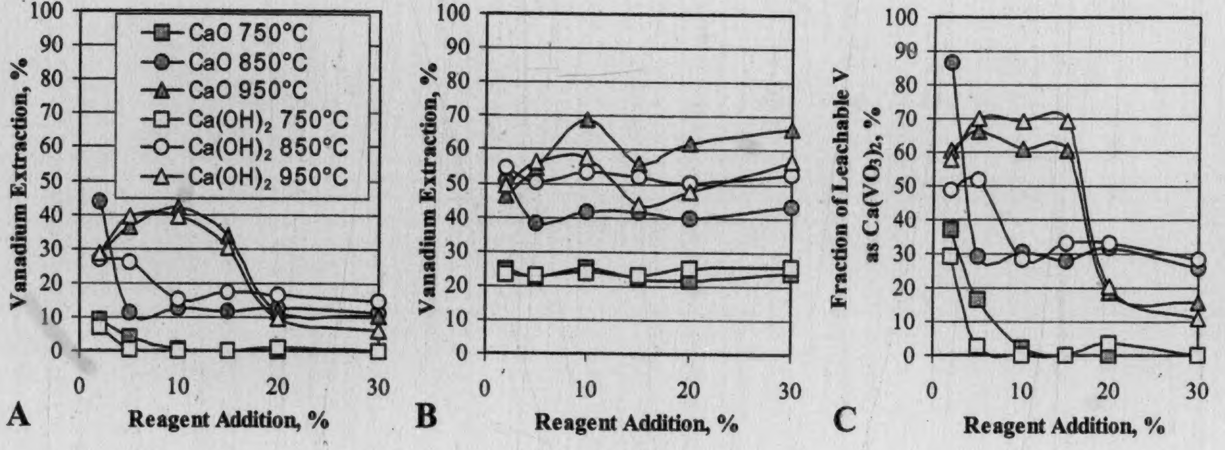

Figure 1

Effect of CaO and Ca(OH)$_2$ Addition and Temperature on Vanadium Extraction after Leaching with Hot Water (A) and 100 g/L Na$_2$CO$_3$ Solution (B) and on the Extent of Ca(VO$_3$)$_2$ Formation (C)

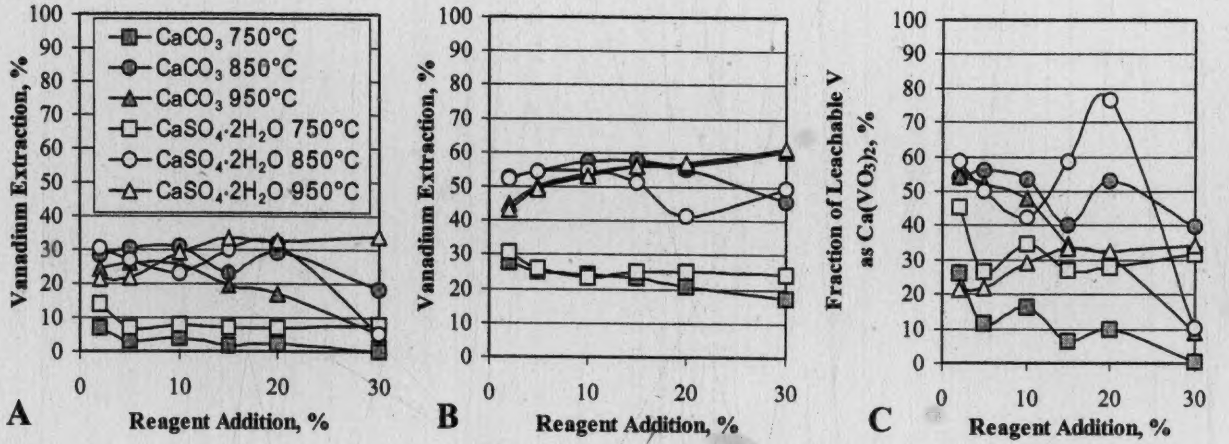

Figure 2

Effect of CaCO$_3$ and Gypsum Addition and Temperature on Vanadium Extraction after Leaching with Hot Water (A) and 100 g/L Na$_2$CO$_3$ Solution (B) and on the Extent of Ca(VO$_3$)$_2$ Formation (C)

Table 2 Summary of Mineral Phases Detected by X-ray Diffraction in Suncor Fly Ash Roasted with Calcium Reagents

Additive	Temperature	Minerals Formed during Roasting
All	750 to 850°C	Poorly crystalline; minor phases (anhydrite ($CaSO_4$), mullite ($Al_6Si_2O_{13}$) and pseudobrookite (Fe_2TiO_5))
$CaCO_3$, Gypsum	950°C	Anorthite($CaAl_2Si_2O_8$) and pseudobrookite (Fe_2TiO_5)
CaO, $Ca(OH)_2$	950°C	Anorthite ($CaAl_2Si_2O_8$) and pseudobrookite (Fe_2TiO_5) at low additions (<10%); decreasing crystallinity with increased additions

By comparing the trends observed in extraction and the extent of calcium metavanadate formation with the changes in mineralogy observed with x-ray diffraction, several important observations can be made from these tests.

First, in the samples roasted with CaO or $Ca(OH)_2$, the formation of calcium metavanadate is preferred at lower additions and with increasing temperature, with other more calcium rich, and less soluble, vanadates preferentially formed at lower temperatures and higher additions. At 950°C, in particular, the noticeable decrease in the fraction of $Ca(VO_3)_2$ formed with increased additions follows closely the decrease in crystallinity observed in x-ray diffraction as the CaO or $Ca(OH)_2$ additions are increased. Increased consumption of CaO or $Ca(OH)_2$ by the reactions to form crystalline calcium aluminosilicates at 950°C may mean that less calcium is available to form more calcium-rich vanadate compounds.

Second, similar trends are not noted for samples roasted with $CaCO_3$ and gypsum as the extraction profiles are either relatively flat, or show only a slight drop in extraction with increasing additions, for a given temperature. Little change is observed in the extraction of vanadium with Na_2CO_3 leaching as the temperature is increased from 850 to 950°C, even with the increase in crystallinity observed using XRD with the increase in temperature.

Third, the maximum vanadium extractions from roasting Suncor oil sands fly ash with calcium reagents are low (i.e., less than 69% for CaO and 56 to 61% for the other reagents) even after leaching with 100 g/L Na_2CO_3 solution and roasting at higher temperatures than were necessary for roasting with NaCl (i.e., 950°C vs. 850°C). These extractions compare poorly to the water leach extractions of 75 to 85% which are regularly obtained when the ash is roasted with NaCl.

Fourth, additional vanadium is not readily leached from the ash; even after leaching with 100 g/L H_2SO_4 (Figure 3), the small to nominal increases in vanadium extraction observed are accompanied by high Al and Si dissolution. (Silicon dissolution increases with decreasing crystallinity of the roasted samples while high dissolution of aluminum is maintained regardless of the degree of sample crystallinity.) This relationship between increased Al and Si dissolution and vanadium extraction may indicate that the remaining vanadium in the fly ash (31 to 44%), which is not readily water or Na_2CO_3 leachable, is associated with the aluminosilicate fraction of the leach residue, or potentially with an acid-insoluble vanadium oxide compound.

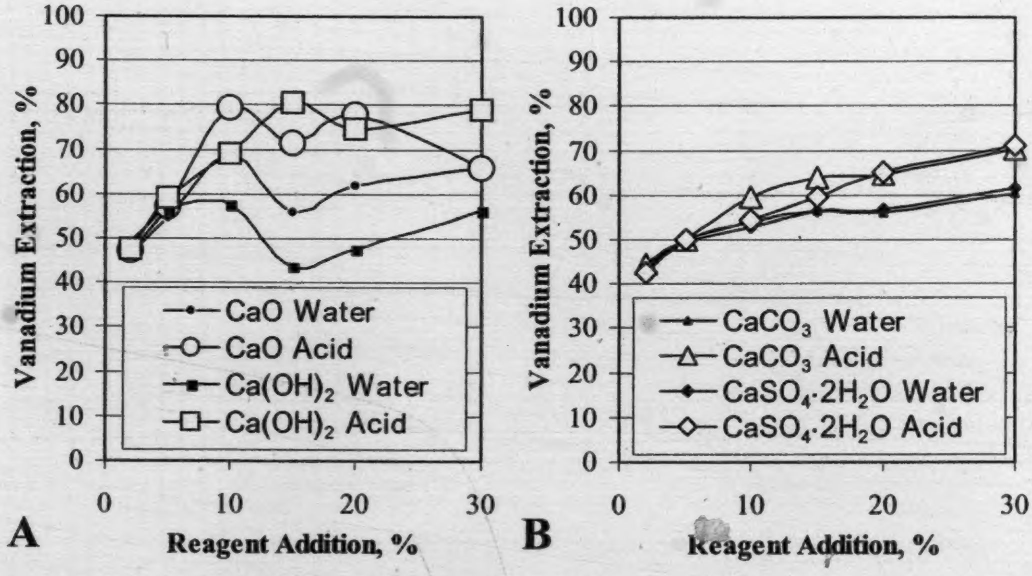

Figure 3 Effect of Reagent Addition at 950°C - Leaching with 100 g/L H_2SO_4

Overall, though, the low extractions and much lower solubility of the vanadates produced would make calcium reagents much less attractive economically than roasting with NaCl.

2.4.1 *Microstructure of Ash Roasted with Calcium Salts*

SEM micrographs of ash roasted with CaO and $Ca(OH)_2$ are shown in Figure 4.

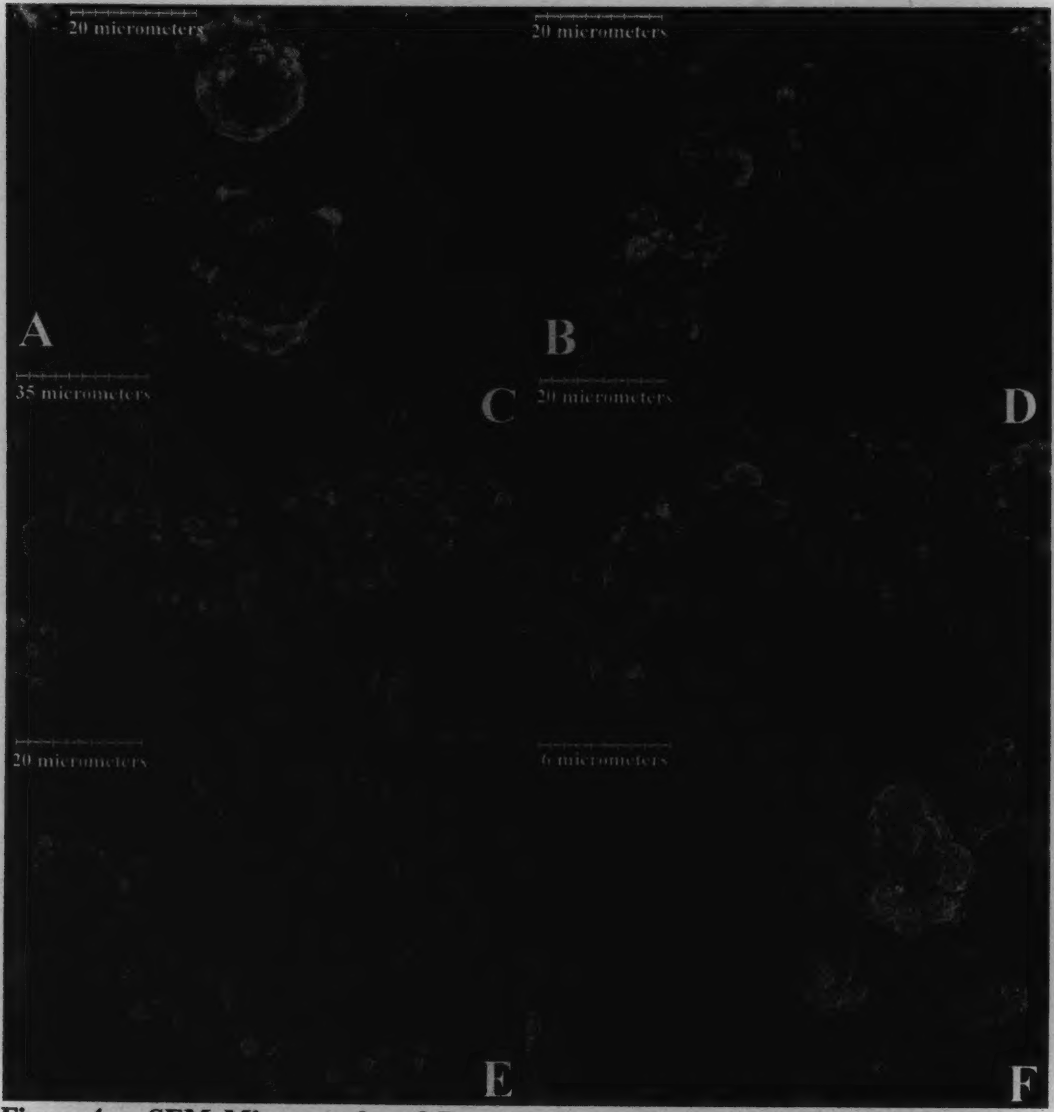
20 micrometers
20 micrometers
A
B
35 micrometers
C
20 micrometers
D
20 micrometers
6 micrometers
E
F

Figure 4 **SEM Micrographs of Roasted Suncor Ash: 10% CaO, 950°C, Water Leach (A,B), 10% CaO, 950°C, Na_2CO_3 Leach (C,D) and 10% $Ca(OH)_2$, 850°C, Na_2CO_3 Leach (E,F)**

At 950°C, most of the cenospheres in the ash have either crystallized to form anorthite, (i.e., irregular shaped crystals) or pseudobrookite (i.e., small elongate crystals) or show signs of alteration (Figure 4A). Cubic crystals of CaO reacting with the ash are visible on the surface of some cenospheres (Figure 4D). More cenospheres are intact in the ash roasted at 850°C, with some showing few signs of alteration (Figure 4E and 4F). Pseudobrookite crystals are also not as well formed in the ash roasted at 850°C.

Ash roasted with $CaCO_3$ and gypsum show signs of more severe alteration than samples roasted with CaO and $Ca(OH)_2$. Cenospheres from ash roasted with $CaCO_3$, where present, show striations pointing to the breakdown, or crystallization, of the cenospheres (Figure 5A) while intact cenospheres are virtually absent from ash roasted with gypsum (Figure 5C). Figure 5D shows a cenosphere, or possibly a pleurosphere, that has extensively recrystallized, but has still retained much of its original hollow spherical shape.

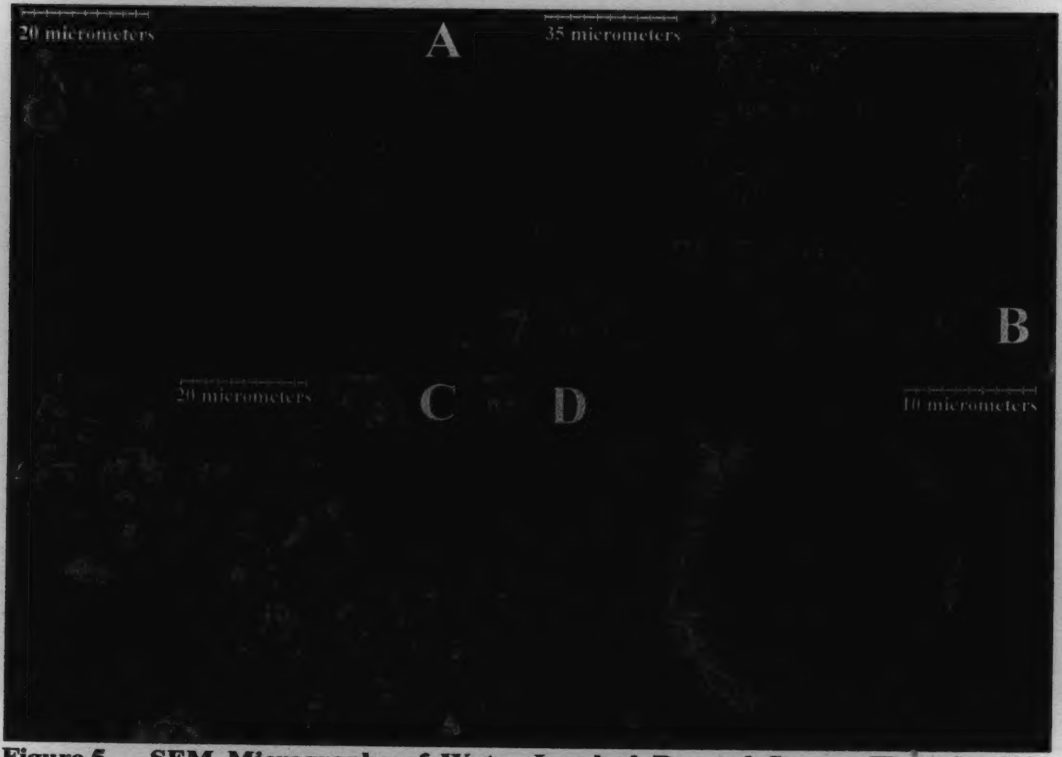

Figure 5 **SEM Micrographs of Water Leached Roasted Suncor Fly Ash: 15% $CaCO_3$ at 950°C (A), 15% Gypsum at 950°C (B,C,D)**

2.5 Roasting with Potassium Reagents

Suncor ash was roasted with varying amounts of KCl, and NaCl for comparison, at 750, 850 and 950°C. The water leach extractions from these tests were then compared on a mass basis (Figure 6) and on a mole basis (Figure 7) to allow direct comparison taking into account the difference in molar mass between K and Na. These figures show that the potassium vanadates formed during roasting are readily soluble in water and similar extractions to those achieved by roasting with NaCl are possible by roasting with KCl.

However, there are two notable trends in the extraction for ash roasted with KCl (Figure 7). First, the maximum vanadium extractions for a given temperature are higher for KCl than NaCl, but higher additions of KCl are required to reach those maxima as the roasting temperature increases. Second, after reaching these maxima, extractions at 750 and 850°C decreased with increasing additions of KCl. Extractions from roasting with NaCl, on the other hand, generally plateau and do not vary significantly with further increases in NaCl addition.

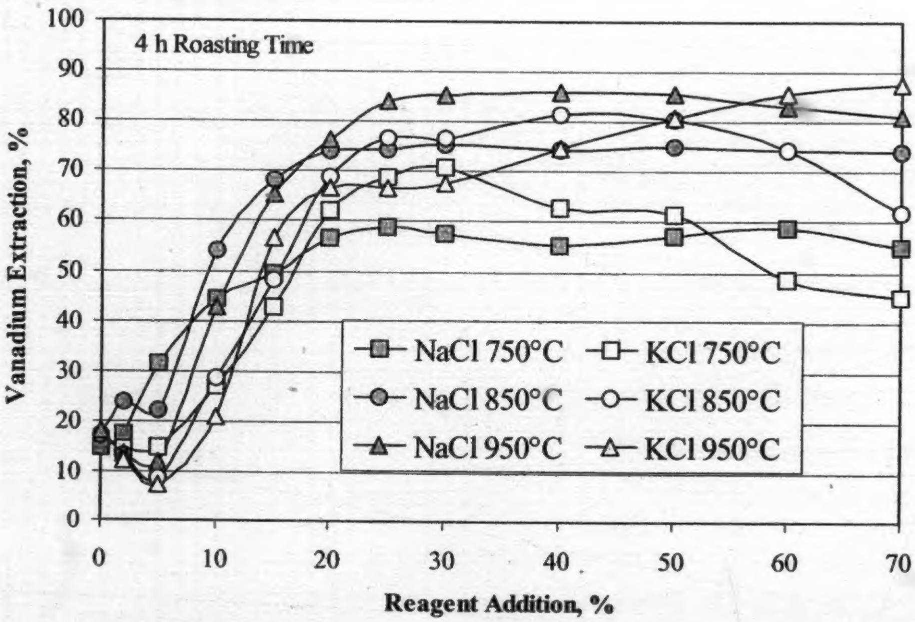

Figure 6 **Effect of KCl and NaCl Addition and Temperature on Vanadium Extraction**

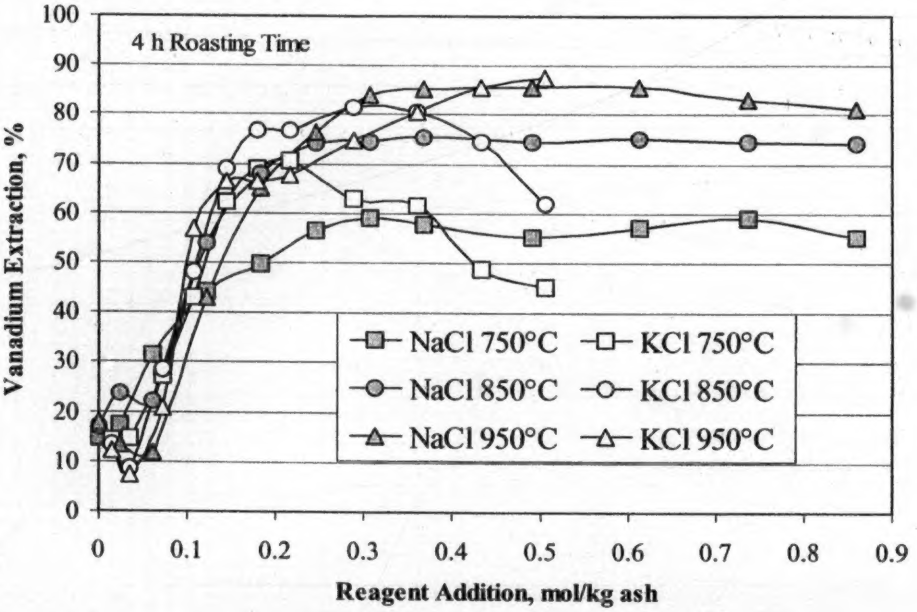

Figure 7 **Vanadium Extraction versus NaCl and KCl Addition (Mole Basis)**

Mineralogically, roasting with KCl is also different. Potassium feldspar, or leucite, ($KAlSi_3O_8$) is the only crystalline aluminosilicate mineral detected at all three temperatures tested using x-ray diffraction in ash roasted with KCl whereas both sodium feldspar, or albite ($NaAlSi_3O_8$), and the feldspathoid hauyne ($Na_4Ca_2Al_6Si_6O_{24}SO_4$) are detected in ash roasted with NaCl. The smaller ionic radius of sodium, and its ability to form a wider range of sodium rich aluminosilicates, including feldspars and feldspathoids, could explain the higher sensitivity to reagent addition and temperature than is observed for roasting with KCl. Pseudobrookite (Fe_2TiO_5) and hematite (Fe_2O_3) are detected using XRD in samples roasted at 750 and 850°C with KCl, but not in samples roasted at 950°C.

Microstructurally, however, the ash roasted with KCl at 850 and 950°C looks very similar to the ash roasted with NaCl at 850°C (Figure 8A) as small elongate pseudobrookite crystals are visible in the midst of a more irregular shaped feldspar (leucite) matrix (Figure 8B and 8C). Only partial or heavily altered cenospheres are present in the ash following roasting with KCl (Figure 8D and 8E). One difference, however, is seen at 850°C where a number of well defined crystals with rhombohedral terminations are observed in the roasted ash that were not observed in ash roasted with NaCl (Figure 8F). These crystals contained Fe and Ti and, thus, based on this and the rhombohedral crystal form, are likely crystals of either ilmenite ($FeTiO_3$) or hematite (Fe_2O_3).

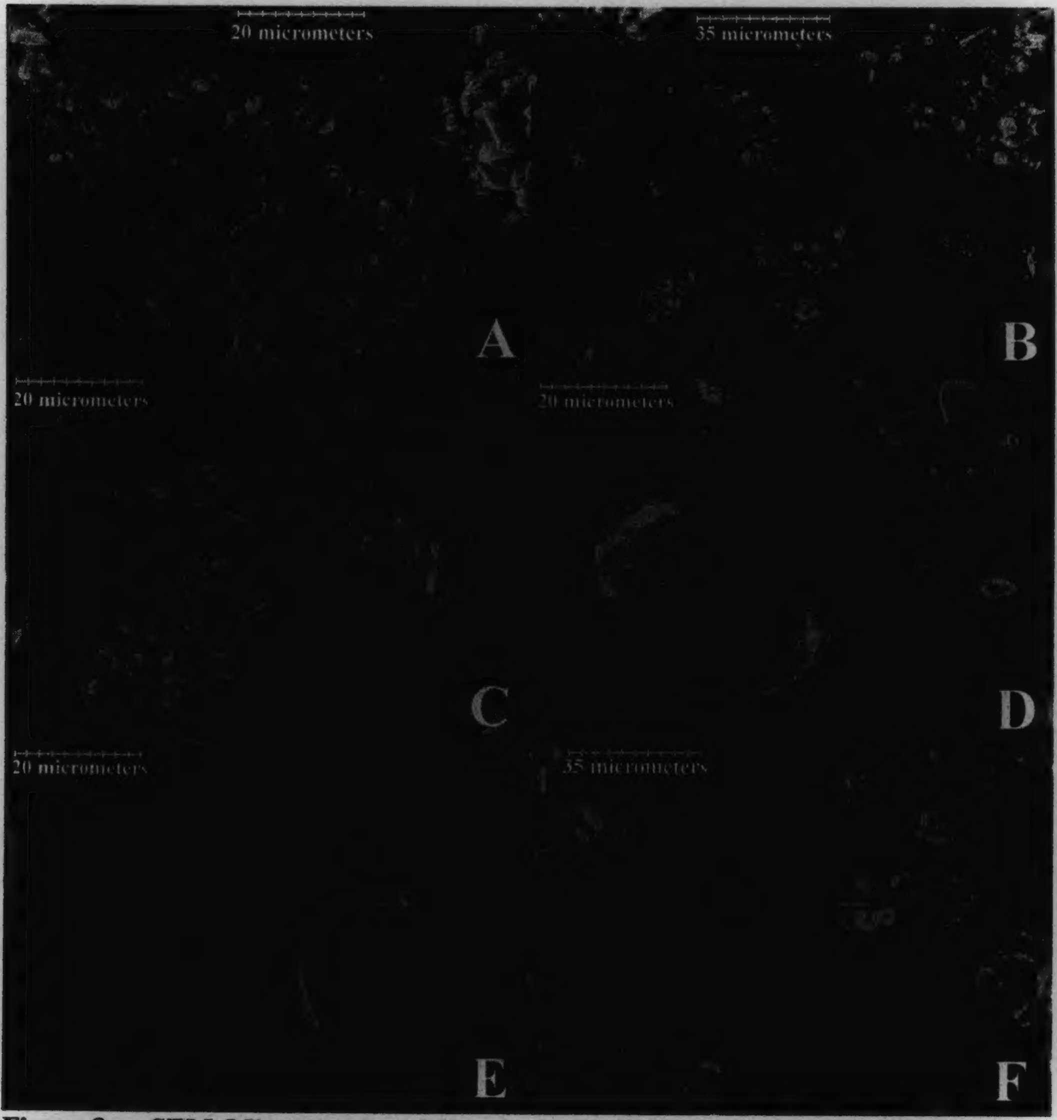
20 micrometers
35 micrometers
A
B
20 micrometers
20 micrometers
C
D
20 micrometers
35 micrometers
E
F

Figure 8 **SEM Micrographs of Water Leached Suncor Fly Ash: 25% NaCl at 850°C (A), 25% KCl at 950°C (B,C) and 25% KCl at 850°C (D,E,F)**

Rate tests where ash was roasted with 25% NaCl or 25% KCl at various times were also performed (Figure 9). Rates and extents of vanadium extraction are very similar at 850 and 950°C for NaCl and KCl. At 750°C, vanadium extractions for ash roasted with KCl reach higher extractions more quickly.

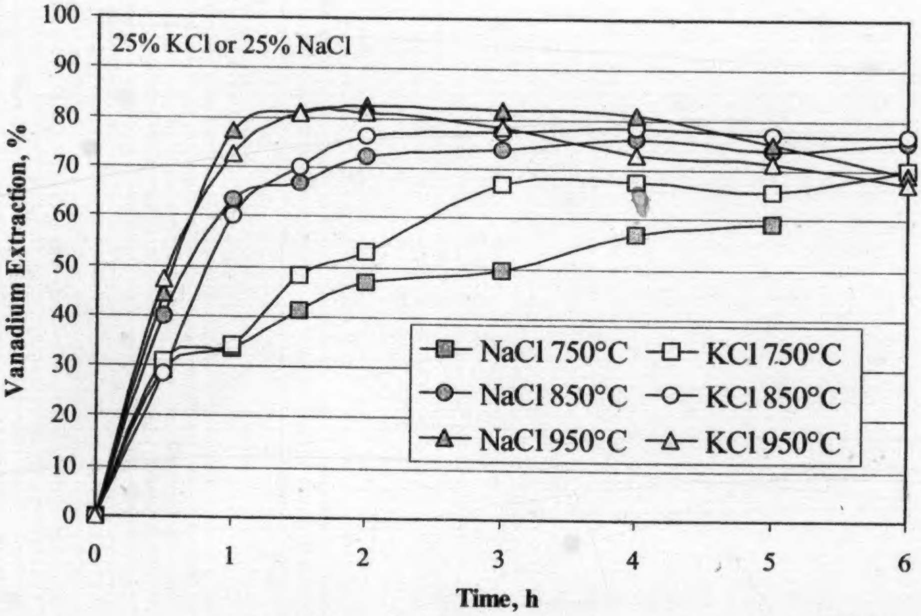

Figure 9 **Effect of Roasting Time and Temperature on Vanadium Extraction**

Overall, similar, or higher, extractions were possible by roasting with KCl compared to roasting with NaCl for a given temperature and similar reaction rates and optimum roasting conditions were observed for both KCl and NaCl. The optimum roasting conditions proposed for NaCl roasting (i.e., additions of 25 to 30%, 850 to 900°C and 3 to 4h) would give an extraction range of 75 to 85% when roasting with KCl.

2.5.1 Integration of KCl into Vanadium Recovery Flowsheet

Based on these encouraging extractions, larger batches of ash were roasted with 25% KCl for 3 h at 850°C and these solids were then leached at 50% solids to generate more concentrated leach solution. This was done to evaluate the use of KCl as a reagent on the subsequent precipitation and salt recovery steps in the process flowsheet proposed for roasting with NaCl (1). However, when the pH of the leach solution was adjusted, or the solution was heated, potassium metavanadate (KVO_3) began to precipitate. This precipitate easily dissolved in water, but even with significant dilution of the leach solution, any adjustment of the solution pH or heating of the solution quickly caused more KVO_3 to precipitate.

Comparison with solubility data for the KCl-KVO_3-H_2O system from the literature (Figure 10) shows that KVO_3 has a much lower solubility in this solution than would be expected, possibly because of the influence of other ions, such as Na^+ and Ca^+, on the solubility. (The leach extraction at 50% solids was also lower at 60% than would be expected from the results from leaching at lower solids concentration; this could also point to a low solubility for KVO_3 in the concentrated leach solution.)

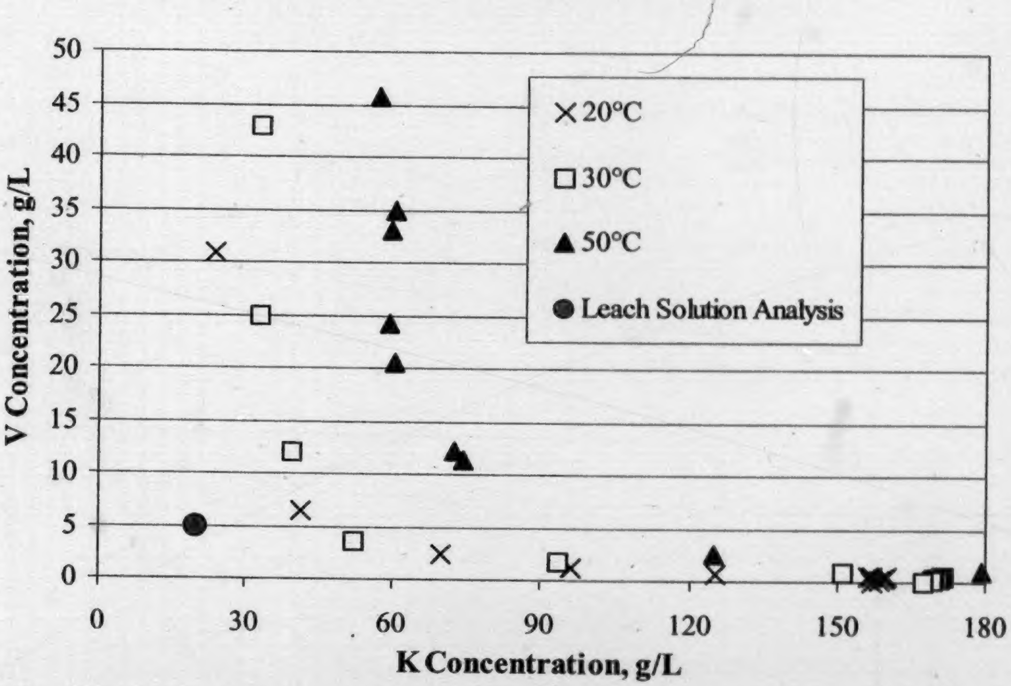

Figure 10 Solubility of Potassium and Vanadium in the KVO_3-KCl-H_2O System[12]

This behaviour has not been noted in ash roasted with NaCl for two reasons. First, the solubility of sodium metavanadate ($NaVO_3$) is less sensitive to NaCl concentration in solution at lower temperatures (12,13). As well, the increase in solubility with temperature for $NaVO_3$ in the $NaVO_3$-$NaCl$-H_2O is much more pronounced and, thus, at higher temperatures, vanadium is highly soluble up to high concentrations of NaCl in solution (12,13).

This low solubility would have significant economic repercussions in trying to integrate KCl into the NaCl roasting flowsheet as increased capital and operating costs would be incurred either by operating with lower solids concentrations and more dilute solutions or by using solvent extraction to concentrate the leach liquor. This, combined with the higher cost of KCl per tonne and the need for similar roasting additions by weight, would preclude the use of KCl as a roasting reagent on economic grounds.

2.6 Conclusions

From the results of these tests, roasting oil sands fly ash with calcium and potassium reagents successfully induced transformations in the minerals in the Suncor fly ash. Through a good understanding of vanadium chemistry and the oil sands fly ash system, reagents containing two different elements were selected, both of which promoted the formation of more soluble vanadate compounds and crystalline aluminosilicate compounds from an ash which was poorly crystalline and had a low vanadium solubility (<1%) in its as-received state. Both types of reagent were able to significantly improve the vanadium solubility over the as-received ash and over ash roasted with no reagents, for all but the lowest roasting temperatures tested. However, due to lower vanadium solubility in the leach solutions derived from ash roasted with calcium or potassium reagents and other economic considerations, potassium and calcium reagents are not likely an economic improvement over NaCl in a roasting process for vanadium recovery.

However, during this study, several important observations were made which could influence the application of this type of process to other materials. First, the relatively low concentration of the element of interest (~3% V) compared with the detection limit of x-ray diffraction (~5%), along with the potential to form more than one vanadate compound, made it difficult to identify vanadium bearing phases using x-ray diffraction and quantify vanadium deportment directly. In particular, for the calcium reagents, diagnostic leaching was required to be able to obtain an idea of the distribution of vanadium between the various vanadate compounds and the aluminosilicates. In addition, differences in the valence state of elements cannot be identified using x-ray diffraction, particularly for elements in low concentrations or in solid solutions, unless phases containing these other valence states are present in sufficient quantity for them to be identified and patterns for these solid solutions or minor phases are available in the x-ray pattern files. (Vanadium present as V^{4+} may be a possible explanation for the lower (i.e., less than 100%) vanadium extractions as V^{4+} would have more of a tendency to substitute in solid solution in the aluminosilicates to form insoluble vanadium oxide compounds.) Thus, it may be difficult to efficiently apply these techniques to optimize metal recovery for metals at low metals concentrations, even with a good understanding of the mineralogy of the material in question, without the use of more complex analytical methods, such as x-ray photoelectron spectroscopy (XPS) or an electron probe micro-analyzer (EPMA).

Second, with the affinity of Na, K and Ca to form both vanadate and aluminosilicate compounds, it was difficult to improve the recovery of vanadium from the ash as each reagent was not particularly selective to either vanadium or the aluminosilicates. As a result, the maximum recovery possible may be the result of two reactions competing for the reactant. However, potentially, the combination of an ionic compound with a higher affinity for the major gangue elements, in combination with another reagent with a high affinity for the metal of interest, may be an alternative that could provide greater selectivity and higher overall metals recoveries. Likely, initial investigations would target maximizing the extraction of a given metal with a single additive, followed by secondary addition of another reagent to either depress the solubility, or recovery, of major impurities or further displace the metal of interest from its associated minerals (i.e., if it is associated in a solid solution with other major impurities).

Third, the amorphous nature of the oil sands fly ash made it necessary to approach the selection of potential reagents for recovering vanadium from an experiential and phenomenological approach, rather than a more fundamental thermodynamic basis. Due to the reliance of these techniques on x-ray diffraction and mineralogical characterization, they would be more easily applied to crystalline materials, though as these tests indicate, crystallinity of the starting material is not essential. With a crystalline material, available thermodynamic data could be used to screen and select potential reagents and roasting temperatures.

3.0 Procedure for Application of Induced Metamorphism to New Materials

Based on the results of these "proof of concept" tests, the next stage of the research focused on trying to apply similar roasting techniques to induce mineralogical transformations in other materials and try to test the limits of the potential applications for transformational roasting.

However, in undertaking this research, several questions immediately arise. Which materials would be better suited to treatment with transformational roasting? How can transformational roasting be applied successfully to new materials, especially those with chemistries that are not well understood? How can the number of potential reagents for testing be reduced to a manageable number in order to expedite the research? What approach can be used that can be systematic and thorough and still be able to eliminate reagents from testing that show little promise? Can the study of the reaction chemistries be effectively balanced with potential economic and process limitations that would occur in the development of any new extraction process?

With these questions in mind, the idea of developing of a generalized procedure, which could be applied consistently to a wide range of materials, was considered the best course of action. This procedure could then be refined and revised, as necessary, by the observations made from applying it to several materials.

3.1 Generalized Procedure for the Application of Transformational Roasting

The following procedure was proposed as the basis for further transformational roasting research to identify promising reagent-mineral systems for further development:

a. **Literature Survey**
b. **Thermodynamic Analysis**
c. **Scoping Roast/Leach Tests**
d. **Design of Experiment (DOE) Tests**
e. **Mineralogical Studies**
f. **Optimization**
g. **Deportment of Minor Elements**

Each stage is described in more detail in the following sections.

3.1.1 Literature Survey

The first step in the procedure would be to perform a comprehensive literature survey on the treatment of each waste that will be studied, along with other related materials. First of all, this will help in understanding the chemistry and mineralogy of the waste in question. Second, the processes proposed for treating each waste can be examined. This allows the advantages and drawbacks, along with any potential environmental or process concerns, for each method of treatment to be identified. Third, through this analysis, the processes that are used commercially for treating these wastes can be distinguished from those that have only been proposed, or have yet to be applied on a commercial scale. Finally, a thorough literature survey will help to identify the novelty of any proposed transformational roasting processes that would be developed in this study and to limit redundancy from repeating research already performed by other researchers.

3.1.2 Thermodynamic Analysis

If the material is crystalline, and its mineralogy readily identified using x-ray diffraction, the next step would be to use available thermodynamic data to identify, or exclude, potential reagents. This will also help examine the tendency of various elements to form oxides, sulphates, arsenates or silicates in a given system and the potential for decomposition of the reagents at temperature. Thermodynamic analysis will also aid in selecting the initial roasting temperatures for the scoping tests.

Naturally, reagent screening would focus on common or cheaper reagents (e.g., alkali metal or alkali earth oxides, carbonates or chlorides), but would not be limited to those reagents. As well, where possible, process conditions would be selected to aim for lower temperatures and, hence, lower energy consumptions, compared with more conventional pyrometallurgical processes, and to aim for primarily solid state reactions (i.e., where the roasted products are not in a molten state).

3.1.3 Scoping Roast/Leach Tests

After selection of potential reagents based on thermodynamics, roasting and recovery tests would then be conducted to screen potential reagents. These tests would involve roasting the dried waste in question with varying amounts of each selected reagent. The roasted waste would then be subjected to either a conventional leaching or mineral processing stage to determine the recovery of the metal of interest, with the lixiviant or separation methods chosen to be appropriate for the recovery of the metal(s) in question for each material. For the sake of time, leaching and roasting times would be selected to be long enough to give the materials time to react, but not necessarily long enough to reach equilibrium. Samples of the roasted waste, before and after this metals recovery/extraction stage, would be taken for XRD and/or SEM analysis and all solids and solutions generated would be analyzed for a spectrum of relevant elements using appropriate analytical methods.

The addition of this step in the procedure has several advantages. First, the number of reagents tested can be quickly reduced to those with the most promising results. Second, the actual mineralogical changes in the material can be determined using SEM or XRD and then compared with the thermodynamic analysis to determine whether the results are consistent with the thermodynamics. Third, by use of fixed roasting times, roasting reactions with very slow reaction kinetics can also be identified and set aside for future reference. Fourth, for unfamiliar systems, the scoping tests can serve to develop and refine the parameters for later testing, such as lixiviant concentration, mineral processing procedures, analytical procedures, roasting temperatures, reagent additions and rate of crucible wear, which would finalize the conditions and methods used in the subsequent design of experiment (DOE) tests.

3.1.4 Design of Experiments (DOE) Tests

Promising reagents, which either improved metals extractions or the deportment of major or minor elements, would then be studied in the Design of Experiments (DOE) stage to try to expand the understanding of the relationship between reagent addition(s), temperature and metals extraction for promising reagent-mineral systems.

Design of Experiments would be used in this portion of the procedure as, especially for an unfamiliar mineral system, the number of potential variables of interest would make sequential testing of each variable inefficient, as well as making it difficult to determine interaction effects between variables. DOE would not only reduce the number of experiments, but would maximize the available information from these experiments and allow for ease in the statistical analysis of the results and in determining more clearly the interrelation of various factors. Given the right selection of the DOE method, more variables can be tested, with more confidence and more information obtained, in less time in the lab.

Variables, such as the type and amount of addition, temperature, secondary reagent additions, or roasting atmosphere, can be tested using the procedures developed during the scoping tests. A variety of data and samples, including minor element analyses, collection of SEM/XRD samples, lixiviant consumption and other measurable variables, would be recorded for future reference and interpretation.

3.1.5 Mineralogical Studies

A combination of XRD and SEM analysis, combined with diagnostic leaching or mineral processing techniques, where necessary, would then be performed to attempt to relate the mineralogical transformations in each material to the metals extractions, or recoveries, observed from the DOE tests. This includes not only the phases formed during roasting, but the phases formed, or consumed, as a result of dissolution or precipitation during leaching, where applicable. Where necessary, quantitative techniques, such as Rietveld refinement, may be necessary to try to determine the relative quantity of each phase and how the quantity is affected by changes in the experimental conditions.

The scanning electron microscope and energy dispersive x-ray analysis (EDX) would then be used to compare the visible phases to those detected using x-ray diffraction. Where possible, trends observed using these methods would then be used to provide direction to further DOE experiments.

3.1.6 Optimization

This stage would involve making adjustments to the experimental conditions established to improve the extent or selectivity of metals extraction from each reagent-mineral system. This could involve adjusting roasting temperatures or reagent additions, changing the roasting atmosphere, or adding secondary additives to enhance extractions, depress major impurities or improve the selectivity in leaching or mineral processing. This could also include screening alternative leaching reagents, testing different mineral processing techniques or conducting rate tests for specific roasting or leaching conditions. Optimization would be expected to be an iterative process between Sections 3.1.3 and 3.1.6.

3.1.7 Deportment of Minor Elements

Once roasting conditions have been optimized for major elements, analysis of the deportment of minor elements to the various phases would then follow. This analysis would be required to determine to which phases valuable or harmful minor elements report. For leached phases, this information would be readily available through analysis of the collected leach solutions; for solid phases, this may require the use of a variety of methods, including chemical analysis, SEM-EDX, diagnostic leaching, electron probe micro-analysis (EPMA) analysis or x-ray photoelectron spectroscopy (XPS).

TCLP (Toxicity Characteristic Leaching Procedure) or other residue stability tests may also be completed during this stage of the research to determine the potential saleability or disposability of residues from the treatment of the waste using these methods.

3.2 Selection of Feed Materials

The range of potential materials for treatment, even only considering the potential number of metallurgical waste streams in industry, is enormous and, thus, for the purpose of this effort, it was important to be able to focus the search for materials to study using transformational roasting.

3.2.1 Feed Selection Criteria

As a starting point, large volume, hazardous wastes from the metallurgical industry with high metals values were targeted in an effort to maximize the economics for any process that may arise from the results of this research. In particular, wastes that have proven difficult to treat using available technology, or that represent disposal problems for the companies that produce them, were considered as ideal candidates for this study.

In addition, wastes with significant minor elements, either in quantity, potential value, potential environmental impact, or potential impact on downstream processing, were also preferred. Although the study of the deportment of these minor elements increases the complexity of the study, the behaviour of these minor elements could significantly influence the economics, or viability, of any process developed and, thus, this behaviour is important to this study.

3.2.2 Selected Feeds

A significant number of interesting materials were identified and in some cases, samples were obtained and preliminary investigations into the related literature and the thermodynamics for potential transformational roasting reactions for these materials were conducted.

However, only three materials were ultimately selected for study in this thesis research for the sake of time and efficiency. Zinc ferrite residue from Doe Run Peru's La Oroya plant, which is a byproduct of electrolytic zinc production, was the first material selected. Electric arc furnace dust from Altasteel in Edmonton, which is a waste produced from the recycling of carbon steels, was the second material selected, due to its mineralogical similarities with the La Oroya zinc ferrite material. Finally, copper residue from Inco's Thompson refinery in northern Manitoba, which is a byproduct of nickel matte electrorefining, was selected as the final waste material for this study. (Blast furnace slag from Doe Run Peru, spent pot liner from Alcan and enargite ore from the Chelopech mine in Bulgaria were also considered, but were not examined to a significant extent because of time and safety constraints.)

4.0 Application of the General Procedure to the Treatment of La Oroya Zinc Ferrite

Zinc ferrite residue from the La Oroya metallurgical complex in Peru was chosen as the first metallurgical waste to be tested using this generalized procedure.

4.1 Feed Material

4.1.1 History of Production of Zinc Ferrite at La Oroya

The La Oroya metallurgical complex is located high in the Andean mountains, 180 km northeast of Lima, Peru (14). It is an integrated lead, zinc and copper smelter where its high altitude (3775 m above sea level) has required significant innovation and adaptation of conventional smelting and refining practices. This plant has been owned and operated by the Doe Run Company since 1997 (14).

The La Oroya ferrite meets the criteria set out earlier in Section 3.2.1. First, the zinc ferrite contains significant Zn, In, Ag and Ga with a combined metals value of between US$500 per tonne (2003) to US$860 per tonne (2005) (15,16,17,18). Second, the zinc ferrite is produced in large quantities (48,000 t/y), of which around 30% is processed using a modified Waelz kiln process (19). The excess, untreated ferrite is stockpiled and, after over 40 years of production, there is, at present, over 1.3 million tonnes of zinc ferrite stockpiled and this amount will continue to grow at current rates of production. Third, since the zinc ferrite comes from an integrated lead-copper-zinc smelter complex, the material contains an assortment of minor elements including potentially valuable metals, such as Ga, In, Ag and harmful metals, like As, Cd, Pb.

Doe Run Peru has evaluated several conventional methods to treat the ferrite in the past, but either high energy consumption or capital costs (i.e., using slag fuming or Waelz kiln processes) or concerns about effluent disposal (i.e., using hot acid leaching), combined with economic factors, have discouraged Doe Run to date from further pursuing those process options. Zinc ferrite is quite resistant to weathering and, thus, does not represent an immediate toxic disposal liability or concern.

4.1.2 Feed Sample

The Doe Run Company was approached in 2002 and their South American branch, Doe Run Peru, supplied a sample of zinc ferrite from their La Oroya operations for testing in early 2003. The analyses provided by Doe Run Peru are shown in Table 3 while Table 4 gives the results of chemical analyses of the feed material performed at the U of A.

Table 3 Chemical Analysis of La Oroya Zinc Ferrite Supplied by Doe Run Peru

Analysis, %						Analysis, ppm			
Al	0.90	Cu	0.62	Mg	0.40	Bi	300	Ge	26
Sb	0.04	Fe	31.6	Mn	1.40	Co	23	Ni	24
As	0.29	In	0.06	Si	4.30	Ga	295	Ag	286
Cd	0.22	Pb	3.50	Zn	20.7				

Table 4 Chemical Analysis of La Oroya Zinc Ferrite Conducted at the University of Alberta

Analysis, %						Analysis, ppm	
Al	0.97	Cu	0.55	Si	4.64	Co	5
As	0.55	Fe	26.6	Na	1.10	F	700
Cd	0.19	Pb	2.98	S	1.50	Ga	407
Ca	0.37	Mg	0.18	Zn	19.5	In	750
C	1.42	Mn	1.22			Ni	9
Cl	0.61	K	0.18				

The as-received ferrite residue had a particle size of 80% passing 45 µm, but with a D_{90} greater than 400 µm. After drying the residue, the oversize was pulverized to give a final particle size of 90% passing 87 µm for the ferrite used in the roasting tests.

X-ray diffraction of the La Oroya ferrite residue showed franklinite ($ZnFe_2O_4$) as the major phase present in this material, with anglesite ($PbSO_4$) observed as a minor phase. Water leaching of the residue gave zinc extractions of about 5 to 10%, indicating that entrained zinc sulphate may also be present in the as-received residue.

Scanning electron microscopy (SEM), along with the use of energy dispersive x-ray analysis (EDX), showed the presence of presence of four distinct phases in the La Oroya ferrite residue (Figure 11). (Imaging with backscattered electrons allows for phases to be distinguished visually by the differences in average atomic number (20.). One large dark grey particle (A) contained K, Al and Si (i.e., a potassium aluminosilicate) while another dark, but more elongate, particle (B) was high in Ca and S (i.e., likely anhydrite ($CaSO_4$)). The very small, very bright particles (C) contained high levels of Pb and S and likely represent anglesite ($PbSO_4$). However, zinc ferrite (D) was the predominant phase observed with the SEM as shown by the abundance of light grey subhedral particles in the backscattered image of Figure 11.

10 micrometers
10 micrometers
C
B
A
SE
BSE

Figure 11 **Secondary Electron (SE) and Backscattered Electron (BSE) Images of La Oroya Zinc Ferrite Feed Sample**

4.2 Literature Survey

4.2.1 Formation of Zinc Ferrite

During oxidative roasting, zinc and iron sulphides oxidize to zinc oxide (ZnO) and hematite (Fe_2O_3). Above 650°C, these minerals react to form zinc ferrite, $ZnFe_2O_4$, which is insoluble in warm dilute acid solution (21,22). The extent to which zinc ferrite is formed depends on roasting temperature, roasting time, the iron content of the ore and the mineralogical association of zinc in the ore (23). Generally, though, roasting zinc concentrates containing iron will lead to some ferrite formation and this material can be a source of significant zinc losses from electrolytic zinc plants, particularly for plants, such as La Oroya, that process predominantly marmatitic ((Zn,Fe)S) zinc ores.

4.2.2 Treatment of Zinc Ferrite

Four main routes have been proposed in literature for the treatment of zinc ferrite residues: the Waelz Process, roasting processes, slag fuming and hot acid leaching. A summary of each of these processes is provided in the following sections, with particular attention paid to the recovery of In, Ga and Ag from these residues.

4.2.2.1 Waelz Process

The Waelz Process involves mixing ore or residues with a solid carbonaceous reductant, such as powdered coke or coal, and feeding the mixture into a horizontal rotary kiln. The carbon in the charge burns to heat the charge and produce a reducing atmosphere close to the charge where zinc, and other volatile metals, are reduced and volatilized. However, the atmosphere in the gas stream above the charge is oxidizing and, thus, CO and metallic gases are then oxidized to carbon dioxide and metallic oxides as they leave the kiln with the metallic oxides recovered as a solid fume in a bag house (24). Operating temperatures range between 1000 and 1300°C depending on the composition of the charge (25). (Lower temperatures are required for higher iron feeds to keep metallic iron from absorbing carbon and causing fusing, melting or accretions from occurring in the kiln (26).) The Waelz process allows for treatment of a wide variety of zinc bearing materials, including mixtures of silicates, ferrites, oxides, sulphides, zinc dust from solution purification for electrolytic zinc, or electric arc furnace (EAF) dust, as well as copper and cadmium bearing wastes.

4.2.2.1.1 Process Chemistry

Komlev and Gareev (27) conducted a detailed study into the chemistry of the Waelz kiln, including deportment of minor elements and mineralogical changes in the charge over the length of the kiln. From this analysis, Komlev and Gareev (27) divide the Waelz kiln into four characteristic zones. (Kashiwada and Kumagai (28) also note similar zones.)

1. **Drying/Heating (0 to 20-25% of kiln length)**
   The charge is heated to reaction temperature and water, whether free or combined, is driven off from the charge.

2. **Sulphate Reduction (25 to 50% of kiln length)**
   Zinc sulphate reacts with carbon in the charge to form a mixture of zinc oxide and zinc sulphide.

   $ZnSO_4 + 4\ C \rightarrow ZnS + 4\ CO$
   $ZnSO_4 + 3\ C \rightarrow ZnO + 3\ CO + \frac{1}{2}\ S_2$

   Zinc oxide combines with silica and alumina in the burden to form zinc silicates and aluminates and cadmium volatilizes.

   $2(Zn,Fe,Mn)O + SiO_2 \rightarrow 2\ (Zn, Fe, Mn)O \cdot SiO_2$
   $ZnO + Al_2O_3 \rightarrow ZnAl_2O_4$

   Ferrite decomposition begins near the end of this zone.

   $3\ ZnFe_2O_4 + C \rightarrow 3\ ZnO + 2\ Fe_3O_4 + CO$

3. **Zinc Sublimation (50 to 83% of kiln length)**
   Ferrite decomposition continues in this stage. The zinc oxide and magnetite products are further reduced to metal with zinc sublimating.

   $ZnO + C \rightarrow Zn_g + CO$
   $ZnO + Fe \rightarrow Zn_g + FeO$
   $ZnS + Fe \rightarrow Zn_g + FeS$
   $Fe_3O_4 + 4\ C \rightarrow 3\ Fe_{met} + 4\ CO$

   Zinc silicates and aluminates react with metallic iron to form metallic zinc.

   $2(Zn,Fe,Mn)O \cdot SiO_2 + Fe \rightarrow Zn_g + 2(Fe, Mn)O\ SiO_2$
   $ZnO \cdot Al_2O_3 + Fe \rightarrow Zn_g + FeAl_2O_4$

4. **Clinker Formation (83 to 100% of kiln length)**
   Zinc sulphides react with copper and a portion of the metallic iron to form a copper-iron matte and to remove zinc by distillation.

   $2\ ZnS + Fe(2Cu) \rightarrow 2\ Zn_g + FeS(Cu_2S)$

4.2.2.1.2 Deportment of Minor Elements

The majority of the zinc in the charge reports to the Waelz oxides. However, from the distribution of metals in the Waelz process reported by Komlev and Gareev (27), the other elements can be grouped into three categories based on their behaviour in the Waelz process.

1. **Sublimates (Cd, In, Tl)**
Virtually all the cadmium volatilizes halfway through the kiln and reports to the Waelz oxides along with zinc. Volatilization of thallium and indium happens later in the kiln with 70 to 80% of the indium and virtually 100% of the thallium reporting to the Waelz oxides.

2. **Mixed Behaviour (Sb, As, Ge, Pb)**
These elements are partially sublimated (As, Sb) or partially sulphidized and then sublimated (Pb, Ge), but also report to the clinker (i.e., As and Sb to matte, Ge to the metallic phase in the clinker and Pb to slag, matte and metallic phases in the clinker).

3. **Clinker Formers (Al, Ca, Cu, Fe, Ga, Mg, Mn, Ni, Si)**
Aluminum reacts with zinc and iron to form zinc or iron aluminates while calcium and magnesium replace lead and zinc in silicates, spinels, etc. and manganese is reduced to MnO and reacts to form silicates. Silicon reacts with oxides to form olivine-type silicates in the first half of the kiln, but converts to glass in the clinker as the kiln temperatures increase. Gallium oxides are not volatilized at the operating temperatures of the kiln and report to the slag (27) or metallic phase of the clinker (29). These six elements report predominantly to the slag phase of the clinker.

Copper, and a portion of the iron, react with sulphur in the charge and become the major components of the sulphide (matte) portion of the Waelz kiln clinker.

Iron is mostly reduced to metallic iron in Waelz processing, but is also present as FeS in the matte phase of the clinker, and as iron silicates in the slag phase of the clinker. Nickel is also reduced to metallic form and is concentrated in the metallic fraction of the clinker.

Metallic iron plays a prominent role in the Waelz kiln reactions as it contributes to the sublimation of zinc from the charge, the reduction and extraction of lead from lead silicates and oxides and the distribution of Ga and Ge in the Waelz kiln (30).

4.2.2.1.3 Plant Practice

The operation of three plants operating commercially using the Waelz process for recovering zinc, and other metals, from zinc ferrite are reported in the literature.

The La Oroya plant in Peru uses a Waelz kiln to process about 40 to 50 tons of zinc ferrite per day (31). The ferrite residue is mixed with 5 to 10% powdered coal and 0.5-1.0% bentonite as a binder and pelletized before roasting at temperatures of up 1050 to 1100°C. Recovery of metals to Waelz oxides are: As 30%, Cd 95%, Cu 6.5%, In 98%, Fe 7%, Pb 50%, Ag 8% and Zn 90%. The Waelz oxides are leached in stages with spent electrolyte or more concentrated sulphuric acid solutions to recover Zn, Cd and In with the lead and silver being concentrated in the leach residue. (The indium rich solution produced is neutralized to make an indium hydroxide concentrate.) Waelz clinker goes through magnetic separation and the iron, copper and silver values are recycled to La Oroya's copper furnaces.

The Nisso Smelting Company processes 80 tons per day of zinc ferrite through two Waelz kilns (28). Recoveries to Waelz oxides of about 96% Zn, 97% Cd, 3% Cu, 4% Fe, 91% Pb and 4% Ag are reported for roasted partially dried residue with 30% coke breeze. The Waelz fume is then chlorinated in rotary kilns to produce a dust rich in cadmium and lead and a relatively pure zinc calcine. The zinc calcine is returned to the zinc plant for leaching in spent electrolyte while the Cd/Pb dust goes through a series of leaching, purification and hydroxide precipitation steps to recover Cd and Pb and allow for the recycle of any residual zinc back to the Waelz kiln. Indium is recovered by leaching the chlorination residue while lead is recovered from the leach residue.

At the Zhouzhou smelter (32), recoveries to Waelz fume of 70% In, 33% Ge, 23% Ga and 60% Tl are reported. After calcination of the fume to remove F, Cl and Tl from the fume at 750 to 850°C, the Waelz oxides are leached. Indium, gallium and germanium are precipitated with zinc dust, redissolved and then separated using solvent extraction.

4.2.2.1.3.1 Use of Additives in Waelz Kiln

Several Russian/Soviet researchers have shown that small chloride additions increase the sublimation of indium during Waelz processing (35-38). Earlier research showed an increase from 60 to 80% recovery of indium to Waelz oxides with very small NaCl additions (0.02 to 0.15%, or even less when using coals with higher chloride contents (33,34)), while more recent work (35-37) indicates that additions of 0.6% NaCl or 0.2 to 1.0% $CaCl_2$ can increase indium recovery to sublimates by 25 to 35% in lab scale operations (37) and 10 to 12% in commercial operation (36). Some of the chloride added reports to the Waelz oxide and, thus, the oxide must be leached with soda (33) or lime (35) to remove Cl before leaching to recover metals from the fume. Some of the same researchers propose using precipitation of basic zinc sulphate or basic zinc chloride to recover indium after leaching from the fume (35,38).

Ivakin et al. (36) also show that CaO additions to give CaO/Fe ratios of 0.45 to 0.80 also increase the recovery of indium to Waelz oxides by 3 to 5%.

4.2.2.1.3.2 Clinker Disposal and Treatment

Waelz clinker is a compact waste with high concentrations of heavy metals in highly reduced (i.e., metallic and sulphidic) phases. In large integrated smelters, such as La Oroya, Waelz clinker can be recycled to compatible streams in copper or lead smelting operations but, in nonintegrated zinc smelters, the disposal of clinker can be a significant environmental issue. A variety of methods have been proposed in the literature for the recovery of metals from this clinker (28,39-47), but will not be discussed here.

4.2.2.1.3.3 Silver Recovery

Silver predominantly reports to the clinker in Waelz processing and, as a result, silver recovery by conventional cyanidation would be difficult without recycling the clinker to a copper smelting circuit. However, several flowsheets have been suggested to recover silver from ferrite residues prior to Waelz processing either by flotation or direct leaching. Flotation recoveries of 70 to 85% and 94%, respectively, are reported in two separate studies (32,48,49) while another study proposed sulphidation of the ferrite residue with Na_2S solution prior to flotation (50) to recover up to 91% of the lead and 99% of the silver from the ferrite. Leaching of silver and gold from ferrites has also been reported using carbon-in-pulp technology and thiourea (51) or using a series of sodium hydroxide and nitric acid leaching steps (52).

4.2.2.2 Roasting Processes

4.2.2.2.1 Sulphation Roast

Sulphation roasting to form water- or weak acid-soluble metal sulphates is another processing route which has been proposed for the recovery of zinc and other metals from ferrite residues and the basic roasting reactions are presented below.

$$ZnFe_2O_4 + H_2SO_4 \rightarrow ZnSO_4 + Fe_2O_3 + H_2O$$
$$ZnFe_2O_4 + (NH_4)_2SO_4 \rightarrow ZnSO_4 + 2\,NH_3 + Fe_2O_3 + H_2O$$

A variety of sulphation reagents for treating zinc ferrite have been proposed. Zinc extractions of less than 50% are reported for Na_2SO_4 and $FeSO_4$ (53), while up to 80% and 94% are reported with SO_2/O_2 mixtures (54) and SO_3 atmospheres (55), respectively. Zinc extractions reported for roasting with $(NH_4)_2SO_4$ vary from 80 to 85% in one study (53,56,57) and as high as 98% in another (58). Using H_2SO_4, or spent electrolyte, zinc extractions of between 91 and 95% are possible, along with extractions of 80% of Cu, In, Cd and Ga and 1 to 6% Fe (53,55,59,60).

4.2.2.2.2 Reduction Roasting

Reduction roasting of zinc ferrites with solid carbon reductants has been proposed as far back as 1929 (61) and the kinetics of this reduction has been discussed in detail (62).

However, several gaseous reducing agents have also been proposed. Park (63,64) showed that zinc ferrite decomposes readily to magnetite and zinc oxide when heated to 700 to 950°C in a vacuum; reduction of the resultant ZnO is possible at low H_2 pressures (0.03 to 0.05 torr), with higher H_2 pressures further reducing magnetite to wustite or metallic iron (64). Sergeev et al. (65,66) effectively reduced zinc ferrite at 950 to 1050°C in a gas mixture containing 15 to 25% SO_2 and 1 to 5% O_2. Reduction with CO, CO/N_2

and CO/CO_2 mixtures has been possible at temperatures between 700 and 1100°C, with either ZnO and Fe_3O_4 or Zn and FeO and/or Fe produced, depending on the CO/CO_2 ratio and overall CO pressure, the reduction temperature and reduction time used (67-71).

Most of the studies on reduction roasting do not indicate how zinc would subsequently be recovered. The one exception is the study by Yamashita et al. (71) which used 25 g/L H_2SO_4 at 80°C to leach the reduced ferrite residue, but leaching was not selective, resulting in high extractions of Fe, Cu and Cd, in addition to zinc.

4.2.2.2.3 Alkali Carbonate Roasting

Zinc ferrite can also be roasted with 13 to 14% Na_2CO_3 and 6 to 7% C at 880°C for 1h, following by leaching the roasted ferrite in NaOH solution, to give zinc extractions of up to 80% (72). The overall reaction proposed for this process is :

$$3\ ZnFe_2O_4 + 3\ Na_2CO_3 + 4\ C \rightarrow 3\ Na_2ZnO_2 + 2\ Fe_3O_4 + 7\ CO$$

Higher temperatures resulted in lower recoveries of zinc to the NaOH leach solution as the zinc oxide was reduced by the carbon and lost as vapour.

4.2.2.3 Ausmelt Slag Fuming

The Ausmelt technology uses an enclosed furnace and the injection of coal or coke and air through a submerged lance to heat, melt and vigorously agitate a ferrite based slag that is created by adding coal and silica to zinc ferrite residue (73,74). The CO gas produced in this process can then react, along with solid C, to reduce and volatilize various metals from the slag bath by the following reactions (73).

$$(MO)_{slag} + C \rightarrow (M)_{gas} + CO$$
$$(MO)_{slag} + CO \rightarrow (M)_{metal} + CO_2$$
$$(M)_{metal} + (Fe_2O_3)_{slag} \rightarrow (MO)_{slag} + 2\ (FeO)_{slag}$$
$$(Fe_2O_3)_{slag} + CO \rightarrow 2(FeO)_{slag} + CO_2$$
$$MSO_4{\cdot}xH_2O \rightarrow MO + SO_2 + 1/2\ O_2 + xH_2O$$

In zinc residue processing, usually two steps are used: the smelting step where fresh feed, silica and coal are added and blown with air or air/O_2 mixtures to produce metallic fume, and a cleaning or reducing step where coal and air are blown into the melt to reduce the remaining volatile metals to low levels in the slag. This two step process allows for the production of off gas with a high SO_2 content which can be treated in existing gas handling systems to recover sulphur while still reducing metal contents in the residue to low levels.

Two companies have tested the application of the Ausmelt technology on ferrite residues. Korea Zinc operates Ausmelt furnaces at its Onsan refinery using temperatures of about 1280°C for its smelting step and about 1310°C for the reducing step and reports recoveries of 82% Zn, 26% Sb, 7.5% Cu, 90% Ge, 70% In, 92% Pb and 72% Ag to fume and recoveries of 41% Sb, 45% Cu and 14% Ag to a copper speiss. (73). The final slag contains 3.5% Zn, 0.1% Sb and less than 3.5% Pb. The Big River Zinc Corporation has also conducted pilot scale Ausmelt tests on their ferrite residue. Operation at higher temperatures of around 1400°C in the reducing step resulted in the recovery of over 99% of Zn, Pb, Cd and Ag and 10% Cu, 5% Ga, 94% Ge, 95% Au and 93% In to the fume (74). The final slag contained only 0.05% Zn, 0.95% Cu, 0.001% Pb and 0.01% S.

4.2.2.4 Hot Acid Leaching

Zinc ferrite is not soluble in warm dilute sulphuric acid solutions or spent electrolyte. However, zinc ferrite can be leached in hot strong sulphuric acid solutions by the following reaction.

$$ZnFe_2O_4 + 4\ H_2SO_4 \rightarrow ZnSO_4 + Fe_2(SO_4)_3 + 4\ H_2O$$

The conditions of hot acid leaching reported in the literature vary little from study to study. Spent electrolyte, or fortified spent electrolyte, containing between 100 to 280 g/L H_2SO_4 is used as the lixiviant and leaching temperatures of 80 to 100°C for atmospheric leaching and up to 260°C for pressure leaching (75,76) and leaching times from 1 to 24 h are reported. (Kinetics of ferrite dissolution are detailed by Ramachandra Sarma et al. (77).)

Most of the novelty in hot acid leaching processes occurs in the methods used to remove dissolved iron from the acidic leach liquor. Three main methods have been developed to precipitate iron either as jarosite ($M[Fe_3(SO_4)_2(OH)_6)$, goethite ($FeOOH$), or hematite (Fe_2O_3).

Jarosite precipitation usually involves the addition of alkali or ammonium ions to acidic leach solutions to promote precipitation of alkali or ammonium jarosite by the following reactions.

$$3\ Fe_2(SO_4)_3 + 14\ H_2O \rightarrow 2\ (H_3O)Fe_3(SO_4)_2(OH)_6 + 5\ H_2SO_4$$
$$3\ Fe_2(SO_4)_3 + 12\ H_2O + X_2SO_4 \rightarrow 2\ XFe_3(SO_4)_2(OH)_6 + 6\ H_2SO_4$$

where X is one of Na^+, K^+, Ag^+, NH_4^+, or 0.5 Pb^{2+}.

Jarosite precipitation is widely used and jarosite processes have been patented by Outokumpu (78,79), Newmont Exploration (80), Norzink (81), Ruhrzink (82), the Electrolytic Zinc Company (83,84) and Asturiana de Zinc (75,76,85,86) Though jarosite filters much more quickly than $Fe(OH)_3$ (87), the high metal content of the jarosite, the high mobility of the toxic metal ions during long term disposal, and the high volume of jarosite produced (0.40 t/t of concentrate (88)) have made jarosite precipitation less attractive to some zinc producers. (Jarosite production was banned in Holland after the year 2000 (89.) Several methods have been proposed in the literature to convert jarosite to a more disposable form of iron, including high temperature pressure leaching (90,91), sulphation roasting of jarosite and residual zinc ferrite to convert jarosite to hematite (92), pressure leaching with $CaCl_2$ to recover residual metals from jarosite to produce a more disposable jarosite residue (87,93), or using Ausmelt technology to remove metals and convert the jarosite to more stable iron silicate slag (94).

Goethite precipitation from hot acid leach solutions has been developed by the Vielle Montagne Company in Belgium (95), the Electrolytic Zinc Company in Australia (96,97) and Akita Zinc (98). Precipitation of goethite, instead of $Fe(OH)_3$, requires a much lower Fe^{3+} concentration (<1 g/L) than is normally present in the hot acid leach solution. Thus, to precipitate goethite, the Fe^{3+} concentration during precipitation must be controlled either by controlling the flow rate of concentrated Fe^{3+} solution into neutralization (Reaction 1) (97) or by reducing all the iron in solution to Fe^{2+} with zinc concentrate and controlling the reoxidation to Fe^{3+} (Reaction 2) (99).

Reaction 1: $Fe_2(SO_4)_3 + H_2O + 3\ ZnO \rightarrow 3\ ZnSO_4 + 2FeOOH$ (Electrolytic Zinc)
Reaction 2: $2\ FeSO_4 + 2\ ZnO + 0.5\ O_2 + H_2O \rightarrow 2ZnSO_4 + 2FeOOH$ (Vielle Montagne)

Hematite precipitation involves the oxidation of Fe^{2+} solutions at 200°C in autoclaves by the reaction below and has also been practiced by Akita Zinc (100) and Ruhr Zink (101).

$2\ FeSO_4 + 2\ H_2O + 0.5\ O_2 \rightarrow Fe_2O_3 + 2\ H_2SO_4$

Where reported, indium and gallium recovery from ferrite residues is generally promoted by high acid additions in hot acid leaching (102-106); solvent extraction or precipitation of indium or gallium as hydroxides is required to recover them from the hot acid leach solutions (102,104).

4.2.3 Conclusions

Based on the literature, the following conclusions can be made about the treatment of zinc ferrite residues.

Hot acid leaching appears to be the industry standard at present because the zinc produced can be readily integrated into electrolytic zinc operations. However, the difficulties encountered with effectively and economically precipitating iron, and the environmental stability of the iron precipitates produced, are the major drawbacks to the use of this process at present.

Waelz kiln and the Ausmelt process are used, but not as widely for the treatment of zinc ferrite residues. Besides having high energy costs due to the higher energy consumption in these processes, the low purity zinc product produced, particularly with respect to Cl, F and Pb, makes it harder to integrate with electrolytic zinc production. However, a major advantage to the Waelz kiln and Ausmelt processes is that both processes are quite robust, in that they can process, and recover metals from, a wider range of waste materials than is possible with hot acid leaching. Unfortunately, the Waelz kiln process produces a solid residue that is difficult to treat further and a poor candidate for stable long term storage due to its highly reduced state. In terms of residue stability and disposability, the residue produced in the Ausmelt process is a significant improvement over both the hot acid leach and Waelz kiln processes.

Finally, the sulphation and reduction roasting that have been proposed in the literature have not yet been commercialized, although whether this is due to economic or technical constraints is not certain from the literature.

However, from this analysis, research on transformational roasting processes has been limited and, thus, the majority of the transformational roasting systems which are presented hereafter would be considered novel.

4.3 Thermodynamic Analysis

Potential reactions for transformational roasting of zinc ferrite were considered based on the following criteria.

a. **Focus on Zinc Recovery** - Franklinite ($ZnFe_2O_4$) is the major component mineral in the ferrite residue and zinc is the major element of interest in the material, both in quantity and percentage of total metals value so, initially, the reactions will focus on zinc recovery, rather than the recovery of Ga, In or Ag.

b. **Formation of Soluble Zinc Minerals** – Zinc would be most easily separated from the zinc ferrite residue if it could be converted to a more soluble form, such as ZnO, $ZnSO_4$ or $ZnCl_2$, and, thus, reactions were selected that had these minerals as products.

c. **Formation of Metal Ferrite Compounds** – In this type of process, the formation of insoluble iron compounds, while forming soluble zinc compounds, would be ideal. In addition, keeping iron in its oxidized ferric state, instead of reduction to ferrous iron compounds or metallic iron, would also have some advantages from a residue disposal standpoint. The formation of non-zinc metal ferrites was, therefore, considered as a possible route to achieve both low iron solubilities and produce a readily disposable residue. Data on the solubility of non-zinc metal ferrites are limited and the limits of solubility, in most cases, would have to be determined experimentally.

Using these criteria and available thermodynamic data, three main types of reactions were identified for further study and are described in further detail overleaf. (All thermodynamic data, including heats and entropies of formation, for this study were obtained from either the FREED (107) or FACTSAGE (108) databases unless otherwise noted.)

4.3.1 Potential Reaction Systems

4.3.1.1 Zinc Replacement Reactions

Roasting in the presence of other metal compounds could induce the formation of other metal ferrites that are more thermodynamically favorable than zinc ferrite and cause zinc to be displaced from the tetrahedral sites of the franklinite structure. This could be possible using metal oxides, carbonates or hydroxides. Generalized chemical reactions are shown in Table 5.

Table 5 Generalized Zinc Replacement Reactions

Reagent Type*	Generalized Replacement Reactions
Metal Oxide (XO)	$Zn(FeO_2)_2 + XO \rightarrow ZnO + X(FeO_2)_2$
Metal Hydroxide ($X(OH)_2$)	$Zn(FeO_2)_2 + X(OH)_2 \rightarrow ZnO + X(FeO_2)_2 + H_2O$
Metal Carbonate (XCO_3)	$Zn(FeO_2)_2 + XCO_3 \rightarrow ZnO + X(FeO_2)_2 + CO_2$

*Where X is a divalent metal ion, or a pair of monovalent metal ions, such as Ca^{2+}, Mg^{2+}, Mn^{2+}, Na_2^{2+}, etc.

Free energy (ΔG^o) is plotted versus temperature for several reagents in Figure 12. From this analysis, most of the reactions listed, except the reactions with MgO and MnO, should be thermodynamically feasible at roasting temperatures of 600 to 1200°C, although minimum temperatures of 820°C and 960°C would be required for roasting with Na_2CO_3 and MnO_2, respectively. From this analysis, a number of reagents, including CaO, $Ca(OH)_2$, $CaCO_3$, MnO, MnO_2, $MnCO_3$, $Mg(OH)_2$, Na_2CO_3, NaOH, were identified for potential scoping tests.

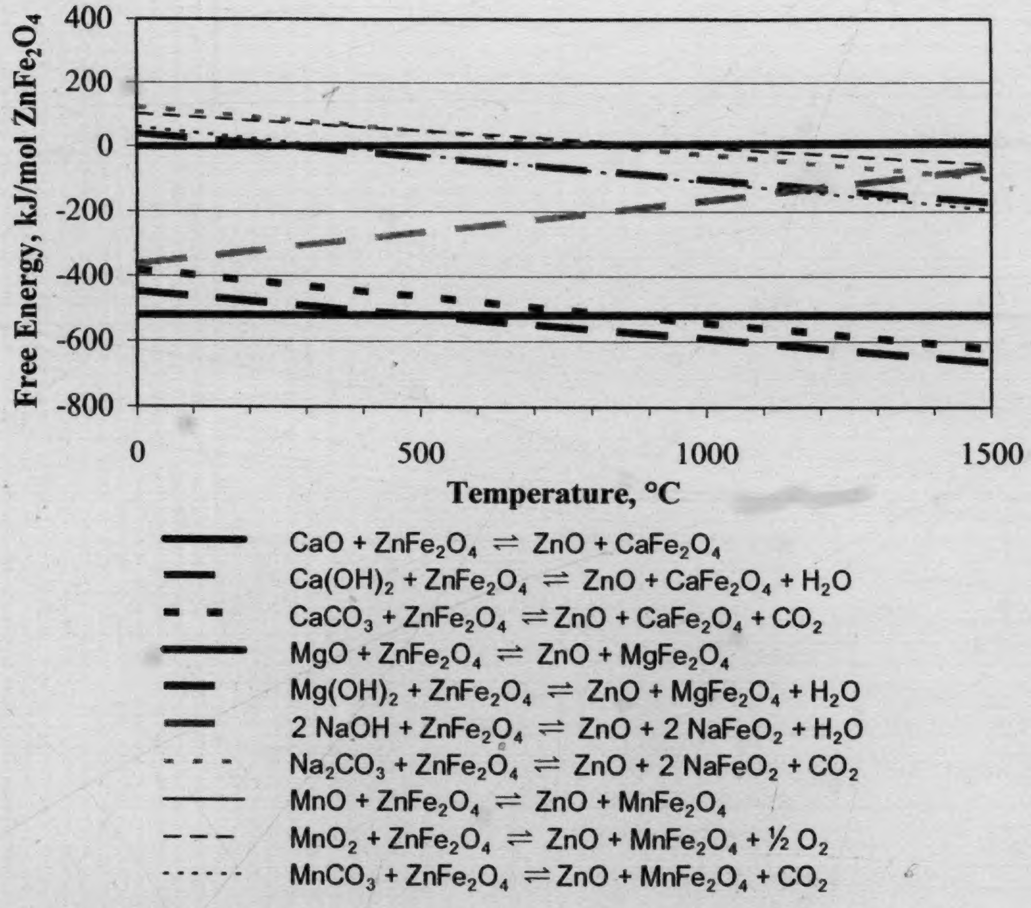

Figure 12 Potential Zinc Replacement Reactions (ΔG° vs. Temperature)

4.3.1.2 Reduction of $ZnFe_2O_4$ and Formation of Non-Zinc Ferrites

Reduction of $ZnFe_2O_4$ using a carbonaceous reagent in the presence of a ferrite forming metal compound is another possible transformational roasting reaction. (This represents a modification of the Waelz kiln process as it aims to form non-zinc ferrites instead of iron oxides or metallic iron.) Generalized chemical reactions for these reagents are shown in Table 6.

Table 6 Generalized Zinc Reduction/Ferrite Formation Reactions

Metallic Reagent Type*	Generalized Zinc Reduction/Ferrite Formation Reactions
Metal Oxide (XO)	$Zn(FeO_2)_2 + C + XO \rightarrow Zn_{(g)} + X(FeO_2)_2 + CO$
Metal Hydroxide ($X(OH)_2$)	$Zn(FeO_2)_2 + C + X(OH)_2 \rightarrow Zn_{(g)} + X(FeO_2)_2 + H_2O + CO$
Metal Carbonate (XCO_3)	$Zn(FeO_2)_2 + C + XCO_3 \rightarrow Zn_{(g)} + X(FeO_2)_2 + CO_2 + CO$

*Where X is a divalent metal ion, or a pair of univalent metal ions, such as Ca^{2+}, Mg^{2+}, Mn^{2+}, Na_2^{2+}, etc.

Figure 13 shows free energy ($\Delta G°$) versus temperature for several reagents. (Two Waelz kiln reactions, including the reduction of $ZnFe_2O_4$ with carbon to form either hematite (Fe_2O_3) or solid iron, are provided for comparison.)

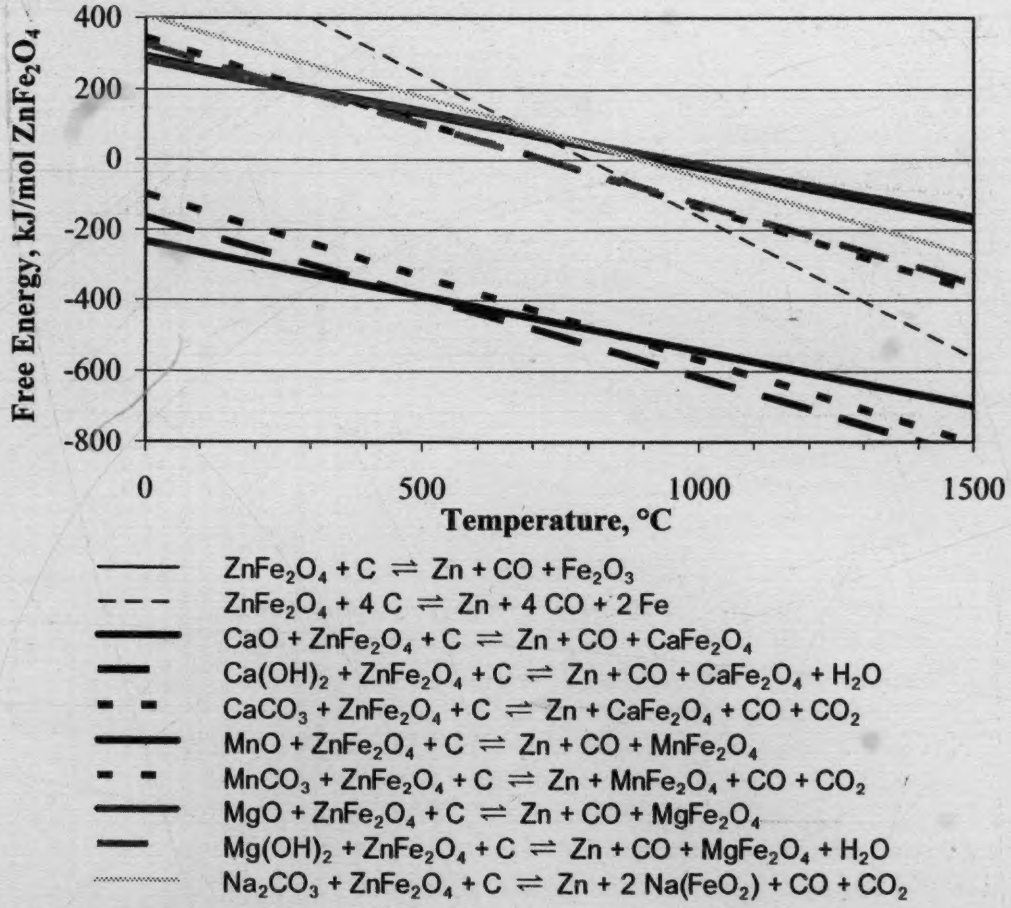

Figure 13 Potential Zinc Reduction/Ferrite Formation Reactions ($\Delta G°$ vs. Temperature)

4.3.1.3 Reaction with Metal Sulphates

Alternatively, reaction with a metal sulphate to produce soluble $ZnSO_4$ is another possibility, following the general reaction: $Zn(FeO_2)_2 + XSO_4 \rightarrow ZnSO_4 + X(FeO_2)_2$. Figure 14 plots free energy (ΔG°) versus temperature for these reactions.

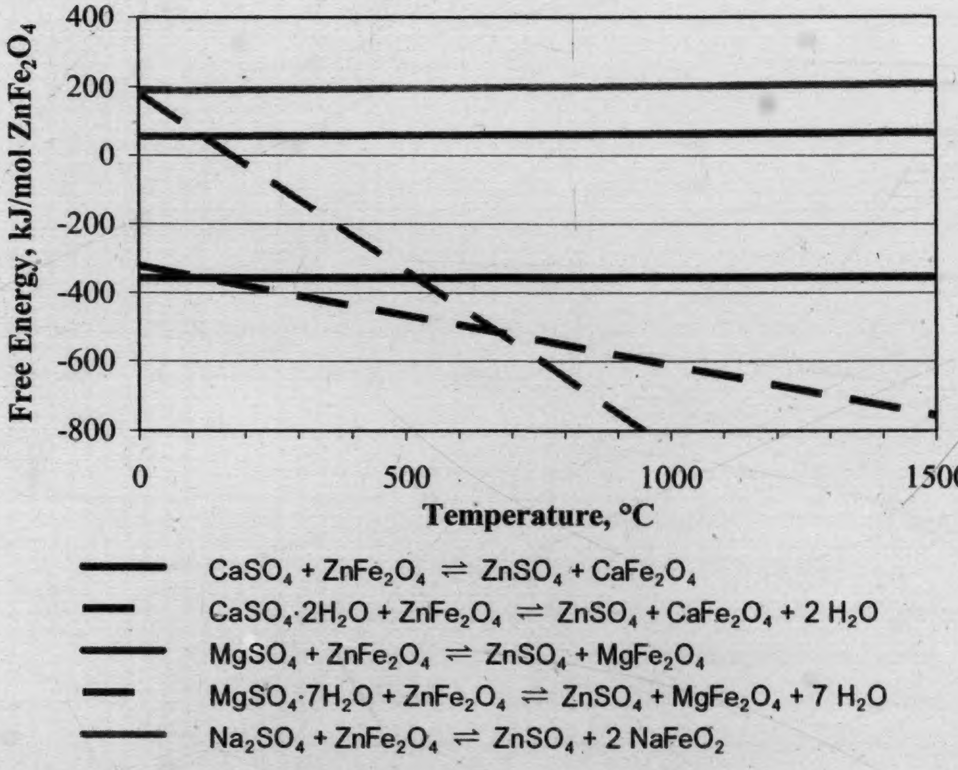

Figure 14 Potential Sulphation Reactions (ΔG° vs. Temperature)

Based on this preliminary analysis, anhydrite ($CaSO_4$), gypsum ($CaSO_4 \cdot 2H_2O$) and epsom salt ($MgSO_4 \cdot 7H_2O$) could be potential reagents. However, on further analysis, the apparent "increase" in spontaneity for the hydrated sulphate salts is from the removal of water from the minerals on heating; thermodynamically, both would be expected to spontaneously dehydrate at temperatures above 120°C. Anhydrite ($CaSO_4$) would not be expected to decompose to form its oxide until over 1500°C, based on the thermodynamics and, thus, could be considered as a reagent for the scoping tests.

4.3.1.4 Reaction with Metal Chlorides

Reaction of the zinc ferrite with metal chlorides to produce soluble ZnO or $ZnCl_2$ is another possible reaction route. Generalized reactions for these reagents are shown in Table 7. Figure 15 plots free energy (ΔG°) versus temperature for these reactions.

Table 7 Generalized Chloridization Reactions

Reagent	Generalized Replacement Reactions
Metal Chloride (XCl_2)	$Zn(FeO_2)_2 + XCl_2 \rightarrow ZnCl_{2(g)} + X(FeO_2)_2$
Metal Chloride + Water Vapor ($XCl_2 + H_2O$)	$Zn(FeO_2)_2 + XCl_2 + H_2O \rightarrow ZnO + X(FeO_2)_2 + 2\ HCl$

*Where X is a divalent metal ion, or a pair of univalent metal ions, such as Ca^{2+}, Mg^{2+}, or Na_2^{2+}, etc.

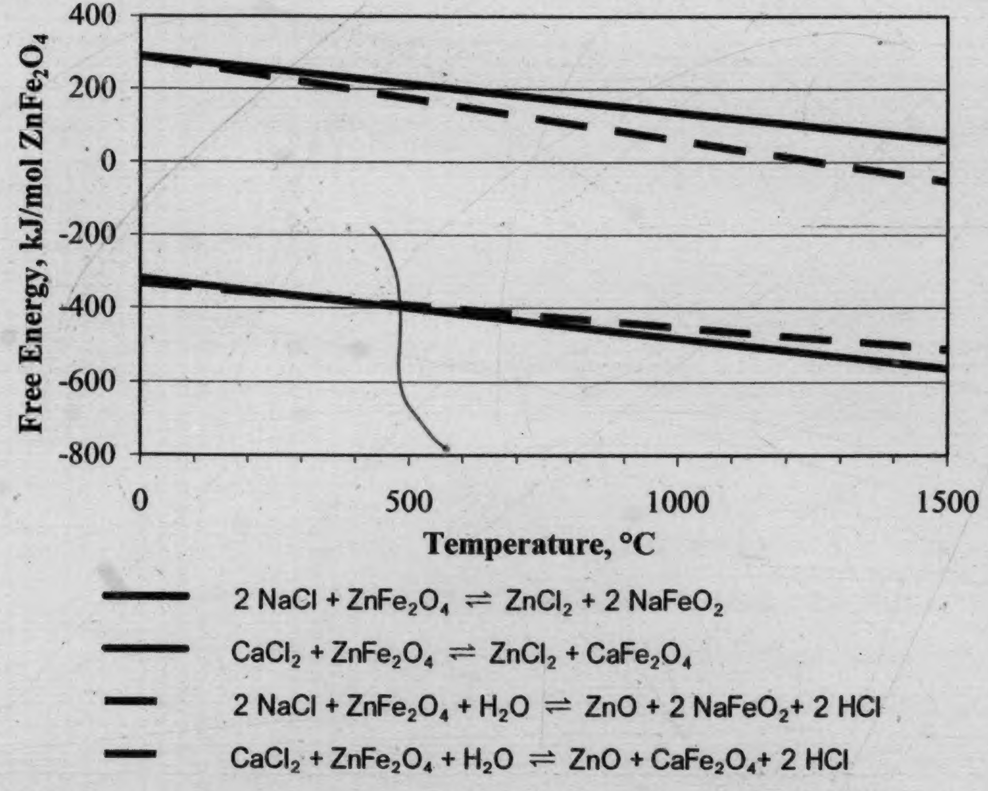

Figure 15 Potential Chloridization Reactions (ΔG° vs. Temperature)

As illustrated, reaction with NaCl is not spontaneous until very high temperatures, but $CaCl_2$ is a reagent that could be considered in the scoping tests.

4.4 Scoping Tests

4.4.1 Roasting and Leaching Procedure

The roasting procedure used was similar to the one used for vanadium recovery by salt roasting. Dried ferrite residue was mixed with the particular reagent, placed in an alumina crucible and heated to the desired temperature for 5 h. (Alumina crucibles did not show significant wear, even after roasting dozens of samples, though some crucibles cracked due to the thermal shock of repeated heating and cooling cycles.) Reagent additions of 50, 100, 150 and/or 200% of stoichiometric, based on the reaction of each reagent with zinc ferrite, were used as a starting point for reagent additions. A roasting time of 5 h was initially selected to screen out reagents at a long, but reasonable, commercial roasting time. (This allowed reactions with poor kinetics to be dropped from testing early in the study.)

After 5 h, the roasted sample was removed from the furnace, air cooled, ground and a subsample taken for XRD and/or SEM analysis. The remainder of the sample was then leached in H_2SO_4 for 1.5 h at room temperature. (Initially, solution containing 100 g/L H_2SO_4 was used, but the acid content was increased to 200 g/L early in the scoping tests to ensure that excess acid remained in solution after leaching.) Sulphuric acid was chosen as the lixiviant because of its low cost and because it was the logical first choice to allow for potential integration of the products and process with zinc electrolytic plants, which operate almost exclusively based on using sulphate chemistry. Higher leaching temperatures were not tested as, since the hot acid leach process is known to decompose $ZnFe_2O_4$ at higher leaching temperatures, leaching at higher temperatures would give an erroneous picture of the effectiveness of roasting to produce acid soluble zinc.

After leaching, the slurry was then filtered and washed with the solids, dried and the filtrate and wash samples collected for analysis. Solutions were analyzed initially for Al, Cu, Ga, In, Pb, Fe, Si and Zn and solids were analyzed for Zn and Fe using atomic absorption spectroscopy (AA). (A single-element Perkin-Elmer 4000 instrument was used for all the analyses.) Scanning electron microscope analysis was performed on selected samples using a Hitachi Model S-2700 Microscope equipped with a GW

Electronics Annular Four-Quadrant Backscattered Electron Detector and a Princeton Gamma Tech (PGT) Prism Intrinsic Germanium (IG) x-ray detector and operating at an accelerating voltage of 20 kV. The digital images were taken using a Princeton Gamma Tech IMIX system.

4.4.2 Scoping Test Results

4.4.2.1 Zinc Replacement Reactions

Figure 16 shows the results of the initial tests involving adding a single additive to try to liberate ZnO and form Ca, Mg or Mn ferrites. The zinc extraction for leaching the unroasted zinc ferrite residue under the same leaching conditions is provided as a baseline for comparison. Extractions were higher than leaching the as-received zinc ferrite in water or sulphuric acid solution (~10%), but were, for the most part, still quite poor and showed little improvement with changes in temperature or reagent addition.

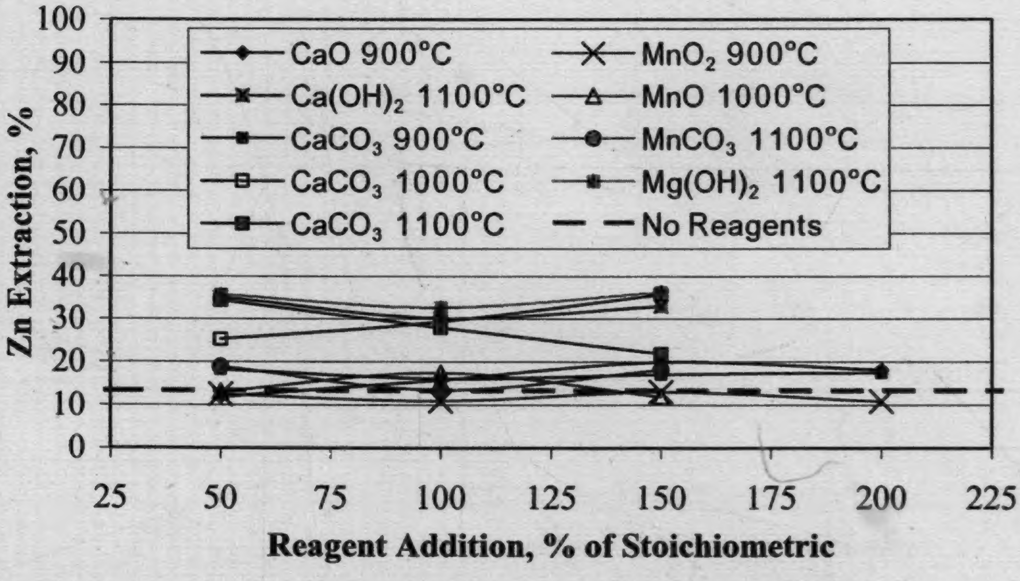

Figure 16 Zinc Extractions for Ca, Mg and Mn Replacement Reactions

Rate tests were conducted with several reagents to determine whether roasting time was the cause of these low extractions. However, increasing or decreasing the roasting time did not significantly affect the zinc extractions for any of the reagents tested (Table 8).

Table 8 Effect of Roasting Time on Zinc Extractions for Various Reagents

Roasting Time	Additive		
	31% $CaCO_3$	35% $MnCO_3$	18% $Mg(OH)_2$
2 h	30.0	17.4	34.6
4 h	28.6	17.7	34.3
7 h	26.5	17.1	32.7
24 h	25.7	19.6	32.8

For all three reagents, x-ray diffraction analysis showed that franklinite ($ZnFe_2O_4$) remained the dominant phase after roasting (Table 9), with some reaction observed between $CaCO_3$ and $Mg(OH)_2$ and silicon to form crystalline Ca- or Mg- silicates. The samples roasted with $MnCO_3$ turned black, which is a color change consistent with the formation of Mn-ferrites or ferrite solid solutions of zinc and manganese. Based on these results, it was concluded that the addition of Ca-, Mg- or Mn-reagents was ineffective in liberating zinc from the franklinite in the ferrite residue under the conditions tested and testing with these reagents alone was not pursued further.

Table 9 Phases Identified in 7 h Roasted Samples with X-ray Diffraction

Reagent	Identified Phases (in order of intensity)
$CaCO_3$	$ZnFe_2O_4$ (major), Hardystonite ($Ca_2ZnSi_2O_7$) , Larnite (Ca_2SiO_4)
$MnCO_3$	$ZnFe_2O_4$ (major)
$Mg(OH)_2$	$ZnFe_2O_4$ (major), Forsterite (Mg_2SiO_4)

Further search of the literature found one study that had done preliminary tests involving the roasting of zinc ferrite with $Ca(OH)_2$ and MgO (109). Even at very long roasting times of 100 h at 950°C, $Ca(OH)_2$ additions of over 200% of stoichiometric and MgO additions of between 120% and 1500% of stoichiometric produced extractions of only 25.7% (CaO) and 38.6% (MgO) of the zinc in the ferrite when leached with 4% acetic acid (109). The magnitude of these extractions is similar to those reported in Table 8 for $CaCO_3$ and $Mg(OH)_2$ additions of 100% of stoichiometric and, if these results from this other study are accurate, further improvements in extraction would not be expected with a significant increase in roasting time or in reagent additions. (X-ray diffraction analysis was not used to determine the phases present after roasting in this other study because of the technological limitations at the time of its writing (i.e., 1927).) This study, though, did report zinc extractions of up to 87% from the zinc ferrite by roasting with CaO additions of almost 430% of stoichiometric, but does not provide a plausible explanation for this improvement in zinc extraction. However, it is unlikely that a process would be economic with such high additions, even if the improvements in zinc extraction that are reported are accurate.

Roasting with sodium compounds to form sodium ferrites, however, gave much more promising results (Figure 17). Roasting with Na_2CO_3 and NaOH gave zinc extractions as high as 98% in the initial tests. Extractions of up to 60% were possible, even at 700°C, with extractions approaching 99% as the reagent addition and temperature were increased.

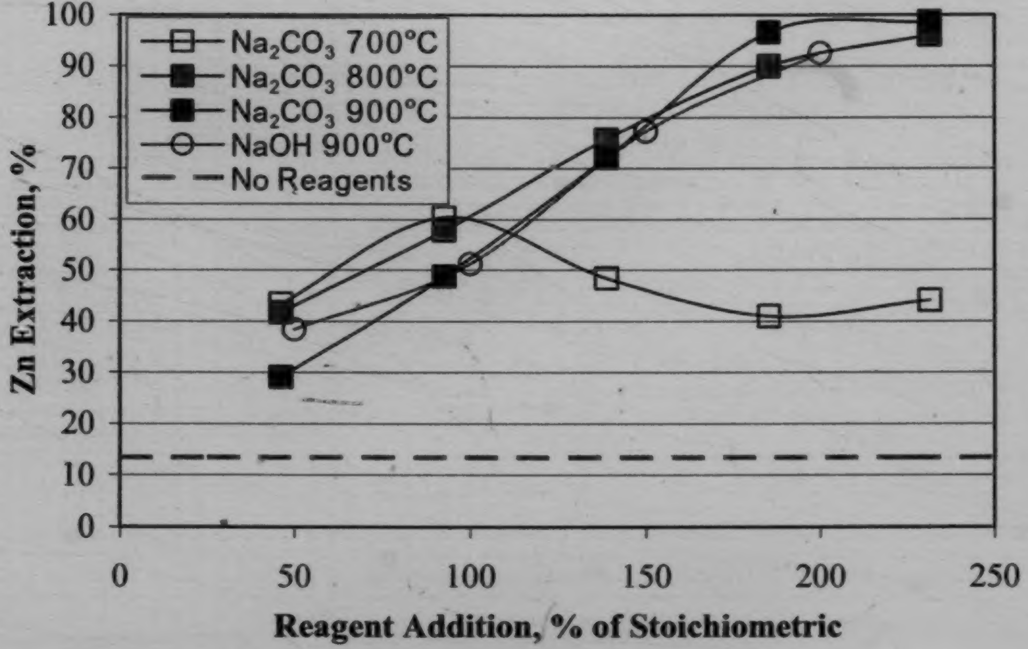

Figure 17 Zinc Extractions for Na Replacement Reactions

However, particularly at higher temperatures, such as 850 or 950°C, the high zinc extractions are also accompanied by extensive dissolution of iron (Figure 18), with up to 85% and up to 99% of the iron leached at 950°C and 850°C, respectively. XRD analysis of the sample roasted at 900°C with a Na_2CO_3 addition of 75% (230% of stoichiometric) showed that zinc occurred as ZnO and Na_2ZnSiO_4 in the roasted ferrite, with the iron present as either α- or β- $NaFeO_2$ and the silicon present as larnite (Ca_2SiO_4). (A phase change between α-$NaFeO_2$ (i.e., rhombohedral crystal structure with space group $R\bar{3}m$) and β-$NaFeO_2$ (i.e., tetragonal crystal structure with space group $Pna2_1$) occurs at 760°C, but, because the phase change transformation is reconstructive and, thus, requires a rearrangement of the oxygen coordination in the structure, there is a potential for slow kinetics, which is consistent with the incomplete transformation observed over the roasting times used in these tests (110). After leaching, the residue is poorly crystalline, with only small peaks for anglesite ($PbSO_4$) and larnite (Ca_2SiO_4) visible. Thus, these x-ray diffraction results would indicate that the sodium ferrite formed in roasting is readily soluble in cold sulphuric acid solutions and, if this system were to be used, steps would have to be taken, either to precipitate the dissolved iron from solution after leaching or to produce less soluble iron compounds during roasting.

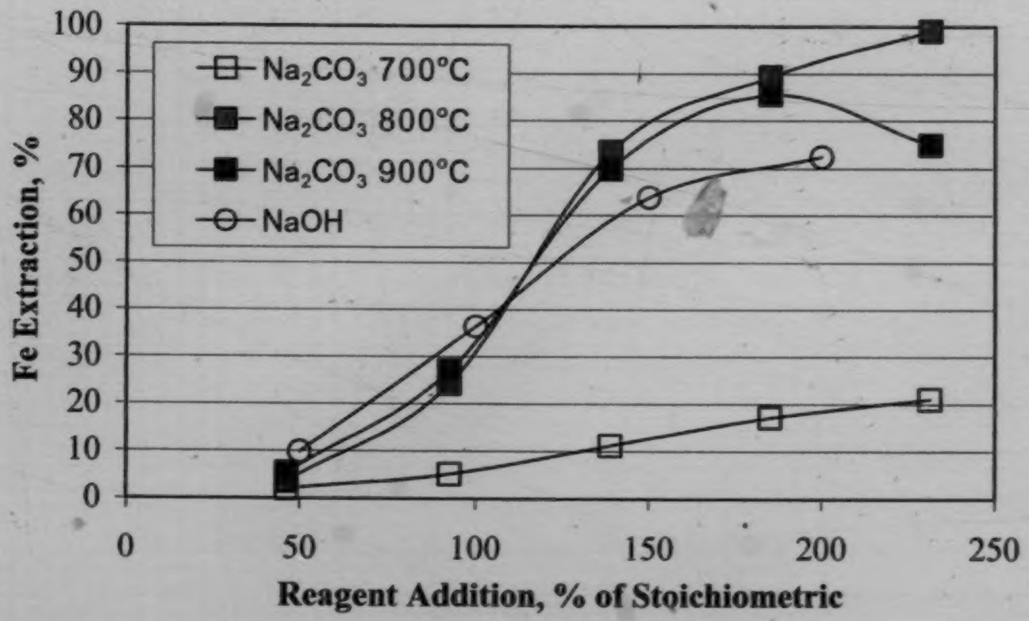

Figure 18 Iron Extractions for Na Replacement Reactions

From those observations, additional roasting tests were performed using a eutectic mixture of Na_2CO_3 and $CaCO_3$ to determine whether the combination of reagents could maintain high zinc extractions, but lower the overall dissolution of iron (Figure 19). Iron extractions were significantly lowered with only minor reductions in zinc extraction.

Mineralogically, the roasted ferrite contained ZnO, α- and β-$NaFeO_2$, srebrodolskite ($Ca_2Fe_2O_5$), Na_2ZnSiO_4 and larnite (Ca_2SiO_4). After leaching, srebrodolskite remained in the residue, along with anglesite ($PbSO_4$) and gypsum. Thus, based on these promising results, the addition of secondary additives to control iron dissolution will be studied further in the DOE tests.

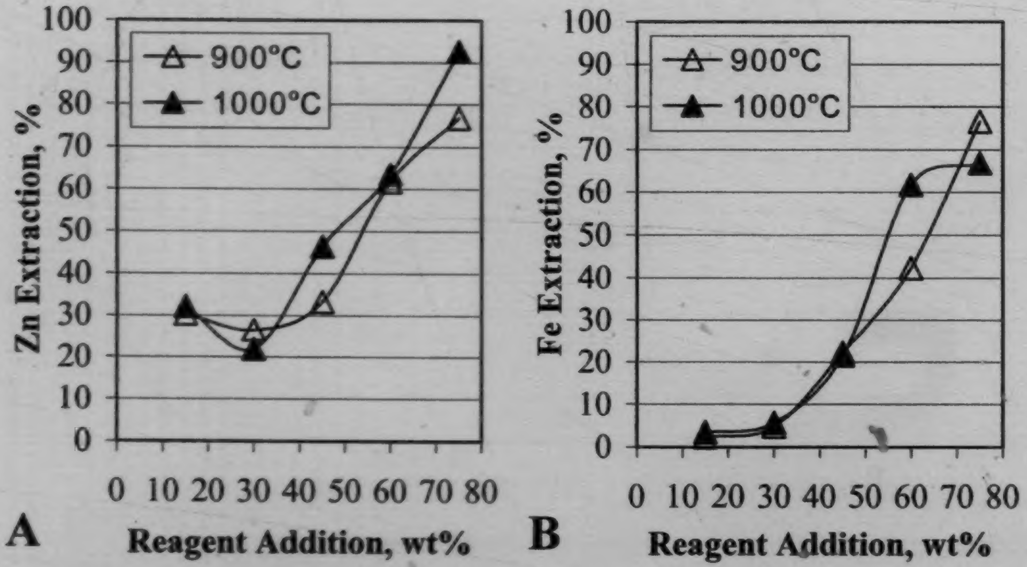

Figure 19 **Effect of Roasting with 60% Na_2CO_3-40% $CaCO_3$ Mixture on A) Zinc and B) Iron Extractions**

4.4.2.2 Reactions for Reduction of $ZnFe_2O_4$ and Formation of Non-Zinc Ferrites

Several samples were roasted with 8% activated charcoal and ferrite-forming reagents (Figure 20). Zinc oxide is produced during these tests and it appears in the roasted samples in the form of white acicular crystals on the surface and edges of the charge and its presence was confirmed using XRD and SEM analysis. In these tests, zinc extractions, which are based on solids analyses and weights, represent the total recoverable zinc (i.e., as fume and as acid-leachable zinc) after roasting.

Most of the reagents tested depressed the amount of zinc extracted, when compared with roasting with activated charcoal with no other reagents, while the addition of activated charcoal only gave marginal improvements in zinc extraction when compared with roasting with these reagents alone. However, roasting with activated charcoal and either $CaCO_3$ and MgO or additions of 150% of stoichiometric for CaO at 1000°C did result in an increase in zinc extraction under these conditions. Thus, these reagents were selected for further study in the subsequent DOE tests.

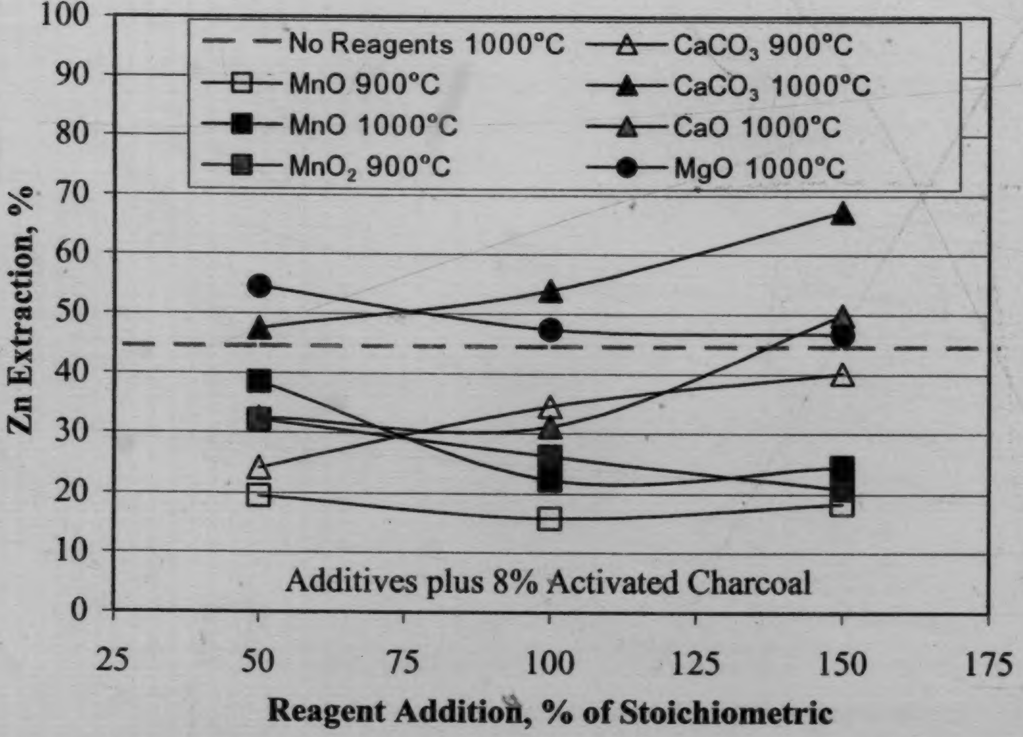

Figure 20 **Zinc Extractions for Roasting with Charcoal and Ferrite-Forming Reagents**

With the addition of carbon as a reagent, several carbon types, including activated charcoal, carbon black or bituminous coal, were also compared in the scoping tests to select carbon source(s) for further testing (Figure 21). In these tests, carbon black gave higher extractions than coal or activated charcoal and, thus, carbon black was selected initially as the reagent to be used in the subsequent DOE tests.

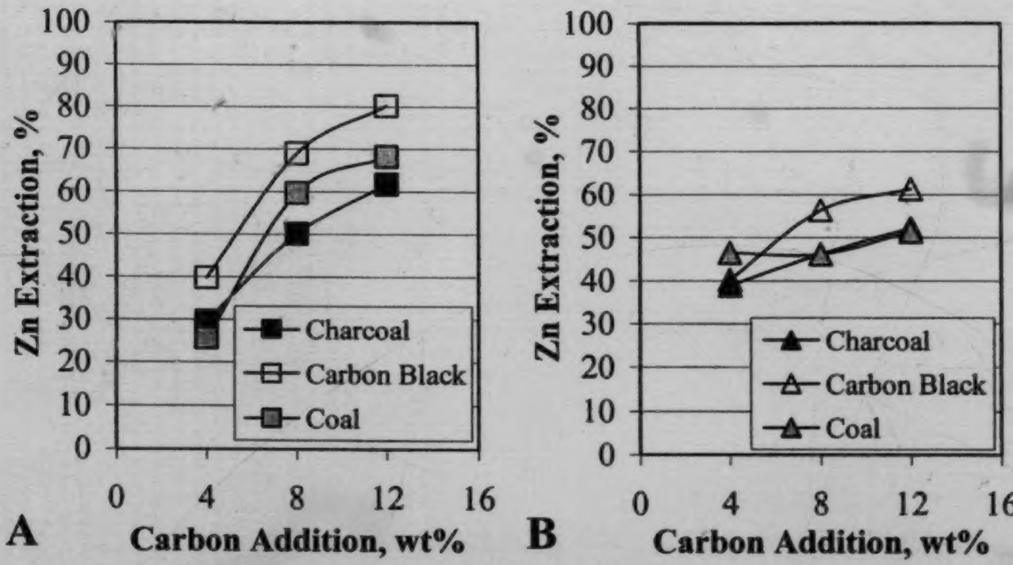

Figure 21 **Zn Extractions for Roasting with Various Types of Carbon at 1000°C with A) CaO (150% of Stoichiometric) and B) MgO (150% of Stoichiometric)**

4.4.2.3 Reactions with Metal Chlorides

Two chloride reagents, $CaCl_2$ and NaCl, were tested in the scoping tests (Figure 22). (Reaction with NaCl should not be spontaneous at 900°C, but was tested for comparative purposes.) In both cases, virtually no zinc was leached from the roasted ferrite, but solids analyses indicated that an additional 22 to 52% of the zinc in the ferrite had been lost, presumably as $ZnCl_2$ fume. However, since this zinc extraction is primarily due to a chlorination reaction, and since $ZnCl_2$ is a product that is not easily integrated into conventional, sulphate-based zinc processes, further investigation into the use of these reagents was not pursued.

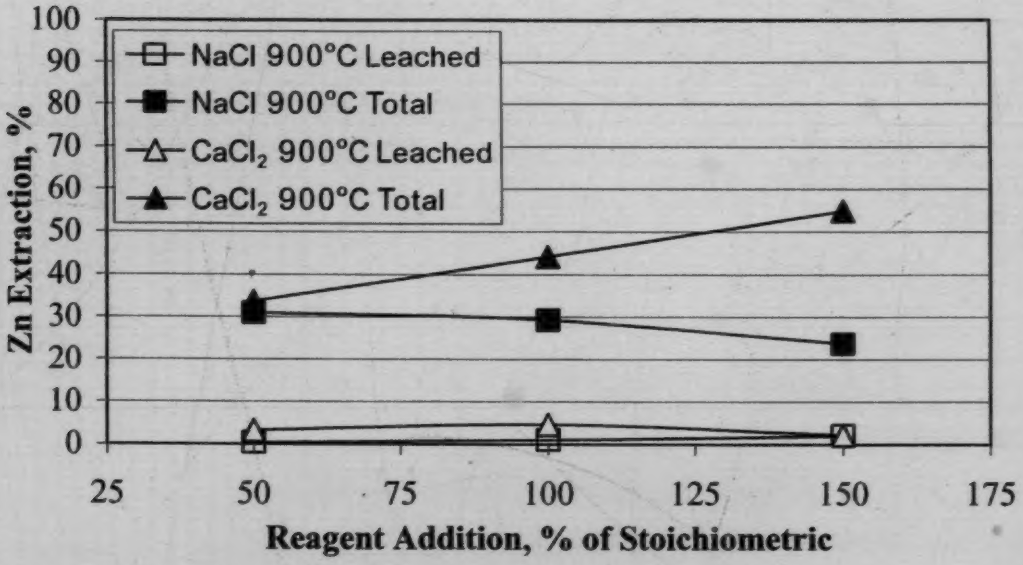

Figure 22 Zinc Extractions from Roasting with NaCl and $CaCl_2$

4.4.2.4 Reactions with Metal Sulphates

Two sulphate reagents, $CaSO_4$ and $MgSO_4$, were tested in the scoping tests (Figure 23). (Reaction with $MgSO_4$ should not be expected to be spontaneous, based on the thermodynamic analysis, but was tested for comparison.)

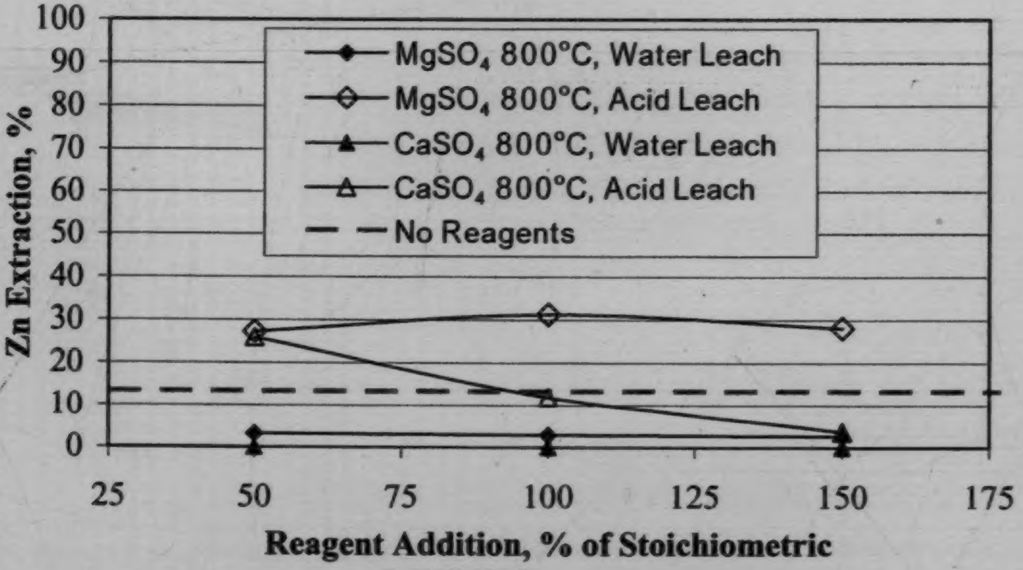

Figure 23 Zinc Extractions from Roasting with $MgSO_4$ and $CaSO_4$

The roasted ferrite was first leached with water to determine whether leachable $ZnSO_4$ had been formed during roasting and then leached under standard conditions with 200 g/L H_2SO_4. Zinc extractions were less than 4% in the water leach, but improved slightly after leaching with H_2SO_4 to between 27 and 31% for $MgSO_4$ and between 3 and 26% for $CaSO_4$. Without particularly encouraging results in these preliminary tests, no further tests were conducted using metal sulphates.

4.5 Design of Experiments (DOE) Tests

Two systems of reagents were identified from the scoping tests for further study in the DOE phase of testing: roasting the ferrite with Na_2CO_3 and roasting with carbonaceous additives and ferrite forming reagents.

4.5.1 Multivariate Experimental Design

Most methods of multivariate experimental design are based on a factorial design, where factors are varied together, rather than individually, and the results are interpreted using statistical methods, such as analysis of variance (ANOVA) or residual analysis. Factorial design is able to handle and quantify factor-factor interactions while greatly reducing the number of tests required if each factor-factor interaction was tested iteratively. (Factorial designs are typically described as 2^k, 3^k, 4^k, etc. with the number referring to the number of levels of each variable tested and the *k* referring to the number of variables tested.)

After examining a number of different DOE techniques, a method called *central composite design* (CCD) was selected for these experiments for two main reasons. First, standard 2^k factorial designs require an assumption of linearity, or that interaction between variables is minimal; nonlinearity is automatically taken into account with higher order (i.e., 3^k or 4^k) designs, but the number of tests required is significantly increased. However, in the central composite design, by adding center points and axial points to the design (Figure 24), the standard 2^k design is enlarged to allow interaction effects, or nonlinearity, to be quantified. In addition, the addition of center and axial points, rather than using a higher order design, also makes CCD a much more efficient design than a 3^k design, especially for higher values of k (Table 10). In short, CCD is able to maximize the information obtained while minimizing the number of tests required in the lab.

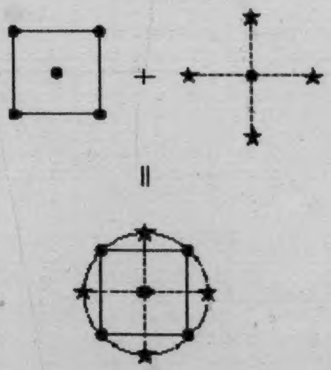

Figure 24 Generation of a Circumscribed Central Composite Design for Two Factors (111)

Table 10 Number of Trials for Various Factorial Designs and Number of Variables

Design	k=2	k=3	k=4	k=5	k=6
2^k	4	8	16	32	64
2^k CCD*	10	16	26	44	78
3^k	9	27	81	243	729

* Using 2 center points

In addition to reducing the number of experiments and quantifying non-linearity, if the initial central composite design is selected properly, the results can then be used in the construction of a response surface model (RSM). This response surface can be used to construct contour plots, which represent essentially a "topographical map" of the variable response and are a powerful tool for response optimization. Response surface modeling is particularly useful when trying to maximize or minimize a response or to map the variable response over a set range of variable space and, hence, is well suited to the objectives of this portion of the roasting research. In addition, another advantage of using a CCD design to produce surface response model designs is that models can be generated for more than one observed variable using the same initial experimental design.

To enable the construction of response surface models, the CCD designs used in this research were designed to be *rotatable* or, in other words, to have a uniformity of prediction error from the centre of the design. In other words, a rotatable design is set up such that the variance of a given point is only dependent on its distance from the design centre (111). The position of the axial points to give rotatability is defined as α; a design is rotatable if $\alpha=(2^k)^{1/4}$ (111). In a rotatable 2^2 design, this corresponds to a situation where all the factorial and axial design points are at a radius $2^{1/2}$ from the center of the design; in a rotatable 2^3 CCD design, the factorial and axial points are arranged on two concentric spheres of radius 1.73 and 1.68, respectively. A software package called DOE XL Pro (112) was purchased to help set up and interpret the results from these tests.

A rotatable central composite design is well suited to the type of roasting tests proposed in the DOE tests portion of the generalized procedure. An elaborate multi-factor factorial design is not required as there are a limited number of variables to investigate (i.e., reagent type(s), amount and temperature) and each variable is known to have an effect on zinc (or other metal) extractions from the results of the scoping tests. In addition, conducting scoping tests before the DOE tests helped to reduce the number of ineffective reagents to be tested in the more elaborate DOE tests and allowed for appropriate ranges of each variable to be determined to provide a basis for the construction of the CCD designs.

The experimental designs used in this research are shown in a generalized form for 2^2 CCD and 2^3 CCD designs in Tables 11 and 12, respectively. (For example, "-1" refers to a decrease of one unit of variance for each variable from the center of the design.) Samples are designated as matrix (M), centre (C), or star (S) points, respectively, depending on their location relative to the centre of the design.

While duplicate tests were not performed for most individual scoping test and DOE test conditions, when samples were repeated, extractions were generally repeatable to within 2 to 3% throughout the testwork for all three materials tested in this research. In the DOE tests, the center points for each DOE test were repeated and the error associated with these repeated tests was incorporated into the response surface model, and is expressed, in combination with the model error in terms of R^2 for each material and set of variables tested .

Table 11 Generalized Experimental Design for a Rotatable 2^2 CCD Design

Sample	Variable A	Variable B
M1	-1	-1
M2	+1	-1
M3	-1	+1
M4	+1	+1
C1	0	0
C2	0	0
S1	0	-1.414
S2	0	+1.414
S3	-1.414	0
S4	+1.414	0

Table 12 Generalized Experimental Design for a Rotatable 2^3 CCD Design

Sample	Variable A	Variable B	Variable C
M1	-1	-1	-1
M2	-1	-1	+1
M3	-1	+1	-1
M4	-1	+1	+1
M5	+1	-1	-1
M6	+1	-1	+1
M7	+1	+1	-1
M8	+1	+1	+1
C1	0	0	0
C2	0	0	0
S1	-1.682	0	0
S2	+1.682	0	0
S3	0	-1.682	0
S4	0	+1.682	0
S5	0	0	-1.682
S6	0	0	+1.682

4.5.2 Results from Design of Experiment Studies and Mineralogical Analysis

For the La Oroya zinc ferrite, two series of DOE tests were performed: one set investigating the roasting of zinc ferrite with Na_2CO_3, with or without the addition of secondary additives to try to inhibit iron dissolution, (Section 4.5.2.1) and the second studying the roasting of zinc ferrite with carbonaceous reagents, with or without the addition of secondary additives to encourage metal ferrite formation (Section 4.5.2.2). The experimental conditions used in these two sets of tests are summarized in Tables 13 and 14, respectively, along with the R^2 values of the response surface models fitted to the metal extractions calculated from the experimental data.

Table 13 Experimental Conditions Used in Experimental Designs for Roasting Zinc Ferrite with Na_2CO_3 and Resulting Model Variance

Range of Variables Tested	Na_2CO_3	Na_2CO_3-$CaCO_3$	Na_2CO_3-$Mg(OH)_2$	Na_2CO_3-$MnCO_3$
Temperature, °C	750-950	750-950	750-950	750-950
Na_2CO_3 Addition, %	40-80	40-80	40-80	40-80
Secondary Addition*, %				
$CaCO_3$	-	7.8-29.5^A	-	-
$Mg(OH)_2$	-	-	4.5-17.1^B	-
$MnCO_3$	-	-	-	8.8-33.3^C
Model R^2				
Zn Extraction	0.969	0.990	0.976	0.969
Fe Extraction	0.959	0.958	0.990	0.970

* Secondary additions represent 25 to 95% of stoichiometric additions assuming formation (A) $CaFe_2O_4$, (B) $MgFe_2O_4$ or (C) $MnFe_2O_4$
Note: All percentages for DOE testing are in weight percent unless otherwise noted.

In some of the extraction plots produced from the response surface models for each set of DOE experiments, a light grey (or yellow for those plots printed in color) region occurs as a contour above the maximum range of extractions. (The plot of zinc extraction in Figure 25A is one example of this, where this region occurs at 950°C and 80% Na_2CO_3.) This region occurs as an artifact of the response surface models. These models determine a surface that will accurately explain the rate of change and range of extractions over a given reaction space, based on experimental results, but are not constrained to values of between 0 and 100% in the process. Since extractions cannot physically exceed 100%, for the purpose of analysis and interpretation, these regions can be considered as regions where extractions approach 100% whenever they occur in figures in subsequent sections.

Table 14 Experimental Conditions Used in Experimental Designs for Roasting Zinc Ferrite with Carbonaceous Reagents and Resulting Model Variance

Range of Variables Tested	Carbon Black	Coal	Coal-$CaCO_3$	Coal-CaO	Coal-$MnCO_3$
Temperature, °C	900-1100	900-1100	900-1100	900-1100	900-1100
Carbon Addition, %					
Carbon Black	12-20	-	-	-	-
Coal	-	12-20	12-20	12-20	12-20
Secondary Addition*, %					
$CaCO_3$	-	-	31-62^A	-	-
CaO	-	-	-	17-34^A	-
$MnCO_3$	-	-	-	-	35-70^B
Model R^2					
Zn Extraction (Total)	0.970	0.954	0.951	0.939	0.934
Zn Fumed	0.839	0.952	0.814	0.886	0.608
Fe Extraction	0.865	0.742	0.924	0.833	0.707

* Secondary additions represent 100 to 200% of stoichiometric additions assuming formation (A) $CaFe_2O_4$ or (B) $MnFe_2O_4$

4.5.2.1 Roasting with Na_2CO_3

Figure 25 shows the results from a 2^2 CCD design showing the relationship of Na_2CO_3 addition and temperature to the zinc and iron extractions. The trends observed are very similar to those from the scoping tests, with maximum zinc extractions of over 90%, and corresponding iron extractions of 70 to 90%.

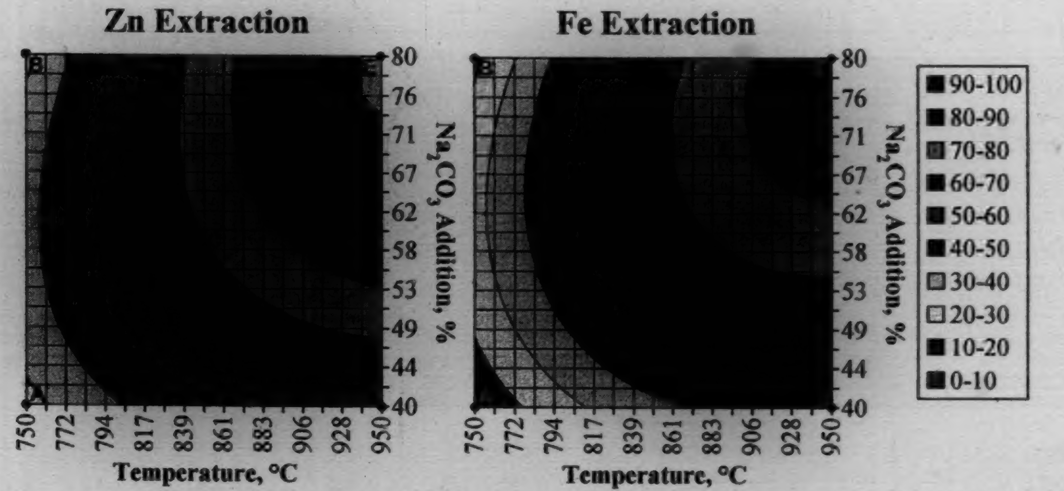

Figure 25 Effect of Temperature and Na_2CO_3 Addition on A) Zinc Extraction and B) Iron Extraction from Roasted La Oroya Zinc Ferrite

Samples at various conditions described by this model, as shown by the points A, B, C, D and E in Figure 25, were analyzed using x-ray diffraction to determine the phase transformations that occurred during roasting at various conditions (Table 15). The diffraction patterns and major phases observed are shown in Figure 26.

Table 15 Phases Identified by X-ray Diffraction Analysis of Zinc Ferrite Roasted with Na_2CO_3

Sample	Identified Phases (in order of intensity)
A	$ZnFe_2O_4$, Na_2CO_3, Pb_5O_8, Ca_2SiO_4 (Larnite), $ZnSO_4\cdot3Zn(OH)_2\cdot0.5\ H_2O$
B	$ZnFe_2O_4$, Na_2CO_3, $PbSO_4$, ZnO
C	$ZnFe_2O_4$, α-$NaFeO_2$, β-$NaFeO_2$, Na_2ZnSiO_4, ZnO, PbO (Massicot)
D	$ZnFe_2O_4$, β-$NaFeO_2$, Na_2ZnSiO_4, PbO (Lithargite), α-$NaFeO_2$
E	β-$NaFeO_2$, ZnO, Na_2ZnSiO_4, Na_2PbO_3, α-$NaFeO_2$

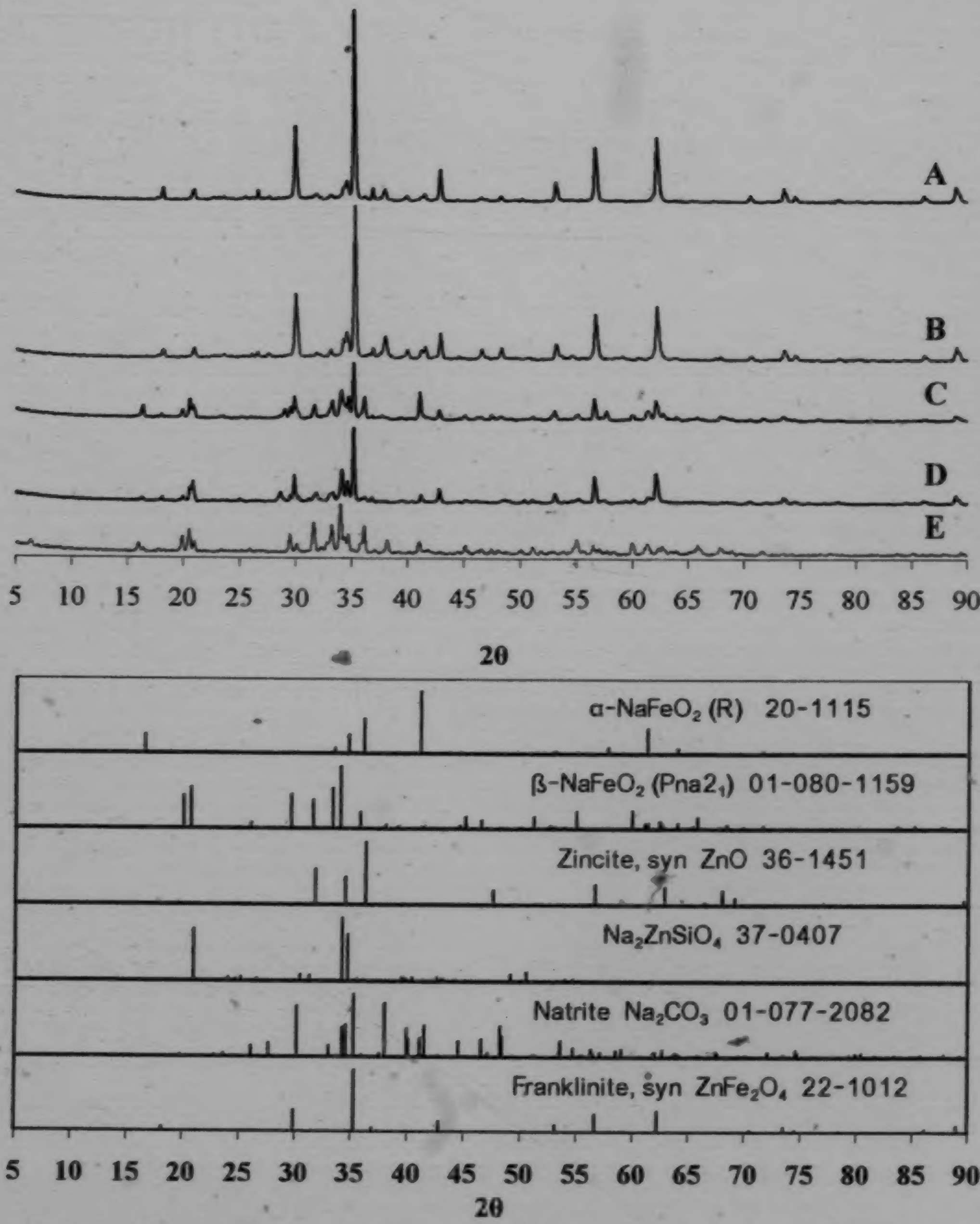

Figure 26 X-ray Diffraction Patterns of Zinc Ferrite Roasted with Na_2CO_3

The x-ray diffraction results show that little reaction occurs at 750°C, as there is significant unreacted Na_2CO_3 in the roasted samples, there is little change in the phases observed from the feed sample and there are only low levels of acid-soluble zinc in these samples. However, above 850°C, $ZnFe_2O_4$ reacts to form $NaFeO_2$, with α-$NaFeO_2$

preferred at 850°C and β-$NaFeO_2$ preferred at 950°C. (Based on the thermodynamic analysis in Section 4.3.1.1, this reaction should become spontaneous above 823°C.) With the release of zinc from the ferrite structure, Na_2ZnSiO_4 and ZnO are also formed, with an indication of an increased preference to form ZnO at higher Na_2CO_3 additions. Decomposition of $ZnFe_2O_4$ is incomplete at lower temperatures or lower Na_2CO_3 additions, but the franklinite peaks disappear at 950°C and 80% Na_2CO_3 (Sample E). These conditions are near the centre of the region where zinc extractions are over 90% in Figure 25, indicating that complete, or near complete, decomposition of $ZnFe_2O_4$ to $NaFeO_2$ is required to achieve high zinc extractions.

Differences between the major phases are also visible with the scanning electron microscope using backscattered electron imaging. Four phases can be clearly identified in Sample E (950°C, 80% Na_2CO_3) in Figure 27. EDX analysis indicates that the bright phase (A) is high in Zn (i.e., ZnO), the light grey phase (B) is high in Na and Fe (i.e., $NaFeO_2$), the dark grey phase (C) contains Ca, Mn, Na, Si and Zn (i.e., a mixture of Ca, Mn and Na-Zn silicates) and the black phase (D) contains Na and S (i.e., residual Na_2CO_3/Na_2SO_4). Texturally, these particles show features consistent with the melting or partial melting of Na_2CO_3 or Na_2SO_4, which would be expected at the roasting temperatures used for this sample.

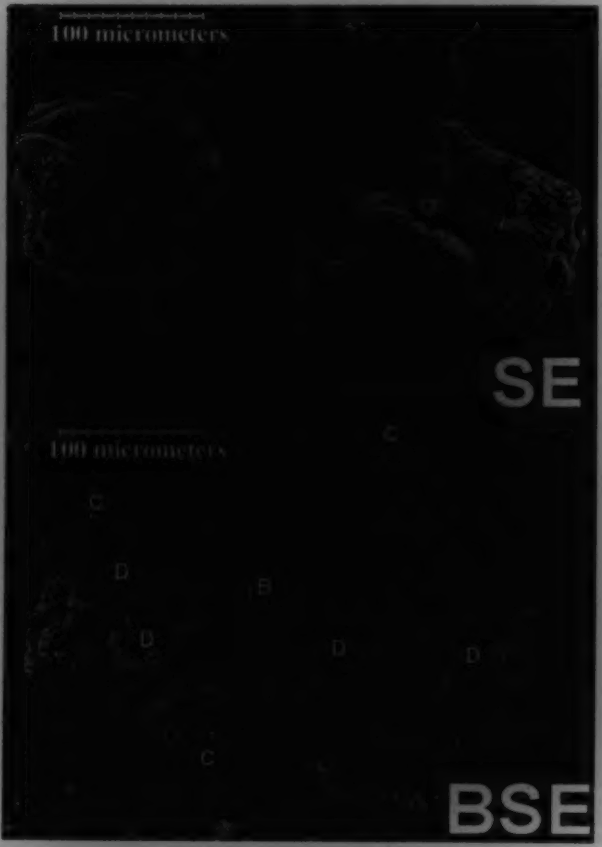

Figure 27
Secondary Electron (SE) and Backscattered Electron (BSE) Images of Zinc Ferrite Roasted at 950°C with 80% Na_2CO_3 (Sample E)

After leaching, anglesite ($PbSO_4$) and unreacted $ZnFe_2O_4$ are the only crystalline phases observed in the leach residues (Figure 28). (The leach residue for sample E, where extractions of 99% Zn and 81% Fe were observed, along with an 87% weight loss during leaching, is poorly crystalline with broad low intensity peaks, but minor $ZnFe_2O_4$ and $PbSO_4$ peaks were identified in this sample as well.)

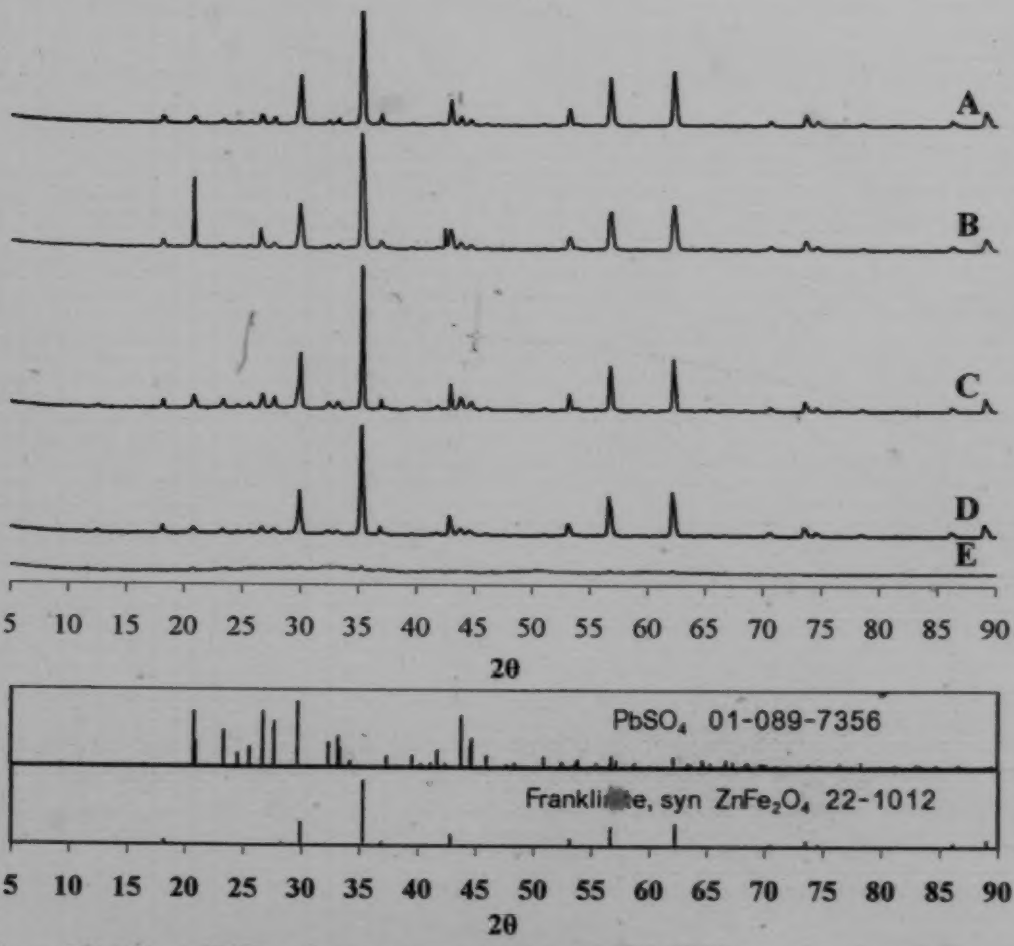

Figure 28 **X-ray Diffraction Patterns of Zinc Ferrite Residue after Roasting with Na_2CO_3 and Leaching with 200 g/L H_2SO_4**

Overall, the analysis of the leach residue confirms the findings of the scoping tests. High iron extractions occur at the conditions required for high zinc extractions which, in turn, correspond to the reaction of $ZnFe_2O_4$ with Na_2CO_3 to form $NaFeO_2$. However, based on these results, these high iron extractions occur because both α- and β-$NaFeO_2$ are highly soluble in cold sulphuric acid solutions. These high iron extractions (80 to 90%) would, of course, be undesirable commercially as the dissolved iron would need to be precipitated as jarosite, goethite or hematite for disposal before any zinc recovery from the leach solution could take place. Without better control of iron dissolution, Na_2CO_3 roasting would have few advantages over the hot acid leaching process described in Section 4.2.2.4, which also results in near quantitative zinc and iron extractions, but is much less energy intensive.

4.5.2.1.1 Potential Secondary Additions to Control Iron Dissolution

Although Na_2CO_3 has been shown to be effective in solubilizing zinc from the La Oroya zinc ferrite, this zinc dissolution is accompanied by near quantitative iron dissolution. Further DOE tests were, therefore, conducted to evaluate the possibility of controlling iron extraction during leaching by forming acid-insoluble metal ferrites during roasting while maintaining high zinc extractions.

Three reagents, $CaCO_3$, $MnCO_3$ and $Mg(OH)_2$, were selected for DOE testing. With the limited reaction of these reagents with $ZnFe_2O_4$ directly, based on the results from Section 4.4.2.1, thermodynamically it was assumed that these reagents would react with $NaFeO_2$ to form either Ca-, Mn- or Mg-ferrites, likely by the reactions shown in Figure 29. From this analysis, the formation of Ca- and Mn-ferrites should be favored at the roasting temperatures used for these tests. The formation of $MgFe_2O_4$, on the other hand, is not favored thermodynamically until 1190°C, but was tested for comparative purposes.

If reaction does not take place during heating, thermodynamically, $CaCO_3$, $Mg(OH)_2$ and $MnCO_3$ would be expected to decompose to their respective oxides at 845, 260, and 360°C, respectively. Reactions showing the reaction of these oxides with $NaFeO_2$ to form Na_2O and metal ferrites are also shown in Figure 29. In all cases, the reaction with the oxides is more favorable thermodynamically at the roasting temperatures tested.

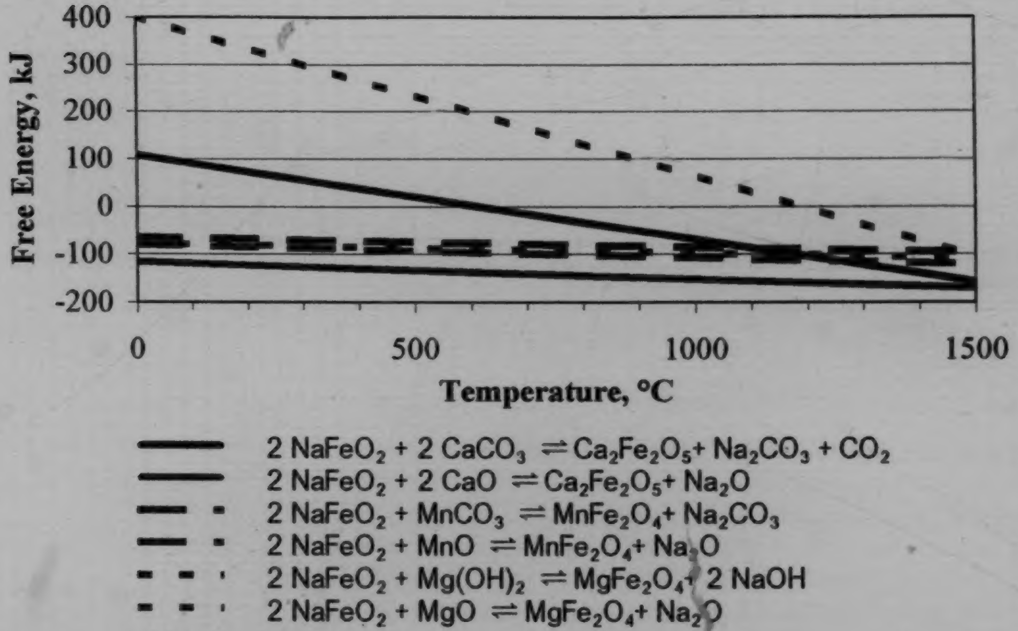

Figure 29 **Potential Reactions of Secondary Reagents with $NaFeO_2$ ($\Delta G°$ vs. Temperature)**

4.5.2.1.1.1 Roasting with $CaCO_3$ as a Secondary Additive

The addition of $CaCO_3$ to the Na_2CO_3 roast produced a shift in the region of maximum zinc extractions to higher temperatures and Na_2CO_3 additions, compared with roasting with Na_2CO_3 alone, such that only the edge of this region is visible in the plots of the conditions tested (Figure 30). In addition, with increasing $CaCO_3$ additions, the "steepness" (i.e.,. the rate of change) of the zinc extraction, particularly with respect to temperature, showed a marked increase as the $CaCO_3$ addition increased.

Over the range of $CaCO_3$ additions tested, zinc extractions increased sharply with increasing Na_2CO_3 additions, but showed only a mild relationship to increases in $CaCO_3$ addition (Figure 31). However, at higher Na_2CO_3 additions, the iron extraction decreases significantly with increasing $CaCO_3$ additions. Thus, this indicates that, by adding up to 29.5% $CaCO_3$, iron extractions can be decreased from 80 to 90% down to 60 to 70% while maintaining zinc extractions in the range of 90 to 100%.

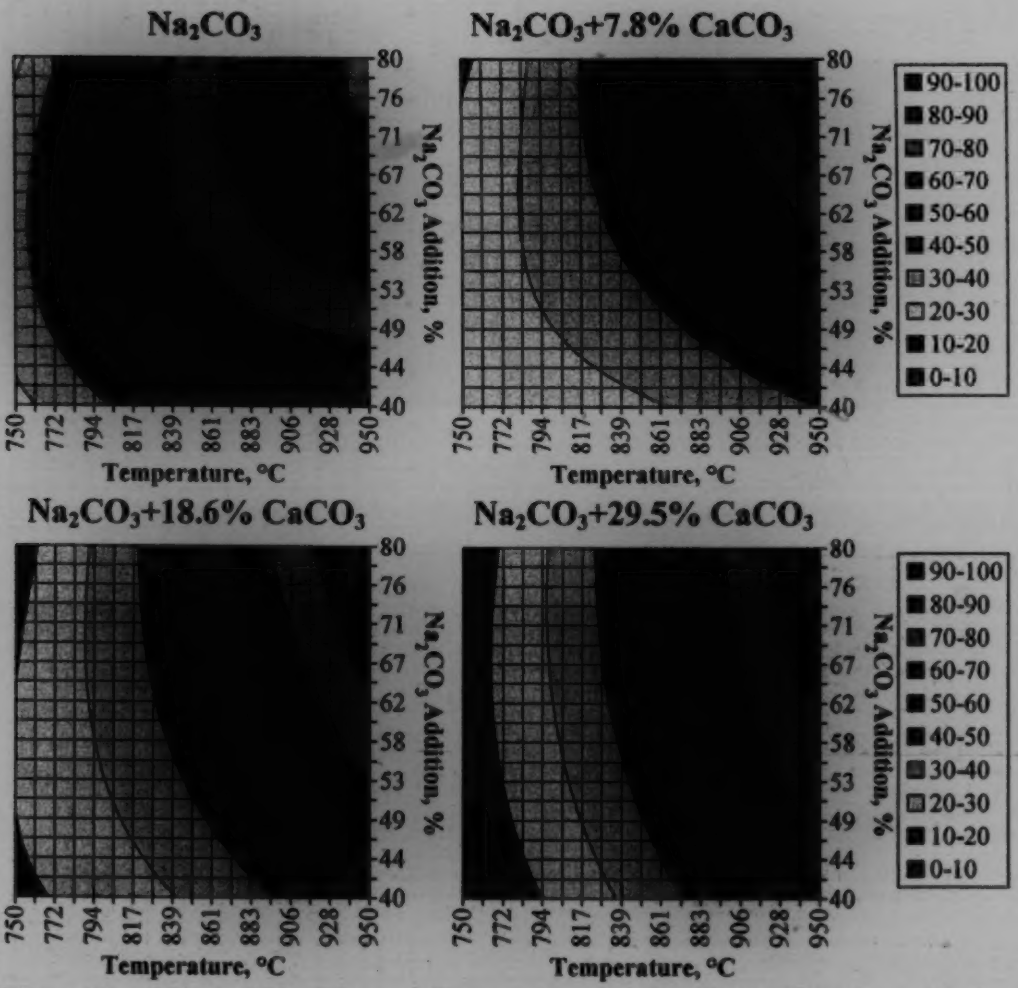

Figure 30 Effect of Na_2CO_3 and Temperature on Zn Extractions from La Oroya Zinc Ferrite Roasted with Various Amounts of $CaCO_3$

Samples at various conditions described by this model were analyzed using x-ray diffraction (Points A, B, C and D on Figure 31C). The identified phases are listed in Table 16 while the diffraction patterns and major phases are shown in Figure 32.

Table 16 Phases Identified by X-ray Diffraction Analysis of Zinc Ferrite Roasted with Na_2CO_3 and $CaCO_3$ at 950°C

Sample	Identified Phases (in order of intensity)
A	$ZnFe_2O_4$, β-$NaFeO_2$, Na_2ZnSiO_4, ZnO, α-$NaFeO_2$, PbO (Massicot)
B	$ZnFe_2O_4$, ZnO, β-$NaFeO_2$, $Ca_2Fe_2O_5$, PbO (Lithargite), Ca_2SiO_4 (Larnite)
C	ZnO, β-$NaFeO_2$, Na_2ZnSiO_4, $Ca_2Fe_2O_5$, α-$NaFeO_2$, $ZnFe_2O_4$, Ca_2SiO_4 (Larnite), Na_2PbO_3
D	ZnO, β-$NaFeO_2$, $Ca_2Fe_2O_5$, α-$NaFeO_2$, $ZnFe_2O_4$, Na_2PbO_3

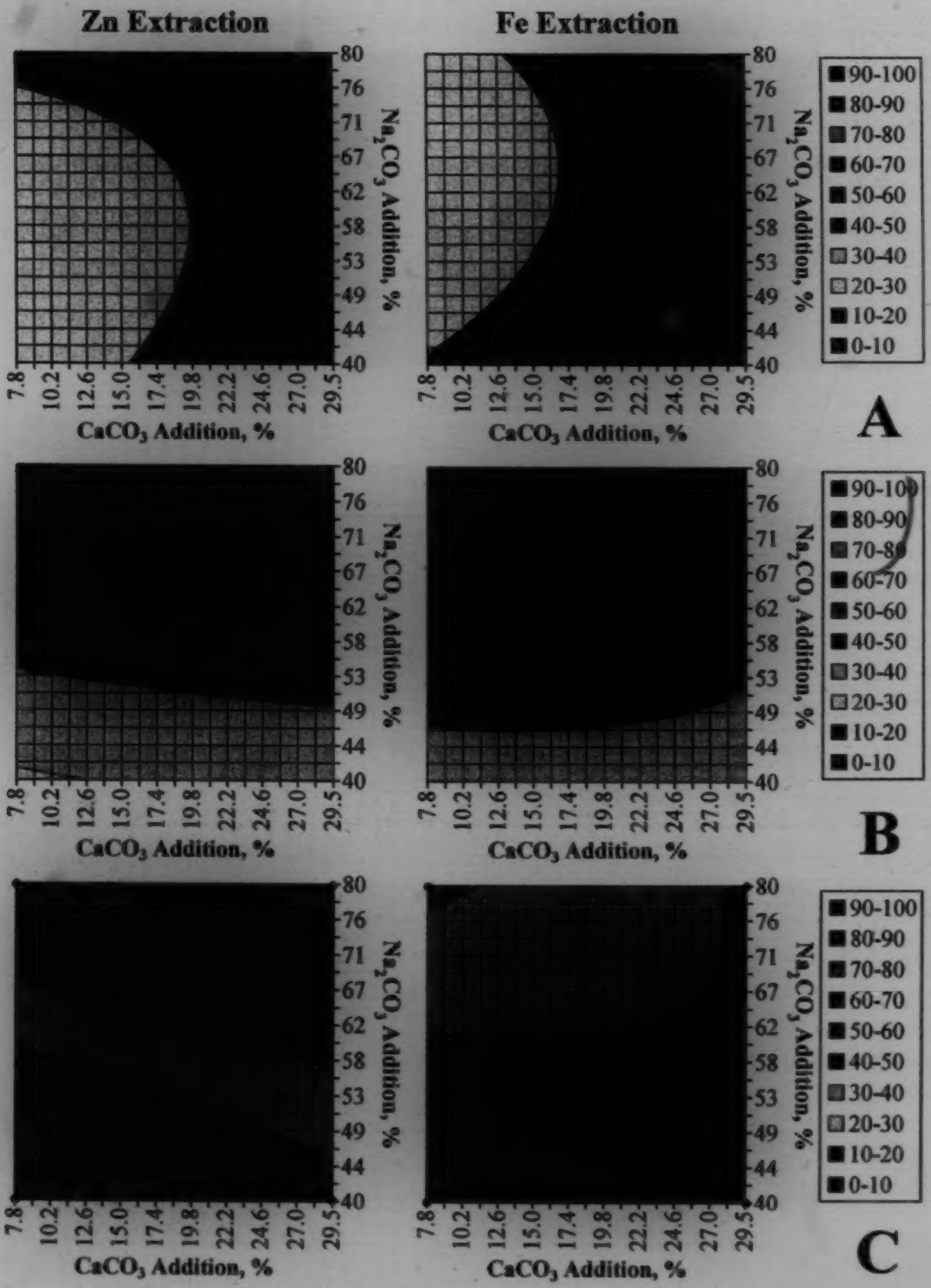

Figure 31 Effect of Na_2CO_3 and $CaCO_3$ Additions on Zinc and Iron Extractions from La Oroya Zinc Ferrite Roasted at A) 750°C, B) 850°C and C) 950°C

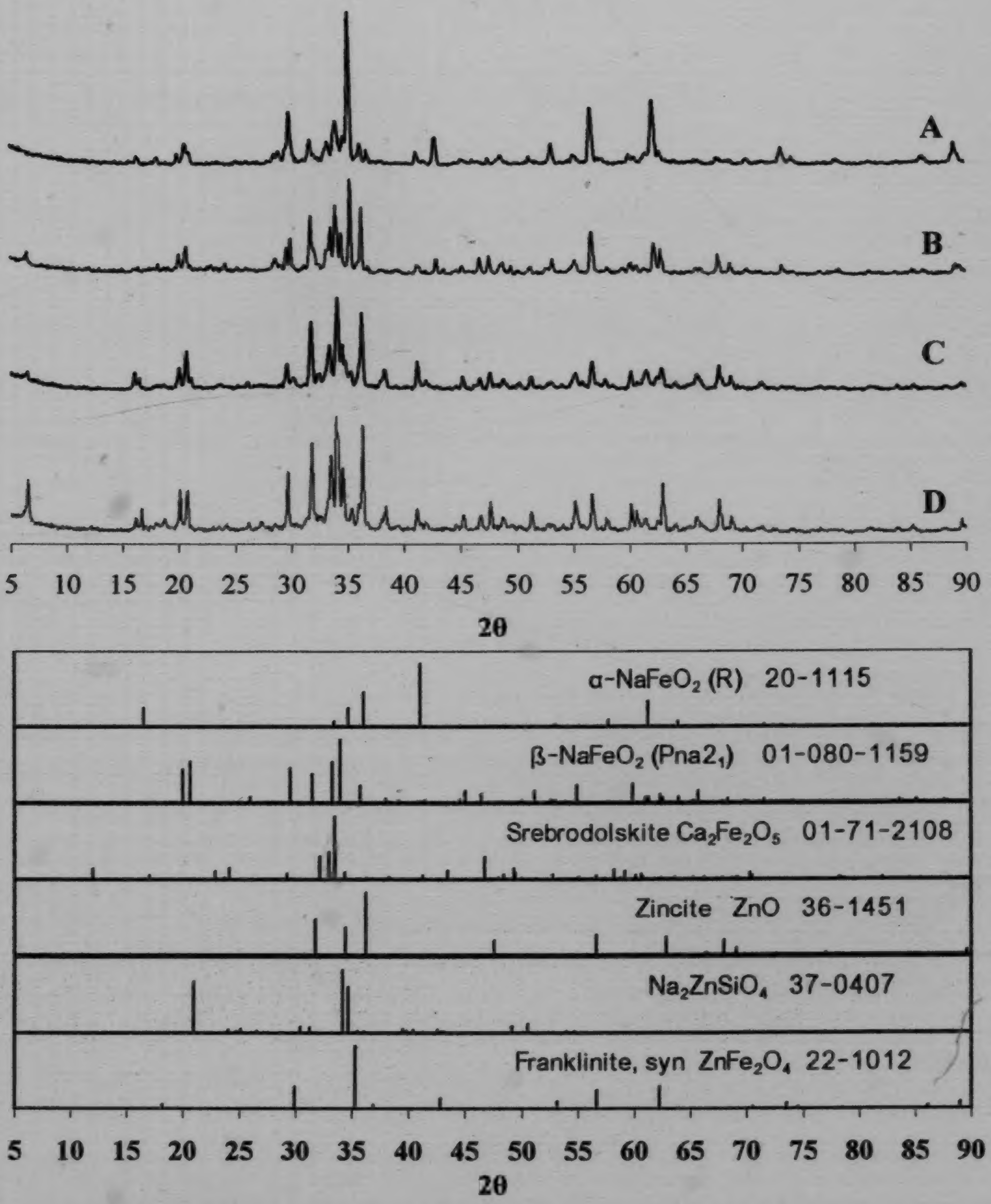

Figure 32 **X-ray Diffraction Patterns of Zinc Ferrite Roasted with Na_2CO_3 and $CaCO_3$**

The phases formed, for the most part, are similar to those observed from roasting with Na_2CO_3 alone. At 950°C, $ZnFe_2O_4$ is decomposed to form α- and β-$NaFeO_2$, ZnO and Na_2ZnSiO_4 as major phases, with the decomposition going toward completion as the Na_2CO_3 addition is increased. The shift of the maximum zinc extraction observed in

Figure 30 to higher temperatures and Na_2CO_3 additions is reflected in the XRD analysis, as residual $ZnFe_2O_4$ is still present in minor quantities after roasting with Na_2CO_3 and $CaCO_3$ at 950°C and 80% Na_2CO_3, conditions where the complete decomposition of $ZnFe_2O_4$ would be observed when roasting with Na_2CO_3 alone. At 950°C, the formation of β-$NaFeO_2$ is preferred as it was when roasting at 950°C without $CaCO_3$ additions.

The major difference in the phases formed is the definite formation of a calcium ferrite, srebrodolskite ($Ca_2Fe_2O_5$), during roasting, with the intensity of the srebrodolskite peaks increasing with increasing Na_2CO_3 and $CaCO_3$ additions. However, this analysis also shows that $NaFeO_2$ is still the predominant iron-bearing phase in the roasted ferrite, indicating that the formation of $Ca_2Fe_2O_5$ from $NaFeO_2$ is far from complete, even with $CaCO_3$ additions of up to 47.5% of stoichiometric for the formation of $Ca_2Fe_2O_5$. The gradual slope of the model, with respect to $CaCO_3$ addition, would mean that a significant increase in $CaCO_3$ would only result in a small decrease in iron extractions.

SEM/EDX analysis of Sample C (950°C, 80% Na_2CO_3, 7.8% $CaCO_3$) shows phases high in Zn and O (i.e., ZnO (A)), high in Na, Fe and O (i.e., $NaFeO_2$ (C)), high in Fe, Na, Pb, S and O (i.e., a mixture of $NaFeO_2$ and $PbSO_4$/Na_2PbO_3 (E)), and high in Ca, Fe, Na, Si, Zn and O (i.e., a mixture of $NaFeO_2$/$Ca_2Fe_2O_5$ and Ca_2SiO_4/Na_2ZnSiO_4 (F)), all of which are consistent with the phases identified using x-ray diffraction (Figure 33). However, additional phases were identified, which were not detected using x-ray diffraction, including phases high in Na, C, S and O (i.e., Na_2CO_3/Na_2SO_4 (B)), high in Fe and O (i.e., Fe_2O_3 or Fe_3O_4 (D)), and high Ca and O (i.e., unreacted $CaCO_3$, likely calcined to CaO (G)).

Sample D (950°C, 80% Na_2CO_3, 29.5% $CaCO_3$) was also examined using SEM/EDX analysis (Figure 34). After comparison with the x-ray diffraction results, phases likely to be ZnO (A), srebrodolskite ($Ca_2Fe_2O_5$) (C), and a mixture of $NaFeO_2$ and $Ca_2Fe_2O_5$ (D) could be identified. However, other phases high in Na, Ca, C, S and O (i.e., a mixture of Na_2CO_3/Na_2SO_4 and $CaCO_3$/$CaSO_4$ (F)), high in Fe and O (i.e., Fe_2O_3 or Fe_3O_4 (E)), high in Ca, Na, Si and O (i.e., a mixture of Ca_2SiO_4 and perhaps Na_2SiO_4 (F)), high in Ca, Si, Fe, Zn and O (i.e., a mixture of Ca_2SiO_4 and unreacted $ZnFe_2O_4$ (G)) and high in Pb, S and O (i.e., $PbSO_4$ and/or PbO (H)) were also observed. One particle (I) showed significant concentrations of As and P, in addition to high levels of Na, Pb and O.

In the residues after leaching with 200 g/L H_2SO_4, gypsum ($CaSO_4 \cdot 2H_2O$), anglesite ($PbSO_4$) and residual $ZnFe_2O_4$ are the major phases; srebrodolskite ($Ca_2Fe_2O_5$) is identified as a minor phase only in Sample D (Table 17 and Figure 35).

Table 17 Phases Identified by X-ray Diffraction Analysis of Zinc Ferrite after Roasting with Na_2CO_3 and $CaCO_3$ and Leaching with 200 g/L H_2SO_4

Sample	Identified Phases (in order of intensity)	Leaching Wt. Loss, %
A	$ZnFe_2O_4$, $PbSO_4$, $CaSO_4 \cdot 2H_2O$	56
B	$ZnFe_2O_4$, $CaSO_4 \cdot 2H_2O$, $PbSO_4$	39
C	$ZnFe_2O_4$, $CaSO_4 \cdot 2H_2O$, $PbSO_4$	78
D	$ZnFe_2O_4$, $CaSO_4 \cdot 2H_2O$, $PbSO_4$, $Ca_2Fe_2O_5$	52

SEM/EDX analysis of Samples C and D after leaching with 200 g/L demonstrates that any ZnO, Na_2ZnSiO_4 or residual Na_2CO_3/Na_2SO_4 have been leached from the samples and also confirms the presence of gypsum ($CaSO_4 \cdot 2H_2O$) and anglesite ($PbSO_4$) in the leach residues (i.e., particles E and F, respectively, in Figure 36 (Sample C), and particles B and A, respectively in Figure 37 (Sample D)). However, at $CaCO_3$ additions of 7.8% (Sample C) where over 80% of the iron was dissolved during leaching, the major iron-bearing phases remaining in the leach residue are either high in Fe and O (i.e., Fe_2O_3/Fe_3O_4 (D)) or high in Fe, Mn and O (i.e.,$MnFe_2O_4$), with unreacted $ZnFe_2O_4$ (A) or $(Zn,Mn)Fe_2O_4$ (B) also present in minor quantities (Figure 36). (Particle G in Figure 36 shows high Pb, Si, Na and O concentrations, possibly indicating the presence of Pb-Na silicate in the leach residue from Sample C). At higher $CaCO_3$ additions (29.5% $CaCO_3$ (Sample D)) where iron extractions were slightly lower at about 72%, only two iron-containing phases are observed in the leach residue: particles high in Ca, Fe and O (i.e.,$Ca_2Fe_2O_5$ (C)) and high in Fe and O (i.e., Fe_2O_3/Fe_3O_4) (Figure 37).

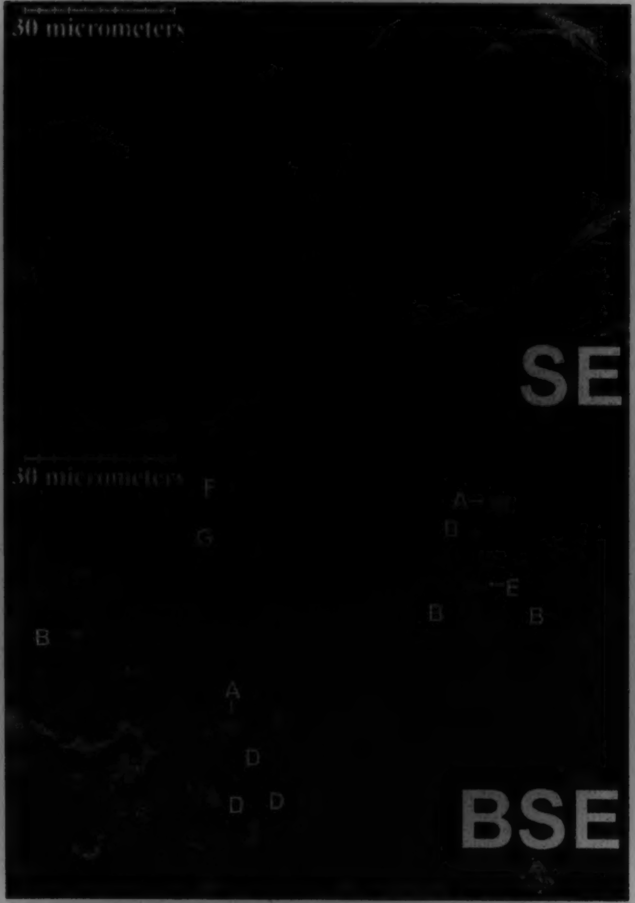
30 micrometers
SE
30 micrometers
F
G
A
B
E
B
B
B
A
D
D
D
BSE

Figure 33
Secondary Electron (SE) and Backscattered Electron (BSE) Images of Zinc Ferrite Roasted at 950°C with 80% Na_2CO_3 and 7.8% $CaCO_3$ (Sample C)

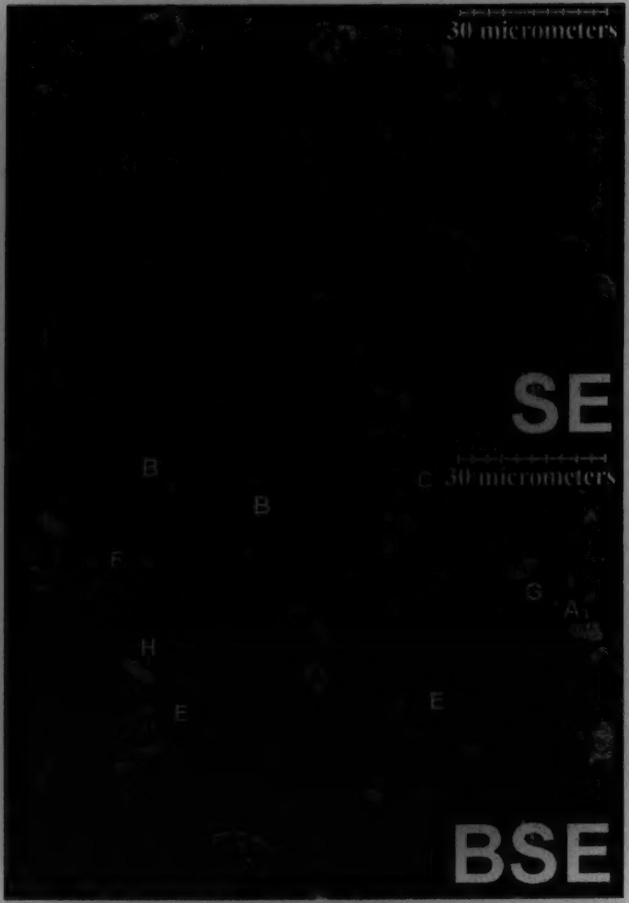
30 micrometers
SE
B
B
C
30 micrometers
F
G
A
H
E
E
BSE

Figure 34
Secondary Electron (SE) and Backscattered Electron (BSE) Images of Zinc Ferrite Roasted at 950°C with 80% Na_2CO_3 and 29.5% $CaCO_3$ (Sample D)

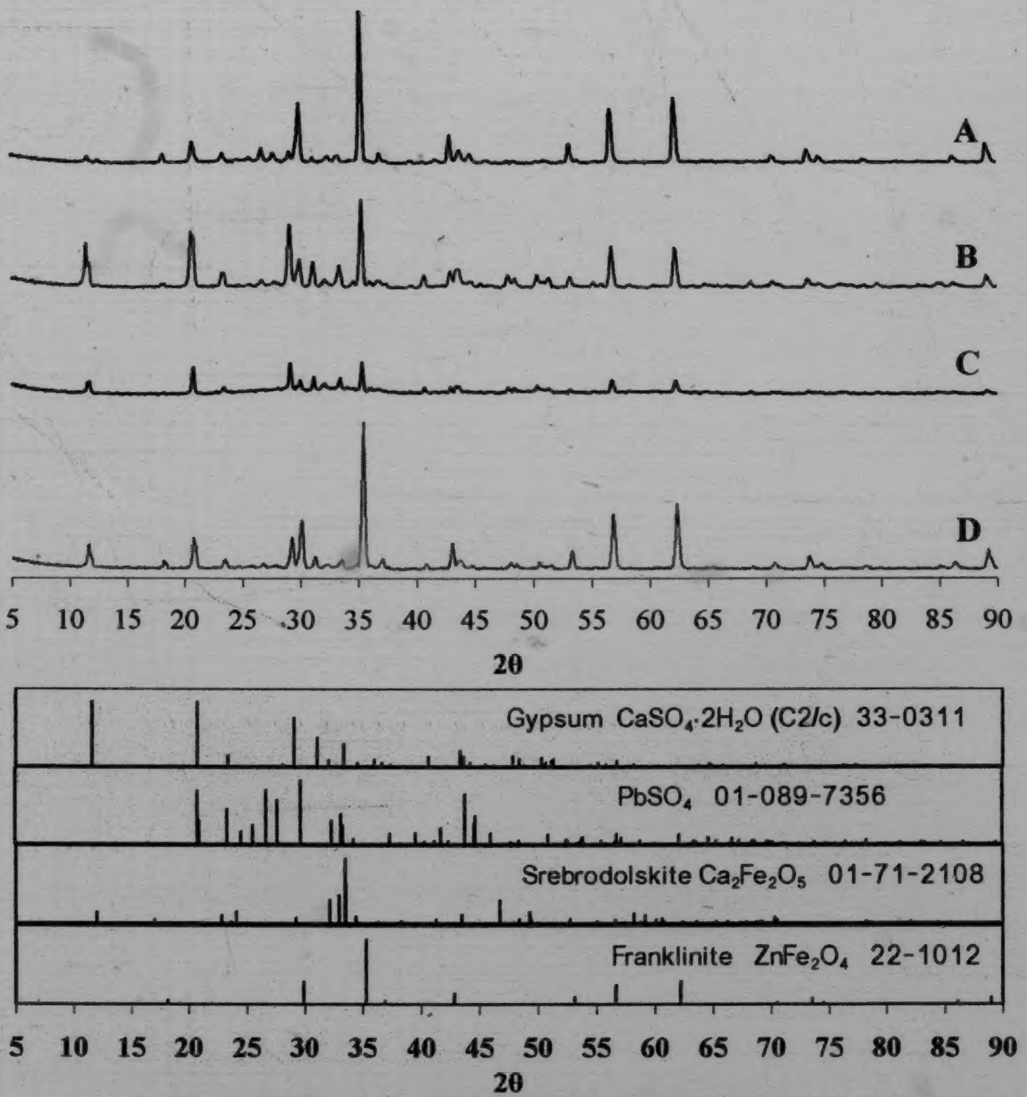

Figure 35 X-ray Diffraction Patterns of Zinc Ferrite Residue after Roasting with Na_2CO_3 and $CaCO_3$ and Leaching with 200 g/L H_2SO_4

Thus, this analysis indicates that the decrease in iron extractions observed between Sample C and Sample D could be the result of the formation of srebrodolskite ($Ca_2Fe_2O_5$) which is not dissolved during the leaching process. However, comparison of the x-ray diffraction patterns before and after leaching indicate that the intensity of the srebrodolskite peaks decrease, or the peaks disappear, after leaching with 200 g/L H_2SO_4. In part, this could be caused by the precipitation of gypsum in the leach residue, which has intense well-defined peaks which could make $Ca_2Fe_2O_5$ harder to detect. However, because srebrodolskite ($Ca_2Fe_2O_5$) is not present in significant quantities in the leach residue using either x-ray diffraction or SEM/EDX analysis, it is likely that $Ca_2Fe_2O_5$ is leached, or partially leached, during leaching with 200 g/L H_2SO_4, and the calcium is then reprecipitated as gypsum under the high sulphate conditions of the leach.

In summary, though the addition of $CaCO_3$ did cause a decrease in the iron extractions of about 10% under the conditions where zinc extraction is greater than 90%, this decrease in iron extraction is significantly lower than would be expected if all the $CaCO_3$ added during roasting reacted to form either $CaFe_2O_4$ or $Ca_2Fe_2O_5$. (If all the $CaCO_3$ reacted, and assuming the calcium ferrites formed are acid insoluble, a decrease in iron extraction of 95% would be expected if $CaFe_2O_4$ was formed and 47.5% if $Ca_2Fe_2O_5$ was formed.) Thus, whether this is a result of poor reaction kinetics for the formation of $CaFe_2O_4$ or $Ca_2Fe_2O_5$, or because the Ca-ferrites formed under these conditions are partially soluble in H_2SO_4 solutions, these results indicate that $CaCO_3$ is not particularly effective as an additive to control, or reduce, the dissolution of iron during roasting of the La Oroya zinc ferrite with Na_2CO_3.

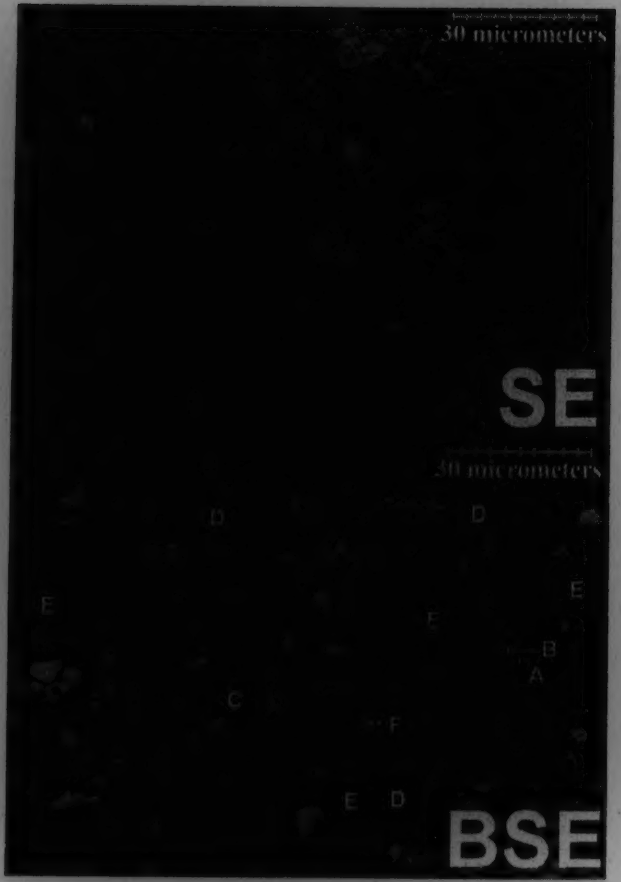

30 micrometers
SE
30 micrometers
D
D
E
E
E
B
A
C
F
E
D
BSE

Figure 36

Secondary Electron (SE) and Backscattered Electron (BSE) Images of Zinc Ferrite Roasted at 950°C with 80% Na_2CO_3 and 7.8% $CaCO_3$ and Leached with 200 g/L H_2SO_4 (Sample C)

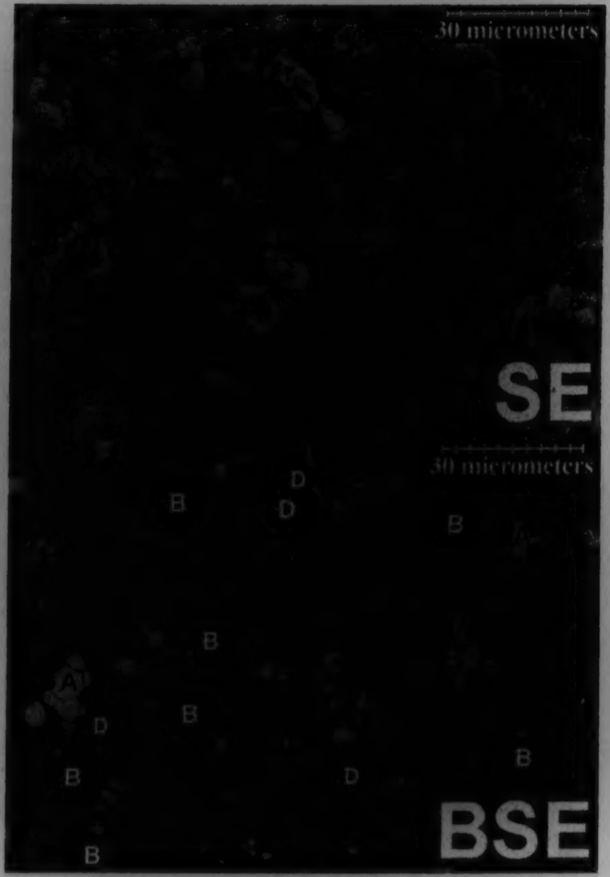

30 micrometers
SE
30 micrometers
D
B
D
B
B
A
D
B
B
D
B
B
BSE

Figure 37

Secondary Electron (SE) and Backscattered Electron (BSE) Images of Zinc Ferrite Roasted at 950°C with 80% Na_2CO_3 and 29.5% $CaCO_3$ and Leached with 200 g/L H_2SO_4 (Sample D)

4.5.2.1.1.2 Roasting with $Mg(OH)_2$ as a Secondary Additive

The addition of $Mg(OH)_2$ to Na_2CO_3 roasting produced a similar shift in the region of maximum zinc extractions to higher temperatures and Na_2CO_3 additions as was observed when roasting with $CaCO_3$ (Figure 38). An increase in the rate of change of the zinc extraction, particularly with respect to temperature, was also evident, although the increase was much smaller than was observed when roasting with $CaCO_3$.

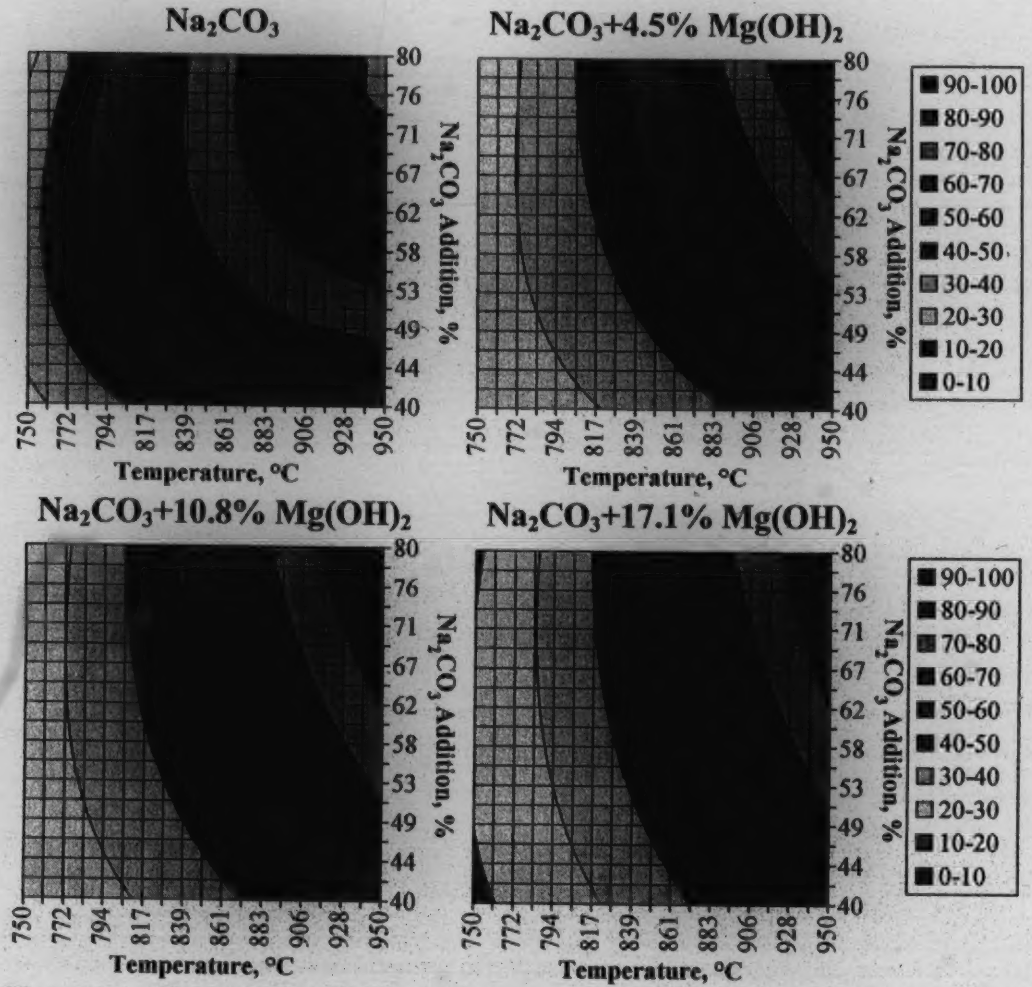

Figure 38 Effect of Na_2CO_3 and Temperature on Zn Extractions from La Oroya Zinc Ferrite Roasted with Various Amounts of $Mg(OH)_2$

Zinc extractions are largely unaffected by $Mg(OH)_2$ additions, with iron extractions showing only a mild decrease with increased $Mg(OH)_2$ additions (Figure 39).

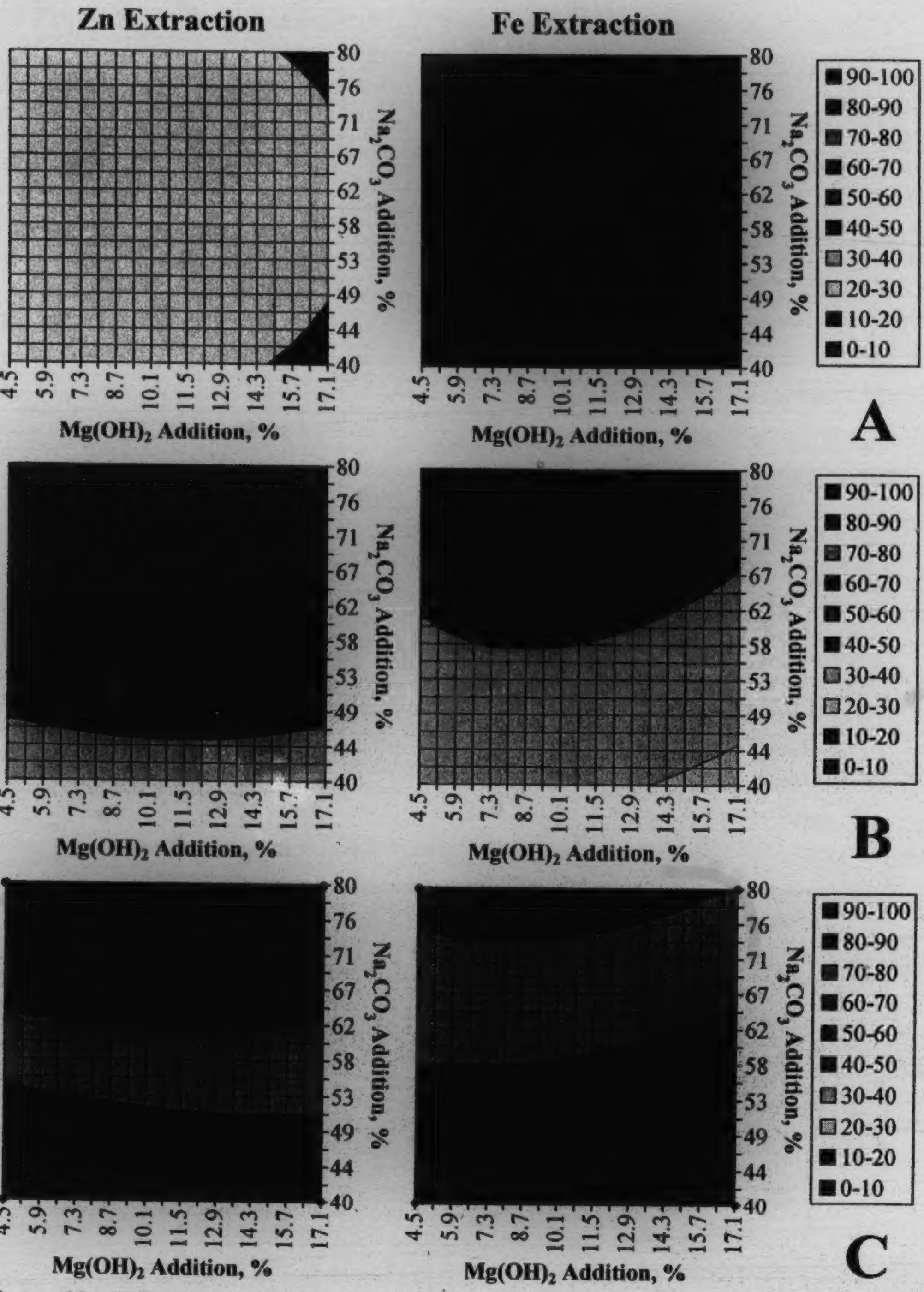

Figure 39 Effect of Na$_2$CO$_3$ and Mg(OH)$_2$ Additions on Zinc and Iron Extractions from La Oroya Zinc Ferrite Roasted at A) 750°C, B) 850°C and C) 950°C

Samples at various conditions described by this model were analyzed using x-ray diffraction (Points A, B, C and D on Figure 39C). The identified phases are listed in Table 18 while the diffraction patterns and major phases are shown in Figure 40.

Table 18 Phases Identified by X-ray Diffraction Analysis of Zinc Ferrite Roasted with Na_2CO_3 and $CaCO_3$ at 950°C

Sample	Identified Phases (in order of intensity)
A	$ZnFe_2O_4$, Na_2ZnSiO_4, β-$NaFeO_2$, α-$NaFeO_2$, PbO (Litharge)
B	$ZnFe_2O_4$, Na_2ZnSiO_4, β-$NaFeO_2$, Ca_2SiO_4 (Larnite), α-$NaFeO_2$, PbO (Litharge)
C	β-$NaFeO_2$, ZnO, Na_2ZnSiO_4, α-$NaFeO_2$, Na_2PbO_3
D	β-$NaFeO_2$, MgO (Periclase), α-$NaFeO_2$, Na_2ZnSiO_4, ZnO, Na_2PbO_3

The phases formed are similar to those observed from roasting with Na_2CO_3 alone or from roasting with Na_2CO_3 and $CaCO_3$, with only changes in the order of measured intensities or in the detection of minor phases. However, in these samples, there was no explicit evidence for the formation of magnesioferrite ($MgFe_2O_4$). In part, this could be due to the close similarity of the x-ray diffraction patterns of $ZnFe_2O_4$ and $MgFe_2O_4$ (Figure 40) which makes it more difficult to confirm the presence of $MgFe_2O_4$ with any confidence or also possibly due to the formation of a $ZnFe_2O_4/MgFe_2O_4$ solid solution. However, the appearance of periclase (MgO) in Sample D would indicate that the majority of the $Mg(OH)_2$ remained unreacted under the conditions tested, as would be expected based on the thermodynamic analysis at the start of Section 4.5.2.1.1.

SEM micrographs of Sample C, and the phases detected, are shown in Figure 41. Energy dispersive x-ray analysis (EDX) of the particles in view showed several differences in composition. Some of the bright particles (A) contained Zn and O (i.e., ZnO) while other bright particles (B) contained Pb and O (i.e., PbO). Particles high in Fe and O (i.e., Fe_2O_3 or Fe_3O_4 (D)), Na, Zn and Si (i.e., Na_2ZnSiO_4 (E)), and Na, O and S (i.e., Na_2SO_4 (F)) were also observed. Still other particles showed a mixture of phases, such as particles (C) containing Ca, Na, Si, S, Zn and O (i.e., a mixture of Na_2ZnSiO_4/Ca_2SiO_4 or $NaSO_4/CaSO_4$), particles (G) containing Fe, Mn, Na, O, Si and Zn (i.e., a mixture of Na_2ZnSiO_4 and $(Zn,Mn)Fe_2O_4$)) and particles (H) containing Fe, Mn, O and Zn (i.e., a mixture of $ZnFe_2O_4$ and $MnFe_2O_4$). No magnesium containing phases were identified in this sample.

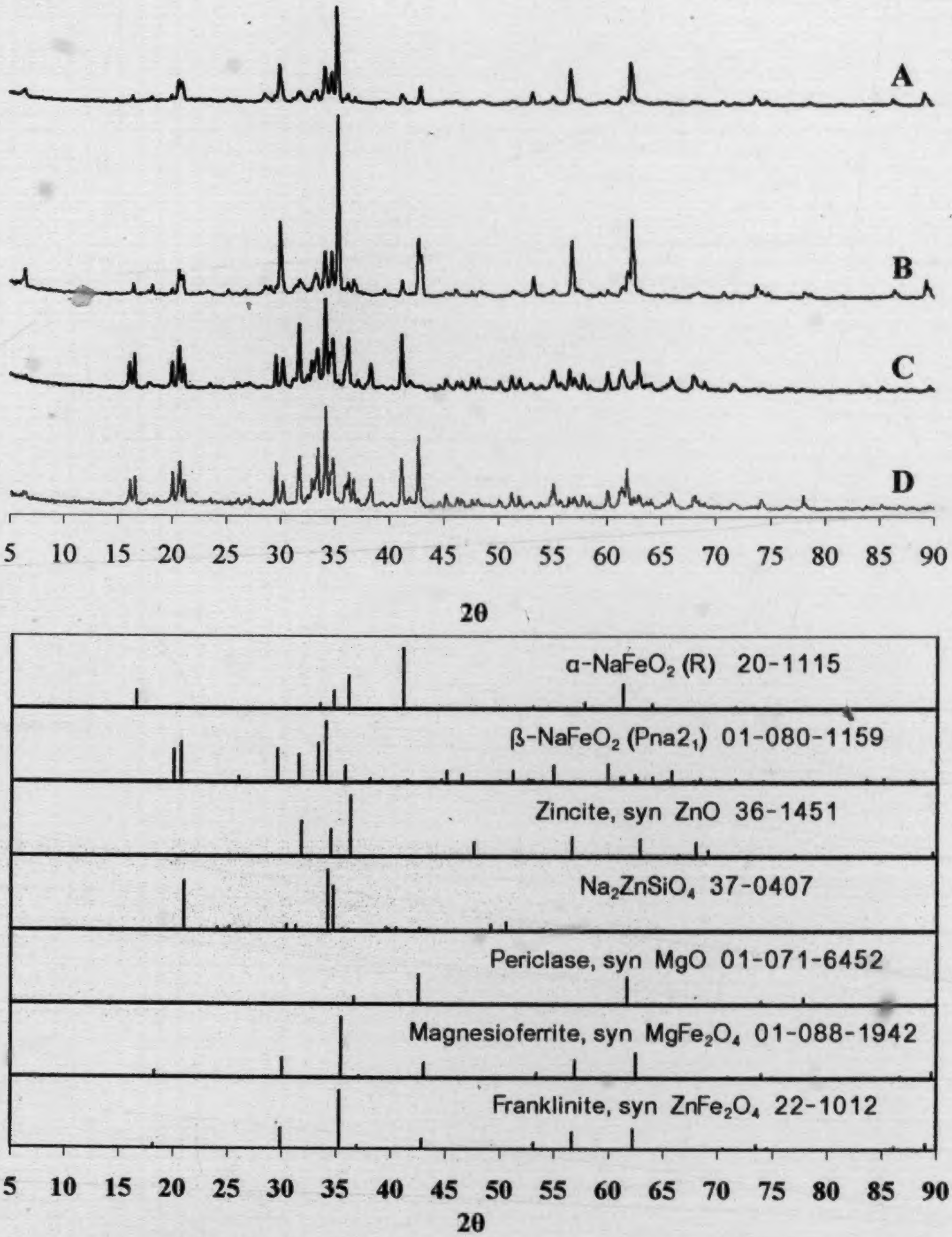

Figure 40 **X-ray Diffraction Patterns of Zinc Ferrite Roasted with Na_2CO_3 and $Mg(OH)_2$**

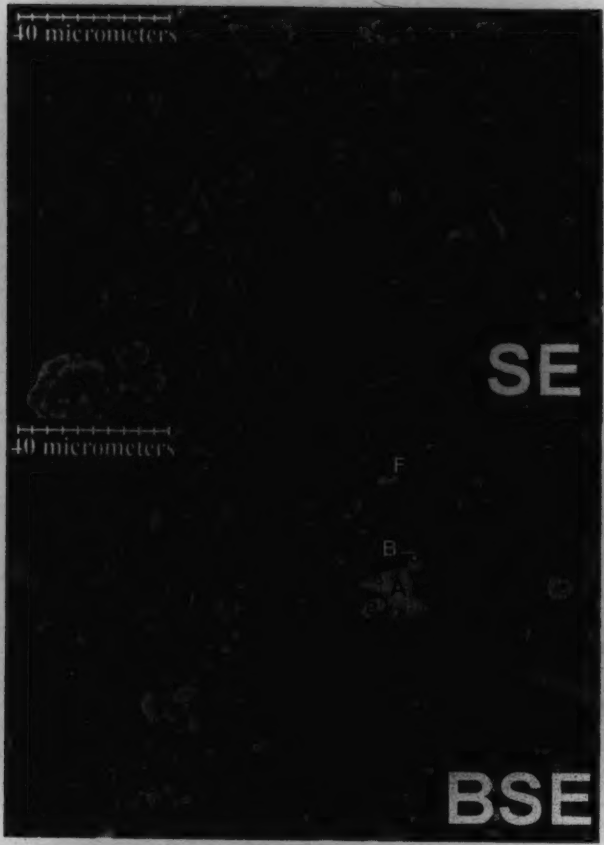

Figure 41
Secondary Electron (SE) and Backscattered Electron (BSE) Images of Zinc Ferrite Roasted at 950°C with 80% Na_2CO_3 and 4.5% $Mg(OH)_2$ (Sample C)

SEM/EDX analysis of Sample D, which was roasted with more $Mg(OH)_2$ (17.1%), shows light grey euhedral octahedral crystals (A), typical of franklinite, that contain Zn, Fe and Mg, indicating that there may be some solid solution of Mg in the spinel structure under these conditions (Figure 42). However, magnesium is also found combined with other metal oxides, likely as periclase (MgO), in bright particles (E) containing Pb, Zn, Mg and O. Besides these phases, other phases consistent with those observed in Sample C, including a Na-Fe-O phase (i.e., $NaFeO_2$ (B)), an Fe-O phase (i.e., Fe_2O_3 or Fe_3O_4 (C)), a Na-S-O phase (i.e., Na_2SO_4 (D)) and a Pb-O phase (i.e., PbO (F)).

After leaching with 200 g/L H_2SO_4, $ZnFe_2O_4$ and $PbSO_4$ were identified in the leach residues from ferrite roasted with lower Na_2CO_3 additions (Samples A and B) while the samples roasted with higher additions (Samples C and D) were poorly crystalline. (Samples C and D experienced a weight loss of at least 85% during leaching.)

SEM micrographs of Sample C after leaching are shown in Figure 43. EDX analysis of this sample shows the presence of sulphate phases ($CaSO_4$ (A) and $PbSO_4$ (C)), quartz (SiO_2 (F)), and iron oxides with varying levels of Mn (i.e., Mn:Fe>1 (B) or Mn:Fe<1 (D)) as major phases. Some particles appear to be a mixture of phases, such as particle E, which is high in Pb, S, Si and O (i.e., likely a mixture of SiO_2 and $PbSO_4$)) and particle G, which is high in Fe, Pb, Mn, O and S (i.e., likely a mixture of $MnFe_2O_4$ and $PbSO_4$). Minor amounts of arsenic and barium were also detected in particle G using EDX analysis.

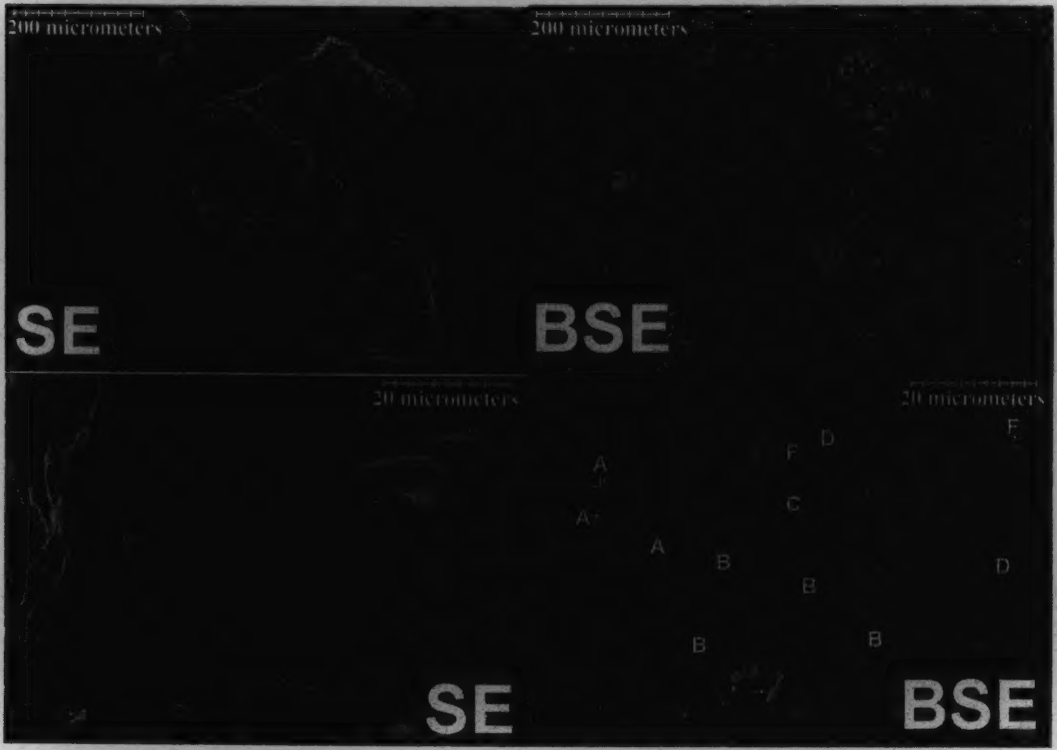

Figure 42 **Secondary Electron (SE) and Backscattered Electron (BSE) Images of Zinc Ferrite Roasted at 950°C with 80% Na_2CO_3 and 17.1% $Mg(OH)_2$ (Sample D)**

SEM/EDX analysis of the residue from the leaching of Sample D was not conducted. However, since this sample experienced a weight loss of 86% and an iron extraction of over 80% upon leaching, it is evident that, even with the potential formation of a Mg-Zn ferrite solid solution in the roasted ash, as identified by the SEM/EDX analysis of the roasted ash, the addition of $Mg(OH)_2$ was not effective in the formation of an acid insoluble metal ferrite. Thus, because $Mg(OH)_2$ proved to be ineffective in controlling the dissolution of iron during roasting of the La Oroya zinc ferrite with Na_2CO_3, no further investigations into this system were made.

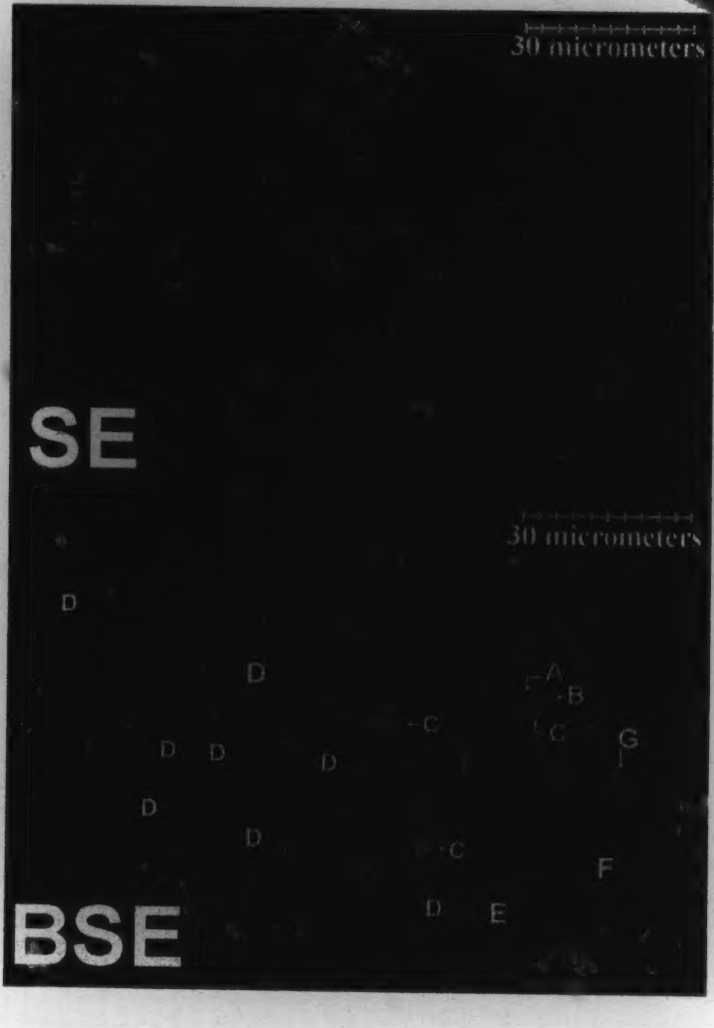
30 micrometers
SE
30 micrometers
D
D
A
B
C
C
G
D
D
D
D
D
C
F
BSE
D
E

Figure 43

Secondary Electron (SE) and Backscattered Electron (BSE) Images of Zinc Ferrite Roasted at 950°C with 80% Na_2CO_3 and 4.5% $Mg(OH)_2$ after Leaching with 200 g/L H_2SO_4 (Sample C)

4.5.2.1.1.3 Roasting with $MnCO_3$ as a Secondary Additive

The addition of $MnCO_3$ did not affect zinc extractions to the same degree as the other two additives tested (Figure 44). The change in zinc extraction with respect to temperature and Na_2CO_3 remained largely unchanged, with only a small shift in the region of maximum zinc extractions to higher temperatures and Na_2CO_3 additions at the low and high additions of $MnCO_3$ tested.

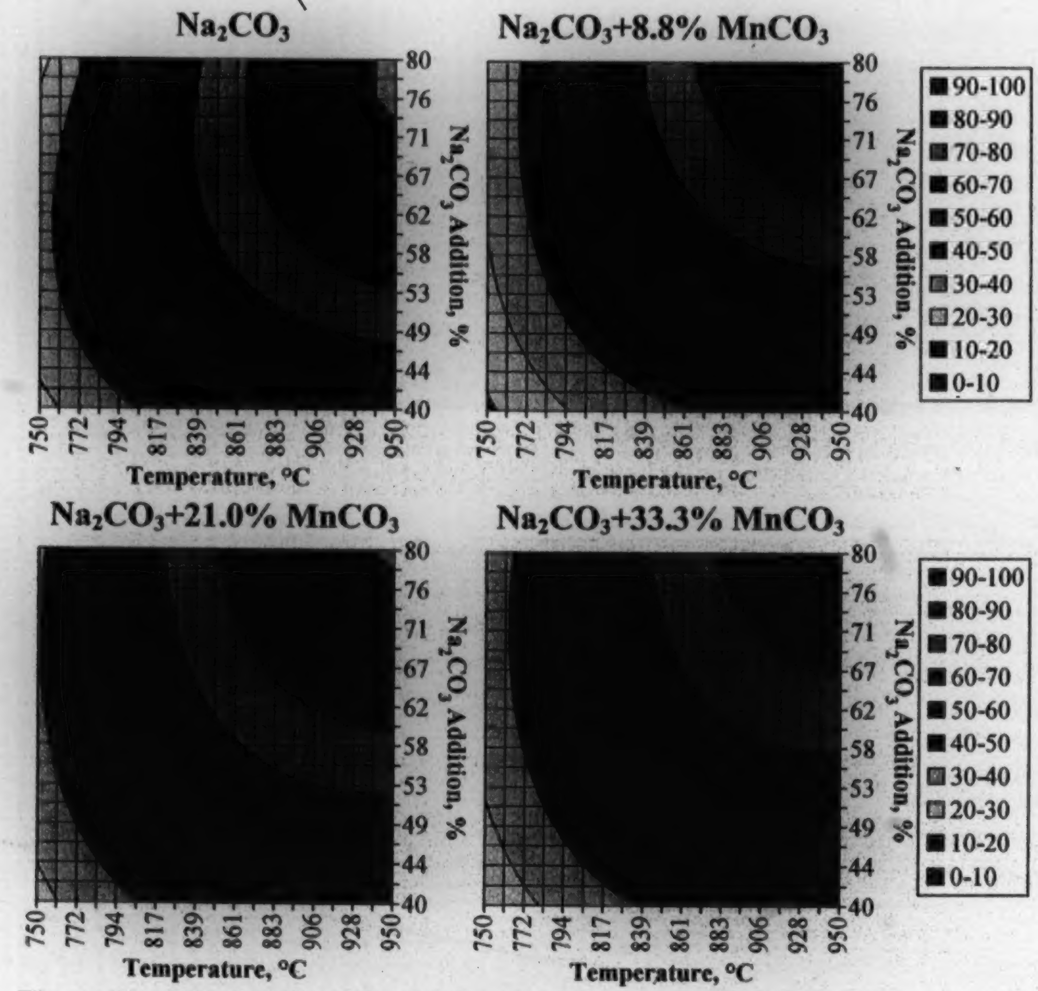

Figure 44 Effect of Na_2CO_3 and Temperature on Zn Extractions from La Oroya Zinc Ferrite Roasted with Various Amounts of $MnCO_3$

The effects of Na_2CO_3 and $MnCO_3$ additions on the zinc and iron extractions from roasting at 750, 850 and 950°C are illustrated in Figure 45.

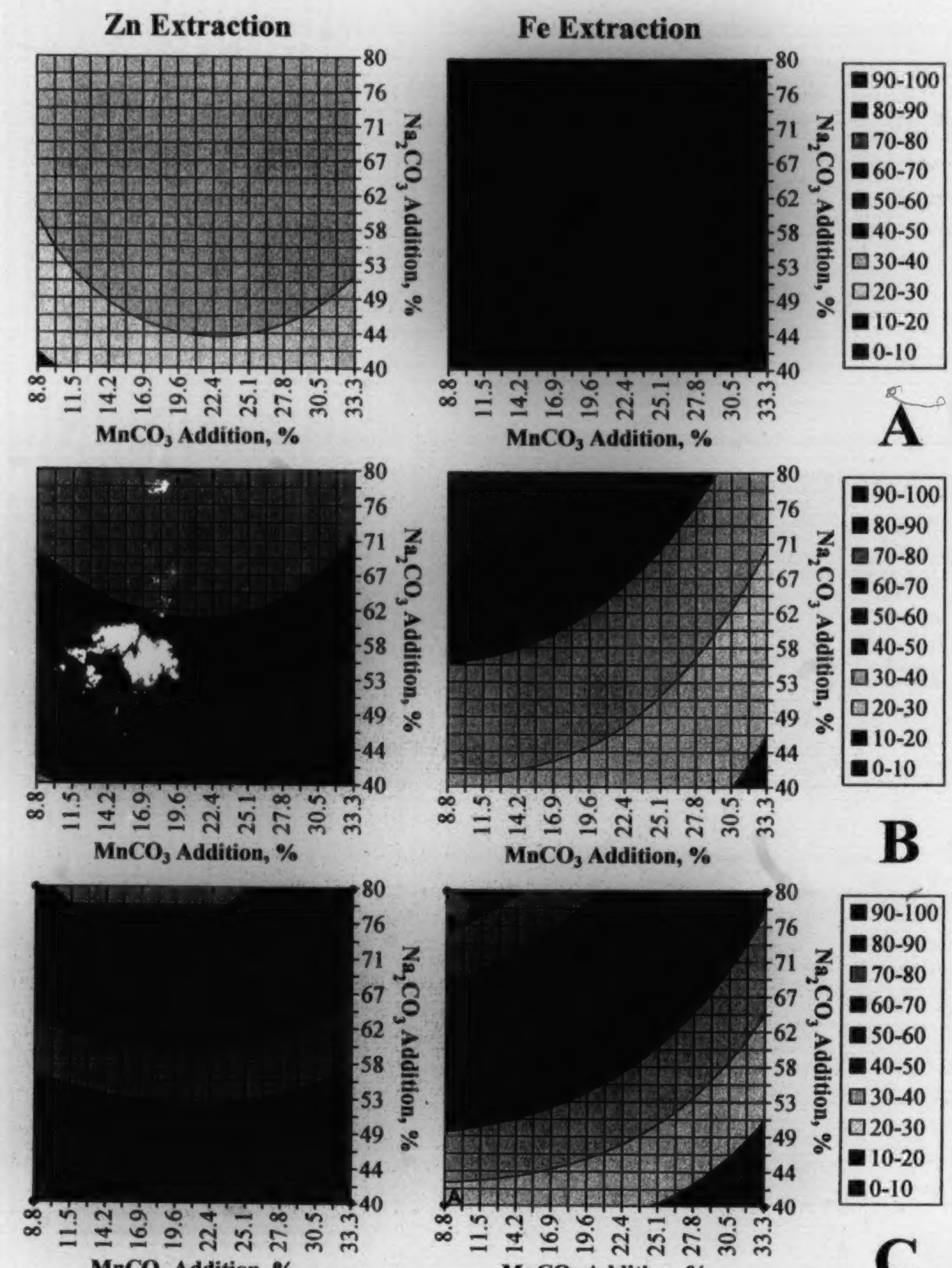

Figure 45 Effect of Na_2CO_3 and $MnCO_3$ Additions on Zinc and Iron Extractions from La Oroya Zinc Ferrite Roasted at A) 750°C, B) 850°C and C) 950°C

Figure 45 demonstrates that, while $MnCO_3$ addition does not have a strong effect on zinc extractions, it has a marked effect on the dissolution of iron. In the region of maximum zinc extraction, iron extractions go from 80 to 90% at 8.8% $MnCO_3$ (25% of stoichiometric) down to 40 to 50% at 33.3% $MnCO_3$ (95% of stoichiometric). Extrapolation of the model shows that iron extractions of less than 40% may be possible by increasing the $MnCO_3$ to near 35% (100% of stoichiometric) while maintaining zinc extractions of over 90%. (Based on the extrapolation of this model, further increases in $MnCO_3$ would be expected to lower zinc extraction to unacceptable levels.)

Samples at various conditions described by this model were analyzed using x-ray diffraction (Points A, B, C and D on Figure 45C). The identified phases are listed in Table 19 while the diffraction patterns and major phases are shown in Figure 46.

Table 19 Phases Identified by X-ray Diffraction Analysis of Zinc Ferrite Roasted with Na_2CO_3 and $CaCO_3$ at 950°C

Sample	Identified Phases (in order of intensity)
A	$ZnFe_2O_4$, Na_2ZnSiO_4, $Na_{0.7}Fe_{0.7}Mn_{0.3}O_2$, PbO (Litharge), Ca_2SiO_4 (Larnite)
B	$ZnFe_2O_4$, $Na_2Mn_3O_7$, Na_2ZnSiO_4, ZnO, $Ca_4Fe_9O_{17}$, Ca_2SiO_4 (Larnite)
C	α-$NaFeO_2$, ZnO, Na_2ZnSiO_4, β-$NaFeO_2$, $Ca_2Fe_2O_5$, $ZnFe_2O_4$
D	$Na_{0.7}Fe_{0.7}Mn_{0.3}O_2$, $Mn_7O_8SiO_4$ (Braunite 1-Q), $MnFe_2O_4$, ZnO, Ca_2SiO_4 (Larnite)

Phase identification for the samples roasted with $MnCO_3$ was less definitive than for ferrite roasted with the other secondary additives as the phases observed are not as consistent from sample to sample, fewer trends in phase transformation are observable and, in several cases, x-ray diffraction peaks of significant intensity could not be positively identified from the available database. (Potentially, since the Na-Fe-Mn-O system has been studied less than the Na-Fe-O or Na-Fe-Ca-O systems, there may be fewer patterns available from which to make positive identifications.)

Zinc oxide and Na_2ZnSiO_4 are still observed in many of the samples, with unreacted $ZnFe_2O_4$ observed at lower Na_2CO_3 additions, as noted previously, and α- and β- $NaFeO_2$ were observed in Sample C. Four types of manganese compounds were identified, including Na-Fe-Mn compounds ($Na_{0.7}Fe_{0.7}Mn_{0.3}O_2$), Na-Mn compounds ($Na_2Mn_3O_7$), Fe-Mn compounds ($MnFe_2O_4$) and a manganese silicate (braunite ($Mn_7O_8SiO_4$)).

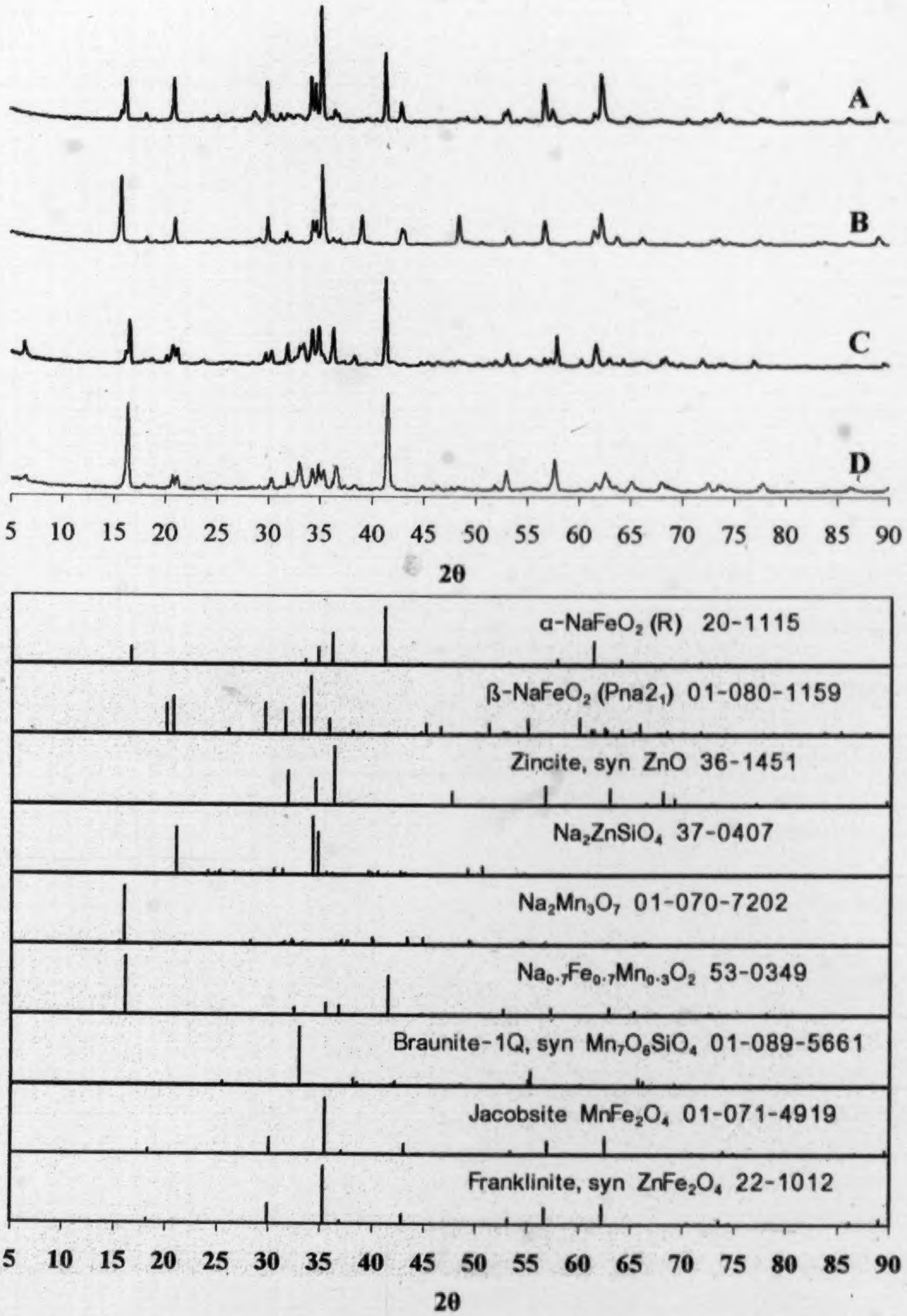

Figure 46 XRD Patterns of Zinc Ferrite Roasted with Na_2CO_3 and $MnCO_3$

Using back scattered electron imaging with the SEM and EDX analysis, the phases present in the roasted ferrite are much clearer (Figure 47). The dark phase (A) visible with the SEM is high in Na, S and O (i.e., a mixture of Na_2SO_4 and residual Na_2CO_3) while the small, very bright particles (E) contain Pb, Zn and O (i.e., a mixture of PbO and ZnO). One mottled area (D) is believed to be a pocket of Na_2ZnSiO_4 due to its high Na, Zn, Si and O content. The rest of the residue that was analyzed was either high in Fe, Mn and O (i.e., jacobsite ($MnFe_2O_4$) (C)) or high in Fe, Mn, Na, Si and O (i.e., possibly a mixture of $Na_{0.7}Fe_{0.7}Mn_{0.3}O_2$ and braunite ($Mn_7O_8SiO_4$), or $MnFe_2O_4$ and Na_2ZnSiO_4 (B)).

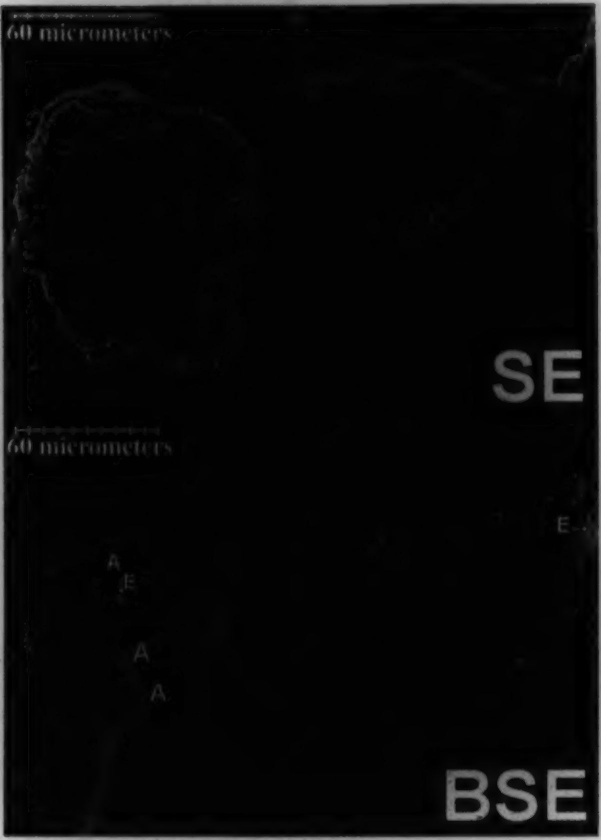

Figure 47
Secondary Electron (SE) and Backscattered Electron (BSE) Images of Zinc Ferrite Roasted at 950°C with 80% Na_2CO_3 and 33.3% $MnCO_3$ (Sample D)

The phase analysis of the leach residues using x-ray diffraction is greatly simplified from the analysis of the roasted ferrite (Table 20 and Figure 48).

Table 20 Phases Identified by X-ray Diffraction Analysis of Zinc Ferrite after Roasting with Na_2CO_3 and $CaCO_3$ and Leaching with 200 g/L H_2SO_4

Sample	Identified Phases (in order of intensity)	Leaching Wt. Loss, %
A	$ZnFe_2O_4$, $ZnMn_3O_7{\cdot}3H_2O$ (Chalcophanite), $PbSO_4$, $Na_2Mn_3O_7$	44
B	$ZnFe_2O_4$, $Na_{0.55}Mn_2O_4{\cdot}1.5\ H_2O$ (Birnessite), $PbSO_4$	35
C	Poorly crystalline; $PbSO_4$, $MnFe_2O_4$	84
D	Poorly crystalline; $MnFe_2O_4$, $PbSO_4$	59

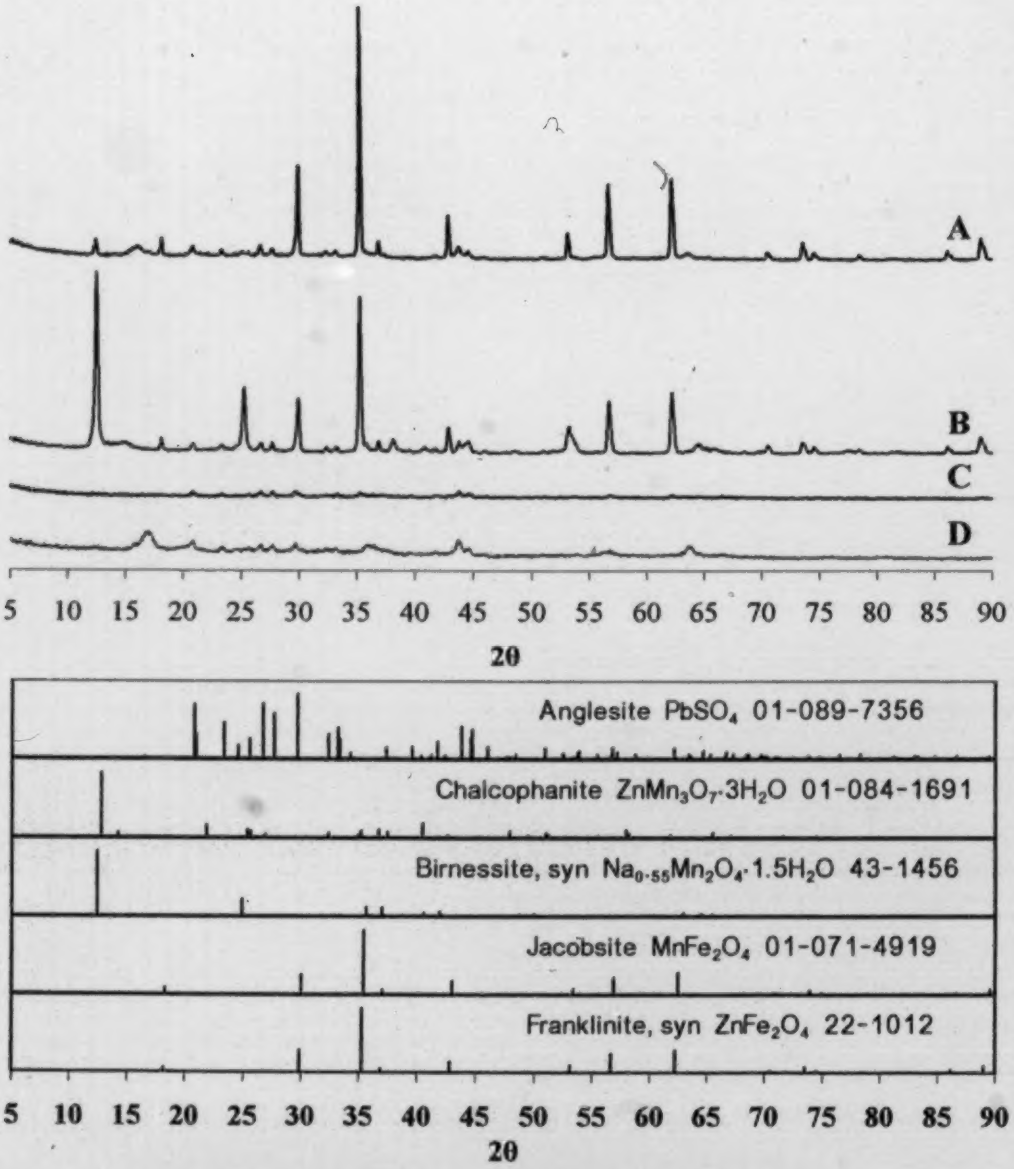

Figure 48 X-ray Diffraction Patterns of Zinc Ferrite Residue after Roasting with Na_2CO_3 and $MnCO_3$ and Leaching with 200 g/L H_2SO_4

Residual $ZnFe_2O_4$ is present in the samples where lower Na_2CO_3 additions were used in roasting (Samples A and B), along with anglesite ($PbSO_4$) and either a hydrated Zn-Mn or Na-Mn compound (chalcophanite ($ZnMn_3O_7{\cdot}3H_2O$) or birnessite ($Na_{0.55}Mn_2O_4{\cdot}1.5\,H_2O$)). The residues from the samples roasted at higher Na_2CO_3 additions (Samples C and D) are both poorly crystalline with low intensity anglesite and jacobsite ($MnFe_2O_4$) peaks detected.

Very little variation in the phases in the residue from Sample D is observed using SEM micrography and EDX analysis (Figure 49). The majority of the residue appears as light grey (A) particles in the backscattered image and these particles contains high levels of Fe, Mn and O, indicating that manganese iron oxides or manganese-iron ferrites are the predominant phase in the leach residue. In addition, the small, very bright particles (C) observed contained Pb, S and O (i.e., $PbSO_4$) while the one large darker particle in the field of view (B) contained Si along with Fe, Mn, Pb, O and S and, thus, was likely a mixture of residual unleached silicates with the other two phases observed.

30 micrometers
SE
30 micrometers
B
C
BSE

Figure 49

Secondary Electron (SE) and Backscattered Electron (BSE) Images of Zinc Ferrite Roasted at 950°C with 80% Na_2CO_3 and 33.3% $MnCO_3$ after Leaching with 200 g/L H_2SO_4 (Sample D)

Since the Fe-Mn oxides observed with the SEM were not identified definitively with x-ray diffraction, this may indicate that these oxides are poorly crystalline. However, the residual texture observed in the SEM (i.e., holes in the Fe-Mn-O particles), the large particle size and well-defined particle shape, along with the similarity in size and shape to the particles observed in the roasted sample, would indicate that these Fe-Mn particles are not leach precipitates. Instead these factors point strongly to the formation of an acid-resistant Fe-Mn oxide during roasting.

Thus, based on the lower iron extractions observed in Figure 45, and evidence of the formation of acid-insoluble Fe-Mn-O particles from the SEM/EDX analysis of the leach residue, roasting with Na_2CO_3 and $MnCO_3$ as a secondary additive appears to be a significant improvement over roasting with Na_2CO_3 alone as high zinc extractions are maintained while reducing iron extractions. In addition, the formation of a stable Fe-Mn residue should also make the residue from this transformational roasting process amenable to long term environmentally safe disposal.

4.5.2.2 Reduction of $ZnFe_2O_4$ to Form Metal Ferrites

4.5.2.2.1 Roasting with Carbon Black or Coal

DOE tests, where the La Oroya zinc ferrite is roasted with carbon black or coal, were conducted to provide a baseline for the comparison of the upcoming results in Sections 4.5.2.2.1.1 and 4.5.2.2.1.2. The experimental conditions used represent a modification of the Waelz kiln process (Section 4.2.2.1), with lower roasting temperatures than those normally employed in Waelz kiln operations and the use of sulphuric acid leaching to dissolve any unfumed, or recondensed, zinc oxide from the roasted zinc ferrite. Figures 50 and 51 show the effect of temperature and the addition of carbon black and coal on the zinc and iron extractions observed.

These models indicate that the maximum zinc extractions (90 to 100%) are favoured at lower temperatures and additions when roasting with carbon black than when roasting with coal. For both types of carbon additive, very little iron was leached from the roasted residue. (None of the samples in the DOE tests showed an iron extraction of more than 2.6%.) Up to 50% of the zinc in the ferrite is removed as zinc fume during roasting, depending on the conditions tested, with coal showing more of a tendency to induce fuming of zinc from the zinc ferrite during roasting than carbon black (Figure 52).

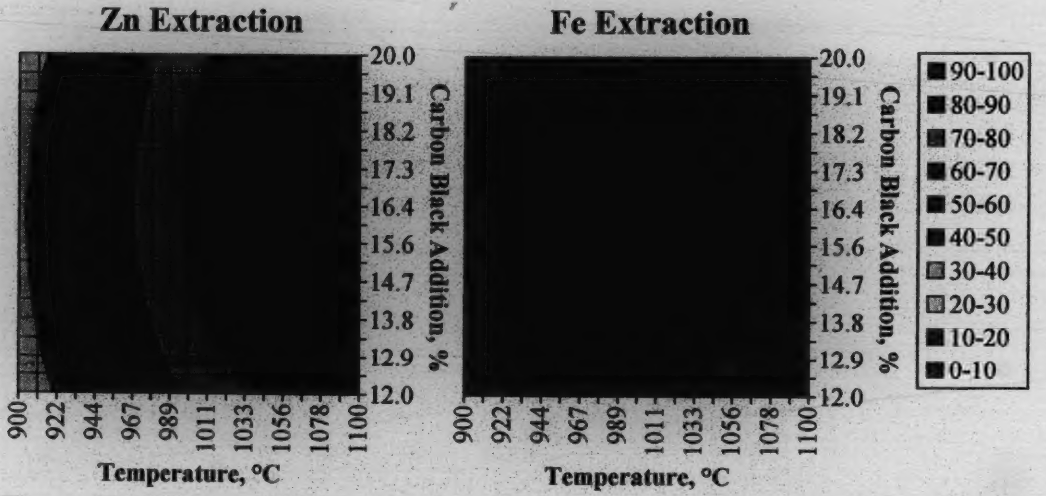

Figure 50 **Effect of Carbon Black Addition and Temperature on Total Zinc and Iron Extractions from Roasted La Oroya Zinc Ferrite**

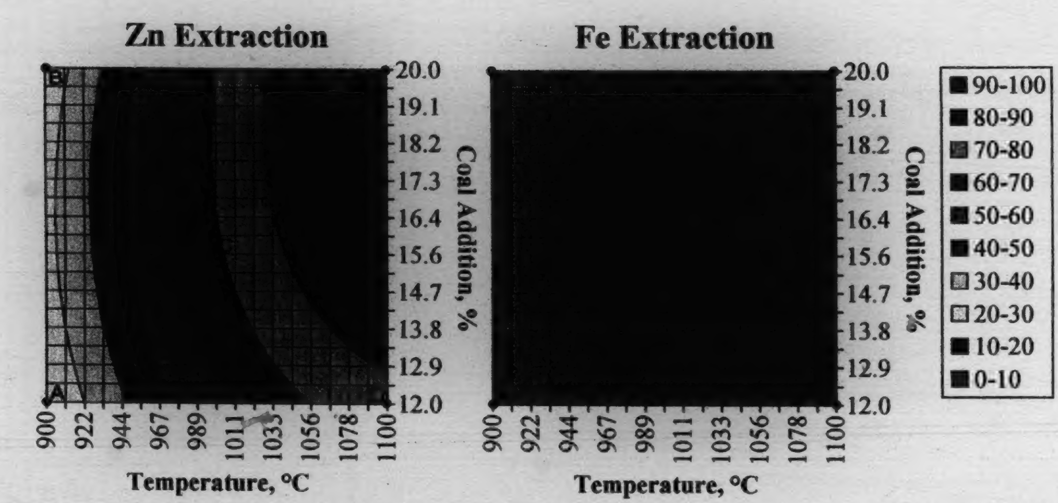

Figure 51 Effect of Coal Addition and Temperature on Total Zinc and Iron Extractions from Roasted La Oroya Zinc Ferrite

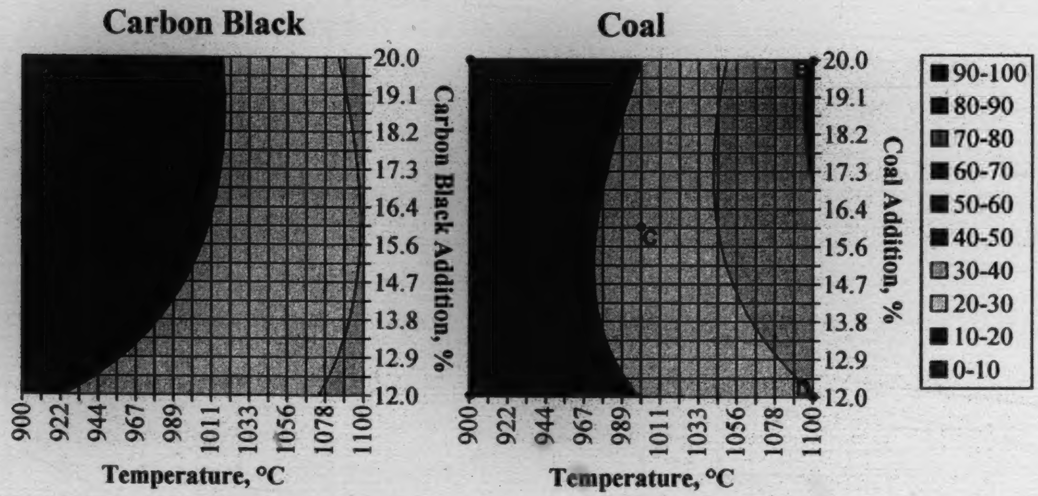

Figure 52 Effect of Temperature and Carbon Black or Coal Addition on the Percentage of Zinc Removed as Fume during Roasting

Samples at various conditions described by the model for roasting with coal were analyzed using x-ray diffraction (Points A through E on Figures 51 and 52). The identified phases are listed in Table 21 while the diffraction patterns and major phases observed are shown in Figure 53. (White acicular zinc oxide crystals were visible to the naked eye in all samples that were roasted at 1000°C or higher, even though ZnO was not always identified in the roasted samples using x-ray diffraction.)

Table 21 Phases Identified by XRD Analysis of Zinc Ferrite Roasted with Coal

Sample	Identified Phases (in order of intensity)
A	$ZnFe_2O_4$, Zn_2SiO_4, SiO_2
B, D	$ZnFe_2O_4$, SiO_2,Zn_2SiO_4
C	ZnO, $ZnFe_2O_4$, Fe_3O_4, Fe_2O_3
E	$ZnFe_2O_4$, SiO_2, Zn_2SiO_4, Fe_3O_4

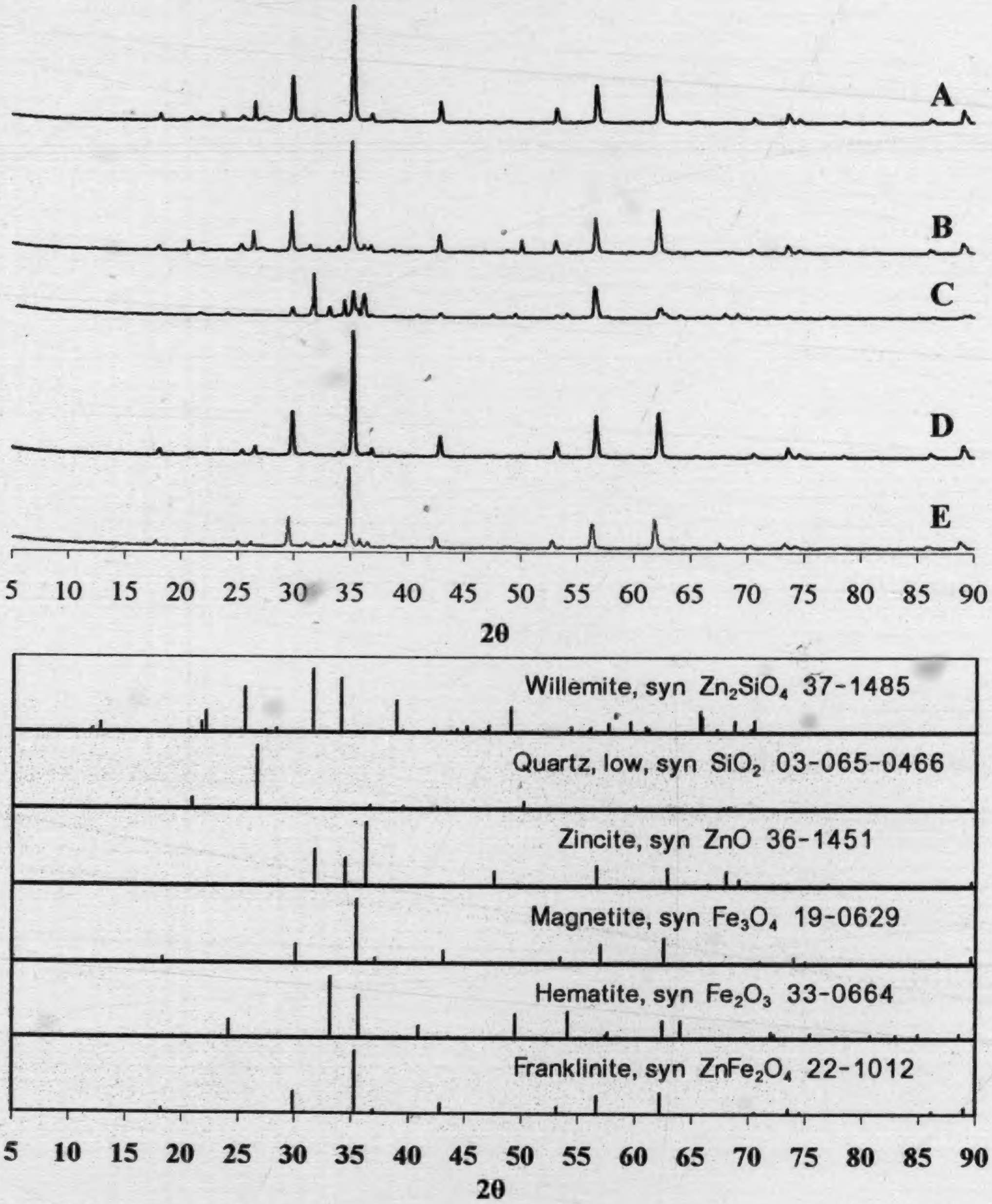

Figure 53 XRD Patterns of Zinc Ferrite Roasted with Coal

Unfumed zinc is present in the roasted ferrite as either willemite (Zn_2SiO_4), zincite (ZnO) or unreacted franklinite ($ZnFe_2O_4$). Zinc-free iron oxide phases, such as hematite (Fe_2O_3) and magnetite (Fe_3O_4), are observed as the reduction of $ZnFe_2O_4$ to $Zn_{(g)}$ and Fe_2O_3 goes to completion.

After leaching with 200 g/L H_2SO_4, zincite (ZnO) or willemite (Zn_2SiO_4) are leached from the roasted ferrite, leaving unreduced zinc ferrite ($ZnFe_2O_4$), anglesite ($PbSO_4$) and, in some cases, quartz (SiO_2) and hematite (Fe_2O_3) present in the leach residue (Table 22 and Figure 54).

Table 22 Phases Identified by X-ray Diffraction Analysis of Zinc Ferrite after Roasting with Coal and Leaching with 200 g/L H_2SO_4

Sample	Identified Phases (in order of intensity)	Leaching Wt. Loss, %
A	$ZnFe_2O_4$, SiO_2, $PbSO_4$	7
B	$ZnFe_2O_4$, SiO_2, $PbSO_4$	13
C	$ZnFe_2O_4$, Fe_2O_3, $PbSO_4$	15
D	$ZnFe_2O_4$, $PbSO_4$	8
E	$ZnFe_2O_4$, $PbSO_4$, Fe_2O_3	10

Although these DOE tests indicate that higher zinc extractions are possible at lower temperatures and additions using carbon black as an additive, and even some preliminary DOE tests were performed using carbon black along with other ferrite forming agents, it was decided to focus on roasting with coal in further DOE experiments as the use of coal would compare more closely to the type and quality of reducing agents that would be used commercially. As such, the results from DOE tests performed with carbon black as a reducing agent will not be presented but, instead, the following sections will focus on the results and analysis from roasting the La Oroya zinc ferrite with coal and either $CaCO_3$ or $MnCO_3$.

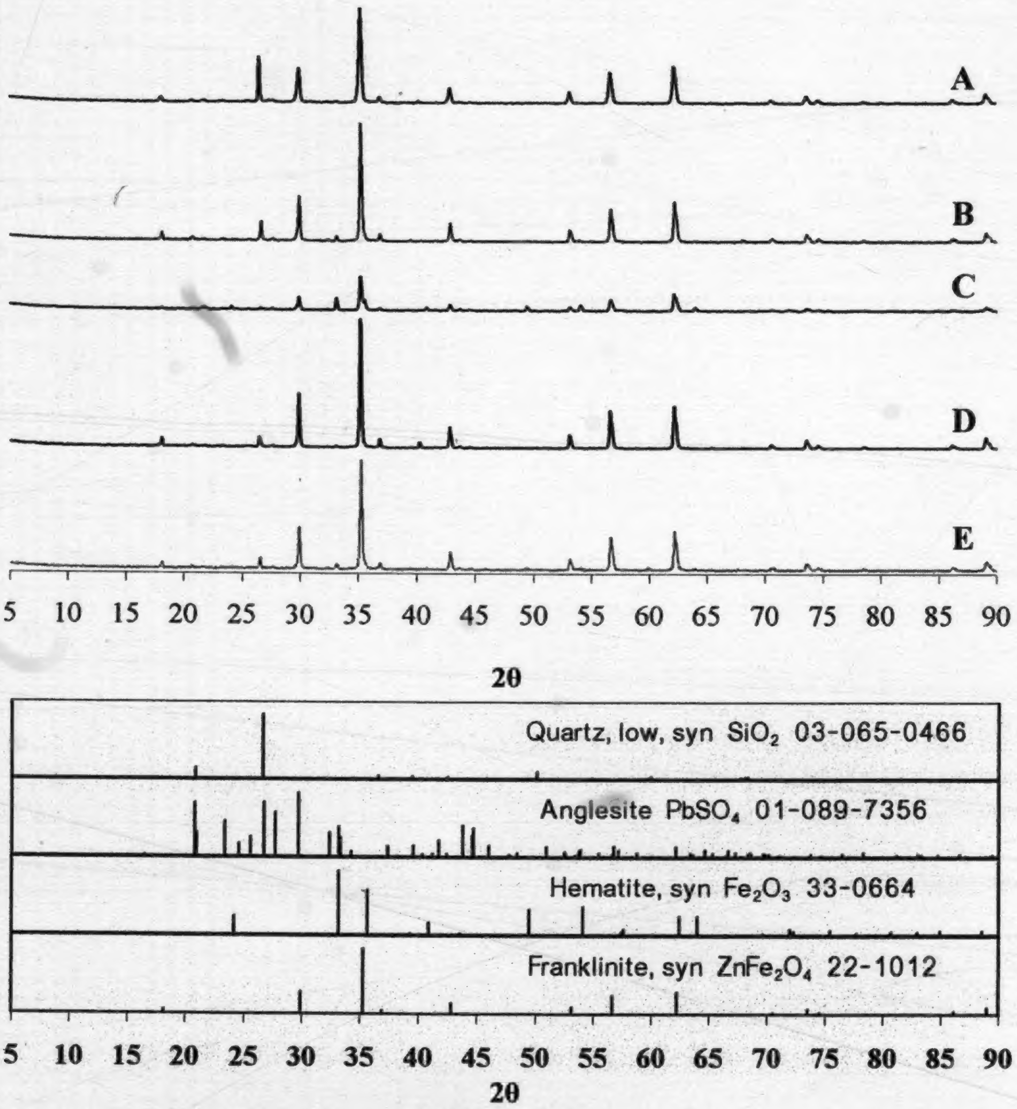

Figure 54 X-ray Diffraction Patterns of Zinc Ferrite Residue after Roasting with Coal and Leaching with 200 g/L H_2SO_4

4.5.2.2.1.1 Roasting with Coal and $CaCO_3$

Compared with roasting without $CaCO_3$, the addition of $CaCO_3$ causes a considerable shift in the region of maximum zinc extraction to higher temperatures and coal additions (Figure 55). This effect becomes more pronounced as the $CaCO_3$ addition is increased. Iron extractions of less than 10% are observed consistently for $CaCO_3$ additions of 46.5% or lower but, at 62.0% $CaCO_3$, iron extractions increase with decreasing temperature or coal additions. At all additions tested, though, iron extractions are consistently less than 10% in the regions of maximum zinc extraction.

The amount of zinc removed as fume during the roasting process is also affected by the increase in $CaCO_3$ addition as illustrated in Figure 56. In general, the degree of fuming increases with increasing temperature, coal addition and $CaCO_3$ addition.

Samples at various conditions described by the model for roasting with coal and 62% $CaCO_3$ were analyzed using x-ray diffraction (Points A through D on Figures 55C and 56C). The identified phases are listed in Table 23 while the diffraction patterns and major phases observed are shown in Figure 57.

Table 23 Phases Identified by XRD Analysis of Zinc Ferrite Roasted with Coal and 62% $CaCO_3$

Sample	Identified Phases (in order of intensity)
A	$ZnFe_2O_4$, $Ca_2Fe_2O_5$, $CaSO_4$, $Ca(OH)_2$, $CaCO_3$, Fe_2SiO_4 (Fayalite), Ca_2SiO_4 (Larnite)
B	$ZnFe_2O_4$, $Ca(OH)_2$, $Ca_2Fe_2O_5$, $CaSO_4$, ZnO, $CaCO_3$, Ca_2SiO_4 (Larnite), SiO_2
C	$ZnFe_2O_4$, $Ca_2Fe_2O_5$, $CaSO_4$, $Ca(OH)_2$, ZnO, CaO, Ca_2SiO_4 (Larnite)
D	ZnO, $Ca_5Si_2O_8SO_4$, $ZnFe_2O_4$, Ca_2SiO_4 (Larnite), $ZnMn_2O_4$ (Hetaerolite), FeO (Wustite)

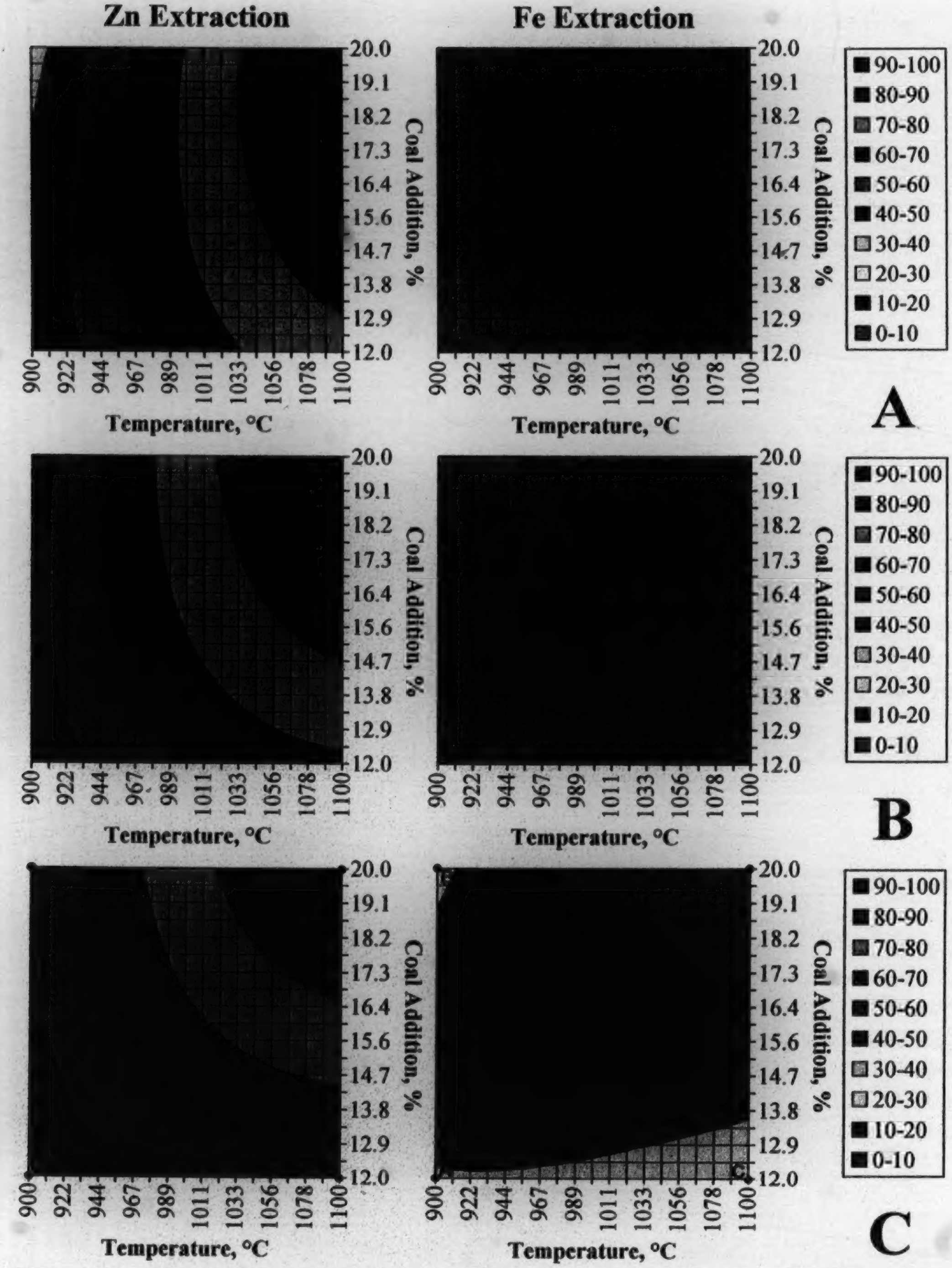

Figure 55 Effect of Coal Addition and Temperature on Zinc and Iron Extractions from La Oroya Zinc Ferrite Roasted with $CaCO_3$ Additions of A) 31.0%, B) 46.5% and C) 62.0%

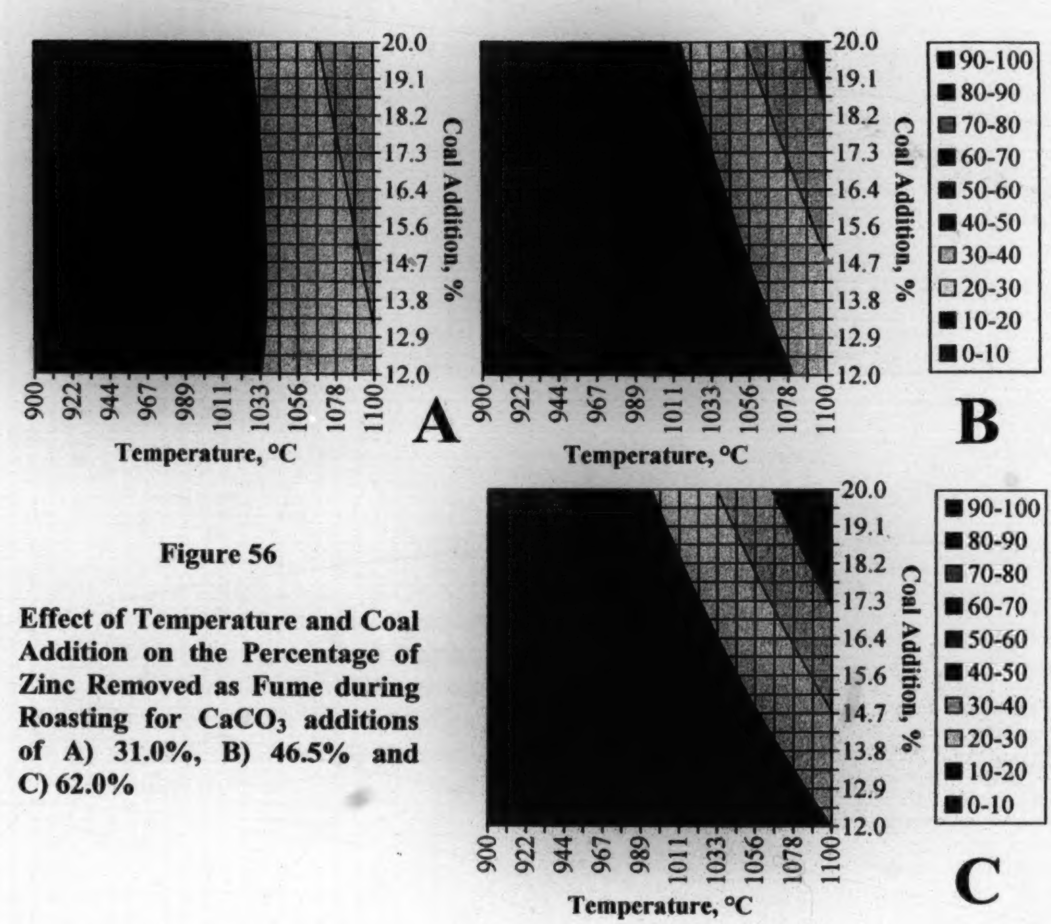

Figure 56

Effect of Temperature and Coal Addition on the Percentage of Zinc Removed as Fume during Roasting for $CaCO_3$ additions of A) 31.0%, B) 46.5% and C) 62.0%

Residual $CaCO_3$, or altered $CaCO_3$ ($Ca(OH)_2$ or CaO), is present in the roasted ferrite, along with reaction products such as anhydrite ($CaSO_4$), srebrodolskite ($Ca_2Fe_2O_5$) and larnite (Ca_2SiO_4) to varying degrees in samples A to C. (At 1100°C and 20% coal (Sample D), silicocarnotite ($Ca_5Si_2O_8SO_4$) and larnite (Ca_2SiO_4) are the only calcium bearing phases identified using x-ray diffraction.) ZnO is identified in all but Sample A; it is the major phase identified in Sample D, even with as much as 60% of the Zn lost as fume (Figure 56C). Franklinite disappears as an identified phase at the highest temperature and coal addition tested (Sample D) and FeO is observed in the roasted ferrite, indicating complete or near complete reduction of $ZnFe_2O_4$ under these conditions.

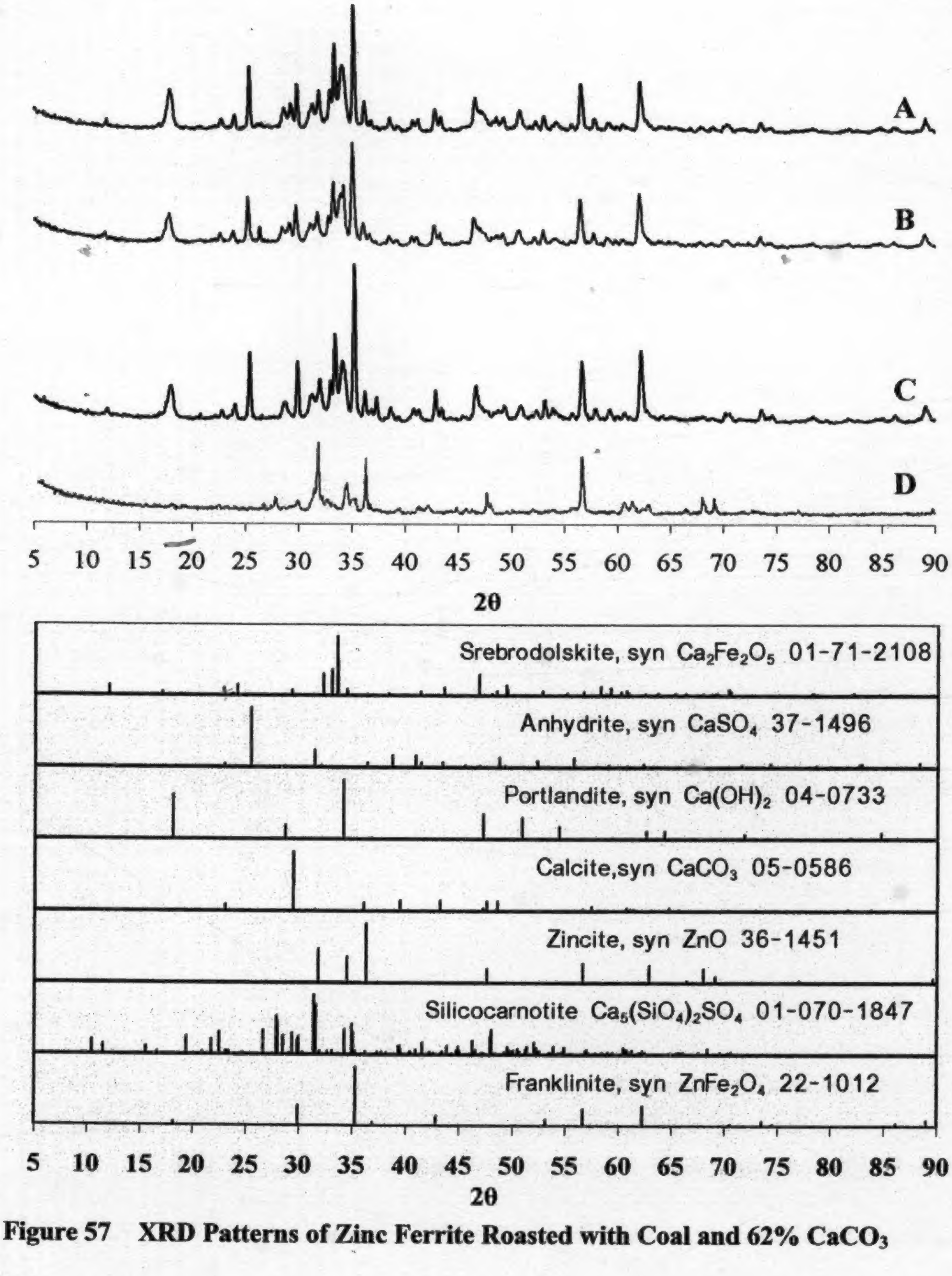

Figure 57 **XRD Patterns of Zinc Ferrite Roasted with Coal and 62% $CaCO_3$**

Phase analysis of Sample C after roasting using SEM micrography and EDX analysis is very consistent with the x-ray diffraction analysis (Figure 58). Numerous particles are identified as being high in Zn and O (i.e., ZnO (A)), Ca and O (i.e., CaO/$Ca(OH)_2$ (B)), Ca, Fe and O (i.e., $Ca_2Fe_2O_5$ (C)), Fe, Zn and O (i.e., $ZnFe_2O_4$ (D)), Ca, Si and O (i.e., Ca_2SiO_4 (E)), and Ca, S and O (i.e., $CaSO_4$ (F)). All of these phases were identified previously using x-ray diffraction. Particle G was the only exception, containing As, as well as Ca and S, possibly due to the formation of a calcium sulphate/arsenate from minor amounts of arsenic in the La Oroya zinc ferrite (0.29% in the feed).

The two main phases identified in Sample D using XRD were also identified using SEM and EDX (Figure 59). The bright tabular phase (A) observed contains Zn and O (i.e., ZnO) and the dark phase (B) is high in Ca, Si, S and O (i.e., silicocarnotite ($Ca_5Si_2O_8SO_4$)). However, a third major phase (C) containing Ca, Fe and O (i.e., likely $Ca_2Fe_2O_5$ or another calcium ferrite) is identified using SEM/EDX that was not identified with XRD. The mottled appearance of some particles (D) analyzes as a mixture of the Ca-Fe-O phase and calcium silicates (i.e., Ca_2SiO_4).

After leaching with 200 g/L H_2SO_4, any unfumed zincite (ZnO) is leached from the roasted ferrite, along with any residual CaO, $Ca(OH)_2$ or $CaCO_3$ which is subsequently precipitates as gypsum ($CaSO_4 \cdot 2\,H_2O$) or $CaSO_4 \cdot 0.67\,H_2O$ (Table 24 and Figure 60). Unreacted $ZnFe_2O_4$ is still present in the leach residue, and, in some cases, unleached fayalite (Fe_2SiO_4), larnite (Ca_2SiO_4) and wustite (FeO) are also detected in the residue using XRD. Although srebrodolskite ($Ca_2Fe_2O_5$) was detected in the roasted ferrite in Samples A, B and C, it is not observed using x-ray diffraction in the residue. Since srebrodolskite ($Ca_2Fe_2O_5$) is the only iron-bearing phase that is not found in the roasted ferrite after leaching, it may be that it is leached, or partially leached, with 200 g/L H_2SO_4, and this behaviour could help explain the increase in iron extraction at lower temperature and coal addition in Figure 55.

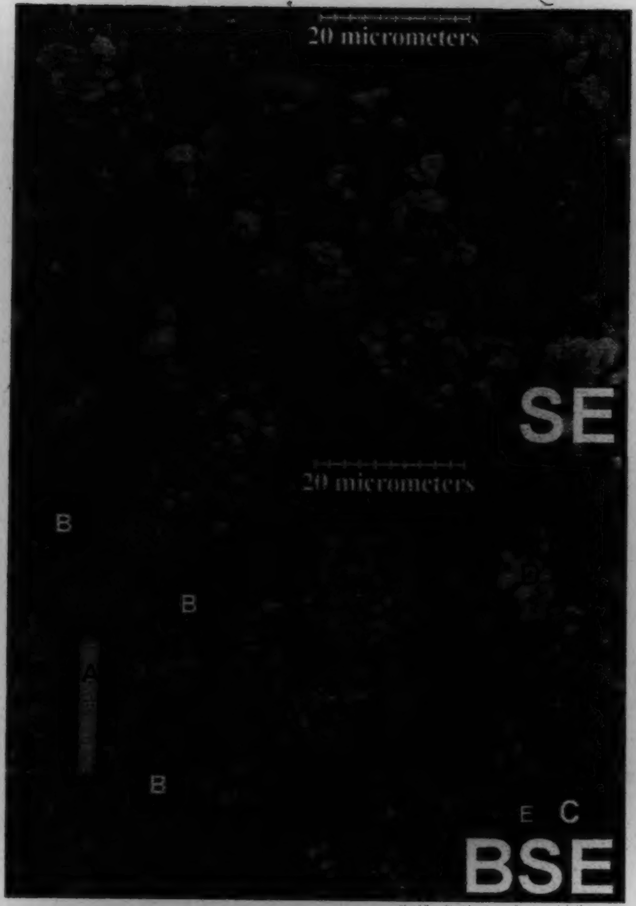
20 micrometers
SE
20 micrometers
B
B
A
D
B
E
C
BSE

Figure 58

Secondary Electron (SE) and Backscattered Electron (BSE) Images of Zinc Ferrite after Roasting at 1100°C with 12% Coal and 62% $CaCO_3$ (Sample C)

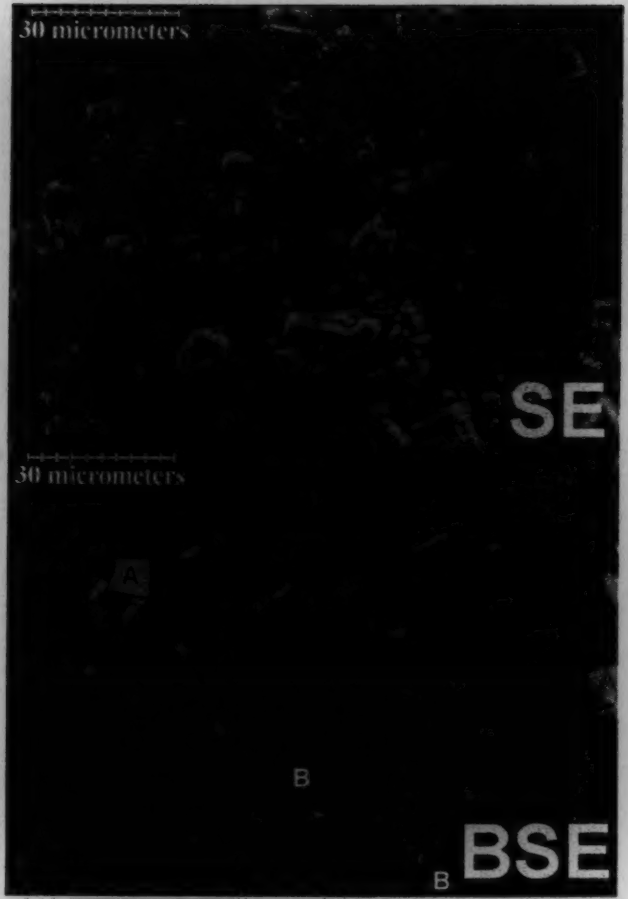
30 micrometers
SE
30 micrometers
A
B
B
BSE

Figure 59

Secondary Electron (SE) and Backscattered Electron (BSE) Images of Zinc Ferrite after Roasting at 1100°C with 20% Coal and 62% $CaCO_3$ (Sample D)

Table 24 **Phases Identified by X-ray Diffraction Analysis of Zinc Ferrite after Roasting with Coal and 62% $CaCO_3$ and Leaching with 200 g/L H_2SO_4**

Sample	Identified Phases (in order of intensity)	Leaching Wt. Gain, %
A, B	$ZnFe_2O_4$, $CaSO_4 \cdot 0.67\ H_2O$, $CaSO_4 \cdot 2\ H_2O$, Fe_2SiO_4 (Fayalite)	13, 12
C	$CaSO_4 \cdot 2\ H_2O$, $ZnFe_2O_4$	19
D	$CaSO_4 \cdot 2\ H_2O$, Ca_2SiO_4 (Larnite), FeO (Wustite)	14

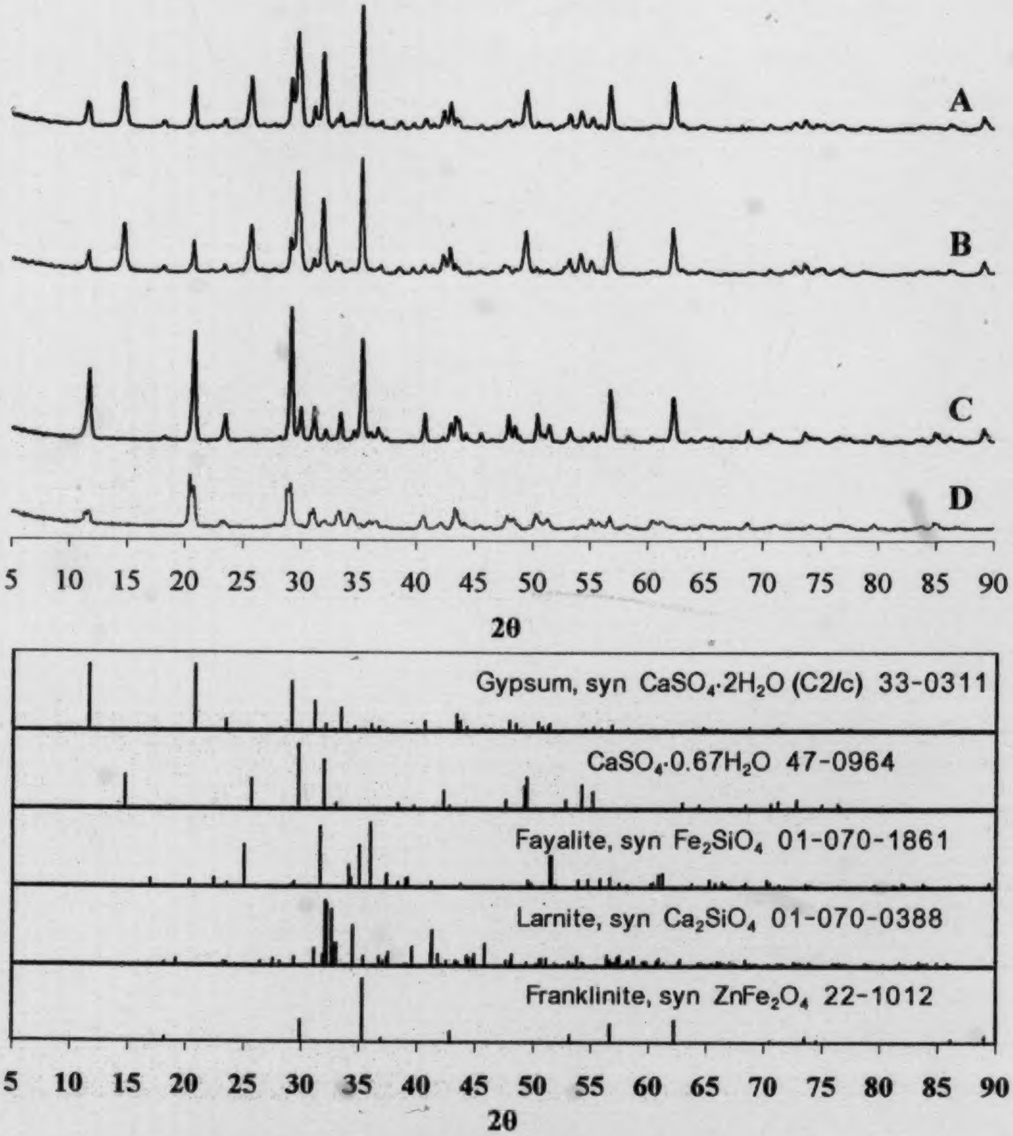

Figure 60 **X-ray Diffraction Patterns of Zinc Ferrite Residue after Roasting with Coal and $CaCO_3$ and Leaching with 200 g/L H_2SO_4**

30 micrometers
SE
30 micrometers
A
BSE

Figure 61

Secondary Electron (SE) and Backscattered Electron (BSE) Images of Zinc Ferrite after Roasting at 1100°C with 20% Coal and 62% $CaCO_3$ and Leaching with 200 g/L H_2SO_4 (Sample D)

SEM images show that two main phases are present in the leach residue from Sample D (Figure 61): the darker needlelike Ca, S and Si rich phase (i.e., a mixture of gypsum ($CaSO_4 \cdot 2H_2O$) and larnite (Ca_2SiO_4), or potentially residual silicocarnotite ($Ca_5Si_2O_8SO_4$)) and a bright phase high in Ca and Fe that could represent calcium ferrites, such as srebrodolskite ($Ca_2Fe_2O_5$), that were not detected using x-ray diffraction. In the field of view, only one particle differed from these two phases (particle A) which contained Ca, Mn, Fe and O and may represent a mixture a Ca-ferrite and $MnFe_2O_4$ in the residue. Since these Ca-Fe-O phases were also found in the Sample D after roasting, and since the iron extraction for Sample D is low (i.e., less than 10%), this could indicate that Ca-ferrites are formed under the roasting conditions for Sample D that are less soluble in H_2SO_4 than those formed at lower temperatures and coal addition. However, since srebrodolskite ($Ca_2Fe_2O_5$) was not detected in the leach residue with XRD, it is likely that it is only present as a minor phase in the roasted ferrite after leaching.

Even with an acid insoluble Ca-Fe-O phase identified in some samples, SEM analysis still indicates that, with $CaCO_3$ additions of 100% of stoichiometric for $Ca_2Fe_2O_5$ formation (62% $CaCO_3$), the majority of the $CaCO_3$ added either does not react to form

Ca-Fe compounds, or that it does not react completely to form acid-insoluble Ca-Fe compounds. This is evident as the majority of the field of view in the SEM, and the dominant phase in XRD, is gypsum, which would be precipitated during acid leaching of any soluble calcium compounds (i.e., unreacted $CaCO_3$ or decarbonized byproducts, such as CaO or $Ca(OH)_2$, dissolved calcium silicates or sulfosilicates, acid soluble calcium-iron compounds, etc.) which, in turn, leads to high acid consumption during leaching. Thus, this would indicate that $CaCO_3$ is not effective enough in forming acid-insoluble ferrites during roasting the La Oroya ferrite under these conditions to be practical commercially and, generally, is less effective than roasting with coal without a secondary additive.

A DOE test was also performed where the La Oroya zinc ferrite was roasted with coal and CaO. However, the zinc and iron extraction and extent of zinc fuming showed little difference from the results obtained using $CaCO_3$. Thus, no further phase analysis or SEM analysis of these samples was conducted and the results were not included in this document.

4.5.2.2.1.2 Roasting with Coal and $MnCO_3$

Increasing additions of $MnCO_3$ causes a dramatic shift in the region of maximum zinc extraction towards higher temperatures and coal additions (Figure 62) such that, at 70.0% $MnCO_3$ addition, the region of 90 to 100% zinc extraction is no longer visible in the range of temperature and coal additions tested. Iron extractions of less than 10% are observed throughout, regardless of the temperature or coal or $MnCO_3$ additions used during roasting. Less zinc is removed as fume, compared both to roasting with coal or roasting with coal and $CaCO_3$ (Figure 63), but the same general trends of an increase in the degree of fuming with increasing temperature, coal addition and $CaCO_3$ addition are observed.

Samples at various conditions described by the model for roasting with coal and 70% $MnCO_3$ were analyzed using x-ray diffraction (Points A through D on Figures 62C and 63C). The identified phases are listed in Table 25 while the diffraction patterns and major phases observed are shown in Figure 64.

Table 25 Phases Identified by XRD Analysis of Zinc Ferrite Roasted with Coal and 70.0% $MnCO_3$

Sample	Identified Phases (in order of intensity)
A	$ZnFe_2O_4$, $MnFe_2O_4$, Fe_3O_4, $CaMnSi_2O_6$ (Johannsenite), $CaMnO_3$, $ZnMn_2O_4$ (Hetaerolite), $PbSO_4$
B	$MnFe_2O_4$, $ZnFe_2O_4$, SiO_2, Zn_2SiO_4, $ZnMn_2O_4$ (Hetaerolite), $ZnSiO_3$
C	$MnFe_2O_4$, ZnO, $Ca_2Fe_{22}O_{33}$
D	$MnFe_2O_4$, ZnO

At lower temperatures, zinc is not only found in unreacted $ZnFe_2O_4$, but also a Zn-Mn ferrite (hetaerolite ($ZnMn_2O_4$)) and zinc silicates. At higher temperatures, the formation of ZnO is promoted and ZnO is detected in the roasted ferrite even with significant fuming of zinc during roasting (Figure 63). Jacobsite ($MnFe_2O_4$) was identified in all the samples tested but, at lower temperatures, residual $ZnFe_2O_4$ and, in Sample A, magnetite (Fe_3O_4) were also detected.

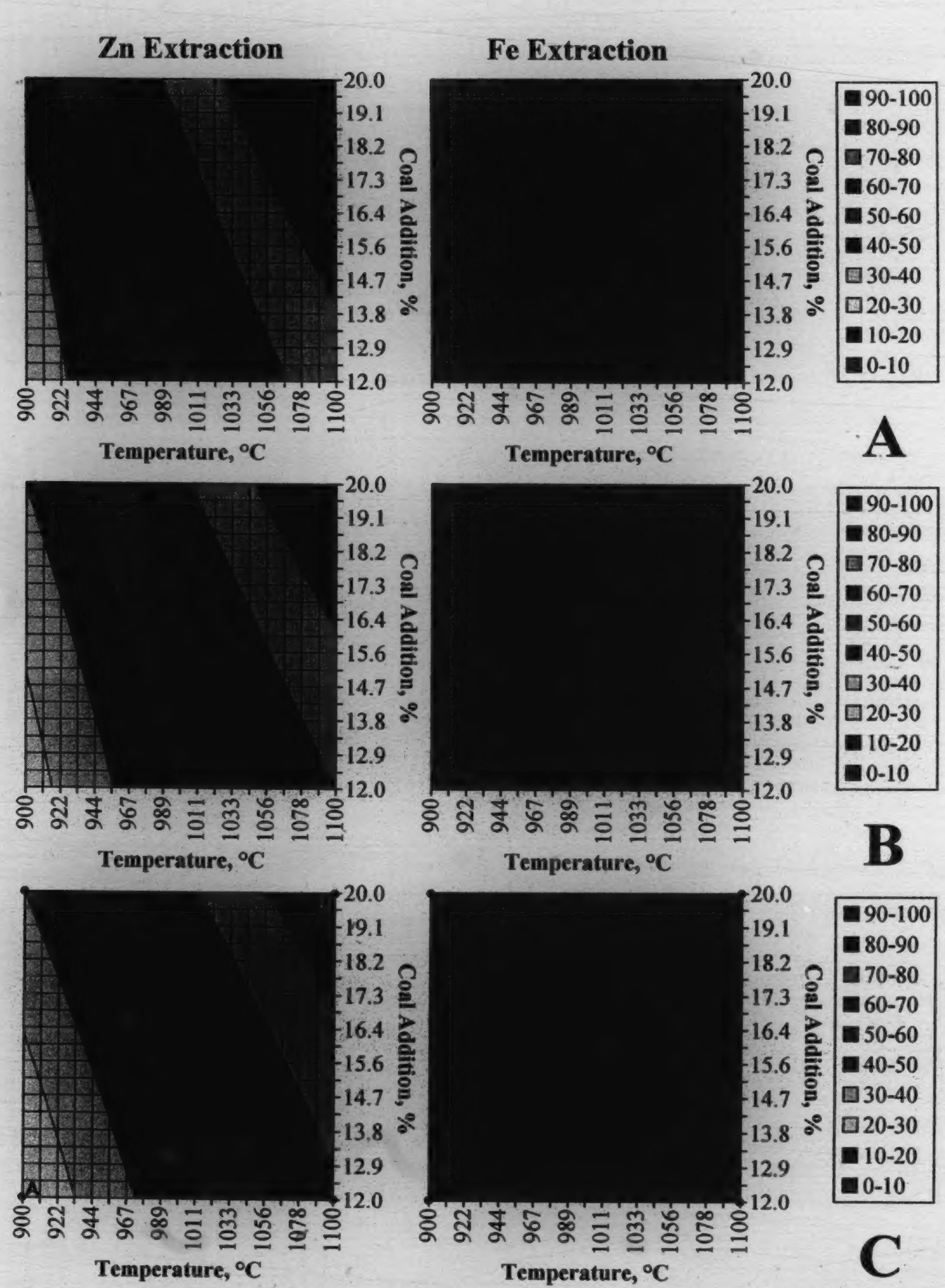

Figure 62 Effect of Coal Addition and Temperature on Zinc and Iron Extractions from La Oroya Zinc Ferrite Roasted with $MnCO_3$ Additions of A) 35.0%, B) 52.5% and C) 70.0%

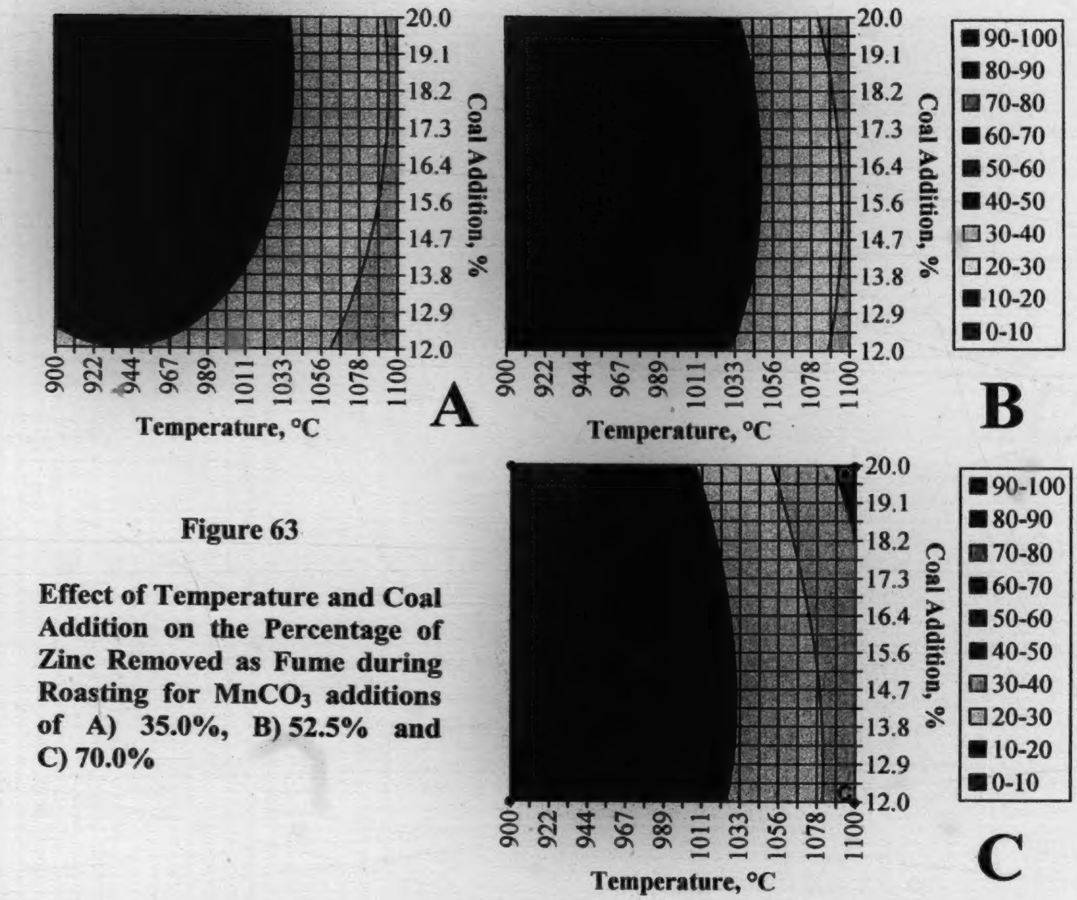

Figure 63

Effect of Temperature and Coal Addition on the Percentage of Zinc Removed as Fume during Roasting for $MnCO_3$ additions of A) 35.0%, B) 52.5% and C) 70.0%

The SEM/EDX analysis of Sample D (Figure 65) showed similar results to the x-ray diffraction analysis, indicating that particles containing Fe, Mn and O (B) (i.e.,$MnFe_2O_4$) were the predominant phase in the roasted ferrite, followed by particles high in Zn and O (C) (i.e., ZnO). Analysis of particle C showed a mixture of Mn and Fe, along with Ca, Si and Pb, likely indicating that it contains a mixture of phases (i.e., likely $MnFe_2O_4$, PbO and Ca-silicates). Particle D was also unusual as it showed high concentrations of Sn and K, as well as Zn, and likely represents a mixture of Zn, Sn and K oxides.

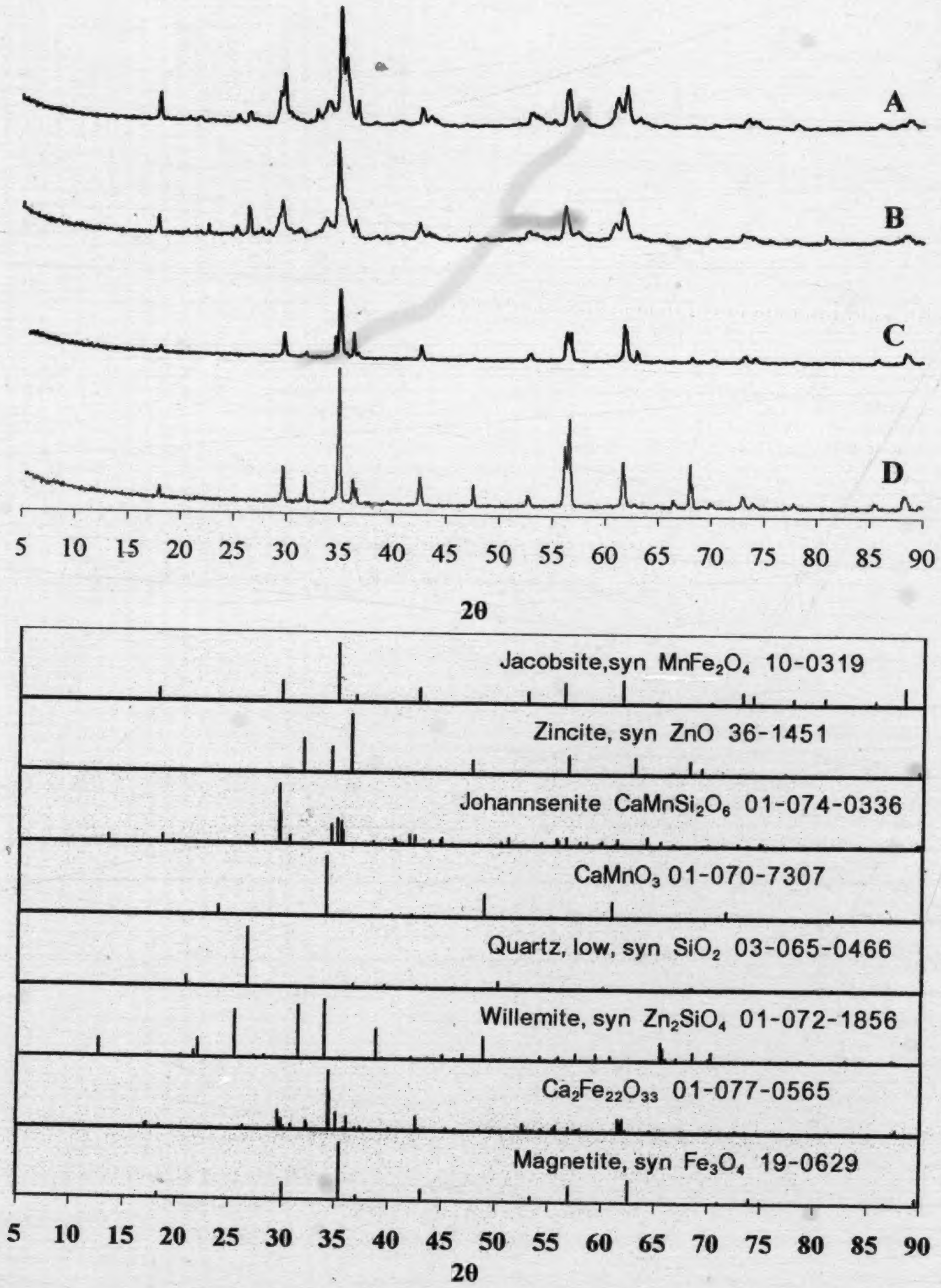

Figure 64 XRD Patterns of Zinc Ferrite Roasted with Coal and 70.0% $MnCO_3$

After leaching with 200 g/L H_2SO_4, any unfumed ZnO in the roasted ferrite has been dissolved, apparently along with Zn or Ca-Mn silicates identified in Table 25, based on the x-ray diffraction analysis of the leach residues (Table 26 and Figure 66).

Jacobsite ($MnFe_2O_4$) is present in all the leach residues along with magnetite (Fe_3O_4), residual franklinite ($ZnFe_2O_4$), quartz (SiO_2) and anglesite ($PbSO_4$). Hetaerolite was also identified in sample A indicating, perhaps, that this Zn-Mn spinel is acid insoluble.

20 micrometers
SE
20 micrometers
BSE

Figure 65
Secondary Electron (SE) and Backscattered Electron (BSE) Images of Zinc Ferrite after Roasting at 1100°C with 20% Coal and 70% $MnCO_3$ (Sample D)

Table 26 Phases Identified by X-ray Diffraction Analysis of Zinc Ferrite after Roasting with Coal and 70.0% $MnCO_3$ and Leaching with 200 g/L H_2SO_4

Sample	Identified Phases (in order of intensity)	Leaching Wt. Loss, %
A	$MnFe_2O_4$, $ZnFe_2O_4$, Fe_3O_4, $PbSO_4$, $ZnMn_2O_4$ (Hetaerolite)	6
B	$ZnFe_2O_4$, $MnFe_2O_4$, Fe_3O_4, SiO_2, $PbSO_4$	13
C	$MnFe_2O_4$, Fe_3O_4, $PbSO_4$	11
D	$MnFe_2O_4$, $PbSO_4$	16

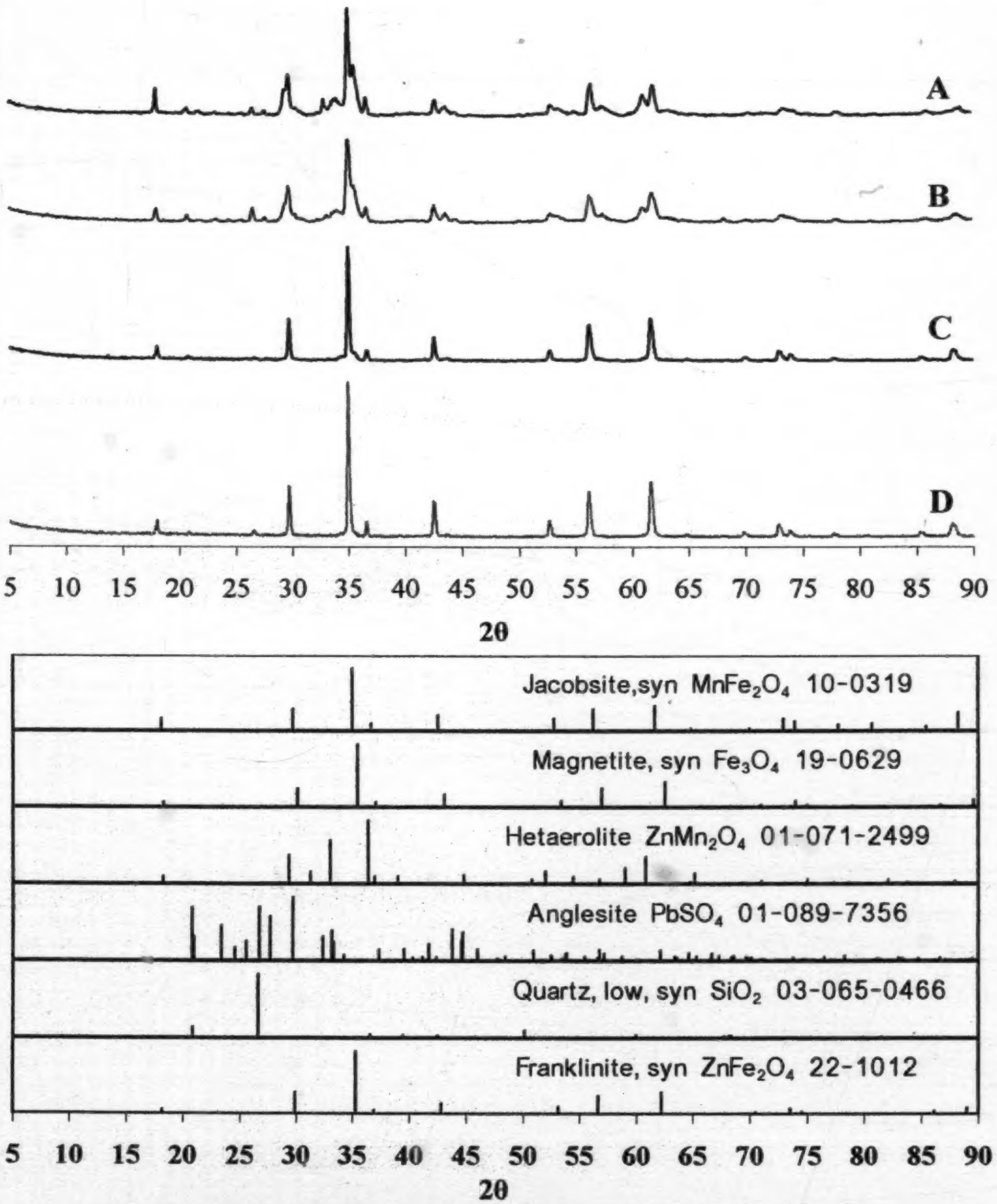

Figure 66 X-ray Diffraction Patterns of Zinc Ferrite Residue after Roasting with Coal and $MnCO_3$ and Leaching with 200 g/L H_2SO_4

SEM micrography and EDX analysis of Sample D (Figure 67) are in good agreement with the x-ray diffraction analyses as the dominant phase (A) is rich in Fe, Mn and O (i.e., $MnFe_2O_4$) and the small bright phase contains Pb, S and O (i.e.,$PbSO_4$). The analysis of one particle (C) was anomalous, as it was found to contain Sn, Zn, Ca and O.

At this point, its mineralogical identity is unknown as, if it were a Sn, Zn or Ca oxide, it would normally be expected to leach during acid leaching.

These results indicate that $MnCO_3$ is an effective ferrite forming reagent as roasting with $MnCO_3$ at 1100°C with 20% coal resulted in near complete conversion of the iron values to jacobsite ($MnFe_2O_4$). However, $MnCO_3$ additions of greater than 100% of stoichiometric decrease the zinc extraction observed at these conditions and, thus, future studies should look more closely at near stoichiometric $MnCO_3$ additions. By using stoichiometric additions (35% $MnCO_3$), less than 1.5% of the iron is solubilized during leaching and zinc recoveries of up to 99% were achieved under the best conditions tested, producing a residue essentially free of zinc and silicates. Following a lead removal step, there may be potential to recover the iron and/or manganese from the ferrite residue pyrometallurgically.

20 micrometers
SE
20 micrometers
C
B
BSE

Figure 67

Secondary Electron (SE) and Backscattered Electron (BSE) Images of Zinc Ferrite after Roasting at 1100°C with 20% Coal and 70% $MnCO_3$ and Leaching with 200 g/L H_2SO_4 (Sample D)

4.6 Department of Minor Elements

Selected solids and solution samples were analyzed to try to understand the deportment of minor elements in the various potential process options identified in this research. Four process options including roasting with Na_2CO_3, $Na_2CO_3/MnCO_3$, coal, and coal/$MnCO_3$ were considered.

Solutions and solids, after fusing with lithium metaborate, were analyzed for As, Na and K using a Varian SpectrAA 220FS atomic absorption spectrometer, with As analyzed using a deuterium lamp for background correction. The silver analysis in the feed solids was determined by fire assay. (Insufficient sample was available to perform fire assays on the leach residues.) Carbon and sulphur were carried out using an EMIA-320V carbon/sulphur analyzer. Chloride and fluoride analyses were analyzed using ion selective electrodes. (Chloride and fluoride analyses on solid samples were performed after fusing the solids with Na_2CO_3/Na_2O_2 in a zirconium crucible and leaching the fusate with H_2SO_4 and HNO_3.) All other analyses were performed using a Perkin-Elmer 4000 atomic absorption (AA) spectrometer.

4.6.1 Roasting with Na_2CO_3

The deportment of minor elements in the La Oroya zinc ferrite during roasting with 80% Na_2CO_3 at 950°C is shown in Table 27. Projected leach solution concentrations are calculated by assuming a solids concentration during leaching to give a maximum sulphate content in the leach solution of 2.29 M, or about 225 g/L H_2SO_4 equivalent. (This is a typical operating concentration for many zinc electrolytic plants.)

As expected the majority of most elements, with the exception of As, Cl, Pb and Ag, reported to the leach solution after Na_2CO_3 roasting and leaching with H_2SO_4. In particular, the high dissolution of iron and sodium limits the solids concentration possible during leaching and, hence, the maximum zinc concentration possible in the leach solution. Iron would have to be precipitated from solution, either as jarosite, hematite or goethite, before zinc could be recovered. Indium and gallium extractions are both high at

87.8% and 84.7%, respectively. These extractions, combined with a zinc extraction of 98.9%, indicate that about 84% of the total value of the valuable metals (i.e., Ga, In, Ag and Zn), or about US$723/tonne of zinc ferrite at 2005 metals prices (15-18), are recoverable in the leach solution. The residue is significantly enriched with respect to lead and silver and it may be possible to recycle this residue to La Oroya's lead smelter for further processing.

Table 27 Deportment of Minor Elements in La Oroya Zinc Ferrite during Roasting with 80% Na_2CO_3 at 950°C

	Element Distribution, %			Composition, % or g/L			
	Solution	Residue	Fume	Feed	Leach Residue	Leach Solution[1]	Fume[1]
Solids, g				1000	199		13.1
Solution, L						7.9	
Elements							
Zn	98.9	1.1	0.0	19.5	1.05	24.4	
Fe	80.6	19.4	0.0	26.6	26	27.1	
Na[2]	95.6	4.4	0.0	1.10	7.97	43.2	
Al	88.7	11.3	0.0	0.97	0.55	1.09	
Cd	95.8	4.2	0.0	0.19	0.04	0.23	
Ca	74.2	25.8	0.0	0.37	0.48	0.35	
Cu	86.3	13.7	0.0	0.55	0.38	0.60	
Pb	4.9	90.7	4.4	2.98	14.3	0.18	10.0
Mg	77.9	22.1	0.0	0.18	0.20	0.18	
Mn	44.6	55.4	0.0	1.22	3.40	0.69	
K	94.4	5.6	0.0	0.18	0.05	0.21	
Si	90.9	9.1	0.0	4.64	2.12	5.33	
As	6.7	3.5	89.8	0.55	0.05	0.047	37.6
Cl	7.0	7.6	85.4	0.608	0.306	0.013	39.6
Co	100.0	0.0	0.0	0.001	n.a.	0.001	
Ga	84.7	15.3	0.0	0.052	0.040	0.056	
F	63.9	10.0	26.1	0.070	0.035	0.004	1.4
In	87.8	12.2	0.0	0.075	0.046	0.083	
Ni	100.0	0.0	0.0	0.001	n.a.	0.001	
Ag	2.1	98.0	0.0	0.030	0.150[3]	0.001	
C[2,4]	30.0	4.0	66.0	1.42	2.10	n.a.	
S[4]	75.6	10.2	14.2	1.50	1.84	n.a.	

[1] Estimated from element distribution, assuming a leach solution of 225 g/L H_2SO_4

[2] Sodium and carbon extractions include Na and C added as Na_2CO_3 during roasting.

[3] Estimated from solids weight and leach extraction

[4] Carbon and sulphur are assumed to be given off as gaseous CO_2 and SO_2.

4.6.2 *Roasting with Na_2CO_3 and $MnCO_3$*

The deportment of minor elements in the La Oroya zinc ferrite during roasting with 80% Na_2CO_3 and 33.25% $MnCO_3$ at 950°C is shown in Table 28.

Table 28 Deportment of Minor Elements in La Oroya Zinc Ferrite during Roasting with 80% Na_2CO_3 and 33.25% $MnCO_3$ at 950°C

	Element Distribution, %			Composition, % or g/L			
	Solution	Residue	Fume	Feed	Leach Residue	Leach Solution[1]	Fume[1]
Solids, g				1000	672		10.5
Solution, L						6.7	
Zn	90.3	9.7	0.0	19.5	3.40	26.2	
Fe	45.4	54.6	0.0	26.6	21.6	18.0	
Na[2]	95.7	4.3	0.0	1.10	2.31	51.0	
Al	81.3	18.7	0.0	0.97	0.27	1.17	
Cd	96.5	3.5	0.0	0.19	0.01	0.27	
Ca	90.0	10.0	0.0	0.37	0.06	0.50	
Cu	52.3	47.7	0.0	0.55	0.39	0.43	
Pb	1.0	93.9	5.1	2.98	4.37	0.04	14.5
Mg	80.1	19.9	0.0	0.18	0.08	0.21	
Mn[2]	4.1	95.9	0.0	1.22	24.4	1.04	
K	84.7	15.3	0.0	0.18	0.04	0.22	
Si	92.8	7.2	0.0	4.64	0.50	6.40	
As	0.7	9.6	89.7	0.55	0.08	0.006	47.1
Cl	46.6	15.2	38.2	0.608	0.137	0.421	22.2
Co	100.0	0.0	0.0	0.001	-	0.001	
Ga	72.8	27.2	0.0	0.052	0.021	0.056	
F	68.4	10.6	21.0	0.070	0.011	0.071	1.4
In	64.1	35.9	0.0	0.075	0.040	0.072	
Ni	100.0	0.0	0.0	0.001	-	0.001	
Ag	6.1	93.9	0.0	0.030	0.040[3]	0.003	
C[2,4]	6.7	0.4	92.9	1.42	0.08	n.a.	-
S[4]	71.8	11.6	16.6	1.50	0.63	n.a.	-

[1] Estimated from element distribution, assuming a leach solution of 225 g/L H_2SO_4

[2] Sodium, manganese and carbon extractions include the sodium, manganese and carbon added as Na_2CO_3 and $MnCO_3$ during roasting.

[3] Estimated from solids weight and leach extraction

[4] Carbon and sulphur are assumed to be given off as gaseous CO_2 and SO_2.

For the most part, extractions are similar to those in the previous section, but the addition of manganese significantly lowers the iron extraction. At these roasting conditions, the

$MnCO_3$ addition also drops the extractions of Cu, Ga, In and Zn. To maintain the extractions of these elements at similar levels to those in Section 4.6.1 for roasting with Na_2CO_3 alone, roasting temperatures would likely have to be increased to 1000°C.

4.6.3 Roasting with Coal

The deportment of minor elements in the La Oroya zinc ferrite during roasting with 20% coal at 1100°C is shown in Table 29.

Table 29 Deportment of Minor Elements in La Oroya Zinc Ferrite during Roasting with 20% Coal at 1100°C

	Element Distribution, %			Composition, % or g/L			
	Solution	Residue	Fume	Feed	Leach Residue	Leach Solution[1]	Fume[1]
Solids, g				1000	610		104.0
Solution, L						1.5	
Zn	61.7	2.9	35.4	19.5	0.84	130.2	66.4
Fe	2.6	97.5	0.0	26.6	37.4	4.7	
Na	8.6	91.4	0.0	1.10	1.65	0.7	
Al	20.8	79.2	0.0	0.97	1.26	1.39	
Cd	0.3	6.8	92.9	0.19	0.00	1.22	1.7
Ca	9.0	91.1	0.0	0.37	0.55	0.23	
Cu	13.4	86.7	0.0	0.55	0.78	0.51	
Pb	0.5	81.3	18.2	2.98	1.55	0.10	5.2
Mg	46.9	53.1	0.0	0.18	0.16	0.58	
Mn	7.5	92.5	0.0	1.22	1.85	0.63	
K	6.5	93.5	0.0	0.18	0.27	0.08	
Si	6.1	93.9	0.0	4.64	7.15	1.94	
As	2.1	4.1	93.8	0.55	0.04	0.079	5.0
Cl	17.1	31.9	51.0	0.608	0.316	2.829	3.0
Co	100.0	0.0	0.0	0.001	n.a.	0.003	
F	17.0	54.0	29.0	0.070	0.062	0.221	0.20
Ga	33.1	66.9	0.0	0.052	0.057	0.118	
In	23.3	39.0	37.7	0.075	0.048	0.314	0.27
Ni	29.0	71.0	0.0	0.001	n.a.	0.002	
Ag	0.4	99.6	0.0	0.030	0.050[2]	0.001	
C	0.0	0.0	100.0[3]	1.42	0.00	n.a.	
S	15.0	8.9	76.1[3]	1.5	0.22	n.a.	

[1] Estimated from element distribution, assuming a leach solution of 225 g/L H_2SO_4 and assuming the fume produced is leached with minimal dissolution of Pb or As

[2] Estimated from solids weight and leach extraction

[3] Carbon and sulphur are assumed to be given off as gaseous CO_2 and SO_2.

As expected from a Waelz kiln type process, cadmium and arsenic are extensively fumed, with Cl, F, In, Pb and Zn partially fumed during the roasting process. Additional indium and zinc are leached from the solids after roasting to give overall zinc and indium extractions of over 97% and 61%, respectively. Gallium is not recovered to a significant extent with only 33% soluble during leaching. Iron extractions are low during leaching and the overall extractions of most elements, relative to zinc, means that higher solids concentrations during leaching should be possible, potentially allowing leach solutions containing up to 130 g/L Zn to be produced.

4.6.4 Roasting with Coal and $MnCO_3$

The deportment of minor elements in the La Oroya zinc ferrite during roasting with 20% coal at 1100°C and 70% $MnCO_3$ is shown in Table 30. The extent of zinc and lead fuming is significantly increased with the addition of $MnCO_3$ but, with the very high $MnCO_3$ additions used in this sample, overall zinc extractions were lowered to around 93%. Indium and gallium extractions are slightly improved to 69 and 39%, respectively. Overall, the extraction of iron and other elements, relative to zinc, are lowered with the addition of $MnCO_3$ which would allow even higher solids concentrations to be used during leaching to nearly enable a solution containing 140 g/L Zn to be produced, or about 93% of the maximum zinc concentration possible for leaching with 225 g/L H_2SO_4.

Lower $MnCO_3$ additions are likely to be used in practice which would significantly reduce the manganese content of the leach residue. The potential for recovering the iron values from the leach residue would be dependent largely on the ability to reduce or deal with the major, potentially deleterious, impurities in the residue, including Cu, Pb, Na and Zn, which will be discussed in more detail in Section 4.7.2.1.

Table 30 Deportment of Minor Elements in La Oroya Zinc Ferrite during Roasting with 20% Coal and 70% $MnCO_3$ at 1100°C

	Element Distribution, %			Composition, % or g/L			
	Solution	Residue	Fume	Feed	Leach Residue	Leach Solution[1]	Fume[1]
Solids, g				1000	1025		169.6
Solution, L						1.3	
Zn	33.6	7.4	59.0	19.5	0.84	139.6	67.8
Fe	1.5	98.5	0.0	26.6	25.6	3.0	
Na	1.4	98.6	0.0	1.10	1.06	0.1	
Al	2.1	97.9	0.0	0.97	0.93	0.16	
Cd	0.4	6.0	93.6	0.19	0.01	1.38	1.0
Ca	0.2	99.8	0.0	0.37	0.36	0.01	
Cu	3.0	97.0	0.0	0.55	0.52	0.13	
Pb	0.3	49.0	50.7	2.98	1.43	0.07	8.9
Mg	34.7	65.3	0.0	0.18	0.11	0.48	
Mn[2]	0.3	99.7	0.0	1.22	33.7	0.03	
K	1.1	98.9	0.0	0.18	0.17	0.01	
Si	2.1	97.9	0.0	4.64	4.44	0.75	
As	2.8	12.7	84.6	0.55	0.07	0.118	2.7
Cl	12.6	62.4	25.0	0.608	0.37	1.77	0.90
Co	83.3	16.7	0.0	0.001		0.003	
Ga	38.9	61.1	0.0	0.052	0.031	0.37	0.18
F	24.3	32.2	43.5	0.070	0.022	0.132	
In	20.8	31.1	48.2	0.075	0.058	0.400	0.21
Ni	0.0	100.0	0.0	0.001		0.000	
Ag	5.6	94.5	0.0	0.030	0.030[3]	0.013	
C	0.0	0.0	100.0[4]	1.42	0.00	n.a.	
S	0.0	2.7	97.3[4]	1.50	0.04	n.a.	

[1] Estimated from element distribution, assuming a leach solution of 225 g/L H_2SO_4 and assuming the fume produced is leached with minimal dissolution of Pb or As

[2] Manganese extractions include the manganese added as $MnCO_3$ during roasting.

[3] Estimated from solids weight and leach extraction

[4] Carbon and sulphur are assumed to be given off as gaseous CO_2 and SO_2.

4.7 Preliminary Evaluation of Potential Processing Options

4.7.1 Roasting with Na_2CO_3 and $MnCO_3$

Roasting with Na_2CO_3 alone has few advantages over direct hot acid leaching. High zinc, indium and gallium extractions are possible, as they are for hot acid leaching. Iron extractions are lower than for hot acid leaching (i.e., 80% versus often over 98% for hot acid leaching). However, because of the higher reaction temperatures and endothermic reactions, involved in the Na_2CO_3 roasting process, roasting with Na_2CO_3 alone would likely provide few advantages, whether in energy, economic or environmental benefits, over hot acid leaching. However, roasting with Na_2CO_3 alone will be discussed in the following sections for comparative purposes with other process options.

Roasting with Na_2CO_3 and $MnCO_3$, with a reduction of almost 50% in the iron extraction from the zinc ferrite, is a more attractive process option, as nearly half of the iron in the original zinc ferrite can be fixed as a Mn-Fe oxide, which is expected to be environmentally stable on disposal with some potential towards recovery of manganese and iron from that residue (Section 4.7.1.2). A possible flowsheet for zinc recovery from the zinc ferrite using Na_2CO_3 and $MnCO_3$ roasting is presented in Figure 68, which should allow the complete integration of the process with Doe Run Peru's existing zinc electrolytic plant at La Oroya. The reactions for each unit operation are provided in Table 31. A similar flowsheet, and chemical reactions, could be proposed for roasting with Na_2CO_3 alone, but less iron would report to the leach residue and more iron would have to be reduced and then precipitated as goethite. (The higher iron extractions that would result, would limit the solids concentration during leaching, which would, in turn, lower the zinc concentration in the leach solution.)

Table 31 Chemical Reactions during the $Na_2CO_3/MnCO_3$ Roast Process

Unit Operation	Chemical Reactions
Na_2CO_3 Roasting	$Na_2CO_3 + ZnFe_2O_4 \rightleftharpoons 2\ NaFeO_2 + ZnO + CO_2$ $2\ NaFeO_2 + MnCO_3 \rightleftharpoons MnFe_2O_4 + Na_2CO_3$
H_2SO_4 Leaching	$H_2SO_4 + ZnO \rightleftharpoons ZnSO_4 + H_2O$ $4\ H_2SO_4 + 2\ NaFeO_2 \rightleftharpoons Na_2SO_4 + Fe_2(SO_4)_3 + 4\ H_2O$
Iron Reduction	$Fe_2(SO_4)_3 + ZnS \rightleftharpoons ZnSO_4 + S^0 + 2\ FeSO_4$
In/Ga Precipitation	$H_2SO_4 + ZnO \rightleftharpoons ZnSO_4 + H_2O$ $(In,Ga)_2(SO_4)_3 + 3\ CaCO_3 + 9\ H_2O \rightleftharpoons 2\ (In,Ga)(OH)_3 + 3\ CaSO_4{\cdot}2H_2O + 3\ CO_2$
FeOOH Precipitation	$2\ FeSO_4 + 2\ ZnO + 0.5\ O_2 + H_2O \rightarrow 2ZnSO_4 + 2FeOOH$
Basic Zinc Sulphate Precipitation	$4\ ZnSO_4 + 3\ CaCO_3 + 13\ H_2O \rightleftharpoons ZnSO_4{\cdot}3Zn(OH)_2{\cdot}4H_2O + 3\ CaSO_4{\cdot}2H_2O + 3\ CO_2$

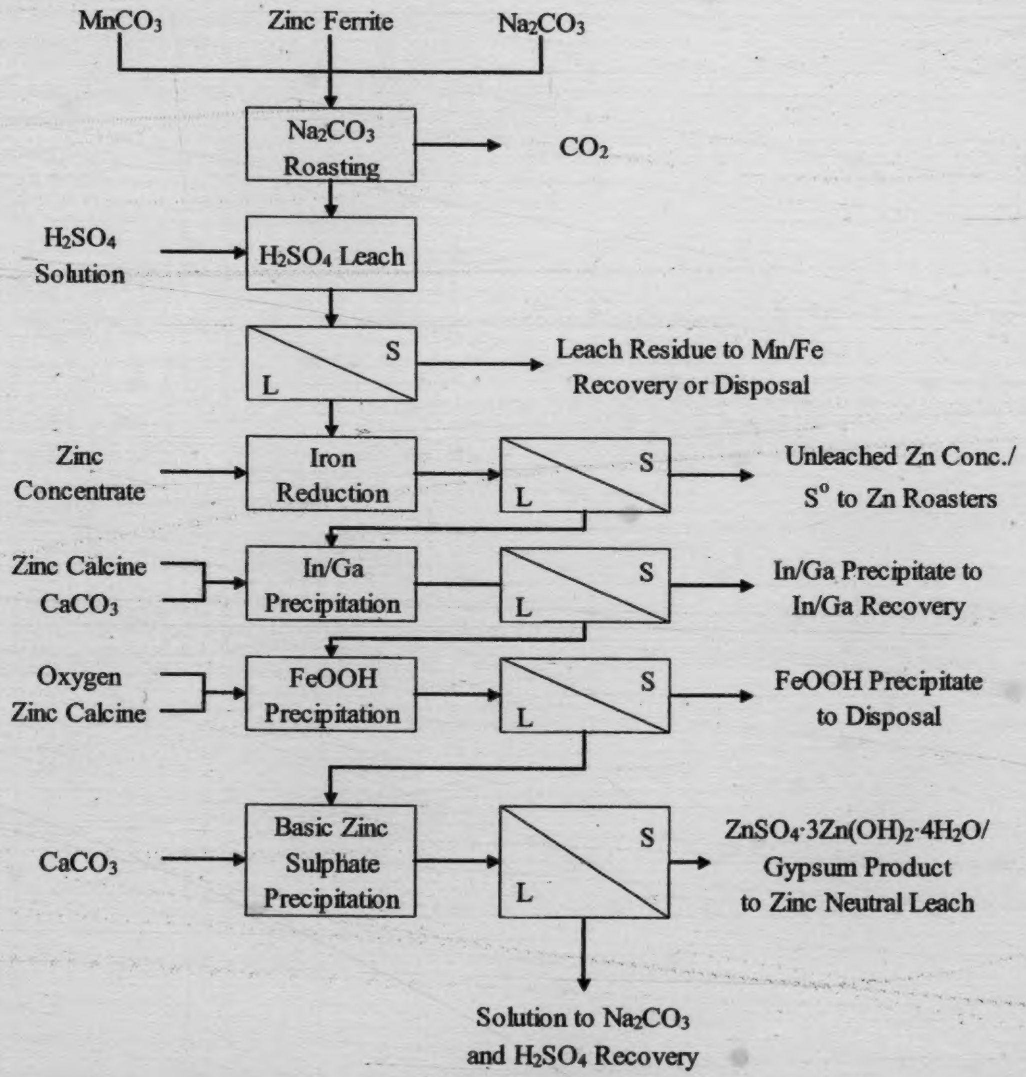
MnCO3
Zinc Ferrite
Na2CO3
Na2CO3 Roasting
CO2
H2SO4 Solution
H2SO4 Leach
S
L
Leach Residue to Mn/Fe Recovery or Disposal
Zinc Concentrate
Iron Reduction
S
L
Unleached Zn Conc./ S° to Zn Roasters
Zinc Calcine
CaCO3
In/Ga Precipitation
S
L
In/Ga Precipitate to In/Ga Recovery
Oxygen
Zinc Calcine
FeOOH Precipitation
S
L
FeOOH Precipitate to Disposal
CaCO3
Basic Zinc Sulphate Precipitation
S
L
ZnSO4·3Zn(OH)2·4H2O/ Gypsum Product to Zinc Neutral Leach
Solution to Na2CO3 and H2SO4 Recovery

Figure 68 **Possible Flowsheet for Na_2CO_3/$MnCO_3$ Roasting and H_2SO_4 Leaching of La Oroya Zinc Ferrite Residue**

In this process flowsheet, the zinc ferrite is roasted with Na_2CO_3 and $MnCO_3$ and then leached in 225 g/L H_2SO_4 solution to give a solution containing about 26 g/L Zn, 18 g/L Fe, 51 g/L Na and less than 5 g/L H_2SO_4. After leaching, the slurry would be filtered from the Mn-ferrite residue, which represents over 50% of the iron values in the original zinc ferrite material, separated from the solution and sent to either disposal or further processing for the recovery of the iron and manganese values (Section 4.7.1.2).

After leaching and filtration, zinc concentrate would be added to reduce Fe^{3+} to Fe^{2+}. Any unreacted zinc concentrate, or S^0 produced during the reduction, would be recycled to the zinc roasters to produce zinc calcine and SO_2 gas for H_2SO_4 production. This step is important for several reasons: first, because it eliminates the possibility of forming sodium jarosite, second, it allows for the recovery of a low iron In/Ga precipitate and, third, it prepares the iron remaining in solution for removal as goethite using the Vielle Montagne process, as described in Section 4.2.2.4 (99).

This solution is then neutralized, first with zinc calcine to neutralize free acid and then with $CaCO_3$ to precipitate indium and gallium from solution as their respective hydroxides in a process similar to that proposed by Maeshiro and Emi (98) or by Benedetto et al. (113). (Aluminum in solution would also likely be precipitated during this step.) The solution pH would be kept below pH 4.5 to minimize the precipitation of basic zinc sulphate during neutralization. The resulting precipitate would then be redissolved and the indium and gallium extracted using solvent extraction flowsheets, such as those described in the literature (113-115), with any coprecipitated zinc and iron recycled to the leach solution.

The solution after precipitation of indium and gallium would then be simultaneously oxidized at temperatures of around 90°C to precipitate iron as goethite (FeOOH) with the acid produced during precipitation, neutralized to give a solution pH of 2.5 to 4.2 (116). (Hematite precipitation is also a possibility, but the higher temperatures and pressures required are unlikely to be practical, especially for a plant operating at high altitudes, such as La Oroya.) Much of the silicon in solution would also be expected to precipitate in the goethite precipitation step (116).

Once iron has been removed from solution, zinc can then be precipitated by raising the solution pH to between pH 6 and 8 with the addition of limestone ($CaCO_3$) or lime (CaO) to precipitate basic zinc sulphate ($ZnSO_4 \cdot 3Zn(OH)_2 \cdot 4H_2O$ (BZS)) (117). This BZS precipitate can then be recycled to the calcine or neutral leach, where roasted zinc ore is normally leached with spent electrolyte, to neutralize acid and recover the contained zinc values. The neutral leach solution would be treated conventionally using zinc dust purification, or other purification methods, before zinc is recovered as super high grade cathode zinc by electrowinning in Doe Run Peru's existing electrolytic plant. Copper and cadmium in solution could be precipitated from the leach solution with the addition of zinc dust before BZS precipitation, depending on their quantity in solution and the desirability of recovering these metals as byproducts.

4.7.1.1 Na_2CO_3 Recovery and H_2SO_4 Regeneration

The addition of Na_2CO_3 during roasting and the consumption of H_2SO_4 during leaching would be substantial operating costs for this process and, thus, recovery of both Na_2CO_3 and H_2SO_4 would improve the economics of Na_2CO_3 roasting of this material. After examination of the available literature, two potential routes for the recycling of these two reagents were identified: Na_2SO_4 metathesis (Figure 69) or solvent extraction/ion exchange of Na_2SO_4 (Figure 70).

With either case, it is likely that the solution after BZS precipitation would be neutralized to pH 10 with lime (CaO) or NaOH to remove most of the remaining impurities in solution (i.e., Al, Cd, Ca, Cl, Co, Cu, F, Pb, Mg, Mn, Ni and Si) and prevent the buildup of these impurities in the Na_2CO_3 recovery circuit or their recycle to acid leaching with the regenerated H_2SO_4. (Potassium would be expected to remain in solution after neutralization.)

In Na_2SO_4 metathesis (Figure 69), sodium sulphate is first crystallized from solution as Glauber's salt ($Na_2SO_4 \cdot 10\ H_2O$) and then further evaporated and crystallized to form Na_2SO_4. The anhydrous Na_2SO_4 is then added to a solution containing 40 to 60% H_2SO_4 and HCl is added to metathesize Na_2SO_4 by the reaction:

$Na_2SO_4 + 2\ HCl \rightleftharpoons 2\ NaCl + H_2SO_4$ (118,119).

The NaCl precipitate can then be separated from the sulphuric acid and a bleed of the sulphuric acid solution diluted and sent to acid leaching.

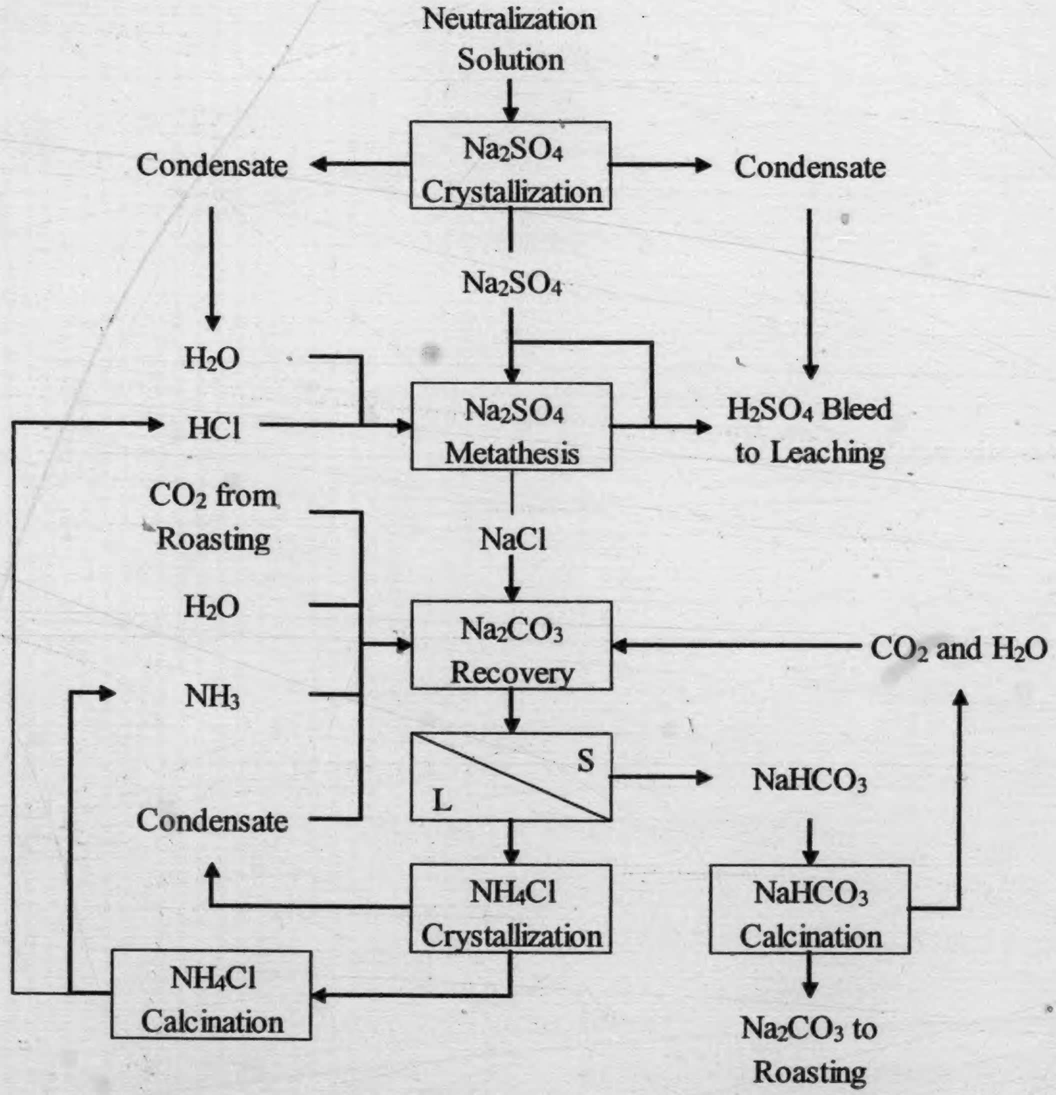
Neutralization Solution
Na2SO4 Crystallization
Condensate
Condensate
Na2SO4
H2O
HCl
Na2SO4 Metathesis
H2SO4 Bleed to Leaching
CO2 from Roasting
NaCl
H2O
Na2CO3 Recovery
CO2 and H2O
NH3
S
L
NaHCO3
Condensate
NH4Cl Crystallization
NaHCO3 Calcination
NH4Cl Calcination
Na2CO3 to Roasting

Figure 69 Na_2CO_3 and H_2SO_4 Regeneration by Low Temperature Metathesis

In solvent extraction or ion exchange of Na_2SO_4 (Figure 70), the Na_2SO_4 solution is contacted with an ion exchange resin in the H^+ form of the resin or an organic solvent, with the resin or solvent stripped with HCl solution to regenerate the resin or solvent and produce a strip solution high in NaCl. (Though research on solvent extraction or ion exchange of sodium solutions is not well documented in the literature, several studies have proposed using ion exchange resins to convert Na_2SO_4 to H_2SO_4 and $NaNO_3$ (120-123).) The H_2SO_4 rich raffinate would be returned to acid leaching with the NaCl solution going on to Na_2CO_3 recovery. (Lowering the pH of the neutralized solution (i.e., pH 10) may be required to maximize the recovery of Na^+ and SO_4^{2-} in this flowsheet.)

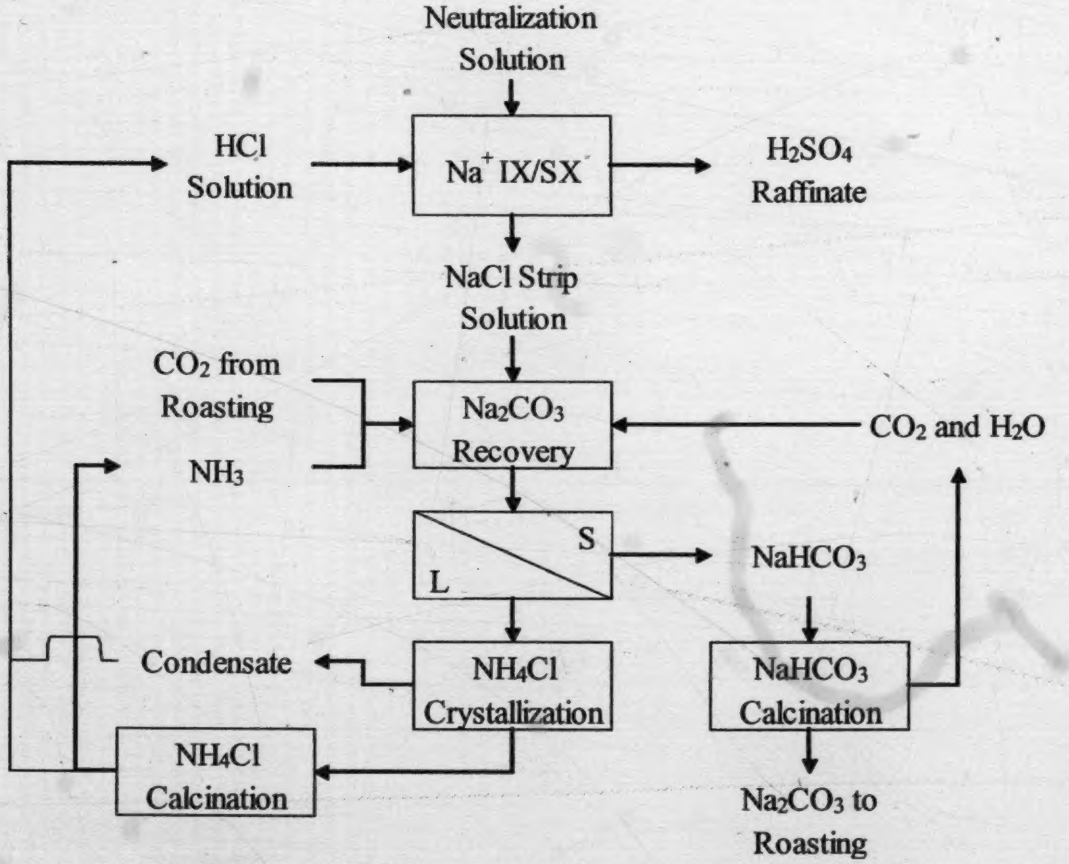
Neutralization Solution
HCl Solution
Na^+ IX/SX
H_2SO_4 Raffinate
NaCl Strip Solution
CO_2 from Roasting
NH_3
Na_2CO_3 Recovery
CO_2 and H_2O
S
L
$NaHCO_3$
Condensate
NH_4Cl Crystallization
$NaHCO_3$ Calcination
NH_4Cl Calcination
Na_2CO_3 to Roasting

Figure 70 Na_2CO_3 and H_2SO_4 Regeneration by Solvent Extraction or Ion Exchange

In both process routes (Figures 69 and 70), Na_2CO_3 would be recovered from solution by adding ammonia (NH_3) to the resulting NaCl solution and bubbling CO_2 gas, a byproduct of the Na_2CO_3 roasting process, through the solution to precipitate sodium bicarbonate ($NaHCO_3$) by the following reaction: $NaCl + H_2O + NH_3 + CO_2 \rightleftharpoons NH_4Cl + NaHCO_3$ (124). The sodium bicarbonate can then be filtered from the solution, calcined to form Na_2CO_3 and recycled to Na_2CO_3 roasting. The NH_4Cl solution can be crystallized to recover NH_4Cl, which can then be decomposed by heating, to recycle HCl and NH_3 to the H_2SO_4 regeneration and Na_2CO_3 recovery steps, respectively.

Even with the capital and operating costs associated with solvent extraction or ion exchange, it is likely that the costs of crystallizing Na_2SO_4 from solution, and the capital cost associated with materials of construction for the high acid concentrations required in the Na_2SO_4 metathesis, would be higher than those for ion exchange or solvent extraction.

The deportment of potassium through either process route is unknown. In the metathesis flowsheet, it is likely that K_2SO_4 would be crystallized along with Na_2SO_4, but would not be metathesized to form H_2SO_4, potentially resulting in a buildup of potassium in solution. In the ion exchange/solvent extraction flowsheet, if potassium is not loaded along with sodium on the resin or solvent, a similar problem would occur and would require either bleeding a portion of the process solution to remove potassium or another alternate potassium removal step. However, if potassium is loaded along with sodium, then it will be stripped as KCl from the resin/solvent. The high solubility of $KHCO_3$ in solution means that $KHCO_3$ would not coprecipitate with $NaHCO_3$ and thus, it would be expected to crystallize from the solution along with NH_4Cl (125). On heating of the crystallized NH_4Cl, $KHCO_3$ would be expected to thermally decompose, releasing CO_2 and water and forming K_2O. The K_2O could be removed from the system as a solid waste and disposed.

4.7.1.1.1 Process Implications and Modifications

In order to minimize sulphate losses as gypsum ($CaSO_4 \cdot 2H_2O$) and maximize the recovery of sulphate as H_2SO_4, it may be advantageous to use Na_2CO_3 instead of limestone ($CaCO_3$) during In/Ga precipitation or BZS precipitation in Section 4.7.1 Any Na_2CO_3 added could be recovered in the Na_2CO_3 recovery portion of the flowsheet.

An alternative to using $CaCO_3$ as a neutralizing agent may be possible using observations made during the roasting of EAF dusts with Na_2CO_3 (Section 5.5.1). In the Na_2CO_3 roasting of EAF dust, water leaching selectively removed chromium from the roasted solids. During hot water leaching, the majority of the sodium added was also leached with sodium extractions of between 70 and 85% to the water leach solution (Sections 5.6.1 and 5.6.2). Analysis of sulphur deportment in the solids indicates that this water leach solution should be very low in sulphate, with the majority of this sulphate associated with zinc and other dissolved impurities. While carbon deportment indicates that some of the sodium in solution is present as Na_2CO_3, likely from Na_2CO_3 that did not react or decompose during roasting, most of the sodium is presumably present as NaOH. (Based on the available analyses, the EAF water leach solution should contain about 1.5% of the sodium as Na_2SO_4, 21% as Na_2CO_3 and 77% as NaOH.) Thus, this solution represents a high sodium, high pH solution which could be used for solution neutralization.

If similar sodium deportments were observed when the La Oroya zinc ferrite is leached with hot water, then it may be possible to modify the process flowsheet to make use of the water leach solution for neutralization. A modified process flowsheet, with the addition of water leaching, is illustrated in Figure 71. The water leach solution could be used as a neutralizing agent in In/Ga precipitation and the precipitation of basic zinc sulphate. Based on the results from Na_2CO_3 roasting of the EAF dust, minor amounts of zinc would also report to the water leach, but reintroduction of the solution as a neutralizing agent would allow this zinc, and any other impurities leached in water leaching, to be recovered or removed as discussed earlier in the unit operations described in Sections 4.7.1 and 4.7.1.1.

Table 32 compares various process options for the processing of La Oroya zinc ferrite, including hot acid leaching and Na_2CO_3 roasting with and without $MnCO_3$ or water leaching based on maximum zinc concentrations in solution and solution volumes. (Zinc concentrations and solution volumes are calculated for the water leach flowsheet assuming that 75% of the sodium added is recovered with water leaching.)

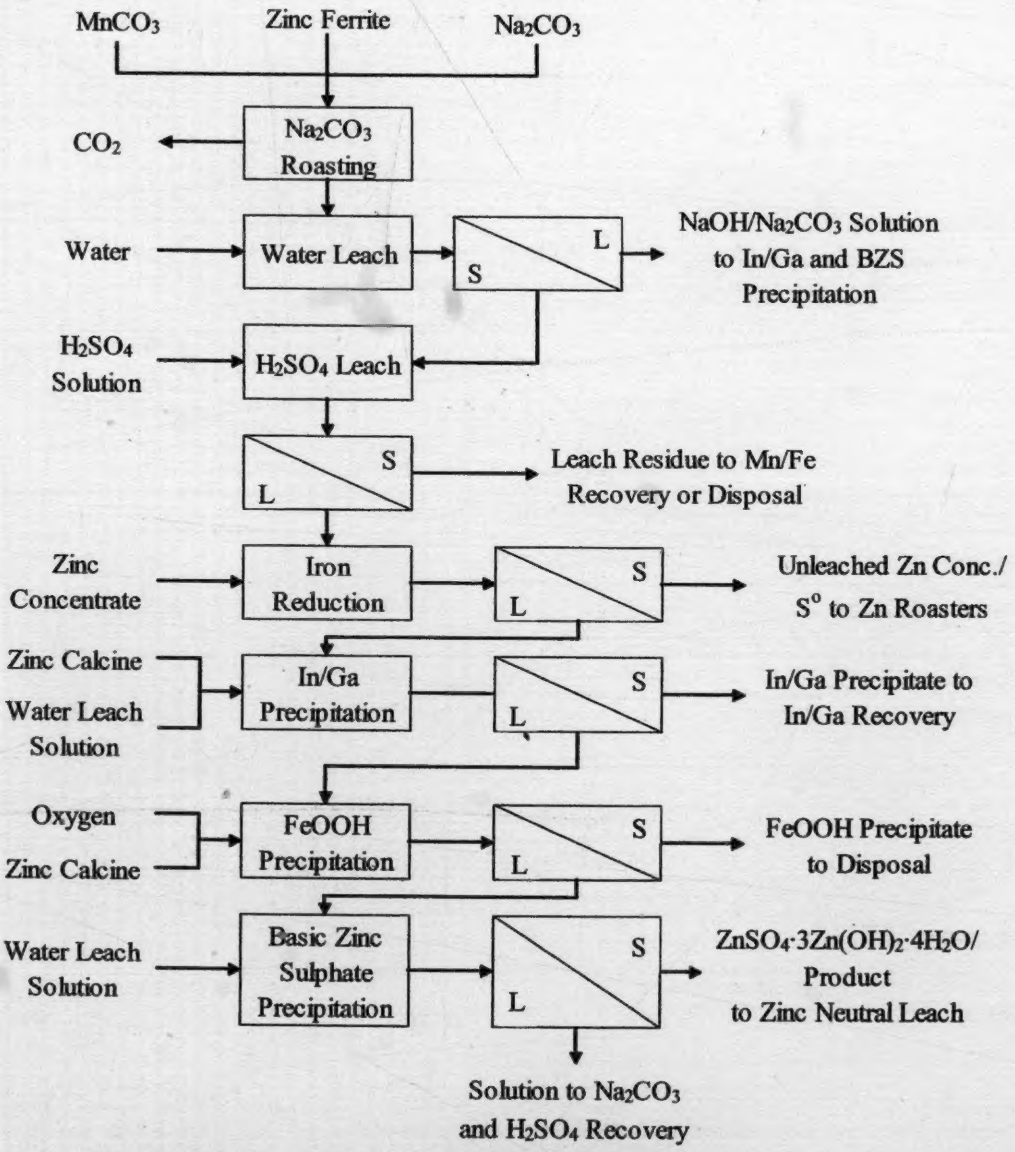

MnCO3
Zinc Ferrite
Na2CO3
CO2
Na2CO3 Roasting
Water
Water Leach
S
L
NaOH/Na2CO3 Solution to In/Ga and BZS Precipitation
H2SO4 Solution
H2SO4 Leach
S
L
Leach Residue to Mn/Fe Recovery or Disposal
Zinc Concentrate
Iron Reduction
S
L
Unleached Zn Conc./ S° to Zn Roasters
Zinc Calcine
Water Leach Solution
In/Ga Precipitation
S
L
In/Ga Precipitate to In/Ga Recovery
Oxygen
Zinc Calcine
FeOOH Precipitation
S
L
FeOOH Precipitate to Disposal
Water Leach Solution
Basic Zinc Sulphate Precipitation
S
L
ZnSO4·3Zn(OH)2·4H2O/ Product to Zinc Neutral Leach
Solution to Na2CO3 and H2SO4 Recovery

Figure 71 Modification of the $Na_2CO_3/MnCO_3$ Roasting Flowsheet to Incorporate Hot Water Leaching into the Process Flowsheet

Much higher zinc concentrations in the leach solution can be obtained with hot acid leaching, due in large part to the high iron extractions observed, and the correspondingly high requirements for zinc concentrate and calcine to be able to reduce and precipitate these iron values. However, because of these high iron extractions, a solution is produced, that with respect to most elements, could potentially be able to be treated directly in electrowinning following zinc dust purification.

Table 32 Comparison of Leach Volumes and Zinc Concentrations for Various Ferrite Treatment Flowsheets

Process Flowsheet	Hot Acid Leach*	Na_2CO_3 Roast	Modified Na_2CO_3 Roast**	Na_2CO_3-$MnCO_3$ Roast	Modified Na_2CO_3-$MnCO_3$ Roast**
Acid Leach Volume, L/kg $ZnFe_2O_4$***	4.6	7.9	5.4	6.7	4.2
Total Zinc Conc. before BZS Precipitation, g/L	141.7	72.0	98.5	57.8	92.9
Zn from $ZnFe_2O_4$, g/L	41.7	24.4	33.4	26.2	42.2
Zn from Zinc Concentrate (ZnS), g/L	33.3	15.9	21.7	10.5	16.9
Zn from Roaster Calcine (ZnO), g/L	66.7	31.7	43.4	21.1	33.8
Distribution of Zn Recovered, %					
$ZnFe_2O_4$	29.4	33.9	33.9	45.4	45.4
Zinc Concentrate (ZnS)	23.5	22.0	22.0	18.2	18.2
Roaster Calcine (ZnO)	47.0	44.1	44.1	36.4	36.4

* Calculated assuming extractions of 99% for Zn and Fe and similar extractions to Na_2CO_3 roasting for all other impurities, except for K, Na and Si
** Flowsheet modified to include water leaching
*** Assuming 225 g/L H_2SO_4 in the leach solution

However, with the relatively high chloride and fluoride concentrations in the La Oroya zinc ferrite, if chloride or fluoride extractions are similar to, or even significantly lower than, the extractions observed in Na_2CO_3 roasting, then the leach solution would contain unacceptably high chloride and fluoride concentrations. (High chloride concentrations (i.e., over 40 mg/L) encourage corrosion of the lead anode (126) while high fluoride concentrations (i.e., over 20 mg/L) can degrade the surface oxide on the aluminum cathode and cause difficulty in stripping of zinc from the cathodes (101,127).) Thus, chloride and fluoride removal would likely be required before this material could be treated directly in electrowinning.

The Na_2CO_3 roasting flowsheets, on the other hand, can easily deal with high chloride and fluoride concentrations as neither element would be expected to precipitate along with basic zinc sulphate.

Modifying the process flowsheet to include water leaching not only decreases acid leach volumes (i.e., decreased capital cost because of decreased equipment size) and significantly increases the zinc concentration in solution (i.e., increased zinc throughput for a certain equipment size), but it also reduces limestone requirements for In/Ga precipitation and BZS precipitation by up to 96% for roasting with Na_2CO_3 alone and up to 100% for roasting with Na_2CO_3 and $MnCO_3$ while eliminating sulphate losses from the system through gypsum precipitation.

While this process modification does appear promising, further research into element deportment during water leaching and the use of water leach solution as a neutralizing agent would have to be performed. The potential impact of hot water leaching on the water balance of the process would also have to be examined.

4.7.1.2 Potential for Iron and Manganese Recovery

From the analyses shown in Section 4.6.2, the leach residue after roasting with 80% Na_2CO_3 and 33.25% $MnCO_3$ at 950°C and leaching with 200 g/L H_2SO_4 would be expected to contain about 3.4% Zn, 21.6% Fe, 0.4% Cu, 2.3% Na, 4.4% Pb and 0.6% S. This residue would represent approximately 55% of the iron in the original zinc ferrite with the remaining iron reporting to the goethite residue after precipitation. These impurity elements have the potential to limit the use of this material for direct reduced iron (DRI) production or recycle. The implications and potential solutions to allow the iron residues to be processed to produce DRI are discussed below.

In most DRI processes, the bulk of the zinc would be expected to be reduced and leave the DRI furnace as zinc fume. If integrated with a zinc smelter, particularly one processing secondary zinc materials, such as zinc ferrites, this zinc could be readily recycled to the zinc plant and the zinc values recovered.

Lead is present as anglesite ($PbSO_4$) in the leach residue, and, as such, might be able to be selectively leached from the residue using either acetic acid, a combination of Na_2CO_3 and acetic acid solutions (128,129) or ammonia (130). Sulphur is largely associated with the lead as $PbSO_4$ and, thus, sulphur levels would be expected to be lowered in the solids as lead is leached from the solids. The lead could then be precipitated and recycled to La Oroya's lead smelter for metal recovery.

Although little mention is made of the deportment of sodium in Waelz kiln or DRI processes, sodium would either report to the slag phase or may be reduced and volatilized, with sodium then reporting to the zinc fume. Thus, the sodium could either be disposed of in the slag or, if fumed, leached and then recovered as Na_2CO_3 in the process flowsheet outlined in Section 4.7.1.

Manganese would be expected to report to the slag phase. The slag phase could then either be leached and manganese precipitated as $MnCO_3$ for recycle to the Na_2CO_3 roasting process or further treated for the production of ferro- or silicomanganese for sale.

So far, these major impurities do not represent insurmountable problems in the operation of an integrated zinc-lead-copper smelter with the addition of DRI capacity. Copper in the residue, however, is the impurity of greatest concern. The Cu:Fe ratio in the feed 0.021:1 which, assuming all the copper added reports to the metal phase during iron production, would result in iron containing nearly 2% Cu. After roasting and leaching, over 50% of the copper is extracted to the solution, but, with only 55% of the iron reporting to the $MnFe_2O_4$ residue, the Cu:Fe ratio is only reduced to 0.018:1 in the $MnFe_2O_4$ residue. If the goethite waste, which would contain Pb, Zn and S as entrained sulphates, was also processed to recover iron, the Cu:Fe ratio would be further reduced to 0.010:1, corresponding to an iron product of about 1% Cu. Based on this analysis, about 88% of the copper in the feed would have to be extracted during leaching in order to lower the copper content of the iron residues produced to levels similar to the allowable copper levels in automobile shredder scrap (0.25%) (131). Roasting with Na_2CO_3 alone caused up to 86% of the copper to be leached from the residue and, thus, increased copper removal may be possible with further optimization of the process conditions (i.e., temperature, Na_2CO_3 and $MnCO_3$ additions). However, further research would be required to determine to what extent copper can be removed and, thus, to what extent iron can be recovered from the iron residues from this process.

4.7.1.3 Silver Recovery

There is no evident economically favorable route for silver recovery from the solids or solutions produced during this process. Thus, it is likely that, if silver were to be recovered, it would have to be recovered using flotation and/or leaching before roasting (Section 4.2.2.1.3.3).

4.7.2 Roasting with Coal and $MnCO_3$ (Modified Waelz Kiln Process)

Roasting with coal and $MnCO_3$ is endothermic but should have a much lower heat requirement for the reaction to form $MnFe_2O_4$ than is necessary for the typical Waelz kiln reaction where $ZnFe_2O_4$ is reduced to form zinc vapor and metallic iron (Table 32).

Table 32 Comparison of Thermodynamics of Waelz Kiln Reactions

Reaction	ΔG° (kJ/mol $ZnFe_2O_4$)
$ZnFe_2O_4 + 4\,C \rightleftharpoons Zn_g + 4\,CO + 2\,Fe$	862 – 0.805T
$ZnFe_2O_4 + C + MnCO_3 \rightleftharpoons Zn_g + MnFe_2O_4 + CO + CO_2$	475 – 0.479T
$ZnFe_2O_4 + C \rightleftharpoons Zn_g + CO + Fe_2O_3$	382 – 0.308T

Based on the thermodynamic analysis, this should reduce the heat required for the reduction reaction by up to 55%. Roasting with $MnCO_3$ is only slightly more endothermic (25%) than the reduction reaction where iron is only reduced to hematite (Fe_2O_3). However, with the difficulty in controlling the temperature and reducing conditions in traditional Waelz kiln operations, reduction to Fe_2O_3, without forming metallic iron, is rare and, thus, the addition of $MnCO_3$ during roasting could be thermodynamically and operationally favorable. In addition, because the leach residue consists predominantly of $MnFe_2O_4$, the residue, unlike the metallic iron residue from normal Waelz processing, should be readily disposable as an environmentally stable residue.

Theoretically, the addition of $MnCO_3$ to limit the reduction of iron values to metallic iron should also reduce the coal requirements during roasting. However, these experiments indicate that coal must be added significantly in excess of stoichiometric requirements for either reaction. This may be a function of the furnace configuration used during these roasting tests; it would be expected that coal requirements would be decreased under a furnace configuration that more closely simulates the atmosphere and temperatures of Waelz kiln operation.

A possible flowsheet for this modified Waelz kiln process of roasting with coal and $MnCO_3$ is presented in Figure 72. Because of the amount of chloride and fluoride in the La Oroya ferrite, and the high recovery of Cl and F to fume and to the leach solution, basic zinc sulphate precipitation would have to be used to minimize the chloride and fluoride concentrations reporting to zinc electrowinning. (The fume and roaster calcine could be leached together in one unit operation if lead or arsenic contamination of the $MnFe_2O_4$ residue can be tolerated.) Overall, though, since the extractions of most elements, including Al, As, Ca, Cd, Cu, Fe, Mg, Mn, K, Si and Na, are considerably lower than those from Na_2CO_3 roasting, much higher solids concentrations can be used in acid leaching, resulting in a much more concentrated zinc solution with lower overall levels of impurities.

Because of the significantly lower iron extractions in solution, much less zinc concentrate and zinc calcine would be needed to reduce and precipitate the iron from solution and less goethite precipitate would be produced. (Less contamination of the In/Ga precipitate by iron would also be expected.) Thus, after removal of In, Ga and Fe, it is likely that this solution would be amenable to be treated directly in zinc electrowinning, following conventional zinc dust purification of the iron-free solution, except for the high chloride and fluoride concentrations in the leach solution.

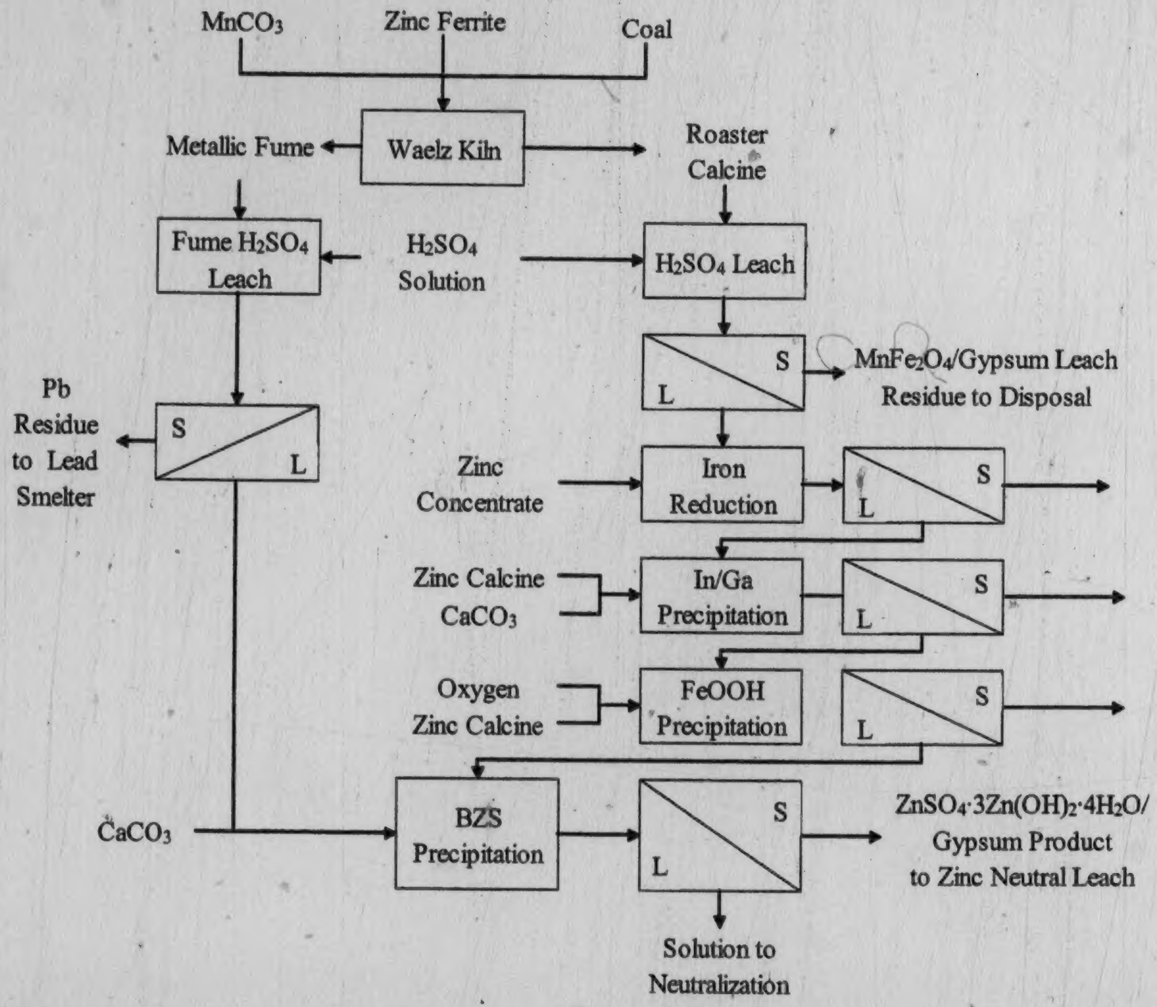
MnCO3
Zinc Ferrite
Coal
Waelz Kiln
Metallic Fume
Roaster Calcine
Fume H2SO4 Leach
H2SO4 Solution
H2SO4 Leach
S
L
MnFe2O4/Gypsum Leach Residue to Disposal
Pb Residue to Lead Smelter
Zinc Concentrate
Iron Reduction
Zinc Calcine
CaCO3
In/Ga Precipitation
Oxygen
Zinc Calcine
FeOOH Precipitation
CaCO3
BZS Precipitation
ZnSO4·3Zn(OH)2·4H2O/ Gypsum Product to Zinc Neutral Leach
Solution to Neutralization

Figure 72 Possible Process Flowsheet for Roasting with Coal and $MnCO_3$ and Leaching with Spent Electrolyte

Under the conditions of the sample analyzed in Table 30 (1100°C, 20% coal, 70% $MnCO_3$), zinc, gallium and indium extractions are relatively low at 93, 39 and 69%, respectively, but extractions of zinc and indium, at least, would be expected to increase with $MnCO_3$ additions closer to stoichiometric, or if slightly higher temperatures or coal additions were used during roasting (Figure 62). However, these extractions indicate that, based on 2005 metal prices (15-18), that, at least, US$543 worth of the Ga, In and Zn values can be recovered by roasting with coal and $MnCO_3$ or about 63% of the total value of Ga, In, Ag and Zn in the ferrite residue.

A major disadvantage for this flowsheet is that there are few options available to recover or recycle the sulphuric acid added during leaching. Some sulphate is lost as gypsum during BZS precipitation and most of the remaining sulphate would likely be lost during neutralization of the barren solution after BZS precipitation to precipitate Cl, F and other elements. This may be acceptable in a zinc plant that produces significant quantities of excess or unsaleable H_2SO_4 from their roasting operations, but would not likely be acceptable economically in most electrolytic zinc plants.

Further research into the possibility of removing chloride and fluoride by leaching the fume and roaster calcine with water or Na_2CO_3 to remove Cl and F should be conducted; if these elements could be removed to lower the Cl and F concentrations to acceptable levels in the leach solution, the solution after goethite precipitation would likely be sufficiently pure, after zinc dust purification to be sent directly to zinc electrowinning.

4.7.2.1 Potential for Iron and Manganese Recovery

Based on the sample analyzed in Table 30 (1100°C, 20% coal, 70% $MnCO_3$), the leach residue would be expected to contain 0.8% Zn, 25.6% Fe, 0.5% Cu, 33.7% Mn, 1.4% Pb, 4.4% Si, 1.1% Na and 0.22% S. (Lower $MnCO_3$ additions during roasting would lower the manganese content in the residue.) Because only 3% of the copper is recovered to the leach solution, the Cu:Fe ratio of the residue does not drop significantly from that of the feed (i.e., 0.021:1 to 0.020:1). Thus, this copper concentration would make recovery of manganese or iron by direct solid state reduction, or other smelting, methods impractical as the iron product would contain unacceptable amounts of copper (i.e., about 2%).

4.7.2.2 Silver Recovery

As discussed in Section 4.7.1.3, there is no evident route for silver recovery in this process as silver is not concentrated in the solids or solutions at any stage of the process. Thus, it is likely that, if silver were to be recovered, it would have to be recovered using flotation and/or leaching before roasting (Section 4.2.2.1.3.3).

4.8 Conclusions

Through the application of the generalized testing procedure to the La Oroya zinc ferrite, two potential reagent systems were identified.

High zinc extractions (>99%) were possible roasting with Na_2CO_3 roasting and leaching with H_2SO_4, but iron extractions were also high at up to 90%. Mineralogical studies indicated that several phases, including α-$NaFeO_2$ β-$NaFeO_2$, Na_2ZnSiO_4, and ZnO, formed during roasting, but, after leaching, only unreacted $ZnFe_2O_4$ and minor amounts of $PbSO_4$ remain in the residue. The addition of secondary reagents during Na_2CO_3 roasting to try to form acid insoluble metal ferrites was also tested. Of the reagents tested, only $MnCO_3$ was effective in significantly lowering iron extractions due to the formation of acid insoluble Mn-ferrites during roasting.

Roasting with coal and ferrite forming additives, such as $CaCO_3$ and $MnCO_3$, was also tested. In both cases, high zinc extractions were possible, but $CaCO_3$ resulted in only limited formation of Ca-ferrites while $MnCO_3$ caused the iron values to be converted nearly quantitatively to jacobsite ($MnFe_2O_4$) during roasting.

The deportment of minor elements in these systems was also detailed and preliminary process flowsheets were developed for each of these promising reagent systems.

5.0 Application of the General Procedure to the Treatment of Altasteel Electric Arc Furnace (EAF) Dust

5.1 Feed Material

A sample of EAF dust produced as a byproduct from processing of carbon steel was obtained from Altasteel. Table 33 shows a summary of the analyses provided by Altasteel while Table 34 presents the analyses performed at the U of A. Elements, such as Cr, F and Pb, are of particular concern, as it is usually based on these elements that the dust fails Toxicity Characteristic Leaching Procedure (TCLP) tests and is then classified as a hazardous waste.

Table 33 Typical Chemical Analysis of EAF Dust Supplied by Altasteel

Analysis	Dust Sample		Analysis	Dust Sample		Extractable Metals	Sample Avg.
	May 04	Aug 04		May 04	Aug 04		
Al, %	0.53	0.48	Ba, ppm	231	255	Strong Acid	
Ca	15.2	11.8	Be	<0.5	10	Hg, ppm	7.8
Cl	0.77	1.01	Co	23	26	Sb	47.1
Cr	0.56	0.36	Mo	179	148	As	40.1
Fe	33.7	34.0	Sr	105	34	Cd	349
Mg	1.83	1.92	Ti	462	<400	Cu	2960
Mn	3.86	4.01	V	100	118	Pb	9990
P	0.04	0.25	Zr	70	8	Ni	300
K	1.16	0.72	SO_4	240	200	Se	5.4
Si	2.80	2.17				Sn	214
Na	0.45	0.63				Water	
S	0.29	0.48				Cr^{6+}, ppm	2.7
Zn	9.18	9.24				F	35

Table 34 Chemical Analysis of As-Received Altasteel EAF Dust

Analysis, %						Analysis, ppm	
Al	0.50	Cr	0.34	K	0.82	Co	70
As	0.04	Cu	0.40	Si	1.92	F	130
Cd	0.03	Fe	31.9	Na	1.32	Mo	150
Ca	7.14	Pb	0.90	S	0.43	Ni	390
C	4.71	Mg	1.39	Zn	9.40	V	80
Cl	1.45	Mn	3.56				

The as-received EAF dust had a particle size of 50% passing 84 μm, but with almost 35% greater than 417 μm. After drying the residue, the oversize was pulverized to give a final particle size of 90% passing 75 μm for the EAF dust used in the roasting tests.

Mineralogically, x-ray diffraction analysis shows that the Altasteel EAF dust contains a mixture of Zn-Mn-Fe spinels ((Zn,Mn,Fe)(Fe,Mn)$_2$O$_4$), $CaCO_3$, NaCl, $CaZn_2(OH)_6 \cdot 2H_2O$ and larnite (Ca_2SiO_4) (Figure 73).

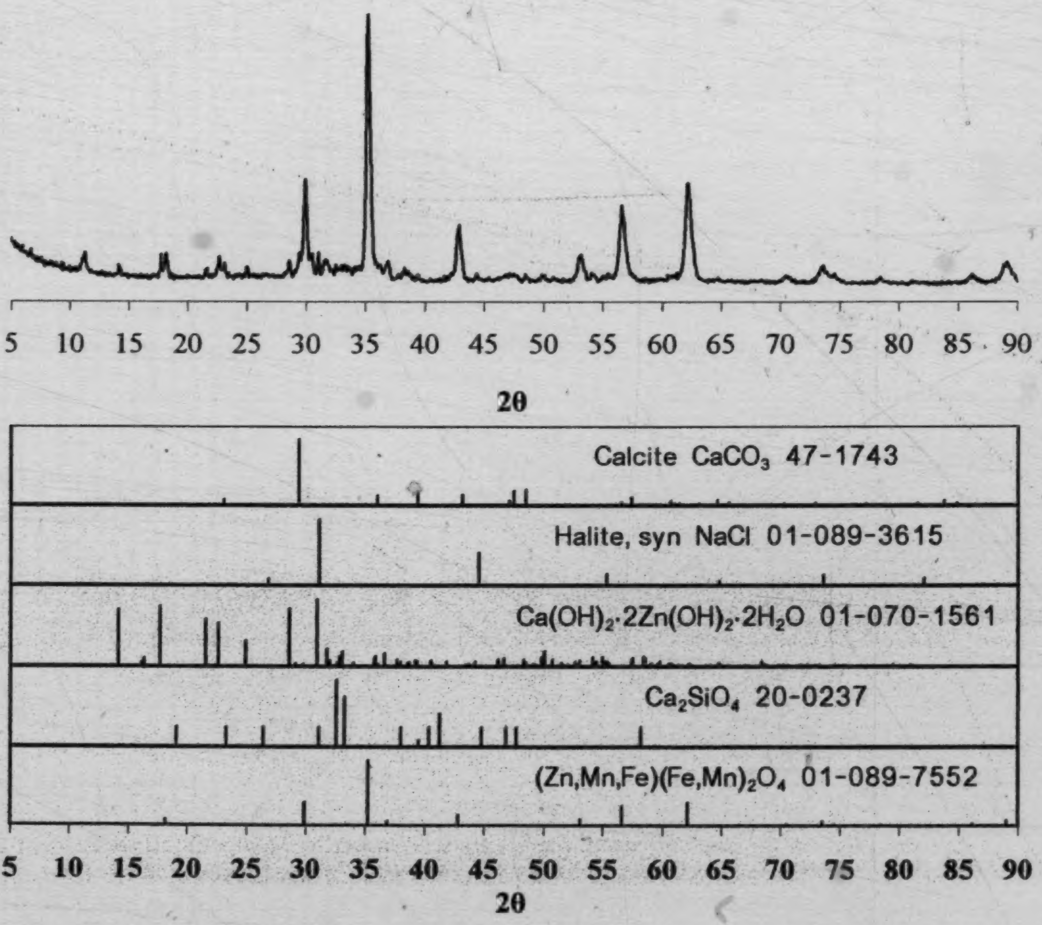

Figure 73 X-ray Diffraction Pattern for Altasteel Electric Arc Furnace Dust

The presence of a hydrated Ca-Zn compound in the dust may indicate that this sample was stored outdoors and was weathered prior to sampling. The x-ray diffraction peaks are less than one third of the intensity of those for the La Oroya ferrite feed, possibly as a result of a lower overall crystallinity in the EAF feed. The poor selectivity observed during diagnostic leaching (i.e., 49% of the zinc dissolved by leaching with sulphuric acid at room temperature, along with a significant portion of the Al, Cd, Cr, Cu, Fe, Ni, Mg, Mn, Mo, V and Si in the EAF dust), particularly with respect to Fe and Mn, is further indication of poor crystallinity in the EAF dust feed.

When viewed with the scanning electron microscope, the EAF dust appears as very fine, often spherical, particles and, in many cases, the texture of the dust shows signs of melting or partial melting (Figure 74), which is likely reflective of the high temperatures at which the dust is produced.

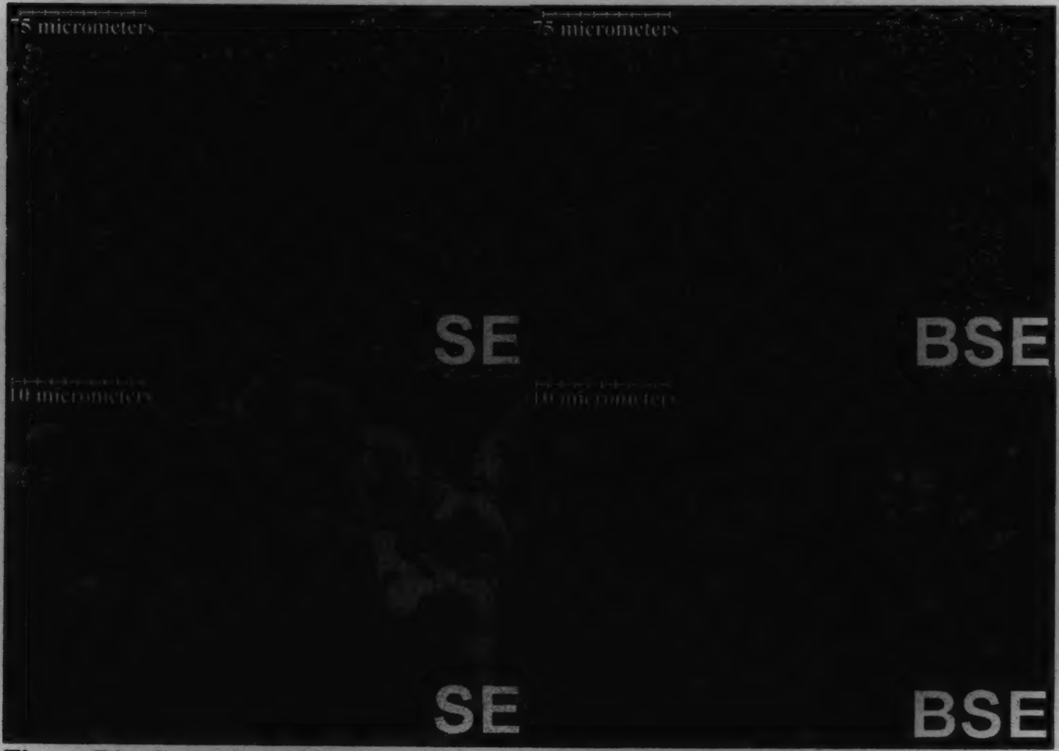

Figure 74 **Secondary Electron (SE) and Backscattered Electron (BSE) Images of Altasteel Electric Arc Furnace Dust Feed Sample**

EDX analysis showed the particles to be quite uniform, containing Ca, Cl, Fe, Pb, Mn, S and Zn, with no visible distinction between phases observed. This is a sharp contrast to the La Oroya ferrite, where major phases existed as distinct particles that could be readily distinguished using SEM/EDX analysis, and is further indication of the lower crystallinity of the EAF dust, relative to the La Oroya ferrite.

5.2 Literature Survey

5.2.1 Mineralogy and Formation of EAF Dust

EAF dust is formed when various molten metallic iron is atomized by the CO released during arc melting and launched into the gas stream where it reacts with volatilized metal oxides, such as Zn, Pb and Cd (132), to form a material containing predominantly a magnetite-franklinite-jacobsite ($Fe_3O_4/ZnFe_2O_4/MnFe_2O_4$) solid solution (133). Depending on the EAF dust sample, other phases such as zincite (ZnO), lime (CaO), periclase (MgO), Fe_2O_3, FeO, Ca_2SiO_4, $Ca_2(Fe,Al)O_4$ and various Ca-Fe-Mn-Zn silicates, along with the occasional entrained metallic iron or coke particle, can also be detected (134-137). Chlorine occurs as NaCl, KCl, $PbCl_2$, $ZnCl_2$ or as Cl-bearing alkali metal oxides while fluorine primarily occurs as CaF_2 or MgF_2 (137). (A number of detailed mineralogical studies on EAF dust have been completed (134-138) and can be consulted for further detail.)

5.2.2 World Production of EAF Dust and Concerns

About 1.2 million tonnes of EAF dust was produced in the US and Canada in 1999 (139), with an additional 500,000 to 600,000 t/y produced in both Europe and Japan (140). This corresponds to between 10 and 20 kg of EAF dust produced per tonne steel (133).

A typical carbon steel EAF dust contains 15 to 25% Zn, 0.5% to 2% Pb, 0.03 to 0.3% Cd, 0.5 to 3% Cl, 0.05 to 0.1% F, 30 to 45% Fe (140). In the developed world, EAF dust is classified as a hazardous waste, as it fails toxicity leaching requirements for Pb, Cd and Cr (133), with the high chloride and fluoride content of the dust causing additional concern, making landfilling of the EAF dust increasingly unpopular. In recent years, it was not uncommon for US EAF plants to spend US$150 to 250 per tonne to dispose of or treat their EAF dust (141); "tipping fees" have been reduced more recently to US$80 to 125 per tonne due to increased competition in the EAF recycling market and improvements in technology (140). Even so, the cost of treating the EAF dust produced during EAF steelmaking can be as high as US$2 to 3 per tonne of steel produced (140). At present, most EAF treatment does not occur locally at the steel mill where the dust is produced, but the dust is instead shipped to a third party for treatment.

5.2.3 Technologies for EAF Treatment

The large tonnages of EAF dust produced worldwide, and the environmental and economic implications of its disposal, has spurred the development of processes to treat EAF dust and there is much more variety than observed for the treatment of ferrite residues from zinc production. Numerous processes have been proposed, developed or piloted; of these, few have been put into production, and several have been tried commercially and abandoned. Tables 35 and 36 list the process type, products and status, as of 2000, of the various EAF treatment technologies.

In general, these processes can be categorized into four categories: pyrometallurgical, hydrometallurgical, hybrid or stabilization processes.

5.2.3.1 Pyrometallurgical Processes

5.2.3.1.1 Waelz Kiln

Waelz kiln processing of EAF dust remains the prominent technology used for the treatment of EAF dusts and other zinc residues, treating 80 to 85% of the EAF dust in the US (141), 83% in Europe and 76% overall worldwide (142). (The Waelz kiln process is discussed in detail in Section 4.2.2.1 and the thermodynamics of the process are presented in detail in the literature (143).) In Europe and Japan, a single stage Waelz kiln process is used, which produces a crude ZnO product which is contaminated with Pb, Cd and halogens. This product is generally treated in Imperial Smelting Process (ISP) plants (Europe) or converted to zinc chemicals or fertilizer (Japan) (141). In the USA and Mexico, most of the EAF dust is treated in a two stage Waelz kiln process, in which the first stage volatilizes Zn, Pb, Cd and halides, and the second kiln is employed to separate a purer zinc oxide from a Pb/Cd halide byproduct (141). Zinc oxide is either processed in zinc electrothermic or leaching plants or used as rubber grade ZnO.

Table 35 **Operating or Developing Technologies for EAF Dust Treatment** (133,141)

Process	Country of Use	Product	Other Products	Fe Recycle	Status (2000)	Process Type
Two Stage Waelz Kiln	US	ZnO[1]		No	Operating	Pyro
Single Stage Waelz Kiln	Europe, Japan, Taiwan	ZnO[1]		No	Operating	Pyro
Two Stage Waelz kiln	Mexico	ZnO[2,3,4]		No	Operating	Pyro
Flame reactor	USA	ZnO[1]		No	Operating	Pyro
MF Furnace	Japan	ZnO[1]		No	Operating	Pyro
Electrothermic Furnace	Japan	ZnO[3]		No	Operating	Pyro
ISF Furnace Tuyere Injection	UK, Germany	PW Zn[5]	Pb	No	Operating	Pyro
Vacuum Heating Reduction	Japan	ZnO[1]		No	Operating	Pyro
EZINEX	Italy	HG Zn[6]	Pb[7], Fe Oxide	Yes	Operating	Hydro
Super Detox (Envirosource)	USA	-		No	Operating	Stabilization
MRP/ASW/PSE	UK, Germany	ZnO[1]		No	Construction	Pyro
BSN	Germany	ZnO[1]		No	Construction	Pyro
CONTOP	Austria, Sweden	ZnO[1]		No	Development	Pyro
HYLSA	Mexico	ZnO[1]		No	Development	Pyro
JCI	South Africa	ZnO[1]		No	Development	Pyro
JCRM, Kawasaki	Japan	Zn		No	Development	Pyro
Midrex Fastmet	Japan	ZnO[1]	DRI	Yes	Development	Pyro
Phoenix Environment	USA	ZnO[1]		No	Development	Pyro
American Metals Recovery (AMR)	USA	ZnO[2]	Pb, DRI	Yes	Development	Hybrid
Hartford Steel	USA	ZnO[2]	Pb	No	Development	Hybrid
Caustic Roasting	Canada, China	Zn	Pb/Cd[7], Fe_2O_3	Yes	Development	Hybrid

[1] Crude ZnO [2] Rubber Grade ZnO [3] Chemical Grade ZnO [4] Fertilizer Grade ZnO [5] Prime Western Grade Zn [6] High Grade Zn [7] Cement

Table 36 **Dormant or Abandoned Technologies for EAF Dust Treatment** (133,141)

Process	Country of Use	Product	Other Products	Iron Recycle	Status (2000)	Process Type
Allmet	USA	PW Zn[5]	Pb	No	Dormant	Pyro
Ausmelt	Australia	ZnO[1]		No	Dormant	Pyro
Enviroplas	South Africa	PW Zn[5]		No	Dormant	Pyro
Envirosource/Metwool	USA	PW Zn[5], ZnO[1]	Pig Iron, Mineral Wool	Yes	Dormant	Pyro
Ammonium Carbonate Leach	Holland	ZnO		No	Dormant	Hydro
Cashman Chloride Leach	USA	HG Zn[6]	Pb[5]	No	Dormant	Hydro
Chloride Pressure Leach	Holland	ZnO		No	Dormant	Hydro
Hatch Acetic Acid Leach	Canada	Impure ZnS		No	Dormant	Hydro
Modified ZINCEX	Spain	SHG Zn	Pb/Cd[7]	No	Dormant	Hydro
Rezada	France	SHG Zn	Pb	No	Dormant	Hydro
Terra Gaia	Canada	ZnS conc.		No	Dormant	Hydro
UBC-Chaparral	Canada	$ZnCO_3$	Pb/Cd[7]	No	Dormant	Hydro
AMAX Roast/Leach	US	Zn		No	Dormant	Hybrid
Elkem	USA	PW Zn[5]	Pb	No	Abandoned	Pyro
HiPlas	UK	Zn	Pig Iron	Yes	Abandoned	Pyro
IMS Plasma	USA	PW Zn[5]	Pb	No	Abandoned	Pyro
Laclede Steel	USA	PW Zn[5]	Pb	No	Abandoned	Pyro
ZTT Ferrolime	USA	ZnO[1]	Ferrolime	Yes	Abandoned	Pyro
MRT I	USA	ZnO[2]	Pb, Fe Oxide	Yes	Abandoned	Hydro
MRT II	USA	ZnO[2]	Pb, Fe Oxide	Yes	Abandoned	Hybrid
IBDR-ZIPP	Canada	SHG Zn	Pb, Pig Iron	Yes	Abandoned	Hybrid
IRC (Nucor), Oregon Steel	USA	-		No	Abandoned	Vitrification

[1] Crude ZnO [2] Rubber Grade ZnO [5] Prime Western Zn [6] High Grade Zn [7] Zinc Dust Cement [8] Super High Grade Zn

In all cases, Waelz kiln processes are energy intensive and produce fairly impure ZnO products and, as such, a number of improvements have been proposed. These include:

a. *Inclined Rotary Reduction Process (IRRP)* -Waelz oxide from a single stage Waelz kiln is pelletized with coal and smelted in a retort with Zn and Pb recovered in an ISP condenser (133).

b. *Pelletization of Feed* – This allows for homogenization and uniformity in the furnace burden (142).

c. *Double Leached Waelz Oxide (DLWO)* – In Europe, the Waelz oxide from the single stage Waelz process is often leached with soda and then water to decrease the halogen content of the oxide and improve its saleability (142).

d. *Optimization of Kiln Heat Pattern* – The zinc in Waelz slag is decreased by controlling the heat pattern of the single stage kiln to minimize FeO formation during reduction (144).

e. *Fluoride Control*– Controlled heating in the single stage Waelz kiln has been proposed to try to fix F as MnF_2 or FeF_2 (145,146).

f. *Slag Treatment* – Magnetic separation to recover magnetite and metallic iron from the Waelz slag, and leaching the non-magnetic fraction to remove heavy metals, has been proposed to improve the disposability/recyclability of the Waelz slag (146).

g. *HTR Process (Japan)/SDHL Process (Germany)* – The single stage Waelz process is modified to operate with a less reducing atmosphere in the latter portion of the kiln (and higher temperatures in the HTR process). In both cases, there is less than 10% metallic iron in the slag, energy and coke requirements are lowered, and higher throughputs are possible for a given kiln (142,147).

h. *Byproduct Usage* – The Horsehead Resource Development Company (HRDC) has marketed the partially metallized Waelz iron slag as road base, road sand and an environmental (heavy metal) absorbent and have developed a hydrometallurgical process to produce cadmium metal and lead sulphate from Pb-Cd residue from the second stage Waelz kiln (148).

5.2.3.1.2 Plasma Based Processes

A number of plasma based processes have been proposed and some have gone to commercialization. The basic process in all cases involves mixing the EAF dust with coke and then passing this mixture through plasma to produce zinc metal and a slag phase. These processes have a number of common problems, including the formation of an alkali halide dross which clogs the metal condenser, the production of low grade metallic zinc (i.e., less than Prime Western grade) and a high Cu and S content in the iron slag which makes it difficult to recycle back to steelmaking (133). With the except of the Plasmadust process, which was operating in 2002 in Sweden and France (149), all the other plasmas based processes that have had plants built, including Hi-Plas, Tetronics Plasma, Enviroplas, IMS Plasma and IBDR-ZIPP, are now shut down with little prospect of reopening (133,141).

5.2.3.1.3 MF and Electrothermic processes

The MF and Electrothermic processes developed in Japan are essentially adaptations of primary zinc smelting processes. Existing facilities were modified to treat EAF dust and both processes would be uneconomic without having similar facilities available for modification (141).

5.2.3.1.4 Flame Reactor

Flash smelting, using the HRDC's Flame Reactor process, produces an iron-rich glassy slag for disposal, and a ZnO product similar in purity to that from a single stage Waelz kiln. This process has the advantage in that it can be operated economically at lower throughput than most Waelz kilns and, thus, has potential to operate on site at large EAF steel operations (133). (The CONTOP process (i.e., a modified KIVCET process) and Inred process are other flash smelting processes that have been proposed or piloted (150).)

5.2.3.1.5 Sealed Arc Furnace Processes

Sealed arc furnace processes, such as Allmet, INMETCO, Elkem, Elkem Multipurpose EAF and Laclede Steel, have similar issues or concerns to other high temperature processes (i.e., high energy consumption, low zinc product quality, and poor recyclability of the iron residues produced), but generally have higher capital costs and are more difficult to operate (133,141).

5.2.3.1.6 Other Pyrometallurgical Processes

In the Metwool process, EAF dust is smelted with coke in a cupola to produce a Zn/Cd/Pb fume, pig iron and a low iron slag which can be spun into mineral wool (141).

Bath smelting (Ausmelt) has been tested on the pilot plant scale, but has yet to be commercialized (151). (The Sirosmelt or Ausmelt technology is discussed in more detail in Section 4.2.2.3.)

5.2.3.2 Hydrometallurgical Processes

5.2.3.2.1 EZINEX and Related Processes

This Italian process is the only hydrometallurgical process in production as of 2002 (141). It uses an ammonium chloride leach to dissolve the zinc, lead and cadmium oxides from the EAF dust, followed by zinc dust cementation to remove Pb and Cd and electrowinning to recover the Zn and allow for recycle of the spent electrolyte. The iron residue is then pelletized with coal and recycled to the EAF (133).

The first MRT process is very similar to the EZINEX process, but zinc is recovered as ZnO instead of electrowon Zn, and no process for recycling the iron values is proposed (141).

5.2.3.2.2 Alkaline Leach Processes

Several processes including the Cardiff, Cebedeau (133) and Rezada processes (141) have been proposed using a caustic leach to leach zinc from the EAF dust, followed by zinc dust cementation of Pb and electrowinning from basic solution to recover Zn. While these processes do not dissolve much iron into solution and make chloride removal easier, only non-ferrite Zn is leached. Therefore, if the residue from these processes were recycled to the EAF, there would be a large recycle of zinc which could affect EAF operation.

In the Ammonium Carbonate process, an ammonia and CO_2 leach is used to recover zinc as zinc ammonium carbonate while the CENIM-LNETI process uses an ammonium carbonate leach, followed by solvent extraction and either $ZnCO_3$ precipitation or electrowinning to recover SHG zinc (133). In both cases, the residue contains zinc ferrite and lead and would require further treatment before recycling to the EAF.

5.2.3.2.3 Sulphuric Acid Leach Processes

Several sulphuric acid leach processes have been proposed. The Modified Zincex process uses a dilute sulphuric acid leach, followed by solvent extraction to separate zinc from the leach solution and electrowinning to recover zinc (133). This process has a low zinc recovery and produces a gypsum residue that would need to be disposed of. AMAX proposed a sulphuric acid leach with autoclave precipitation of hematite to reject iron from solution. Other researchers, such as the Warren Spring Laboratory and Cruells and Nunez, were able to adjust conditions to achieve up to 90% zinc extraction, but produce a solution high in iron that would require neutralization prior to disposal (133). In all these processes, a lead-bearing iron residue is produced which could not be recycled to steelmaking.

5.2.3.2.4 Sulphide Precipitation Processes

The Hatch Acetic Acid Leach is a modification of the UBC-Chaparral process (Section 5.2.3.2.5) and uses an acetic acid leach followed by precipitation of a mixed Cu, Pb and Zn sulphide as its major zinc product (133). Low extractions (i.e., less than 76% Zn and Pb), a low purity and low value product, and a significant recycle of Cu, Pb and Zn in the iron residue, due to the low extractions, have made this process unattractive economically.

Terra Gaia, another Canadian technology, proposes the leaching of EAF dust in an acidic $FeCl_3$ oxidizing pressure leach followed by precipitation of a mixed sulphide to recover the metals values (141). The relatively pure hematite residue would then be recycled to ironmaking or discarded.

5.2.3.2.5 Other Processes

The Cashman $CaCl_2$ pressure leach process was adapted from the treatment of arsenic and copper wastes and produces a Pb/Cd cement along with ZnO as products. This process only recovers non-ferrite Zn and thus recoveries are low (133).

The UBC-Chaparral process has a complex flowsheet with a lime leach, ammonia leach, calcium recovery and recovery of zinc as $ZnCO_3$ (133). While this process produces a non-toxic residue, it suffers from low zinc and lead recoveries (60%).

5.2.3.3 Hybrid Processes

The second MRT process is a modification of the original MRT process where a rotary hearth prereduction step before leaching is used to produce a metallized iron product for recycle (141). (The Hartford Steel process proposed by other researchers (152) is virtually identical to the revised MRT process.)

The other hybrid processes have only reached the development stage. The AMAX Roast/Leach Process involves roasting EAF dust with 10% coke at 950°C, followed by a caustic leach (133). (Recoveries of over 80% Zn and over 90% Cl, Na and K are possible with low lead extractions.) Ye (153), among other researchers (150), proposed sulphation roasting as a possibility for trying to reduce the fluoride in the leach solution after roasting.

Caustic roasting has recently been proposed in two studies as an option for the treatment of EAF dust. Xia and Pickles (154) roasted EAF dust with NaOH at 350 to 450 C and then leached the calcine in 4 M NaOH. Extractions of over 95% Zn, 89% Cd, 65% Pb, 80% Cr, and less than 1% Fe are reported and iron is reported to be present as hematite in the residue. High NaOH additions (200 to 400%) are required to achieve high extractions, but the proposed flowsheet does provide for some recovery of NaOH during basic zinc electrowinning. Youcai and Stanforth (155) report a similar roasting and leaching process, but lower NaOH additions and lower temperatures produced lower zinc recoveries.

Soda ash roasting, followed by hot water leaching to recover the metal values in EAF dust, has also been proposed (156). High extractions of Zn, Pb and Sn (99.6 to 99.8%) were achieved by roasting for 3 h at 850 to 900°C, with little soluble iron and a residue containing predominantly hematite. However, the low iron content (22%) and high metals content (22% Zn, 18.6% Sn and 12.5% Pb) would indicate that this is not a typical carbon steel EAF dust since it would have a much lower ferrite content (i.e., less than 60% $ZnFe_2O_4$) and, therefore, much of the metals would be present as their respective oxides.

5.2.3.4 Stabilization Processes

The Super Detox process was developed and patented by Bethelehem Steel in 1990 (157) and the chemically stabilized EAF dust (CSEAFD) produced was delisted by the EPA in 1995 (158). In this process, EAF dust is mixed with fly ash and lime kiln dust or hydrated lime and then mixed with $Fe(OH)_2/CaSO_4$ solution to produce a viscous paste which is then left to harden. The reactions during this "cementing" process cause the heavy meals in the ash to be immobilized in a calcium aluminosilicate matrix. The resulting CSEAFD contains roughly 33% EAF dust by weight. Since its invention, the Super Detox process has been used to treat over two million tonnes of EAF dust in the United States (159).

Pyroconsolidation by roasting of pyrite cinders with up to 10% EAF in oxygen at 1200°C has been tested as a method to stabilize EAF dusts (160). D'Souza et al. (161) also report a reduction in Cr solubility by heating stainless steel EAF dusts to 1200°C in air.

Several vitrification processes, including the CANMET process (162) and the Oregon Steel process (163), have been developed where EAF dust is mixed with glass forming agents, heated and the melt quenched to produce residues that comply with TCLP or other environmental leaching regulations. At present, vitrification is not practiced commercially (140).

5.2.3.5 Recycling

With the observed difficulties and disadvantages of the various EAF treatment technologies, research has also looked into minimization of EAF dust production by recycling the dust to the EAF. This represents a significant recycling load of zinc, lead and other contaminants which could be detrimental in the long term on steel quality.

To try to remedy this, several processes have been proposed. The Argonne National Lab (164) has developed a process to remove zinc from scrap before charging to the EAF furnace; Mantovani and Takano(165) and McCrea and Pickles (166) promote pelletization of EAF dust with binders such as limestone, Portland Cement or molasses to enhance zinc removal during recycle to the EAF. Sandstroem et al. (167) propose a simple NaCl/HCl leach to recover about 60% of the Zn by precipitation as $ZnCO_3$ to lower the Zn content of the recycled EAF dust, which would then be pelletized with coal and returned to the EAF.

5.2.4 Summary

From this summary of the various technologies developed for the treatment of EAF dust, the following conclusions can be made.

Pyrometallurgical methods using carbon as a reducing agent remain the dominant technology for treating EAF dusts, in spite of high energy consumption, the production of relatively low quality zinc products and the general inability to recycle the iron values from the dust back to the steel furnaces. For the predominant technology of the Waelz kiln, the economics dictate the non-localized treatment of the dust and nearby electrothermic or ISP zinc smelters that can accept the zinc product. However, the high metal recoveries of Zn, Pb and Cd using these processes and their ability to treat a wide variety of zinc residues still make them the first choice for EAF dust treatment.

Hydrometallurgical technologies, with a few exceptions, falter as a result of either poor zinc extractions under less aggressive leaching conditions and poor selectivity between zinc and iron under more aggressive leaching conditions. The leached iron must then be precipitated in a cheap and disposable form, resulting in similar concerns to those experienced in the hot acid leaching of zinc ferrite residues. (Those processes with lower iron extractions generally still have residues containing significant amounts of lead.) Thus, though higher purity, and higher value, zinc products are often possible with hydrometallurgical processes, the residues produced are potentially even more troublesome than the EAF dust and iron recycle to steel furnaces is still not possible.

To date, hybrid processes have either been pursued to try to fix problems in existing hydro- or pyrometallurgical processes or have not gone beyond the development stage. With the predominant industry emphasis on pyrometallurgical methods, less time has been spent on researching these types of techniques; as a result, the only processes described in the literature are unlikely to be economic, or have already been tested without success in the treatment of other similar materials. However, because the advantages of hydrometallurgical and pyrometallurgical processes are potentially complimentary, hybrid processes appear to be the best place to place future research efforts into the recovery of metals from EAF dust.

5.3 Thermodynamic Analysis

As franklinite ($ZnFe_2O_4$) is the zinc bearing major phase in EAF dust, just as it is in the La Oroya zinc ferrite residue, the thermodynamic analysis of the decomposition follows that described previously in Section 4.3. However, the experience gained from applying transformational roasting to the La Oroya zinc ferrite residue can be used to practically limit the number of reagents tested in the scoping and DOE tests. In particular, these tests will focus on metals recovery using either Na_2CO_3 roasting or the reduction of $ZnFe_2O_4$ with carbonaceous reagents to form metal ferrites.

5.4 Scoping Tests

Roasting the EAF dust with Na_2CO_3 was initially evaluated in a scoping test to determine its feasibility and any differences in behaviour from the La Oroya zinc ferrite. In addition, since roasting with sodium salts has been used as a method to recover chromium from ores, a hot water leach of the roasted EAF dust was added to the experimental procedure that was used for the roasting and leaching of the La Oroya zinc ferrite (Section 4.4.1) to determine whether chromium was made water soluble in the roasting process. Sodium carbonate additions of 10, 20, 40, 60 and 80% and a roasting temperature of 900°C were used in the scoping test. (Solutions were analyzed for Cr, Cu, Fe, Pb, Mo, Si, V and Zn while solid samples were fused with lithium metaborate before analyzing for Cr, Fe and Zn.) The results of this test are shown in Figure 75.

These results show that roasting with Na_2CO_3 followed by water leaching can effectively remove up to 98% of the chromium from the EAF dust. Water leaching is quite selective to chromium as less than 1% Fe, 9% Si and 4% Zn are dissolved at the maximum chromium extraction. Molybdenum and vanadium, which are present only in trace quantities in the dust, are quantitatively removed from the ash with water leaching. Chromium extraction then drops off with higher Na_2CO_3 additions and silicon dissolution is dramatically increased, possibly due to the formation of water soluble sodium silicates.

Acid leaching of the water leach residue recovered up to 89% of the zinc in the EAF dust to solution. These zinc extractions show a peak in extraction at 60% Na_2CO_3, similar to that observed with earlier with water soluble chromium. The iron extractions observed are considerably lower (i.e., less than 58%) than the 80 to 90% regularly observed with the Na_2CO_3 roasting of the La Oroya zinc ferrite. However, the lower zinc content of the EAF dust still means that there is a Zn:Fe ratio of 2:1, by weight, in the leach solution, indicating that increased iron removal through the addition of secondary additives during roasting would be desirable for this material.

Because Waelz kiln processing (i.e., carbonaceous reduction) of EAF dust is used internationally for a wide range of dust compositions, scoping tests using carbonaceous reductants were not performed. Instead, a DOE test, where the Altasteel EAF dust is roasted with coal, was conducted to provide a baseline for further DOE tests using these reagents and a basis of comparison with the results from similar tests on the La Oroya zinc ferrite. Thus, this test was conducted using the same conditions that were used for similar tests with zinc ferrite (Section 4.5.2.2.1).

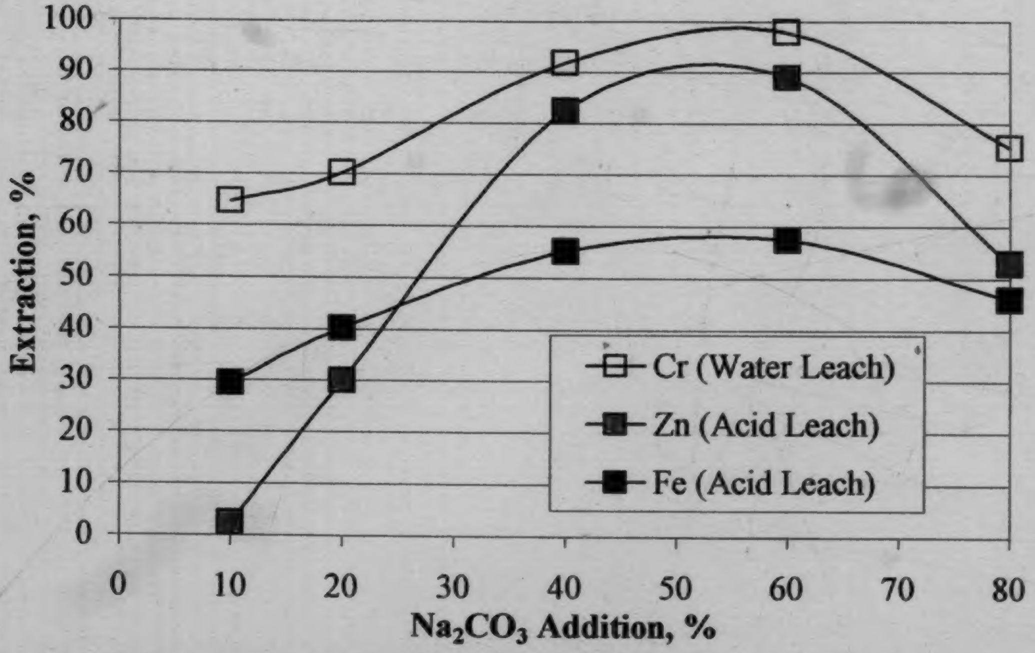

Figure 75 **Effect of Na_2CO_3 Addition on the Extraction of Cr, Zn and Fe from Altasteel EAF Dust**

5.5 Design of Experiment (DOE) Tests for Altasteel EAF Dust

For the Altasteel EAF dust, two series of DOE tests were performed: one set investigating the roasting of zinc ferrite with Na_2CO_3, with or without secondary additives to try to inhibit iron dissolution, (Section 5.5.1) and the second studying the roasting of zinc ferrite with carbonaceous reagents, with or without secondary additives to encourage metal ferrite formation (Section 5.5.2). Systems of reagents that were shown to be ineffective (e.g., Na_2CO_3-$Mg(OH)_2$) for the La Oroya zinc ferrite were not included in the DOE tests for the EAF dust. The experimental conditions used in these two sets of tests are summarized in Tables 37 and 38, respectively, along with the R^2 values of the response surface models fitted to the resulting metals extraction data.

Table 37 **Experimental Conditions Used in Experimental Designs for Roasting EAF Dust with Na_2CO_3 and Resulting Model Variance**

Range of Variables Tested	Na_2CO_3	Na_2CO_3-$CaCO_3$	Na_2CO_3-$MnCO_3$
Temperature, °C	750-950	800-1000	800-1000
Na_2CO_3 Addition, %	40-80	50-90	50-90
Secondary Addition*, %			
$CaCO_3$	-	3.7-14.1^A	-
$MnCO_3$	-	-	4.3-16.3^B
Model R^2			
Zn Extraction	0.895	0.898	0.884
Cr Extraction	0.941	0.765	0.765
Fe Extraction	0.972	0.945	0.986

* Secondary additions represent 25 to 95% of stoichiometric additions assuming formation (A) $CaFe_2O_4$ or (B) $MnFe_2O_4$ from the $ZnFe_2O_4$ in the EAF dust

Table 38 **Experimental Conditions Used in Experimental Designs for Roasting EAF Dust with Carbonaceous Reagents and Resulting Model Variance**

Range of Variables Tested	Coal	Coal-$CaCO_3$
Temperature, °C	900-1100	850-1050
Coal Addition, %	12-20	12-20
$CaCO_3$ Addition*, %	-	3.7-14.1
Model R^2		
Zn Extraction (Total)	0.836	0.923
Zn Fumed	0.702	0.426
Fe Extraction	0.781	0.950

* Secondary additions represent 100 to 200% of stoichiometric additions assuming formation of $CaFe_2O_4$ from the $ZnFe_2O_4$ in the EAF dust

5.5.1 Roasting with Na_2CO_3

After roasting with Na_2CO_3, hot water leaching allows chromium to be selectively leached from the roasted EAF dust (Figure 76). The DOE tests show that 90 to 100% of the chromium can be extracted, with the region of high chromium extraction occurring at around 950°C and Na_2CO_3 additions of about 40%. Hot water leaching is relatively selective to chromium, with less than 6% Zn dissolved, although about 51% of the silicon and almost 100% of the trace amounts of Mo and V in the EAF dust are also dissolved.

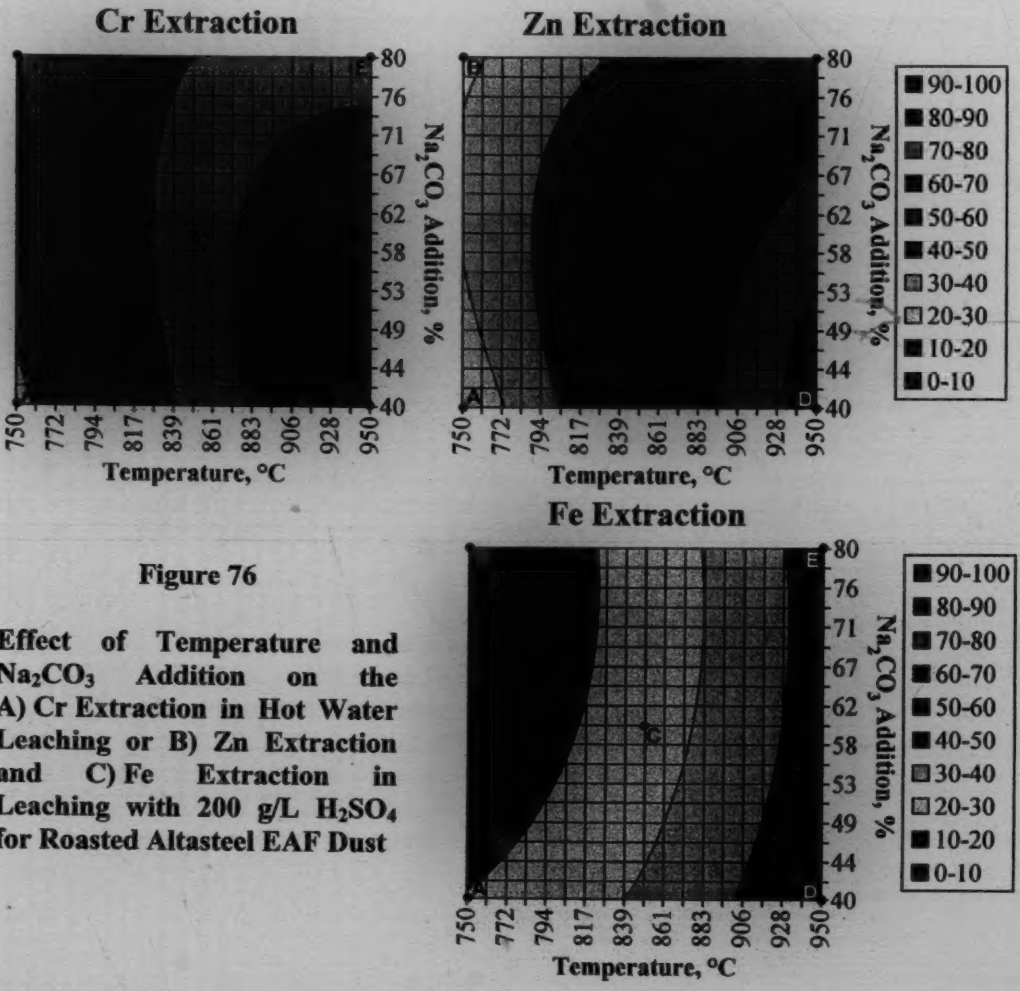

Figure 76

Effect of Temperature and Na_2CO_3 Addition on the A) Cr Extraction in Hot Water Leaching or B) Zn Extraction and C) Fe Extraction in Leaching with 200 g/L H_2SO_4 for Roasted Altasteel EAF Dust

Subsequent leaching with 200 g/L H_2SO_4 results in maximum zinc extractions of 80 to 90% in a region occurring around 950°C and 40% Na_2CO_3 (Figure 77). At these conditions, chromium extractions with hot water leaching are 90 to 100% and iron extractions with 200 g/L H_2SO_4 leaching are 40 to 50%. The magnitude of the zinc, iron and chromium extractions, and the Na_2CO_3 additions required to achieve them, are consistent with the results from the scoping tests; however, these extractions are observed at 950°C, instead of 900°C in the scoping tests. Compared to roasting the La Oroya ferrite with Na_2CO_3, lower Na_2CO_3 additions are required to achieve high zinc extractions during roasting of the EAF dust although, in both cases, the Na_2CO_3 additions required to achieve high zinc extractions correspond to additions of around 250% of stoichiometric for the reaction of Na_2CO_3 with $ZnFe_2O_4$. Based on this response surface model, higher roasting temperatures would be required to reach zinc extractions of over 90% for the EAF dust. The iron extraction from the EAF dust is much lower throughout and shows a much stronger dependence on temperature than on Na_2CO_3 addition.

Samples at various conditions described by the model for roasting with Na_2CO_3 were analyzed using x-ray diffraction (Points A through E on Figure 76). The identified phases are listed in Table 39 while the diffraction patterns are shown in Figure 77.

Table 39 Phases Identified by XRD Analysis of EAF Dust Roasted with Na_2CO_3

Sample	Identified Phases (in order of intensity)
A	$(Zn,Mn,Fe)(Fe,Mn)_2O_4$, $Ca_2Fe_2O_5$, α-$NaFeO_2$, ZnO, Ca_2SiO_4
B	$(Zn,Mn,Fe)(Fe,Mn)_2O_4$, Na_2CO_3, α-$NaFeO_2$, $Ca_2Fe_2O_5$, Ca_2SiO_4, ZnO
C	α-$NaFeO_2$, $(Zn,Mn,Fe)(Fe,Mn)_2O_4$, ZnO, $Ca_2Fe_2O_5$, Ca_2SiO_4
D	α-$NaFeO_2$, $Ca_2Fe_2O_5$, ZnO, β-$NaFeO_2$, Ca_2SiO_4
E	$(Zn,Mn,Fe)(Fe,Mn)_2O_4$, α-$NaFeO_2$, $Ca_2Fe_2O_5$, ZnO, β-$NaFeO_2$, Ca_2SiO_4

The phases observed with x-ray diffraction show some similarities to those observed during Na_2CO_3 roasting of the La Oroya zinc ferrite. Little reaction occurs at 750°C, with the mixture of spinels ($(Zn,Mn,Fe)(Fe,Mn)_2O_4$) as the major phase and α-$NaFeO_2$ as a minor phase, in Samples A and B. (Unreacted Na_2CO_3 is also observed in Sample B.) As the temperature increases, the conversion to $NaFeO_2$ from $(Zn,Mn,Fe)(Fe,Mn)_2O_4$ increases, but α-$NaFeO_2$ is present in greater quantities than β-$NaFeO_2$ at all temperatures tested. (In Na_2CO_3 roasting of the La Oroya ferrite, the formation of β-$NaFeO_2$ is preferred at temperatures of 950°C and higher.) Zinc oxide is detected in all samples.

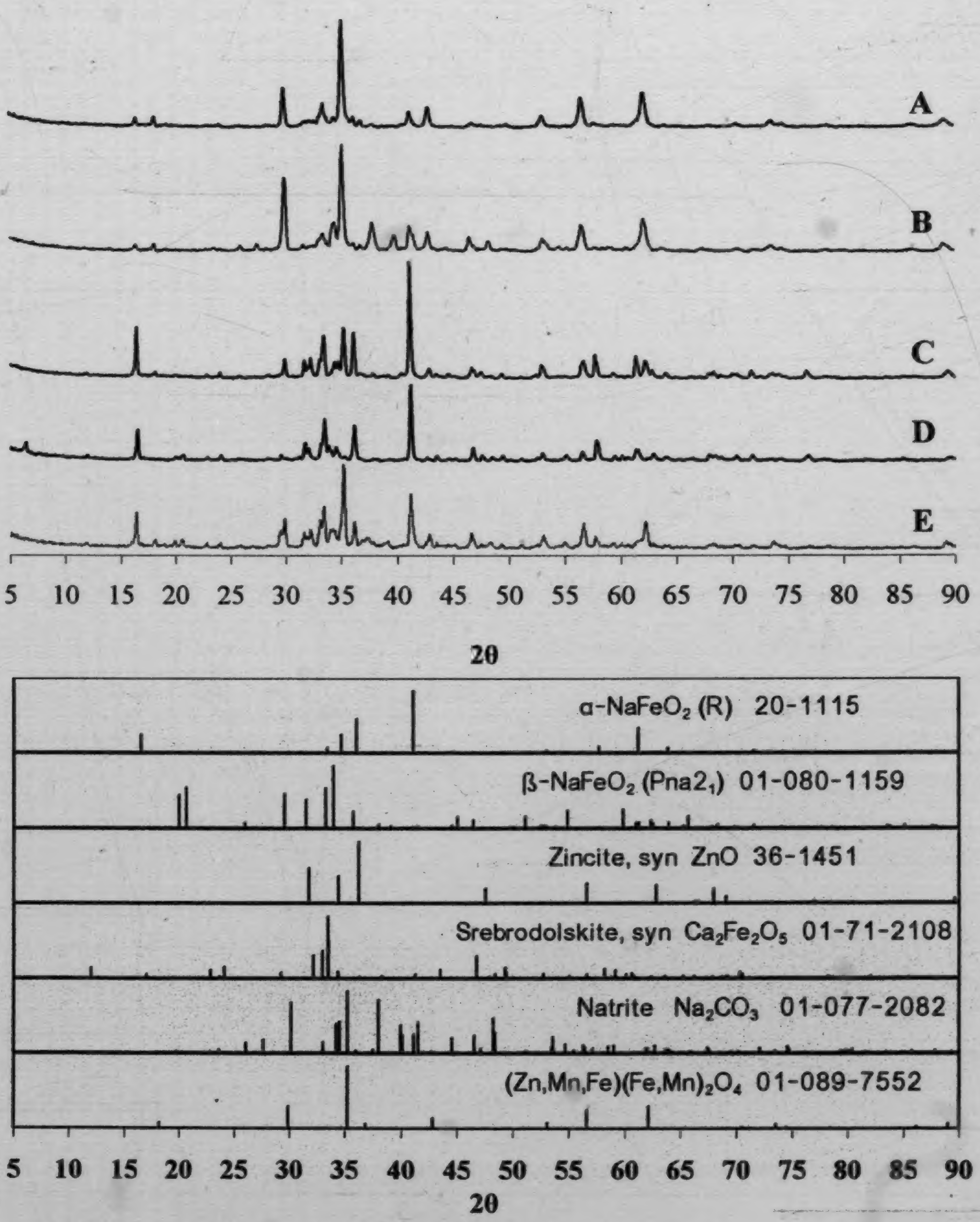

Figure 77 XRD Patterns of EAF Dust Roasted with Na_2CO_3

Larnite (Ca_2SiO_4), which is present in the dust before roasting, appears to be the major silicate phase in the roasted EAF dust. Calcium which is not associated with silicon appears to react, either with the $NaFeO_2$ formed during roasting or with magnetite

(Fe_3O_4) in the dust, to form srebrodolskite ($Ca_2Fe_2O_5$), which is present in all the samples analyzed.

Samples D (950°C, 40% Na_2CO_3) and E (950°C, 80% Na_2CO_3) were both examined using SEM/EDX analysis after roasting and a number of distinct particles were detected (Figures 78 and 79).

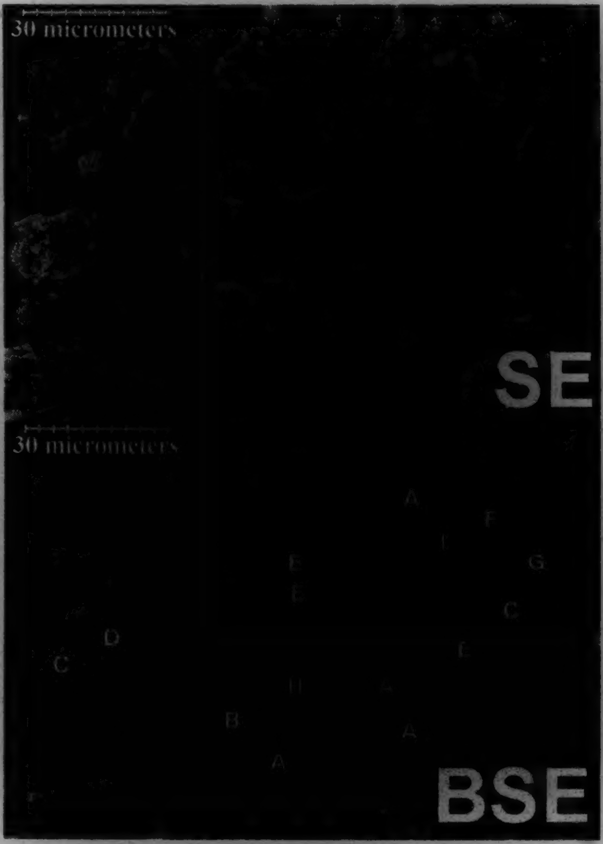

Figure 78
Secondary Electron (SE) and Backscattered Electron (BSE) Images of EAF Dust after Roasting at 950°C with 40% Na_2CO_3 (Sample D)

In Sample D (Figure 78), the bright phase is identified as zinc oxide (A) and the presence of an assortment of metal ferrites are indicated by the EDX analysis. Particles high in Fe, Mn, Zn and O (i.e., (Zn, Mn)Fe_2O_4 (B)), Ca, Fe and O (i.e., $Ca_2Fe_2O_5$ (C)) and Mn, Fe and O (i.e., $MnFe_2O_4$ (D)) were observed along with several particles which appear to be mixtures of ferrite phases, which included particles high in Fe, Mn, Na and O (i.e., $MnFe_2O_4$/$NaFeO_2$ (E)) and high in Ca, Fe, Mn, Na and O (i.e., $Ca_2Fe_2O_5$/$MnFe_2O_4$/$NaFeO_2$ (F)). One particle (G) contained a significant amount of magnesium, along with Na, Fe and O, which may indicate that the magnesium in the dust becomes associated with the soluble $NaFeO_2$ phase during roasting. The darker particles in the field of view in Figure 78 are either silicates, aluminosilicates or aluminates, with particles high in Ca, Si and O (i.e.,

Ca_2SiO_4 (H)) and high in Al, Ca, Fe, Si and O (i.e., a mixture of Ca- or Fe- silicates, aluminates or aluminosilicates (I)).

In Sample E, zinc oxide was not visible as a distinct phase in the field of view of Figure 79, even though it was detected in this sample using x-ray diffraction. Instead, the bright phase (F) observed in Figure 79 is high in Pb and O (i.e., PbO). Iron is associated with two phases: the larger light grey particles (D), which are high in Fe and O (i.e., Fe_3O_4), and the smaller, more euhedral light grey particles (E), which are high in Mn and Fe, but contain low levels of Zn (i.e.,$(Zn,Mn)Fe_2O_4$). The darker particles in Figure 79 are either high in Na, K and S (i.e., $(Na,K)_2SO_4$ (A)), high in Na and O (i.e., Na_2O or Na_2CO_3 (B)), or high in Ca and Si (i.e.,Ca_2SiO_4 (C)). No particles containing Cr, Cl or F were identified in Samples D or E.

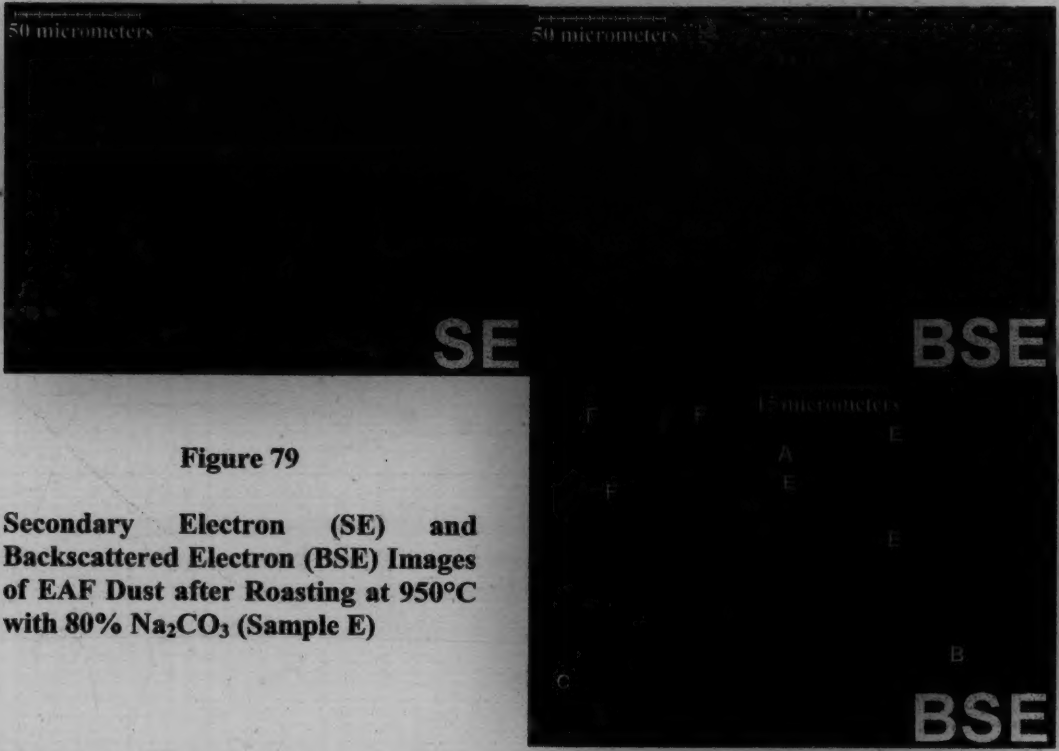

Figure 79

Secondary Electron (SE) and Backscattered Electron (BSE) Images of EAF Dust after Roasting at 950°C with 80% Na_2CO_3 (Sample E)

After leaching Sample E with hot water, the sodium-bearing phases (i.e., $(Na,K)_2SO_4$, Na_2O or Na_2CO_3) are dissolved while the other phases remain (Figure 80). Particles high in Fe and O (i.e., Fe_3O_4 (A)), Zn, Mn, Fe and O (i.e., $(Zn,Mn)Fe_2O_4$ (B)), Fe, Mn and O (i.e., $MnFe_2O_4$ (C)), Ca and Si (i.e., Ca_2SiO_4 (D)) and Pb and O (i.e., PbO (E)) are observed in this sample after water leaching.

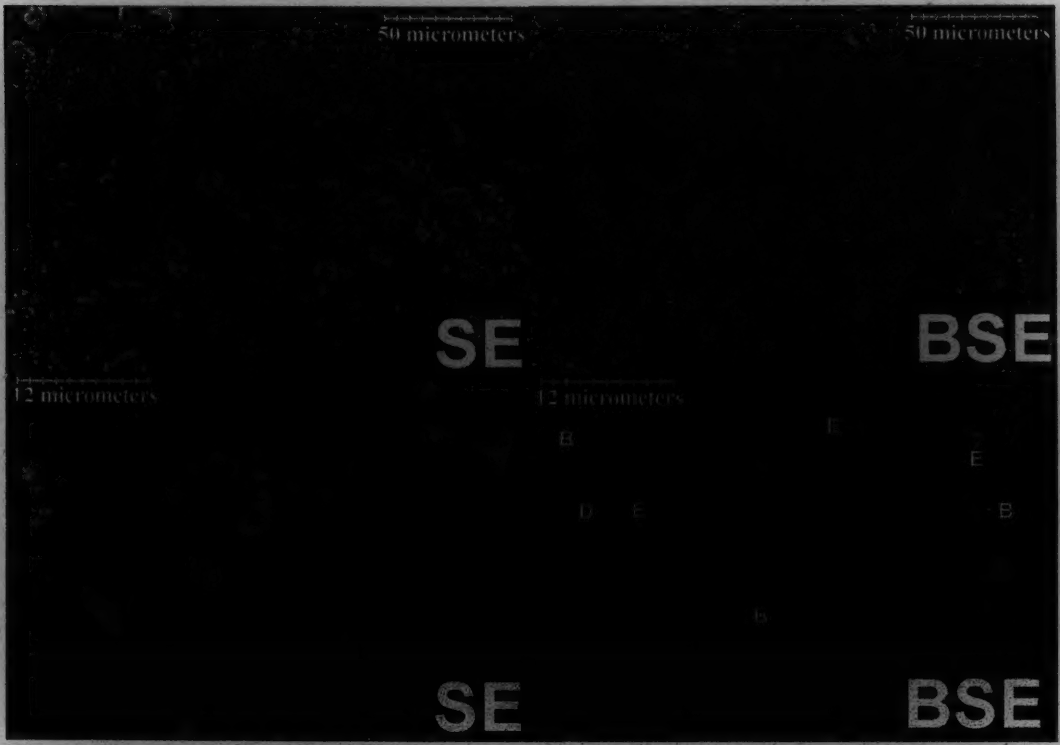

Figure 80 **Secondary Electron (SE) and Backscattered Electron (BSE) Images of EAF Dust after Roasting at 950°C with 80% Na_2CO_3 and Leaching with Hot Water (Sample E)**

After leaching with 200 g/L H_2SO_4, $(Zn,Mn,Fe)(Fe,Mn)_2O_4$, magnetite (Fe_3O_4) and gypsum ($CaSO_4\cdot 2H_2O$) are identified with XRD in the residues (Table 40 and Figure 81).

Table 40 **Phases Identified by X-ray Diffraction Analysis of EAF Dust after Roasting with Na_2CO_3 and Leaching with 200 g/L H_2SO_4**

Sample	Identified Phases (in order of intensity)	Leaching Wt. Loss, %
A	$(Zn,Mn,Fe)(Fe,Mn)_2O_4$, $CaSO_4\cdot 2H_2O$	27[1], 29[2]
B	$(Zn,Mn,Fe)(Fe,Mn)_2O_4$, $CaSO_4\cdot 2H_2O$	44[1], 56[2]
C	Fe_3O_4, $CaSO_4\cdot 2H_2O$	16[1], 58[2]
D	Fe_3O_4, $CaSO_4\cdot 2H_2O$,	40[1], 48[2]
E	$CaSO_4\cdot 2H_2O$, $(Zn,Mn,Fe)(Fe,Mn)_2O_4$	32[1], 53[2]

[1] Hot Water Leach [2] Acid Leach

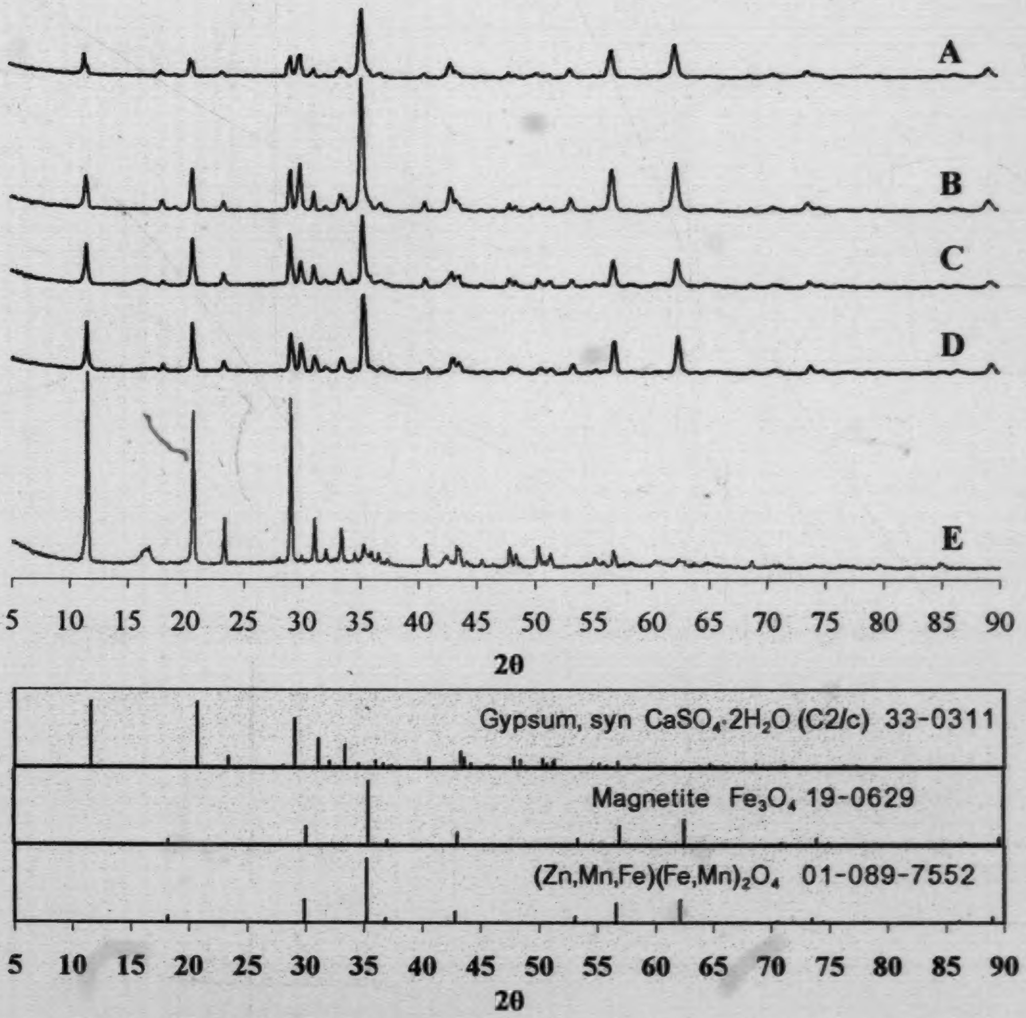

Figure 81 **XRD Patterns of EAF Dust Residue after Roasting with Na_2CO_3 and Leaching with 200 g/L H_2SO_4**

Samples D (950°C, 40% Na_2CO_3) and E (950°C, 80% Na_2CO_3) were both examined using SEM/EDX analysis after acid leaching (Figures 82 and 83). SEM/EDX analysis of sample D (Figure 82) showed gypsum to be the major phase (C), with particles high in Fe, Mn and O (i.e., $MnFe_2O_4$ (A)) being the major iron-bearing phase and particles high in Fe, Mn, Zn and O (i.e., residual, unreacted $(Zn,Mn)Fe_2O_4$ (B)) also present to a lesser degree. In Sample E (Figure 83), gypsum is again the major phase (A), but particles high in Ca, Mn, Fe and O (i.e., possibly a mixture of $Ca_2Fe_2O_5$ and $MnFe_2O_4$ (B)) represent the major iron-bearing phase, with particles high in Mn, Fe, Zn and O (i.e.,

$(Zn,Mn)Fe_2O_4$ (D)) also present. (Particles with the label C in Figure 83 represent a mixture of gypsum (A) and the Mn-ferrites (B).)

30 micrometers
30 micrometers
C
B
D
C
C
C
SE
BSE

Figure 82 Secondary Electron (SE) and Backscattered Electron (BSE) Images of EAF Dust after Roasting at 950°C with 40% Na_2CO_3 and Leaching with 200 g/L H_2SO_4 (Sample D)

50 micrometers
50 micrometers
SE
BSE
10 micrometers
10 micrometers
C
A
A
C
A
D
A
SE
BSE

Figure 83 Secondary Electron (SE) and Backscattered Electron (BSE) Images of EAF Dust after Roasting at 950°C with 80% Na_2CO_3 and Leaching with 200 g/L H_2SO_4 (Sample E)

Larnite (Ca_2SiO_4) was not observed in SEM/EDX analysis of the residue, while srebrodolskite ($Ca_2Fe_2O_5$) is only perhaps present in mixtures of metal ferrites in the SEM/EDX analysis of the residue, even though both phases were consistently detected in the roasted samples with x-ray diffraction and SEM/EDX. This may indicate that the Ca ferrites and/or Ca-silicates formed during roasting may have been either dissolved or partially dissolved during sulphuric acid leaching, with much of the calcium reprecipitating from solution as gypsum.

Iron deportment in the Na_2CO_3 roasting and sulphuric acid leaching of the EAF dust is considerably different from that observed during roasting of the La Oroya ferrite. For example, in Sample C, iron extractions are only 40 to 50%, in a region where zinc extractions are greater than 80%, but this level of iron extraction is maintained in Sample D, even with much lower zinc extractions, and, hence, much lower conversions of $ZnFe_2O_4$ to $NaFeO_2$ and ZnO. Since the EAF dust contains iron as franklinite ($ZnFe_2O_4$), magnetite (Fe_3O_4) and jacobsite ($MnFe_2O_4$), while iron is only present in the La Oroya ferrite as franklinite, this difference in the leaching behaviour may be caused by the reaction of these other iron minerals with Na_2CO_3 during roasting.

To test this hypothesis, a rough iron balance was conducted, using the available results from leaching, XRD and SEM/EDX analysis, to try to explain the deportment of iron in the EAF dust with the results shown in Table 41. Figure 84 plots free energy versus temperature for several potential reactions.

The iron balance for the feed is calculated assuming 100% of Zn and Mn in the feed are present as $ZnFe_2O_4$ and $MnFe_2O_4$ and the balance of the iron is present as Fe_3O_4. The iron balance for Samples A to E is calculated using zinc extractions to determine the conversion of $ZnFe_2O_4$ to $NaFeO_2$ and assuming that all unleached manganese is present as $MnFe_2O_4$, that Fe_3O_4 formed during roasting is insoluble under the acid leaching conditions used and that all calcium that is not associated with silicon as Ca_2SiO_4 reacts with Fe_3O_4 to form srebrodolskite ($Ca_2Fe_2O_5$). (Thermodynamically, reaction with Fe_3O_4 should be preferred over reaction with $NaFeO_2$ formed from reaction of Na_2CO_3 with

$ZnFe_2O_4$ (Figure 84). Since ferrous iron is not detected in any of the leach solutions by the addition of diphenylamine, and no oxidant is used during leaching, it is likely that any ferrous iron is oxidized during roasting. For the iron balance, srebrodolskite ($Ca_2Fe_2O_5$) was assumed to leach completely in sulphuric acid and the magnetite content of Sample E was assumed to be greater than zero, but less than the detection limit for phases using x-ray diffraction (i.e., 5%).

Table 41 Deportment of Iron Minerals during Na_2CO_3 Roasting and H_2SO_4 Leaching of Altasteel EAF Dust

Iron Minerals	% of Total Iron in Feed					
	Feed	Sample A	Sample B	Sample C	Sample D	Sample E
$ZnFe_2O_4$	50.3	38.2	42.5	23.7	5.0	27.5
$MnFe_2O_4$	22.7	22.3	22.2	22.2	22.0	22.1
Fe_3O_4	27.0	19.7	19.7	19.7	19.7	4.0
$Ca_2Fe_2O_5$	0.0	7.3	7.3	7.3	7.3	7.3
$NaFeO_2$	0.0	12.6	8.3	27.1	46.0	39.1
Total	100.0	100.0	100.0	100.0	100.0	100.0
Fe Extraction						
Projected, %*		19.8	15.6	34.4	53.3	46.4
Actual, %		21.2	9.5	28.8	54.2	46.5
Difference, %		-1.4	6.1	5.6	-0.9	-0.1

* Calculated assuming the total dissolution of $NaFeO_2$ and $Ca_2Fe_2O_5$ during leaching

The projected iron extraction from this balance (Table 41) is quite close to the measured iron extraction for these samples. From this analysis, it becomes quite apparent that the srebrodolskite phase ($Ca_2Fe_2O_5$) formed during roasting at these temperatures must be soluble, or partially soluble, during leaching, as the iron extractions observed at low temperatures (Samples A and B) cannot be accounted for by the formation and dissolution of $NaFeO_2$ from the reaction of Na_2CO_3 with $ZnFe_2O_4$. At higher temperatures and Na_2CO_3 additions in Sample E, the conversion of $ZnFe_2O_4$ to $NaFeO_2$ and the leaching of $Ca_2Fe_2O_5$ only account for the extraction of 30.1% of the iron in the dust, compared to an actual iron extraction of 46.5% during leaching. This discrepancy may indicate that, at the higher temperatures and Na_2CO_3 additions used in roasting

Sample E, magnetite (Fe_3O_4) may react with Na_2CO_3 to form $NaFeO_2$, resulting in additional acid soluble iron. (Because some Fe-O minerals (i.e., Fe_3O_4) are observed in Sample E after roasting, it is likely that this reaction is incomplete, but occurs to a sufficient extent to decrease the intensity of magnetite peaks so that magnetite cannot be readily identified using x-ray diffraction.) Since Na_2CO_3 is added well in excess of the stoichiometric amount required to react with $ZnFe_2O_4$ in Sample D, it is possible that magnetite also partially reacts with Na_2CO_3 in Sample D. However, because magnetite (Fe_3O_4) is observed using x-ray diffraction in the leach residue of Sample D, and high zinc extractions are achieved during leaching, it is likely that this reaction is not extensive under those conditions.

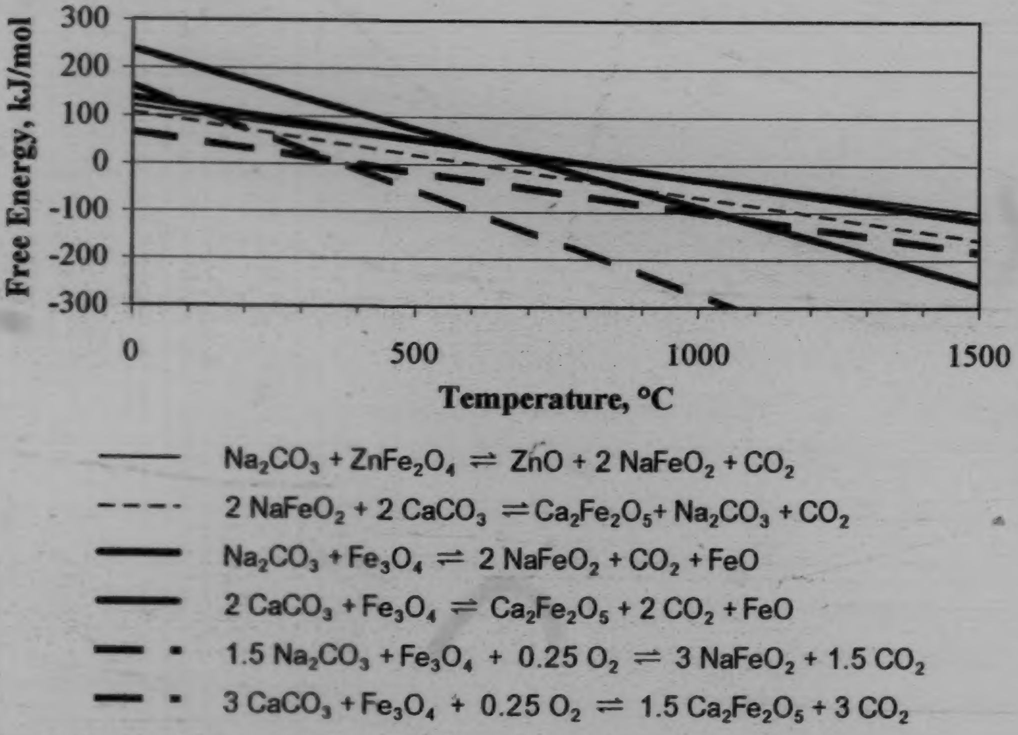

Figure 84 Reactions of $ZnFe_2O_4$ and Fe_3O_4 with Na_2CO_3 and $CaCO_3$

Thus, this analysis indicates that, though the iron extractions for Samples D and E are similar in magnitude, the iron extractions observed are caused, in part, by the preferential reaction of Na_2CO_3 with different minerals at high and low Na_2CO_3 additions. Based on this analysis, it appears that, at 950°C, the reaction of $ZnFe_2O_4$ with Na_2CO_3 is preferred at lower Na_2CO_3 additions while reaction of Na_2CO_3 with Fe_3O_4 is preferred at higher Na_2CO_3 additions. However, in both samples, the abundance of Mn-ferrite particles in the SEM micrographs, both before and after leaching, would indicate that the lower iron extractions during leaching are a result of the formation of insoluble Mn-ferrites during roasting.

5.5.1.1 Secondary Additions to Control Iron Dissolution

Further DOE tests were performed to try to further depress iron extractions through the addition of secondary additives to form insoluble metal ferrites during roasting. The thermodynamics for the formation of these metal ferrites is discussed in Section 4.5.2.1.1. Secondary additions of $CaCO_3$ and $MnCO_3$ were tested. Additions of $Mg(OH)_2$ were not tested because of its ineffectiveness as a secondary additive in the Na_2CO_3 roasting of La Oroya zinc ferrite.

Based on the results of the DOE test where the EAF dust was roasted with Na_2CO_3, the temperature range and Na_2CO_3 additions were increased to 800 to 1000°C and 50 to 90%, respectively, to try to increase the zinc extractions observed during roasting. To allow easier comparison with the results from Sections 5.5.1.1.1 and 5.5.1.1.2, Figure 85 shows the extrapolation of the response surface models for Cr, Zn and Fe for the roasting of EAF dust with Na_2CO_3.

Lower additions of $CaCO_3$ (3.7 to 14.1%) and $MnCO_3$ (4.3 to 16.3%) were made than were used during the DOE tests using secondary additives for the La Oroya zinc ferrite. These additions were determined based on the stoichiometric additions that would be required to form $CaFe_2O_4$ or $MnFe_2O_4$ from the zinc ferrite in the EAF dust.

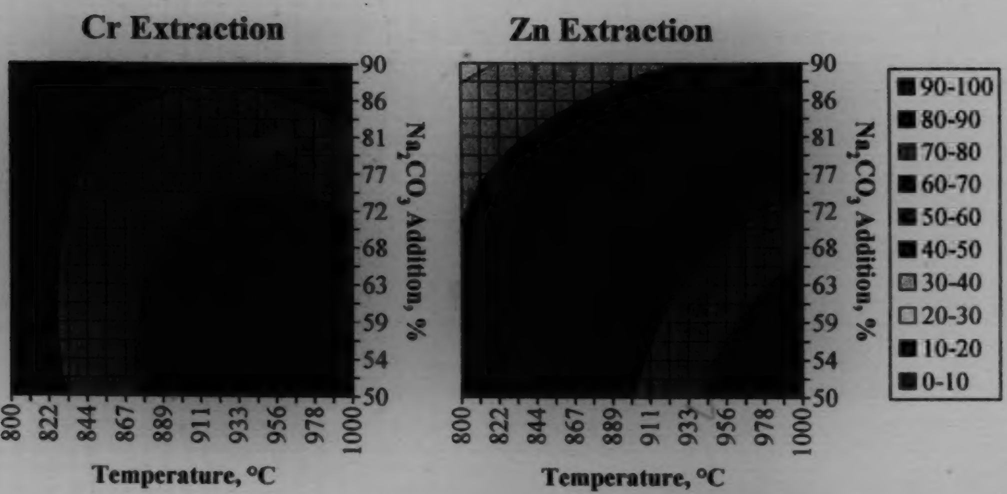

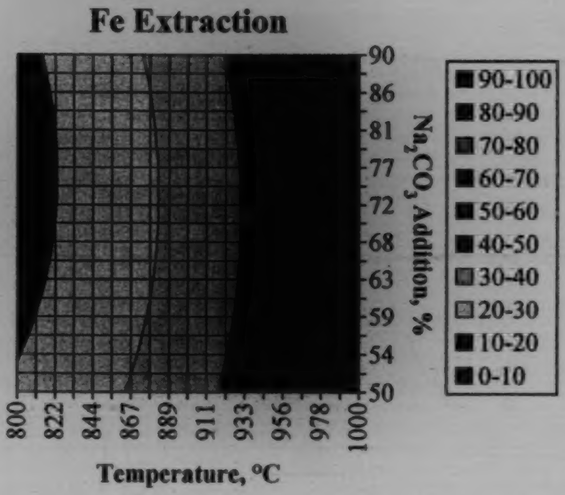

Figure 85

Extrapolation of the Response Surface Models Describing the Effect of Temperature and Na$_2$CO$_3$ Addition on the A) Chromium Extraction in Hot Water Leaching or B) Zinc Extraction and C) Iron Extraction in Leaching with 200 g/L H$_2$SO$_4$ for Roasted Altasteel EAF Dust

5.5.1.1.1 Roasting with $CaCO_3$ as a Secondary Additive

Compared with roasting with Na_2CO_3 alone (Figure [illegible]), roasting with $CaCO_3$ as a secondary additive significantly broadened the area of maximum chromium extraction (90 to 100%) possible with water leaching (Figure 86) at the $CaCO_3$ additions tested, making these extractions possible over a wider range of temperatures and Na_2CO_3 additions. However, this model also indicates that the size of this region decreases as $CaCO_3$ additions are increased.

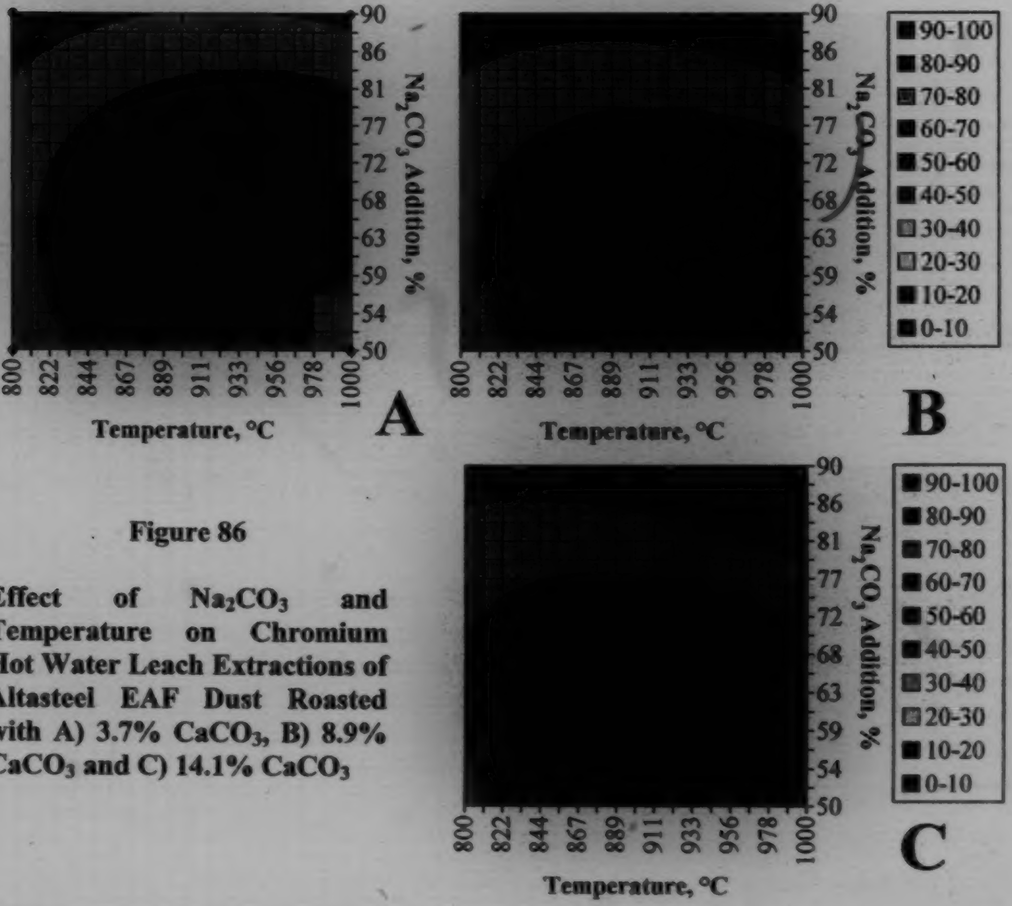

Figure 86

Effect of Na_2CO_3 and Temperature on Chromium Hot Water Leach Extractions of Altasteel EAF Dust Roasted with A) 3.7% $CaCO_3$, B) 8.9% $CaCO_3$ and C) 14.1% $CaCO_3$

The shape of the zinc extraction model for leaching the roasted ash with 200 g/L H_2SO_4 closely follows the trends in extraction observed in the scoping tests and roasting with Na_2CO_3 alone (Figure 85), with a maximum around 50% Na_2CO_3 and a decrease in extractions at higher Na_2CO_3 additions (Figure 87). (Figures 85 and 87 indicate that the increase in roasting temperature to around 1000°C makes zinc extractions of over 90% possible.) With increasing $CaCO_3$ additions, the region of 90 to 100% zinc extraction increases in size, making these extractions possible at lower temperatures and a broader range of Na_2CO_3 additions. Chromium extractions from water leaching are consistently greater than 90% in the regions where zinc extractions are over 90%.

The addition of $CaCO_3$ greatly affects the extraction of iron from the EAF dust during leaching. For roasting with Na_2CO_3 alone, iron extractions were 50 to 60% in the region of 90 to 100% zinc extraction (Figure 85), but iron extractions for that same range of zinc extractions when roasting with Na_2CO_3 and $CaCO_3$ increase from 60 to 80% to 60 to 90% with increasing $CaCO_3$ additions (Figure 87). As well, the model indicates that, for roasting the EAF dust with Na_2CO_3 and $CaCO_3$, the iron extraction is dependent both on temperature and Na_2CO_3 addition, with increasing temperature and decreasing Na_2CO_3 additions causing an increase in the iron extraction observed. This differs significantly from the trend in Figure 85, which showed a strong dependence of the iron extraction on the roasting temperature, but little effect of Na_2CO_3 addition on the extraction.

Samples at various conditions described by the model for roasting with Na_2CO_3 and the lowest $CaCO_3$ addition tested (3.7%) were analyzed using x-ray diffraction (Points A through D on Figures 86A and 87A). The identified phases are listed in Table 42 while the diffraction patterns and major phases observed are shown in Figure 88.

Table 42 Phases Identified by XRD Analysis of EAF Dust Roasted with Na_2CO_3 and 3.7% $CaCO_3$

Sample	Identified Phases (in order of intensity)
A	α-$NaFeO_2$, $Ca_2Fe_2O_5$, $(Zn,Mn,Fe)(Fe,Mn)_2O_4$, ZnO
B	$Ca_2Fe_2O_5$, $(Zn,Mn,Fe)(Fe,Mn)_2O_4$, α-$NaFeO_2$, ZnO
C	α-$NaFeO_2$, $Ca_2Fe_2O_5$, ZnO, β-$NaFeO_2$, $CaCO_3$
D	$(Zn,Mn,Fe)(Fe,Mn)_2O_4$, α-$NaFeO_2$, $Ca_2Fe_2O_5$, β-$NaFeO_2$, ZnO

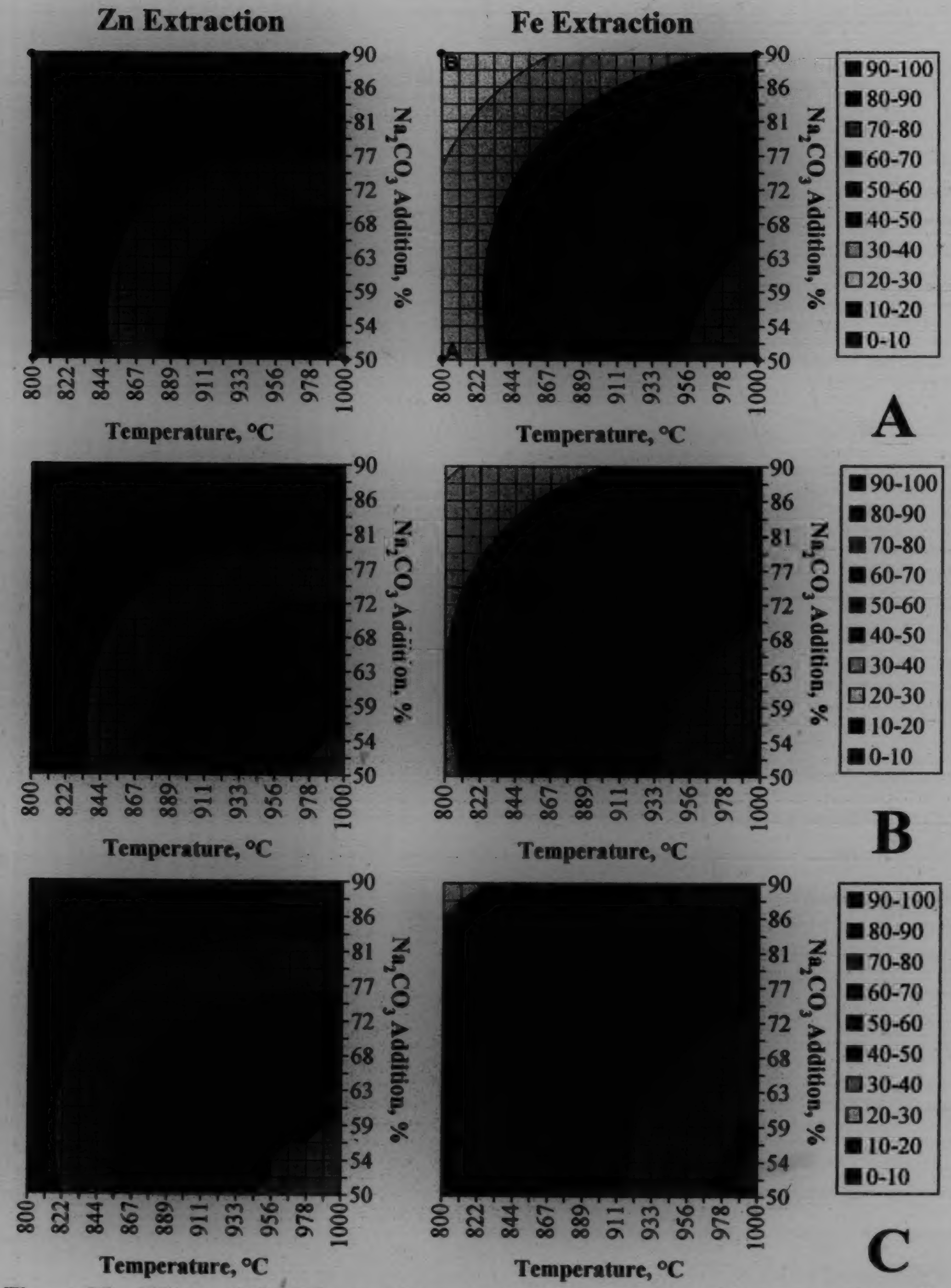

Figure 87 Effect of Na$_2$CO$_3$ and Temperature on Zinc and Iron Extractions from Altasteel EAF Dust Roasted with A) 3.7% CaCO$_3$, B) 8.9% CaCO$_3$ and C) 14.1% CaCO$_3$ after Leaching with 200 g/L H$_2$SO$_4$

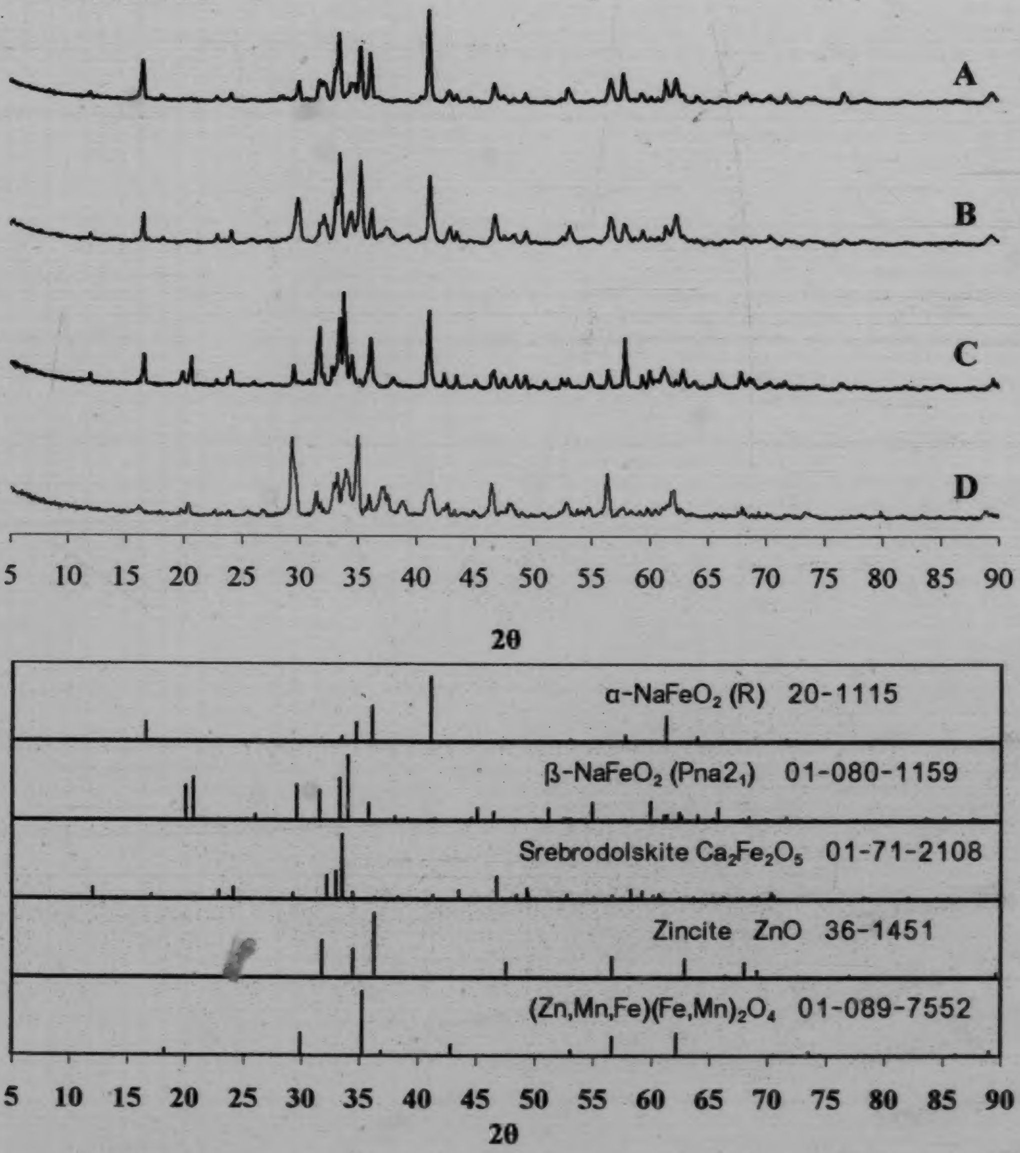

Figure 88 **XRD Patterns of EAF Dust Residue after Roasting with Na_2CO_3 and $CaCO_3$**

With the increase in the range of roasting temperatures, significant reaction of the $ZnFe_2O_4$ in EAF dust occurred and, as a result, $NaFeO_2$ and ZnO were present in all the samples tested using XRD. However, as noted previously for roasting EAF dust with Na_2CO_3, the formation of α-$NaFeO_2$ is predominant, even at higher temperatures, which differs from the behaviour observed in roasting the La Oroya zinc ferrite where β-$NaFeO_2$ is preferred at temperatures of 950°C and higher. Srebrodolskite is observed in all four samples, and is the major phase in Samples B and C, likely forming from the preferential reaction of free calcium with magnetite (Fe_3O_4) or $NaFeO_2$ as noted in Section 5.5.1. No spinel-type compounds are observed in the x-ray diffraction pattern of Sample C, where zinc extractions of 90 to 100% were achieved, while $(Zn,Mn,Fe)(Fe,Mn)_2O_4$ remains as the major phase at higher Na_2CO_3 additions in Sample D. Specific silicate phases could not be identified using x-ray diffraction but, based on the phases observed in Section 5.5.1 and in the EAF dust feed, it is likely that the majority of silicon is present in the roasted dust as larnite (Ca_2SiO_4)

A number of different particles can be observed in Sample C (1000°C, 50% Na_2CO_3, 3.7% $CaCO_3$) after roasting using back-scattered SEM imaging and EDX analysis (Figure 89). The zinc oxide (A) and srebrodolskite (C) phases identified using XRD are visible with the SEM, but a distinct Na-Fe phase (i.e., $NaFeO_2$) was not detected in the field of view. Other phases that are observed, include particles high in Pb, Ca and O (i.e., PbO and CaO (B)), high in Ca, Mn, Fe and O (i.e., likely a mixture of $MnFe_2O_4$ and $Ca_2Fe_2O_5$ (D)), and high in Fe and O (i.e., Fe_3O_4 (E)), as well a darker phase containing Na, K and O (i.e., likely $(Na,K)_2O$ (F)).

20 micrometers
SE
20 micrometers
BSE

Figure 89
Secondary Electron (SE) and Backscattered Electron (BSE) Images of EAF Dust after Roasting at 1000°C with 50% Na_2CO_3 and 3.7% $CaCO_3$ (Sample C)

After leaching with 200 g/L H_2SO_4, the only three phases detected using XRD analysis (Table 43 and Figure 90) in the leach residue were $(Zn,Mn,Fe)(Fe,Mn)_2O_4$, gypsum ($CaSO_4{\cdot}2H_2O$) and srebrodolskite ($Ca_2Fe_2O_5$).

Table 43 Phases Identified by X-ray Diffraction Analysis of EAF Dust after Roasting with Na_2CO_3 and $CaCO_3$ and Leaching with 200 g/L H_2SO_4

Sample	Identified Phases (in order of intensity)	Leaching Wt. Loss, %
A	$(Zn,Mn,Fe)(Fe,Mn)_2O_4$, $CaSO_4{\cdot}2H_2O$	24^1, 67^2
B	$(Zn,Mn,Fe)(Fe,Mn)_2O_4$, $CaSO_4{\cdot}2H_2O$	42^1, 52^1
C	$Ca_2Fe_2O_5$, $CaSO_4{\cdot}2H_2O$	14^1, 41^2
D	$(Zn,Mn,Fe)(Fe,Mn)_2O_4$, $CaSO_4{\cdot}2H_2O$, $Ca_2Fe_2O_5$	41^1, 45^2

[1] Hot Water Leach [2] Acid Leach

Samples C (1000°C, 50% Na_2CO_3, 3.7% $CaCO_3$) and D (1000°C, 90% Na_2CO_3, 3.7% $CaCO_3$) were examined using SEM/EDX analysis after leaching with 200 g/L H_2SO_4 (Figures 91 and 92) to try to better understand the iron deportment in this system. Gypsum ($CaSO_4{\cdot}2H_2O$) is the major phase in the field of view in both samples and is labeled as phase G in both Figures 91 and 92.

However, a number of phases containing iron are identified in Sample C (Figure 91), including particles high in Ca, Fe and O (i.e., $Ca_2Fe_2O_5$ (E)) and high in Fe, Mn, Zn and O (i.e., residual unreacted $(Zn,Mn)Fe_2O_4$ (D)). Several particles were found to be high in Fe, Mn and O, but the ratio of manganese to iron in the EDX intensities differed, with some particles showing a ratio of intensities of Mn:Fe of between 2:1 and 3:1 (A, B) and others with a ratio of about 0.33:1 to 0.5:1 (C). Thus, this would indicate that some manganese may substitute for ferric iron in the Mn-ferrite structure, resulting in Mn-ferrites closer to the composition of Mn_2FeO_4 (Particles A and B) while other Mn-ferrites are more typical of jacobsite ($MnFe_2O_4$) (Particles C and F). Particle B contains Ca, Pb and S, in addition to Mn, Fe and O, and is likely a mixture of Mn_2FeO_4, gypsum and anglesite ($PbSO_4$) while Particle F contains Ca, Mn, Fe and O and is likely a mixture of $MnFe_2O_4$ and $Ca_2Fe_2O_5$. From a similar analysis for Sample D (Figure 92), similar particles likely representing $(Zn,Mn)Fe_2O_4$ (A), $MnFe_2O_4$ (C), $Ca_2Fe_2O_5$ (D) and a mixture of Mn_2FeO_4 and gypsum (E) were identified. However, in Sample D, Phase A ($(Zn,Mn)Fe_2O_4$) is much more abundant, due to the lower zinc extractions in this sample, and Phase E ($Mn_2FeO_4/CaSO_4 \cdot 2H_2O$) is not observed as frequently as in Sample C.

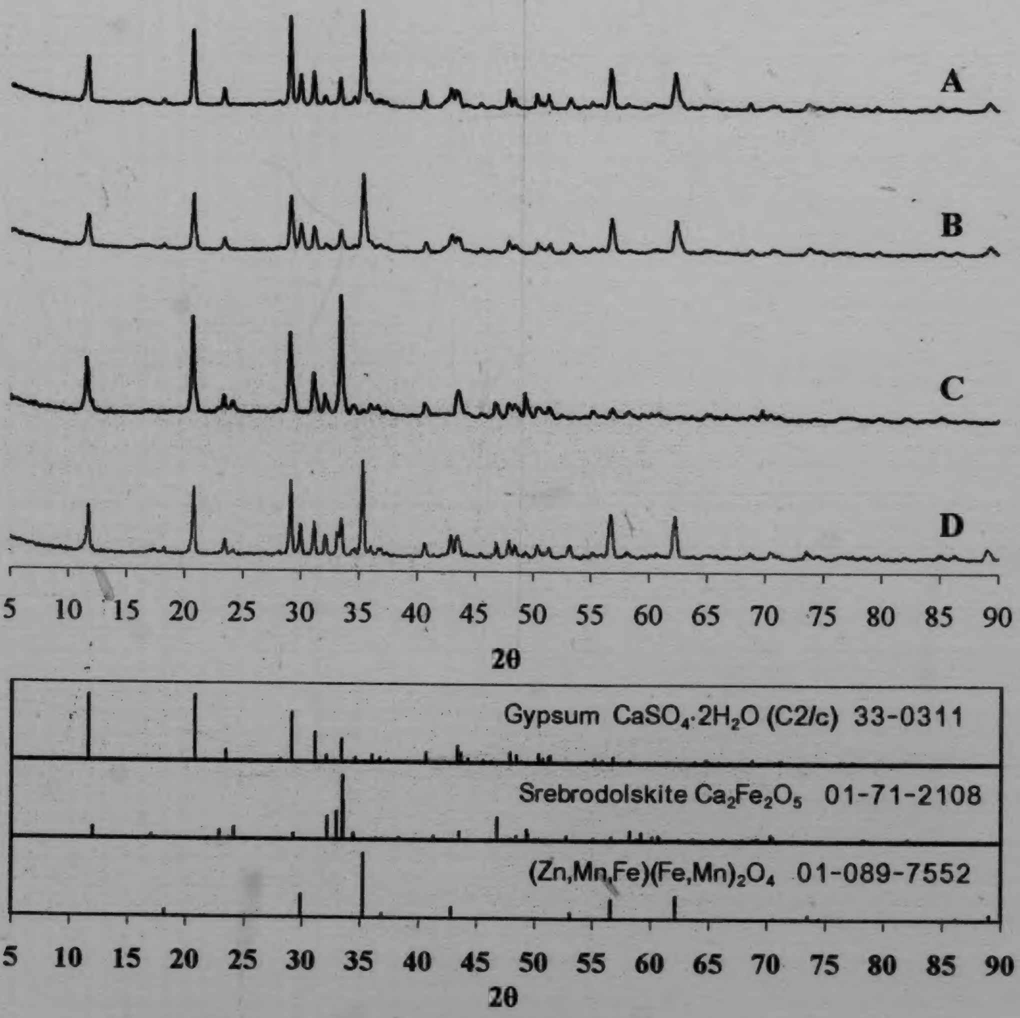

Figure 90 **XRD Patterns of EAF Dust Residue after Roasting with Na_2CO_3 and $CaCO_3$ and Leaching with 200 g/L H_2SO_4**

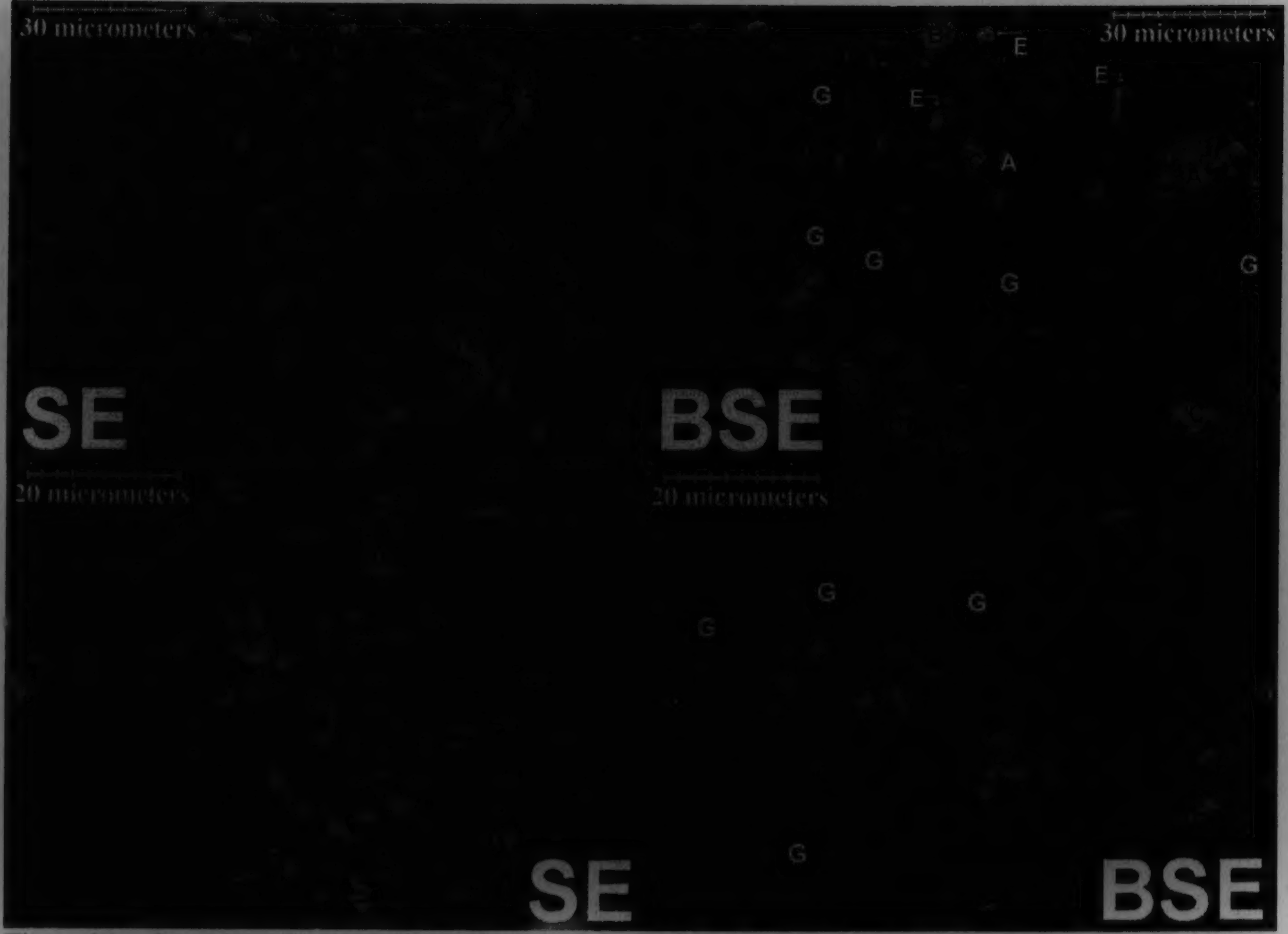
30 micrometers
30 micrometers
E
E
G
E
A
G
G
G
G
SE
BSE
20 micrometers
20 micrometers
G
G
G
G
SE
BSE

Figure 91 Secondary Electron (SE) and Backscattered Electron (BSE) Images of EAF Dust after Roasting at 1000°C with 50% Na_2CO_3 and 3.7% $CaCO_3$ and Leaching with 200 g/L H_2SO_4 (Sample C)

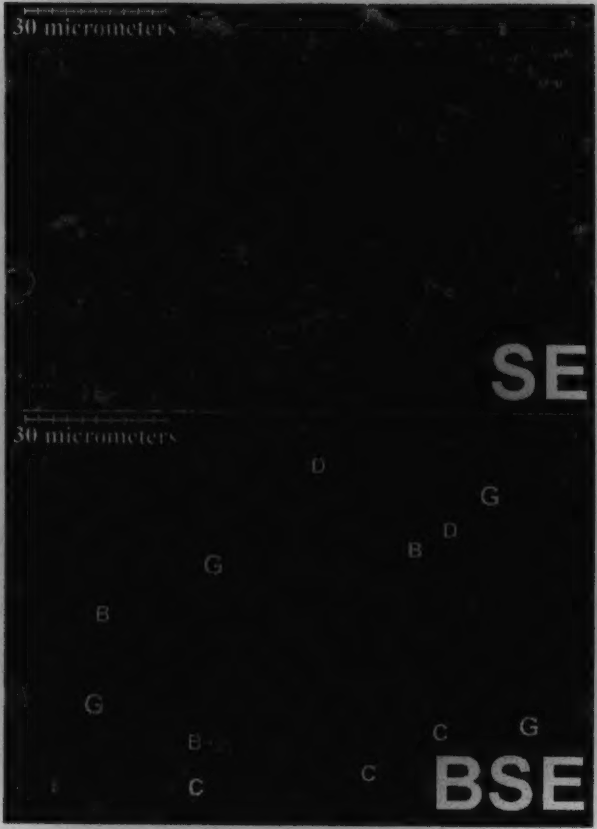

Figure 92
Secondary Electron (SE) and Backscattered Electron (BSE) Images of EAF Dust after Roasting at 1000°C with 90% Na_2CO_3 and 3.7% $CaCO_3$ and Leaching with 200 g/L H_2SO_4 (Sample D)

Using similar methods to those employed in Section 5.5.1, an iron balance for the roasting of EAF dust with Na_2CO_3 and $CaCO_3$ was constructed (Table 44). However, several adjustments to the assumptions made for the iron balance constructed for roasting with Na_2CO_3 alone were made. First, because srebrodolskite ($Ca_2Fe_2O_5$) is observed in the XRD and SEM/EDX analysis of the leach residue from Samples C and D, but not in Samples A and B, it was assumed that the $Ca_2Fe_2O_5$ formed at high temperatures was insoluble, but was still assumed to be leached completely in Samples A and B. Second, the assumption that 100% of the available calcium reacts with magnetite to form $Ca_2Fe_2O_5$ led to a significant overestimate of the iron extraction in Samples A and B; thus, it was assumed for this balance that the unreacted calcium in the feed reacts with Fe_3O_4 to form $Ca_2Fe_2O_5$ while the $CaCO_3$ added during roasting reacted with $NaFeO_2$ to form $Ca_2Fe_2O_5$. Third, even if complete leaching of $Ca_2Fe_2O_5$ and complete conversion of magnetite (Fe_3O_4) to $NaFeO_2$ were assumed in Sample C, the iron extraction predicted by the balance would still be significantly lower than actual leaching extraction. Thus, it was assumed, based on the SEM/EDX phase analysis for Samples C and D, that some of the iron was present as Mn_2FeO_4, instead of as $MnFe_2O_4$, with the remaining iron reacting with Na_2CO_3 to form $NaFeO_2$. With these assumptions, the balance agrees reasonably well with the iron extractions observed.

Table 44 Deportment of Iron Mineral during Roasting of EAF Dust with Na_2CO_3 and $CaCO_3$ and Leaching with 200 g/L H_2SO_4

Iron Minerals	% of Total Iron in Feed				
	Feed	Sample A	Sample B	Sample C	Sample D
$ZnFe_2O_4$	50.3	20.9	24.1	2.0	30.7
$MnFe_2O_4$	22.7	22.1	22.1	1.1[a]	13.5[b]
Mn_2FeO_4	0.0	0.0	0.0	5.3[a]	2.3[b]
Fe_3O_4	27.0	20.3	20.3	0.0	0.0
$Ca_2Fe_2O_5$	0.0	13.8	13.8	13.8	13.8
$NaFeO_2$	0.0	22.9	19.7	77.8	39.8
Total	100.0	100.0	100.0	100.0	100.0
Fe Extraction					
Projected, %		36.7[1]	33.5[1]	77.8[2]	39.8[2]
Actual, %		38.9	24.1	79.3	39.6
Difference, %		-2.2	9.4	-1.5	0.2

[a] Calculated assuming 90% of Mn is present as Mn_2FeO_4

[b] Calculated assuming 40% of the Mn is present as Mn_2FeO_4

[1] Calculated assuming the total dissolution of $NaFeO_2$ and $Ca_2Fe_2O_5$ during leaching

[2] Calculated assuming only the dissolution of $NaFeO_2$ during leaching

The apparent decrease in srebrodolskite ($Ca_2Fe_2O_5$) solubility with increasing temperature is consistent with the findings in Section 5.5.2.2 where, with the addition of $CaCO_3$ during roasting with coal, the results indicate that the solubility of the srebrodolskite ($Ca_2Fe_2O_5$) formed is heavily dependent on the temperature of formation, with much less iron dissolved after roasting at higher temperatures and evidence of $Ca_2Fe_2O_5$ in the leach residue.

Evidence for the decomposition of magnetite (Fe_3O_4) to form $NaFeO_2$ and $Ca_2Fe_2O_5$ has been noted earlier in Section 5.5.1.1, although the results from this test show that the extent of decomposition increases significantly with the increase in temperature and Na_2CO_3 addition used in this test.

However, some phenomena, such as the formation of $Mn(Fe,Mn)_2O_4$ spinels, or the increase in zinc and chromium extractions with the addition of $CaCO_3$ during roasting, are not as easily explained. For example, for the Mn-spinels, if some of manganese is present in the EAF dust as Mn^{3+} or Mn^{4+}, then the formation of predominantly jacobsitic ($MnFe_2O_4$) spinels, as observed during roasting with Na_2CO_3, would require reduction of the manganese present. On the other hand, if the manganese in the EAF dust is present entirely as Mn^{2+}, then the formation of more $Mn(Fe,Mn)_2O_4$ spinels would require the oxidation of manganese to Mn^{3+} or Mn^{4+}. Research on manganese iron spinels indicates that the formation of Mn_2FeO_4 is more likely where, instead of direct substitution of Mn^{3+} for Fe^{3+} in the octahedral sites, a combination of Mn^{4+} and Fe^{2+} are found in the octahedral sites, with Mn^{2+} remaining in the tetrahedral sites (168). Oxidation of Mn^{2+} is probably more likely, given that all the roasting is done in air, but it is uncertain why this latter phase would be favored, and why this phase is observed after the addition of $CaCO_3$ to the roasting system.

Likewise, the increases in zinc and chromium extraction with the addition of $CaCO_3$ could occur because if $CaCO_3$ reacts as expected ($2\ NaFeO_2 + 2\ CaCO_3 \rightarrow Ca_2Fe_2O_5 + Na_2CO_3 + CO_2$), then it is possible that more Na_2CO_3 would be available for reaction. However, because Na_2CO_3 is added in considerable excess during roasting, and zinc extractions are depressed by higher Na_2CO_3 additions, this seems unlikely. Alternatively, the combined reactions of Na_2CO_3 and $CaCO_3$ may work synergistically to cause more of the spinel phases in the EAF dust to be decomposed at lower temperatures, resulting in available zinc and chromium available for extraction using H_2SO_4 and hot water, respectively. Additional characterization and phase identification would be required to be able to explain these phenomena and will be the subject of future research.

These unexplained behaviours could also be connected to the low crystallinity of the EAF dust, which was discussed in Section 5.1. If portions of the EAF dust are indeed metastable, then crystallization would be expected on heating and, thus, if crystallization occurs in the presence of other ionic compounds, such as $CaCO_3$, the distribution of elements, such as iron, may be affected differently than if those same additives were added to a crystalline material, such as the La Oroya zinc ferrite.

5.5.1.1.2 Roasting with $MnCO_3$ as a Secondary Additive

Compared with roasting with Na_2CO_3 alone (Figure 85), roasting with $MnCO_3$ as a secondary additive does broaden the area of maximum chromium extraction (90 to 100%) possible with water leaching (Figure 93), but not as much as when roasting with $CaCO_3$. The size of this region also increases with increasing $MnCO_3$ additions.

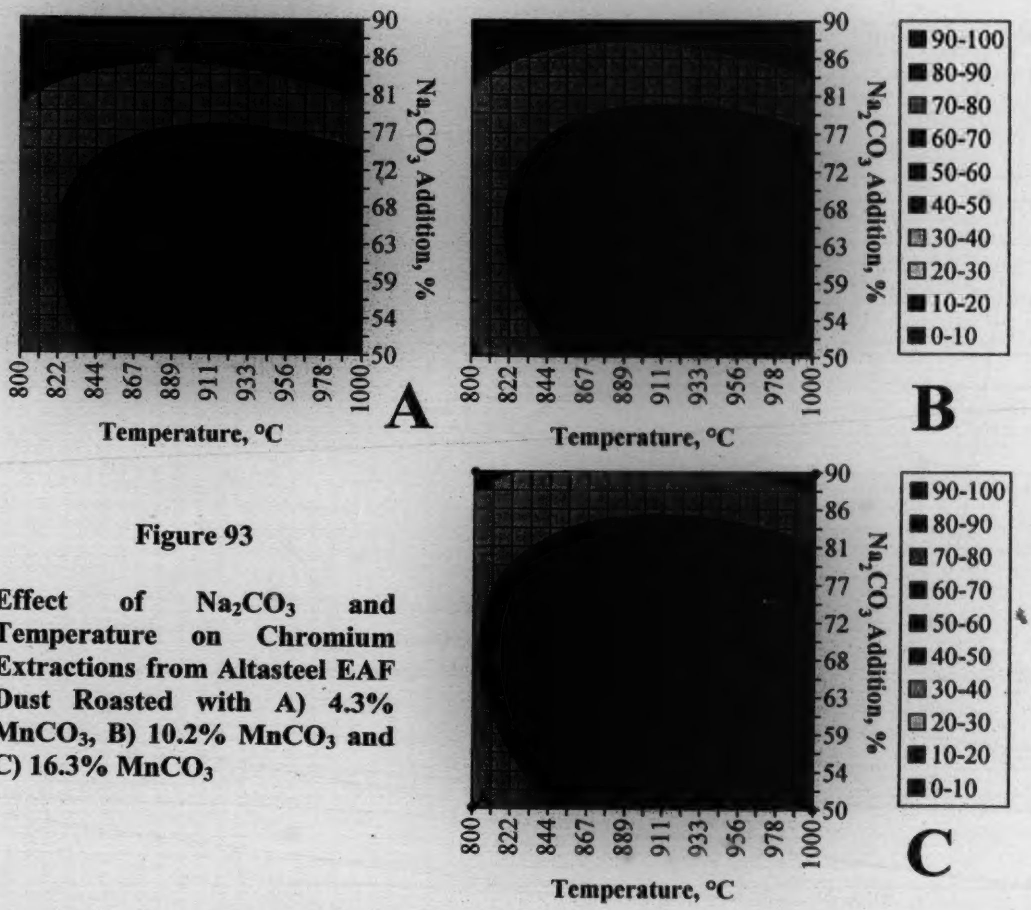

Figure 93

Effect of Na_2CO_3 and Temperature on Chromium Extractions from Altasteel EAF Dust Roasted with A) 4.3% $MnCO_3$, B) 10.2% $MnCO_3$ and C) 16.3% $MnCO_3$

The shape of the zinc extraction model for leaching the roasted ash with 200 g/L H_2SO_4 (Figure 94) follows closely the trends in extraction observed in the scoping tests from roasting with Na_2CO_3 (Figure 85) or Na_2CO_3-$CaCO_3$ (Figure 87), with a maximum around 50% Na_2CO_3 and a decrease in extractions at higher Na_2CO_3 additions.

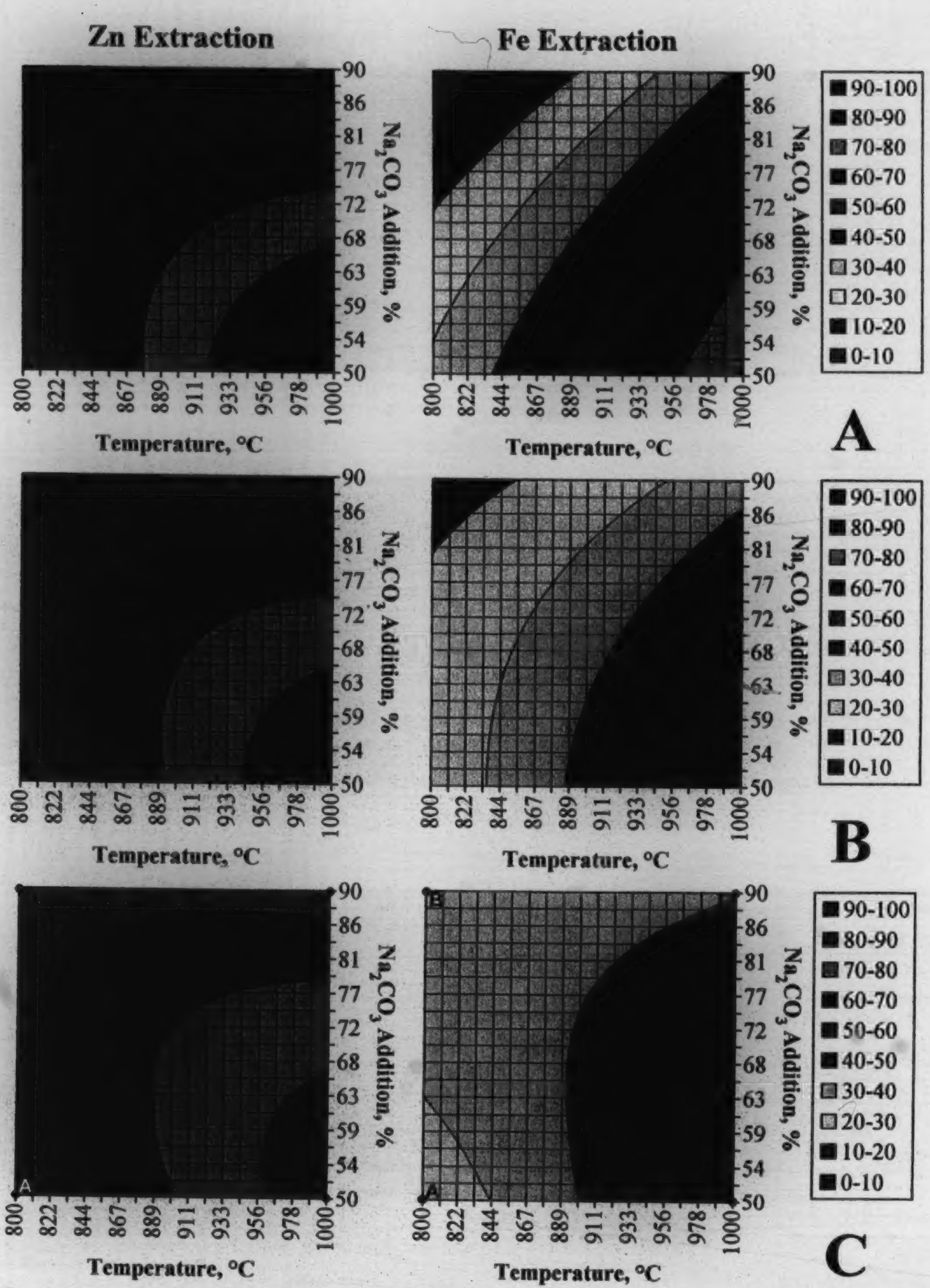

Figure 94 Effect of Na_2CO_3 and Temperature on Zinc and Iron Extractions from Altasteel EAF Dust Roasted with A) 4.3% $MnCO_3$, B) 10.2% $MnCO_3$ and C) 16.3% $MnCO_3$

Samples at various conditions described by the model for roasting with Na_2CO_3 and the highest $MnCO_3$ addition tested (16.3%) were analyzed using x-ray diffraction (Points A through D on Figures 93C and 94C). The identified phases are listed in Table 45 while the diffraction patterns and major phases observed are shown in Figure 95.

Table 45 Phases Identified by XRD Analysis of EAF Dust Roasted with Na_2CO_3 and $MnCO_3$

Sample	Identified Phases (in order of intensity)
A	α-$NaFeO_2$, $(Zn,Mn,Fe)(Fe,Mn)_2O_4$, ZnO, $Ca_2Fe_2O_5$
B	α-$NaFeO_2$, ZnO, $(Zn,Mn,Fe)(Fe,Mn)_2O_4$, ZnO, $Ca_2Fe_2O_5$
C	α-$NaFeO_2$, $Ca_2Fe_2O_5$, $(Zn,Mn,Fe)(Fe,Mn)_2O_4$, ZnO
D	α-$NaFeO_2$, ZnO, $Ca_4Mn_3O_{10}$, $Ca_2Fe_2O_5$, β-$NaFeO_2$

As with the x-ray diffraction analysis of La Oroya ferrite roasted with Na_2CO_3 and $MnCO_3$ (Section 5.5.1.1.2), phase identification for the EAF dust samples roasted with $MnCO_3$ was less definitive than for EAF dust roasted with Na_2CO_3 or Na_2CO_3-$CaCO_3$. In several cases, x-ray diffraction peaks of significant intensity could not be positively identified from the available database. However, it was possible to positively identify several phases with x-ray diffraction including α-$NaFeO_2$, $(Zn,Mn,Fe)(Fe,Mn)_2O_4$, zincite (ZnO) and srebrodolskite ($Ca_2Fe_2O_5$), which are found in most of the samples tested. In Sample D, a calcium-manganese oxide ($Ca_4Mn_3O_{10}$) was also identified along with trace amounts of β-$NaFeO_2$.

Phase analysis of Sample C (1000°C, 50% Na_2CO_3, 16.3% $MnCO_3$) using backscattered electron imaging in the scanning electron microscope and EDX analysis is much clearer (Figure 96). Zinc oxide is visible as bright particles in the backscattered images (A). Ferrites containing Mn, Fe and O (i.e., $MnFe_2O_4$ (B)) are the dominant iron bearing phase identified, but particles high in Ca, Fe and O (i.e., $CaFe_2O_5$ (C)) are also identified and both are consistent with the phases detected using x-ray diffraction. In addition, some darker particles were shown to be high in Ca, Si and O (i.e.,Ca_2SiO_4 (D)) or high in Ca and O (i.e., $CaO/Ca(OH)_2$ (E)). Texturally, the particles in view in some of the SEM micrographs are quite interesting, showing what appear to be lamellar type layers of $MnFe_2O_4$ and ZnO in some particles.

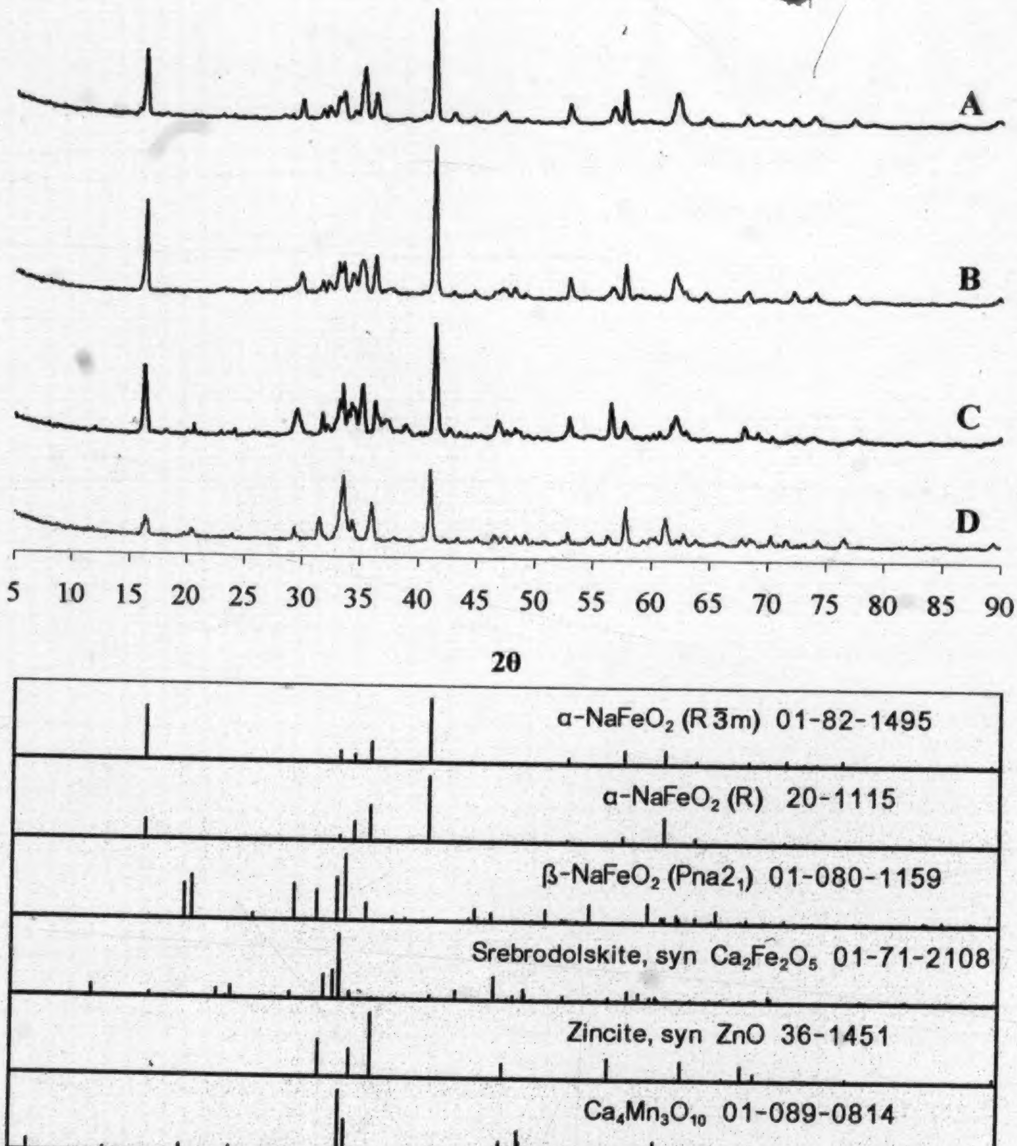

Figure 95 **XRD Patterns of EAF Dust Roasted with Na_2CO_3 and $MnCO_3$**

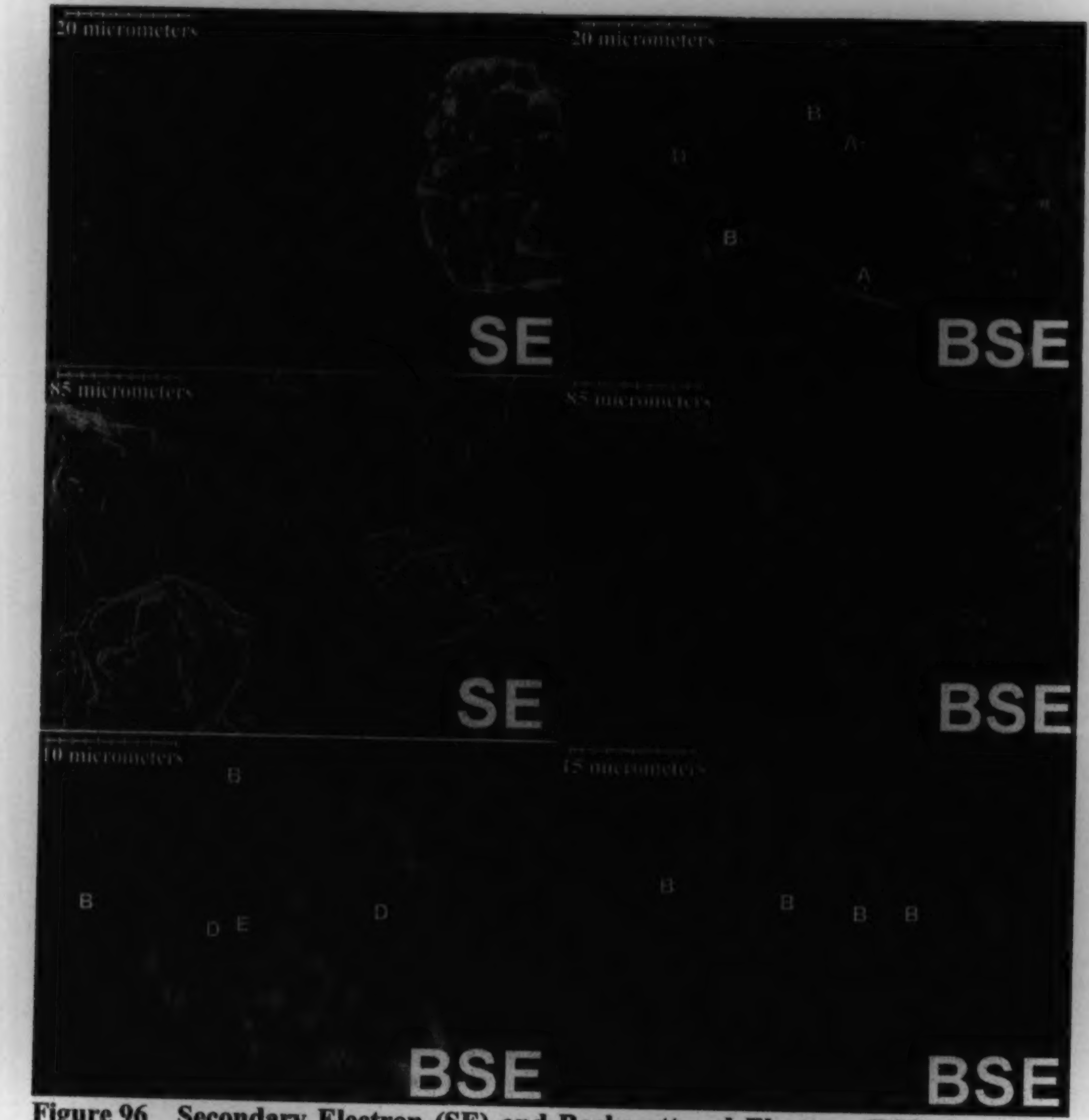
20 micrometers
SE
20 micrometers
B
A
B
B
A
BSE
85 micrometers
SE
85 micrometers
BSE
10 micrometers
B
B
D
E
D
BSE
15 micrometers
B
B
B
B
BSE

Figure 96 Secondary Electron (SE) and Backscattered Electron (BSE) Images of EAF Dust after Roasting at 1000°C with 50% Na_2CO_3 and 16.3%$MnCO_3$ (Sample C)

After leaching with 200 g/L H_2SO_4, zincite (ZnO) and $NaFeO_2$ are dissolved and gypsum ($CaSO_4 \cdot 2H_2O$) and spinel phases, such as $(Zn,Mn,Fe)(Fe,Mn)_2O_4$, $MnFe_2O_4$ or Fe_3O_4, are the only phases which could be positively identified using x-ray diffraction in the leach residue (Table 46 and Figure 97). Several peaks could not be identified using the database and software available.

Table 46 **Phases Identified by X-ray Diffraction Analysis of EAF Dust after Roasting with Na_2CO_3 and $MnCO_3$ and Leaching with 200 g/L H_2SO_4**

Sample	Identified Phases (in order of intensity)	Leaching Wt. Loss, %
A	$CaSO_4{\cdot}2H_2O$, $(Zn,Mn,Fe)(Fe,Mn)_2O_4$	19^1, 72^2
B	$CaSO_4{\cdot}2H_2O$, $(Zn,Mn,Fe)(Fe,Mn)_2O_4$	34^1, 54^2
C	$CaSO_4{\cdot}2H_2O$, $MnFe_2O_4/Fe_3O_4$	9^1, 62^2
D	$CaSO_4{\cdot}2H_2O$, $(Zn,Mn,Fe)(Fe,Mn)_2O_4$, $MnFe_2O_4/Fe_3O_4$	35^1, 50^2

[1] Hot Water Leach [2] Acid Leach

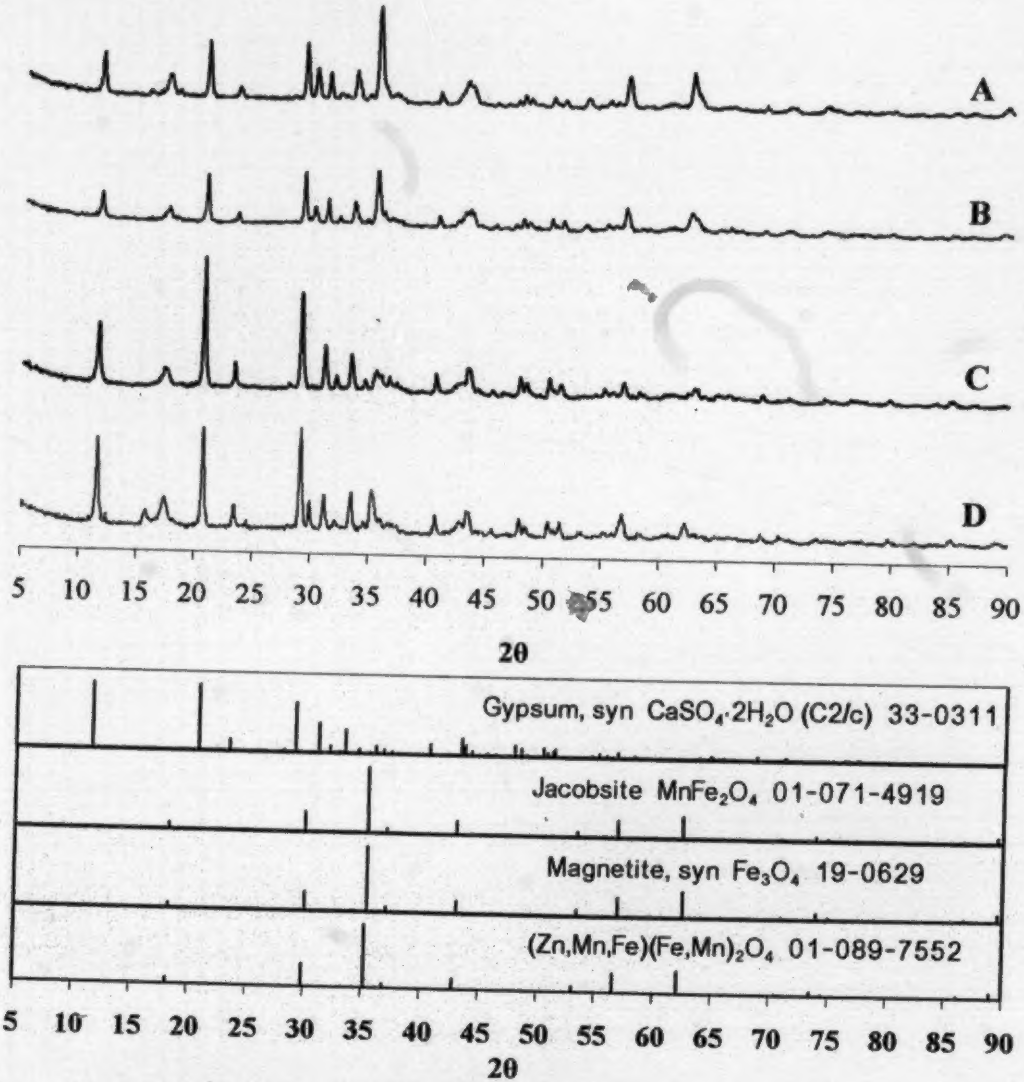

Figure 97 **XRD Patterns of EAF Dust Residue after Roasting with Na_2CO_3 and $MnCO_3$ and Leaching with 200 g/L H_2SO_4**

SEM/EDX analysis of the leach residue for Sample C (1000°C, 50% Na_2CO_3, 16.3% $MnCO_3$) again showed gypsum (A), present as fine elongate crystals, as the major phase in roasted EAF dust after leaching, likely due to the dissolution of larnite (Ca_2SiO_4) and reprecipitation of the dissolved calcium as gypsum during leaching (Figure 98). Iron is present mostly as metal ferrites, with particles high in Fe, Mn and O (i.e., $MnFe_2O_4$ (B)) or high in Fe, Mn, Zn and O (i.e., $(Zn,Mn)Fe_2O_4$ (C)) being the most common in the SEM micrograph and particles high in Ca, Fe and O (i.e., $Ca_2Fe_2O_5$ (E)) present in smaller quantities. The presence of significant amounts of $(Zn,Mn)Fe_2O_4$ would be expected, due to the lower zinc extractions (i.e., less than 80%) observed with these roasting conditions. However, iron is also found in Particle D, which contains Mn, Si and O as well as Fe, likely as a Mn-Fe silicate.

60 micrometers
60 micrometers
A
A
A
SE
BSE
10 micrometers
20 micrometers
A
A
A
SE
BSE

Figure 98 **Secondary Electron (SE) and Backscattered Electron (BSE) Images of EAF Dust after Roasting at 1000°C with 50% Na_2CO_3 and 16.3%$MnCO_3$ and Leaching with 200 g/L H_2SO_4 (Sample C)**

From this analysis, and previous findings in Sections 4.5.2.1.1.3 and 4.5.2.2.1.2, it is evident that the addition of $MnCO_3$ promotes the formation of acid insoluble Mn-ferrites during roasting. This is indicated, first of all, by the detection of Mn ferrites using SEM/EDX analysis both before and after leaching and, second, by the decrease in iron extractions observed with increased $MnCO_3$ additions during roasting. However, for roasting the EAF dust with Na_2CO_3 and $MnCO_3$, several phenomena remain unexplained.

First, small additions of $MnCO_3$ (4.3%) cause an initial increase in the iron extractions observed, compared to those from roasting with Na_2CO_3 alone, while additions of up to 16.3% are required to reduce iron extractions to the low levels that are possible when roasting with Na_2CO_3 alone. In roasting with low $CaCO_3$ additions in Section 5.5.1.1.1, significant amounts of Mn_2FeO_4, or other manganese rich ferrites, formed which meant that less iron was associated with manganese and, thus, more iron could react with Na_2CO_3 and become acid soluble. A similar phenomenon may occur during the roasting of the EAF dust with $MnCO_3$, resulting, initially, in higher iron extractions, due to the formation of more manganese rich spinels and the associated increase in the amount of iron reacting to form $NaFeO_2$, and, then, in a steady decrease in iron extractions with higher $MnCO_3$ additions as $MnCO_3$ reacts with $NaFeO_2$ to form $MnFe_2O_4$.

Also, the addition of $MnCO_3$ decreases the zinc extractions possible at a given temperature, but much more significantly than was observed in Section 4.5.2.1.1.3 for the roasting of the La Oroya ferrite. This could be connected to the presence of a $(Zn,Mn)Fe_2O_4$ solid solution in the EAF dust, or its formation during roasting, either by crystallization of the EAF dust after heating in the presence of the manganese in the dust or Mn added as $MnCO_3$, or by reaction of franklinite in the EAF dust with the manganese added as $MnCO_3$. If the majority of the zinc is present as a solid solution in $(Zn,Mn)Fe_2O_4$, then it is possible that the increase in manganese content could decrease the activity of $ZnFe_2O_4$ in the roasting reactions, which, in turn, could decrease the zinc extractions possible during roasting.

To examine this possibility, calculations were made to determine the effect of $ZnFe_2O_4$ activity on the thermodynamics of the roasting reaction ($ZnFe_2O_4 + Na_2CO_3 \rightarrow 2\ NaFeO_2 + ZnO + CO_2$) using the equation, $\Delta G=\Delta G^{\circ}+RT\ln K$. Several assumptions were made in these calculations, including assuming that all the manganese in the feed, and that added as $MnCO_3$ during roasting, reacts to form a solid solution of $(Zn,Mn)Fe_2O_4$, that the activity of $ZnFe_2O_4$ in that solid solution is defined by Raoult's law (i.e., ideal solution), that P_{CO_2} is approximately 1 atm close to the reaction surface, that little change occurs in the activities of the other solids in the equilibrium constant over the temperature range considered (i.e., $a_{solids} \approx 1$, and, thus, $K \approx 1/a_{ZnFe_2O_4}$) and that the maximum zinc extraction occurs where the activity of $ZnFe_2O_4$ is decreased enough to cause ΔG to equal zero for a given temperature. Based on these assumptions, Figure 99 was constructed to compare the theoretical maximum extractions from these activity and thermodynamic calculations with the maximum extractions observed for each temperature from the response surface models (Figure 94) for each level of $MnCO_3$ used in the DOE tests

Figure 99 clearly shows a shift in the theoretical zinc extraction with an increase in the $MnCO_3$ addition, which is a trend that is consistent with the experimental results, as is the observed trend of increasing maximum zinc extraction with increasing roasting temperature. At low $MnCO_3$ additions, though, the maximum theoretical and experimental zinc extractions do not agree closely. However, as the $MnCO_3$ additions are increased, the discrepancy between the maximum theoretical and experimental zinc extractions, particularly at higher roasting temperatures, decreases until at 16.3% $MnCO_3$ the theoretical and experimental extraction curves almost coincide. (For all $MnCO_3$ additions, the zinc extractions for EAF dust roasted with 50% Na_2CO_3 agree more closely to the theoretical than the maximum extractions from the response surface model.) Thus, this indicates that, as $MnCO_3$ additions are increased during the roasting of EAF dust with Na_2CO_3, the activity of $ZnFe_2O_4$ in the $(Zn,Mn)Fe_2O_4$ spinel solid solution does affect the maximum zinc extractions possible at a given temperature, making it increasingly difficult to obtain high zinc extractions during transformational roasting of the EAF dust with high $MnCO_3$ additions.

From this analysis, roasting EAF dust with Na_2CO_3 and $MnCO_3$ as a secondary additive has no advantages over roasting the EAF dust with Na_2CO_3 alone. With increasing

$MnCO_3$ additions, zinc extractions are lower for a given roasting temperature and iron extractions are not improved over roasting with Na_2CO_3 alone. As a result, no further study of this system was conducted. From these results, it was decided that the addition of $MnCO_3$ as a secondary addition during the roasting of EAF dust with coal would not be tested, as similar effects, with regard to the formation of $MnFe_2O_4$ or $(Zn,Mn)Fe_2O_4$, and the decrease in zinc recoveries that would follow, would be expected.

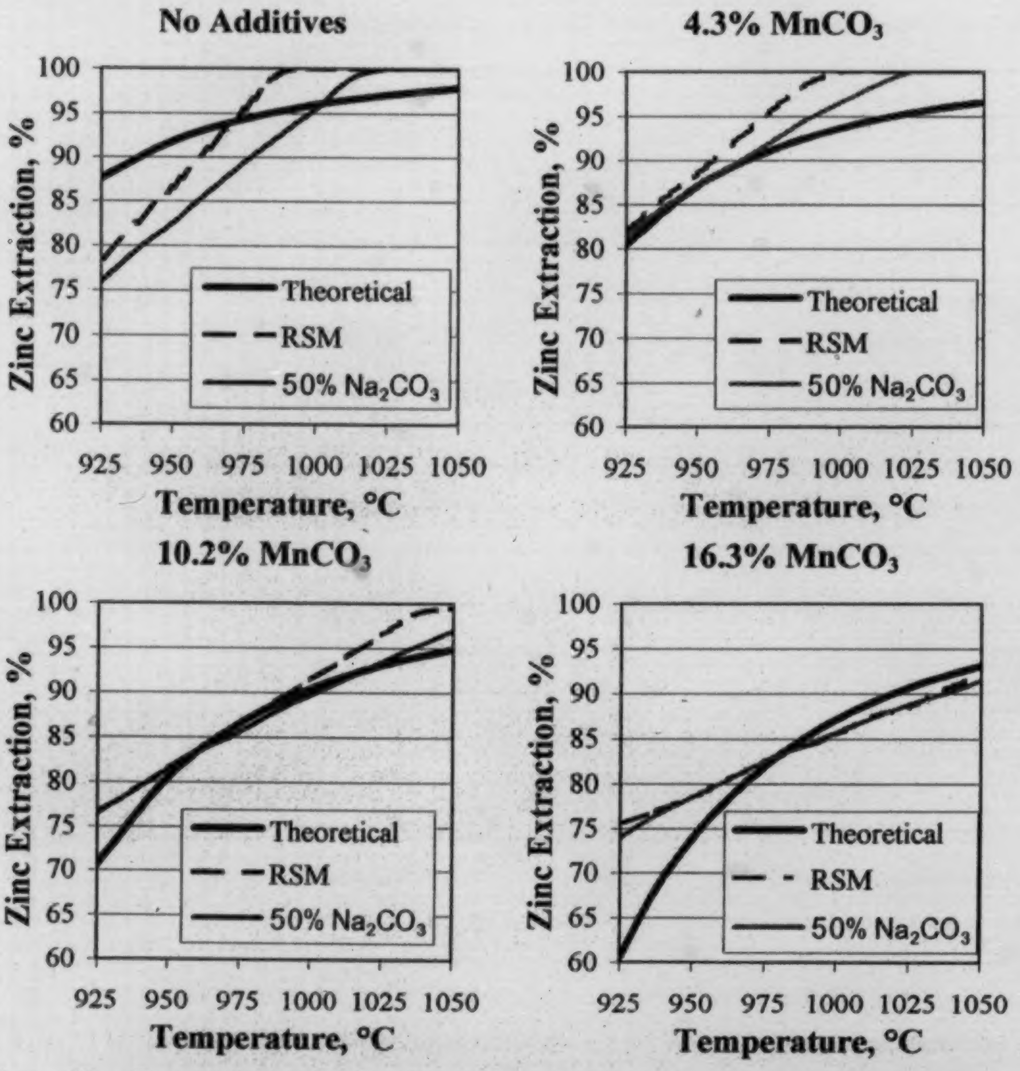

Figure 99 Comparison of Maximum Zinc Extractions and Zinc Extractions at 50% Na_2CO_3, from the Response Surface Models (RSM) with Maximum Extractions Calculated from the Change in Activity in a $(Zn,Mn)Fe_2O_4$ Solid Solution

5.5.2 Reduction of EAF Dust to Form Metal Ferrites

5.5.2.1 Roasting with Coal

Zinc extractions after roasting the Altasteel EAF dust with coal showed a much larger area of maximum extractions than observed for roasting the La Oroya zinc ferrite, with extractions of over 90% Zn possible at temperatures as low as 970°C and coal additions as low as 14.5% (Figure 100A). The increase in the zinc lost as fume (Figure 100C) was a major contributor to this increase as the amount of zinc fumed varied from 30 to 70% in the region of maximum zinc extraction, compared with a range of only 30 to 50% for the La Oroya ferrite. Iron extractions from the EAF dust are consistent with those from the La Oroya ferrite at less than 10% for all the roasting conditions tested (Figure 100B).

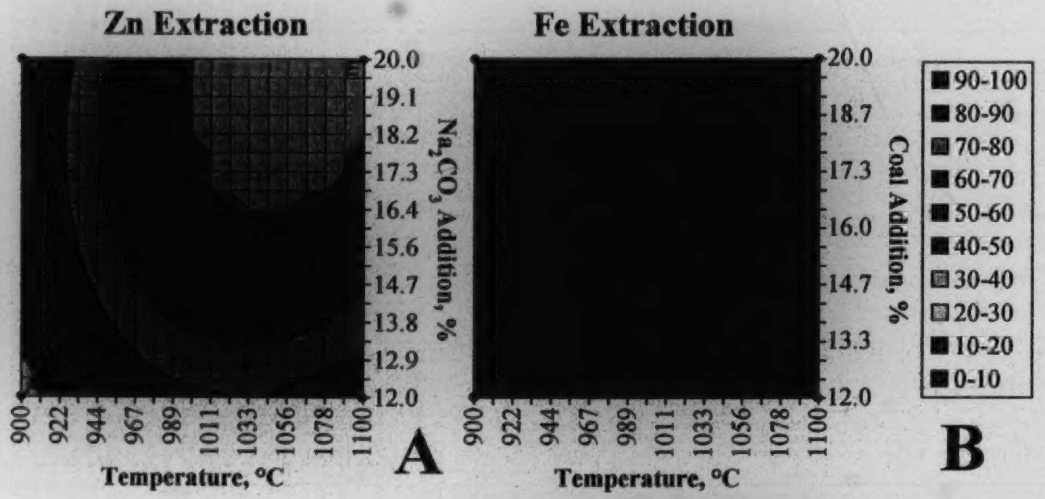

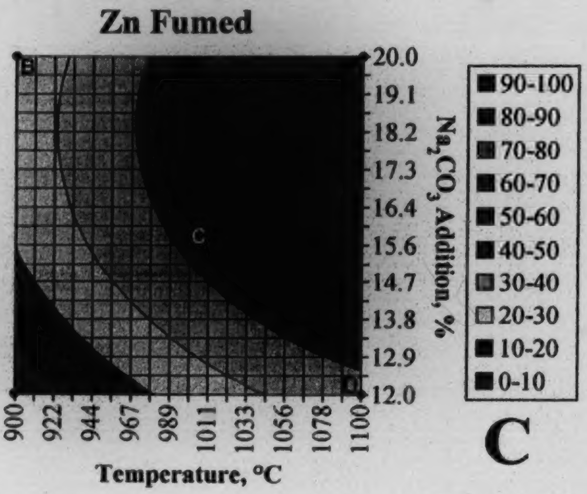

Figure 100

Effect of Coal Addition and Temperature on the A) Zn Extraction and B) Fe Extractions after Leaching with 200 g/L H_2SO_4 and C) the Amount of Zinc Fumed during Roasting from the Roasted Altasteel EAF Dust

The reduction in the coal required is likely related in part to the lower concentration of zinc in the feed (i.e., 9.4% vs. 19.5% for the La Oroya ferrite). However, the need for both lower coal additions and lower roasting temperatures indicates that the zinc in the EAF dust is more easily reduced by coal than the La Oroya zinc ferrite. The higher temperature of formation, and the resulting poorer crystallinity, of the EAF dust may be connected to this behaviour, with zinc more readily reduced from a metastable, poorly crystalline matrix than from a more crystalline zinc ferrite material.

Samples at various conditions described by the model for roasting with coal were analyzed using x-ray diffraction (Points A through E on Figure 100). The identified phases are listed in Table 47 while the diffraction patterns and major phases observed are shown in Figure 101.

Table 47 Phases Identified by XRD Analysis of EAF Dust Roasted with Coal

Sample	Identified Phases (in order of intensity)
A	(Zn,Mn,Fe)(Fe,Mn)$_2$O$_4$, $Ca_4Fe_{14}O_{25}$, ZnO, Ca_2SiO_4 (Larnite), $Ca_2Fe_2O_5$
B	(Zn,Mn,Fe)(Fe,Mn)$_2$O$_4$, ZnO, $Ca_4Fe_{14}O_{25}$, Fe_2O_3, Ca_2SiO_4 (Larnite)
C	ZnO, (Zn,Mn,Fe)(Fe,Mn)$_2$O$_4$, $Ca_4Fe_{14}O_{25}$, Ca_2SiO_4 (Larnite)
D	(Zn,Mn,Fe)(Fe,Mn)$_2$O$_4$, ZnO, $Ca_4Fe_{14}O_{25}$, Fe_2O_3, Ca_2SiO_4 (Larnite)
E	(Zn,Mn,Fe)(Fe,Mn)$_2$O$_4$, ZnO, Fe_2O_3, $Ca_4Fe_{14}O_{25}$, Ca_2SiO_4 (Larnite)

The phases observed are quite consistent from sample to sample, with zincite (ZnO), a mixture of metal ferrites (Zn,Mn,Fe)(Fe,Mn)$_2$O$_4$, $Ca_4Fe_{14}O_{25}$ and larnite (Ca_2SiO_4) observed in varying quantities in all samples, with srebrodolskite ($Ca_2Fe_2O_5$) and hematite (Fe_2O_3) observed as minor phases in some samples. (Less zincite is observed in Sample E than in Sample C, due to the extensive zinc fuming in Sample E.)

Using these identified phases, an iron balance was conducted to estimate the distribution of iron in the various phases after roasting (Table 48). The balance was calculated using the total zinc extractions (i.e., from leaching and fuming) to determine the amount of $ZnFe_2O_4$ that had reacted, and assuming that all the calcium that is not associated with larnite (Ca_2SiO_4) is present as either $Ca_4Fe_{14}O_{25}$ or $Ca_2Fe_2O_5$ and that any iron from the decomposition of $ZnFe_2O_4$ either reacts to form a calcium ferrite or is present as hematite (Fe_2O_3) in the roasted EAF dust.

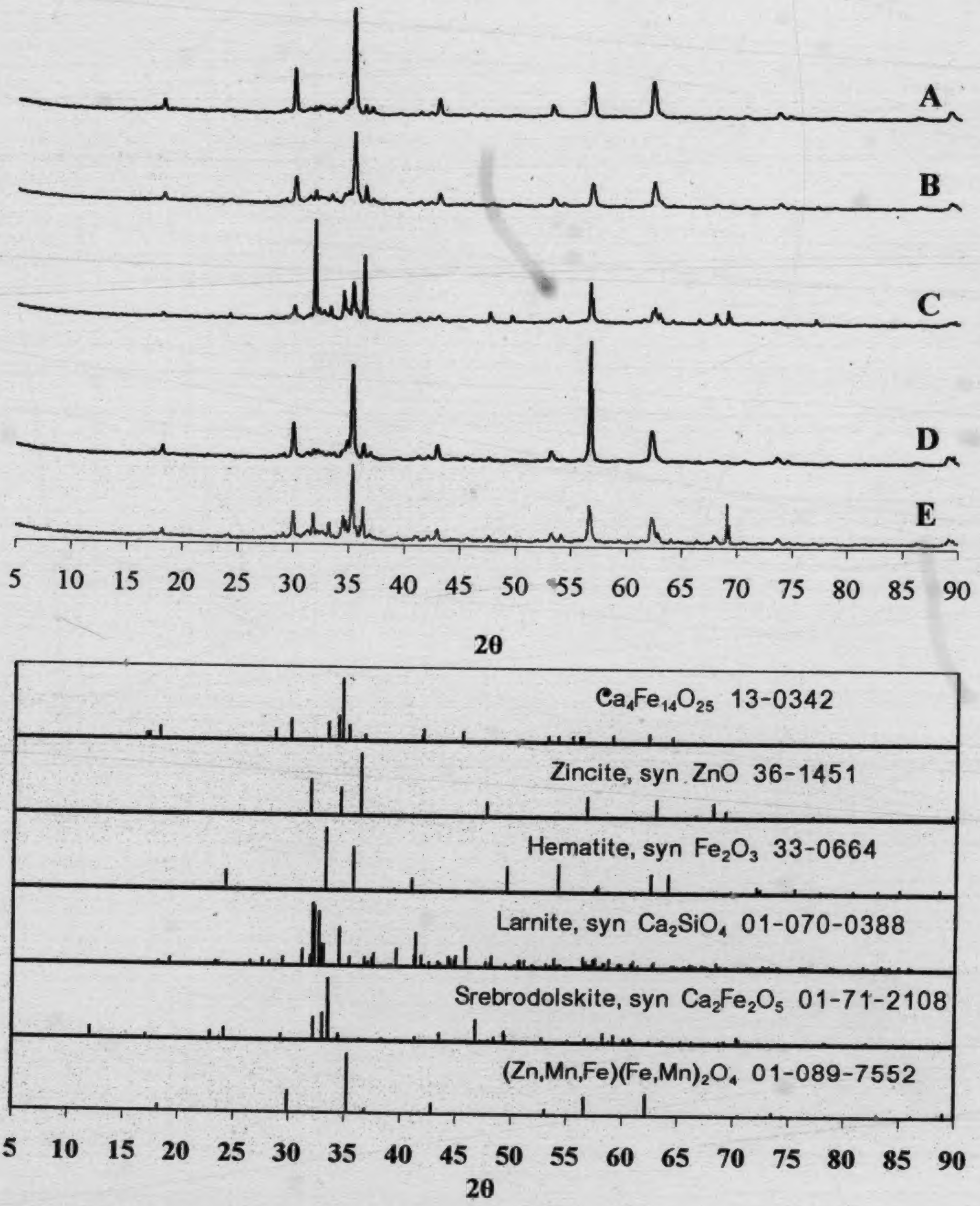

Figure 101 XRD Patterns of EAF Dust Roasted with Coal

Table 48 Estimated Distribution of Iron in Mineral Phases after Roasting of EAF Dust with Coal

Iron-Bearing Minerals	% of Total Iron in Feed					
	Feed	Sample A	Sample B	Sample C	Sample D	Sample E
$ZnFe_2O_4$	50.3	36.1	22.8	33.7	4.8	2.8
$MnFe_2O_4$	22.7	22.7	22.7	22.7	22.7	22.7
Fe_3O_4	27.0	27.0	27.0	27.0	27.0	27.0
$Ca_4Fe_{14}O_{25}$	0.0	11.4	21.3	14.7	21.3	21.3
Fe_2O_3	0.0	0.0	6.3	0.0	24.3	26.3
$Ca_2Fe_2O_5$	0.0	2.8	0.0	1.9	0.0	0.0
Total	100.0	100.0	100.0	100.0	100.0	100.0
Extraction, %						
Zn		28.2	54.8	33.0	90.5	94.5
Fe		4.2	3.8	2.7	2.8	2.0
Ca-Ferrites Leached*, %		29.5	18.0	16.0	13.3	9.3

* Extraction assuming 100% of the iron extracted comes from the leaching of $Ca_4Fe_{14}O_{25}$ or $Ca_2Fe_2O_5$

The balance agrees quite well with the results from x-ray diffraction, with $ZnFe_2O_4/MnFe_2O_4/Fe_3O_4$ as the major phase identified, and with $Ca_4Fe_{14}O_{25}$, $Ca_2Fe_2O_5$ and Fe_2O_3 present in the samples where predicted from the balance, except where these phases are present below XRD detection limits (<<5%). This balance confirms that, stoichiometrically, with larnite as the major silicate phase in the as-received and roasted EAF dusts, the amount of calcium available for reaction with iron during the reduction of $ZnFe_2O_4$ is low and, thus, the formation of a more calcium deficient Ca-ferrite ($Ca_4Fe_{14}O_{25}$) is favored over more calcium rich ferrites, such as $Ca_2Fe_2O_5$, in these samples.

SEM/EDX analysis was conducted on Sample C (1000°C, 16% coal) and Sample E (1100°C, 20% coal) after roasting. The SEM micrographas for these samples are shown in Figures 102 and 103, respectively.

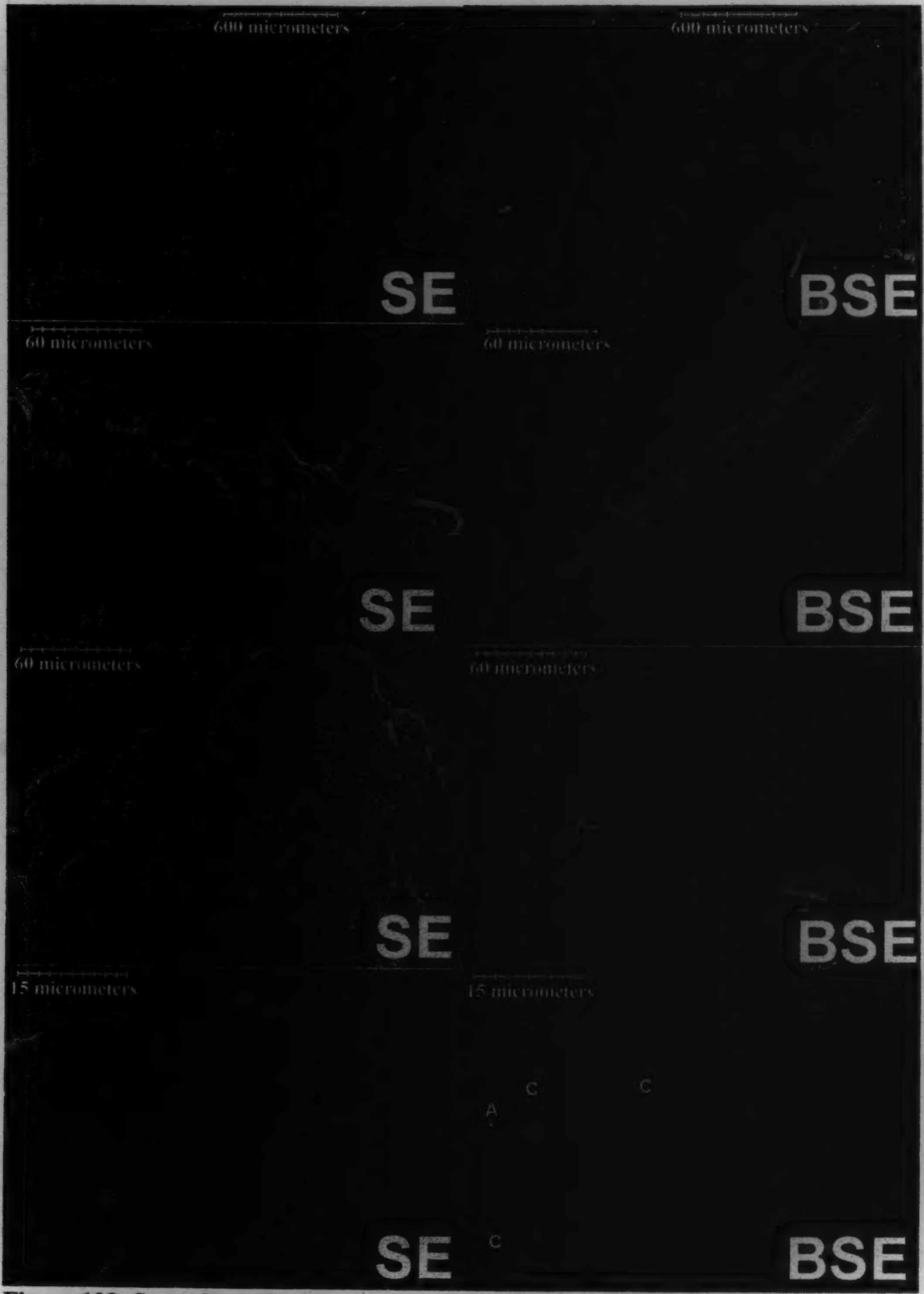
600 micrometers
600 micrometers
SE
BSE
60 micrometers
60 micrometers
SE
BSE
60 micrometers
60 micrometers
SE
BSE
15 micrometers
15 micrometers
C
C
A
C
SE
BSE

Figure 102 Secondary Electron (SE) and Backscattered Electron (BSE) Images of EAF Dust after Roasting at 1000°C with 16% Coal (Sample C)

50 micrometers
50 micrometers
SE
BSE
10 micrometers
10 micrometers
C
C
C
C
SE
BSE

Figure 103 Secondary Electron (SE) and Backscattered Electron (BSE) Images of EAF Dust after Roasting at 1100°C with 20% Coal (Sample E)

Bright, elongate or bladed particles (A) are observed in both samples and are likely zincite (ZnO), due to their high Zn and O content. In Figure 102, the hexagonal pyramidal crystal structure of the zincite crystals is quite evident in these micrographs, and the large size and extensive branching of these crystals, combined with their visibility to the naked eye on the surface of the roasted samples, are indicative of vapor phase deposition of the zinc oxide during roasting of the EAF dust.

In Sample C (Figure 102), two major iron-bearing phases are detected: particles high in Ca, Fe, Mn and O (i.e., likely a mixture of $(Mn,Fe)(Fe,Mn)_2O_4$ and $Ca_4Fe_{14}O_{25}$ (B)) and particles high in Fe and O (i.e., Fe_2O_3 or Fe_3O_4 (C)). In Sample E (Figure 103), only one type of iron-containing particle was identified, which contained Ca, Fe, Mn Zn and O (B), and, thus, is likely a mixture of $(Zn,Mn,Fe)(Fe,Mn)_2O_4$ and $Ca_4Fe_{14}O_{25}$. (The dark grey phase (C) observed in Sample E is high in Ca, Al, Si and S and, thus, is likely a mixture of larnite (Ca_2SiO_4) along with $CaSO_4$ and/or Ca-aluminates, which were not identified with x-ray diffraction.)

After leaching with 200 g/L H_2SO_4, zincite (ZnO) and larnite (Ca_2SiO_4) are no longer detected using x-ray diffraction in any of the samples, indicating that these phases were dissolved during leaching (Table 49 and Figure 104). $Ca_4Fe_{14}O_{25}$ is only detected as a minor phase in Sample B, which may point towards the partial dissolution of this phase during leaching, as indicated in Table 48. The majority of the dissolved calcium likely reprecipitates as gypsum ($CaSO_4{\cdot}2H_2O$), which is observed as a major phase in the x-ray diffraction patterns of all the samples. Iron, and zinc that did not fume or leach, are predominantly present as Zn-Fe-Mn ferrites in the leach residue. (Hematite (Fe_2O_3) and jacobsite ($MnFe_2O_4$) are detected as minor phases, in addition to $(Zn,Mn,Fe)(Fe,Mn)_2O_4$, in samples with higher overall zinc extractions (Samples C and E).)

Table 49 Phases Identified by X-ray Diffraction Analysis of EAF Dust after Roasting with Coal and Leaching with 200 g/L H_2SO_4

Sample	Identified Phases (in order of intensity)	Leaching Wt. Loss, %
A	$(Zn,Mn,Fe)(Fe,Mn)_2O_4$, $CaSO_4{\cdot}2H_2O$	-3.6
B	$(Zn,Mn,Fe)(Fe,Mn)_2O_4$, $CaSO_4{\cdot}2H_2O$, Fe_2O_3, $Ca_4Fe_{14}O_{25}$	3.1
C	$CaSO_4{\cdot}2H_2O$, $(Zn,Mn,Fe)(Fe,Mn)_2O_4$, Fe_2O_3, $MnFe_2O_4$	1.2
D	$(Zn,Mn,Fe)(Fe,Mn)_2O_4$, $CaSO_4{\cdot}2H_2O$	-1.2
E	$CaSO_4{\cdot}2H_2O$, $(Zn,Mn,Fe)(Fe,Mn)_2O_4$, Fe_2O_3, $MnFe_2O_4$	1.6

SEM/EDX analysis of Sample C (1000°C, 16% coal) after leaching with 200 g/L H_2SO_4 shows that gypsum (A) is the principal phase visible in the field of view (Figure 105). EDX analysis indicates that silicon from the dissolution of larnite also appears to have precipitated along with the gypsum. Metal ferrites are visible as bright particles in the backscattered electron images, with all iron bearing particles containing Fe and Zn and some containing lower concentrations of Ca and Mn (B) and some with high Ca and Mn concentrations (C).

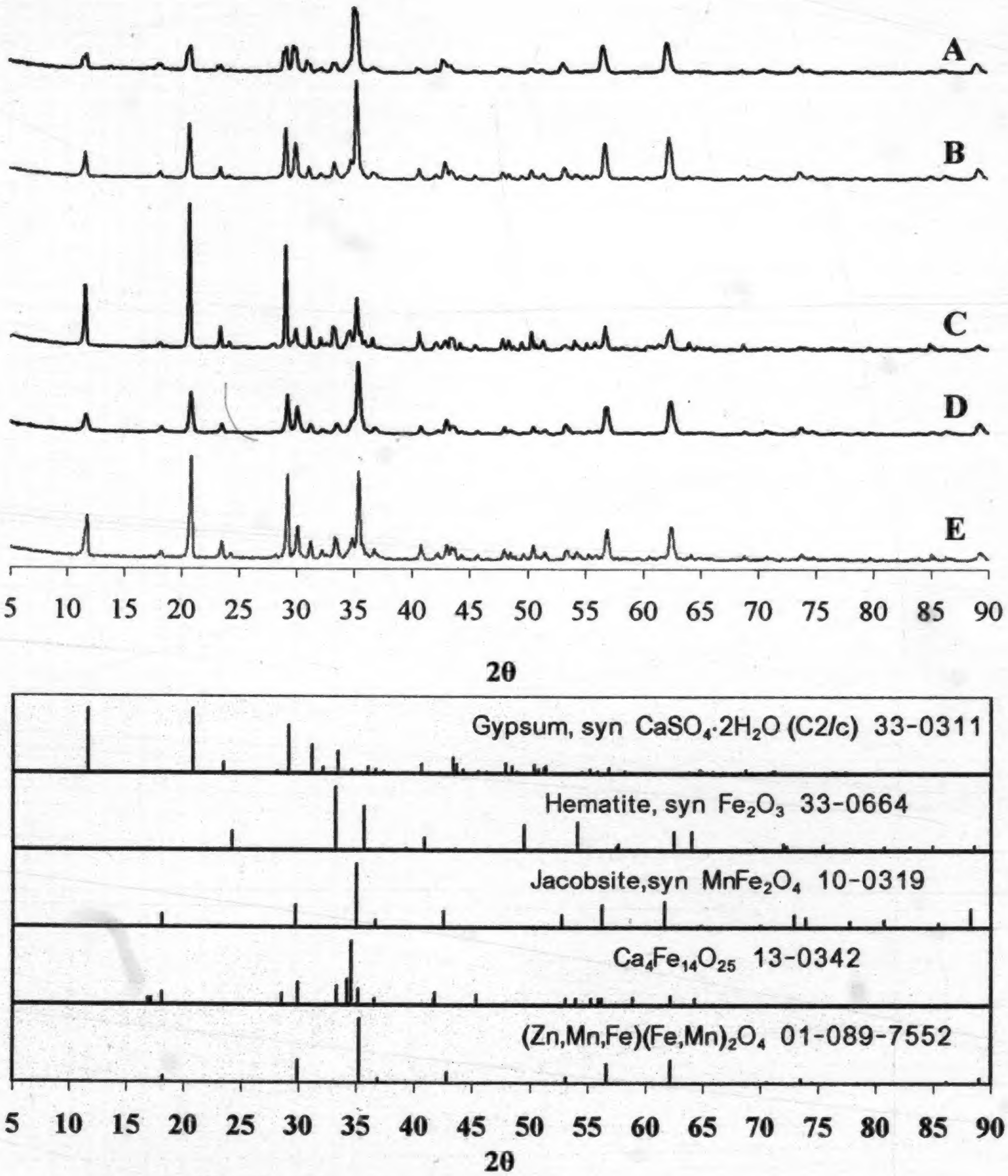

Figure 104 **XRD Patterns of EAF Dust Residue after Roasting with Coal and Leaching with 200 g/L H_2SO_4**

60 micrometers
60 micrometers
SE
BSE
15 micrometers
15 micrometers
A
B
A
A
A
SE
BSE

Figure 105 **Secondary Electron (SE) and Backscattered Electron (BSE) Images of EAF Dust after Roasting at 1000°C with 16% Coal and Leaching with 200 g/L H_2SO_4 (Sample C)**

These results indicate that the Altasteel EAF dust is highly amenable to roasting with coal to recover zinc through a combination of fuming and leaching. As discussed for the La Oroya zinc ferrite in Section 4.5.2.2.1, this DOE test should mean similar zinc recoveries are possible as would be expected during Waelz kiln processing of this material, although the methods used here require much lower temperatures to achieve the high zinc extractions than are typical for Waelz kiln operations. Because of the low temperatures, metallic iron is not formed during roasting, as it would be in most Waelz kiln processes, but, instead, a combination of Zn-Mn-Fe spinels, larnite (Ca_2SiO_4) and calcium ferrites are formed. During leaching, the iron oxides or Zn-Mn-Fe spinels are insoluble, with less than 4% of the iron extracted in most samples, while recovering up to 99% of the zinc by leaching or as fume.

It is possible, with an experimental setup more consistent with the rotary kilns used in Waelz kiln processing and, with increased air flow by the dust samples during roasting, that more of the zinc recovered in these tests by leaching the roasted EAF dust could leave the sample as fume during roasting rather than redepositing on the surface of the sample from the gas phase. This would eliminate the need for leaching of the roasted dust and, thus, would eliminate any potential concerns with the dissolution of the Ca-silicates and Ca-ferrites in the roasted dust during leaching, or with the amount of acid consumed to dissolve these compounds and to precipitate the dissolved calcium as gypsum. However, additional tests to optimize the zinc recoveries by fuming were not performed during these tests and will be the subject of future study.

Further analysis of the deportment of minor elements to the fume, the leach solutions and the leach residue will be discussed in Section 5.6.

5.5.2.2 Roasting with Coal and $CaCO_3$

Because of the large region of high zinc extractions over the conditions tested in Section 5.5.2.1, the temperatures and coal additions were lowered for the next DOE test. A temperature range of 850 to 1050°C and coal additions of 12 to 18% were used when the EAF dust was roasted with both coal and $CaCO_3$.

As Figure 106 indicates, the addition of $CaCO_3$ drastically depresses the overall zinc extractions during roasting of the EAF dust, compared with roasting with coal alone. A small area where the zinc extraction is greater than 90% is visible with an addition of 3.7% $CaCO_3$, but this area is pushed to higher temperatures and coal additions with increasing $CaCO_3$ addition, such that only a small region of 80 to 90% zinc extraction is visible at the highest $CaCO_3$ addition tested. This is in stark contrast to the results from roasting EAF dust with coal alone, where extractions of greater than 90% were possible at temperatures as low as 970°C and coal additions as low as 14.5%.

In Figure 106, iron extractions in the areas of maximum zinc extractions are all less than 10% which is consistent with extractions observed for roasting EAF dust, or La Oroya ferrite, with coal alone. However, a significant increase in the iron extraction in samples roasted at lower temperatures is observed as the addition of $CaCO_3$ is increased. A similar effect was observed during the roasting of the La Oroya ferrite with coal and $CaCO_3$ at very high (62%) $CaCO_3$ additions (Section 4.5.2.2.1.1). However, during roasting of EAF dust with coal and $CaCO_3$, this effect is observed even at very low $CaCO_3$ additions (3.7% $CaCO_3$) and becomes more pronounced as the $CaCO_3$ addition is increased.

The R^2 value for the response surface model for the amount of zinc fumed was very low (i.e., 0.426), but the contour plots of this model were included for comparative purposes (Figure 107). This model shows that 50% is the maximum amount of zinc fumed during roasting with coal and $CaCO_3$; this is a significant drop from roasting the EAF dust with coal alone, where up to 70% of the zinc was removed from the EAF dust as fume.

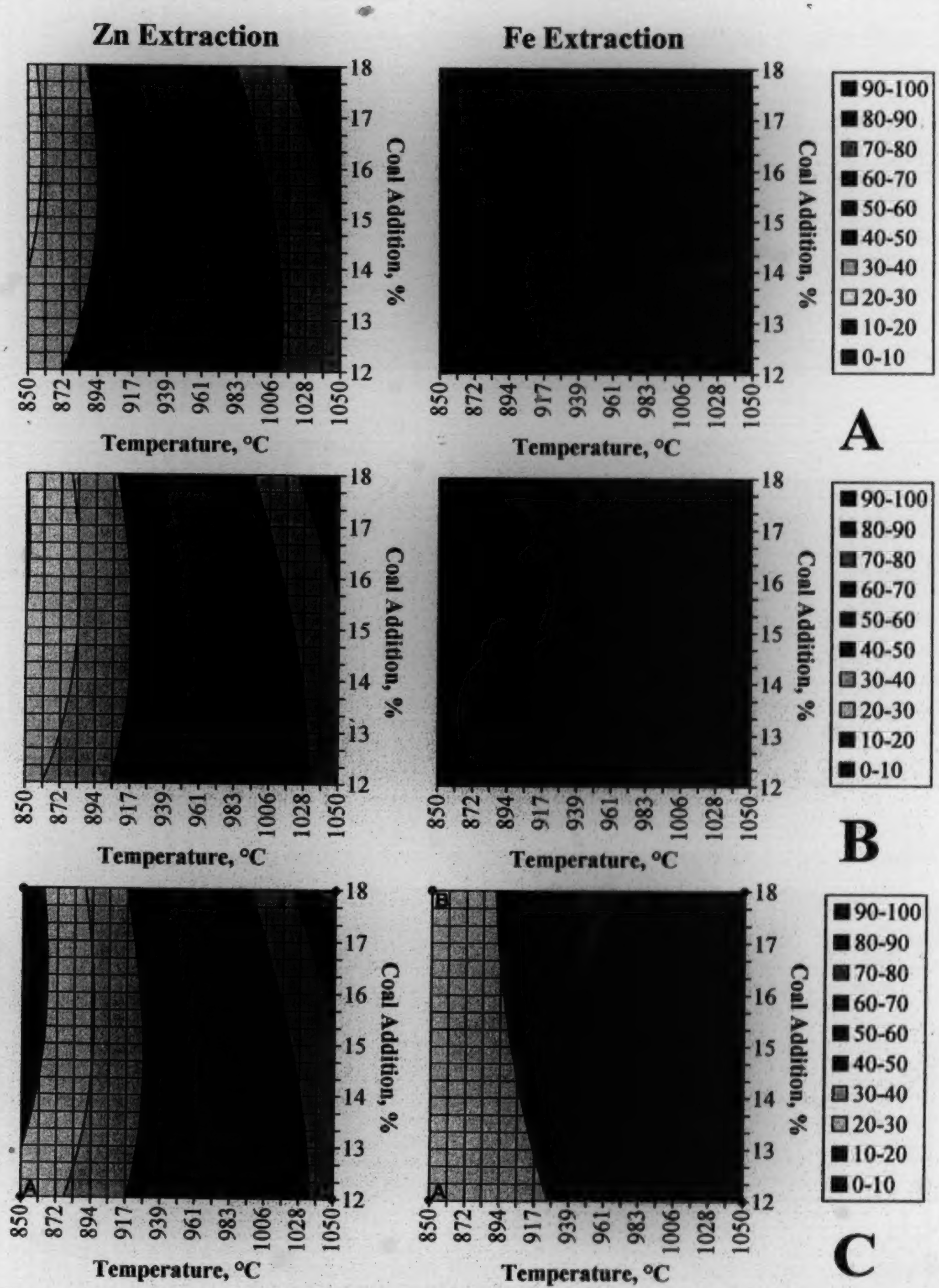

Figure 106 Effect of Coal Addition and Temperature on Zinc and Iron Extractions from Altasteel EAF Dust Roasted with $CaCO_3$ Additions of A) 3.7%, B) 8.9% and C) 14.1%

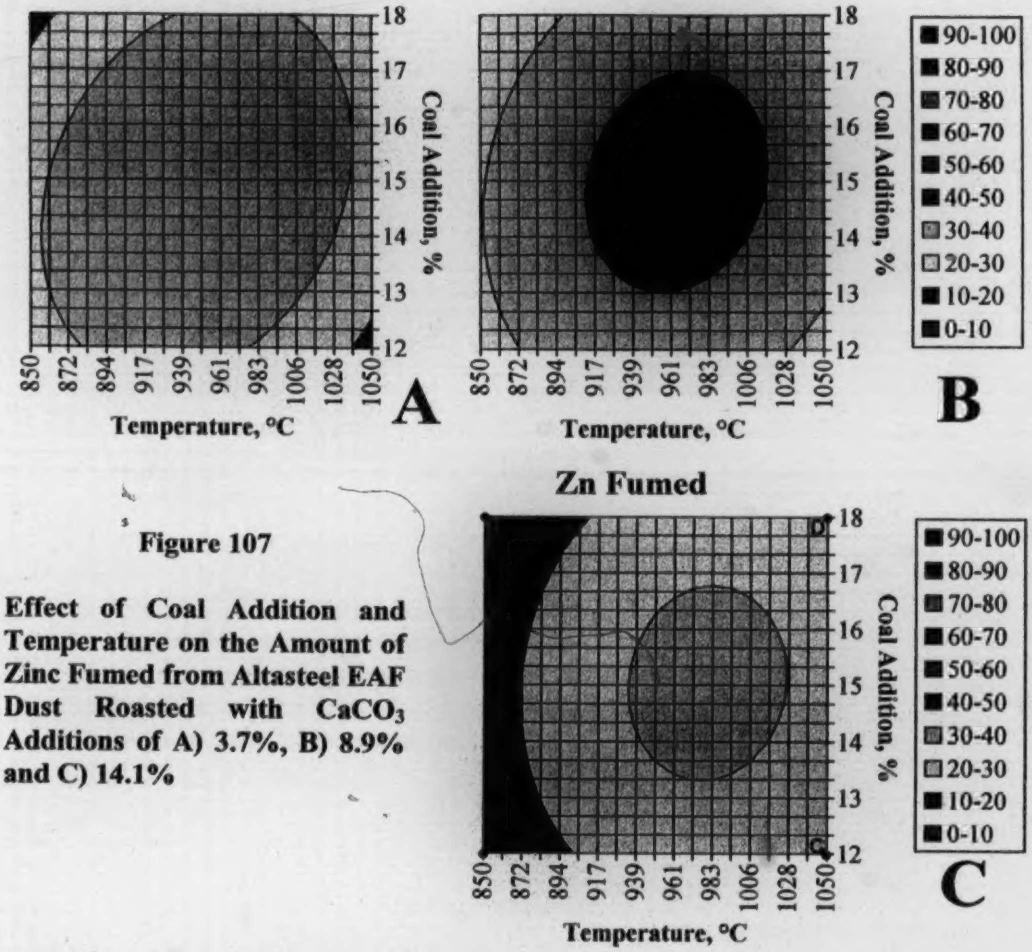

Figure 107

Effect of Coal Addition and Temperature on the Amount of Zinc Fumed from Altasteel EAF Dust Roasted with $CaCO_3$ Additions of A) 3.7%, B) 8.9% and C) 14.1%

Samples at various conditions described by the model for roasting with coal and 14.1% $CaCO_3$ were analyzed using x-ray diffraction (Points A through D on Figures 106C and 107C). The identified phases are listed in Table 50 while the diffraction patterns and major phases observed are shown in Figure 108.

Table 50 Phases Identified by XRD Analysis of EAF Dust Roasted with Coal and 14.1% $CaCO_3$

Sample	Identified Phases (in order of intensity)
A	$(Zn,Mn,Fe)(Fe,Mn)_2O_4$, $Ca_2Fe_2O_5$, Pb_3O_5
B	$(Zn,Mn,Fe)(Fe,Mn)_2O_4$, $Ca_2Fe_2O_5$, Ca_2SiO_4 (Larnite),
C	ZnO, $(Zn,Mn,Fe)(Fe,Mn)_2O_4$, $Ca_2Fe_2O_5$, Ca_2SiO_4 (Larnite)
D	ZnO, $(Zn,Mn,Fe)(Fe,Mn)_2O_4$, $Ca_2Fe_2O_5$, Ca_2SiO_4 (Larnite)

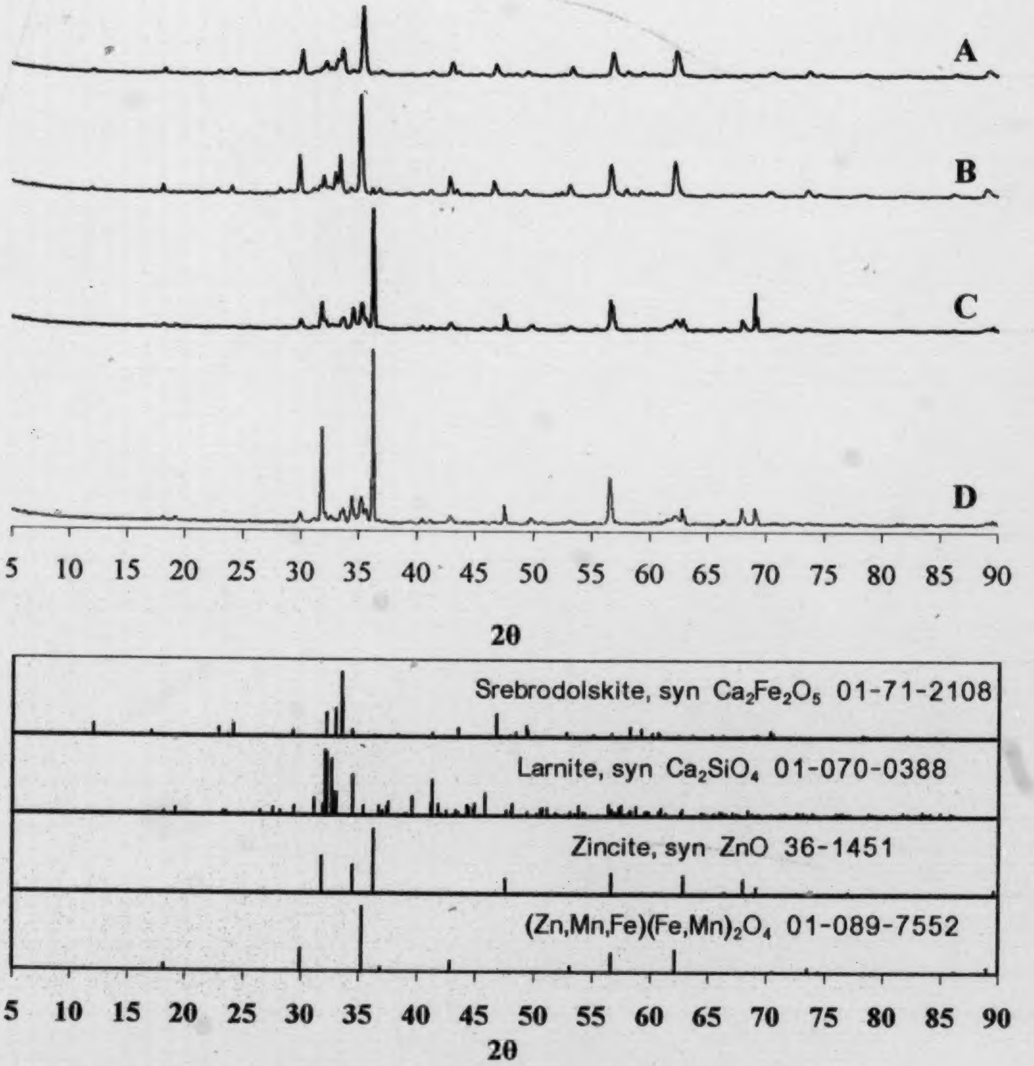

Figure 108 XRD Patterns of EAF Dust Roasted with Coal and $CaCO_3$

Zincite (ZnO) is present only in the samples roasted at 1050°C (Samples C and D) as the samples at lower temperatures only had zinc extractions of between 10 and 30%. (When roasting with coal alone, zincite was visible in even the samples roasted at 850°C as the zinc extractions were significantly higher at 30 to 60%.) The mixture of zinc and manganese ferrites is still the predominant iron-bearing phase in the EAF dust roasted with coal and $CaCO_3$ but, with the increase in calcium in the dust due to the addition of $CaCO_3$, the formation of srebrodolskite ($Ca_2Fe_2O_5$) is favored in all samples, instead of the less calcium-rich ferrite, $Ca_4Fe_{14}O_{25}$, or unreacted hematite (Fe_2O_3), observed in the EAF dust when roasted with coal alone. Larnite (Ca_2SiO_4) remains the major silicate phase in the roasted dust as it is observed in most of the samples with x-ray diffraction.

Using these phases as a starting point, an iron balance was constructed to estimate the distribution of iron among the iron minerals present in the roasted EAF dust (Table 51).

Table 51 Estimated Distribution of Iron in Mineral Phases after Roasting of EAF Dust with Coal and $CaCO_3$

Iron-Bearing Minerals	% of Total Iron in Feed				
	Feed	Sample A	Sample B	Sample C	Sample D
$ZnFe_2O_4$	50.3	43.7	44.8	14.0	6.2
$MnFe_2O_4$	22.7	22.7	22.7	22.7	22.7
Fe_3O_4	27.0	2.8	1.8	27.0	27.0
$Ca_2Fe_2O_5$	0.0	30.7	30.7	30.7	30.7
Fe_2O_3	0.0	0.0	0.0	5.6	13.4
Total	100.0	100.0	100.0	100.0	100.0
Extraction, %					
Zn		13.1	11.0	72.2	87.6
Fe		25.6	23.5	5.8	4.7
$Ca_2Fe_2O_5$ Leached*, %		83.4	76.5	18.8	15.4

* Extraction assuming 100% of the iron extracted comes from the leaching of $Ca_2Fe_2O_5$

The balance was calculated using the total zinc extractions (i.e., from leaching and fuming) to determine the amount of $ZnFe_2O_4$ that had reacted and assuming that all the calcium that is not associated with larnite (Ca_2SiO_4) reacts with either Fe_2O_3 from $ZnFe_2O_4$ decomposition or with magnetite (Fe_3O_4) to form $Ca_2Fe_2O_5$ and that all of the iron from the decomposition of $ZnFe_2O_4$ either reacts to form a calcium ferrite or is present as hematite (Fe_2O_3) in the roasted EAF dust. Once again, the balance reflects the phases observed in x-ray diffraction and their relative quantity. However, the balance indicates that, at lower temperatures, excess calcium is likely to react with magnetite (Fe_3O_4) to form srebrodolskite ($Ca_2Fe_2O_5$). Based on the magnitude of the iron extractions observed when roasting at 850°C (Samples A and B), this reaction must occur to a significant extent, and the resulting srebrodolskite ($Ca_2Fe_2O_5$) that is formed at these lower temperatures must be highly soluble, since iron equivalent to over 76% of the $Ca_2Fe_2O_5$ in the dust is dissolved during leaching with 200 g/L H_2SO_4 solutions. However, this balance also indicates $Ca_2Fe_2O_5$ formed at higher temperatures is less soluble in H_2SO_4 solution as with the equivalent of less than 19% of the iron present in $CaFe_2O_5$ is leached from those samples.

A number of different phases can be identified using backscattered electron imaging in the SEM and EDX analysis of Sample D (1050°C, 18% coal, 14.1% $CaCO_3$) after roasting (Figure 109). The bright elongate, or platelike, phase (A) observed is high in Zn and O (i.e., ZnO) while the other light grey phases are likely mixtures of calcium and/or manganese ferrites as they were found to contain either Ca, Mn, Fe and O (E), or Ca, Fe and O (F). Particles containing Ca, Si and O (B) and Ca, Mg, Si and O (C) were also observed and are likely calcium- or calcium-magnesium-silicates. (The long dark grey particle (D), however, is unique in the field of view in Figure 109, as it contains Cr, K, Na, S and O, possibly representing a mixture of Na- or K-sulphates and/or Na- or K-chromates).

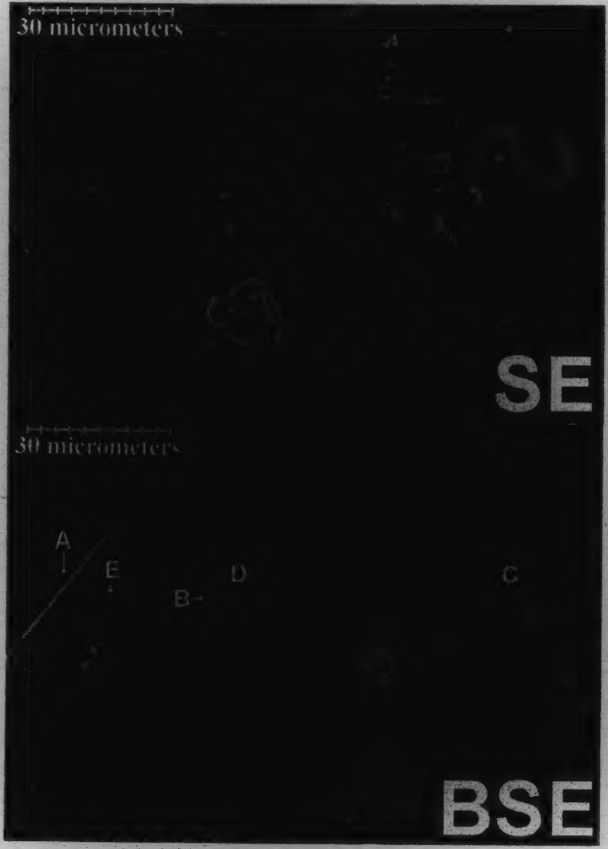

Figure 109
Secondary Electron (SE) and Backscattered Electron (BSE) Images of EAF Dust after Roasting at 1050°C with 18% Coal and 14.1% $CaCO_3$ (Sample D)

As observed in Section 5.5.2.1, zincite (ZnO) and larnite (Ca_2SiO_4) are no longer detected using x-ray diffraction on any of the samples, indicating that these phases were dissolved during leaching (Table 52 and Figure 110). Gypsum ($CaSO_4 \cdot 2H_2O$) is again identified as a major phase in the roasted EAF dust, forming due to the reprecipitation of dissolved calcium in the H_2SO_4 leach, and unleached iron is present primarily as Zn-Fe-Mn ferrites in the leach residue. Srebrodolskite ($Ca_2Fe_2O_5$) and $CaFe_2O_4$ are also observed in the x-ray diffraction patterns in the leach residues of Samples C and D, but not in the samples roasted at lower temperatures. This is consistent with the higher iron extractions at lower roasting temperatures seen in Figure 106 and the results of the iron balance in Table 51 and likely indicates that the calcium-iron oxides formed at higher temperatures are less soluble in H_2SO_4 than those formed at lower roasting temperatures.

Table 52 Phases Identified by X-ray Diffraction Analysis of EAF Dust after Roasting with Coal and 14.1% $CaCO_3$ and Leaching with 200 g/L H_2SO_4

Sample	Identified Phases (in order of intensity)	Leaching Wt. Loss, %
A	$(Zn,Mn,Fe)(Fe,Mn)_2O_4$, $CaSO_4 \cdot 2H_2O$	-7.0
B	$(Zn,Mn,Fe)(Fe,Mn)_2O_4$, $CaSO_4 \cdot 2H_2O$	-12.7
C	$CaSO_4 \cdot 2H_2O$, $(Zn,Mn,Fe)(Fe,Mn)_2O_4$, $Ca_2Fe_2O_5$, $CaFe_2O_4$	2.5
D	$CaSO_4 \cdot 2H_2O$, $(Zn,Mn,Fe)(Fe,Mn)_2O_4$, $CaFe_2O_4$, $Ca_2Fe_2O_5$	7.8

SEM/EDX analysis of Sample D (1050°C, 18% coal, 14.1% $CaCO_3$) after leaching showed that gypsum ($CaSO_4 \cdot 2H_2O$) was present in the leach residue as fine needlelike particles (A) and, again, is the principal phase in the field of view (Figure 111). Several iron oxide phases are also identified in the leach residue, including particles high in Mg, Mn and Ca (i.e., a mixture of $(Mg,Mn)Fe_2O_4$ and $Ca_2Fe_2O_5$ (B)), high in Zn and Mn (i.e., unreacted $(Zn,Mn)Fe_2O_4$ (C)) and high in Ca and Fe (i.e., $Ca_2Fe_2O_5$ (D)).

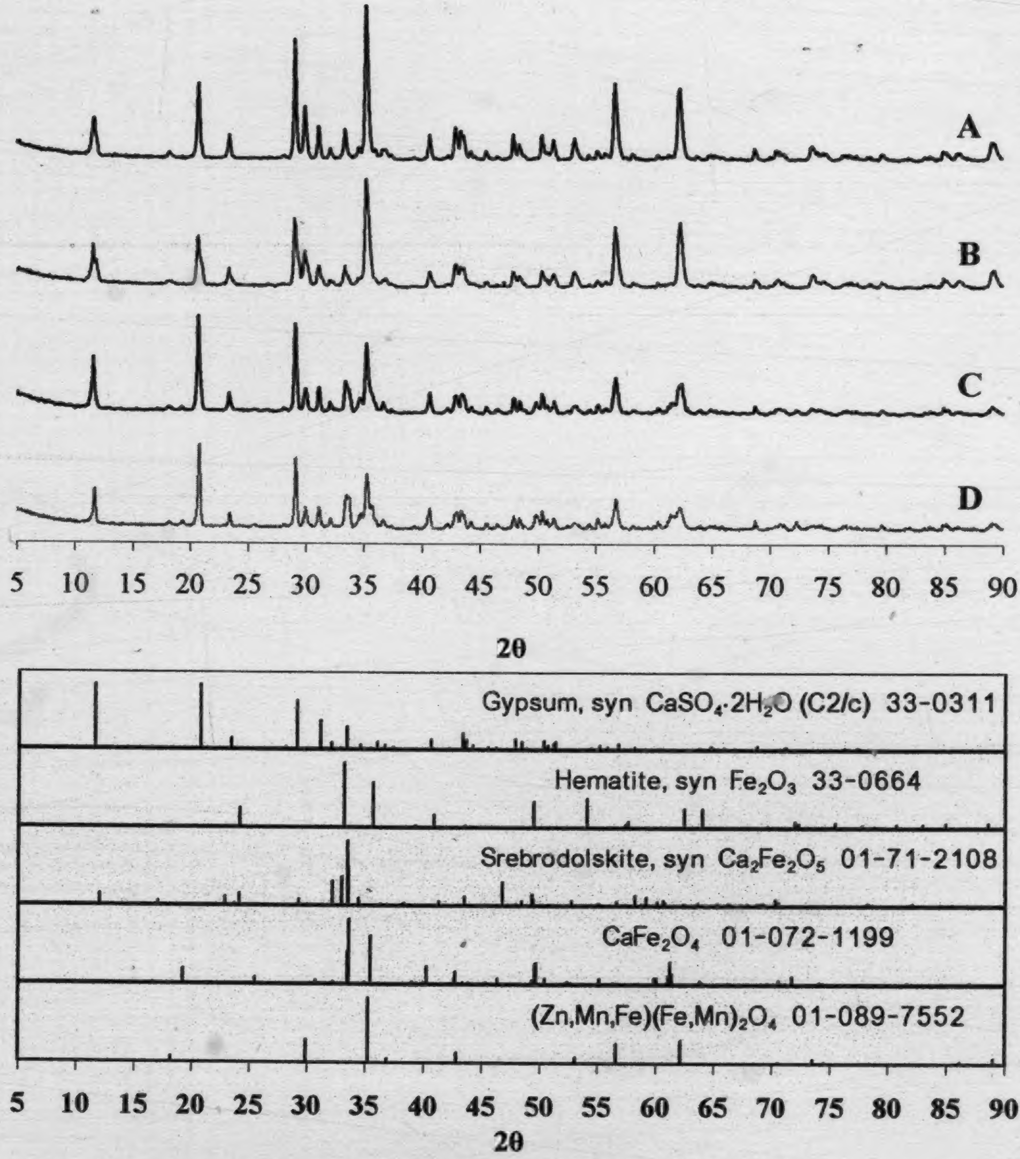

Figure 110 XRD Patterns of EAF Dust Residue after Roasting with Coal and $CaCO_3$ and Leaching with 200 g/L H_2SO_4

Thus, this DOE test indicates that adding $CaCO_3$ during roasting of EAF dust with coal can aid in the formation of acid-insoluble calcium ferrites, but roasting temperatures of over 1050°C would be necessary to maintain zinc extractions of greater than 90%. At those roasting temperatures, based on the observations from this DOE test, the combination of $MnFe_2O_4$, srebrodolskite ($CaFe_2O_5$), magnetite (Fe_3O_4) and hematite (Fe_2O_3) in the residue should only have a limited solubility, with iron extractions of less than 5% expected at the conditions required to maximize zinc extractions. These results indicate that operating at lower temperatures, not only lowers the zinc extraction possible during leaching, but may encourage side reactions with the magnetite (Fe_3O_4) in the dust and the formation of srebrodolskite ($Ca_2Fe_2O_5$) with a higher solubility in H_2SO_4 solutions.

However, roasting with $CaCO_3$ and coal has little advantage over roasting with coal alone for the Altasteel EAF dust since lower temperatures can be used to achieve higher zinc extractions without the use of $CaCO_3$. Because of the lower energy costs for roasting at lower temperatures, roasting with coal alone would be more likely to be pursued commercially than roasting with coal and $CaCO_3$.

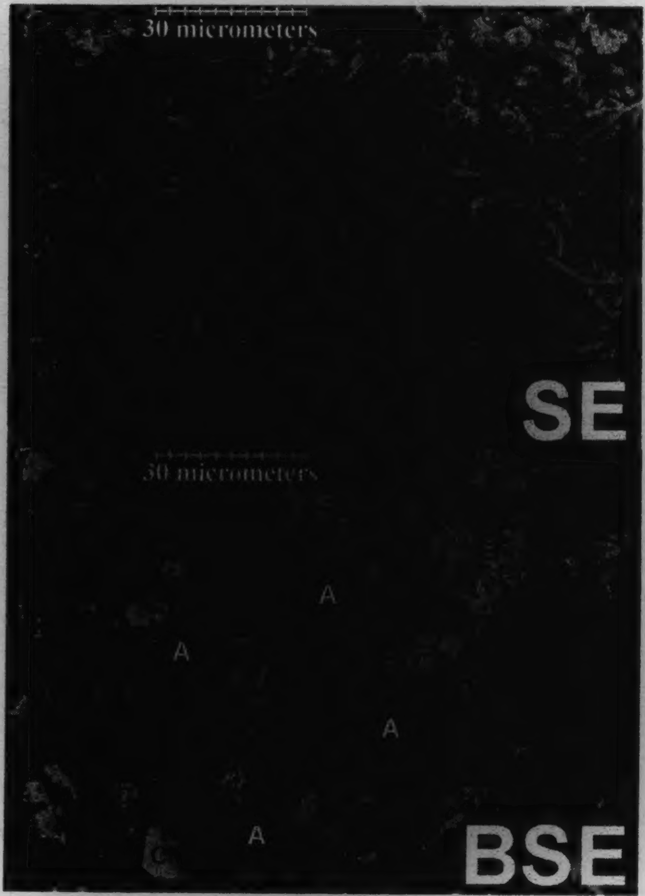

Figure 111
Secondary Electron (SE) and Backscattered Electron (BSE) Images of EAF Dust after Roasting at 1050°C with 18% Coal and 14.1% $CaCO_3$ and Leaching with 200 g/L H_2SO_4 (Sample D)

5.6 Deportment of Minor Elements

Selected solids and solution samples were analyzed to try to understand the deportment of minor elements in the various possible process options identified in this research. From this work, only two process options were selected: roasting with Na_2CO_3 and lower temperature (i.e., 1000°C) roasting with coal.

Solutions and solids, after fusing with lithium metaborate, were analyzed for As, Na and K using a Varian SpectrAA 220FS atomic absorption spectrometer, with As analyzed using a deuterium lamp for background correction. Carbon and sulphur were analyzed using an EMIA-320V carbon/sulphur analyzer. Chloride and fluoride analyses were analyzed using ion selective electrodes. (Chloride and fluoride analyses on solids samples were performed after fusing the solids with Na_2CO_3/Na_2O_2 in a zirconium crucible and leaching the fusate with H_2SO_4 and HNO_3.) All other analyses were performed using a Perkin-Elmer 4000 atomic absorption (AA) spectrometer.

5.6.1 Roasting with Na_2CO_3

Table 53 shows the deportment of minor elements during roasting of Altasteel EAF dust with 40% Na_2CO_3 at 950°C. With the exception of K, Na and Cr, only minor levels of impurities are dissolved into solution during water leaching and only 2% of the zinc is leached in hot water. Chromium is selectively and extensively leached in water leaching as are molybdenum and vanadium. Sodium is also leached to a significant extent in the water leach solution.

Overall zinc extractions are low (89.7%) in this sample; higher roasting temperatures are necessary to reach higher zinc extractions as noted in Section 5.5.1.1. Gypsum formation during leaching results in a very high sulphur content in the leach residue.

Table 53 Deportment of Minor Elements in Altasteel EAF Dust during Roasting with 40% Na_2CO_3 at 950°C

	Element Distribution, %			Composition, % or g/L			
	Water Leach Solution	Acid Leach Solution	Residue	Feed	Leach Residue	Water Leach Solution[1]	Acid Leach Solution[2]
Solids, g				1000	652.8	-	-
Solution, L				-	-	1.6	3.2
Zn	3.1	86.6	10.3	9.4	1.05	1.8	25.6
Fe	0.0	56.6	43.4	31.9	21.2	-	56.7
Na[3]	82.0	11.9	6.1	1.32	1.37	96.2	7.0
Al	34.7	30.1	35.2	0.50	0.27	1.09	0.47
Cd	0.0	22.7	77.3	0.03	-	0.00	0.02
Ca	0.0	2.1	97.9	7.14	10.7	0.00	0.47
Cr	91.7	2.5	5.8	0.34	0.03	1.96	0.03
Cu	0.2	59.0	40.8	0.40	0.25	0.01	0.74
Pb	2.3	2.2	88.0	0.90	1.35	0.13	0.06
Mg	0.0	40.0	60.0	0.98	0.90	0.00	1.23
Mn	0.0	3.1	96.9	3.56	5.28	0.00	0.35
K	88.5	8.8	2.7	0.82	0.035	4.56	0.23
Si	10.5	63.3	26.2	1.92	0.77	1.27	3.82
As	9.4	4.1	1.5	0.039	-	0.023	0.005
Cl	4.3	27.4	24.6	1.45	0.55	0.392	1.25
Co	2.4	53.4	44.2	0.007	-	0.001	0.012
F	5.5	5.6	88.9	0.013	0.0028	0.016	0.027
Ni	0.4	25.9	73.7	0.039	-	0.001	0.032
Mo	100.0	0.0	0.0	0.015	-	0.094	0.000
V	66.9	29.8	3.3	0.008	-	0.034	0.007
C	9.2	6.2	0.3	4.71	0.04	n.a.	n.a.
S	94.2	0.0	0.0	0.43	6.59	n.a.	n.a.

[1] Estimated from element distribution and assuming a solids concentration of 625 g/L

[2] Estimated from element distribution and assuming a leach solution of 225 g/L H_2SO_4

[3] Sodium extractions include the sodium added as Na_2CO_3 during roasting.

* For 1000 g of feed, 1.2 g of fume would be expected to be produced containing 57.9% Pb and 28.5% As as their respective oxides. (7.5% of Pb and 85% of As report to this fume.) 84.3% of the carbon and 5.8% of the sulphur are also lost to the gas stream.

5.6.2 Roasting with Coal

Table 54 shows the deportment of minor elements during roasting of Altasteel EAF dust with 16% coal at 1000°C. The carbon content of the as-received EAF dust is quite high (4.7%) and this carbon content could explain the lower coal additions required to achieve high extractions as noted in Section 5.5.2.1. Because of the low zinc concentration in the feed, a maximum for the solids concentration during leaching of 1000 g/L was set for the acid leach, which corresponds to an acid leach concentration of about 180 g/L H_2SO_4.

Table 54 Department of Minor Elements in Altasteel EAF Dust during Roasting with 16% Coal at 1000°C

	Element Distribution, %			Composition, % or g/L			
	Solution	Residue	Fume	Feed	Leach Residue	Leach Solution[1]	Fume
Solids, g				1000	1019		56.6
Solution, L						1.0	
Zn	51.9	48.1	43.1	9.4	1.00	89.3	71.7
Fe	2.0	98.0	0.0	31.9	36.6	6.38	
Na	32.6	67.4	0.0	1.32	1.04	4.30	
Al	53.4	46.6	0.0	0.50	0.27	2.67	
Cd	0.4	5.6	94.0[2]	0.03	n.a.	0.28	0.5
Ca	1.9	98.1	0.0	7.14	8.2	1.36	
Cr	8.9	91.1	0.0	0.34	0.36	0.30	
Cu	2.6	97.4	0.0	0.40	0.32	0.10	
Pb	1.4	48.7	49.9	0.90	0.52	0.13	7.9
Mg	7.6	92.4	0.0	0.98	1.06	0.74	
Mn	1.8	98.2	0.0	3.56	4.09	0.64	
K	20.9	79.1	0.0	0.82	0.76	1.71	
Si	30.5	69.5	0.0	1.92	2.89	5.86	
As	12.7	2.3	85.0[2]	0.039	n.a.	0.050	0.6
Cl	0.3	19.4	80.3	1.45	0.33	11.7	
Co	9.9	90.1	0.0	0.007	n.a.	0.007	
Ni	1.2	98.8	0.0	0.039	n.a.	0.005	
Mo	100.0	0.0	0.0	0.015	n.a.	0.150	
V	99.2	0.8	0.0	0.008	n.a.	0.079	
F	93.3	6.7	0.0	0.13	0.001	0.121	
C	0.0	0.0	100.0	4.71	0.0	n.a.	n.a.
S	-[3]	-[3]	0.0	0.43	4.16	n.a.	n.a.

[1] Estimated from element distribution and assuming a solids concentration of 1000 g/L in leaching and assuming the fume produced is leached with no dissolution of Pb or As

[2] Estimated

[3] More sulphur is present in the residue than in the feed due to gypsum formation during leaching.

5.7 Preliminary Evaluation of Potential Processing Options

Because of the low volume of EAF dust produced by Altasteel (15000 t/y), it is unlikely that any process could be operated to economically recover zinc or other metals because of the unfavorable economics of having to operate at such a small scale. However, the implications of the processing, assuming the availability of larger tonnages of EAF dust, using the roasting processes proposed here will be discussed.

5.7.1 Roasting with Na_2CO_3

A possible process flowsheet for the processing of electric arc furnace dust with Na_2CO_3 roasting is illustrated in Figure 112.

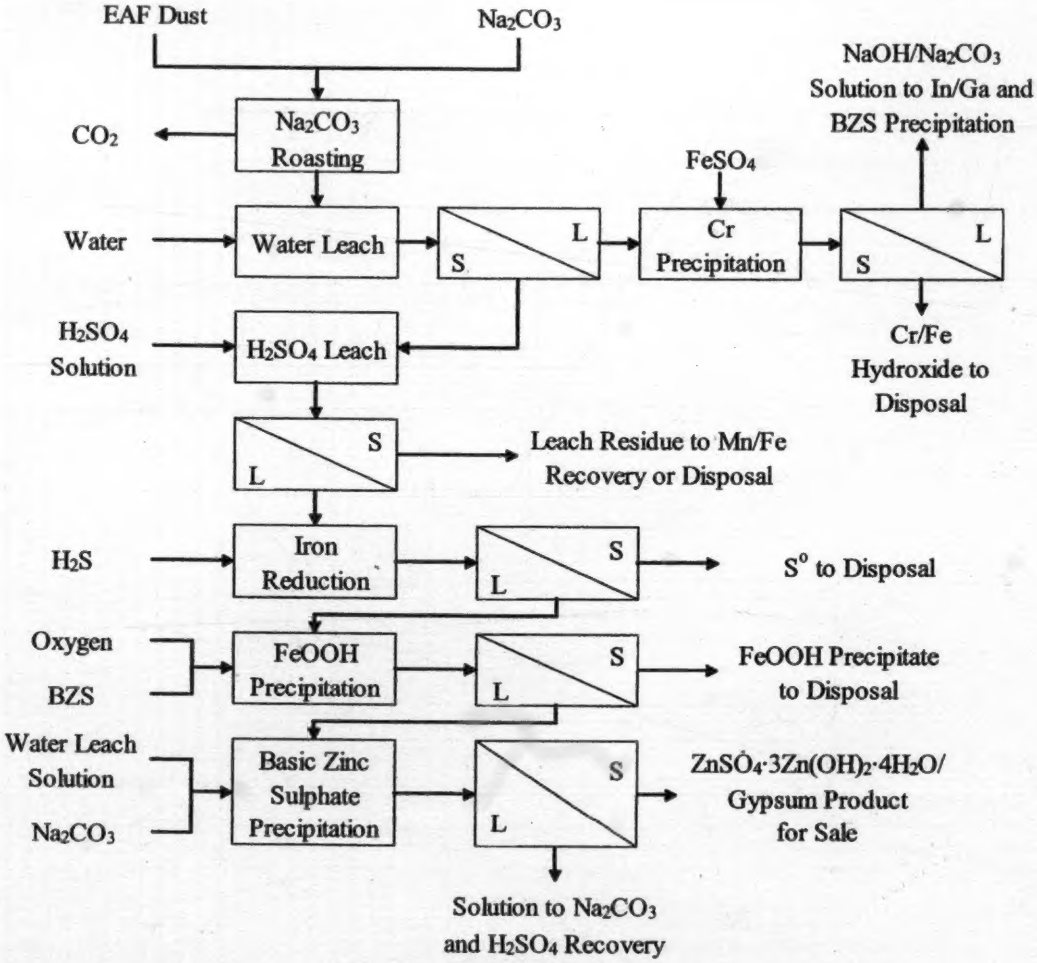
EAF Dust
Na2CO3
CO2
Na2CO3 Roasting
NaOH/Na2CO3 Solution to In/Ga and BZS Precipitation
FeSO4
Water
Water Leach
S
L
Cr Precipitation
S
L
H2SO4 Solution
H2SO4 Leach
Cr/Fe Hydroxide to Disposal
S
L
Leach Residue to Mn/Fe Recovery or Disposal
H2S
Iron Reduction
S
L
S° to Disposal
Oxygen
BZS
FeOOH Precipitation
S
L
FeOOH Precipitate to Disposal
Water Leach Solution
Na2CO3
Basic Zinc Sulphate Precipitation
S
L
ZnSO4·3Zn(OH)2·4H2O/ Gypsum Product for Sale
Solution to Na2CO3 and H2SO4 Recovery

Figure 112 Possible Process Flowsheet for Na_2CO_3 Roasting of EAF Dust

Sodium recovery and H_2SO_4 regeneration would be carried out by the methods outlined in Section 4.7.1.1.

This flowsheet is very similar to the one presented in Section 4.7.1.1.1 for roasting La Oroya zinc ferrite with Na_2CO_3 and $MnCO_3$ followed by water and acid leaching, but the following changes were made. (

First, because of the high chromium extraction in water leaching, chromium precipitation would be required before the water leach solution could be used as a neutralizing agent later on in the process. A variety of methods for the removal of chromium from solution have been proposed, or are being used commercially, as chromium is a major impurity in waste streams from leather tanning (169). However, the simplest method for chromium removal from this solution appears to be adding $FeSO_4$ to form a mixed Cr/Fe hydroxide. All of the chromium in the water leach solution is initially present as Cr^{6+} but, at the high pH of the water leach solution (i.e., pH 11 in the DOE test water leach solution), upon reduction of Cr^{6+}, Cr^{3+} would readily precipitate from solution. A scoping test on a small volume of water leach solution from the DOE tests showed that the addition of $FeSO_4$ readily reduced Cr^{6+} to Cr^{3+} and both Cr^{3+} and Fe^{3+} precipitated from solution as their respective hydroxides, with less than 0.1 mg/L Cr detected in the solution after precipitation. The hydroxide precipitate was easily separated from the solution by vacuum filtration.

Second, because the integration of an EAF dust treatment facility with an existing zinc smelter is unlikely, the flowsheet had to be modified to reflect the availability of various reagents. For example, without zinc concentrate available to use in iron reduction, another reductant, such as H_2S, would have to be used to reduce Fe^{3+} to Fe^{2+} to allow for goethite precipitation. A significant proportion of the basic zinc sulphate precipitated would have to be recycled to goethite precipitation to neutralize the acid produced during precipitation. Finally, because of the low sodium addition required during roasting, the sodium content of the water leach solution is lower and, thus, the water leach solution has less neutralizing capacity than the water leach solution from the roasting of zinc ferrite.

Based on the solution analyses presented in Section 5.6.1, the water leach solution would be expected to meet 56% of the neutralization requirements for BZS precipitation and the remaining neutralization requirement would have to be made up with Na_2CO_3 or $CaCO_3$.

Without integration with a zinc smelter, basic zinc sulphate would be the primary zinc product produced for sale. While this is a saleable product, and easily integrated into existing zinc smelter flowsheets, it would command a considerably lower price than zinc metal and, thus, this would affect the economics of any plant using this process.

Another of the major hindrances of treating the Altasteel EAF dust is the low zinc content and the high iron content of the as-received material. If treatment were considered, it may be valuable to test the feasibility of magnetic separation to remove magnetite (Fe_3O_4) values from the EAF dust prior to Na_2CO_3 roasting. Given the morphology of the as-received EAF dust (Figure 74), it is uncertain whether this would be possible, but if low-zinc iron oxides can be rejected, then the grade of zinc in roasting could be increased while decreasing the amount of material treated using Na_2CO_3 roasting and possibly decreasing the amount of iron reacting with sodium during roasting and reporting to the acid leach solution.

5.7.1.1 Iron and/or Manganese Recovery

The leach residue after Na_2CO_3 roasting contains 1.1% Zn, 21.2% Fe, 1.1% Al, 10.7% Ca, 1.4% Pb, 1.3% Na, 5.3% Mn, 0.8% Si and 6.6% S. As discussed previously in Sections 4.7.1.2 and 4.7.2.1, various impurities in the residue, including Cu, Pb, Na and S, would determine the potential to recover the iron or manganese values using a direct reduced iron (DRI) or an iron smelting process.

Sulphur, mostly present in the leach residue as gypsum ($CaSO_4 \cdot 2H_2O$), is a major impurity in the leach residue from the roasting of EAF dust. While it is possible that the iron values could be separated from the gypsum in the residue using magnetic separation or other mineral processing techniques, it is still likely that sulphur contamination could be an issue with further processing of this material.

Copper in the EAF dust is much lower than in the zinc ferrite with a Cu:Fe ratio of 0.013:1 in the as-received EAF dust. However, the Cu:Fe ratio is not significantly improved in the leach residue (0.012:1), though it is improved if the iron and copper content of the goethite and leach residue are combined (0.005:1). However, in all cases, the Cu:Fe ratio is higher than the allowable copper levels in automobile shredder scrap (0.25%), and it is unlikely that a marketable steel product could be produced from these residues as a result.

5.7.2 Roasting with Coal (Waelz Kiln Processing)

A possible flowsheet for roasting with coal following by water leaching is presented in Figure 113. This flowsheet is very similar to that presented in Section 4.7.2, but with the following modifications. H_2S is used instead of zinc concentrate as a reducing agent in iron reduction, basic zinc sulphate is recycled to goethite precipitation to neutralize the acid produced during precipitation, and basic zinc sulphate is the zinc product produced for sale. (Iron extractions are low during acid leaching and, thus, reduction and neutralization requirements for goethite precipitation, and the amount of goethite precipitate, would be low for this process flowsheet.) The high calcium content of the EAF dust would be expected to cause significant sulphate losses through the precipitation of gypsum during acid leaching.

Again, the low zinc grade of the EAF dust limits the solids concentration possible during acid leaching. As mentioned earlier, any concentration of the zinc values in the EAF dust prior to roasting (i.e., by removal of magnetite values) would be advantageous to this process flowsheet as well.

The high sulphur content (4.2%) of the residue because of gypsum precipitation during leaching and the Cu:Fe ratio in the leach residue (0.009:1) are likely to make further processing of the leach residue to recover iron or manganese undesirable.

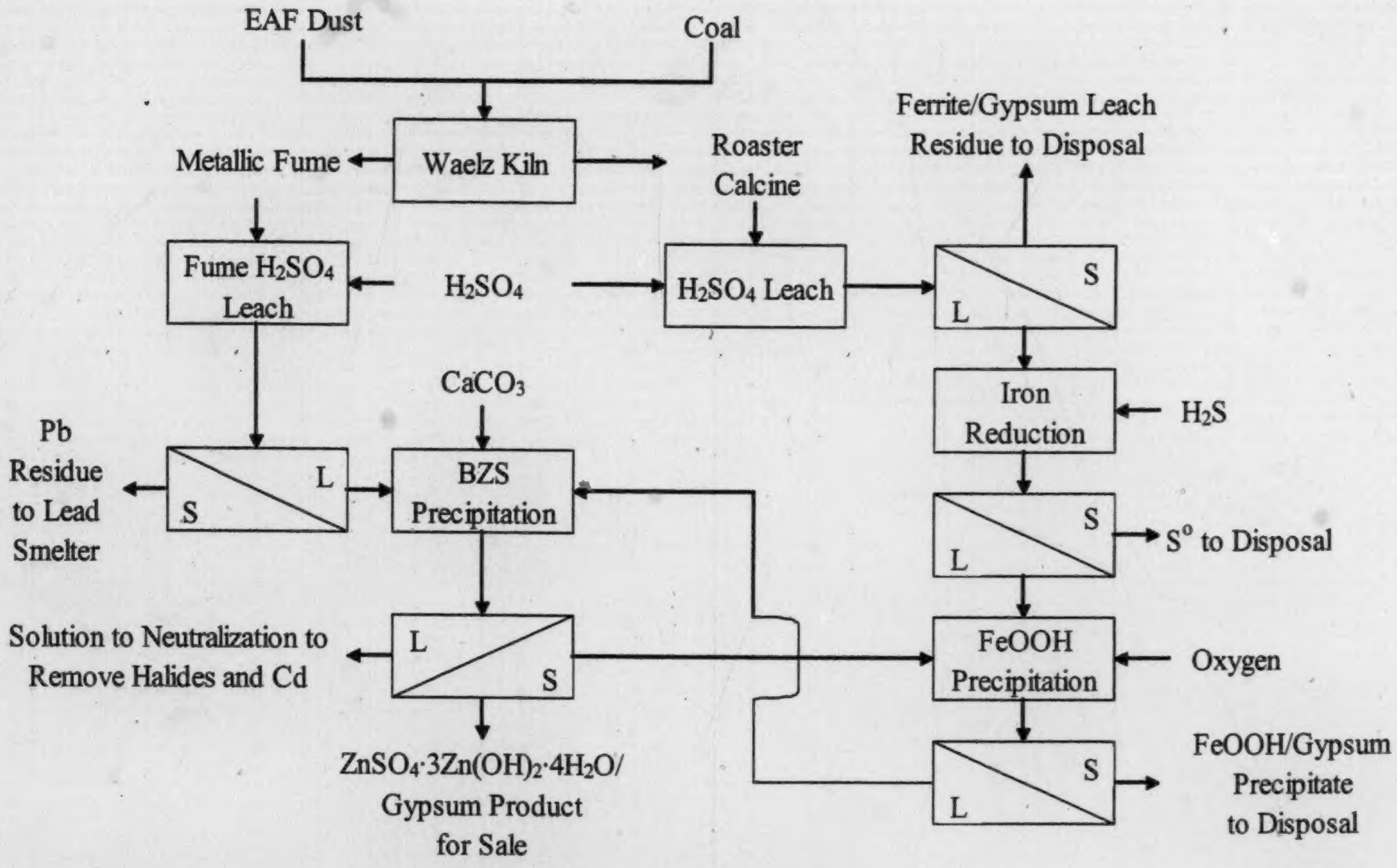
EAF Dust
Coal
Waelz Kiln
Metallic Fume
Roaster Calcine
Ferrite/Gypsum Leach Residue to Disposal
Fume H_2SO_4 Leach
H_2SO_4
H_2SO_4 Leach
S
L
Iron Reduction
H_2S
$CaCO_3$
Pb Residue to Lead Smelter
L
S
BZS Precipitation
S
L
S^o to Disposal
Solution to Neutralization to Remove Halides and Cd
L
S
FeOOH Precipitation
Oxygen
$ZnSO_4 \cdot 3Zn(OH)_2 \cdot 4H_2O$/ Gypsum Product for Sale
S
L
FeOOH/Gypsum Precipitate to Disposal

Figure 113 Potential Process Flowsheet for Roasting of EAF Dust with Coal

Overall, processing this material by roasting with coal and then acid leaching has few advantages over traditional Waelz kiln processing. Without integration with a zinc plant, recovery or regeneration of H_2SO_4 would be difficult and, thus, fresh acid would have to be added continuously in this flowsheet which would significantly increase operating costs for this process. The high carbon content of the EAF dust makes this material highly amenable to conventional Waelz kiln processing; increased roasting temperatures would cause most of the zinc to be removed as fume and the high manganese content of the EAF dust would reduce the amount of iron reduced to metallic iron and, thus, would improve the thermodynamics of the Waelz kiln process, as described in Section 4.7.2.

Based on this analysis, without integration with an existing zinc smelter, and without larger tonnages of dust available for treatment, processing of EAF dusts by these processes (i.e. Na_2CO_3 roasting or coal roasting/acid leaching) would be difficult to operate economically. Thus, as discussed in the literature survey of EAF treatment processes in Section 5.2.3, traditional Waelz kiln processing appears to be the most feasible method of treatment investigated to date for this material.

5.8 Conclusions

Only one potentially novel transformational roasting system was identified through the application of the generalized procedure to the Altasteel EAF dust. Sodium carbonate roasting of the EAF dust resulted in zinc extractions of over 90% while leaching 50 to 60% of the iron into solution. The addition of secondary additives to further reduce the iron extraction was ineffective for this material.

Mineralogically, the EAF dust behaved with much more complexity than the La Oroya zinc ferrite. This study points to the low crystallinity of the EAF dust feed, the formation of $(Zn,Mn)Fe_2O_4$ solid solutions and the reaction of other non-$ZnFe_2O_4$ iron compounds with Na_2CO_3 during roasting as potential reasons for this behaviour.

After minor element analysis and preliminary flowsheet development, Waelz kiln processing appears to be the most feasible process option for treating this waste material.

6.0 Application of the General Procedure to the Treatment of Inco Copper Residue

Two samples of copper residue from Inco's Thompson Refinery were obtained in 2005, one from Inco's research facilities in Mississauga, ON and another directly from Thompson, MN. This material is byproduct of the electrorefining of nickel matte and is produced at a rate of 4000 t/y and, at present, is not treated further for metals recovery, resulting in an accumulation of about 100 000 t in containment ponds at Inco's Thompson refinery (170). Analyses of the samples obtained are presented in Table 55 below.

Table 55 Analysis of INCO Copper Residue

Sample	Analysis, %							
	Al	As	Cu	Ni	Fe	Pb	Si	S
1	0.06	1.93	30.8	4.74	0.25	0.17	0.21	19.1
2	0.13	3.04	29.7	3.80	0.31	0.61	0.31	28.1

At 2005 metal prices (171,172), the contained copper and nickel would be valued at between US$1660 and $1840 per tonne.

The particle size distribution of Feed #1 was analyzed using a Malvern Mastersizer 2000 and this sample showed a bimodal distribution with a D_{90} of 98.8 μm and a D_{50} of 24.8 μm. Due to the fine particle size of this sample, it was used directly in the roasting tests without further grinding.

SEM micrographs of Feed #1 of the Inco copper residue feed are shown in Figure 114 with micrographs of Feed #2 shown in Figure 115. The material in Feed #1 (Figure 114) is extremely fine and platelike and, with imaging with back-scattered electrons, the coloration of the residue is very uniform, indicating a high degree of homogeneity. EDX analysis of the feed showed the presence of Cu, Ni, S and Cl, with minor amounts of arsenic, but no distinct phases could be identified in the feed using EDX. Even though the second feed sample is also very fine, more distinct phases can be observed using backscattered electron imaging (Figure 115). The dipyramidal crystals (A) contain sulphur and the crystal shape of the particles is consistent with that expected for elemental sulphur. Other particles include sulphides, including particles high in Cu and As (B), Ni and Cu (C) and Ni, Cu and As (D), and sulphates with varying Ni:Cu ratios in the EDX analysis (i.e., 1:1 Ni:Cu (E) and 2:1 Ni:Cu (F). Some of the sulphidic particles also contain low levels of chloride (i.e., particles B and D).

20 micrometers
20 micrometers
SE
BSE
5 micrometers
5 micrometers
SE
BSE

Figure 114 Secondary Electron (SE) and Backscattered Electron (BSE) Images of As-Received Inco Copper Residue (Feed #1)

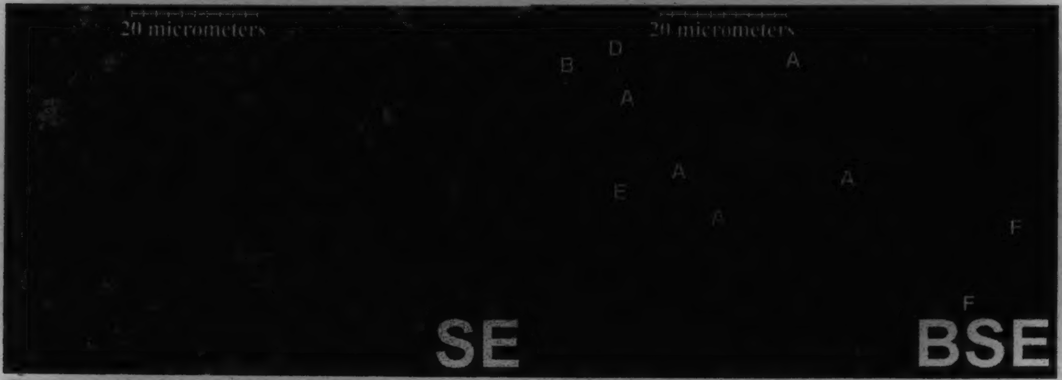
20 micrometers
20 micrometers
D
B
A
A
A
E
A
A
F
F
SE
BSE

Figure 115 Secondary Electron (SE) and Backscattered Electron (BSE) Images of As-Received Inco Copper Residue (Feed #2)

X-ray diffraction of the two feed samples was also performed and the results are reported in Table 56 and Figure 116. This analysis showed the presence of a number of hydrated copper and nickel phases, likely as the result of the drying of entrained electrorefining solution in the solids. Leaching with hot water confirmed this, as up to 24% Cu, 82% Ni, 85% As and 11% S were soluble from Feed #1 and up to 6.5% Cu, 66% Ni, 68% As and 23% S were soluble from Feed #2. These water leached samples were also analyzed with XRD and the phases found were also reported in Table 56 and Figure 116.

Table 56 Phases Identified by XRD Analysis of Copper Residue Feed Samples

Sample	Identified Phases (in order of intensity)
Feed #1	CuS (Covellite), $NiSO_4 \cdot 6H_2O$ (Retgersite), NiS_2 (Vaesite), $Cu_3(AsO_4)_2$, $Cu_2Cl(OH)_3$ (Atacamite), PbS (Galena), $NiCl_2 \cdot 4H_2O$, S, $BaSO_4$ (Barite), As_2S_3 (Orpiment)
Feed #1 Water Leach	CuS (Covellite), NiS_2 (Vaesite), $Pb_3O_2SO_4$, S
Feed #2	CuS (Covellite), NiS_2 (Vaesite), Cu_3AsS_4 (Enargite), S, $CuSO_4 \cdot 3H_2O$, $Cu_4SO_4(OH)_6$ (Brochantite), $Cu_2Cl(OH)_3$ (Atacamite), PbS (Galena), $BaCl_2 \cdot 2H_2O$
Feed #2 Water Leach	CuS (Covellite), NiS_2 (Vaesite), $Pb_3O_2SO_4$, Cu_3AsS_4 (Enargite), S

Covellite (CuS) is the major phase, and major copper phase, in both samples, with the remaining copper present as either soluble copper arsenate, chloride or sulphate or as enargite (Cu_3AsS_4). Nickel is present in the residue primarily as entrained nickel sulphates or chlorides in both samples, with the remaining nickel present as vaesite (NiS_2). Arsenic is present in Feed #1 as $Cu_3(AsO_4)_2$ and orpiment (As_2S_3), with $Cu_3(AsO_4)_2$ as the major phase, as shown by the high solubility of arsenic in hot water for this sample; in Feed #2, the only arsenic phase identified is enargite (Cu_3AsS_4) but, since up to 68% of the arsenic is soluble in hot water, there are likely other unidentified arsenate compounds in this feed sample. Phases containing minor elements, such as barium (i.e., barite ($BaSO_4$) and $BaCl_2 \cdot 2H_2O$) and lead (galena (PbS)), are also identified in both samples. Sulphur is present primarily in the nickel and copper sulphides, but also as elemental sulphur (S), particularly in Feed #2.

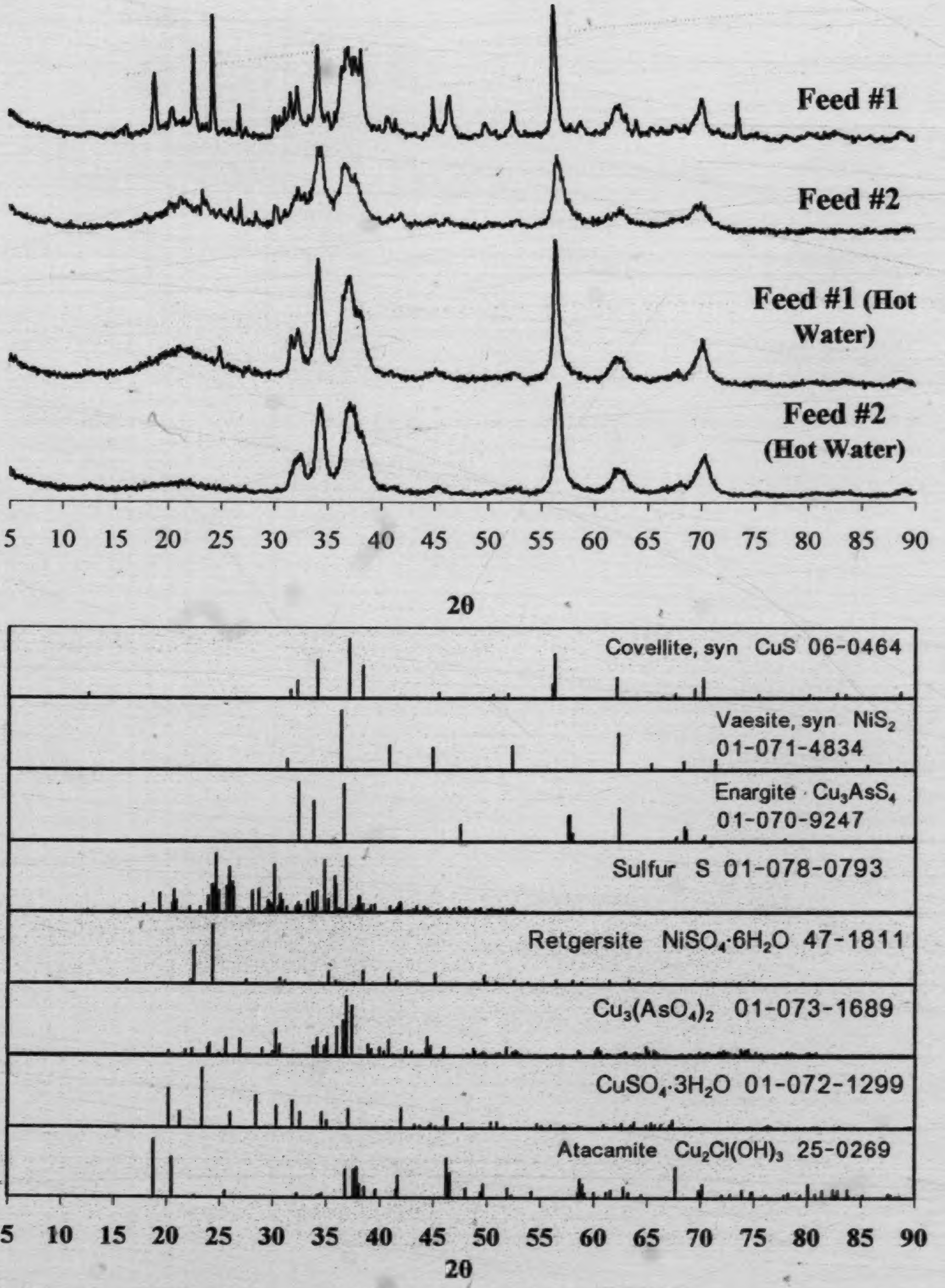

Figure 116 XRD Patterns of Copper Residue Samples before and after Leaching with Hot Water

6.1 Literature Survey

No reference could be found in the literature on the treatment of solid residues from the electrorefining of nickel matte. However, there have been a number of research studies that have examined the application of transformational roasting processes to the treatment of sulphide concentrates. This research falls into three main categories, including lime roasting of copper concentrates, lime roasting of refractory gold concentrates and Na_2CO_3 roasting of refractory gold concentrates, and each will be discussed in the following sections. In addition, sodium carbonate roasting has been proposed as a method to treat metallurgical wastes containing metal selenides, tellurides and arsenides and, thus, the treatment of these materials has also been summarized. However, based on this review of available literature, none of the materials listed appear to be treated commercially using transformational roasting processes at present.

6.1.1 Lime Roasting of Copper Concentrates

Research into lime roasting of copper sulphide concentrates was conducted in the 1970's, and piloted on a commercial scale by Kennecott (173) as an alternative processing route due to concerns that sulphide smelting might become legally prohibited because of the release of SO_2 and other gaseous emissions. The lime roasting reaction is shown below.

$$2\ CuFeS_2 + 4\ Ca(OH)_2 + 8.5\ O_2 \Rightarrow 2\ CuO + Fe_2O_3 + 4\ CaSO_4 + 4\ H_2O$$

Haver and Wong (174) with the US Bureau of Mines were the first to publish details on a lime roasting process for copper concentrates. They proposed roasting a chalcopyrite ore (26% Cu, 25% Fe, 28% S, 1% Mo) with 57% $Ca(OH)_2$ (88% of stoichiometric) by allowing the ore to oxidize spontaneously after ignition to give roasting temperatures of about 500 to 600°C. Then, using a 20% HCl leach, extractions of 99% Cu, 96% Mo and 87% Fe were achieved while retaining up to 98% of the sulphur in the solids during roasting. (The formation of $CuFe_2O_4$ during roasting, which is insoluble in H_2SO_4, is cited as the reason for selecting HCl as the lixiviant (175).) Molybdenum was then removed from the leach solution with activated carbon, copper was recovered by iron powder cementation and the resulting $FeCl_2$ solution was injected into a spray reactor at 500°C to convert $FeCl_2$ to Fe_2O_3 and recover HCl as a vapor for recycle to the process. Further testing and optimization looked at pelletization of the feed, particle size, air flow, roaster configuration and roasting and leaching conditions (175). From this optimization, a range of operating temperatures (600 to 900°C) was selected to both minimize the formation of $CaSO_3$ at lower temperatures and prevent the decomposition of $CaSO_4$ at higher temperatures. Large scale pilot plant testing produced results consistent with the smaller batch tests with 97% of the sulphur retained in the solids during roasting and extractions of 99% Cu, 73% Fe, 91% Mo and 81% Ag possible after leaching with boiling 20% HCl. After roasting, near quantitative gold recovery was possible through cyanidation of the leach residue.

Similarly, Bartlett and Haung from Stanford (176) also studied the possibility of using lime roasting to treat chalcopyrite concentrates in the early 1970's. They showed that roasting at 500°C with $Ca(OH)_2$ additions of 88% of stoichiometric could be used to fix over 95% of the sulphur in the solids while allowing over 98% of the copper to be recovered by leaching with H_2SO_4 solution. Less than stoichiometric $Ca(OH)_2$ additions are possible due to the partial sulphation of copper during roasting. Better temperature control and lower roasting temperatures prevented the formation of $CuFe_2O_4$ during roasting. This research eventually led to a US patent (177) and further research into fluidized bed roasting of lime-concentrate pellets was also performed (178).

In later years, other similar studies on lime roasting of copper concentrates have also been published in South Africa (179,180), India (181) and, most recently, in China (182) and, generally, report similar reaction conditions and results to what either Haver and Wong or Bartlett and Haung reported.

More recently, however, another study was performed to try to better understand and optimize the lime roasting of a chalcopyrite concentrate (28% Cu, 26% Fe, 32% S) by looking at a variety of process variables (183-186). The best copper extractions were found to occur when pellets of 0.75 to 1.25 mm in diameter with 38 to 43% porosity and

92% CaO additions (200% of stoichiometric) were roasted at 500°C for 50 min with an air flow rate of 24 L/h and leached in dilute sulphuric acid solutions (185). In a later study, Riveros (187) indicated that similar results could be achieved using activated limestone ($CaCO_3$) instead of lime (CaO) as the roasting reagent. Chalcocyanite ($CuSO_4$), dolerophanite ($CuO{\cdot}CuSO_4$), anhydrite ($CaSO_4$) and hematite (Fe_2O_3) are the major phases present in the ore roasted under these conditions (185). Roasting at 500°C was selected as roasting below 600°C was necessary to avoid $CuFe_2O_4$ formation and maintain the heat balance of the reaction (184).

Mineralogically, after chalcopyrite ($CuFeS_2$) decomposes to covellite (CuS) and FeS, covellite breaks down on heating in air in the following sequence (186):

covellite → digenite → cuprite → tenorite → dolerophanite → chalcocyanite
$CuS \rightarrow Cu_{1.8}S \rightarrow Cu_2O \rightarrow CuO \rightarrow CuO{\cdot}CuSO_4 \rightarrow CuSO_4$

If water is adding during pellet production, the formation of tenorite (CuO) is favored over dolerophanite ($CuO{\cdot}CuSO_4$). Iron oxidizes from FeS to Fe_2O_3 while calcium reacts either to form anhydrite ($CaSO_4$) directly or to form CaS as an intermediary before reacting further to form anhydrite. (No CaS was formed when covellite (CuS) or digenite ($Cu_{1.8}S$) were roasted in air, indicating that iron plays a role in the formation of CaS during roasting (185).)

The same research group also reported using lime to capture arsenic and sulphur emissions during the roasting of a sample of enargite (Cu_3AsS_4) at 700°C (188). Arsenic was captured as either CaAs or $Ca_3(AsO_4)_2$, with sulphur captured as CaS or $CaSO_4$. (The formation of calcium arsenates is preferred over copper arsenates at all the temperatures tested.) Complete removal of arsenic and conversion of enargite to digenite ($Cu_{1.8}S$) is possible in 30 minutes of roasting with longer roasting times encouraging the formation of cuprite (Cu_2O), tenorite (CuO) and dolerophanite ($CuO{\cdot}CuSO_4$). Lime layers of up to 400% by volume or 140% by weight, relative to the enargite ore, were required to ensure no arsenic or sulphur is emitted during roasting (i.e., about 95% of stoichiometric).

Another study proposed lime roasting as a possible process route for recovering copper from copper smelter flue dust (173). Roasting a sample of flue dust (15% Cu, 7% S, 8% As, 30% H_2O) at 650°C for 2 h, followed by leaching with NH_3/NH_4Cl or $NH_3/(NH_4)NO_3$ solutions for 24 h, resulted in copper extractions of 60 to 64% while extracting less than 0.3% As. Heap leaching of roasted pelletized feed for up to 25 days increased copper extractions to up to 77% from this material.

6.1.2 Transformational Roasting of Gold Concentrates

6.1.2.1 Lime Roasting of Refractory Gold Concentrates

Refractory gold concentrates are ores where most of the gold is trapped within sulphide minerals, such as pyrite (FeS_2) or arsenopyrite (FeAsS), and, thus, the gold cannot be recovered by direct cyanidation of the ore. In most cases, the ores need to be oxidized in order to make the gold in the ores more recoverable. The oxidation reactions for the roasting of pyrite and arsenopyrite are provided in Table 57

Table 57 Pyrite and Arsenopyrite Oxidation (9)

	Pyrite Reactions	Arsenopyrite Reactions
Dissociation	$FeS_2 = FeS + S_{(g)}$	$FeAsS = FeS + As_{(g)}$
FeS Oxidation	$3\ FeS + 5\ O_{2(g)} = Fe_3O_4 + 3\ SO_{2(g)}$ $4\ Fe_3O_4 + O_{2(g)} = 6\ Fe_2O_3$	$3\ FeS + 5\ O_{2(g)} = Fe_3O_4 + 3\ SO_{2(g)}$ $4\ Fe_3O_4 + O_{2(g)} = 6\ Fe_2O_3$
S/As Oxidation	$S_{(g)} + O_{2(g)} = SO_{2(g)}$	$S_{(g)} + O_{2(g)} = SO_{2(g)}$ $4\ As_{(g)} + 3\ O_{2(g)} = 2\ As_2O_{3(g)}$
Total Reaction	$2\ FeS_2 + 5.5\ O_{2(g)} = Fe_2O_3 + 4\ SO_{2(g)}$	$2\ FeAsS_2 + 7\ O_{2(g)} = Fe_2O_3 + 4\ SO_{2(g)} + As_2O_{3(g)}$

Since both of these overall reactions produce noxious gases (i.e., SO_2 and As_2O_3), oxidation of pyrite and arsenopyrite by roasting has been largely abandoned in favor of aqueous pressure or bacterial oxidation, which not only oxidize the ores but, with further processing of the leach solutions, enable sulphur and arsenic to be precipitated in an environmentally stable form (i.e., gypsum ($CaSO_4{\cdot}2H_2O$), calcium arsenate ($Ca_3(AsO_4)_2$) or ferric arsenate ($FeAsO_4$)) (9).

However, lime roasting of refractory gold ores, where the addition of calcium, in the form of CaO, $CaCO_3$ or $Ca(OH)_2$, would be used to eliminate sulphur and arsenic emissions through the formation of $CaSO_4$ and $Ca_3(AsO_4)_2$ during roasting, was first proposed in the early 1990's as a possible alternative process route to aqueous pressure or bacterial oxidation. The additional roasting reactions for the capture of sulphur and arsenic during the lime roasting of pyrite and arsenopyrite are shown in Table 58.

Table 58 **Lime Roasting Reactions for Pyrite and Arsenopyrite** (9)

	Pyrite Reactions	Arsenopyrite Reactions
S Fixation	$CaO + SO_{2(g)} = CaSO_3$ $2\ CaSO_3 + O_{2(g)} = 2\ CaSO_4$	$CaO + SO_{2(g)} = CaSO_3$ $2\ CaSO_3 + O_{2(g)} = 2\ CaSO_4$
As Fixation		$3\ CaO + As_2O_{3(g)} = Ca_3(AsO_3)_2$ $Ca_3(AsO_3)_2 + O_{2(g)} = Ca_3(AsO_4)_2$
Total Roasting Reaction	$4\ FeS_2 + 8\ CaO + 15\ O_{2(g)} = 2\ Fe_2O_3 + 8\ CaSO_4$	$2\ FeAsS + 5\ CaO + 7\ O_{2(g)} = Fe_2O_3 + 2\ CaSO_4 + Ca_3(AsO_4)_2$

Early on in this research, Taylor et al. (9) found that $Ca(OH)_2$ was more effective than CaO or $CaCO_3$ in reducing sulphur and arsenic emissions from the roasting of pyrite and arsenopyrite and most subsequent research has focused primarily on $Ca(OH)_2$ as the roasting reagent for these applications.

Taylor et al. (9) conducted process and mineralogical studies on lime roasting of both pyrite and arsenopyrite. For the roasting of pyrite (FeS_2), sulphur retentions of over 98% were reported for roasting with 108% $Ca(OH)_2$ at 650°C for 60 minutes (9). Subsequent mineralogical studies showed that, when roasting above 600°C in the presence of $Ca(OH)_2$, pyrite is converted stepwise, first to pyrrhotite ($Fe_{1-x}S$) and then to hematite (Fe_2O_3), with the sulphur released reacting with calcium to form either anhydrite ($CaSO_4$), CaS or $CaSO_3$ (189). Roasting the same mixtures at 400°C showed no reaction while pyrite roasted at 500°C showed an unreacted pyrite core surrounded by a low porosity rim of hematite (189). Roasting about 700°C caused sintering of the particles to occur, with essentially no porosity present in particles after roasting at 850°C (190).

Roasting of arsenopyrite (FeAsS) with 90% $Ca(OH)_2$ at 650°C for 60 minutes produced similar results with over 98% of the sulphur and 99.9% of the arsenic retained during roasting (9). Mineralogically, during roasting, arsenopyrite converts from FeAsS to pyrrhotite ($Fe_{1-x}S$) to magnetite (Fe_3O_4) and, finally, to hematite (Fe_2O_3). The sulphur released reacts to form CaS and anhydrite ($CaSO_4$) during roasting, with lower $Ca(OH)_2$ additions and roasting temperatures promoting the formation of CaS (189,190).

For both pyrite and arsenopyrite, roasting at 650°C and 60 min produced porous residues suitable for gold recovery by cyanidation. Roasting a sample of refractory gold ore (0.55 oz/t Au) at these conditions gave gold extractions of up to 87% with cyanidation, with extractions of up to 97% possible with regrinding of the roasted ore (190).

Several less detailed studies on lime roasting of refractory gold concentrates are reported in the literature. Agar (191) patented a process for $CaO/Ca(OH)_2$ roasting of sulphide/arsenide gold concentrates to reduce, but not eliminate, sulphur and arsenic emissions. This process used additions of at least 75% of the stoichiometric $CaO/Ca(OH)_2$ addition to fix up to 75% of the arsenic and sulphur in the ore while roasting for 2 to 4 h at 550 to 650°C. Lime roasting was also tested on a gold concentrate (3.5% S, 1.3% As) from Ashanti Goldfields, which could not be treated using aqueous pressure oxidation because the high carbon content in the oxidation residue caused lower than acceptable gold recoveries by cyanidation (192,193). After agglomeration with between 16.5 and 22.0% $Ca(OH)_2$, the ore was roasted at 700°C, with over 95% of the sulphur retained in the calcine and gold extractions of over 90% possible using cyanidation. Another study (194) used an industrial waste, containing 92% $Ca(OH)_2$, to fix arsenic and sulphur from a Chinese refractory gold concentrate (11% As, 32% S, 31% Fe, 19 g/t Au, 80 g/t Ag) with up to 95% of the arsenic and 93% of the sulphur retained in the roasted ore and gold extractions of 94% possible using cyanidation.

6.1.2.1.1 Lime Roasting for Selective Control of Arsenic Emissions from Refractory Gold Ores

Zeng et al.(195) used a slightly different approach, using lower additions of $Ca(OH)_2$ to preferentially eliminate arsenic emissions during roasting of a carbonaceous pyrite/arsenopyrite concentrate (1% As, 21% S, 1% Sb, 3% C) while allowing the majority of the SO_2 produced to be liberated from the ore. In this process, over 78% of the sulphur in the ore was volatilized, but up to 92% of the arsenic was retained in the roasted ore and up to 92% of the gold in the ore could be recovered by cyanidation.

Similarly, Liu et al. (196) used mixtures of $FeSO_4$ and CaO to selectively reduce arsenic emissions during the roasting of a refractory pyrite/arsenopyrite ore (57 g/t Au, 2 g/t Ag, 1% Sb, 1% As, 22% Fe, 21% S). Using a 9:1 mole ratio of $Ca(OH)_2$:$FeSO_4$ and additions of 10% by weight, up to 92% of the arsenic, but only 22% of the sulphur, was retained in the roasted ore, which would then allow the SO_2 produced to be recovered for the production of sulphuric acid. To avoid the formation of low melting point antimony compounds, a two-stage roast using temperatures of 450°C in the first stage and 650°C in the second stage was used to maximize gold recovery at between 89 and 91% using cyanidation. The resultant residue passed TCLP tests for arsenic.

6.1.2.2 Sodium Carbonate/Sodium Hydroxide Roasting of Refractory Gold Ores

Following similar principles to those used for lime roasting, sodium carbonate has been proposed as another possible reagent for controlling the emission of sulphur and arsenic during roasting of sulphide and arsenic sulphide concentrates. Roasting with Na_2CO_3 is reported in several studies as a possible treatment method for refractory gold ores containing pyrite, arsenopyrite and stibnite (Sb_2S_3). The following illustrate the reactions involved during Na_2CO_3 roasting of these minerals:

$$2\ FeS_2 + 4\ Na_2CO_3 + 7.5\ O_2 \rightleftharpoons Fe_2O_3 + 4\ Na_2SO_4 + 4\ CO_2$$
$$2\ FeAsS + 5\ Na_2CO_3 + 7\ O_2 \rightleftharpoons Fe_2O_3 + 2\ Na_2SO_4 + 2\ Na_3AsO_4 + 5\ CO_2$$
$$Sb_2S_3 + 7\ O_2 + 3\ Na_2CO_3 \rightleftharpoons Sb_2O_5 + 3\ Na_2SO_4 + 3\ CO_2$$

Taylor and Yin (197,198) looked at roasting gold ores containing stibnite or arsenopyrite with Na_2CO_3, as it gave higher sulphur retentions than roasting with $Ca(OH)_2$, but did not cause fusion of the roasting charge like NaOH. Roasting stibnite at 550°C for 90 minutes with 101% Na_2CO_3 (108% of stoichiometric) gave retentions of over 99.9% Sb and 95% S, with over 85% of the sulphur converted to soluble Na_2SO_4. Similarly, roasting of arsenopyrite at 550°C for 90 min. with the addition of 134% Na_2CO_3 (110% of stoichiometric) resulted in retentions of over 99.9% As and 97% S. Up to 97% of the arsenic in the roasted arsenopyrite residue was soluble in distilled water adjusted to pH 13 with NaOH. (Less arsenic is dissolved in solution with lower pH, which likely indicates that arsenic is present as a mixture of sodium and either ferrous or ferric arsenate in the roasted ore, as the iron arsenates would be expected to leach more readily as the pH of the solution is increased.) Arsenic solubility is also affected by roasting temperature, with a maximum at 550°C, a minimum at 625°C and another increase at higher temperatures. The melting of sodium arsenite at 600°C followed by its oxidation at higher temperatures to produce more soluble arsenic compounds is proposed as the mechanism for this behaviour. Arsenic and sulphur were then precipitated from the arsenopyrite leach solutions as Ca_2AsO_4OH and $CaSO_4$ by adding $CaCl_2$.

Five other studies on Na_2CO_3/NaOH roasting of pyrite/arsenopyrite refractory gold ores are also reported in the literature. Wu (199) roasted an ore, containing 39 g/t Au, 13% As, 11% S and 17% Fe, with 100% NaOH at 700°C to retain up to 96% of the arsenic in the solids during roasting. Zhang et al. (200) roasted another ore (20 g/t Au, 10 g/t Ag, 7% As, 31% S) with Na_2CO_3 or NaOH at 650 to 700°C for 1 to 3 h to convert up to 85% of the sulphur to sulphate and allow up to 88% of the gold to be recovered using cyanidation. (Zhang et al. (200) also propose the use of $MgCO_3$ and $Mg(OH)_2$ as potential sulphur-fixing agents.) Luganov et al. (201,202) roasted a carbonaceous arsenopyrite/pyrite ore (7 g/t Au, 6% As, 12% S, 14% Fe, 13% C) with 150 to 200% Na_2CO_3 at 600°C for 1 h; 98% of the As and 99% of the S were retained in the ore after roasting while leaching the residue at 70°C with water recovered between 95 and 97% of the arsenic and sulphur to solution. (Dundua and Dobrokhotov (203) report a similar roasting and leaching procedure in their study.) After water leaching, 70 to 75% of the gold could be recovered by direct cyanidation and up to 96% of the gold was recoverable after treating the ore with SO_2 prior to cyanidation. Finally, Xue (204) reports cyanidation recoveries of up to 98% Au, 70% Ag and 93% Cu from a pyritic refractory gold concentrate (55 g/t Au, 150 g/t Ag, 24% S, 28% Fe and 0.12% As) roasted with Na_2CO_3.

6.1.2.3 Roasting of Refractory Gold Ores with Iron Sulphates

Iron sulphate was also used in another study (205) where refractory sulphide/arsenide ores are roasted in an oxygen enriched atmosphere at 500 to 575°C to enable up to 92% of the gold to be recovered by cyanidation while producing a disposable ferric arsenate ($FeAsO_4$). Further modifications of this process include using additional fuel sources (e.g. S, FeS_2, etc.) to improve the heat balance of the process (206) and using one roasting stage to oxidize and volatilize arsenic and a second roasting stage to react the arsenic gas from the first stage with a metal (e.g., Ba, Ca, Mn or Fe) oxide, sulphate, chloride or hydroxide in an oxygen enriched atmosphere to form insoluble metal arsenates (207).

6.1.3 Sodium Carbonate Roasting of Other Related Materials

6.1.3.1 Copper Electrolytic Slimes

Sodium carbonate roasting has also been proposed for the treatment of copper electrolytic slimes, which generally contain a mixture of copper selenides or tellurides

Makhmetov (208) and Tishchenko an Smirnov (209) proposed adding CaO or Na_2CO_3 to copper electrolytic slimes to reduce the volatilization of Se during oxidative roasting.

In a review paper on the recovery of selenium and tellurium from copper electrolytic slimes (i.e., typically 5 to 25% Se, 2 to 10% Te), Hoffmann (210) reports that roasting with Na_2CO_3 at 530 to 650°C converts both selenium and tellurium to Se^{6+} and Te^{6+}, respectively, so that the sodium selenate readily dissolves selectively in water, leaving tellurium in the solids. The sodium selenate solution is then crystallized, with the crystals mixed with charcoal, reduced to Na_2Se and then oxidized to elemental form in solution with air sparging; tellurium is recovered from the original water leach residue by sulphuric acid leaching, with the dissolved tellurium converted to elemental tellurium either by HCl reduction and precipitation with SO_2 or by reduction and precipitation of TeO_2 with $NaSO_3$, followed by dissolution in NaOH solution and electrowinning.

6.1.3.2 Speiss

Speiss is a metallurgical term for a mixture of arsenic compounds produced as a byproduct of smelting high arsenic ores. Two studies have been published on roasting nickel, copper or cobalt speiss with sodium compounds to remove arsenic from the speiss.

The first study (211) involved roasting a mixture of nickelite (NiAs) and cloanthite ($NiAs_2$), grading 31% Ni and 48% As, at 400 to 500°C with a mixture of NaOH and $NaNO_3$ ($NaOH:NaNO_3$ mole ratio of 0.68 to 0.85). However, extremely high additions (i.e., 700 to 780% of stoichiometric) are required and only 91% of the arsenic could be removed from the speiss by hot water leaching, resulting in a product grading 53 to 60% Ni and 7 to 10% As.

The journal article from the second study (212) was not available, but the abstract indicates that a speiss containing nickel, copper and cobalt was roasted with 66% Na_2CO_3 and 2% of a catalyst at 800°C for 2.5 h. Arsenic is removed by leaching with hot water while up to 97% Cu, 99% Ni and 92% Co are recovered, presumably by leaching the water leach residue in H_2SO_4 solution.

6.1.4 Conclusions

From this analysis, it is clear that both $Ca(OH)_2$ and Na_2CO_3 can be effective reagents in capturing or limiting sulphur and arsenic emissions during the roasting of sulphide ores. Although high additions of these compounds are required during roasting to limit these emissions, these roasting reactions are possible at relatively low temperatures and the metals of interest are readily recovered by subsequent leaching of the roasted ores.

All research to date has focused on the recovery of copper or precious metals from traditional copper or refractory gold concentrates. No research has been conducted on the roasting of arsenic-bearing base metal sulphides with Na_2CO_3 and only limited research has been conducted on roasting these materials with $Ca(OH)_2$. Thus, this indicates that roasting of the Inco copper residue with Na_2CO_3 to capture sulphur and arsenic and enhance metals recovery is a novel approach to processing this material. Because of the extensive research on lime roasting of copper sulphides, comparison of the results of roasting with Na_2CO_3 and with $Ca(OH)_2$ may be valuable to allow for comparison of the effectiveness of the two reagents.

6.2 Thermodynamic Analysis

Using available thermodynamic data, three main types of reactions were identified for further study. Where possible, thermodynamic data, including heats and entropies of formation, were taken from either the FREED or FACTSAGE databases (107,108). Exceptions include: ΔH_f° for $FeAsO_4 \cdot 2H_2O$ and Na_3AsO_4 (213), S_{298}° for Na_3AsO_4 (214), S_{298}° for $FeAsO_4$ (215) and ΔH_f° and S_{298}° for $Fe(OH)_3$ (147). (With no data available in the literature, the ΔH_f° for $FeAsO_4$ was estimated from the ΔH_f° for $FeAsO_4 \cdot 2H_2O$ and the S_{298}° for $FeAsO_4 \cdot 2H_2O$ was estimated from the S_{298}° for $FeAsO_4$ by adjusting the values for the presence or absence of water. (This approximation was based on the observed difference in ΔH_f° and S_{298}° between $CaSO_4$ and $CaSO_4 \cdot 2H_2O$.)) No thermodynamic data for atacamite ($Cu_2Cl(OH)_3$), brochantite ($Cu_4SO_4(OH)_6$), or enargite (Cu_3AsS_4) were available in the literature.

6.2.1 Roasting of As_2S_3

Free energy (ΔG°) is plotted versus temperature for several potential reactions for the roasting of As_2S_3 in Figure 117. Arsenic sulphide can be roasted readily in air to form sulphur dioxide (SO_2) and arsenic trioxide (As_2O_3) (Reaction 1, Figure 117). However, neither product is particularly desirable as both represent significant environmental concerns if they are not captured and converted to a more disposable form.

Based on the results reported for roasting arsenopyrite concentrates (198), it may be possible to roast materials containing As_2S_3 in the presence of oxygen and Na_2CO_3 to capture sulphur and arsenic in the roasting residue as sodium sulphate (Na_2SO_4) and sodium arsenate (Na_3AsO_4), respectively (Reaction 2, Figure 117). The residue could then be leached with water to dissolve these two compounds. The SO_4^{2-} ions could then be precipitated as gypsum ($CaSO_4 \cdot 2H_2O$) by adding lime or limestone and the AsO_4^{3-}

ions could be precipitated either as calcium arsenate ($Ca_3(AsO_4)_2$) or ferric arsenate ($FeAsO_4$). (Sodium could be recovered from solution using a modified version of the Solvay process (124).)

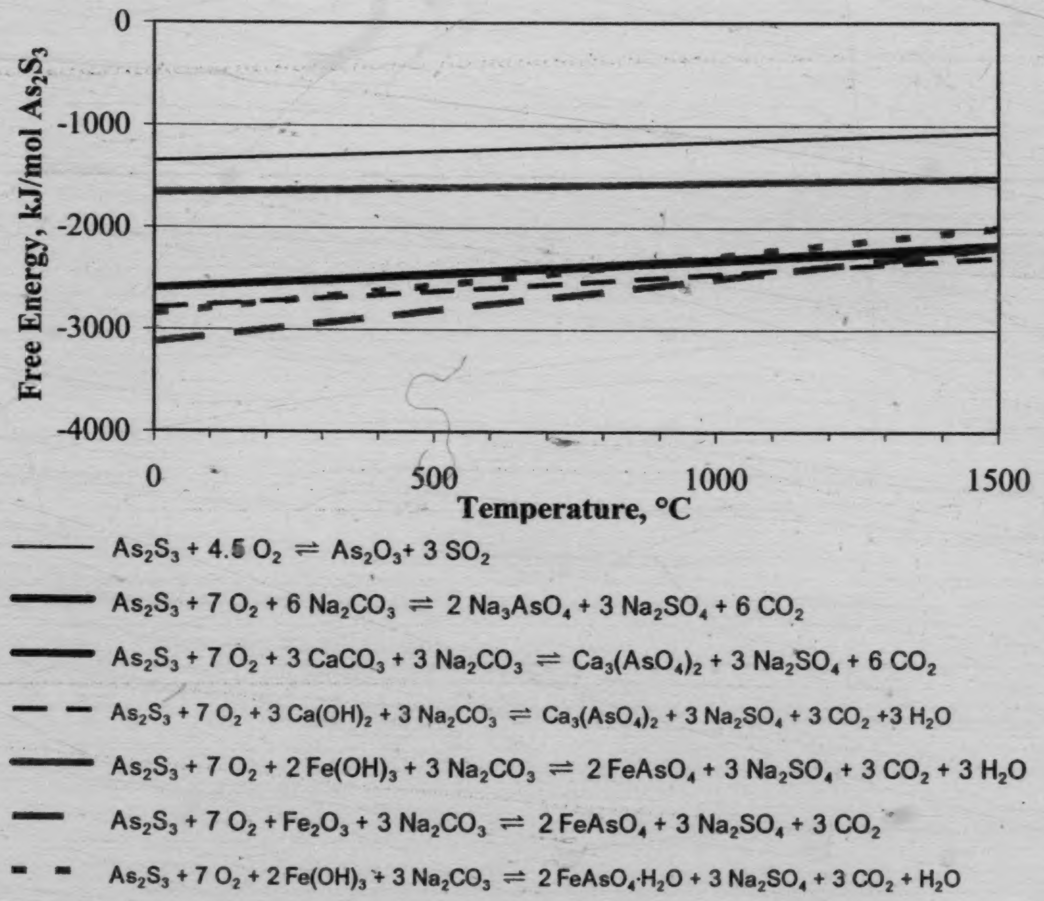

Figure 117 Potential Reactions for Roasting As_2S_3 ($\Delta G°$ vs. Temperature)

However, calcium arsenate or ferric arsenate precipitated at low temperatures from aqueous solution may not be stable enough to allow for long term disposal of this residue (25). To improve the stability of these compounds, precipitation is often carried out at higher temperatures and pressures in precipitation autoclaves. However, the possibility of roasting with sodium carbonate, along with an additional reagent which is added specifically to promote the formation of more stable, higher temperature arsenic compounds directly during roasting, also warrants investigation. Since calcium and iron

(III) both form arsenates with low solubilities, potential reactions for forming both compounds are proposed (Reactions 3 to 7, Figure 117).

All the reactions presented are not only highly exothermic, but thermodynamically possible at between 200 and 1500°C and the free energies in each case are lower than for the direct oxidation of As_2S_3. An oxidizing atmosphere, however, would be required in all cases for these reactions to proceed.

6.2.2 Roasting of Copper and Nickel Sulphides

Free energy (ΔG^o) is plotted versus temperature for several potential reactions for the roasting of covellite (CuS), vaesite (NiS_2), retgersite ($NiSO_4{\cdot}6H_2O$) and bonattite ($CuSO_4{\cdot}3H_2O$) with Na_2CO_3 in Figure 118.

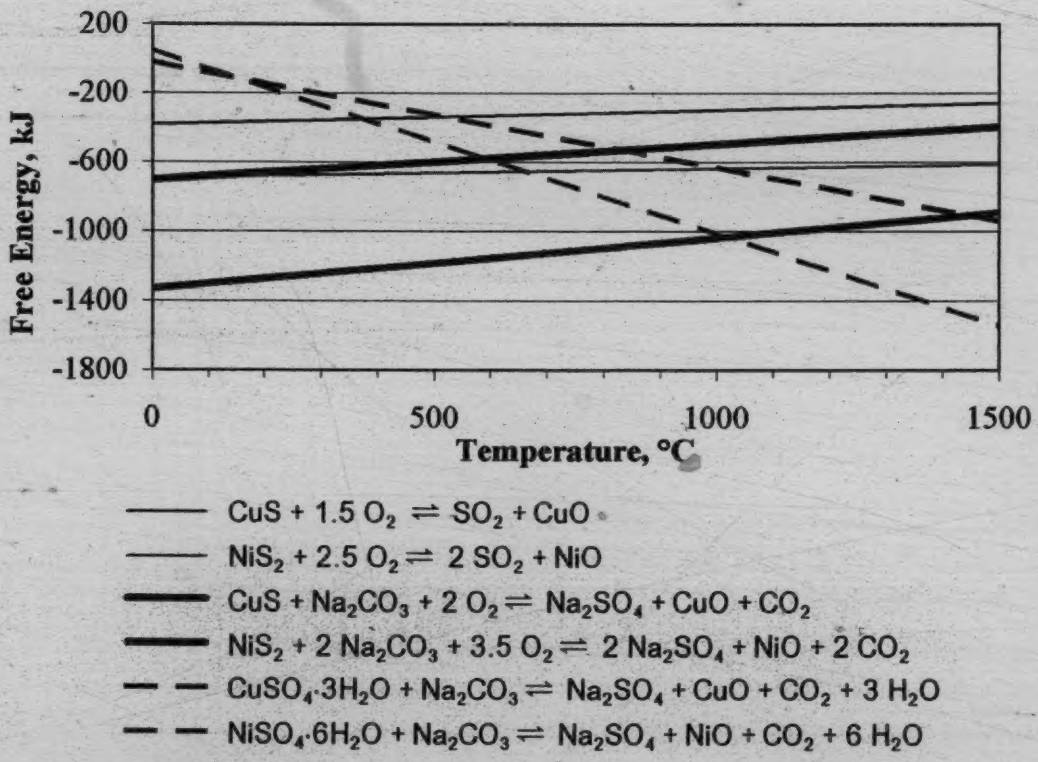

Figure 118 Potential Reactions for Roasting Copper and Nickel Sulphides (ΔG^o vs. Temperature)

Reactions 1 and 2 show the expected reaction for roasting the copper and nickel sulphides in air while Reactions 3 and 4 show the proposed reactions for oxidative roasting of these sulphides in the presence of Na_2CO_3. For both sulphides, all the reactions are exothermic and the free energy for roasting with Na_2CO_3 is significantly lower than for roasting in air alone. Reactions 5 and 6 show the potential reactions of two of the hydrated nickel and copper sulphates found in the samples of the copper residue feed. These reactions are mildly endothermic, but should be spontaneous at temperatures above 50°C.

Thus, this analysis indicates that roasting of the Inco copper residue with Na_2CO_3 should be thermodynamically feasible at all temperatures above 50°C.

6.3 Scoping Tests

6.3.1 Experimental Procedure

For the first batch of scoping tests and the first DOE tests, a Lindberg split-tube furnace was used in the configuration shown in Figure 119A. For all subsequent tests, a Thermolyne tube furnace was used, where one end of the furnace was sealed off with refractory, in the configuration illustrated in Figure 119B.

The furnace set point was adjusted so that the centre of the hot zone of the furnace was equal to the desired reaction temperature. The samples boats were inserted so that the center of the sample coincided with the centre of the hot zone. Measurements of the temperature distribution in the tube furnaces used showed a variation of less than 10°C from the center to either end of the sample during roasting.

Dried copper residue was mixed with the particular reagent(s), placed in an alumina boat and inserted into the tube furnace which had been preheated to the desired reaction temperature. Once inserted, the tube was sealed and air flow to the furnace was started and adjusted to give a continuous flow of 2.4 to 3.3 L/min of air through the furnace tube. (This flow was selected due, in part, to constraints in the flowmeters available, but was set to ensure that air was supplied in significant excess to ensure that the oxidation reaction could proceed.) The sample was then roasted in the furnace for 4 h. After roasting, the sample was removed from the furnace, air cooled, ground and a subsample taken for chemical, XRD and SEM analysis.

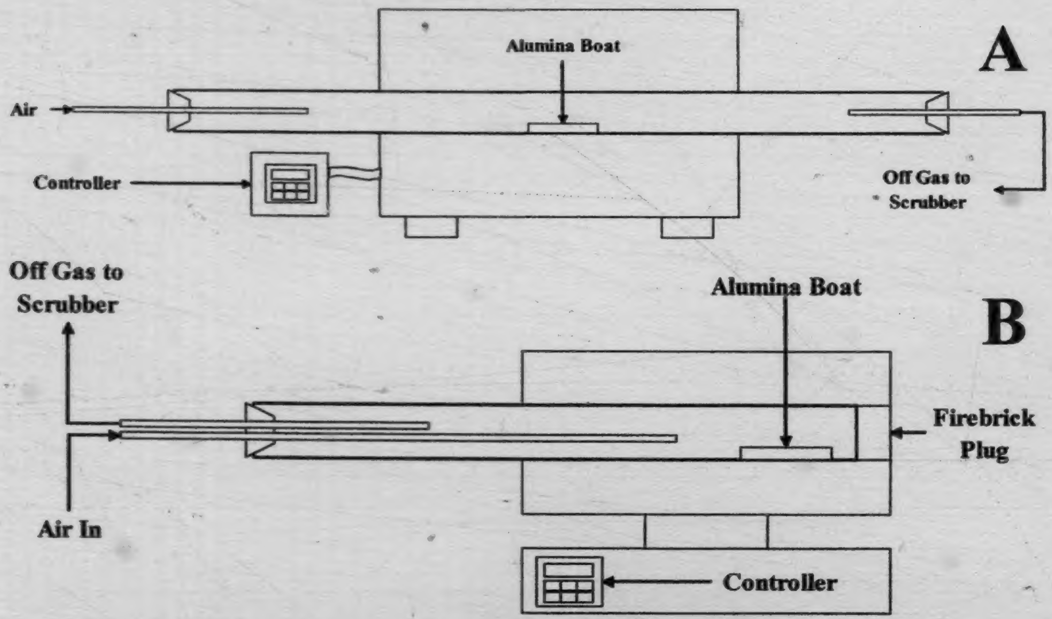

Figure 119 **Setup for Tube Furnaces Used in Roasting Tests for A) Preliminary Scoping Tests and DOE Tests and B) All Other Roasting Tests (Not Drawn to Scale)**

The remainder of the sample was then leached in water at 95 to 97°C for 1 h. After hot water leaching, the leach slurry was filtered with the filtrate collected for chemical analysis and the solids were then washed three times with distilled water with the wash solution collected for analysis. The filter cake was then dried at 80°C overnight before being ground in a mortar and pestle. A subsample of the water leach residue was taken for chemical, XRD and SEM analysis.

The remainder of the sample was then leached in 200 g/L H_2SO_4 at room temperature for 1.5 h. After leaching, the leach slurry was filtered with the filtrate collected for analysis and the solids washed twice with water adjusted to pH 2 with H_2SO_4 and twice with distilled water with the wash solution collected for analysis. The filter cake was then dried at 80°C overnight before being ground in a mortar and pestle.

Solutions were analyzed initially for Cu, Ni, Fe and Pb using a Perkin-Elmer 4000 atomic absorption (AA) spectrometer and then for arsenic using a Varian SpectrAA 220FS atomic absorption spectrometer with a deuterium lamp for background correction.

Solids were fused with lithium metaborate in a two stage fusion process, where the first stage, involving oxidation of the solid sample with $NaNO_3$ or $LiNO_3$ at 700°C, is followed by a second stage where the oxidized sample is fused with lithium metaborate at 950°C. After the fusion, the samples are dissolved in concentrated HCl, with HNO_3 added where necessary, to ensure complete dissolution of the fused samples. The dissolved solids fusion samples were then analyzed for Cu, Ni and As as indicated for the solution samples in the previous paragraph. Solid samples were also analyzed for sulphur using a Horiba EMIA-320V carbon/sulphur analyzer.

Scanning electron microscope analysis was performed on selected samples using a Hitachi Model S-2700 microscope equipped with a GW Electronics annular four-quadrant backscattered electron detector and a Princeton Gamma Tech (PGT) prism intrinsic germanium (IG) x-ray detector and operating at an accelerating voltage of 20 kV. Digital images were taken using a Princeton Gamma Tech IMIX system.

6.3.2 Results from Scoping Tests

6.3.2.1 Na_2CO_3 Roasting Tests

Inco copper residue (Feed #1) was roasted with 100% Na_2CO_3 at 600, 700 and 800°C in the initial scoping tests. The deportment of Cu, Ni, As and S during roasting, water leaching and leaching with 200 g/L H_2SO_4 are summarized in Figures 120 to 123.

With the addition of 100% Na_2CO_3, all of the sulphur in the residue is retained in the solids during roasting; the majority of the sulphur in the roasted residue was soluble in water, indicating the formation of sulphates, but the amount of sulphur leached decreases with increasing roasting temperature (Figure 120). Essentially no sulphur is soluble in sulphuric acid solution, meaning that the remaining unleached sulphur is likely present as sulphides that are not oxidized during roasting.

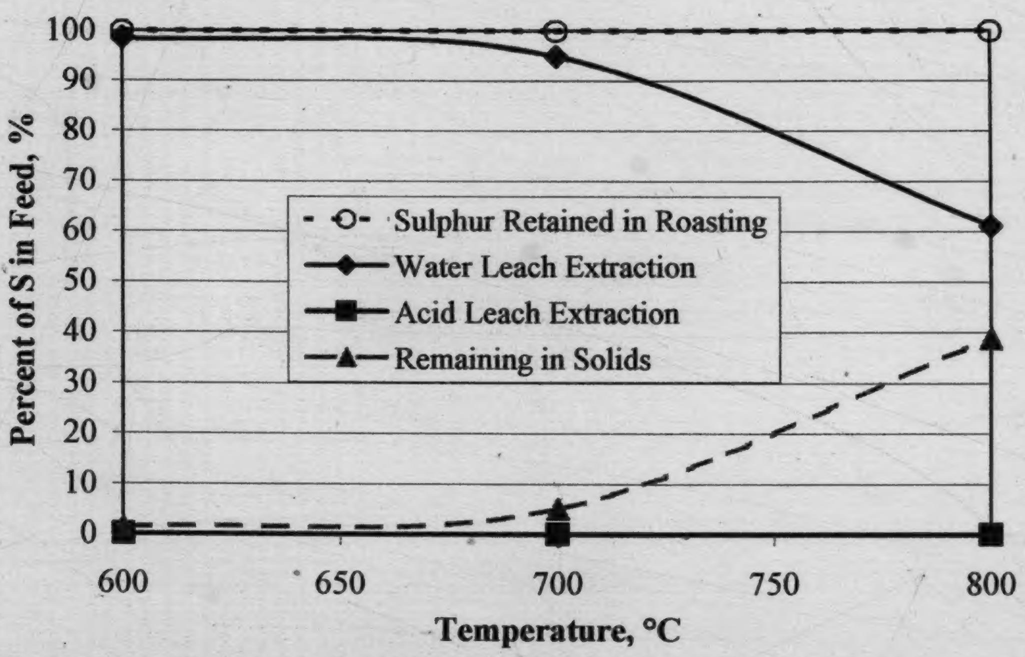

Figure 120 Deportment of Sulphur during Scoping Roasting and Leaching Tests on Inco Copper Residue (Feed #1)

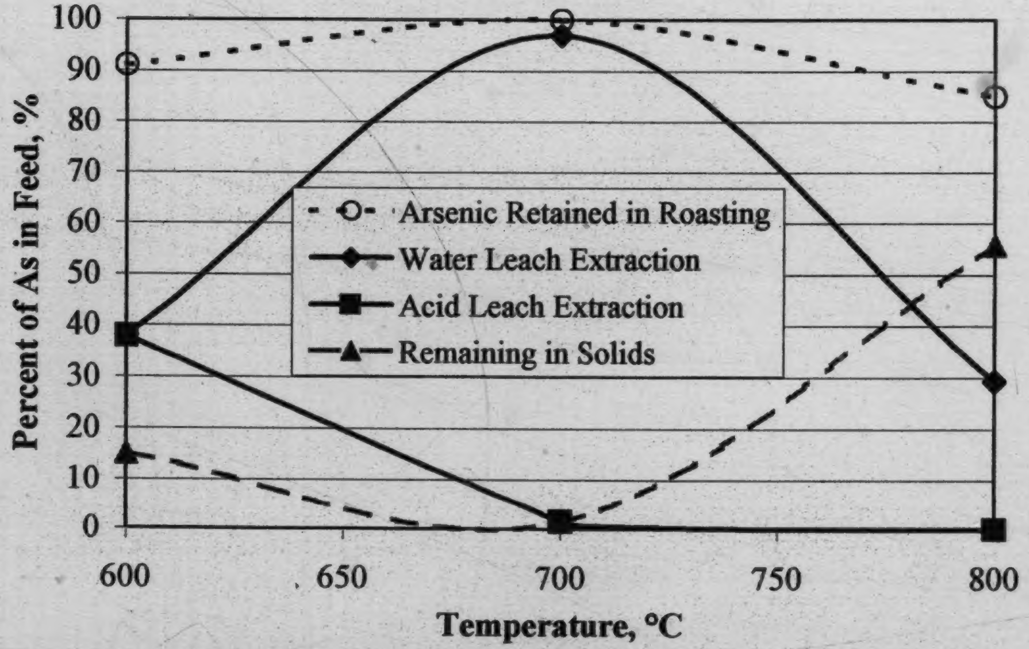

Figure 121 Deportment of Arsenic during Scoping Roasting and Leaching Tests on Inco Copper Residue (Feed #1)

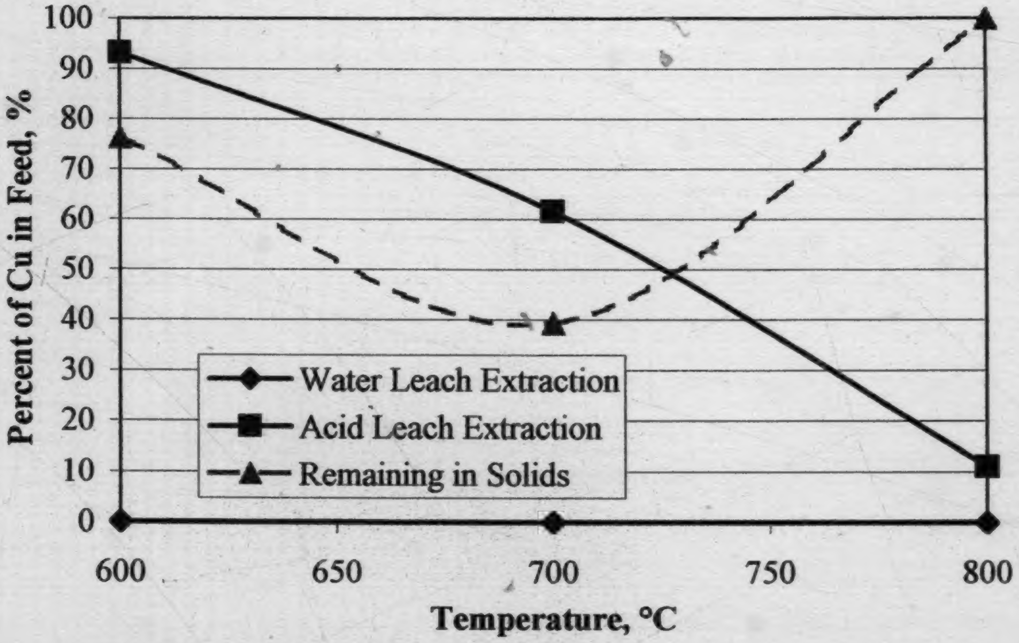

Figure 122 Deportment of Copper during Scoping Roasting and Leaching Tests on Inco Copper Residue (Feed #1)

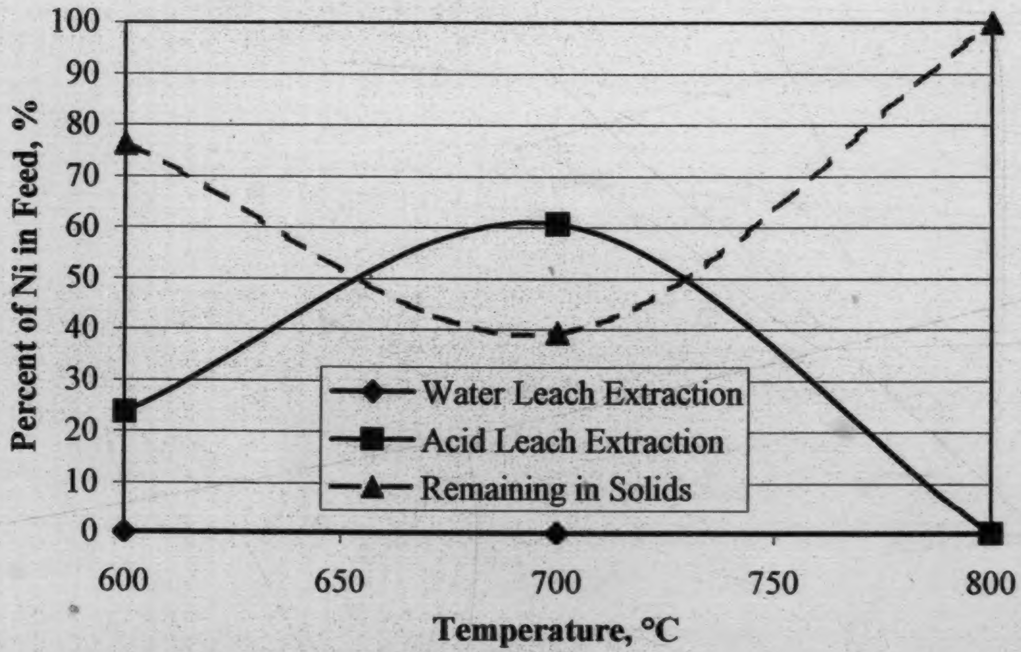

Figure 123 Deportment of Nickel during Scoping Roasting and Leaching Tests on Inco Copper Residue (Feed #1)

Over 85% of the arsenic is retained in the solids during roasting, with a maximum observed at 700°C in these tests (Figure 121). A similar maximum is observed during water leaching with nearly 97% water soluble arsenic after roasting at 700°C, but much lower extractions at higher and lower temperatures (29 to 38%). An additional 38% and 1.6% of the arsenic is leached from samples roasted at 600°C and 700°C, respectively, with 200 g/L H_2SO_4 to give overall arsenic extractions of 88 to 100%. Over 55% of the arsenic remains in the solids after roasting at 800°C and leaching, compared to only 15% for the sample roasted at 600°C and 1.4% for the sample roasted at 700°C.

Neither copper nor nickel volatilized during roasting and virtually no copper or nickel were soluble in subsequent water leaching. The copper extractions after leaching with 200 g/L H_2SO_4 showed a steady decrease with increasing temperature, with over 93% of the copper leached from the sample roasted at 600°C and only 11% leached from the 800°C sample. Nickel extraction reached a maximum of 61% at 700°C; some nickel extraction was observed at 600°C, but no nickel was extracted at 800°C. Extensive sintering of the sample was observed in the sample roasted at 800°C, which could perhaps explain the poor oxidation of Cu, Ni, As and S observed in this sample.

Thus, these preliminary results indicate that sulphur and arsenic emissions can be reduced or eliminated by roasting with Na_2CO_3 and that there is significant potential to be able to selectively leach arsenic and sulphur in water and then subsequently recover the majority of the copper and nickel by leaching in sulphuric acid solutions. However, lower temperatures should be used for subsequent tests to try to avoid the poor results achieved by roasting at 800°C.

6.3.2.2 Screening of Secondary Reagents

After the first DOE test (Section 6.4.1.1) was completed, four roasting/leaching tests with Feed #1 of the Inco copper residue were conducted to try to screen potential reagents that could be used to form insoluble, and potentially stable, arsenic compounds during roasting. Samples were roasted for 4 h at 550°C with 80% Na_2CO_3 and either $FeCl_3$, $FeSO_4{\cdot}7H_2O$, $CaCO_3$ or $Ca(OH)_2$, which were added to give additions of 200% of stoichiometric for the formation of $FeAsO_4$ or $Ca_3(AsO_4)_2$ from the arsenic in the copper residue. The samples were then leached with hot water and then 200 g/L H_2SO_4 at room temperature. Table 59 shows the elemental deportment from these tests.

Table 59 Elemental Deportment from Roasting and Leaching of Inco Copper Residue (Feed #1) with Na_2CO_3 and Various Secondary Additives

Secondary Additive	None*	$FeCl_3$	$FeSO_4 \cdot 7H_2O$	$CaCO_3$	$Ca(OH)_2$
Addition, %	--	8.1	13.9	7.5	5.6
Sulphur					
Retained, %	93	100	100	100	100
Water Leach, %	90	97.6	97.6	92.4	94.8
Acid Leach, %	0	2.1	2.0	0.0	0.0
Total, %	90	99.7	99.5	92.4	94.8
Arsenic					
Retained, %	89	100	99.4	100	93.0
Water Leach, %	16	1.1	0.6	3.7	7.0
Acid Leach, %	62	66.0	74.7	85.4	76.6
Total, %	78	67.1	75.3	89.1	83.6
Copper					
Water Leach, %	2	0.0	0.0	0.0	0.0
Acid Leach, %	92	92.2	94.3	98.2	98.0
Total, %	94	92.2	94.3	98.2	98.1
Nickel					
Water Leach, %	16	0.0	0.0	0.0	0.0
Acid Leach, %	36	30.5	38.6	31.9	30.6
Total, %	52	30.5	38.6	32.0	30.6

* Results estimated from response surface models from first DOE test (6.4.1.1)

All the secondary reagents show slight increases in sulphur and arsenic retention from the DOE results. (The former likely occurs because more Na_2CO_3 is liberated to react with sulphur instead of reacting with arsenic.) Sulphur is soluble in hot water up to almost 98% after roasting with the iron reagents and between 92 and 95% for the calcium reagents. Copper extractions are quite similar to the DOE results for the iron reagents and slightly higher at around 98% for the calcium reagents. Nickel extractions are consistently lower than the DOE results, which are already relatively low because of the low temperatures used during acid leaching. Changes in the acid leach conditions, as employed in Sections 6.4.1.2 and 6.4.3, would be expected to significantly improve the extraction of nickel.

However, overall arsenic extractions are only lowered, compared to the results of the DOE tests, when iron reagents are added during roasting, with a decrease of about 3% for $FeSO_4 \cdot 7H_2O$ and 11% for $FeCl_3$. (Though these results indicate that calcium indeed does form calcium-arsenic compounds, these compounds appear to be readily soluble in H_2SO_4 solutions at room temperature.) These results were not particularly promising, but these reagents were selected as potential reagents to try to fix arsenic as an acid insoluble iron compound during roasting. (A few DOE samples were roasted with $FeCl_3$ but, with the higher arsenic content of the second sample of Inco copper residue and the range of $FeCl_3$ additions used (200 to 400% of stoichiometric), fuming of copper chlorides was observed as some copper reported to the scrubber solution during roasting. Thus, as a result, further tests with $FeCl_3$ were not performed and the DOE test in Section 6.4.3 was performed with $FeSO_4 \cdot 7H_2O$ as the secondary additive.)

6.4 Design of Experiment (DOE) Tests

For the Inco copper residue, four DOE tests were performed. The first involved roasting the copper residue (Feed #1) with Na_2CO_3, followed by hot water leaching and leaching with 200 g/L H_2SO_4 at room temperature (Section 6.4.1.1). However, because of low nickel extractions in this first test, a second test was then performed under the same conditions with the second sample of Inco copper residue, expect that H_2SO_4 leaching was performed at higher temperatures (95 to 97°C) (Section 6.4.1.2). A third test was then performed to look at the potential for the addition of secondary additives to produce stable acid insoluble iron arsenate compounds (Section 6.4.3). Finally, the last DOE test involved roasting the Inco copper residue with $Ca(OH)_2$ under similar conditions to the first two DOE tests to provide a comparison between the results from lime and sodium carbonate roasting of this material (Section 6.4.2). The experimental conditions used in these tests are summarized in Table 60 along with the R^2 values of the response surface models fitted to the resulting metals extraction data. (The same procedure as described in Section 6.3.1 was used in the scoping tests, except for the modifications in the exact conditions used, such as roasting times, temperatures and additions and acid leach concentrations, which are documented in Table 60.)

Table 60 Experimental Conditions Used in Experimental Designs for Roasting Inco Copper Residue with Na_2CO_3 and Resulting Model Variance

Range of Variables Tested	Na_2CO_3 (Cold Acid)	Na_2CO_3 (Hot Acid)	Na_2CO_3-$FeSO_4 \cdot 7H_2O$	$Ca(OH)_2$
Temperature, °C	550-700	550-700	450-600	550-700
Roasting Time, h	4	4	5	4
Na_2CO_3 Addition, %	50-150	50-150	50-150	-
$Ca(OH)_2$ Addition, %	-	-	-	38-113%
$FeSO_4 \cdot 7H_2O$ Addition, %	-	-	45-90%*	-
Acid Leach Temp., °C	25	95-97	95-97	95-97
H_2SO_4 Conc., g/L	200	200	200	300
Model R^2				
Arsenic				
Emitted/Retained	0.890	0.851	0.768	0.583
Water Extraction	0.962	0.960	0.888	0.896
Acid Extraction	0.989	0.987	0.673	0.638
Total Extraction	0.938	0.968	0.773	0.644
Sulphur				
Emitted/Retained	0.735	0.925	0.967	0.713
Water Extraction	0.952	0.969	0.825	0.860
Acid Extraction	--	--	--	0.858
Total Extraction	0.687	0.933	0.871	0.952
Copper				
Water Extraction	0.722	0.964	0.961	0.888
Acid Extraction	0.986	0.955	0.946	0.698
Total Extraction	0.994	0.950	0.749	0.945
Nickel				
Water Extraction	0.938	0.850	0.680	0.985
Acid Extraction	0.685	0.955	0.741	0.842
Total Extraction	0.817	0.973	0.951	0.724

*** Secondary additions represent 200 to 400% of stoichiometric additions assuming the formation of $FeAsO_4$**

6.4.1 Roasting with Na_2CO_3

6.4.1.1 Roasting of Inco Copper Residue (Feed #1) with Na_2CO_3

6.4.1.1.1 Roasting Behaviour

The emission of sulphur and arsenic from the copper residue is highly dependent on Na_2CO_3 addition (Figure 124). No sulphur was lost if Na_2CO_3 additions of over 100% were used; lowering of arsenic emissions to similar levels required Na_2CO_3 additions of closer to 150%. In both cases, these additions are higher than the stoichiometric Na_2CO_3 addition for this material of 71%. Sulphur emissions showed very little dependence on temperature while arsenic emissions showed a slight dependence, reaching a maximum at around 600°C and then decreasing with increasing or decreasing temperature

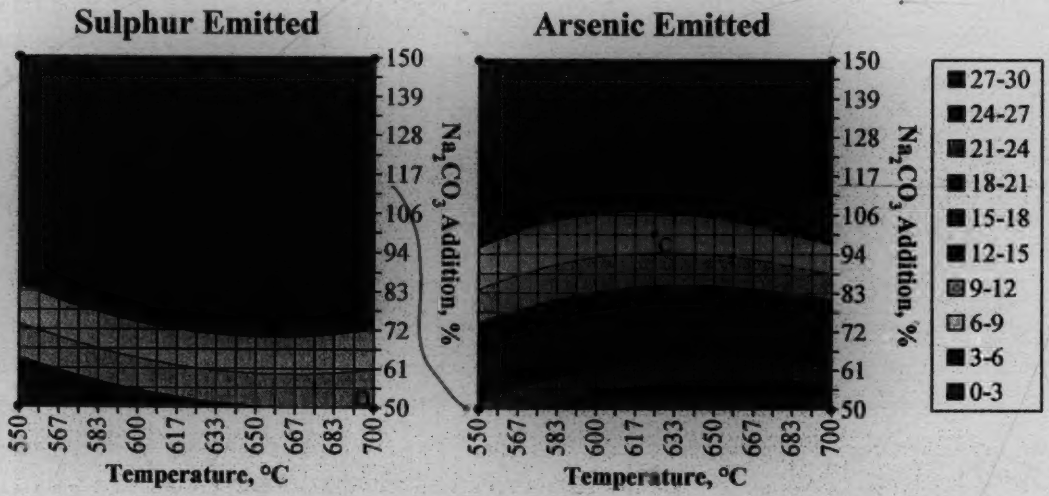

Figure 124 Effect of Na_2CO_3 Addition and Temperature on Sulphur and Arsenic Emissions During Roasting of Inco Copper Residue (Feed #1)

The phases formed during roasting were identified using x-ray diffraction analysis of selected samples (Points A through E on Figures 124, 127, 128 and 129). The identified phases for the copper residue after roasting are listed in Table 61 while the diffraction patterns for the samples and major phases observed are shown in Figure 125.

As the results from Figure 125 indicate, the sulphur in the copper residue reacts readily with the Na_2CO_3 added during roasting to form sodium sulphate (Na_2SO_4), which is the major phase in both samples B and E after roasting. Some unreacted, or partially reacted, Na_2CO_3 is observed in these samples either as Na_2CO_3 or $Na_4CO_3SO_4$.

Table 61 Phases Identified by XRD Analysis of Copper Residue Roasted at 700°C with Na_2CO_3

Sample	Identified Phases (in order of intensity)
B	Na_2SO_4, CuO (Tenorite), NiO (Bunsenite), Na_2CO_3 (Gregoryite), $Cu_{1.96}S$ (Chalcocite-Q)
E	Na_2SO_4, CuO (Tenorite), NiO (Bunsenite), $Cu_{1.96}S$ (Chalcocite-Q), $Na_4CO_3SO_4$, Na_3AsO_4

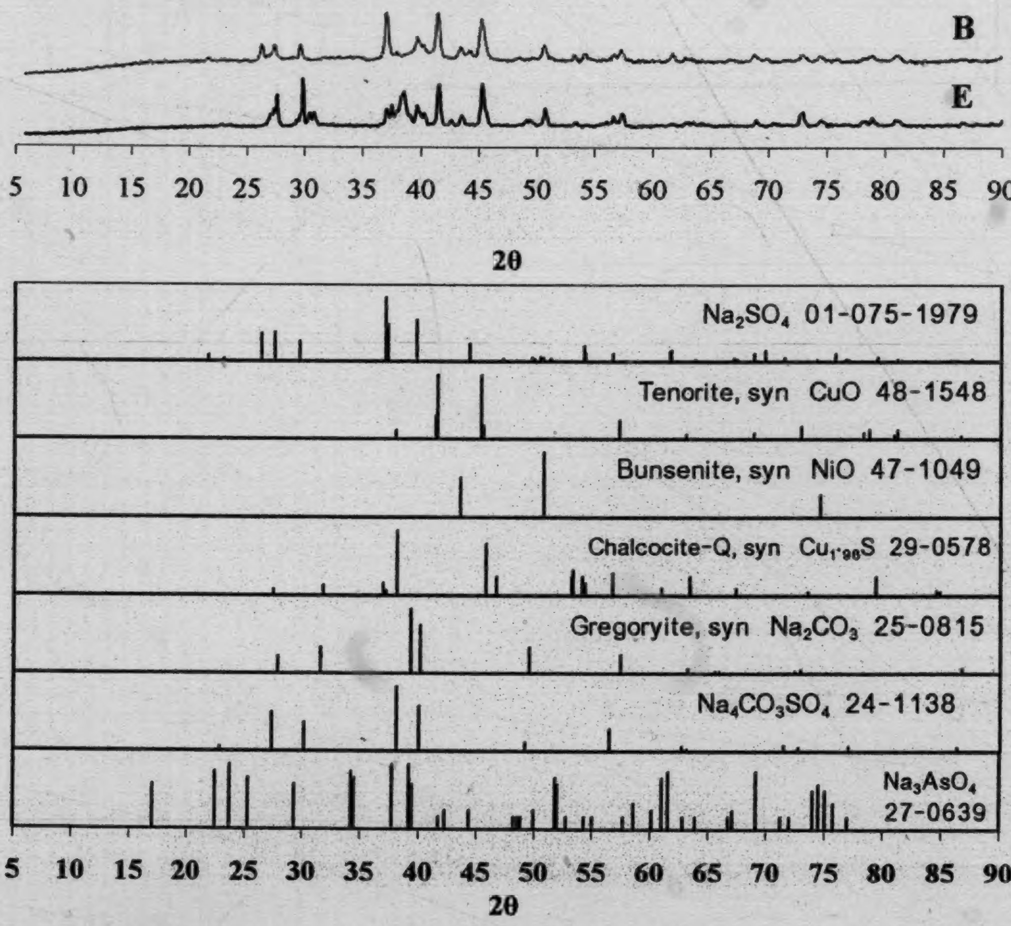

Figure 125 XRD Patterns of Inco Copper Residue (Feed #1) after Roasting with Na_2CO_3

Copper and nickel are predominantly converted to their respective oxides (i.e., tenorite (CuO) and bunsenite (NiO)), but some residual copper sulphide (i.e., $Cu_{1.96}S$) is also present in both samples. The conversion from covellite (CuS) to this form of chalcocite shows that significant oxidation of covellite has occurred and, thus, chalcocite likely represents an intermediate step in the oxidation of covellite to tenorite (CuO), likely falling in between covellite and digenite ($Cu_{1.8}S$) on the reaction series described in Section 6.1.1 (185). (Chalcocite-Q is a high temperature tetragonal polymorph of monoclinic chalcocite (Chalcocite-M). It would be expected to revert to the monoclinic form at room temperature over time.) Sodium arsenate (Na_3AsO_4) is also detected as a minor phase in the x-ray diffraction patterns of Sample E.

Backscattered electron imaging and EDX analysis of Sample B (550°C with 150% Na_2CO_3) confirm the presence of many of the phases detected using x-ray diffraction (Figure 126). The darker particles, identified as either Na_2SO_4 (B) or Na_2CO_3/Na_2SO_4 (A), are the predominant phases in the field of view with the smaller brighter particles representing unreacted, or partially reacted, copper sulphides (E) or mixtures of copper and nickel sulphides (D). EDX analysis of Particle C showed that it contained As, Na, Cl, S and O and, thus, likely represents a mixture of NaCl, Na_2SO_4 and Na_3AsO_4.

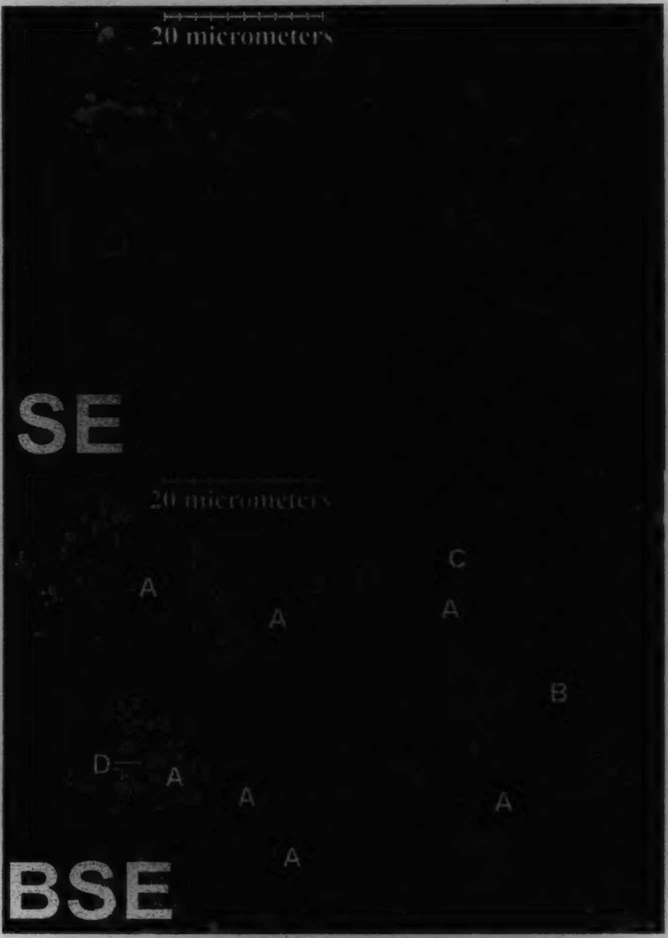

Figure 126
Secondary Electron (SE) and Backscattered Electron (BSE) Images of Inco Copper Residue (Feed #1) after Roasting at 550°C with 150% Na_2CO_3 (Sample B)

6.4.1.1.2 Hot Water Leaching and Room Temperature Acid Leaching

Since the majority of the sulphur retained in the solids is present as Na_2SO_4, it follows that most of the sulphur in the roasted residue is readily soluble in hot water (Figure 127).

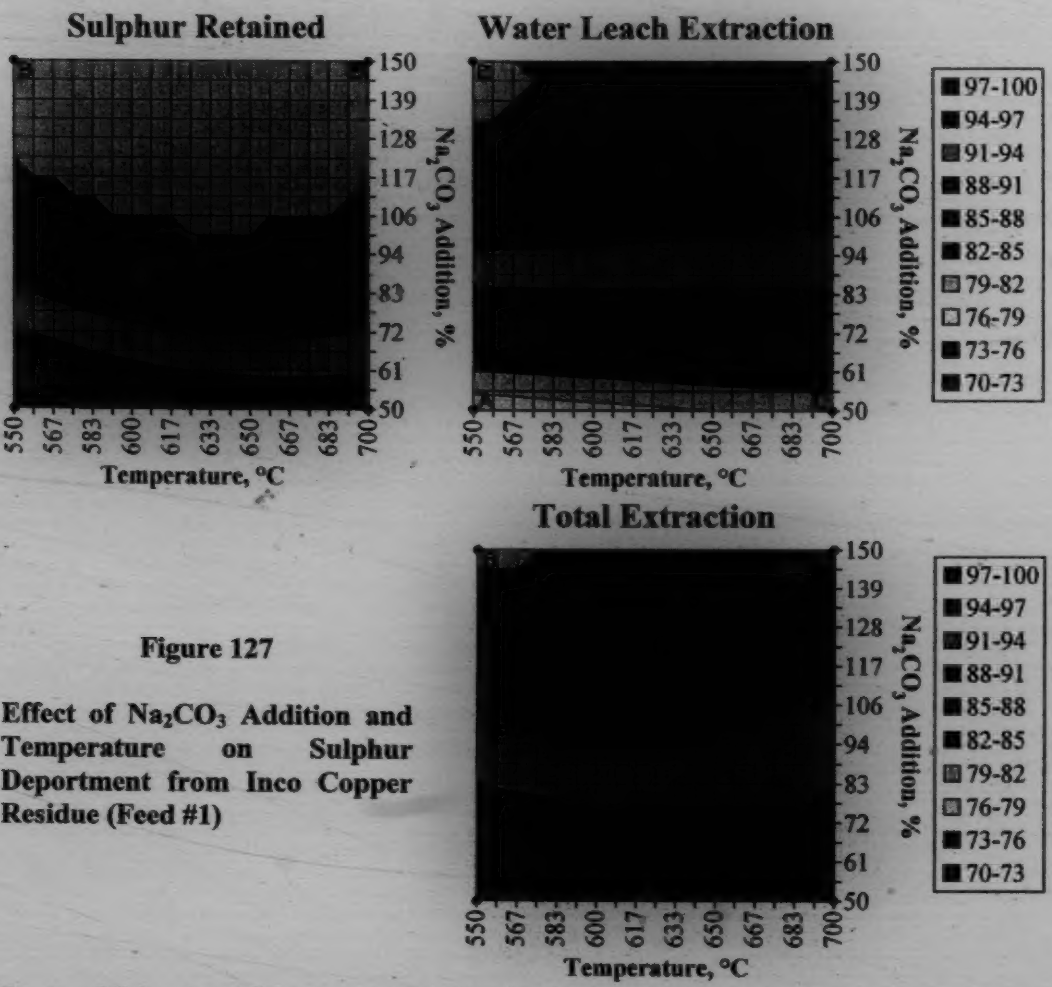

Figure 127

Effect of Na_2CO_3 Addition and Temperature on Sulphur Deportment from Inco Copper Residue (Feed #1)

Some additional sulphur is extracted by leaching with 200 g/L H_2SO_4 from samples roasted with low Na_2CO_3, likely due to the formation of copper or nickel oxysulphates during roasting when insufficient sodium was present to form Na_2SO_4 from all of the sulphide sulphur. Because any unleached sulphur in the solids is likely present as sulphides, the response surface model for the total extraction of sulphur can also be used to explain the degree of oxidation of sulphides during roasting. This model demonstrates, first, that higher Na_2CO_3 additions encourage the formation of water soluble Na_2SO_4 during roasting and, second, that higher conversions of sulphur to sulphate are observed at lower temperatures. The drop in conversion at higher temperatures may be due either to sintering of the residue as the roasting temperature approaches the melting point of Na_2CO_3 (851°C) or to kinetic concerns (i.e., the formation of reaction products which limit the rate at which oxygen reaches the sulphide surface).

Very different trends are observed in the deportment of arsenic during hot water and room temperature H_2SO_4 leaching (Figure 128). Increasing Na_2CO_3 addition and temperature both strongly promote the formation of hot water soluble arsenic such that, while less than 10% As is converted to a water soluble form at 550°C and 50% Na_2CO_3, (Sample A) nearly 100% is water soluble after roasting at 700°C and 150% Na_2CO_3 (Sample E). (Sodium arsenate (Na_3AsO_4) was identified in the x-ray diffraction patterns for the residue sample roasted under the latter conditions (Sample E) which explains the high arsenic extraction observed during water leaching for this sample.) Additional arsenic is then dissolved by leaching with 200 g/L H_2SO_4, where the extent of leaching is inversely related to the roasting temperature, but is largely unaffected by Na_2CO_3 additions. The response surface model for the overall arsenic extraction shows that, for most of the region where over 90% of the arsenic is retained during roasting, over 70% of the arsenic can be removed from the residue by water and/or acid leaching.

Less than 3.5%, and generally less than 0.3%, of the copper in the feed, and up to 30% of the nickel in the feed, can be leached in hot water (Figure 129). These extractions are highest when low Na_2CO_3 additions were used, possibly pointing to the formation of copper or nickel sulphates when not enough Na_2CO_3 was added to completely react with the sulphide sulphur during roasting. In the regions of greater than 90% sulphur and arsenic retention, copper and nickel water leach extractions are negligible.

Acid leaching of the water leach residues resulted in copper extractions of up to 96% and overall extractions of up to 98%, with the best conversions of copper to an acid soluble form in samples that had been roasted at temperatures of 575°C or lower (Figure 129). Under these same conditions, only 50% of the nickel is leached in the H_2SO_4 solution and overall nickel extractions only reach 60%, with the highest extractions observed at the lowest Na_2CO_3 additions and temperatures tested.

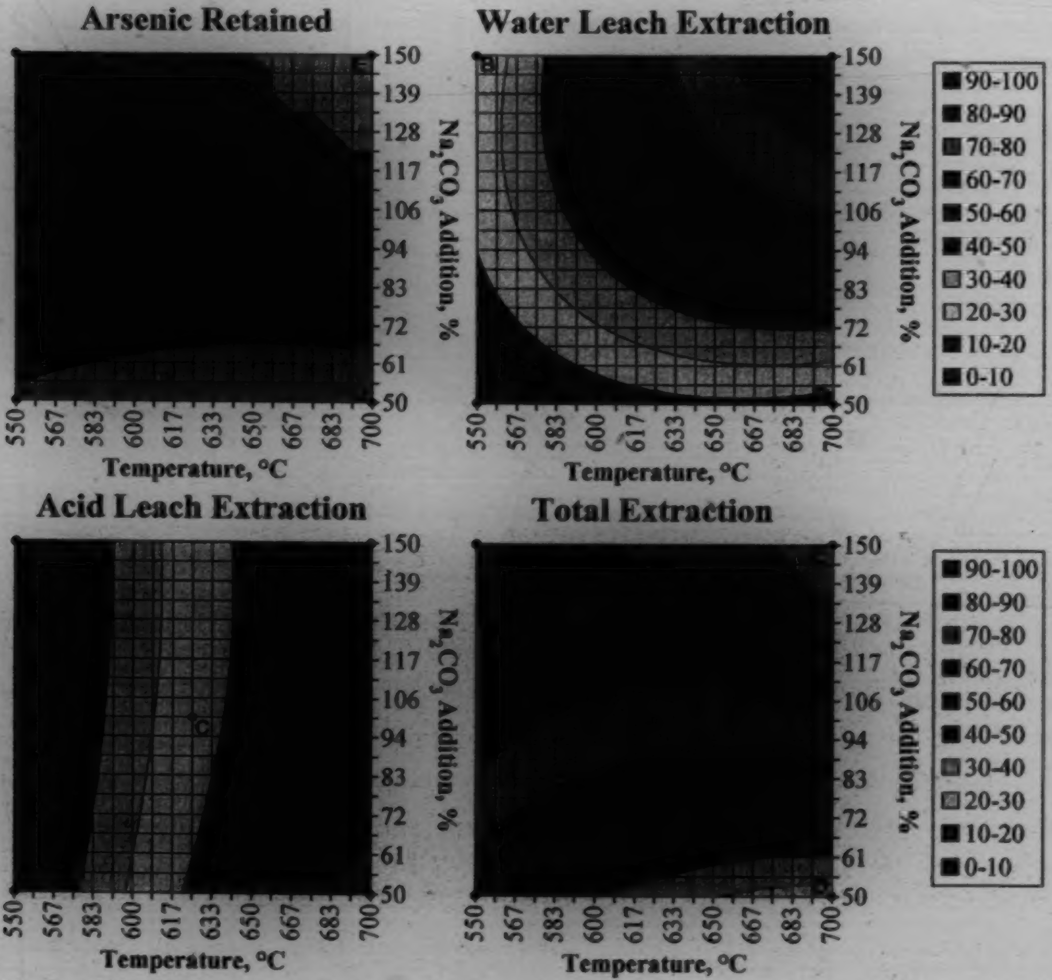

Figure 128 Effect of Na_2CO_3 Addition and Temperature on Arsenic Deportment from Inco Copper Residue (Feed #1)

The phases present in the copper residue after leaching with hot water and after leaching with 200 g/L H_2SO_4 solution are summarized in Tables 62 and 63, respectively while the diffraction patterns and major phases observed are shown in Figures 130 and 131.

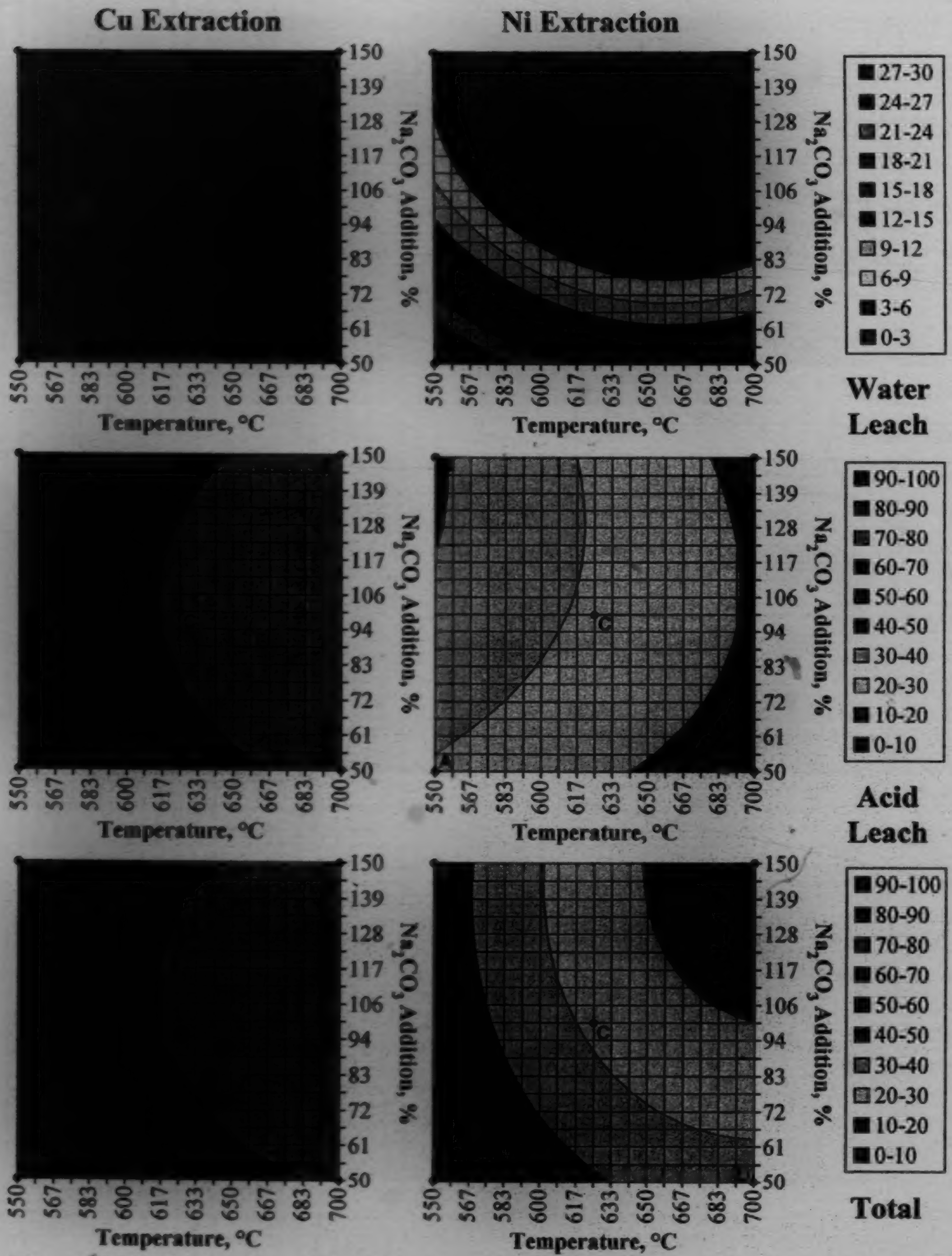

Figure 129 Effect of Na$_2$CO$_3$ Addition and Temperature on Copper and Nickel Extractions from Inco Copper Residue (Feed #1)

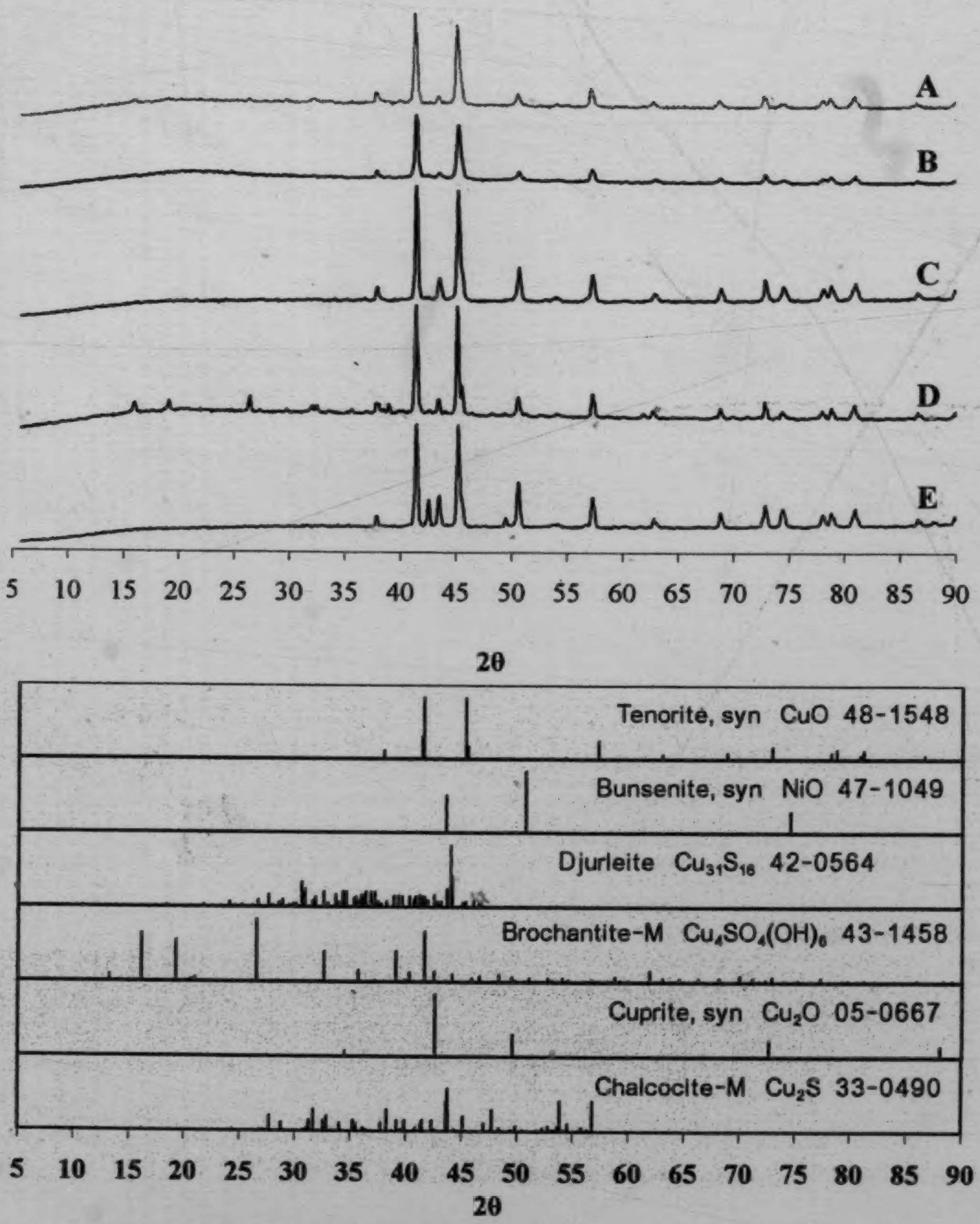

Figure 130 XRD Patterns of Inco Copper Residue (Feed #1) after Roasting with Na_2CO_3 and Leaching with Hot Water

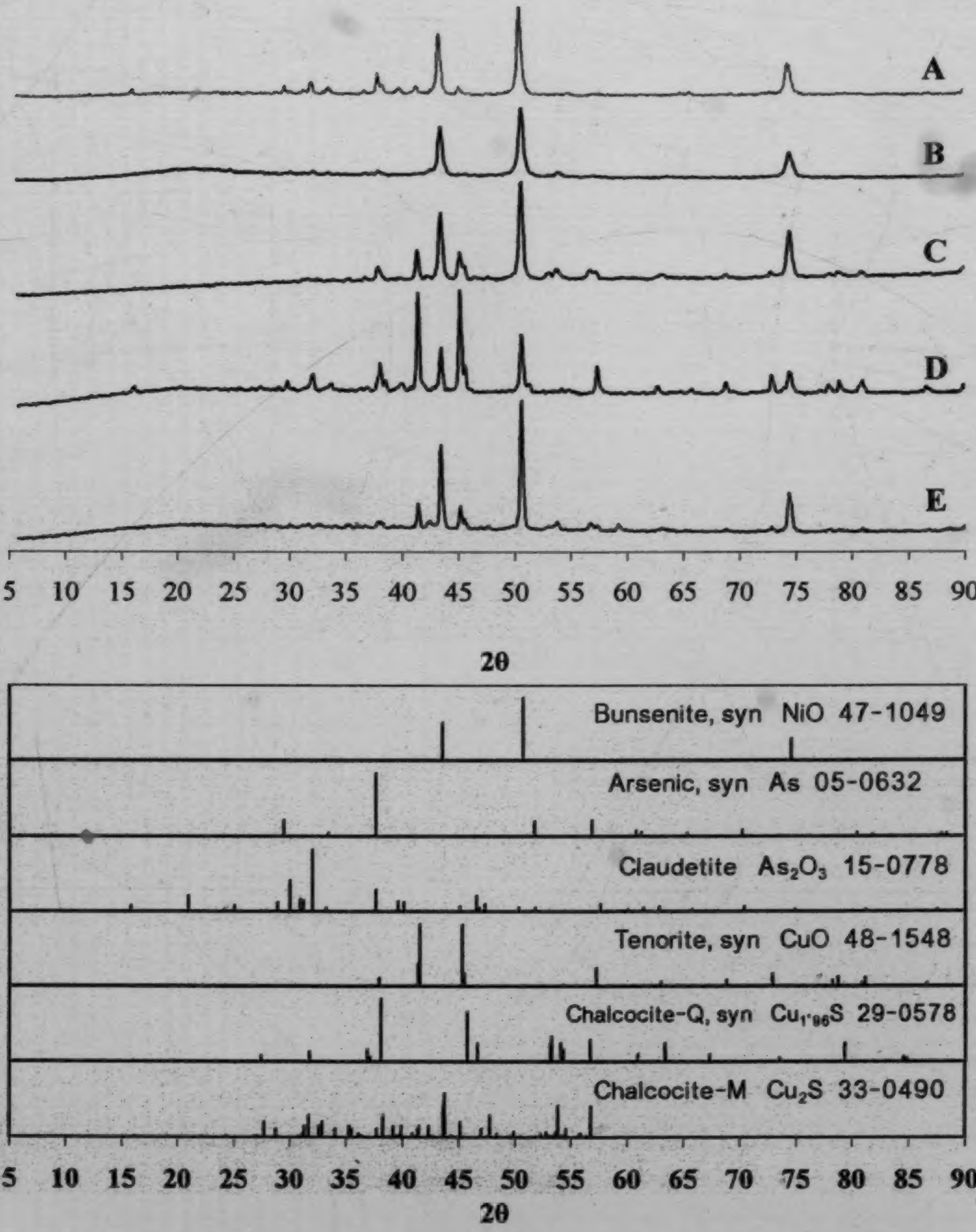

Figure 131 XRD Patterns of Inco Copper Residue (Feed #1) after Roasting with Na_2CO_3 and Leaching with 200 g/L H_2SO_4 at Room Temperature

Table 62 Phases Identified by XRD Analysis of Inco Copper Residue (Feed #1) Roasted with Na_2CO_3 and Leached with Hot Water

Sample	Identified Phases (in order of intensity)	Leaching Wt. Loss, %
A	CuO (Tenorite), NiO (Bunsenite), As_2O_3 (Claudetite)	62
B	CuO (Tenorite), NiO (Bunsenite)	75
C	CuO (Tenorite), NiO (Bunsenite)	70
D	CuO (Tenorite), NiO (Bunsenite), $Cu_4SO_4(OH)_6$ (Brochantite-M)	64
E	CuO (Tenorite), NiO (Bunsenite), Cu_2O (Cuprite), Cu_2S (Chalcocite-M)	77

Table 63 Phases Identified by XRD Analysis of Inco Copper Residue (Feed #1) Roasted with Na_2CO_3 and Leached with 200 g/L H_2SO_4 at Room Temperature

Sample	Identified Phases (in order of intensity)	Leaching Wt. Loss, %
A	NiO (Bunsenite), As, As_2O_3 (Claudetite), CuO (Tenorite), $BaSO_4$ (Barite)	85
B	NiO (Bunsenite), Cu_2S (Chalcocite-M)	84
C	NiO (Bunsenite), CuO (Tenorite), $Cu_{1.96}S$ (Chalcocite-Q), Cu_2S (Chalcocite-M), $Ni_{3.11}S_2$	64
D	CuO (Tenorite), NiO (Bunsenite), As_2O_3 (Claudetite), $BaSO_4$ (Barite), $PbSO_4$ (Anglesite)	58
E	NiO (Bunsenite), CuO (Tenorite), Cu_2S (Chalcocite-M)	51

After leaching with hot water, any Na_2SO_4 or residual Na_2CO_3 is dissolved along with any water soluble As, Ni or Cu to leave tenorite (CuO) and bunsenite (NiO) as the major phases identified in all the water leach residues. Claudetite (As_2O_3) and brochantite ($Cu_4SO_4(OH)_6$) are also identified in Samples A and D, which were roasted with low Na_2CO_3 additions. (Claudetite (As_2O_3) is likely formed by the decomposition of As_2S_3 to S and As and the subsequent oxidation of As to As_2O_3 (25) under conditions where less sodium was available to react to form other arsenic compounds.) Two intermediate phases in the oxidation of covellite (CuO) were also observed in Sample E as chalcocite (Cu_2S) and cuprite (Cu_2O) were identified. SEM/EDX analysis of Sample B (550°C, 150% Na_2CO_3) reflects the findings of the XRD analysis as particles containing either Cu and O (i.e., CuO (tenorite) (A)), Ni, Cu and O (i.e., a mixture of NiO and CuO (C)), or Ni, Cu, O and As (i.e., NiO, CuO and/or possibly copper or nickel arsenates or arsenites (B)), were identified (Figure 132).

After leaching with 200 g/L H_2SO_4 at room temperature, both bunsenite (NiO) and tenorite (CuO) are still major phases in most of the samples. Arsenic (As) and As_2O_3 appear to be largely unleached in the acid conditions as they are identified in the acid leach residues from samples roasted with low Na_2CO_3 additions (Samples A and D). Several intermediate phases from covellite and vaesite oxidation, such as Cu_2S, $Cu_{1.96}S$ and $Ni_{3.11}S_2$, are also observed in several samples. Insoluble sulphates, such as barite ($BaSO_4$) and anglesite ($PbSO_4$), are also present in several samples, likely as the result of dissolution, and reprecipitation, of lead and barium compounds during H_2SO_4 leaching. SEM/EDX analysis of Sample B (550°C, 150% Na_2CO_3) also indicates that nickel oxide (C) are the major phase in the acid leach residue, with minor amounts of nickel and copper sulphides with Cu:Ni ratios varying between 1:1 (A) and 3:1 (B) also observed (Figure 133) .

From this analysis, it is evident that good control of sulphur and arsenic emissions, high sulphur extractions by water leaching and high copper extractions by subsequent H_2SO_4 leaching are all possible by roasting with Na_2CO_3 under these conditions. However, the presence of unleached bunsenite (NiO) and tenorite (CuO) after acid leaching indicates that changes in the leaching procedure are necessary to maximize nickel and copper extractions. Thus, a second DOE test was carried out using identical conditions, except that H_2SO_4 leaching was conducted at 95 to 97°C, instead of room temperature. This second test was performed using the second sample of Inco copper residue because previous testing had depleted the small first sample that had been obtained from Inco.

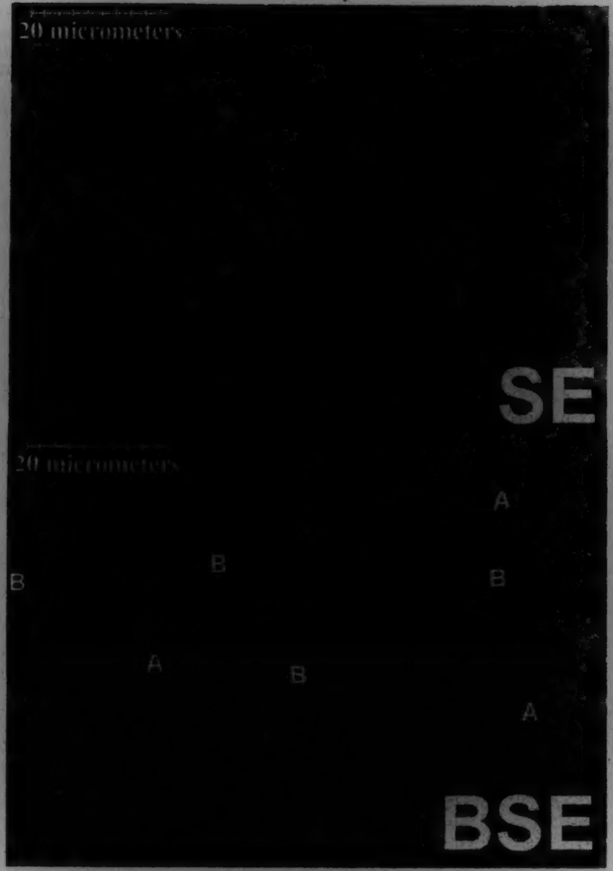
20 micrometers
SE
20 micrometers
A
B
B
B
A
B
A
BSE

Figure 132

Secondary Electron (SE) and Backscattered Electron (BSE) Images of Inco Copper Residue (Feed #1) after Roasting at 550°C with 150% Na_2CO_3 and Leaching with Hot Water (Sample B)

20 micrometers
SE
20 micrometers
A
B
A
BSE

Figure 133

Secondary Electron (SE) and Backscattered Electron (BSE) Images of Inco Copper Residue (Feed #1) after Roasting at 550°C with 150% Na_2CO_3 and Leaching with 200 g/L H_2SO_4 at Room Temperature (Sample B)

6.4.1.2 Roasting of Inco Copper Residue (Feed #2) with Na_2CO_3

6.4.1.2.1 Roasting

The response surface models for roasting of Feed #2 of the Inco copper residue indicates that, while the Na_2CO_3 additions used in this DOE test were able to reduce sulphur emissions to zero at higher Na_2CO_3 additions (i.e., greater than about 125% Na_2CO_3), they were not effective in reducing arsenic emissions to zero during roasting (Figure 134). Extrapolation of the response surface model indicates that Na_2CO_3 additions of over 170% would be required to eliminate arsenic emissions during the roasting of this sample. This is not entirely unexpected as, stoichiometrically, an addition of 111% Na_2CO_3 (i.e., 98% for reaction with sulphur and 13% for reaction with arsenic) would be required to completely react with these two elements in the second sample of Inco copper residue. This is a significant increase from the stoichiometric requirement for the first sample of Inco copper residue (71%) and is due, in large part, to the high elemental sulphur and arsenic content of this second residue sample.

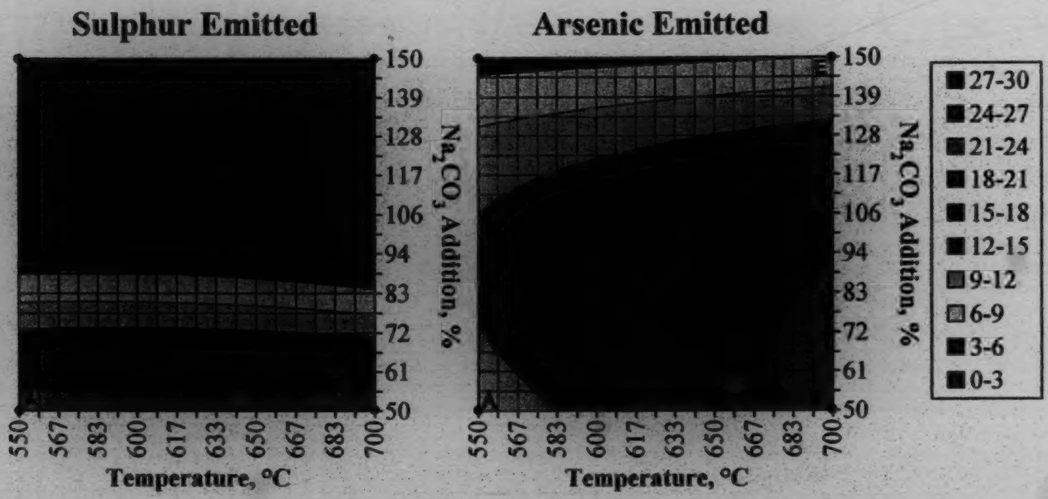

Figure 134 Effect of Na_2CO_3 Addition and Temperature on Sulphur and Arsenic Emissions During Roasting of Inco Copper Residue (Feed #2)

The amount of arsenic emitted during roasting this sample is also much more dependent on temperature, particularly at lower Na_2CO_3 additions and does not show a peak in emission at 600°C as observed in the roasting of Feed #1. This is likely due to the differences in arsenic mineralogy in this material, with enargite (Cu_3AsS_4) being the major arsenic phase identified, instead of $Cu_3(AsO_4)_2$ and orpiment (As_2S_3).

The phases formed during roasting were identified using x-ray diffraction analysis of selected samples (Points A through E on Figures 134, 136, 137 and 138). The identified phases for the copper residue after roasting are listed in Table 64 while the diffraction patterns and major phases observed are shown in Figure 135.

Table 64 Phases Identified by XRD Analysis of Inco Copper Residue (Feed #2) Roasted with Na_2CO_3

Sample	Identified Phases (in order of intensity)
A	CuO (Tenorite), Na_2SO_4, $CuAsO_3(OH)\cdot H_2O$ (Geminite), $Na_2As_4O_{11}$, S, $Cu_3(AsO_4)_2\cdot 4H_2O$ (Rollandite), $CuSO_4$ (Chalcocyanite)
B	Na_2SO_4, CuO (Tenorite), NiO (Bunsenite)
C	Na_2SO_4, CuO (Tenorite), Cu_2S (Chalcocite-Q), $Na_4CO_3SO_4$, NiO (Bunsenite)
D	Na_2SO_4, CuO (Tenorite), Na_2CO_3 (Gregoryite), Cu_2S (Chalcocite-Q), $Na_4CO_3SO_4$, NiO (Bunsenite), $BaCO_3$ (Cerussite), $CuAsO_3(OH)\cdot H_2O$ (Geminite)
E	$Na_4CO_3SO_4$, CuO (Tenorite), Na_2SO_4, $NaCu_4(AsO_4)_3$, NiO (Bunsenite), Cu_2S (Chalcocite-M), Na_3AsO_4, $BaCO_3$ (Cerussite)

Generally, the copper, nickel and sulphur phases observed after roasting the second sample of the Inco copper residue are very similar to those observed after roasting the first sample. The sodium carbonate added reacts readily with the sulphur from the elemental sulphur and sulphides to form Na_2SO_4 and, thus, sodium sulphate is a major phase in all the samples analyzed, but some unreacted, or partially reacted, Na_2CO_3 is also present in Samples C, D and E, either as Na_2CO_3 or $Na_4CO_3SO_4$. Tenorite (CuO) and bunsenite (NiO) are the major copper and nickel phases, respectively, in the roasted residue, but intermediate phases in the oxidation of covellite (CuS), such as tetragonal and monoclinic chalcocite, are also observed in the samples roasted above 625°C. Chalcocyanite ($CuSO_4$) is also formed in Sample A, likely because of sulphation due to the lower addition of Na_2CO_3 relative to the sulphur content in this sample.

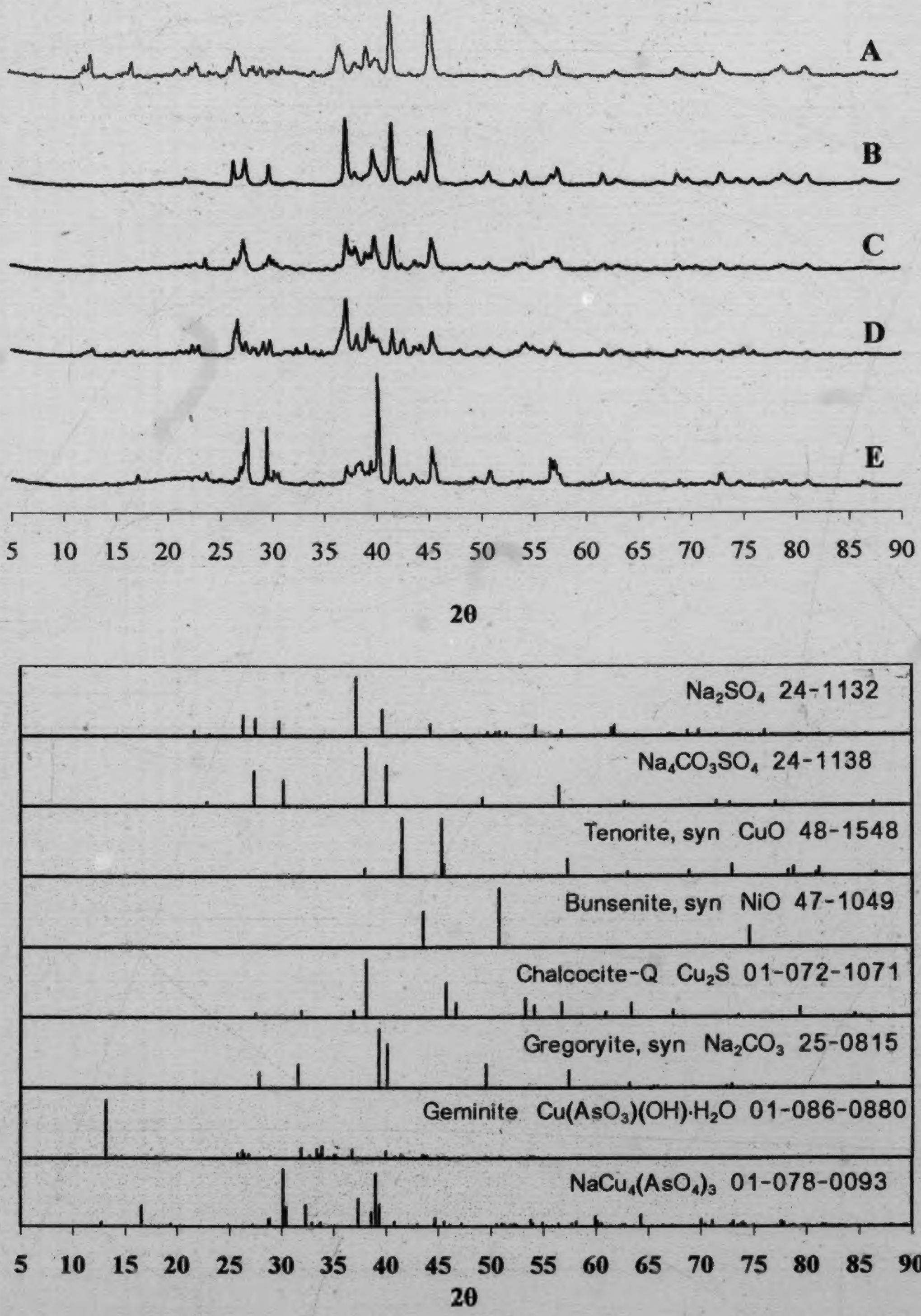

Figure 135 XRD Patterns of Inco Copper Residue (Feed #2) after Roasting with Na_2CO_3

However, a wider range of arsenic minerals are observed after roasting the second copper residue sample from Inco. Arsenic compounds in the roasted residues consist mostly of copper or sodium arsenates or arsenites, with $CuAsO_3(OH)\cdot H_2O$ (Geminite), $Na_2As_4O_{11}$ and $Cu_3(AsO_4)_2\cdot 4H_2O$ (Rollandite) detected at lower Na_2CO_3 additions in Samples A and D and $NaCu_4(AsO_4)_3$ and Na_3AsO_4 identified at higher Na_2CO_3 additions in Sample E.

6.4.1.2.2 Hot Water Leaching and Hot Acid Leaching

Though the majority of the sulphur in the solids is soluble by hot water leaching, the overall water leach extractions from this second sample of copper residue are much lower than those observed for the roasting and leaching of Feed #1 (Figure 136).

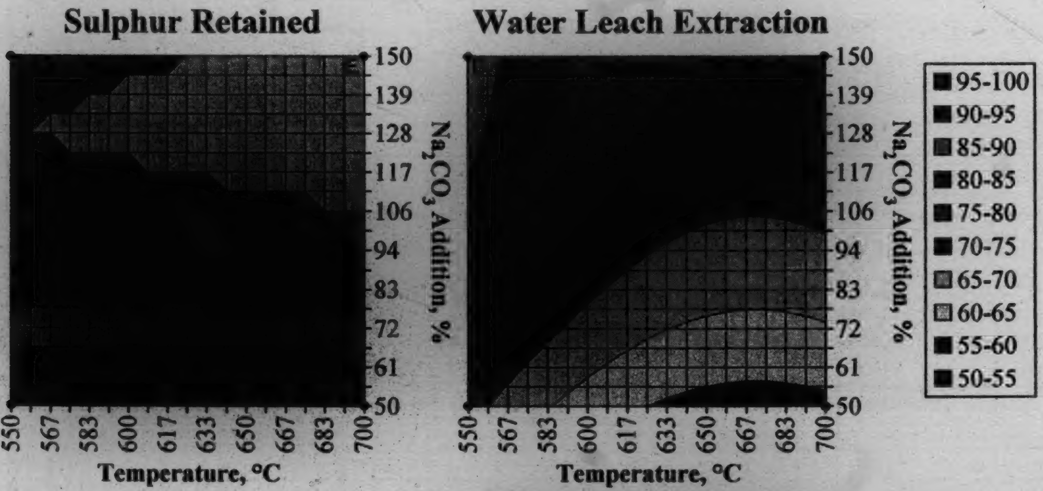
Sulphur Retained

Water Leach Extraction

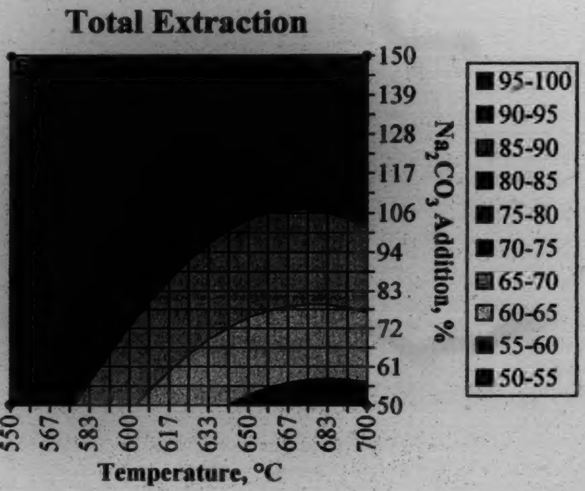
Total Extraction

Figure 136

Effect of Na_2CO_3 Addition and Temperature on Sulphur Deportment from Inco Copper Residue (Feed #2)

Between 55 and 90% of the sulphur is soluble from the second Inco copper residue sample over this range of roasting conditions while between 76 and 100% could be extracted under similar conditions from Feed #1 and little additional sulphur is leached with 200 g/L H_2SO_4. Thus, these overall extractions represent an approximate range of sulphide conversion of only 55 to 90%, which is quite low given the long roasting time and high air flow used in these experiments. However, since roasted residue samples from this DOE test showed a significant degree of sintering, particularly at higher roasting temperatures. it is possible that the high sulphur, and particularly elemental sulphur, content of this feed sample, in combination with the proximity of the roasting temperatures to the melting point of Na_2CO_3 (851°C), encouraged sintering of the roasting charge, and, as a result, could have inhibited the effective oxidation of sulphide sulphur during roasting.

The leaching of arsenic with hot water shows a similar trend to that observed when roasting Feed #1 as the arsenic extraction increases with increasing temperature and Na_2CO_3 addition (Figure 137). However, the maximum arsenic extraction by hot water leaching only reaches 70% which is considerably lower that that observed from roasted Feed #1 (i.e., up to 90%). This is likely related to the low Na_2CO_3 addition, relative to the sulphur and arsenic content of this material, which not only reduced the amount of arsenic captured, compared to roasting the first feed sample, but also would reduce the amount of sodium available for the formation of water soluble sodium arsenates or arsenites. Subsequent extraction of arsenic by leaching with hot 200 g/L H_2SO_4 shows that the arsenic extractions by acid leaching increase strongly with decreasing temperature and Na_2CO_3 additions. This trend is nearly the opposite of that observed in water leaching, and, thus, high overall arsenic extractions of between 60 to 100% are possible, with the highest overall extractions occurring at lower roasting temperatures.

Up to 12% of the copper and nickel extractions are leached by hot water from this feed sample, but only at lower Na_2CO_3 additions during roasting; water leach extractions are negligible when enough Na_2CO_3 is added to reduce sulphur emissions to less than 3% (Figure 138). As mentioned previously, this water soluble copper and nickel is likely a result of the partial sulphation of the copper or nickel sulphides under conditions where insufficient Na_2CO_3 was present to promote the formation of Na_2SO_4 from sulphide sulphur. Maximum water leach extractions were significantly higher for nickel (i.e., up to 30%) for the first feed sample. About 15% more of the nickel was soluble in hot water leaching of the as-received sample of Feed #1, likely as retgersite ($NiSO_4 \cdot 6H_2O$), and it is possible that this compound is not completely converted to NiO during with lower Na_2CO_3 additions.

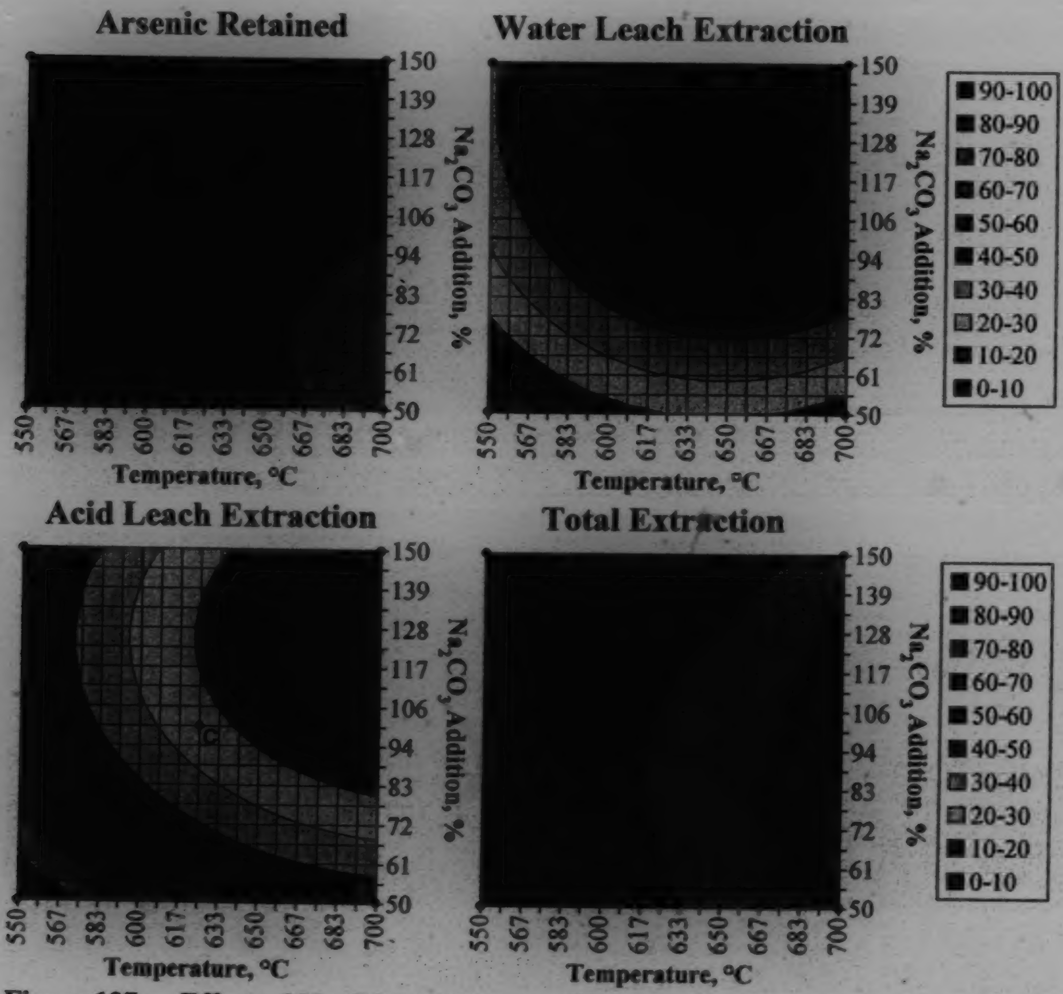

Figure 137 Effect of Na_2CO_3 Addition and Temperature on Arsenic Deportment from Inco Copper Residue (Feed #2)

Acid leaching extractions for copper and nickel follow closely the trends observed for the acid leach extraction of arsenic from the samples of roasted residue. Both copper and nickel extractions show an increase with decreasing temperature and, to a lesser degree, decreasing Na_2CO_3 addition, though the nickel extraction shows less dependence overall on the Na_2CO_3 addition (Figure 138). Acid leach and overall copper extractions are decreased across the reaction space from Feed #1 to Feed #2, with acid leach extractions ranging from 10 to 90%, and overall extractions from 10 to 100%, which is considerably lower than the range of 70 to 100% observed under similar roasting conditions for Feed #1. However, leaching with hot sulphuric acid solutions greatly improved the recovery of nickel, with up to 90% recovered by acid leaching and up to 100% overall for these roasting conditions.

The phases present in the copper residue after leaching with hot water and after leaching with 200 g/L H_2SO_4 solution at 95 to 97°C are summarized in Tables 65 and 66, respectively, while the diffraction patterns and major phases observed are shown in Figures 139 and 140. Because of a high weight loss during leaching, insufficient sample of the acid leach residue of Sample A was available for analysis.

Table 65 Phases Identified by XRD Analysis of Inco Copper Residue (Feed #2) Roasted with Na_2CO_3 and Leached with Hot Water

Sample	Identified Phases (in order of intensity)	Leaching Wt. Loss, %
A	CuO (Tenorite), $Cu_4SO_4(OH)_6$ (Brochantite-M), $Cu_3SO_4(OH)_4$ (Antlerite), NiO (Bunsenite), $NaCu_4(AsO_4)_3$ (Bradaczekite)	60
B	CuO (Tenorite), NiO (Bunsenite), Cu_2S (Chalcocite-M)	76
C	CuO (Tenorite), Cu_2S (Chalcocite-M), NiO (Bunsenite), $Cu_{1.96}S$ (Chalcocite-Q), Ni_3S_2 (Heazlewoodite), $Ba(OH)_2 \cdot H_2O$	68
D	CuO (Tenorite), Cu_2O (Cuprite), NiO (Bunsenite), Cu_2S (Chalcocite-M), $Cu_{1.96}S$ (Chalcocite-Q), Cu_3AsS_4 (Enargite), $BaSO_4$ (Barite)	61
E	CuO (Tenorite), NiO (Bunsenite), Cu_2S (Chalcocite-M)	76

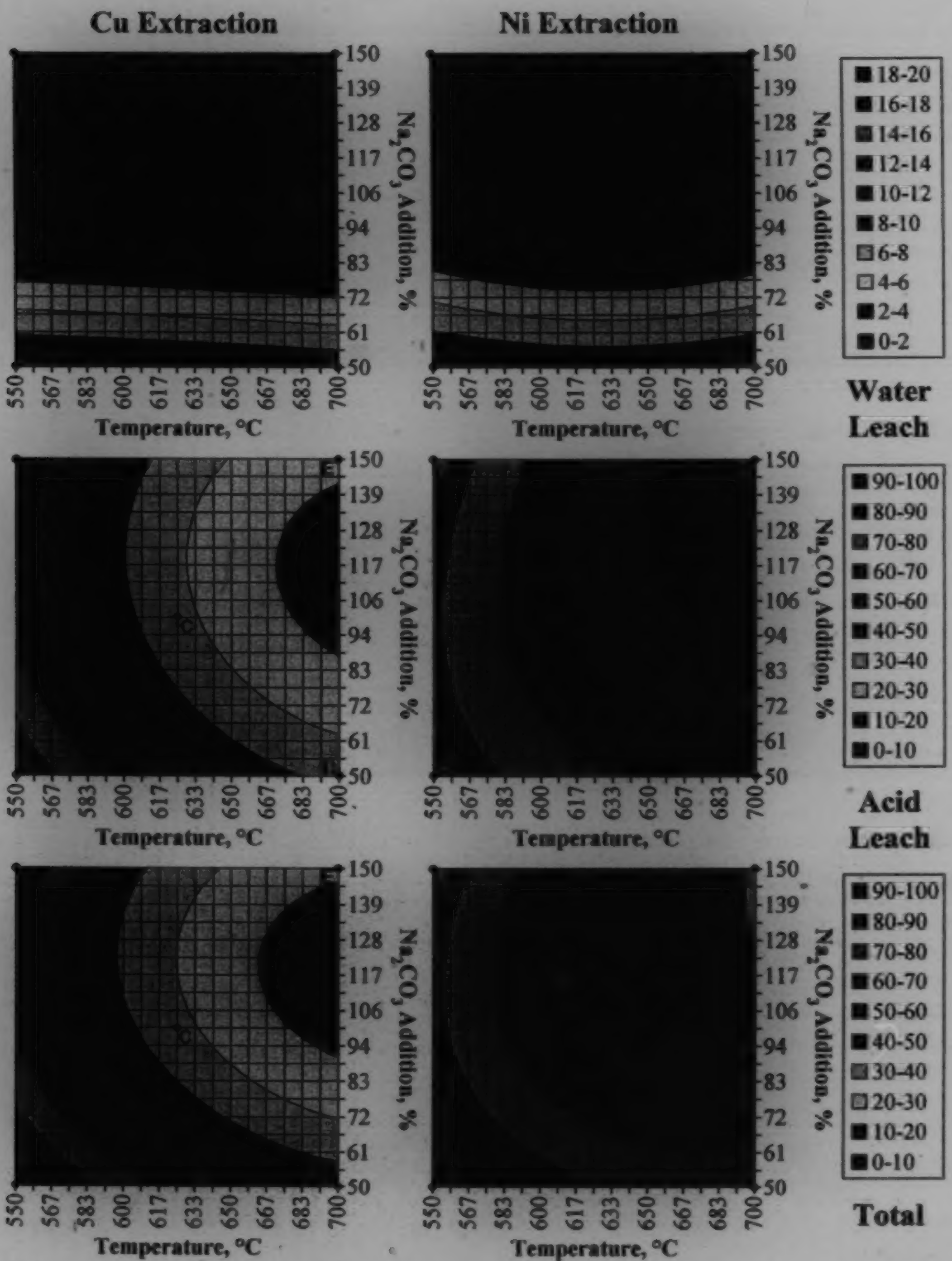

Figure 138 Effect of Na$_2$CO$_3$ Addition and Temperature on Copper and Nickel Extractions from Inco Copper Residue (Feed #2)

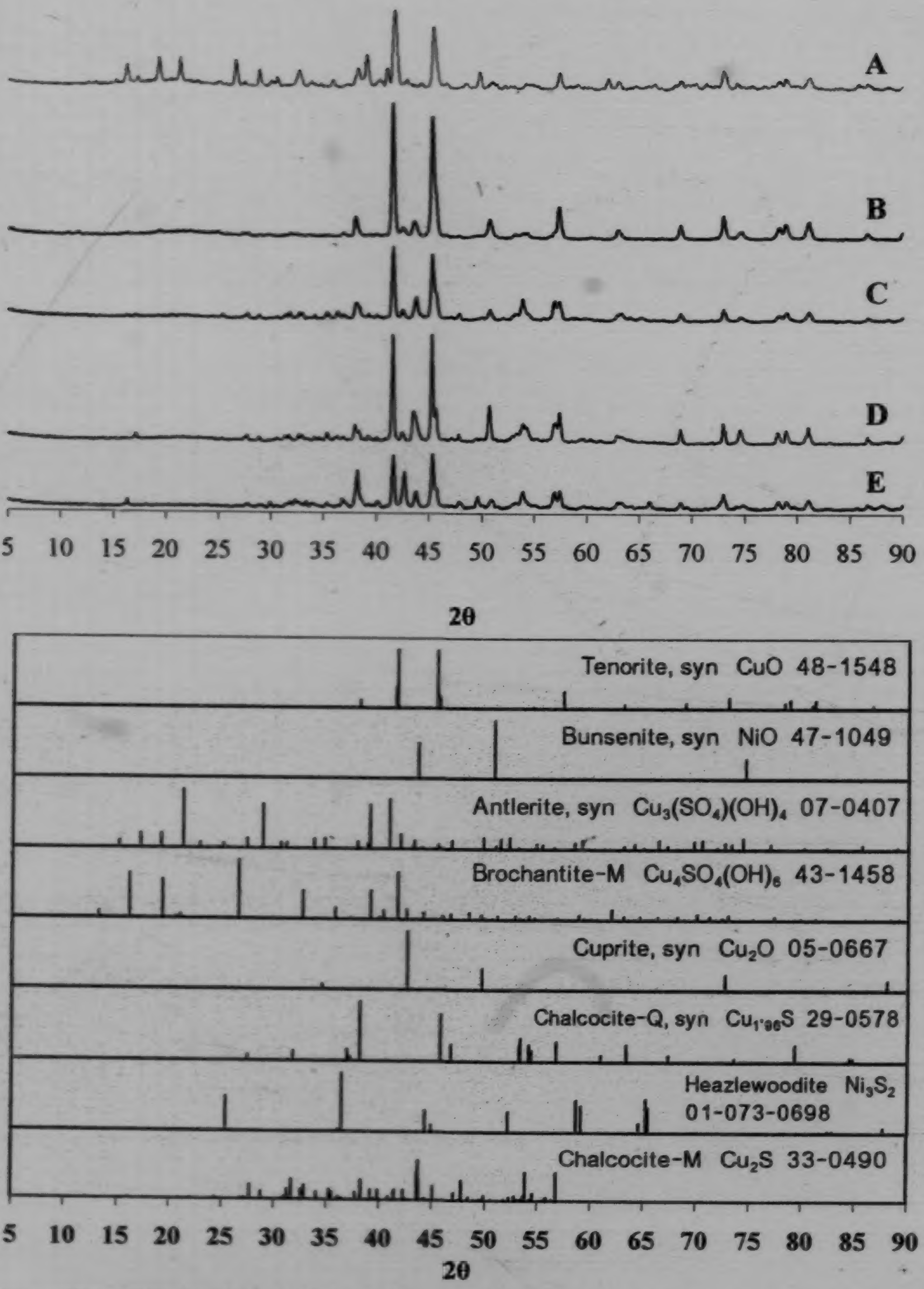

Figure 139 XRD Patterns of Inco Copper Residue (Feed #2) after Roasting with Na_2CO_3 and Leaching with Hot Water

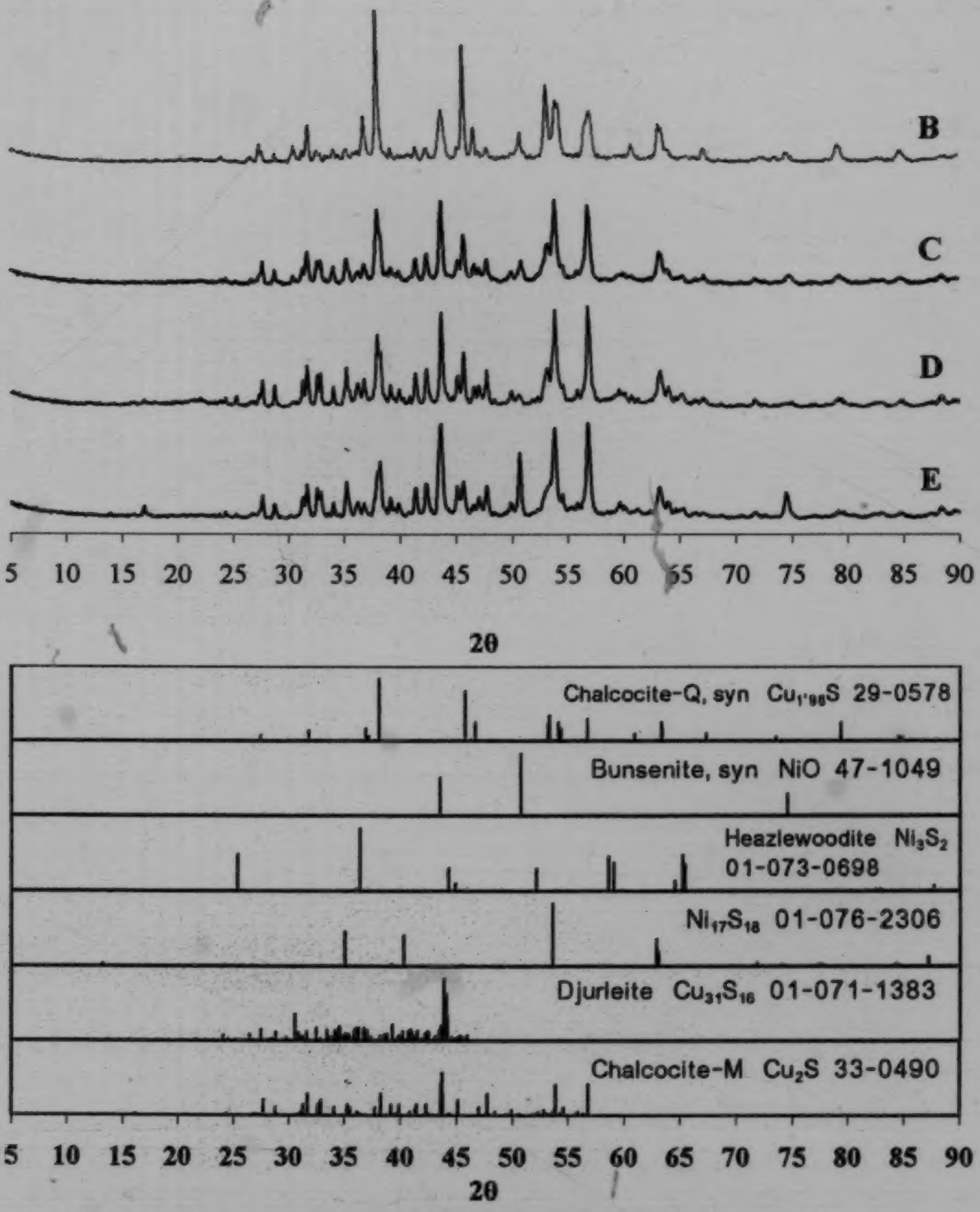

Figure 140 XRD Patterns of Inco Copper Residue (Feed #2) after Roasting with Na_2CO_3 and Leaching with 200 g/L H_2SO_4 at 95 to 97°C

Table 66 Phases Identified by XRD Analysis of Inco Copper Residue (Feed #2) Roasted with Na_2CO_3 and Leached with 200 g/L H_2SO_4 at 95 to 97°C

Sample	Identified Phases (in order of intensity)	Leaching Wt. Loss, %
B	$Cu_{1.96}S$ (Chalcocite-Q), Cu_2S (Chalcocite-M), NiO (Bunsenite), $Cu_{31}S_{16}$ (Djurleite)	99
C	Cu_2S (Chalcocite-M), $Cu_{1.96}S$ (Chalcocite-Q), Ni_3S_2 (Heazlewoodite), $Ni_{17}S_{18}$	79
D	Cu_2S (Chalcocite-M), $Cu_{1.96}S$ (Chalcocite-Q), NiO (Bunsenite)	35
E	Cu_2S (Chalcocite-M), $Cu_{1.96}S$ (Chalcocite-Q), NiO (Bunsenite)	27

After leaching in hot water, a number of phases are no longer detected that were detected in the roasted copper residue, including Na_2SO_4, $Na_4CO_3SO_4$, Na_2CO_3, Na_3AsO_4, $Na_2As_4O_{11}$, $CuAsO_3(OH)\cdot H_2O$ (Geminite), $Cu_3(AsO_4)_2\cdot 4H_2O$ (Rollandite), and $CuSO_4$ (Chalcocyanite); all are believed to be phases that are readily soluble and, thus, are likely dissolved during the hot water leaching stage. After hot water leaching, tenorite (CuO) is the major phase present in all five samples analyzed with XRD while bunsenite (NiO) is again identified as the predominant nickel-bearing phase. Intermediate products in the covellite reactions series are observed in all but Sample A, including both monoclinic chalcocite (Cu_2S), tetragonal chalcocite ($Cu_{1.96}S$) and cuprite (Cu_2O). Heazlewoodite (Ni_3S_2), likely an intermediate product in vaesite oxidation, is also identified in Sample C and some unreacted enargite (Cu_3AsS_4) is also detected as a minor phase in Sample D. In Sample A, after water leaching, copper is also present as basic copper sulphates, such as brochantite ($Cu_4SO_4(OH)_6$) and antlerite ($Cu_3SO_4(OH)_4$), and as a sodium-copper arsenate ($NaCu_4(AsO_4)_3$). Barium is present in trace quantities in the feed and barium compounds are observed in trace quantities in Samples C and D, with $Ba(OH)_2\cdot 2H_2O$ detected at lower Na_2CO_3 additions and barite ($BaSO_4$) detected at higher additions.

Backscattered electron imaging with the scanning electron microscope and EDX analysis of Sample B (550°C, 150% Na_2CO_3) show more variation in the phases present than were observed using x-ray diffraction (Figure 141). Copper sulphides (i.e., chalcocite (Cu_2S) (A)) and copper and nickel oxides (i.e., tenorite (CuO) (D) or mixtures of CuO and NiO (C)) are indeed present, as indicated by the x-ray diffraction analysis, but other particles high in Cu, S and As (i.e., enargite (Cu_3AsS_4 (B)), high in Ni, Cu, O and C (i.e., possibly a mixture of CuO, NiO and $NiCO_3$ (E)) and high in Ni, Cu, As, O and C (i.e., possibly a mixture of the phases in Particle E with a copper arsenate (F)).

After leaching with 200 g/L H_2SO_4 at 95 to 97°C, reaction products of covellite (CuS) and vaesite (NiS_2), such as tetragonal chalcocite ($Cu_{1.96}S$), monoclinic chalcocite (Cu_2S), djurleite ($Cu_{31}S_{16}$), heazlewoodite (Ni_3S_2) and $Ni_{17}S_{18}$, are the major phases in the acid leach residue, indicating that, although partial oxidation of the sulphides has occurred, oxidation is incomplete for the roasting conditions tested as was proposed earlier from analysis of the overall sulphur and copper extractions. SEM/EDX analysis of Sample B (550°C, 150% Na_2CO_3) confirms these findings, as copper sulphides (A) and nickel sulphides (B) are the only phases visible in the field of view for the acid leach residue from Sample B (Figure 142). Some unleached bunsenite (NiO) is still present in the acid leach residue, but the amount has been significantly reduced through the change in acid leaching conditions for this sample.

The results from roasting both Feed #1 and Feed #2 of the Inco copper residue with Na_2CO_3, followed by hot water and H_2SO_4 leaching, indicate that lower roasting temperatures should be used to maximize copper and nickel extractions during roasting. In addition, these tests indicate that Na_2CO_3 additions of over 125% of stoichiometric are required to eliminate the emission of sulphur during roasting with additional Na_2CO_3 additions of between 230 and 600% of the stoichiometric requirement for arsenic capture required to effectively eliminate arsenic emissions. (The wide variation reported here may be caused by the differences in the arsenic minerals present in Feed #1 and #2.) If enough Na_2CO_3 is added to eliminate sulphur emissions, it is then possible to selectively extract the majority of the sulphur from the roasted residue by hot water leaching with minimal dissolution of copper and nickel.

20 micrometers
SE
20 micrometers
C
F
D
A
C
E
BSE

Figure 141

Secondary Electron (SE) and Backscattered Electron (BSE) Images of Inco Copper Residue (Feed #2) after Roasting at 550°C with 150% Na_2CO_3 and Leaching with Hot Water (Sample B)

20 micrometers
SE
20 micrometers
A
BSE

Figure 142

Secondary Electron (SE) and Backscattered Electron (BSE) Images of Inco Copper Residue (Feed #2) after Roasting at 550°C with 150% Na_2CO_3 and Leaching with 200 g/L H_2SO_4 at 95 to 97°C (Sample B)

The formation of water soluble arsenic is promoted at higher roasting temperatures and Na_2CO_3 additions for both copper residue samples. However, since higher roasting temperatures, particularly for Feed #2, reduce the amount of copper and nickel that can be recovered from this material, further research, possibly using oxygen enrichment of the roasting atmosphere, would be necessary to try to improve the water solubility of arsenic and, hence, its selective removal from copper and nickel during water leaching after roasting at lower overall roasting temperatures.

6.4.2 Roasting of Inco Copper Residue (Feed #2) with $Ca(OH)_2$

Since a number of studies have reported the results of roasting sulphide concentrates with hydrated lime (Sections 6.1.1 and 6.1.2.1), one DOE test was conducted to produce response surface models which could then be used to allow comparisons to be made between the effectiveness of $Ca(OH)_2$ and Na_2CO_3 as roasting reagents, and to be able to compare these results more effectively with those reported from lime roasting. The results of this test are described in the following section. Slightly higher acid concentrations of 300 g/L H_2SO_4 were used during acid leaching to ensure that unreacted $Ca(OH)_2$ would not be able to completely neutralize the available acid from the leach solution.

6.4.2.1 Roasting

The roasting results agree quite well with those reported in the literature (175-177). Sulphur emissions are effectively eliminated at all additions above the stoichiometric requirement for $Ca(OH)_2$ additions (68.5%) (Figure 143). While capture of the arsenic should require an additional 4.5% $Ca(OH)_2$, based on the stoichiometry, arsenic emissions were negligible (0.0 to 0.3%) for the entire range of $Ca(OH)_2$ additions and temperatures tested.

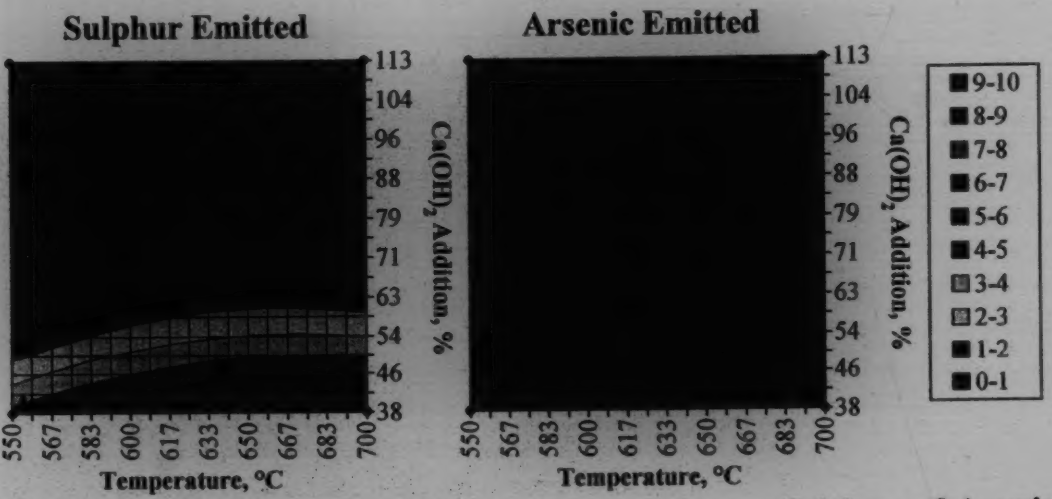

Figure 143 Effect of $Ca(OH)_2$ Addition and Temperature on Sulphur and Arsenic Emissions During Roasting

The phases formed during roasting were identified using x-ray diffraction analysis of selected samples (Points A through E on Figures 143, 145, 146 and 147). The identified phases for the copper residue after roasting are listed in Table 67 while the diffraction patterns and major phases observed are shown in Figure 144.

Table 67 Phases Identified by XRD Analysis of Copper Residue (Feed #2) Roasted with $Ca(OH)_2$

Sample	Identified Phases (in order of intensity)
A	$CaSO_4$ (Anhydrite), CuO (Tenorite), Cu_2OSO_4 (Dolerophanite), $CuSO_4$ (Chalcocyanite), CaO (Lime), $CaHAsO_4 \cdot H_2O$ (Haidingerite)
B	$CaSO_4$ (Anhydrite), CuO (Tenorite), NiO (Bunsenite), Cu_2OSO_4 (Dolerophanite), $CuSO_4$ (Chalcocyanite), $Ba_2Cu_5O_{8.54}$, $CaHAsO_4$ (Weilite)
C	$CaSO_4$ (Anhydrite), CuO (Tenorite), NiO (Bunsenite), Cu_2S (Chalcocite-M)
D	$CaSO_4$ (Anhydrite), CuO (Tenorite), NiO (Bunsenite), $CuSO_4$ (Chalcocyanite), $CaHAsO_4$ (Weilite)
E	$CaSO_4$ (Anhydrite), CuO (Tenorite), CaO (Lime), NiO (Bunsenite), $Cu_{31}S_{16}$ (Djurleite)

During roasting the sulphur in the sulphides and elemental sulphur are oxidized and react with $Ca(OH)_2$ to form anhydrite ($CaSO_4$) which is the major phase in all the roasted residue samples. (Some unreacted lime (CaO), which would form from $Ca(OH)_2$ upon heating, was also detected as a minor phase in Samples A and E.) Tenorite (CuO) and bunsenite (NiO) are the major copper and nickel phases identified, respectively. Copper sulphates or copper oxysulphates, such as chalcocyanite ($CuSO_4$) or dolerophanite (Cu_2OSO_4), are also formed as minor phases, particularly in samples roasted at lower temperatures or with lower $Ca(OH)_2$ additions (Samples A, B and D). Copper sulphides, including monoclinic chalcocite (Cu_2S) and djurleite ($Cu_{31}S_{16}$), which are intermediate phases in covellite oxidation, are also detected in samples roasted at higher temperatures and $Ca(OH)_2$ additions (Samples C and E). Arsenic is detected in the roasted residue samples as either haidingerite ($CaHAsO_4 \cdot H_2O$) or weilite ($CaHAsO_4$).

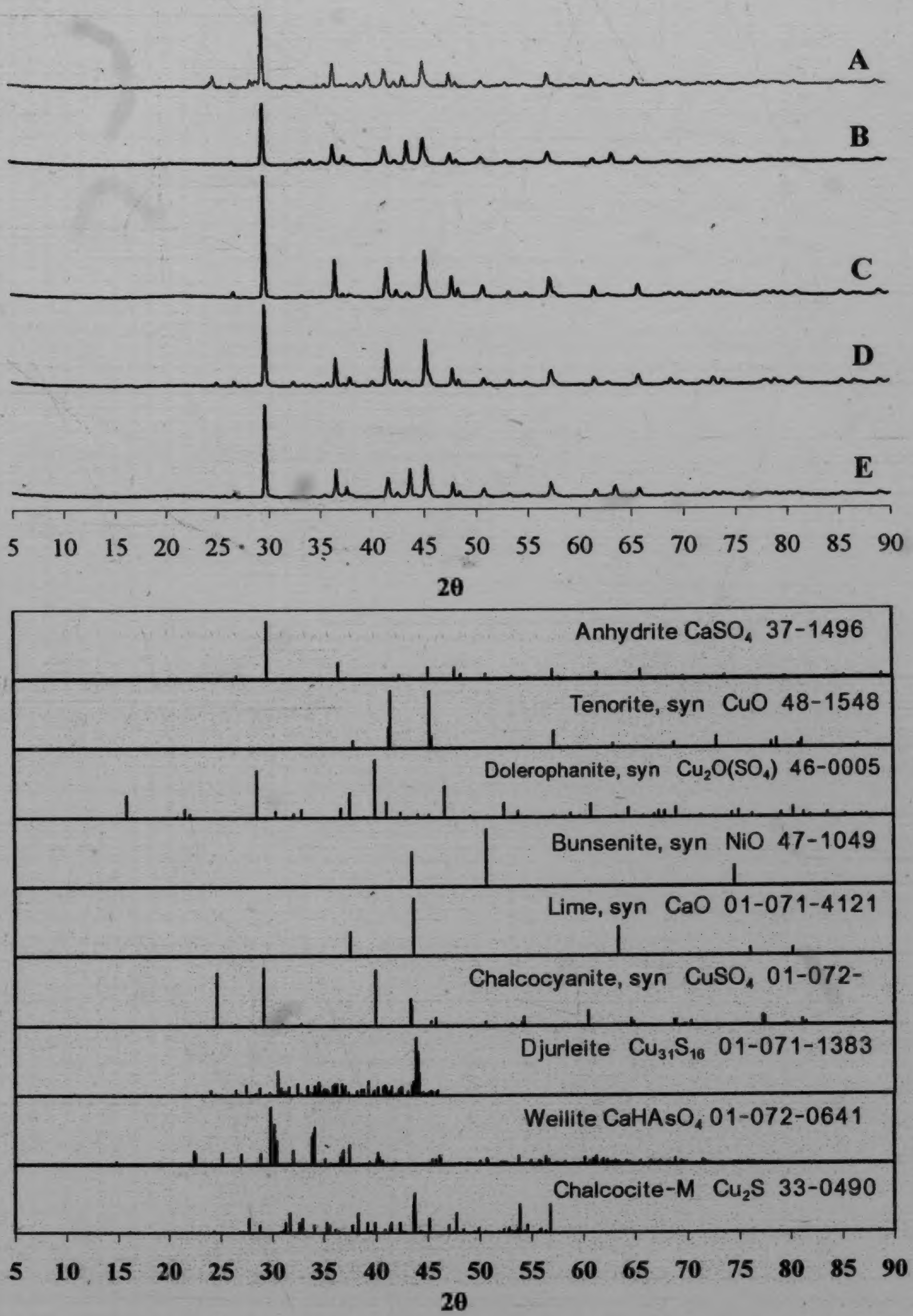

Figure 144 XRD Patterns of Inco Copper Residue after Roasting with $Ca(OH)_2$

6.4.2.2 Hot Water Leaching and Hot Acid Leaching

Between 30 and 50% of the sulphur is leached with hot water (Figure 145), with the increase in sulphur extraction observed with decreasing $Ca(OH)_2$ additions due to the formation of water soluble copper or nickel sulphates under these roasting conditions (Figure 147). Up to an additional 30% of the sulphur in the residue was dissolved during leaching with 300 g/L H_2SO_4 to give an overall extraction of 30 to 70%.

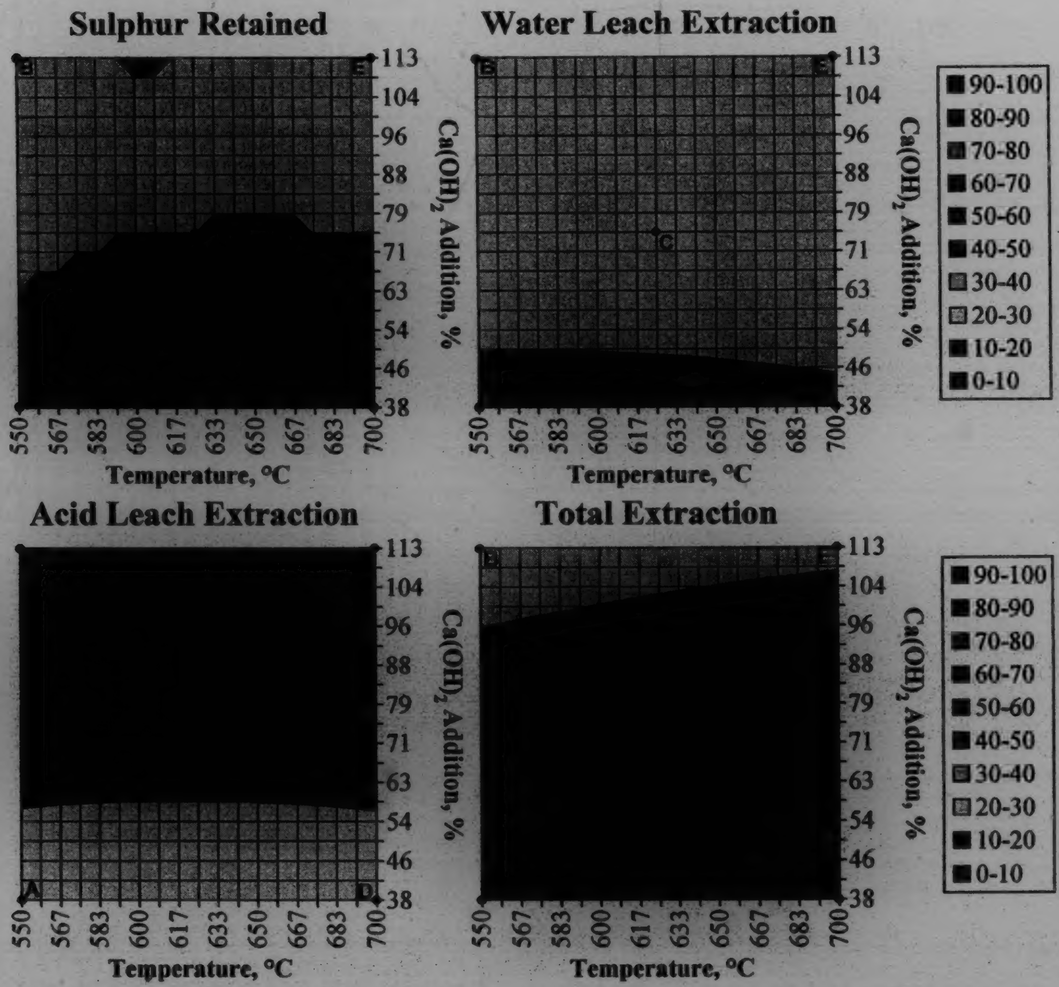

Sulphur Retained

Water Leach Extraction

Acid Leach Extraction

Total Extraction

Figure 145 Effect of $Ca(OH)_2$ Addition and Temperature on Sulphur Deportment

As noted earlier, essentially all of the arsenic is retained in the solids after roasting and, similarly, no arsenic is dissolved during leaching with hot water (Figure 141). Between

90 and 98% of the arsenic in the water leach residue is then dissolved with 200 g/L H_2SO_4 solutions with increased extractions with decreasing $Ca(OH)_2$ additions.

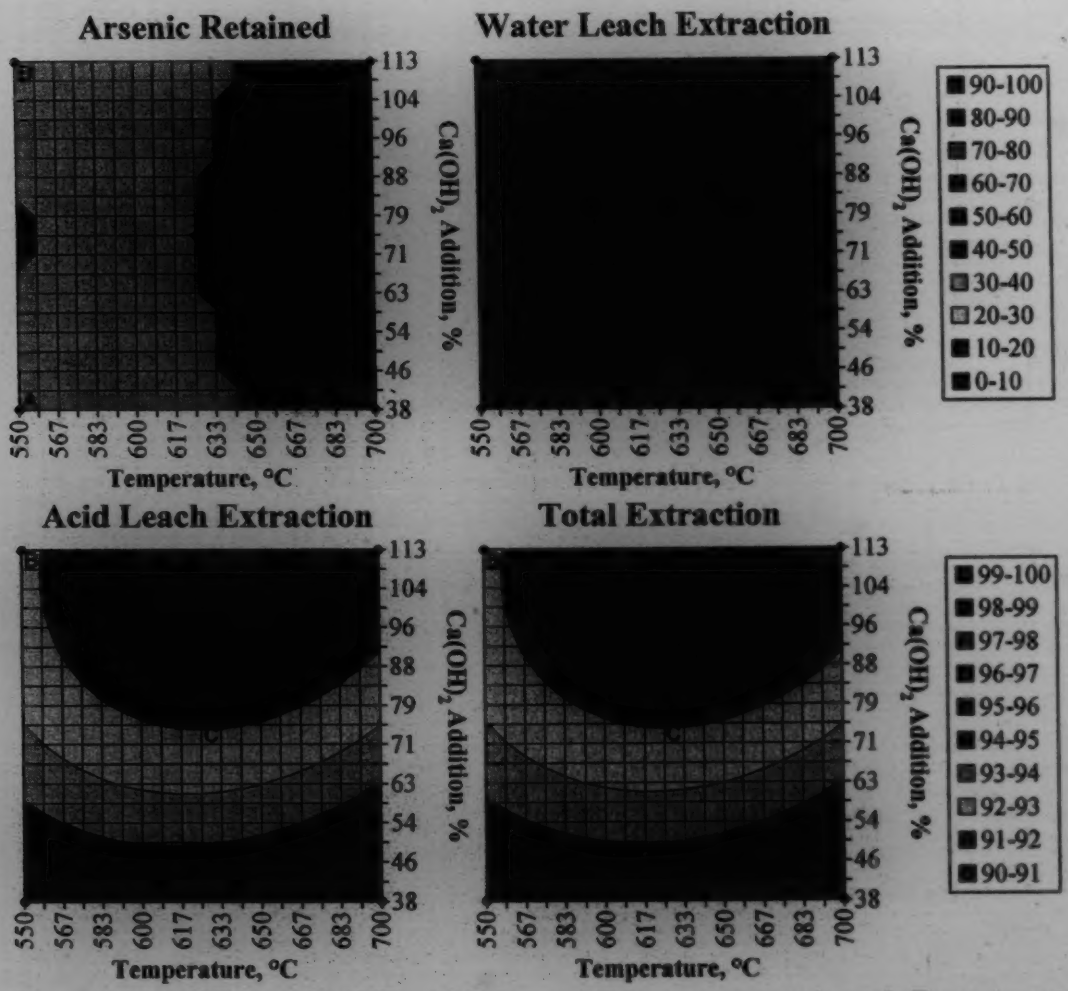

Figure 146 Effect of $Ca(OH)_2$ Addition and Temperature on Arsenic Deportment

Up to 12% of the copper and up to 36% of the nickel are dissolved during leaching with hot water with the extractions increasing with decreasing $Ca(OH)_2$ additions (Figure 142). However, over the region where sulphur emissions are zero, copper and nickel water leach extractions are negligible, indicating that sulphur reacts preferentially with calcium to form anhydrite ($CaSO_4$) and these soluble nickel or copper sulphates are formed, likely by direct sulphation of copper and nickel sulphides, only when insufficient calcium is present to react with all the sulphur present. These results follow a pattern similar to that observed during Na_2CO_3 roasting, except that, at low additions of $Ca(OH)_2$, nickel sulphation is more extensive than for roasting with low levels of Na_2CO_3 (i.e., up to 36% water soluble Ni for $Ca(OH)_2$ compared with up to 12% for roasting with Na_2CO_3).

Between 85 and 100% of the copper is leached with the sulphuric acid solution, with a maximum occurring around 75% $Ca(OH)_2$ and 670°C. These extractions, when combined with the water leach extractions, result in an overall copper extraction of up to 100%, with the overall copper extraction decreasing with increasing $Ca(OH)_2$ addition and decreasing roasting temperature.

The behaviour of nickel during acid leaching is significantly different from that of copper. Nickel extractions increase with decreasing temperature and increasing $Ca(OH)_2$ additions, but do not exceed 90% over the range of roasting conditions tested. When combined with the water leach extractions, overall nickel extractions increase with decreasing $Ca(OH)_2$ additions and temperature to give a maximum of over 90% at 550°C and 38% $Ca(OH)_2$.

The phases present in the copper residue after leaching with hot water and after leaching with 300 g/L H_2SO_4 solution are summarized in Tables 68 and 69, respectively while the diffraction patterns and major phases observed are shown in Figures 148 and 149.

Table 68 Phases Identified by XRD Analysis of Copper Residue Roasted with $Ca(OH)_2$ and Leached with Hot Water

Sample	Identified Phases (in order of intensity)	Leaching Wt. Loss, %
A	$CaSO_4$ (Anhydrite), $Cu_3SO_4(OH)_4$ (Antlerite)	17
B	$CaSO_4$ (Anhydrite), CuO (Tenorite), $Ca(OH)_2$ (Portlandite), Cu_2S (Chalcocite-M), NiO (Bunsenite), $BaPbO_3$	1
C	$CaSO_4$ (Anhydrite), CuO (Tenorite), NiO (Bunsenite), $CaHAsO_4 \cdot 3\,H_2O$	4
D	$CaSO_4$ (Anhydrite), CuO (Tenorite), NiO (Bunsenite), CuS (Covellite), $Cu_4SO_4(OH)_6$ (Brochantite)	12
E	$CaSO_4$ (Anhydrite), CuO (Tenorite), $Ca(OH)_2$ (Portlandite), NiO (Bunsenite)	1

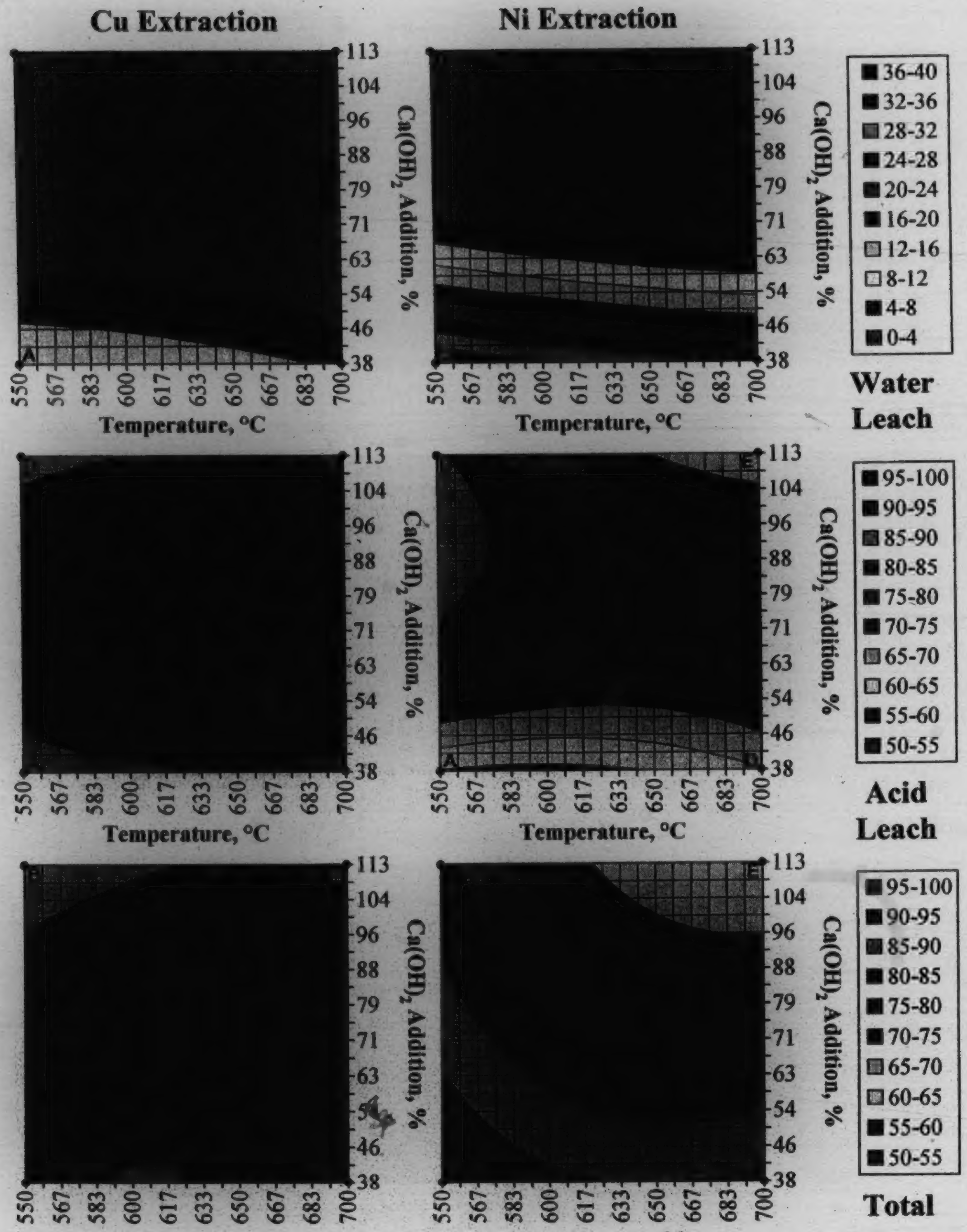

Figure 147 Effect of Ca(OH)$_2$ Addition and Temperature on Copper and Nickel Extractions

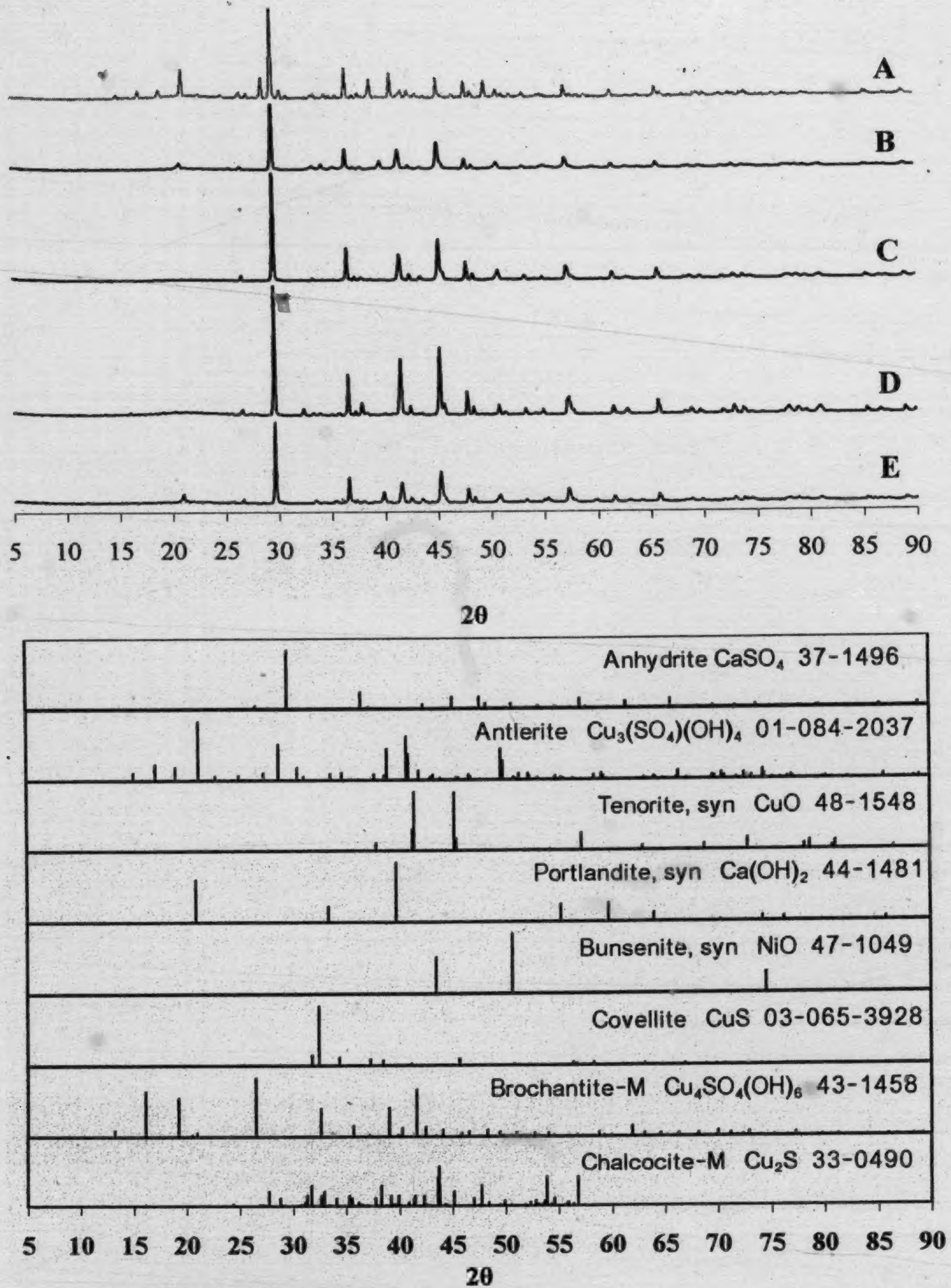

Figure 148 **XRD Patterns of Inco Copper Residue after Roasting with $Ca(OH)_2$ and Leaching with Hot Water**

Table 69 Phases Identified by XRD Analysis of Copper Residue Roasted with $Ca(OH)_2$ and Leached with 300 g/L H_2SO_4 at 95 to 97°C

Sample	Identified Phases (in order of intensity)	Leaching Wt. Loss, %
A	$CaSO_4$ (Anhydrite), NiO (Bunsenite)	57
B	$CaSO_4$ (Anhydrite)	13
C	$CaSO_4$ (Anhydrite)	34
D	$CaSO_4$ (Anhydrite), NiO (Bunsenite)	51
E	$CaSO_4$ (Anhydrite), NiO (Bunsenite)	15

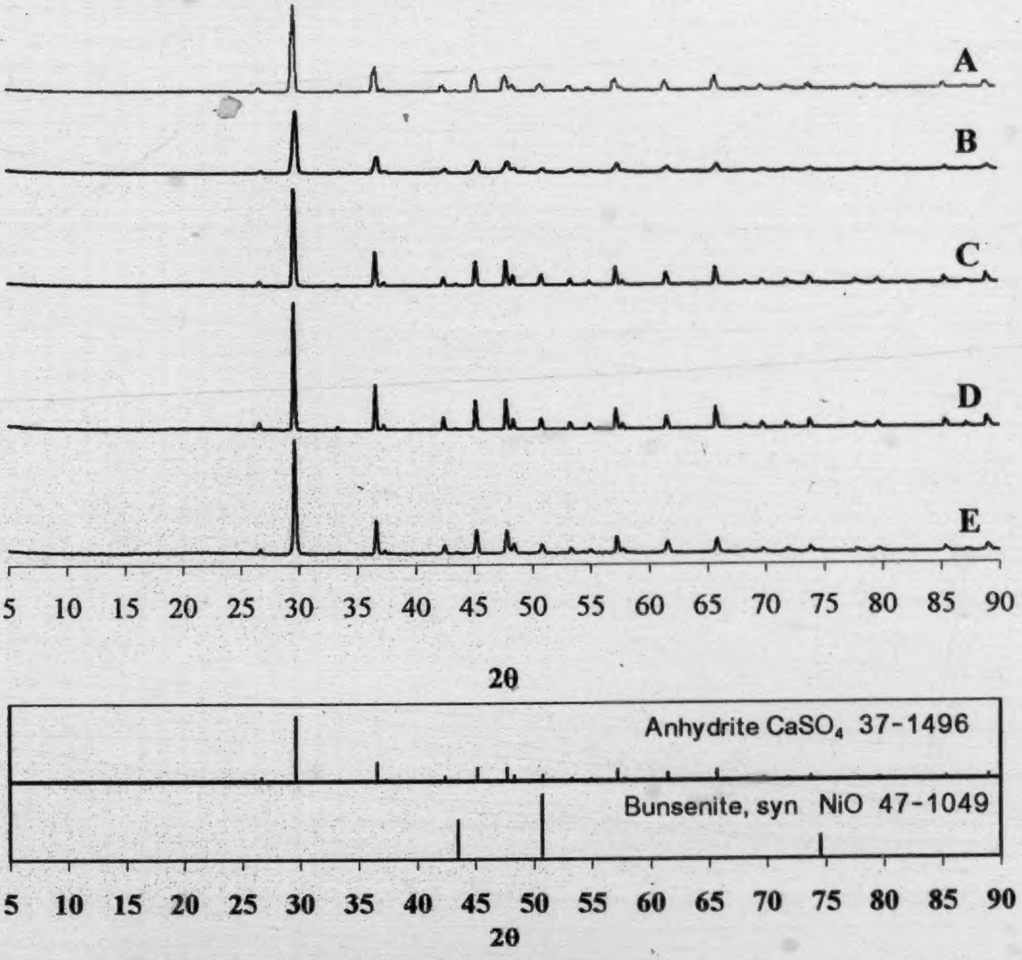

Figure 149 XRD Patterns of Inco Copper Residue after Roasting with $Ca(OH)_2$ and Leaching with 300 g/L H_2SO_4 at 95 to 97°C

After water leaching, anhydrite ($CaSO_4$) is still the major phase in all the samples analyzed and chalcocyanite ($CuSO_4$) and any nickel sulphates have been leached from the solids. Unreacted $Ca(OH)_2$, which had been calcined to CaO, and subsequently rehydrated during water leaching, is also observed in samples where excess $Ca(OH)_2$ was added during roasting (Samples B and E). Tenorite (CuO) is the major copper phase, in all but Sample A, where antlerite ($Cu_3SO_4(OH)_4$) is the only phase other than anhydrite present. Sample B contains monoclinic chalcocite (Cu_2S) and Sample D contains unreacted covellite (CuS) and brochantite ($Cu_4SO_4(OH)_6$), all in trace quantities. Bunsenite (NiO) is the only nickel phase and haidingerite ($CaHAsO_4{\cdot}H_2O$) the only arsenic compound identified in any of the samples using XRD.

However, after leaching with 300 g/L H_2SO_4, the only phases that can be identified in the leach residues are anhydrite ($CaSO_4$) and bunsenite (NiO), which points to the dissolution of the other phases observed after water leaching, such as CuO, $Ca(OH)_2$, $Cu_3SO_4(OH)_4$, NiO and $CaHAsO_4{\cdot}3H_2O$. Copper sulphides, such as covellite (CuS) and chalcocite (Cu_2S) would be expected to remain unleached, but may not be present in large enough quantities, particularly with the high concentration of anhydrite ($CaSO_4$) in the leach residue, to be detected using XRD. It should be noted that bunsenite is only detected in samples where low nickel extractions where observed during acid leaching (Samples A, D and E) . Thus, with further modification of the leaching conditions, it may be possible to dissolve the remaining NiO from these samples and further improve the nickel extractions possible from $Ca(OH)_2$ roasting of this material.

Overall, this test indicates that roasting with $Ca(OH)_2$ is very effective in controlling the emissions of sulphur and arsenic, with essentially no sulphur or arsenic released from the copper residue during roasting with a $Ca(OH)_2$ addition very close to the stoichiometric requirements for sulphur and arsenic capture. With proper selection of the roasting conditions, not only can sulphur and arsenic emissions be eliminated, but over 95% of the copper can be recovered from the roasting residue with acid leaching. Depending on the exact roasting conditions selected, nickel extractions would be expected to be between 75 and 85%, based on this analysis.

However, although $Ca(OH)_2$ was very effective in capturing arsenic during roasting, and did form arsenic compounds that were not soluble during water leaching, the compounds formed are highly soluble when leached with 200 g/L H_2SO_4; the overall arsenic extractions for roasting with $Ca(OH)_2$ were considerably higher than those observed for roasting with Na_2CO_3 (Sections 6.4.1.1.2 and 6.4.1.2.2). Thus, this indicates, that at least under the roasting conditions tested, the calcium-arsenic compounds formed are not sufficiently stable to permit recovery of nickel and copper by acid leaching to leave an acid insoluble arsenic residue for disposal. Arsenic would be expected to leach extensively during acid leaching and would then have to be precipitated as either a calcium or ferric arsenate in a subsequent effluent disposal/arsenic fixation process.

Sulphur also cannot be selectively removed from the copper and nickel in the roasted residue with water leaching. Between 30 and 40% of the sulphur in the feed is dissolved in water leaching and an additional 10 to 20% during acid leaching under these conditions, resulting in a leach residue containing only 40 to 60% of the sulphur originally in the feed. This dissolved sulphur would have to be precipitated from the H_2SO_4 leach solution for disposal in a gypsum precipitation unit operation possibly before solvent extraction or electrowinning of nickel or copper to prevent the precipitation of gypsum from solution in these metals recovery processes.

Roasting the second sample of Inco copper residue with $Ca(OH)_2$ did not result in the same problems with sintering that were observed in Section 6.4.1.2. Thus, the sintering problems observed at these temperatures may be specific to roasting with Na_2CO_3. It is possible that the formation of a low melting point, or eutectic, phase with Na_2CO_3 and either elemental sulphur or one of the sulphide phases occurs which inhibits the transport of oxygen to the reaction surface or otherwise slows the rate of oxidation of the sulphides in the residue.

Thus, these results indicate that roasting of this material with hydrated lime could be an effective treatment method. Its major advantage over Na_2CO_3 roasting, at this stage of the research, is its effective control of arsenic emissions with only low reagent additions during roasting. However, higher roasting temperatures are necessary [illegible] achieve high copper extractions, but those temperatures are less than optimum for maximum nickel recovery. Roasting with either Na_2CO_3 and $Ca(OH)_2$ would require precipitation of sulphur and arsenic from the leach solutions for disposal; however, the major potential advantage for roasting with Na_2CO_3 is that, with some optimization and improvement, it may be possible to selectively leach sulphur and arsenic from the copper residue, such that this solution can be dealt with separately for arsenic and sulphur disposal without any concern about interference with the recovery of nickel and copper. However, if further research into Na_2CO_3 roasting cannot overcome the potential concerns about arsenic capture and selective water leaching of arsenic, then the use of $Ca(OH)_2$ as a secondary arsenic-capturing agent may be worth further consideration and study.

6.4.3 Roasting with Secondary Additives to Fix Arsenic

One additional DOE test was performed to determine whether $FeSO_4 \cdot 7H_2O$ could be added as a secondary additive during Na_2CO_3 roasting to try to produce stable, acid insoluble ferric arsenates during roasting, which, after copper and nickel extraction, could then be disposed of safely. Similar Na_2CO_3 additions to those used in Section 6.4.1 at 50 to 150% were made, but roasting temperatures were lowered to between 450 and 600°C to try to further improve nickel and copper extractions based on the trends observed in the DOE tests in Section 6.4.1.

6.4.3.1 Roasting

The addition of $FeSO_4 \cdot 7H_2O$ means that additional sulphur is added to the roasting system and, thus, the stoichiometric requirement for Na_2CO_3 to control sulphur emissions is shifted from 98% with no $FeSO_4 \cdot 7H_2O$ added, to 107% with 22.6% $FeSO_4 \cdot 7H_2O$ and 116% with 45.2% $FeSO_4 \cdot 7H_2O$. For $FeSO_4 \cdot 7H_2O$ additions of 22.6%, sulphur emissions can be eliminated by roasting at Na_2CO_3 additions of 135% or higher (125% of stoichiometric for sulphur capture), but at higher $FeSO_4 \cdot 7H_2O$ additions, while sulphur emissions approach zero as Na_2CO_3 additions approach 150%, minor losses of sulphur (i.e., 2 to 3%) to atmosphere still occur in this region (Figure 150).

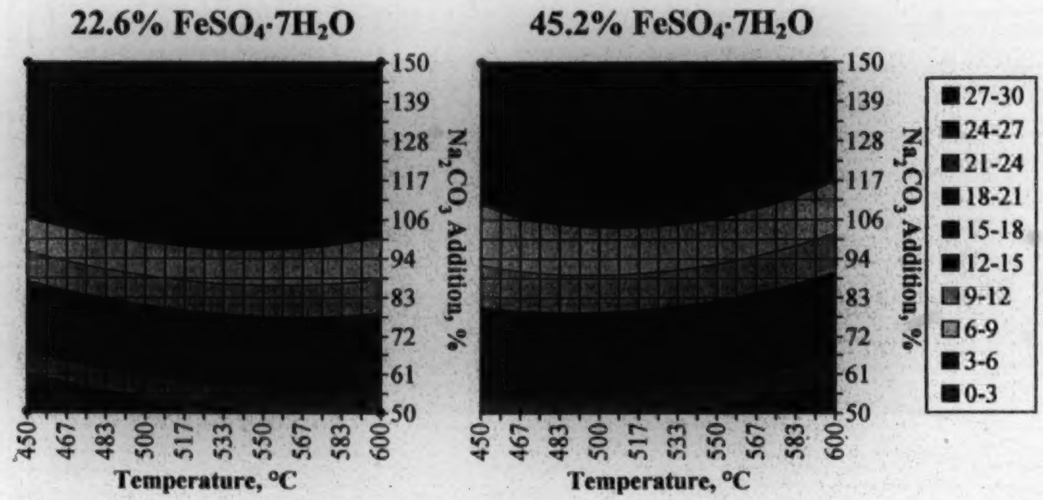

Figure 150 Effect of Na_2CO_3 Addition and Temperature on Sulphur Emissions During Roasting with 22.6 and 45.2% $FeSO_4 \cdot 7H_2O$

The addition of $FeSO_4{\cdot}7H_2O$ also has a dramatic effect on the effects of Na_2CO_3 addition and temperature on arsenic emissions (Figure 151). From extrapolation of the response surface model for roasting with Na_2CO_3 alone (Figure 134), the elimination of arsenic emissions, without the addition of $FeSO_4{\cdot}7H_2O$, would occur only at high Na_2CO_3 additions (i.e., above 170%) or at very low roasting temperatures (i.e., less than 300°C). However, with the addition of 22.6% $FeSO_4{\cdot}7H_2O$, arsenic emissions are reduced to zero at higher temperatures and lower Na_2CO_3 additions as the response surface model shown in Figure 151 shows an elliptical minimum centered around 475°C and 70% Na_2CO_3, with arsenic emissions increasing as the temperature and Na_2CO_3 additions move away from this point. At high $FeSO_4{\cdot}7H_2O$ additions (45.2%), arsenic emissions are reduced to as low as 1%, but are not completely eliminated, and the region of minimum arsenic emission shrinks in size and shifts to higher temperatures and Na_2CO_3 additions (530°C and 125% Na_2CO_3)

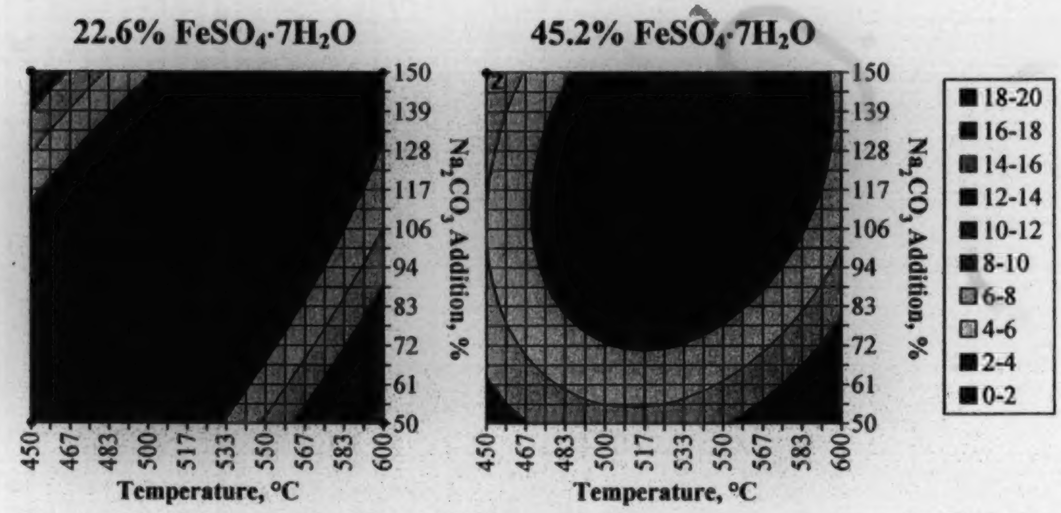

Figure 151 Effect of Na_2CO_3 Addition and Temperature on Arsenic Emissions During Roasting with 22.6 and 45.2% $FeSO_4{\cdot}7H_2O$

The phases formed during roasting with 22.6% $FeSO_4{\cdot}7H_2O$ were identified using x-ray diffraction analysis of selected samples (Points A through D on Figures 150, 151, 153, 154, 155 and 156). The identified phases for the copper residue after roasting are listed in Table 70 while the diffraction patterns and major phases observed are shown in Figure 152.

Table 70 Phases Identified by XRD Analysis of Copper Residue (Feed #2) Roasted with Na_2CO_3 and 22.6% $FeSO_4 \cdot 7H_2O$

Sample	Identified Phases (in order of intensity)
A	CuO (Tenorite), Na_2SO_4, $Fe_4(OH)_3(AsO_4)_3 \cdot 6H_2O$ (Pharmacosiderite), $CuSO_4$ (Chalcocyanite), $BaCO_3$ (Witherite), $Na_2As_4O_{11}$, $Cu_3(AsO_4)_2 \cdot 4H_2O$ (Rollandite), Na_5FeO_4, $Na_2Cu(SO_4)_2 \cdot 2H_2O$ (Kroenhkite)
B	Na_2SO_4, CuO (Tenorite), $CuSO_4$ (Chalcocyanite), NiO (Bunsenite), Fe_2O_3 (Hematite), Cu_2OSO_4 (Dolerophanite), $BaSO_4$ (Barite)
C	CuO (Tenorite), Na_2SO_4, $CuNa_2(CO_3)_2 \cdot 3H_2O$ (Chalconatronite), Na_5FeO_4, $Na_2As_4O_{11}$, $Na_3H(SO_4)_2$, NiO (Bunsenite), $Fe_2(SO_4)_2(OH)_2 \cdot 7H_2O$ (Hohmannite), $Cu_3(AsO_4)_2 \cdot 4H_2O$ (Rollandite)
D	CuO (Tenorite), Na_2SO_4, $Na_6CO_3(SO_4)_2$ (Burkeite), Fe_2O_3 (Hematite), NiO (Bunsenite)

Sodium reacts with the sulphur in the copper residue, forming Na_2SO_4 as the major sulphur and sodium phase, but also forming burkeite ($Na_6CO_3(SO_4)_2$) and $Na_3H(SO_4)_2$ in certain roasted samples. Sodium also reacts with iron and arsenic to form Na_5FeO_4 and $Na_2As_4O_{11}$, respectively, in Samples A and C where Na_2CO_3 additions during roasting were lower. Sodium also reacts with copper in these samples to form either kroenhkite ($Na_2Cu(SO_4)_2 \cdot 2H_2O$) or chalconatronite ($CuNa_2(CO_3)_2 \cdot 3H_2O$); both of these phases would be expected to be water soluble in hot water leaching.

The primary phase in all but one sample, and the major copper phase in all the samples, is again tenorite (CuO). In addition to the sodium-copper compounds listed earlier, copper also forms $CuSO_4$ (Chalcocyanite), Cu_2OSO_4 (Dolerophanite), or $Cu_3(AsO_4)_2 \cdot 4H_2O$ (Rollandite) in the samples roasted at lower temperatures and/or Na_2CO_3 additions (Samples A, B and C). Bunsenite (NiO) was the only nickel phase identified by x-ray diffraction once again.

Arsenic is found as $Fe_4(OH)_3(AsO_4)_3 \cdot 6H_2O$ (Pharmacosiderite), $Na_2As_4O_{11}$, or $Cu_3(AsO_4)_2 \cdot 4H_2O$ (Rollandite) in samples roasted at low temperatures and Na_2CO_3 additions (Samples A and C); no arsenic-bearing phases are detected in Samples B and D, which were roasted with higher Na_2CO_3 additions. Iron is also found as hematite (Fe_2O_3) in the samples roasted with higher Na_2CO_3 additions (Samples B and D) and as Na_5FeO_4 and/or hohmannite ($Fe_2(SO_4)_2(OH)_2 \cdot 7H_2O$) in samples roasted with lower additions (Samples A and C).

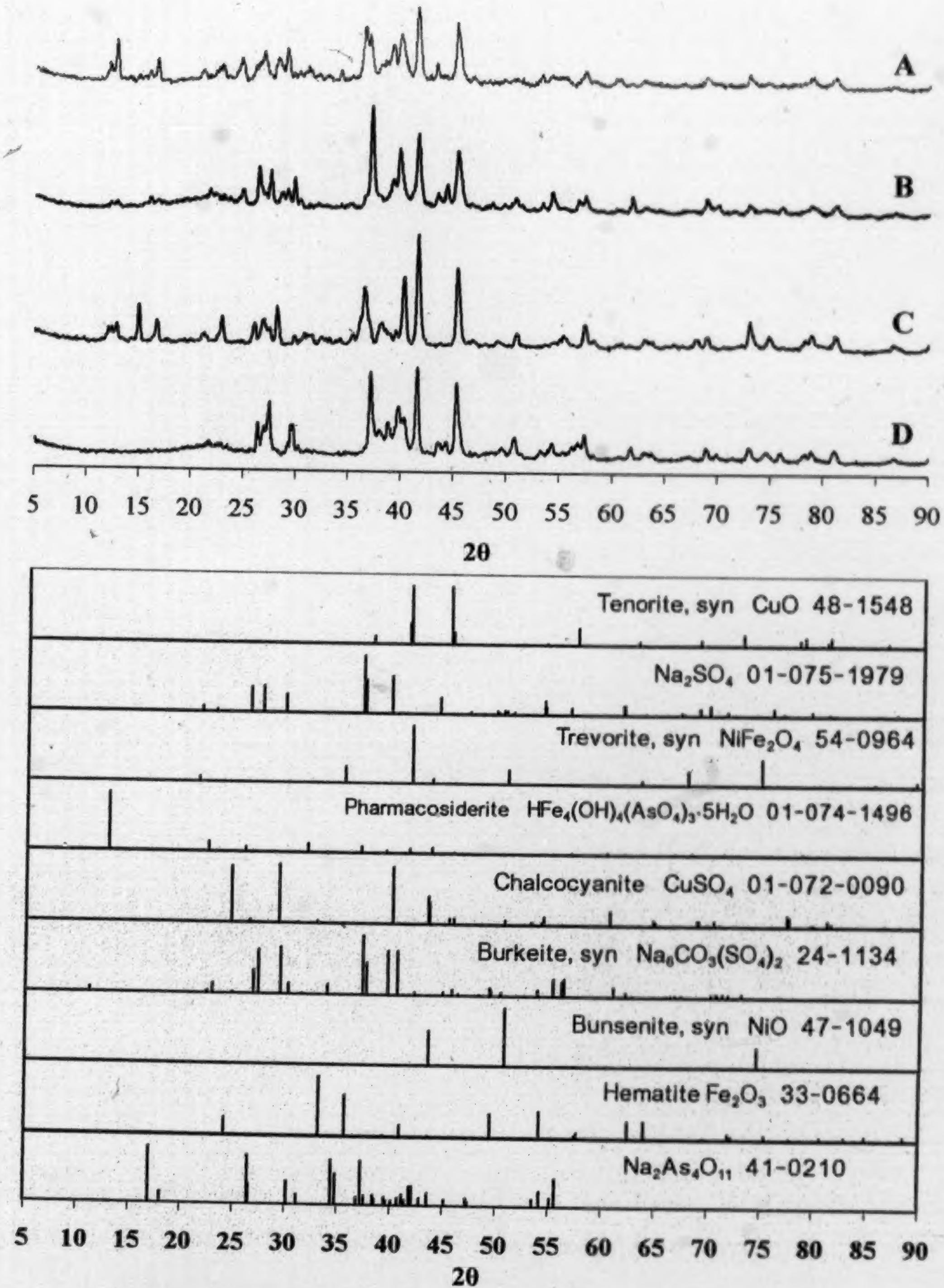

Figure 152 **XRD Patterns of Inco Copper Residue after Roasting with Na_2CO_3 and 22.6% $FeSO_4 \cdot 7H_2O$**

6.4.3.2 Hot Water and Acid Leaching of Inco Copper Residue (Feed #2) Roasted with Na_2CO_3 and $FeSO_4 \cdot 7H_2O$

The leaching behaviour of sulphur with both lixiviants is similar at both of the $FeSO_4 \cdot 7H_2O$ additions shown in Figure 153. Most of the sulphur in the roasted ash can be leached in hot water as, in the region where over 94% of the sulphur is retained in the solids during roasting, hot water leach extractions of between 84 and 96% S are observed. After leaching with 200 g/L H_2SO_4 solution, up to an additional 10% of the sulphur can be dissolved to give an overall sulphur extraction in this region of between 84 and 100%. The model shows that for both $FeSO_4 \cdot 7H_2O$ additions shown in Figure 153, the maximum conversion to soluble sulphur occurs at high Na_2CO_3 additions as the roasting temperature approaches 450°C.

The solubility of arsenic during water leaching is dramatically reduced with the addition of $FeSO_4 \cdot 7H_2O$ during roasting (Figure 154). From the extrapolation of the response surface model shown in Figure 137, arsenic extractions by water leaching would be expected to be between 0 and 60% when roasting with Na_2CO_3 alone under these conditions. However, after roasting with $FeSO_4 \cdot 7H_2O$, maximum arsenic extractions by water leaching are only 24% and 15% for roasting with 22.6% and 45.2% $FeSO_4 \cdot 7H_2O$, respectively. Though the arsenic extractions by water leaching still increase with increasing temperature and Na_2CO_3 additions, as they did in Figure 137 without the addition of $FeSO_4 \cdot 7H_2O$, arsenic extractions are less than 3% for most of the roasting conditions tested.

Arsenic extractions after leaching with 200 g/L H_2SO_4, though, cover a much wider range of extractions with a minimum extraction of 64% for roasting with 22.6% $FeSO_4 \cdot 7H_2O$ and 76% for roasting with 45.2% $FeSO_4 \cdot 7H_2O$, compared with a minimum of less than 10% for roasting without $FeSO_4 \cdot 7H_2O$. The arsenic extractions during acid leaching increase with decreasing temperature and Na_2CO_3, following a similar trend to that observed when roasting with Na_2CO_3 alone (Figure 137). As a result, overall arsenic extractions of between 74 and 100% are possible from this material, depending on the exact roasting temperature and Na_2CO_3 and $FeSO_4 \cdot 7H_2O$ additions used.

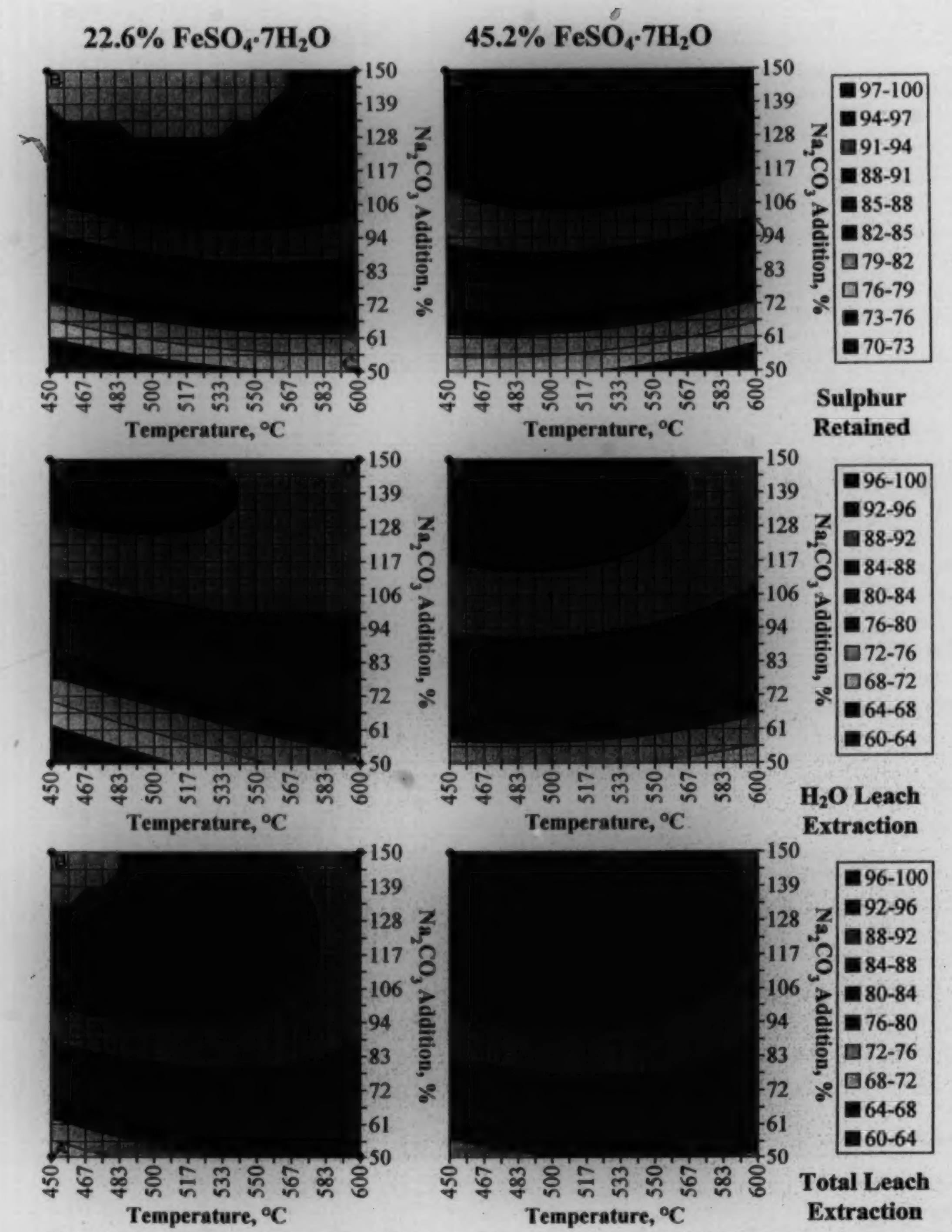

Figure 153 Effect of Na_2CO_3 Addition, Temperature and $FeSO_4 \cdot 7H_2O$ Additions on Sulphur Deportment

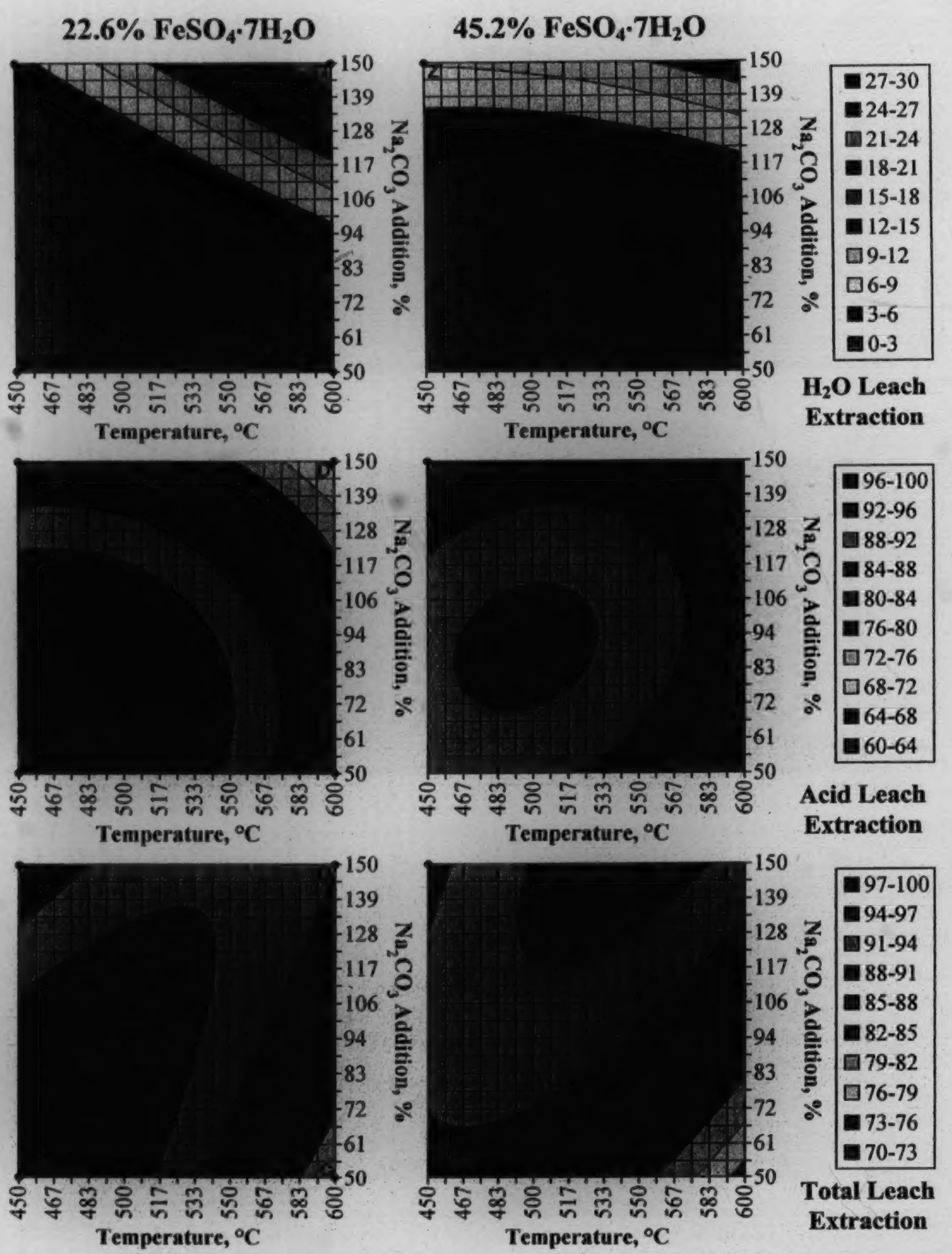

Figure 154 Effect of Na_2CO_3 Addition, Temperature and $FeSO_4 \cdot 7H_2O$ Additions on Arsenic Deportment

Copper water leach extractions (Figure 155) also follow similar trends to those observed in Figure 138 for roasting without $FeSO_4 \cdot 7H_2O$. Water leach extractions are negligible over the regions of the reaction space where sulphur emissions are a minimum, with an increase with lower Na_2CO_3 additions. Water leach extractions of copper are much higher than in Figure 138 (i.e., up to 32% instead of a maximum of 12%). Though it is possible that copper sulphation is increased with lower roasting temperatures, it is more likely that the increase in water soluble copper is due to sulphation of copper by reacting with the sulphate ions available from the $FeSO_4 \cdot 7H_2O$ added during roasting, as well as by direct oxidation of some copper sulphides to $CuSO_4$. As noted in previous sections, this appears to happen more readily under conditions where less than stoichiometric amounts of Na_2CO_3 are added to the residue during roasting, indicating that, when available, the sulphur in the copper sulphides in this residue will react preferentially with sodium, instead of forming $CuSO_4$ directly.

Copper, which is not leached in hot water, is leached with 200 g/L H_2SO_4, such that overall copper extractions of 96 to 100% and 94 to 100% are observed after roasting with 22.6% and 45.2% $FeSO_4 \cdot 7H_2O$, respectively (Figure 155). The overall copper extractions increase with increasing temperatures, but are very high over the entire region of Na_2CO_3 addition and temperature tested in this DOE test. These high extractions, and the high corresponding sulphur extractions, indicate that the majority of the copper sulphide in the residue (i.e., 94 to 100%) is oxidized and converted to a water and/or acid soluble form during roasting. These extractions are significantly improved from those obtained in Section 6.4.1.2 and this increase in copper extractions is likely due, in large part, to the decrease in roasting temperature and, hence, the reduction of sintering during roasting rather than to the addition of $FeSO_4 \cdot 7H_2O$. From these results, copper extractions appear to be largely independent of the amount of $FeSO_4 \cdot 7H_2O$ added during roasting.

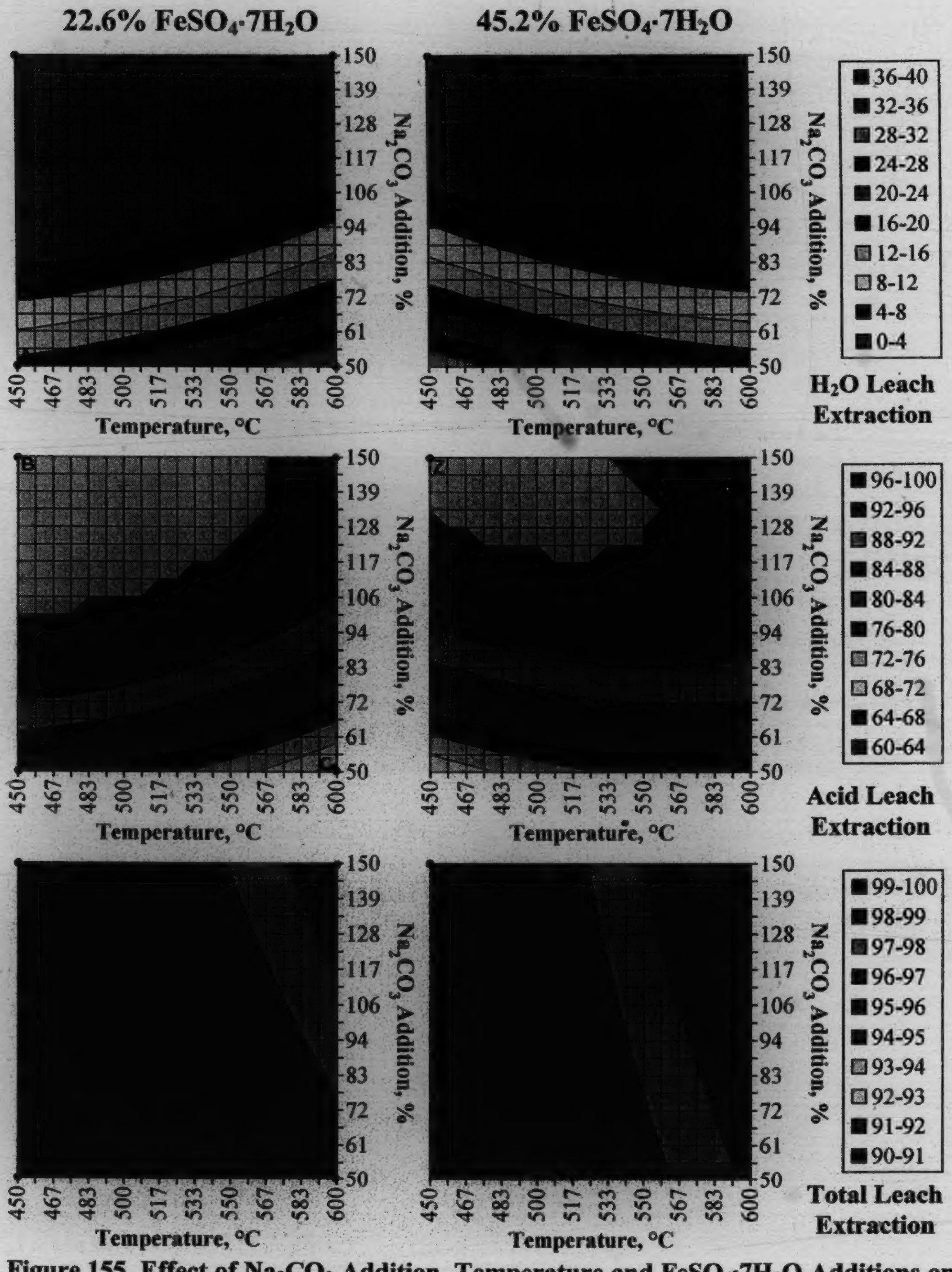

Figure 155 Effect of Na_2CO_3 Addition, Temperature and $FeSO_4 \cdot 7H_2O$ Additions on Copper Extractions

Nickel extractions by water leaching, however, are affected much more dramatically by the addition of $FeSO_4 \cdot 7H_2O$ (Figure 156). Nickel water leach extractions of less than 12% are reported in Figure 139 for Na_2CO_3 alone while nickel extractions of up to 35% and 50% are possible by water leaching for roasting additions of 22.6 and 45.2% $FeSO_4 \cdot 7H_2O$, respectively. As with copper sulphation, nickel sulphation is more prevalent at lower Na_2CO_3 additions, but with high additions of $FeSO_4 \cdot 7H_2O$, nickel sulphation is enhanced, particularly at higher roasting temperatures, even where Na_2CO_3 additions are in excess of the stoichiometric requirements to react with, and capture, sulphur. Thus, though direct sulphation of nickel sulphides by oxidation still likely contributes to the overall nickel water leach extraction, the strong dependence of this extraction on the $FeSO_4 \cdot 7H_2O$ addition indicates that most of the observed increase in nickel water leach extractions occurs because nickel reacts with the sulphate in the ferrous sulphate to form water soluble nickel sulphates during roasting.

Leaching the water leach residue with 200 g/L H_2SO_4 extracted an additional 50 to 96% of the nickel in the copper residue (Figure 156) with the acid leach extraction increasing significantly with decreasing temperature and increasing Na_2CO_3 additions. Thus, this results in overall nickel extractions of 76 to 96% for roasting with 22.6% $FeSO_4 \cdot 7H_2O$ and 64 to 100% for roasting with 45.2% $FeSO_4 \cdot 7H_2O$ (Figure 156). As with the overall copper extraction, the overall nickel extraction is dependent primarily on roasting temperature, with nickel extractions of over 90% possible below 550°C and below 515°C for $FeSO_4 \cdot 7H_2O$ additions of 22.6 and 45.2%, respectively.

The phases present in the copper residue after leaching with hot water and after leaching with 300 g/L H_2SO_4 solution are summarized in Tables 71 and 72, respectively while the diffraction patterns and major phases observed are shown in Figures 157 and 158.

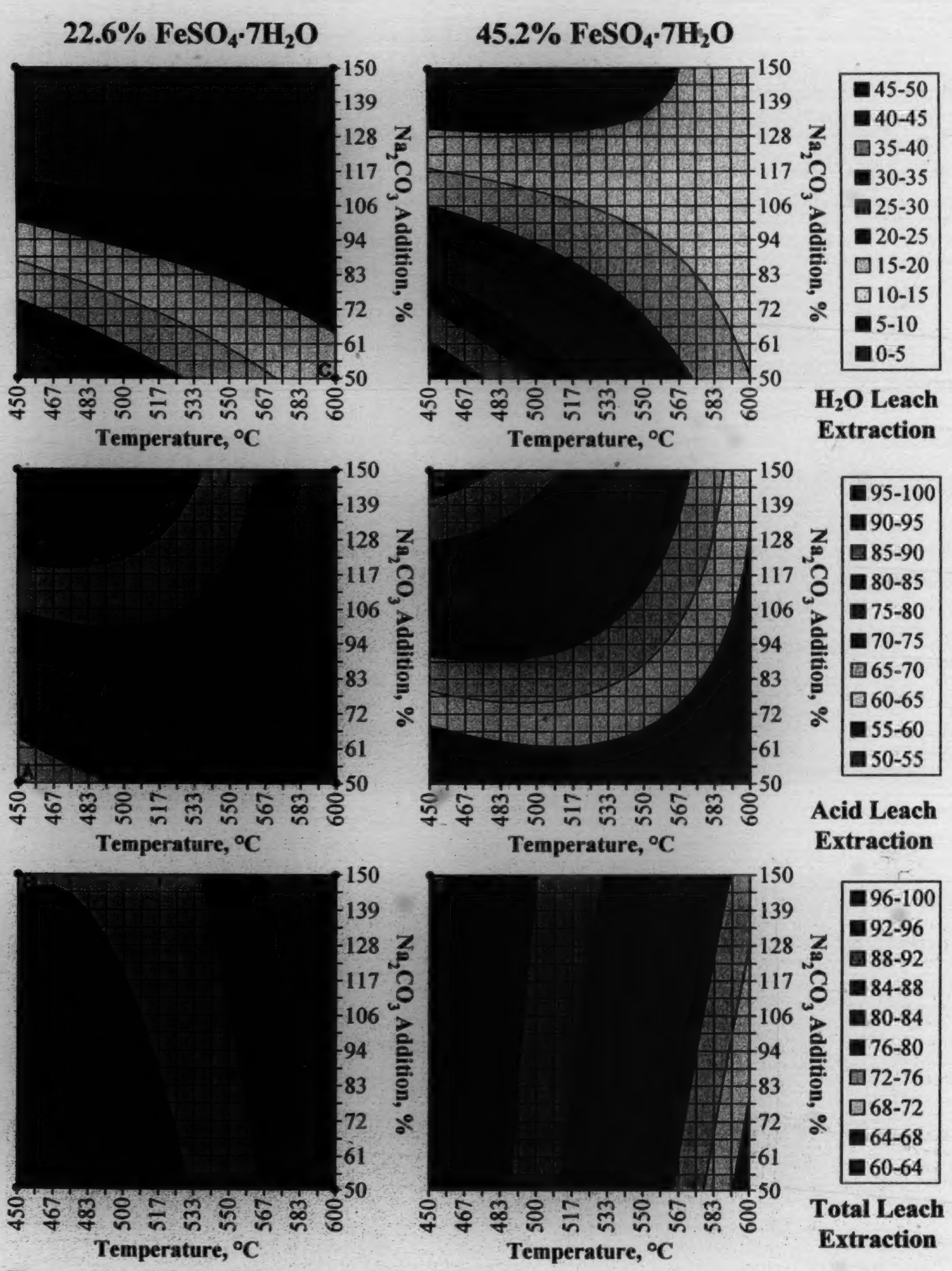

Figure 156 Effect of Na_2CO_3 Addition, Temperature and $FeSO_4{\cdot}7H_2O$ Additions on Nickel Extractions

Table 71 Phases Identified by XRD Analysis of Copper Residue Roasted with Na_2CO_3 and 22.6% $FeSO_4 \cdot 7H_2O$ and Leached with Hot Water

Sample	Identified Phases (in order of intensity)	Leaching Wt. Loss, %
A	$Cu_3SO_4(OH)_4$ (Antlerite), $Cu_4SO_4(OH)_6$ (Brochantite), Cu_2S (Chalcocite-Q), Fe_7S_8 (Pyrrhotite-4M)	59
B	$Cu_3SO_4(OH)_4$ (Antlerite), $NiFe_2O_4$ (Trevorite), $Cu_4SO_4(OH)_6$ (Brochantite), Fe_2O_3 (Hematite)	75
C	CuO (Tenorite), $Cu_3SO_4(OH)_4$ (Antlerite), $Fe_{21}(OH)_{32}$ (Maghemite), Fe_2O_3 (Hematite), $CuFe_2S_3$ (Cubanite), FeOOH (Goethite)	66
D	CuO (Tenorite), NiO (Bunsenite), Cu_2S (Chalcocite-M), Fe_2O_3 (Hematite), $Cu_{1.96}S$ (Chalcocite-Q), Cu_5FeS_4 (Bornite)	74

Table 72 Phases Identified by XRD Analysis of Copper Residue Roasted with Na_2CO_3 and 22.6% $FeSO_4 \cdot 7H_2O$ and Leached with 200 g/L H_2SO_4 at 95 to 97°C

Sample	Identified Phases (in order of intensity)	Leaching Wt. Loss, %
A	--*	95
B	--*	92
C	$NiFe_2O_4$ (Trevorite), Fe_2O_3 (Hematite), $(Ba,Pb)SO_4$ (Barite, plumbian)	82
D	Cu_9S_5 (Digenite), NiO (Bunsenite), Cu_5FeS_4 (Bornite), $Cu_{31}S_{16}$ (Djurleite)	61

***Insufficient sample to conduct x-ray diffraction analysis**

A wider range of copper minerals is found in the residue after hot water leaching than was observed in the previous DOE tests. Tenorite (CuO) is only found in samples roasted at 600°C (Samples C and D), with antlerite ($Cu_3SO_4(OH)_4$) as the second most prominent phase in Sample C which was roasted with lower Na_2CO_3 additions. In Samples A and B which are roasted at 450°C, antlerite is the major copper phase and copper is also present as brochantite ($Cu_4SO_4(OH)_6$). Tetragonal chalcocite (Cu_2S) is found in Sample A and is found along with monoclinic chalcocite in Sample D. Bunsenite (NiO) is only detected by XRD in Sample D.

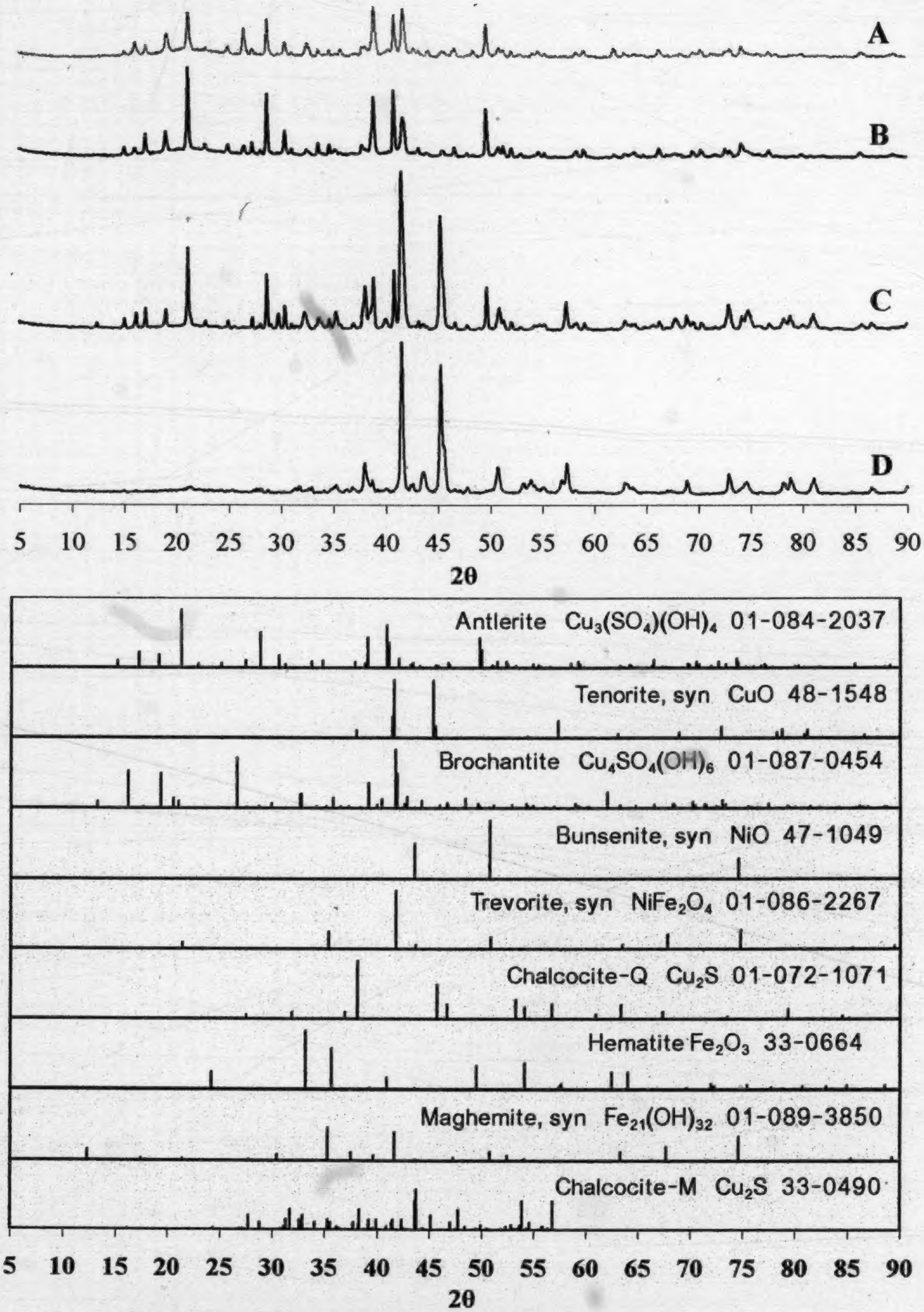

Figure 157 XRD Patterns of Inco Copper Residue after Roasting with Na_2CO_3 and 22.6% $FeSO_4 \cdot 7H_2O$ and Leaching with Hot Water

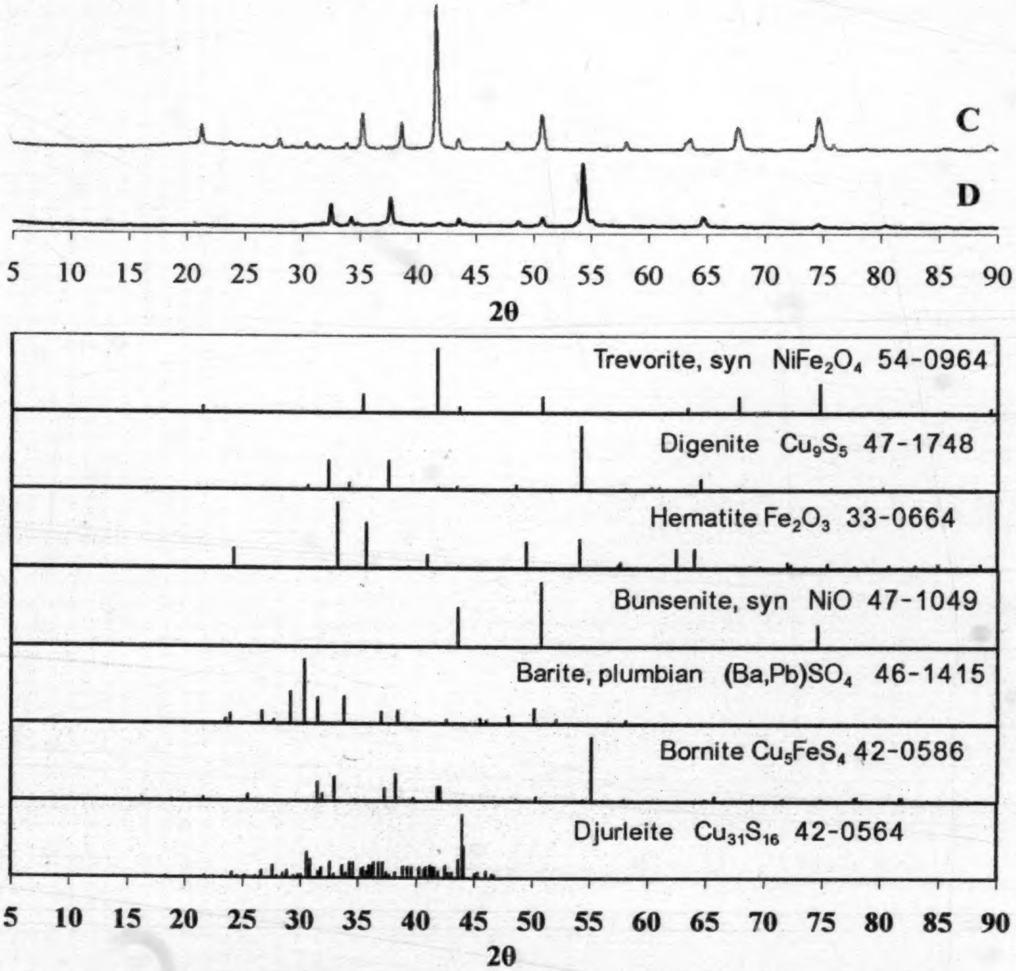

Figure 158 XRD Patterns of Inco Copper Residue after Roasting with Na_2CO_3 and 22.6% $FeSO_4 \cdot 7H_2O$ and Leaching with 200 g/L H_2SO_4 at 95 to 97°C

The addition of iron, however, results in the formation of a variety of phases that have not been observed in previous XRD studies of this material after roasting. While these phases are minor relative to the quantity of tenorite or antlerite in the roasted residue, iron is detected as pyrrhotite (Fe_7S_8) in Sample A, as trevorite ($NiFe_2O_4$) and hematite (Fe_2O_3) in Sample B, as maghemite ($Fe_{21}(OH)_{32}$), hematite (Fe_2O_3), cubanite ($CuFe_2S_3$) and goethite (FeOOH) in Sample C and hematite (Fe_2O_3) and bornite (Cu_5FeS_4) in Sample D. The formation of copper-iron sulphides or nickel ferrites during roasting is of particular concern as it has the potential to detrimentally affect nickel and copper extractions during acid leaching through the formation of potentially acid insoluble copper or nickel compounds during roasting.

Because of the high extractions, and weight loss, during acid leaching, x-ray diffraction analysis could not be performed on the acid leach residues for Samples A and B. At 600°C and 50% Na_2CO_3 (Sample C), trevorite ($NiFe_2O_4$) is the major unleached phase, with hematite (Fe_2O_3) and insoluble barium-lead sulphates also detected. In Sample D which was also roasted at 600°C, but with 150% Na_2CO_3, digenite (Cu_9S_5) was the major phase present, with lesser amounts of NiO and minor amounts of bornite (Cu_5FeS_4) and djurleite ($Cu_{31}S_{16}$). Since copper and nickel extractions for these samples are quite high (i.e., over 97% and 76%, respectively) and iron extractions are only 60 to 70%, the quantity of iron minerals detected does not seem to be consistent with that expected from the chemical analyses. Thus, it is possible that a portion of the iron in these leach residues is poorly crystalline and, thus, is not identified using x-ray diffraction analysis.

SEM/EDX analysis was conducted on Sample Z (450°C, 150% Na_2CO_3, 45.2% $FeSO_4 \cdot 7H_2O$) (Figure 159). After water leaching, the overall EDX analysis shows high concentrations of Cu, Fe, Ni, As and O. The brighter particles (Particles B and C) both contain barium, either as a mixture of $BaSO_4$, CuO and NiO (i.e., high in Ba, S and O, with minor Cu and Ni (C)) or as $BaSO_4$ alone (B). Iron-bearing particles were identified to be oxides using EDX, indicating that iron is likely present as hematite (Fe_2O_3), or possibly $Fe_{21}(OH)_{32}$ (Maghemite) or goethite (FeOOH), but is found in particles that also either contain minor amounts of Cu and Ni (i.e., likely as a mixture of CuO, NiO and Fe_2O_3 (C)) or significant Cu and minor amounts of As (i.e., likely as either a copper or iron arsenate (D)). Particles containing only Cu and O (i.e., CuO (E)) are identified as well along with particles containing predominantly NiO (F) but with minor amounts of CuO also present.

After leaching of Sample Z in 200 g/L H_2SO_4, the overall EDX analysis indicates that this material contains Fe and O and minor amounts of Ni and S (Figure 160). Bright particles are found to be high in Ba, S and O (i.e., $BaSO_4$ (A)). Other particles either contain Fe and O (i.e., Fe_2O_3 (B)), Ni and S (i.e., likely a partially oxidized nickel sulphide such as heazlewoodite (Ni_3S_2) (C)) and Ni, Fe and O (i.e., likely $NiFe_2O_4$ (Trevorite) (D)).

The results from this DOE test indicate that, by lowering the roasting temperature very high copper extractions of between 94 and 100% and high nickel extractions are possible from this material. By examining the response surface models for Cu, Ni and S, it should be possible, with proper selection of roasting conditions (e.g., 450°C and 140% Na_2CO_3) to eliminate sulphur emissions while being able to selectively remove up to 96% of the sulphur from the solids during hot water leaching and to achieve copper extractions of over 99% and nickel extractions of up to 96% with less than 1% copper or nickel dissolved during water leaching. All these results are extremely promising and have considerable potential for future study and process development.

Arsenic deportment, however, continues to be a concern. Based on these results, $FeSO_4 \cdot 7H_2O$ is less effective in capturing arsenic then either $Ca(OH)_2$ or high levels of Na_2CO_3 and the arsenic compounds produced are not significantly less soluble in 200 g/L H_2SO_4 than those formed by reaction with Na_2CO_3 or $Ca(OH)_2$. This means that arsenic dissolved during acid leaching would still need to be precipitated in a subsequent arsenic fixation step, which would also be required for roasting with Na_2CO_3 and $Ca(OH)_2$, based on the analyses made at the ends of Sections 6.4.1.2.2 and 6.4.2.2. Thus, without being able to form stable acid insoluble iron arsenates during roasting, there appears to be no advantage to using $FeSO_4 \cdot 7H_2O$ as a secondary reagent during roasting. Future research should focus on improving arsenic capture and the conversion of arsenic to a water soluble form during roasting with Na_2CO_3; arsenic precipitation from the resultant water leach solution could then be dealt with using conventional arsenic precipitation technologies to form stable, disposal arsenic residues.

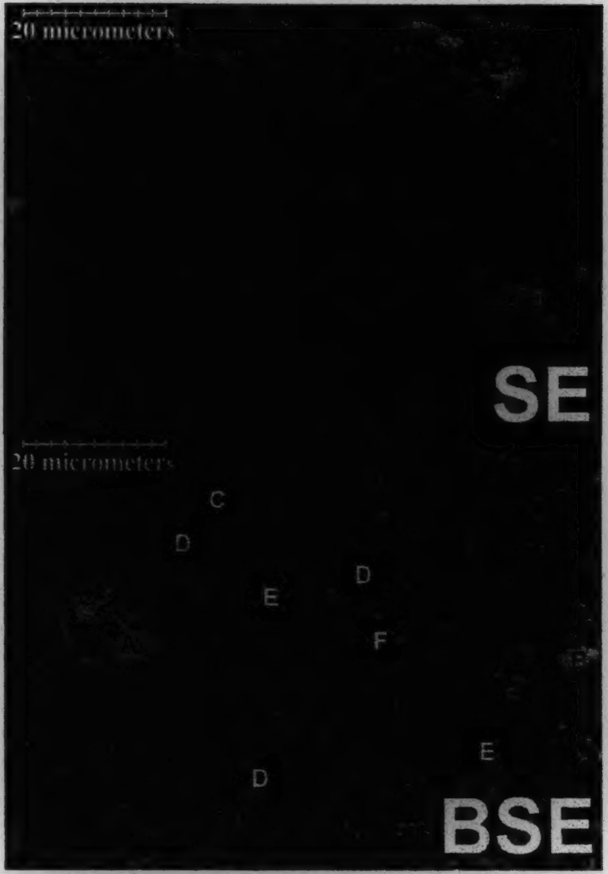
20 micrometers
SE
20 micrometers
C
D
E
D
F
E
D
BSE

Figure 159

Secondary Electron (SE) and Backscattered Electron (BSE) Images of Inco Copper Residue (Feed #2) after Roasting at 450°C with 150% Na_2CO_3 and 45.2% $FeSO_4{\cdot}7H_2O$ and Leaching with Hot Water (Sample Z)

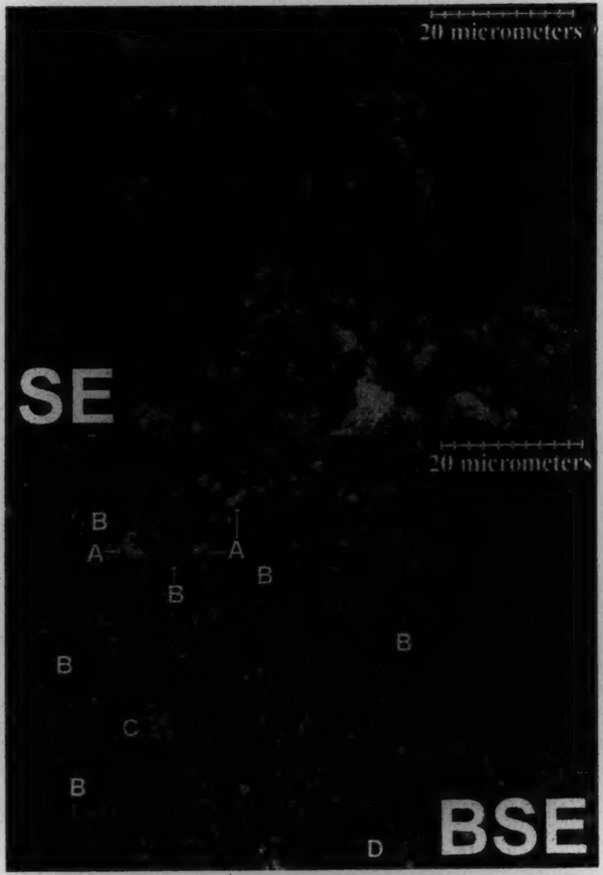
20 micrometers
SE
20 micrometers
B
A
A
B
B
B
B
C
B
D
BSE

Figure 160

Secondary Electron (SE) and Backscattered Electron (BSE) Images of Inco Copper Residue (Feed #2) after Roasting at 450°C with 150% Na_2CO_3 and 45.2% $FeSO_4{\cdot}7H_2O$and Leaching with 200 g/L H_2SO_4 at 95 to 97°C (Sample Z)

6.5 Deportment of Minor Elements

Two further batch tests were performed to generate solids and solutions for minor element analysis under conditions more typical of the projected optimum roasting conditions for this material and allow a preliminary evaluation of the potential of using an oxygen enriched atmosphere during roasting to improve arsenic deportment. These samples were roasted for 4 h at 450°C with 170% Na_2CO_3 with either an air or oxygen flow rate of 2.5 to 3.3 L/min in the second furnace configuration shown in Figure 119B. The results of these tests are shown in Table 74.

Table 73 Element Deportment from Roasting and Leaching of Inco Copper Residue (Feed #2) with 170% Na_2CO_3 at 450°C in Air and in Oxygen

Atmosphere	Air	O_2	Atmosphere	Air	O_2
Sulphur			Arsenic		
Retained, %	100.0	100.0	Retained, %	100.0	100.0
Water Leach, %	90.9	90.5	Water Leach, %	43.6	61.5
Acid Leach, %	0.0	6.9	Acid Leach, %	55.5	38.4
Total, %	90.9	97.4	Total, %	99.1	99.9
Copper			Nickel		
Water Leach, %	1.3	0.4	Water Leach, %	0.4	0.1
Acid Leach, %	72.7	89.2	Acid Leach, %	85.1	98.0
Total, %	74.0	89.6	Total, %	85.5	98.1

As expected, all the sulphur and arsenic in the copper residue were retained in the solids with the increase in Na_2CO_3 addition to 170%. The majority of the sulphur reports to the water leach solution and the sulphur remaining in the acid leach residue would be expected to be present as unoxidized, or partially oxidized, sulphides. While the use of oxygen does not significantly affect the amount of sulphur reporting to the water leach solution, the conversion of sulphide sulphur to sulphate is about 6.5% higher for the sample roasted with oxygen. Roasting in oxygen did improve the amount of arsenic extracted by water leaching by about 19% with overall arsenic extractions of over 99% achieved for both roasting in air and in oxygen.

Copper and nickel extractions are lower than predicted by extrapolation of the response surface models in Section 6.4.1.2.2, but this is not unexpected as these roasting conditions are well outside of the model conditions tested previously for roasting with Na_2CO_3 alone. Water leaching extractions for both metals are very low and both nickel and copper extractions in acid leaching appear to be improved by roasting with oxygen instead of air. Combined with the increase in water soluble arsenic, roasting with an oxygen atmosphere appears to be promising, but further testing at lower temperatures and higher Na_2CO_3 additions, including testing of the roasting atmosphere and the effect of pelletizing would be required to optimize roasting conditions for this material.

The deportment of minor elements after roasting with air and oxygen are shown in Tables 74 and 75, respectively.

Table 74 Deportment of Minor Element in Inco Copper Residue (Sample #2) after Roasting with 170% Na_2CO_3 at 450°C in Air

	Element Distribution, %			Composition, % or g/L			
	Water Leach Solution	Acid Leach Solution	Residue	Feed	Leach Residue	Water Leach Solution[1]	Acid Leach Solution[2]
Solids, g				1000	138.0	-	-
Solution, L				-	-	6.8	2.9
Cu	1.3	72.7	26.0	29.7	60.0	0.59	73.7
Ni	0.4	85.1	14.5	3.80	4.00	0.02	11.0
As	43.6	55.5	1.0	3.04	0.23	1.96	5.76
S	90.9	0.0	9.1	28.1	20.7	37.8	0.0
Na	99.6	0.2	0.2	0.25	1.07	108.8	0.62
Al	15.2	63.6	21.2	0.13	0.20	0.029	0.28
Cd	1.2	85.0	13.8	0.02	0.020	0.0003	0.058
Ca	0.7	97.5	1.8	0.45	0.060	0.0044	1.50
Cl	95.3	1.6	3.1	0.45	0.10	0.64	0.024
Co	1.0	82.9	16.1	0.06	0.070	0.0009	0.17
F[3]	71.4	11.0	4.1	0.081	0.024	0.10	0.031
Fe	0.2	93.3	6.5	0.31	0.15	0.0009	0.98
Pb[3]	1.8	40.9	6.5	0.61	0.36	0.016	0.85
Mg	0.1	99.0	0.9	0.39	0.025	0.0008	1.31
Mn	0.3	88.7	11.0	0.025	0.020	0.0001	0.076
K	37.6	9.8	52.6	0.055	0.21	0.031	0.018
Si	2.9	86.0	11.1	0.31	0.25	0.013	0.94
Zn	0.7	83.6	15.7	0.035	0.040	0.0003	0.10

[1] Estimated from element distribution and assuming a solids concentration of 400 g/L

[2] Estimated from element distribution and assuming a leach solution of 150 g/L H_2SO_4

[3] 51.8% of the Pb and 13.5% of the F in the feed were fumed during roasting

Table 75 Deportment of Minor Elements in Inco Copper Residue (Sample #2) after Roasting with 170% Na_2CO_3 at 450°C in Oxygen

	Element Distribution, %			Composition, % or g/L			
	Water Leach Solution	Acid Leach Solution	Residue	Feed	Leach Residue	Water Leach Solution[1]	Acid Leach Solution[2]
Solids, g				1000	51.7	-	-
Solution, L				-	-	6.8	3.6
Cu	0.4	89.2	10.4	29.7	66.0	0.16	73.4
Ni	0.1	98.0	1.9	3.8	1.40	0.005	10.3
As	61.5	38.4	0.1	3.04	0.055	2.77	3.24
S	90.5	6.9	2.6	28.1	15.9	37.7	5.37
Na	98.7	1.2	0.1	0.25	1.50	107.7	2.55
Al	0.0	82.1	17.9	0.13	0.45		0.30
Cd	0.9	94.8	4.3	0.02	0.020	0.0003	0.052
Ca	0.7	98.7	0.6	0.45	0.050	0.0045	1.23
Cl	96.7	2.7	0.6	0.45	0.050	0.65	0.034
Co	1.1	94.6	4.3	0.06	0.050	0.0010	0.16
F	86.4	12.2	1.4	0.081	0.023	0.10	0.028
Fe	0.2	96.8	3.0	0.31	0.15	0.0011	0.83
Pb[3]	1.8	45.0	7.8	0.61	0.92	0.020	0.76
Mg	0.2	99.5	0.3	0.39	0.022	0.0010	1.074
Mn	0.4	95.5	4.1	0.025	0.020	0.0001	0.066
K	40.1	11.0	48.9	0.055	0.52	0.033	0.017
Si	4.0	90.0	6.0	0.31	0.36	0.018	0.77
Zn	0.8	96.3	3.0	0.035	0.020	0.0004	0.093

[1] Estimated from element distribution and assuming a solids concentration of 400 g/L

[2] Estimated from element distribution and assuming a leach solution of 150 g/L H_2SO_4

[3] 44.6% of the Pb in the feed was fumed during roasting

Overall, extractions in water leaching are low for all elements, except for As, Cl, F, K, Na and S while the majority of the other elements present in the copper residue were dissolved to a significant extent during acid leaching.

6.6 Preliminary Evaluation of Potential Processing Options

6.6.1 Roasting and Leaching Unit Operations

A proposed flowsheet outlining the roasting and leaching steps for Na_2CO_3 roasting of this material is provided in Figure 161. Roasting and leaching reactions for each unit operation are shown in Table 76.

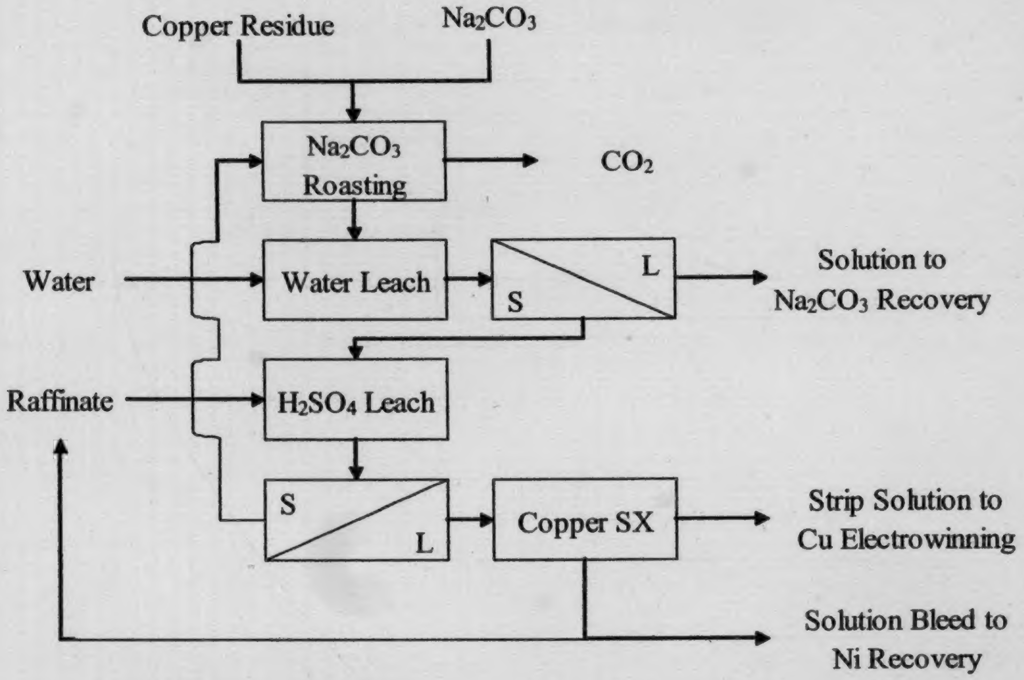
Copper Residue
Na_2CO_3
Na_2CO_3 Roasting
CO_2
Water
Water Leach
S
L
Solution to Na_2CO_3 Recovery
Raffinate
H_2SO_4 Leach
S
L
Copper SX
Strip Solution to Cu Electrowinning
Solution Bleed to Ni Recovery

Figure 161 Proposed Roasting and Leaching Flowsheet for Na_2CO_3 Roasting of the Inco Copper Residue

Table 76 Roasting and Leaching Reactions Expected during Na_2CO_3 Roasting

Unit Operation	Chemical Reactions
Na_2CO_3 Roasting	$Na_2CO_3 + CuS + 2\ O_2 \rightleftharpoons Na_2SO_4 + CuO + CO_2$ $2\ Na_2CO_3 + NiS_2 + 3.5\ O_2 \rightleftharpoons 2\ Na_2SO_4 + NiO + 2\ CO_2$ $11\ Na_2CO_3 + 2\ Cu_3AsS_4 + 17.5\ O_2 \rightleftharpoons 8\ Na_2SO_4 + 2\ Na_3AsO_4 +$ $6\ CuO + 11\ CO_2$
Water Leaching	$Na_2SO_{4(s)} \rightleftharpoons Na_2SO_{4(aq)}$ $Na_3AsO_{4(s)} \rightleftharpoons Na_3AsO_{4(aq)}$ $NiSO_{4(s)} \rightleftharpoons NiSO_{4(aq)}$ $CuSO_{4(s)} \rightleftharpoons CuSO_{4(aq)}$
H_2SO_4 Leaching	$H_2SO_4 + CuO \rightleftharpoons CuSO_4 + H_2O$ $H_2SO_4 + NiO \rightleftharpoons NiSO_4 + H_2O$

In this flowsheet, after roasting with Na_2CO_3 and leaching in hot water and hot acid solutions, the acid leach residue which, from the results presented in 6.4.2.2, is largely composed of unleached oxides or partially reacted copper sulphides, would be recycled back into roasting in order to maximize copper and nickel recoveries in the process.

Further optimization of the process conditions through ongoing batch testing will, of course, be performed in order to maximize extractions on the "first pass" through the process flowsheet, but the nature of the process chemistry would allow for the possibility of recycling unreacted sulphides or oxides to roasting without any major process concerns.

Because of the low acid concentrations expected after acid leaching, copper recoveries during solvent extraction are expected to be high (216); ideally, the raffinate would be completely barren of copper after solvent extraction, but this may not be practical from an operational standpoint. Thus, the solution treatment options outlined in subsequent sections would have to consider the possibility of the removal of copper during the treatment of the raffinate for nickel recovery.

The raffinate would be recycled to acid leaching, with the sulphuric acid generated in the raffinate during loading of the copper in solvent extraction used to leach additional copper and nickel from the water leach solids. With this recycle of raffinate solution, the solution strength would be adjusted to allow for higher concentrations of nickel and other elements in the acid leach solution. To prevent the buildup of these elements in solution, a portion of the raffinate would then be bled to recover elements such as nickel and sodium and to allow for removal and disposal of arsenic from solution. A high recycle rate would minimize the volume of the solution bleed treated, which would, in turn, minimize sulphate losses during the treatment of the raffinate bleed.

6.6.2 Nickel Recovery from the Raffinate Bleed

There are two main process options that might be used to recover nickel from the raffinate bleed: precipitation as $Ni(OH)_2$ or precipitation of nickel sulphide. These process options are outlined in Sections 6.6.2.1 and 6.6.2.2, respectively.

6.6.2.1 Precipitation of Nickel Hydroxide from the Raffinate Bleed

A possible flowsheet for the recovery of nickel from the raffinate bleed as $Ni(OH)_2$ is shown in Figure 162. Reactions for the various unit operations in this flowsheet are outlined in Table 77.

The high pH of the solution from water leaching should allow it to be used as a neutralizing agent in a similar fashion as was proposed during process development for the Na_2CO_3 roasting of the La Oroya zinc ferrite or the Altasteel EAF dust (Sections 4.7.1.1.1 and 5.7.1). Using this solution would reduce the reagents costs (i.e., lime or limestone use) in neutralization, would eliminate sulphate losses to gypsum and should minimize nickel or cobalt losses due to entrainment in the gypsum or iron solids precipitated in this process flowsheet.

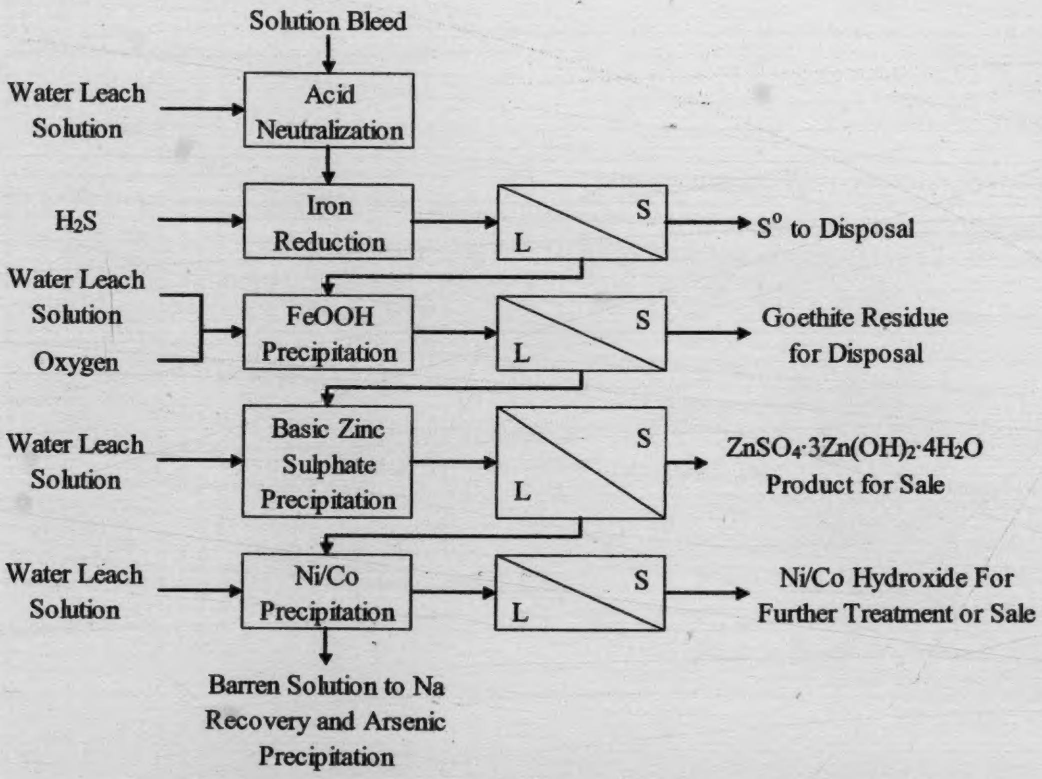
Solution Bleed
Water Leach Solution
Acid Neutralization
H2S
Iron Reduction
S
L
S° to Disposal
Water Leach Solution
Oxygen
FeOOH Precipitation
S
L
Goethite Residue for Disposal
Water Leach Solution
Basic Zinc Sulphate Precipitation
S
L
ZnSO4·3Zn(OH)2·4H2O Product for Sale
Water Leach Solution
Ni/Co Precipitation
S
L
Ni/Co Hydroxide For Further Treatment or Sale
Barren Solution to Na Recovery and Arsenic Precipitation

Figure 162 **Proposed Flowsheet for the Precipitation of Nickel Hydroxide from the Raffinate Bleed from Na_2CO_3 Roasting of Inco Copper Residue**

Table 77 Reactions during Nickel Hydroxide Precipitation of the Raffinate Bleed

Unit Operation	Chemical Reactions
Acid Neutralization	$NaOH + H_2SO_4 \rightleftharpoons H_2O + Na_2SO_4$
Iron Reduction	$Fe_2(SO_4)_3 + H_2S \rightleftharpoons H_2SO_4 + 2\ FeSO_4 + S°$
FeOOH Precipitation	$2\ FeSO_4 + 2\ ZnO + 0.5\ O_2 + H_2O \rightarrow 2ZnSO_4 + 2FeOOH$
Basic Zinc Sulphate Precipitation	$4\ ZnSO_4 + 3\ CaCO_3 + 13\ H_2O \rightleftharpoons ZnSO_4{\cdot}3Zn(OH)_2{\cdot}4H_2O + 3\ CaSO_4{\cdot}2H_2O + 3\ CO_2$
Ni/Co Precipitation	$NiSO_4 + 2\ NaOH \rightleftharpoons Ni(OH)_2 + Na_2SO_4$

Following a similar procedure to that described in Section 4.7.1.1.1, free acid is neutralized at about pH 2, followed by reduction of iron to Fe^{2+} with H_2S, then precipitation of goethite at pH 2.5 to 4.2 and finally precipitation of basic zinc sulphate at up to pH 6.5. A lower precipitation pH for BZS precipitation would have to be used to minimize coprecipitation of nickel and cobalt. Nickel and cobalt hydroxide precipitation would then be conducted at pH 7.0 to 7.5 (217).

Even with a high raffinate recycle rate, the volumes of iron and zinc precipitates would be expected to be small and, economically, separate removal steps may not be desirable. However, both elements should be removed to minimize contamination of the Ni/Co hydroxide produced. Precipitation of both zinc and iron in a single step would lead to significant soluble zinc in the resulting residue.

Based on the deportment of minor elements, the nickel/cobalt hydroxide produced would be expected to have a Ni:Co ratio of about 65:1 and would likely also be contaminated with significant amounts of manganese and magnesium (217). The low cobalt content would likely make cobalt recovery uneconomic, but cobalt would have to be removed from the nickel in order to produce a high purity nickel product.

In this flowsheet, copper from the raffinate would likely precipitate as copper hydroxide over the pH range used for goethite precipitation. This goethite residue could be recycled to acid leaching to recover copper, but goethite would also likely dissolve or partially dissolve. The inability to effectively recover copper from this material could lead to unacceptable copper losses from the raffinate bleed.

Aluminum and silicon would also be expected to precipitate along with goethite, as indicated previously in Section 4.7.1, but some arsenic may also precipitate with iron in goethite or be absorbed on the surface of the iron precipitate. Arsenic contamination of the goethite would be undesirable as goethite is unlikely to have the stability required for long term arsenic disposal.

Finally, the nickel/cobalt hydroxide would require additional processing steps (i.e., releaching and hydrogen reduction and/or solvent extraction/electrowinning) to recover nickel from the Inco copper residue on site at the Thompson refinery as this material does not integrate well with the existing nickel recovery methods (i.e., converting and matte electrorefining) used at Inco's Thompson refinery. The hydroxide product should be a saleable nickel product, and could possibly be treated in Inco's Sudbury refinery or possibly sold to a third party for further treatment for nickel recovery.

6.6.2.2 Sulphide Precipitation of the Raffinate Bleed

A possible flowsheet for the precipitation of copper, arsenic and nickel from the raffinate bleed stream is shown in Figure 163. Reactions for the respective unit operations are provided in Table 78.

Research performed on refinery bleed streams at the Kennecott Utah smelter indicate that copper can be removed from acidic copper solutions while minimizing the sulphidization and coprecipitation of arsenic (218). Based on this study, the first stage of sulphide precipitation in this process flowsheet would involve the controlled addition of H_2S to precipitate any residual copper from solution along with a portion of the arsenic in solution (218). This copper/arsenic sulphide would then be recycled to Na_2CO_3 roasting to recover the copper values. (In the current roasting flowsheet, at least a portion of the arsenic recycled to roasting would be expected to report to the water leach solution and, thus, not all the arsenic recycled to roasting would be expected to report to the raffinate bleed.) After filtration to recover this residue, a second stage of sulphide precipitation would be performed to remove any remaining arsenic from solution. This precipitate would provide an additional bleed of arsenic from the acid leach solution. The arsenic sulphide would then be sent to sodium and arsenic precipitation unit operations for further processing (Section 6.6.2.3).

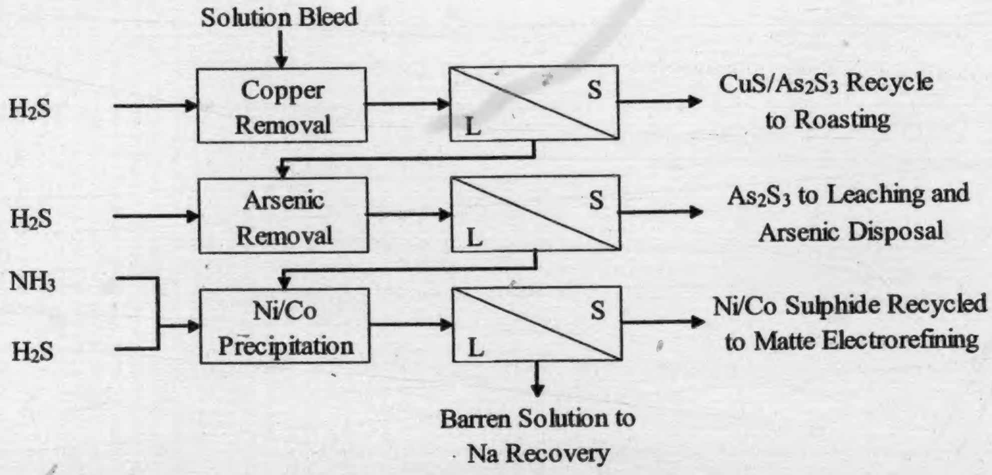
Solution Bleed
H2S
Copper Removal
S
L
CuS/As2S3 Recycle to Roasting
H2S
Arsenic Removal
S
L
As2S3 to Leaching and Arsenic Disposal
NH3
H2S
Ni/Co Precipitation
S
L
Ni/Co Sulphide Recycled to Matte Electrorefining
Barren Solution to Na Recovery

Figure 163 **Proposed Flowsheet for Sulphide Precipitation of Copper, Arsenic and Nickel from the Raffinate Bleed from Na_2CO_3 Roasting of Inco Copper Residue**

Table 78 Reactions during Sulphide Precipitation of Raffinate Bleed

Unit Operation	Chemical Reactions
Copper Removal	$CuSO_4 + H_2S \rightleftharpoons CuS + H_2SO_4$ $2\ HAsO_2 + 3\ H_2S \rightleftharpoons As_2S_3 + 4\ H_2O$ $Fe_2(SO_4)_3 + H_2S \rightleftharpoons H_2SO_4 + 2\ FeSO_4 + S$
Arsenic Removal	$2\ HAsO_2 + 3\ H_2S \rightleftharpoons As_2S_3 + 4\ H_2O$ $2\ H_3AsO_4 + 5\ H_2S \rightleftharpoons As_2S_5 + 8\ H_2O$
Ni/Co Precipitation	$NiSO_4 + H_2S + NH_3 \rightleftharpoons NiS + (NH_4)_2SO_4$ $CoSO_4 + H_2S + NH_3 \rightleftharpoons CoS + (NH_4)_2SO_4$

Since acidic conditions are required for both copper and arsenic precipitation (218) and the pH of the bleed solution is already low, no neutralization of the bleed solution would be required before performing sulphide precipitation. A number of other elements, such as Cd, Pb and Zn, would also be expected to precipitate with the addition of H_2S but, without further study, the deportment of these elements (i.e., to the copper or arsenic sulphides) cannot be confirmed at this time.

After filtering the arsenic sulphide from the Cu- and As-free raffinate bleed solution, ammonia would be added to raise the solution pH and buffer it during sulphide precipitation, and a mixed nickel-cobalt sulphide would be precipitated by the addition of H_2S. As in the Ni/Co hydroxide, the Ni:Co ratio in the sulphide would be expected to be around 65:1 and the low cobalt content would likely make cobalt recovery uneconomical. However, this nickel sulphide precipitate could then be dried and added to the matte produced daily at the Thompson refinery, with the nickel recovered in Inco's existing matte electrorefining operations. This eliminates the need to build and design separate nickel recovery equipment (i.e., hydrogen reduction or solvent extraction/electrowinning) for the treatment of this material.

After precipitation of nickel and cobalt, the resulting impure $(NH_4)_2SO_4$ solution would then be combined with the water leach solution to allow the sodium and NH_3 in solution to be recovered and the Al, F, Cl, Fe, Mg, Mn and Si from solution to be removed in the subsequent Na_2CO_3 recovery and arsenic precipitation steps.

The valent state of arsenic in the acid leach solution is, at present, unknown. While As^{3+} and As^{5+} should both be precipitated as sulphides, precipitation of As^{5+} is slower and often reduction to As^{3+} is proposed prior to sulphide precipitation (219). (Some of the As^{5+} is often reduced to As^{3+} by the H_2S during precipitation (219).) Further study will be required to determine the valence of arsenic in solution and the efficiency of arsenic sulphide precipitation from these process solutions. Most of the accepted methods of arsenic precipitation for long term storage require all the arsenic to be present as As^{5+}, and, thus, if complete reduction of the arsenic to As^{3+} could be avoided, it would be helpful in later processing.

Overall, the sulphide precipitation flowsheet has several advantages over the hydroxide precipitation flowsheet as it allows for copper to be recovered from the bleed solution and recycled into the process, it produces a nickel byproduct that can be integrated easily into Inco's existing operations, it eliminates sulphate losses by neutralization and it produces an intermediate arsenic product which can then be processed further and precipitated in a more stable form. Thus, the potential sodium recovery and arsenic precipitation steps considered in the following section will assume that the raffinate bleed solution has been treated by sulphide precipitation.

6.6.2.3 Sodium Recovery and Arsenic Precipitation

A possible process flowsheet for the recovery of sodium and the precipitation of arsenic in a stable form is presented in Figure 164. Reactions for the various unit operations are provided in Table 79.

Table 79 Reactions during Sodium Recovery and Arsenic Precipitation

Unit Operation	Chemical Reactions
As Precipitate Leaching	$As_2S_3 + 12\ NaOH + 7\ O_2 \rightleftharpoons 2\ Na_3AsO_4 + 3\ Na_2SO_4 + 6\ H_2O$ $As_2S_5 + 16\ NaOH + 10\ O_2 \rightleftharpoons 2\ Na_3AsO_4 + 5\ Na_2SO_4 + 8\ H_2O$
Al/Fe Precipitation	$H_2SO_4 + NaOH \rightleftharpoons Na_2SO_4 + H_2O$ $Al_2(SO_4)_3 + 6\ NaOH \rightleftharpoons 2\ Al(OH)_3 + 3\ Na_2SO_4$ $2\ FeSO_4 + 0.5\ O_2 + 4\ NaOH + H_2O \rightleftharpoons 2\ Fe(OH)_3 + 2\ Na_2SO_4$
Primary Na_2CO_3 Recovery	$Na_2SO_4 + 2\ H_2O + 2\ NH_3 + 2\ CO_2 \rightleftharpoons (NH_4)_2SO_4 + 2\ NaHCO_3$ $NaOH + CO_2 \rightleftharpoons NaHCO_3$ $NaHCO_3 + NaOH \rightleftharpoons Na_2CO_3 + H_2O$
Gypsum/APHAP Precipitation	$(NH_4)_2SO_4 + Ca(OH)_2 \rightleftharpoons CaSO_4{\cdot}2H_2O + 2\ NH_3$ $10\ Ca(OH)_2 + 5.25\ H_3PO_4 + 0.75\ Na_3AsO_4 \rightleftharpoons$ $Ca_{10}(As_{0.125}P_{0.875}O_4)_6(OH)_2 + 2.25\ NaOH + 15.75\ H_2O$
$NaHCO_3$ Calcination	$2\ NaHCO_3 \rightleftharpoons Na_2CO_3 + H_2O + CO_2$
Secondary Na_2CO_3 Recovery	$NaOH + HCl \rightleftharpoons NaCl + H_2O$ $Na_2CO_3 + 2\ HCl \rightleftharpoons 2\ NaCl + CO_2 + H_2O$ $NaCl + H_2O + NH_3 + CO_2 \rightleftharpoons NH_4Cl + NaHCO_3$
NH_4Cl Calcination	$NH_4Cl \rightleftharpoons NH_3 + HCl$

The arsenic sulphide precipitate produced in the arsenic removal step of sulphide precipitation should be readily soluble at the high pH of the water leach solution (220). Oxygen would be introduced to aid the oxidation of these sulphides, and, if necessary, more aggressive oxidants, such as chlorine or ozone, would be used to ensure all the arsenic is present in solution as As^{5+} (221).

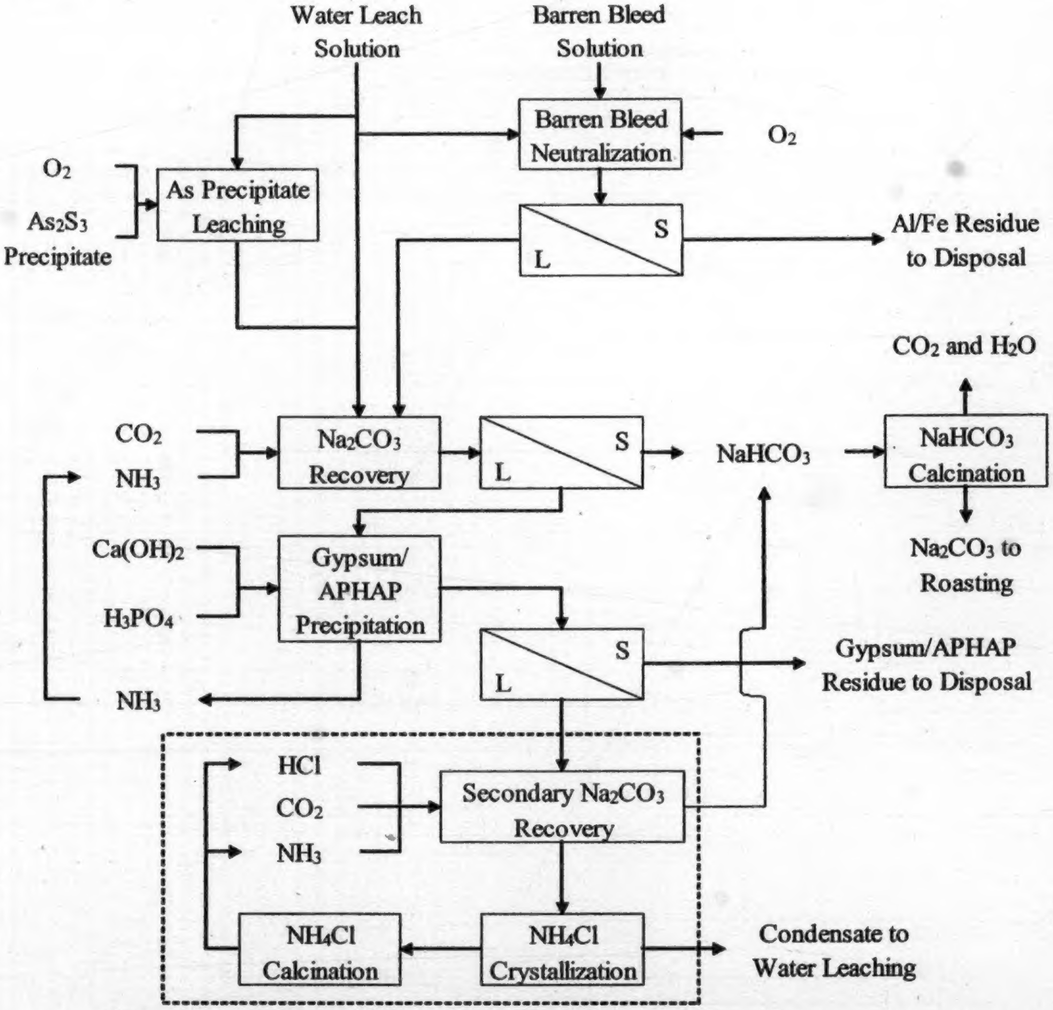
Water Leach Solution
Barren Bleed Solution
Barren Bleed Neutralization
O2
O2
As2S3 Precipitate
As Precipitate Leaching
S
L
Al/Fe Residue to Disposal
CO2 and H2O
CO2
NH3
Na2CO3 Recovery
S
L
NaHCO3
NaHCO3 Calcination
Na2CO3 to Roasting
Ca(OH)2
H3PO4
Gypsum/ APHAP Precipitation
S
L
Gypsum/APHAP Residue to Disposal
NH3
HCl
CO2
NH3
Secondary Na2CO3 Recovery
NH4Cl Calcination
NH4Cl Crystallization
Condensate to Water Leaching

Figure 164 Proposed Flowsheet for Sodium Recovery and Arsenic Precipitation from the Barren Solutions from Na_2CO_3 Roasting of the Inco Copper Residue

The barren raffinate solution would then be neutralized with water leach solution to neutralize free acid and precipitate Al, Fe and possibly Si from the leach solution to minimize contamination of the Na_2CO_3 produced in the subsequent Na_2CO_3 recovery step. After filtration to remove the Al/Fe precipitate, this solution would then be combined with the rest of the water leach solution and the solution from leaching of the arsenic sulphide precipitate, and the combined solution forwarded to primary Na_2CO_3 recovery.

The high Na_2CO_3 addition required to eliminate arsenic emissions during Na_2CO_3 roasting results in a water leach solution slightly different from that obtained from water leaching of roasted zinc ferrite or EAF dust. (In the flowsheets outlined in Sections 4.7.1.1.1 and 5.7.1, the water leach solution is first used as a neutralization agent to convert all the sodium in solution to Na_2SO_4 and the sodium is then converted to NaCl in solvent extraction/ion exchange.) Based on the available analyses, the water leach solution from Na_2CO_3 roasting of the Inco copper residue is expected to contain about 50% of the sodium as Na_2SO_4, 1.5 to 2.5% as Na_3AsO_4, 30% as Na_2CO_3 and the remainder as NaOH. This is not a typical solution used in the Solvay, or other related, processes, where NaCl is the predominant sodium mineral in solution, and, thus, few details are available in the literature on the behaviour of this solution upon the addition of NH_3 and CO_2. However, based on available thermodynamic data, it should be possible to precipitate $NaHCO_3$ from both Na_2SO_4 and NaOH though, potentially, the $NaHCO_3$ formed could react with NaOH to produce additional Na_2CO_3 in solution. (Use of the water leach solution to neutralize the raffinate bleed solution would reduce the NaOH concentration in the water leach solution, but not enough to completely convert NaOH to Na_2SO_4 in solution.) However, thermodynamically, aqueous Na_2CO_3 should not react with CO_2 or H_2O in solution to form $NaHCO_3$, but would be expected to remain in solution after $NaHCO_3$ precipitation from the other sodium species is complete. Thus, it may be possible to remove up to 70% of the sodium in solution during this primary Na_2CO_3 recovery step, but the remaining sodium would remain in the solution entering the subsequent gypsum/APHAP precipitation unit operation. Thermodynamic data for $(NH_4)_3AsO_4$ were not available and, thus, the behaviour of Na_3AsO_4 in this process is uncertain at present.

There are several possible methods for precipitating arsenic from process solutions. Precipitation of arsenic sulphides and ferric arsenate require low solution pH which, for the process solution in this process, would require expensive acidification and, then, reneutralization for solution disposal after precipitation (221). In addition, arsenic sulphides are not environmentally stable and the high iron additions required for ferric arsenate precipitation results in large volumes of arsenic precipitates (221). Calcium arsenate precipitation is possible at high pH, but the precipitates produced are not suitable for long term disposal (221,222).

However, in recent years, the possibility of precipitating arsenic in a hydroxyapatite ($Ca_{10}(PO_4)_6(OH)_2$) structure has been investigated at Montana Tech (222,223). In this process, phosphoric acid (H_3PO_4) is added to solution to give a P:As ratio of 7:1 or greater and the solution is adjusted to over pH 12 with lime to precipitate arsenatephosphatehydroxyapatite ($Ca_{10}(As_xP_yO_4)_6(OH)_2$) (APHAP)). The precipitation of arsenic as APHAP down to less than 15 mg/L in solution has been successful from a variety of process and wastewater solutions and the APHAP precipitate has been shown to be very stable with arsenic concentrations in solution of between 3 and 43 mg/L observed after 18 months of air sparging and as low as 2 mg/L after eight years in anaerobic conditions (223). Thus, based on these reported results, and the high solution pH of the solution that is expected, APHAP precipitation appears to be the most promising method for precipitation of arsenic from the solution from primary Na_2CO_3 recovery.

With the addition of lime (CaO) or hydrated lime ($Ca(OH)_2$), the ammonium sulphate in solution would also react to liberate ammonia (NH_3) for recycle to the Na_2CO_3 recovery step while precipitating the sulphate ions as gypsum ($CaSO_4{\cdot}2H_2O$). At the high pH conditions of APHAP precipitation, Cl, F, Mg and Mn would also be expected to be precipitated out of solution and be bled from the system. In these basic conditions, carbonate ions would be expected to precipitate as $CaCO_3$, producing a solution containing NaOH as its major component.

After gypsum/APHAP precipitation, the resulting solution would then have to be treated to recover the remaining Na_2CO_3 from solution. It may be possible to precipitate $NaHCO_3$ directly from this NaOH solution, but, because of the potential of forming

Na_2CO_3 by reaction of $NaHCO_3$ and NaOH in the process, this possibility would have to be tested experimentally. Alternatively, the solution be treated for Na_2CO_3 recovery by neutralizing the solution with HCl to produce a NaCl solution which could then be treated in a secondary Na_2CO_3 recovery step (i.e., modified Solvay process) similar to that proposed in Sections 4.7.1.1.1 and 5.7.1. This type of neutralization could not be performed before primary Na_2CO_3 recovery without losses of sulphate or chloride to the solids during gypsum/APHAP precipitation. Both options would likely require evaporation/crystallization of the solution, which is not a desirable process option, if avoidable, and the process used would be selected based on purity of the product that could be produced and the capital and operating costs associated with each process option. However, a recent publication indicates that it may be possible to regenerate ammonia and HCl from NH_4Cl using activated carbon (224). To date, this NH_4Cl regeneration process has only been conducted on a small scale, but if this process proves to be effective on a commercial scale, it would greatly reduce the energy requirements for NH_4Cl crystallization and calcination and could be applied similarly to eliminate the NH_4Cl crystallization step in the flowsheets proposed in Sections 4.7.1.1.1 and 5.7.1.)

6.6.2.4 Optimization of Arsenic Deportment and Flowsheet Implications

Further optimization of the arsenic deportment during roasting, and subsequent leaching operations, would be expected to further simplify the process flowsheet described earlier.

If roasting conditions were adjusted so that all the arsenic reports to the water leach solution, then the arsenic precipitation step of the raffinate bleed treatment and the arsenic sulphide dissolution step in the sodium recovery/arsenic precipitation flowsheet could be eliminated. An arsenic free copper precipitate could be produced from the raffinate bleed treatment which could be recycled to roasting without adding a recirculating load of arsenic into Na_2CO_3 roasting.

Alternatively, if $Ca(OH)_2$ were added during roasting as a secondary additive to selectively capture arsenic, then it is likely that lower Na_2CO_3 additions during roasting would be required. This would decrease the amount of sodium to be recovered in the two

Na_2CO_3 recovery steps and, depending on the amount of Na_2CO_3 and NaOH in solution, could possibly eliminate the need for a secondary Na_2CO_3 recovery step. However, the addition of calcium could potentially lead to the formation of some anhydrite ($CaSO_4$) during roasting or to increased calcium in the acid leach solution which could lead to gypsum formation during acid leaching. If copper and nickel extractions were not complete after roasting and leaching, then the leach residue would contain unleached oxides and sulphides contaminated with anhydrite and/or gypsum. Modification of leaching procedures to ensure complete dissolution of oxide particles and the possibility of using flotation to recover unreacted sulphides from the gypsum/anhydrite in the residue would have to be investigated if this flowsheet modification were to be used.

The addition of $Ca(OH)_2$ during roasting should convert all the leachable arsenic to an acid soluble form. Thus, all the arsenic would report to the acid leach solution where it would be precipitated as arsenic sulphides during the treatment of the raffinate bleed. This would consolidate all the arsenic in the process into one byproduct, which could then be redissolved and treated separately from the other process solutions using any of the current technologies available for the precipitation and disposal of arsenic.

6.6.2.5 Process Evaluation

Since there are currently no existing or competing processes for treating matte electrorefining wastes reported in the literature with which to compare the Na_2CO_3 roasting process, it is still important to objectively look at the Na_2CO_3 roasting process developed and point out potential strengths and shortcomings.

The roasting process itself is an advantage to this process. There should be sufficient heat generated by the oxidation of the sulphides in this material to allow roasting to continue autogenously and the roasting equipment should not be very capital intensive, particularly without the need to have an extensive system for gas handling or the need for an acid plant. (Scrubbers would still likely be put in place for safety purposes to trap any fugitive emissions due to roaster upset or sudden changes in roaster feed, but would not have to be used heavily if the roasting process is operating properly.) The roaster calcine would be quenched for heat recovery and the steam generated could be used to heat other process solutions. Heat recovery from roaster off gases is also a possibility.

One disadvantage of the roasting process is that all the sulphur is converted to sulphate and, eventually, to gypsum. While this is better economically than producing H_2SO_4, which is capital intensive and unlikely to be economic for the remote location of the Thompson smelter, the opportunity to convert some of the sulphur to elemental sulphur, instead of the sulphate, such as would be expected in any pressure leaching flowsheet for this material, would be an advantage and would reduce the volume of solid gypsum waste produced, and lower costs for lime for neutralization. If roasting in an oxygen atmosphere is required, the need to produce oxygen, and potentially build an oxygen plant, would also be a disadvantage, though any pressure leaching operation would also likely need to operate with oxygen as its primary oxidant.

With the exceptions of H_2S, lime and phosphoric acid (H_3PO_4), all other reagents are regenerated for reuse in roasting or leaching, and, thus, costs for makeup H_2SO_4, Na_2CO_3, NH_3 or HCl would be minimal. The primary waste from this process would be the gypsum/APHAP residue, with a much volume of Al/Fe residue also produced.

However, the process for regenerating Na_2CO_3 from this solution requires a number of different unit operations and several different process chemistries. If NH_4Cl could be regenerated to NH_3 and HCl using activated carbon, or the second stage of Na_2CO_3 recovery can be eliminated, the process flowsheet would become much more attractive. However, this process would have to be compared based on economic and operational factors with other potential alternative processes to determine its feasibility relative to other process options. Because of the relatively simple sulphides present in the Inco copper residue, aqueous pressure oxidation of the copper residue, with copper recovered by solvent extraction and electrowinning, arsenic precipitated as a sulphide for further processing and nickel precipitated as a sulphide for recycle to matte electrorefining, may be a possible alternate technology for the recovery of copper and nickel from this material and may warrant further study.

6.7 Conclusions

From the application of the generalized transformational roasting procedure to the treatment of the Inco copper residue, it was shown that roasting with Na_2CO_3 could be used to eliminate sulphur and arsenic emissions during roasting of this material, while achieving high nickel and copper extractions during subsequent sulphuric acid leaching. Sulphur converted to sulphate sulphur could be readily and selectively removed from copper and nickel by water leaching. The deportment of arsenic was mixed, with some reporting to the water leach solution and some to the acid leach solutions. Further optimization of the operating conditions, including to roasting temperature, roasting times, oxygen content in gas stream during roasting, and leaching reagents and temperatures, would be required to further improve on the results reported here.

Roasting with $Ca(OH)_2$ was also effective in eliminating sulphur and arsenic emissions and high copper extractions were also possible from acid leaching the residue. Nickel extractions were slightly lower (<90%). However, based on these results, higher roasting temperatures would be required to achieve higher nickel and copper extractions from this material than are necessary for roasting with Na_2CO_3. The possibility of using small $Ca(OH)_2$ additions to control arsenic emissions, along with Na_2CO_3 to control sulphur emissions, was proposed and would be studied in future testing.

Several calcium and iron compounds were added to try to form acid insoluble arsenate compounds during roasting, but, while Ca-As and Fe-As compounds were formed, as shown by the stark change in arsenic deportment, these materials readily dissolved in sulphuric acid. Thus, without further improvements, most future work would have to focus on precipitation and disposal from the leach solutions produced.

The deportment of minor elements and preliminary process flowsheet development for Na_2CO_3 roasting were also conducted, with several potential flowsheet options identified and areas for future research identified.

7.0 Evaluation of Transformational Roasting Techniques

7.1 Is the Procedure Proposed for the Application of Transformational Roasting Techniques to New Materials Effective?

The procedure used proved to be quite effective to be able to obtain the desired types of mineralogical transformations and the desired deportment of many major and minor elements. However, after applying these techniques to several different materials, several observations can be made.

First, limited thermodynamic data, particularly for less common elements or less studied chemical systems, can limit the ability to predict accurately the chemical reactions that are observed during roasting. This was observed in this research when studying reactions with arsenic compounds; thermodynamic data were not readily available for common arsenate or arseno-sulphate compounds, even those that are commonly used for arsenic disposal, such as $Ca_3(AsO_4)_2$ or $FeAsO_4$, let alone for arsenite compounds, scorodite ($FeAsO_4 \cdot 2H_2O$), enargite (Cu_3AsS_4), ammonium arsenate or arsenatephosphatehydroxyapatite. Without this data, selection of roasting reagents and conditions, and selection of subsequent solution treatment options, must be done on an entirely empirical basis which, with the number of variables potentially involved in transformational roasting processes, would be extremely time consuming and difficult.

Second, some of the tests conducted may call into question the accuracy of high temperature thermodynamic data. In Section 4.4.2.1, though the thermodynamics for the formation of non-zinc ferrites, such as $CaFe_2O_4$, are extremely favorable, roasting times of up to 24 h at 1100°C were unable to cause any significant observable conversion of $ZnFe_2O_4$ to $CaFe_2O_4$. In fact, in later testing, the formation of $Ca_2Fe_2O_5$, which is much less thermodynamically favorable, was more readily formed and $CaFe_2O_4$ was seldom observed using XRD on the roasted ferrite or EAF residues. Though it is possible that this is an issue of kinetics or caused by potential reverse reactions during cooling, this research would tend to indicate that the franklinite mineral ($ZnFe_2O_4$) is much more stable, and the formation of other metal ferrites much less favorable, than the available thermodynamic data would indicate. This difficulty also makes it hard to accurately predict the phases formed during transformational roasting.

Third, though thermodynamic data for some compounds are available, often solubility data for these compounds are not. For example, no solubility data for $NaFeO_2$ and srebrodolskite ($Ca_2Fe_2O_5$), which are minerals that were commonly formed during transformational roasting of the La Oroya zinc ferrite and Altasteel EAF dust, were available in the literature. Empirically, it was quickly discovered, based on the iron extractions observed during leaching of the roasted zinc ferrite or EAF dust, that these compounds were either highly soluble or that their solubility appeared to vary depending on the temperature of formation of these compounds. The lack of accurate solubility data makes it difficult to target desirable transformational roasting reactions (i.e., reactions that produce acid insoluble, stable residues). Determining these solubilities empirically requires extensive characterization of the roasted and leached materials using SEM and XRD techniques and, because of the complex mineral assemblages present in the materials tested, often these solubilities must be inferred from calculated metals extractions rather than measured directly.

Fourth, the scoping tests were very effective in screening roasting reagents and selecting roasting conditions. However, because of the amount and accuracy of the information possible through DOE testing, and time constraints during testing, sometimes the testing was pushed towards DOE tests before enough experience with the process chemistry had been gained and before a sufficient understanding of more optimum roasting or leaching conditions could be obtained. This problem would be expected to decrease as further materials are tested and more experience is gained in the treatment of various types of materials and the effectiveness of various reagents. However, particularly when testing an unfamiliar material, the process of running scoping tests should not be rushed; more time testing the roasting conditions before performing DOE tests produce results from the DOE tests that are more useful in optimizing the roasting and leaching conditions, and in understanding the roasting reactions taking place at the temperatures tested.

Fifth, using design of experiments (DOE) techniques worked very well with the testing of transformational roasting processes. Although the DOE tests require conducting a significant amount of experiments, DOE testing is much more effective and efficient than testing each variable iteratively, particularly in new systems with several potentially important process variables and, with proper design of the tests, a vast amount of information on various measurable output variables can be obtained from each DOE test. Integration of DOE testing with mineralogical analysis also produced a very good understanding, in most cases, of the stability of various compounds and the effectiveness of various roasting conditions to produce the desired mineralogical transformations.

Sixth, the integration of SEM, XRD and DOE tests to perform mineralogical studies of the roasting and leaching reactions was very effective, but also very analytically intensive. For some companies the amount of XRD and SEM time, and the associated cost with these two methods, may make some companies reluctant to use this integrated approach to process mineralogy. However, the use of both techniques in tandem along with the DOE test results proved to be very powerful and it would have been very difficult to get an accurate picture of the process chemistry and roasting reactions that occurred during transformational roasting without their use.

Seventh, in order to be most effective, the feedback provided by x-ray diffraction analyses needs to be available consistently throughout the scoping and DOE testing steps of this procedure. Equipment failure and low availability of x-ray diffraction equipment at times during this research made it difficult to be able to accurately gauge the effectiveness of the transformational roasting processes tested. (Fewer tests would need to have been conducted, and better results obtained in places, if more consistent feedback of the phases formed during roasting had been available.) Thus, the study of transformational roasting processes using this procedure is not very effective without ready availability of XRD analysis.

Eighth, because of the number of variables that needed to be investigated or set in order to make the process chemistry work in these processes, it often made it difficult to be able to effectively optimize roasting or leaching times over the course of this research. (In most cases, these variables were altered more by necessity (e.g., increasing the leaching temperature for the roasted Inco copper residue), where clear XRD results indicated that changes needed to be made, or by conjecture (e.g. lengthening roasting times for some of the Inco copper residue tests).) Kinetic studies for promising systems would need to be performed in future research to determine the effectiveness and efficiency of the roasting processes used.

Finally, the study of the deportment of minor elements in all these materials was extremely valuable; significant changes in the process flowsheets proposed for the treatment of these materials were required in order to minimize the potential effects of various deleterious minor elements on downstream processing or metals recovery.

7.2 Is Transformational Roasting a Realistic Option for Processing of Metallurgical Wastes?

As expected, for some materials, transformational roasting does appear to be a potential alternative to other available metals recovery processes. Transformational roasting processes would be expected to be more energy intensive than most leaching processes, but less energy intensive than most smelting processes. In general, transformational roasting also appears to have a greater potential to form more disposable solid wastes than most hydrometallurgical processes and some pyrometallurgical processes though, in general, the solid wastes produced at high temperatures in smelting tend to be highly stable. From these studies, transformational roasting should also have the potential to develop low waste processes, as most of the reagents used in processes should be able to be recycled and reused in the roasting process. The synergistic use of hydrometallurgy and pyrometallurgical processing also provides more potential opportunities to effectively recycle or treat process byproducts, which might not be available in a stand alone hydro- or pyrometallurgical plant. For the materials tested to date, with proper process selection, integration of transformational roasting processes with existing pyro- or hydrometallurgical operations seems relatively easy as, in most cases, these processes can be designed to recover metal in a readily recyclable form and can be designed to make use of synergies with existing operations. To date, some of the residues from these processes are produced hydrometallurgically and some pyrometallurgically, giving an overall waste stability between that of pyro- and hydrometallurgical processes.

There are several disadvantages to transformational roasting processes, though, that are observed from this study. First, many of the reactions involve high-temperature equilibria and, in many cases, limits to the effectiveness of these reactions, or the ability to push these reactions to completion, were observed. It is possible that a better understanding of the process chemistry or solid solutions involved in the mineralogical transformations taking place during roasting may lead to improvements in the roasting and leaching results; in some cases, these kinetic or equilibrium constraints may make it difficult to make further improvements for some process options. Second, the lack of available solubility data often made it difficult to consistently form insoluble solid minerals during roasting. It is possible that using a wider range of lixiviants and leaching conditions could minimize this dissolution, but this would potentially increase the complexity and cost of the processes developed. Third, if the reagent added does not form an insoluble solid during roasting, which can then be disposed of safely, a more complex flowsheet is then required, where possible, to try to recover these additives. This recovery is a necessity both economically (i.e., to minimize overall reagent consumption and costs) and environmentally (i.e., to minimize the impact of a potentially large volume of liquid effluent). The ability to effectively recover these reagents from process water prior to disposal and recycle them into roasting would likely make or break the technical and economic feasibility of any potential transformational roasting process.

From this study, the development of viable transformational roasting processes is, at present, hampered by the limited amount of research available in the literature on these types of processes. Although, in some cases, the high temperature reactions observed during roasting, and perhaps even the response of the various minerals formed during roasting to subsequent leaching operations, may be documented in the literature, the literature is largely void of references on the purification or treatment of the process solutions produced during transformational roasting. This became quite apparent during the development of potential process flowsheets for these processes; process conditions and the effects of various impurity elements in solution treatment had to be drawn from a wide range of sources, including references to the Solvay process and the treatment of waste solutions from tanning operations, because the assemblages of dissolved elements were generally fairly unique, and are virtually unreported in the literature. From the study of the available literature, good potential process options were proposed in all the flowsheets presented in this document, but a lot of additional research would be needed to be confident of the behaviour of the various elements in solution through the various solution treatment processes proposed after the roasting and leaching operations. This should not be unexpected, as, if the development of these transformational roasting processes is novel, then the development of solution treatment options for these same processes would be expected to be relatively novel as well. However, at present, this lack of information in the available literature does severely limit the ability to properly evaluate the overall viability of the process options discussed in this study.

As with any metallurgical process, some materials are more amenable than others to treatment using a particular method. The best example from this research is the treatment of the Inco copper residue. Though the leaching and roasting flowsheet is relatively straightforward, the solution purification and Na_2CO_3 recovery flowsheets for Na_2CO_3 roasting are much more involved. Although pressure leaching can be capital cost intensive, hydrometallurgical processing could also be effective in recovering copper and nickel while being able to use a relatively simple, and fairly conventional, process flowsheet. Aqueous pressure oxidation testing of this material would be required to confirm this possibility. (Process selection and the advantages and disadvantages of each process could then be made using a combination of economic and operational factors.)

In future transformational roasting research, it would likely be preferable to primarily target materials for testing which do not already have an economically and environmentally viable pyro- or hydrometallurgical process option, or materials where a more limited amount of research has been performed on those types of materials. This would likely mean targeting materials such as complex oxides or silicates, precipitates from leaching processes, or other less studied materials, such as arsenides, tellurides or selenides, for future testing.

8.0 Future Work

The objective of this testwork was to evaluate the effectiveness of transformational roasting processes on the treatment of several different materials and to identify promising systems for further study. From this research, a number of systems were identified which have the potential for development into processes for the recovery of metals from these materials and improve the disposability of the residues produced. These systems include:

La Oroya Zinc Ferrite: Roasting with Na_2CO_3, $Na_2CO_3/MnCO_3$ or coal/$MnCO_3$
Altasteel EAF Dust: Roasting with Na_2CO_3 or with coal at lower roasting temperatures
Inco Copper Residue: Roasting with Na_2CO_3, $Ca(OH)_2$ or $Na_2CO_3/Ca(OH)_2$

Additional testing would be required for each of these systems before the processes developed for the three main materials examined in this study could be considered for pilot plant testing or commercial application. Kinetic studies and rate tests should be conducted at the optimum conditions for each of the roasting systems identified to allow for the optimization of the roasting and leaching times required for each system. The effect of pelletizing the feed materials and additives, which would likely be used in any commercial operation, and evaluation of potential refractories for use in processing should also be investigated in any future work.

Though the roasting and leaching portion of the proposed process flowsheets have been studied quite extensively in this study, the portions of the flowsheet involving purification or treatment of the process solutions would need to be tested to determine their effectiveness, and evaluate the technical and economic viability of the processes proposed in this study and the deportment of minor elements in each process step. After these studies are complete, an economic analysis of each process option could then be constructed and the process economics compared with other competing process options.

A number of specific areas for further research were also identified over the course of this research. These items include:

- Feasibility of silver recovery from the La Oroya zinc ferrite by flotation
- Potential advantages/feasibility of magnetic separation to upgrade EAF dust prior to Waelz kiln processing or Na_2CO_3 roasting
- Optimization of roasting conditions for Inco copper residue, particularly at lower roasting temperatures
- Testing of the addition of $Ca(OH)_2$ as a secondary additive for the control of arsenic emissions during the Na_2CO_3 roasting of the Inco copper residue
- Testing of the feasibility of aqueous pressure oxidation of the Inco copper residue, and the possibility of using solvent extraction and sulphide precipitation to recover copper and nickel, respectively, from the leach solutions
- Determination of the valence and mineralogical association of unleached vanadium in oil sands fly ash after transformational roasting
- Development of a Na_2CO_3 roasting flowsheet for the recovery of vanadium and molybdenum from oil sands fly ash
- Investigate the potential of adding fluxes or controlling the partial pressure of CO_2 during roasting to improve the reaction kinetics for roasting with calcium reagents
- Investigate the possibility of using microwave processing for transformational roasting applications

Finally, the techniques and procedures for applying transformational roasting to the treatment of these four metallurgical wastes have the potential for much wider application. As with any type of metallurgical process, not all materials will be amenable to transformational roasting, but additional research to apply these techniques to a wider range of metallurgical wastes would develop an increased understanding of the limits, and potential benefits, of these techniques to the recovery of metals from or the disposability of these types of materials. Similar techniques may also be applicable to other non-metallurgical systems, such as the control of heavy metals or volatile elements during coal or coke combustion.

9.0 Conclusions

Over the course of this research, transformational roasting was able to induce changes in the minerals in the four metallurgical wastes tested to produce at least one of the following desirable process results:

a) an increase in the solubility of valuable elements during leaching (e.g., V in the oil sands fly ash, Ga, In and Zn from the La Oroya zinc ferrite, Zn from the Altasteel EAF dust and Cu and Ni from the Inco copper residue)
b) a decreased solubility of a major impurity (e.g., Fe in the La Oroya zinc ferrite and Altasteel EAF dust)
c) a differential solubility between valuable and harmful elements (e.g., Zn and Cr in the Altasteel EAF dust), and
d) control of the emission of volatile elements during roasting (e.g., As and S in the Inco copper residue)

The range of materials tested and the range of different process results that were possible using transformational roasting techniques show the immense potential for using transformational roasting processes to solve problems encountered in the metallurgical industry.

In this research, transformational roasting was applied to a number of complex materials that have not traditionally been considered candidates for this type of roasting process. As a result, a number of promising transformational roasting systems were identified for each waste material tested. Process flowsheets were then developed, based on the roasting, leaching and mineralogical testing completed in the research, for each promising system. Through the application of transformational roasting to these materials, these process flowsheets showed the potential of producing either saleable products from these waste materials, or byproducts which could be readily integrated with the existing hydro- or pyrometallurgical operations where these wastes are produced. The composition of the process solutions produced showed the potential for the recovery of most the reagents used during roasting or solution treatment for recycle back into the process. In addition, through the application of transformational roasting, solid wastes were produced from some materials that would be expected to be highly amenable to long term storage or disposal.

The generalized procedure proposed for applying transformational roasting to new materials proved to be effective. This procedure not only helped streamline the process of identifying and screening potential reagents or narrowing down process conditions, but allowed for a very good understanding of the mineralogical transformations that occur during the roasting process and the behaviour and solubility of these minerals in subsequent leaching operations. The study of actual metallurgical process wastes also allowed a good understanding of the deportment of minor elements through the transformational roasting processes and provided the basis for the construction of process flowsheets for the roasting systems identified. With minor refinements and improvements, this procedure could continue to be used to apply transformational roasting to the recovery of metals or stabilization of wastes for an even wider range of materials.

References

1 Holloway, Preston Carl. Vanadium recovery from oil sands fly ash [M.Sc. Thesis]. Edmonton, Alberta, Canada: University of Alberta, 2003.

2 Holloway, P. C. and Etsell, T. H., Salt roasting of Suncor oil sands fly ash, Metallurgical and Materials Transactions B, 35(6), 2004, p.1051-1058.

3 Holloway, P. C. and Etsell, T. H., Process for the complete utilization of oil sands fly ash, Canadian Metallurgical Quarterly, 45(1), 2006, p.25-32.

4 Goddard, J. B. and Fox, J. S., Salt roasting of vanadium ores, Extractive Metallurgy of Refractory Metals: Proceedings of a the 110th AIME Annual Meeting, H. Y. Sohn, O. N. Carlson, and J. T. Smith, eds. Warrendale, PA: Metallurgical Society of AIME, 1981. p.127-145.

5 Downing, J. H., Deeley, P. H., and Fichte, R., Chromium and chromium alloys, Ullmann's Encyclopedia of Industrial Chemistry, A7, 6th ed. New York, NY: Wiley Interscience, 2002.

6 Sebenik, R. F., Burkin, A. R., Dorfler, R. R., Laferty, J. M., Leichtfried, G., Meyer-Gruenow, H., Mitchell, P. C. H., Vukasovich, M. S., Church, D. A., Van Riper, G. G., Gilliland, J. C., and Thielke, S. A., Molybdenum and molybdenum compounds, Ullmann's Encyclopedia of Industrial Chemistry, A16, 6th ed. New York, NY: Wiley Interscience, 2002.

7 Nielsen, R., Zirconium and zirconium compounds, Ullmann's Encyclopedia of Industrial Chemistry, A28, 6th ed. New York, NY: Wiley Interscience, 2002.

8 Wietelmann, U. and Bauer, R. J., Lithium and lithium Compounds, Ullmann's Encyclopedia of Industrial Chemistry, A15, 6th ed. New York, NY: Wiley Interscience, 2002.

9 Taylor, P. R., Yin, Z. B., Bell, S. L., and Bartlett, R. W., Lime roasting of refractory precious metal ores, EPD Congress 91, D. R. Gaskell, ed. Warrendale, Pa: Minerals, Metals & Materials Society, 1991. p.725-42.

10 Schneider, L. G. and George, Z. M., Recovery of vanadium and nickel from oil sands coke ash, Extractive Metallurgy of Refractory Metals, H. Y. Sohn, O. N. Carlson, and J. T. Smith, eds. Warrendale, PA: Metallurgical Society of AIME, 1981. p.413-20.

11 George, Z. M., Schneider, L. G., and Kessick, M. A., Effect of calcium hydroxide upon Athabasca oil sands bitumen upgrading, The Future of Heavy Crude and Tar Sands: Second International Conference, R. F. Meyer, J. C. Wynn, and J. C. Olson, eds. New York, NY: Coal Age Mining Information Services, McGraw-Hill, 1984. p.1171-4.

12 Trypuc, M., Bialowicz, K., and Mazurek, K., Solubility in the KVO_3-KCl-H_2O System from 293 to 323 K, Industrial Engineering Chemistry Research, 41(4174-77), 2002.

13 Linke, W. F., Solubilities, Inorganic and Metal-Organic Compounds; a Compilation of Solubility Data from the Periodical Literature, 4th ed. Washington D.C.: American Chemical Society, 1958. p. 1177 .

14 Chadwick, J., La Oroya, Mining Magazine, 178(2), 1998, p.106, 108-11.

15 Gabby, P. N., Zinc, Mineral Commodity Summaries 2006, Washington, DC: United States Department of the Interior, 2006, p. 190-91.

16 Carlin Jr., J. F., Indium, Mineral Commodity Summaries 2006, Washington, DC: United States Department of the Interior, 2006, p. 82-3.

17 Kramer, D. A., Gallium, Mineral Commodity Summaries 2006, Washington, DC: United States Department of the Interior, 2006, p. 66-7.

18 Brooks, W. E., Silver, Mineral Commodity Summaries 2006, Washington, DC: United States Department of the Interior, 2006, p. 152-3.

19 Reyes, Jose. FW: Questions about zinc plant waste streams. E-mail to: Preston Holloway. 2004 Apr 26.

20 Analyze This! L.L.C. Analyze This! Specialists in Electron Probe Microanalysis - FAQ's [Web Page]. 2002; Accessed Apr. 6, 2006. Available at: http://www.analyzethis1.com/faqs.htm.

21 Hopkins, D. W., A reaction between solids: the formation of zinc ferrite from zinc oxide and ferric oxide, Journal of the Electrochemical Society, (96), 1949, p.195-203.

22 Hopkins, D. W., Factors affecting the rate of formation of zinc ferrite from zinc oxide and ferric oxide, Bulletin - Institution of Mining and Metallurgy, (515), 1949, p.1-21.

23 Liddell, Donald Macy, Handbook of nonferrous metallurgy, 2nd ed. New York, London: McGraw-Hill Book Company, inc., 1945.

24 Mathewson, Champion Herbert, Zinc: the science and technology of the metal, its alloys and compounds, New York, NY: Reinhold Pub. Corp., 1959.

25 Graf, G. G., Zinc, Ullmann's Encyclopedia of Industrial Chemistry, A28, 6th ed. New York, NY: Wiley Interscience, 2002.

26 Feinman, J., Chapter 11 - Direct Reduction and Smelting Processes, Making, Shaping and Treating of Steel, 11th ed. Pittsburgh, PA: Association of Iron and

Steel Engineers, 1999, p. 741-77.

27 Komlev, G. A. and Gareev, V. N., Chemistry of processing zinc cake in rotary kilns, Tsvetnye Metally (Moscow, Russian Federation), 37(3), 1964, p.22-9.

28 Kashiwada, M. and Kumagai, T., Waelz process for leach residues at Nisso Smelting Company Limited, Aizu, Japan, AIME World Symposium on Mining and Metallurgy of Lead and Zinc, C. H. Cotterill, ed. New York, NY: AIME, 1970. p.409-22.

29 Huang, Z., Yang, Y., Cai, J., Guo, Y., Li, G., Jiang, T., and Qiu, G., Comprehensive utilization of zinc-leaching residue and concentration mechanism of gallium, Zhongnan Gongye Daxue Xuebao, Ziran Kexueban, 33(2), 2002, p.133-136.

30 Komlev, G. A. and Gareev, V. N., Iron in Waelz treatment of zinc mud, Tsvetnye Metally (Moscow, Russian Federation), 39(7), 1966, p.50-3.

31 Koenig, H. J., Treatment of zinc leach residues in a Lurgi rotary kiln, operated by Cerro de Pasco Corporation, Erzmetall, 23(3), 1970, p.108-13.

32 Huang, Z., The recovery of silver and scarce elements at Zhuzhou Smelters, Lead-Zinc '90, T. S. Mackey and R. D. Prengaman, eds. Warrendale, PA: TMS - Minerals, Metals & Materials Society, 1990. p.239-50.

33 Pilipchuk, N. A., Tulenkov, I. P., Leitsin, V. A., and Voloshina, A. N., Increasing the extraction of indium during rotary-kiln processing of zinc cakes at the Chelyabinsk Zinc Plant, Tsvetnye Metally (Moscow, Russian Federation), (2), 1978, p.15-16.

34 Pilipchuk, N. A., Tulenkov, I. P., Leitsin, V. A., and Voloshina, A. N., Processing of indium-containing products by reduction roasting, SU 548049, May 25, 1978.

35 Kazanbayev, L. A., Kozlov, P. A., and Kubasov, V. L., Integrated process of zinc concentrate treatment with indium recovery and its subsequent electrochemical refining, Electrometallurgy 2001, Proceedings of 31st Annual Hydrometallurgy Meeting, J. A. Gonzalez, J. E. Dutrizac, and G. H. Kelsall, eds. Montreal, Quebec: Canadian Institute of Mining, Metallurgy and Petroleum, 2001. p.307-317.

36 Ivakin, D. A., Kazanbaev, L. A., Kozlov, P. A., and Kolesnikov, A. V., Effect of calcium oxide and chlorine-containing reagents on indium recovery during Waelz-furnace processing of zinc cakes, Izvestiya Vysshikh Uchebnykh Zavedenii, Tsvetnaya Metallurgiya, 3(7-10), 2002.

37 Ivakin, D. A., Kazanbaev, L. A., Kozlov, P. A., and Kolesnikov, A. V., Selective sublimation of valuable components during Waelz-furnace processing of cakes from electrowinning of zinc, Izvestiya Vysshikh Uchebnykh Zavedenii, Tsvetnaya Metallurgiya, (3), 2002, p.16-20.

38 Geikhman, V. V., Kazanbaev, L. A., Kozlov, P. A., Skudnyi, A. I., and Girshengorn, A. P., Improvement of the Waelz-oxide prepartion for hydrometallurgical recovery of zinc, cadmium and indium, Tsvetnye Metally (Moscow), (5), 2000, p.27-30.

39 Kharitidi, G. P., Skopov, G. V., and Kolmachikhin, V. N., Low-waste processing of zinc-plant clinker at Ural copper smelters, Tsvetnye Metally (Moscow, Russian Federation), (4), 1991, p.5-7.

40 Fel'man, R. I., Autogenous shaft smelting of clinker, Tsvetnye Metally (Moscow, Russian Federation), (4), 1991, p.10-13.

41 Mechev, V. V., Myzenkov, F. D., and Glupov, O. V., Complex recovery of valuable components from clinker of the UKSTsK plant, Tsvetnye Metally (Moscow, Russian Federation), (4), 1991, p.7-9.

42 Dobrev, N., Shishkov, P., and Iliev, G. R., Recovery of nonferrous metals from Waelz clinker, Tsvetnye Metally (Moscow, Russian Federation), (11), 1989, p.53-5.

43 Belykh, V. L., Technology for processing of zinc-manufacturing clinker and depletion of converter slags, Tsvetnye Metally (Moscow, Russian Federation), (4), 1991, p.9-10.

44 Maiskii, O. V., Voronin, V. G., and Petunin, V. I., Pilot-plant tests of a method of clinker processing by chloride-sublimation roasting, Tsvetnye Metally (Moscow, Russian Federation), (11), 1980, p.39-43.

45 Okunev, A. I., Shugol, L. S., Nagirnyak, F. I., Fridman, S. E., and Gagarin, E. S., Collective-selective magnetic separation of zinc-plant clinker, Tsvetnye Metally (Moscow, Russian Federation), 36(1), 1963, p.30-5.

46 Zabolotskaya, V. L., Behavior of indium and germanium in the treatment of clinker, Tsvetnye Metally (Moscow, Russian Federation), 37(6), 1964, p.81-3.

47 Riskin, M. A., Shpil'berg, B. A., and Getskin, L. S., Pilot-plant studies of clinker smelting in a zinc plant, Tsvetnye Metally (Moscow, Russian Federation), 37(12), 1964, p.38-43.

48 Anonymous, Silver recovery from leaching residues in the zinc hydrometallurgical process by direct flotation without tailing water discharge, Youse Jinshu, 35(2), 1983, p.73-9.

49 Otrozhdennova, L. A., Maksimov, I. I., Khodov, N. V., Kuznetsov, O. K., Malinovskaya, N. D., and Sataev, I. Sh., Combined technology for silver recovery from zinc cakes of zinc electric smelting, Gornyi Zhurnal, (4), 1997, p.39-40.

50 Rastas, J., Leppinen, J., Hintikka, V., and Fugleberg, S., Recovery of lead, silver and gold from zinc process residues by a sulfidization-flotation method, Lead-Zinc

'90, T. S. Mackey and R. D. Prengaman, eds. Warrendale, PA: TMS - Minerals, Metals & Materials Society, 1990. p.193-209.

51 Rosato, L. I., Stanley, R. W., Berube, M., Blais, M., Leroux, G., and Shink, D., Precious metal recovery from zinc plant residue by thiourea leaching, Lead-Zinc '90, T. S. Mackey and R. D. Prengaman, eds. Warrendale, PA: TMS - Minerals, Metals & Materials Society, 1990. p.109-20.

52 Bakanova, M. A. and Kharlamov, M. N., Coarse gold-containing zinc residues, SU 210371, Sept. 5, 1968.

53 Sahoo, P. K., Karra, V. K., and Jena, P. K., Recovery of zinc from moore cake, Transactions of the Indian Institute of Metals, 26(5), 1973, p.18-21.

54 Lenchev, A., Sulfatizing roasting of zinc ferrites, Metalurgiya (Sofia), 31(12), 1976, p.21-3.

55 Sterkx, J. V. M. and Lemaitre, C. A., Recovery of nonferrous metals in a residue rich in goethite, France FR 2463189, Feb. 20, 1981.

56 Sahoo, P. K., Das, S. C., and Jena, P. K., Extraction of lead and zinc from zinc plant residue, Transactions of the Indian Institute of Metals, 31(5-6), 1978, p.465-7.

57 Sahoo, P. K., Das, S. C., and Sengupta, D. K., Sulfation of Moore cake by ammonium sulfate, Transactions of the Indian Institute of Metals, 34(4), 1981, p.309-12.

58 Gaprindashvili, V. N. and Shaorshadze, M. P., Decomposition of zinc ferrite by sintering it with ammonium sulfate, Pererab. Margantsevykh Polimetal. Rud Gruz., 1970, p.257-61.

59 Shakhtakhtinskii, G. B., Shakarov, G. A., and Geidarov, A. A., Recovery of valuable components from retort residues of zinc production, Izvestiya Akademii Nauk Gruzinskoi SSR, Seriya Khimicheskaya, 10(3), 1984, p.205-8.

60 Hosokura Kogyo K. K., J., Recovery of valuable metals in zinc ore leaching residue by roasting with sulfuric acid, JP 58064327, Apr. 16, 1983.

61 Tafel, V. and Grosse, H., The reduction of zinc ferrite, Metall Und Erz, (26), 1929, p.354-7.

62 Mrowiec, J., Reduction of zinc ferrite in the presence of carbon, Rudy i Metale Niezelazne, 11(11), 1966, p.575-9.

63 Park, P. C., Reduction of zinc ferrite with hydrogen. I., Kumsok Hakhoe Chi, 10(1), 1972, p.56-60.

64 Park, P. C., Reduction of zinc ferrite with hydrogen. II., Kumsok Hakhoe Chi, 10(2), 1972, p.135-46.

65 Sergeev, G. I., Hudyakov, I. F., Lykasov, A. A., and D'yachuk, V. V., Effect of roasting parameters on the reduction of zinc ferrite by sulfur dioxide in roasted zinc concentrates, Kompleksnoe Ispol'Zovanie Mineral'Nogo Syr'Ya, (1), 1990, p.72-6.

66 Sergeev, G. I., Khudyakov, I. F., Lykasov, A. A., Bakin, I. V., and Davletshina, S. G., Kinetics of reduction of ferrite zinc in a roasted zinc concentrate by sulfur dioxide in a fluidized bed, Kompleksnoe Ispol'Zovanie Mineral'Nogo Syr'Ya, (2), 1990, p.50-5.

67 Lee, F. T. and Hayes, P. C., The gaseous reduction of zinc ferrite, Publications of the Australasian Institute of Mining and Metallurgy, (4/94(6th AusIMM Extractive Metallurgy Conference, 1994)), 1994, p.149-54.

68 Latkowska, A. and Donizak, J., Reduction of zinc ferrite with carbon monoxide-carbon dioxide-nitrogen gaseous mixture, Zeszyty Naukowe Akademii Gorniczo-Hutniczej Im. Stanislawa Staszica, Metalurgia i Odlewnictwo, (109), 1987, p.135-45.

69 Gvelesiani, G. G., Konyshkova, T. E., and Chizhikov, D. M., Kinetics and mechanism of the reduction of zinc ferrite with carbon monoxide, Izvestiya Akademii Nauk SSSR, Otdelenie Tekhnicheskikh Nauk, Metallurgiya i Toplivo, (1), 1959, p.50-4.

70 Chen, T. and Dutrizac, J., A mineralogical study of the reductive roasting of zinc ferrite residues--a potential zinc recycling technology, Materials Transactions, 42(12), 2001, p.2511-2518.

71 Yamashita, S., Hata, K., and Goto, S., Reduction roasting for effective leaching of zinc from calcine or zinc leaching residue, Zinc & Lead '95, T. Azakami, ed. Tokyo, Japan: Mining and Materials Processing Institute of Japan, 1995. p.818-827.

72 Bhattacharyya, A., Bhattacharya, S., and Roy, D. L., Recovery of zinc from Moore cake, Transactions of the Indian Institute of Metals, 31(1), 1978, p.54-5.

73 Choi, C. Y. and Lee, Y. H., Treatment of zinc residues by Ausmelt technology at Onsan zinc refinery, REWAS '99--Global Symposium on Recycling, Waste Treatment and Clean Technology, I. Gaballah, J. Hager, and R. Solozabal, eds. Warrendale, Pa: Minerals, Metals & Materials Society, 1999. p.1613-1622.

74 Altepeter, M. and James, S., Proposed treatment of neutral leach residue at Big River Zinc, Residues and Effluents: Processing and Environmental Considerations, R. G. Reddy, W. P. Imrie, and P. B. Queneau, eds. Warrendale, PA: Minerals, Metals & Materials Society, 1992. p.449-59.

75 Pickering, R. W. and Whayman, E., Recovering zinc from zinc ferrite, US 3143486, Aug. 4, 1964.

76 Pickering, R. W. and Haigh, C. J., Recovering zinc in solution with little iron from zinc ferrite formed in roasting sulfide ore., US 3493365, Feb. 3, 1970.

77 Sarma, V. N. R., Deo, K., and Biswas, A. K., Dissolution of zinc ferrite samples in acids, Hydrometallurgy, 2(2), 1976, p.171-84.

78 Rastas, Jussi K., Bjorkqvist, Lars-Goran, Gisler, Raija-Leena, Liukkonen, and Simo S., Process for the recovery of zinc, copper and cadmium in the leaching of zinc calcine, US 4383979, May 17, 1983.

79 Rastas, Jussi Kalevi, Huggare, Tor-Leif Johannes, Fugleberg, and Sigmund Peder, Hydrometallurgical extraction of zinc, copper, and cadmium from ferrites, US 3959437, May 25, 1976.

80 DeGuire, M. F. and Wirag, J. H., Treatment of zinc calcines for zinc recovery, US 4128617, Dec. 5, 1978.

81 Von Roepenack, A., Wuethrich, H., and Schmidt, W., Process for the recovery of zinc from zinc- and iron-containing materials, US 3691038, Sept. 12, 1972.

82 Von Roepenack, A., Wiegand, V., and Smykalla, G., Treating residues from the leaching of roasted zinc blende, US 4107265, Aug. 15, 1978.

83 Pammenter, Robert V., Haigh, and Curzon J., Process for precipitating iron as jarosite with a low non-ferrous metal content , US 4192852 , Mar. 11, 1980.

84 Pammenter, Robert V., Haigh, and Curzon J., Process for precipitating iron as jarosite with a low non-ferrous metal content , US 4305914, Dec. 15, 1981.

85 Menendez, F. J. S. and Fernandez, V. A., Process for recovering zinc from ferrites, US 3434798, Mar. 25, 1969.

86 Menendez, Francisco Javier Sitges, Fernandez, and Vicente Arregui, Process for recovering zinc from ferrites, US 3985857 , Oct. 12, 1976.

87 Peters, M. A., Hazen, W. W., and Reynolds, J. E., Process for recovering metal values from jarosite solids, PCT International Application WO 8803911, June 2, 1988.

88 Habashi, Fathi, A textbook of hydrometallurgy, Sainte Foy, Quebec: Metallurgie Extractive Quebec, Enr., 1993.

89 Cook, Fred. Sale of the Century Zinc Project, Issues Brief 19 1996-97 [Web Page]. 1997 Apr 2; Accessed Dec. 12, 2005. Available at: http://www.aph.gov.au/library/pubs/CIB/1996-97/97cib19.htm.

90 Rastas, Jussi K., Fugleberg, Sigmund P., Heimala, Seppo O., Hultholm, Sitg-Erik, Poijarvi, and Jaakko T. I., Hydrometallurgical process for the treatment of oxides and ferrites which contain iron and other metals, US 4219354 , Aug. 26, 1980.

91 Rastas, Jussi K., Nyberg, Jens R., Karpale, Kauko J., Bjorkqvist, and Lars-Goran, Hydrometallurgical process for the treatment of a raw material which contains oxide and ferrite of zinc, copper and cadmium, US 4362702, Dec. 7, 1982.

92 Rastas, Jussi K., Saikkonen, Pekka J., Honkala, and Risto J., Process for the treatment of a raw material which contains oxide and ferrite of zinc, copper and cadmium, US 4355005 , Oct. 19, 1982.

93 Peters, M. A. and Hazen, W. W., Process for recovering metal values from ferrite wastes, PCT International Application WO 8803912, June 2, 1988.

94 Masters, I. M., Piret, N. L., and Short, W., Combined Dynatec and Ausmelt technologies for zinc refining, Erzmetall, 55(7), 2002, p.345-59.

95 Delvaux, R., Leaching of calcined zinc ores by the Goethite process, Metallurgie (Mons, Belgium), 16(3), 1976, p.154-63.

96 Allan, R. W., Haigh, C. J., and Hamdorf, C. J., Removal of trivalent iron from solutions containing it, DE 2111737, Dec. 16, 1971.

97 Allan, R. W., Haigh, C. J., and Hamdorf, J., Method of removing dissolved ferric iron from iron-bearing solutions, US 3781405, Dec. 25, 1973.

98 Maeshiro, I. and Emi, M., Gallium, germanium, and iron recovery from zinc extraction residue, JP 53021006, Feb. 27, 1978.

99 Davey, P. T. and Scott, T. R., Formation of goethite (FeOOH) and iron oxide (Fe_2O_3) in the goethite process, Transactions of the Institution of Mining and Metallurgy, Section C: Mineral Processing and Extractive Metallurgy, 84(June), 1975, p.C83-86.

100 Abe, H., Yamada, T., and Okada, S., Recovery of gallium and indium at Dowa Mining, Joint Meeting MMIJ-AIME, 1980. New York, NY: AIME, 1982. p.65-76.

101 Buban, K. R., Collins, M. J., and Masters, I. M., Iron control in zinc pressure leach processes, JOM, 51(12), 1999, p.23-25.

102 Doran, H. M., Jackson, M. A., and Alf, A. I., Recovery of indium, US 2384610, Sept. 11, 1945.

103 Harbuck, D. D., Morrison, J. W., and Davidson, C. F., Optimization of gallium and germanium extraction from hydrometallurgical zinc residues, Light Metals, 1989, p.983-9.

104 Harbuck, D. D., Gallium and germanium recovery from domestic sources, Report of Investigations (United States. Bureau of Mines), RI 9419, 1992, p.29 pp.

105 Wardell, M. P. and Davidson, C. F., Acid leaching extraction of gallium and germanium, Journal of Metals, 39(6), 1987, p.39-41.

106 Khan, O. A., Saprygin, A. F., Gusar, L. S., Mal'tsev, V. I., Ren, A. I., Guterman, Yu. P., and Ushakov, N. N., Development of the technology for hydrometallurgical processing of zinc cakes and sublimates with extraction of rare metals, Sbornik Nauchnykh Trudov - Vsesoyuznyi Nauchno-Issledovatel'Skii Gornometallurgicheskii Institut Tsvetnykh Metallov, (25), 1975, p.223-5.

107 Freed, [Freed], Richard Luu, Arthur E. Morris, Freed. Version 6.0, THERMART; 2002 Sep 20; c2000.

108 FactSageThermafact/CRCT and GTT-Technologies. Version 5.3, Montreal, Canada/Aachen, Germany: Thermafact/CRCT; GTT-Technologies; 2004; c1976-2004.

109 Swartz, C. E. and Krauskopf, F. C., Formation and decomposition of ferrite, American Institute of Mining, Metallurgical and Petroleum Engineers Technical Publication, No. 40, 1927, p.19 pp.

110 Okamoto, S., Crystallization and phase transformation of sodium orthoferrites, Journal of Solid State Chemistry, 39, 1981, p.240-5.

111 NIST/SEMATECH e-Handbook of Statistical Methods [Web Page]. Accessed Aug. 11, 2005. Available at: http://www.itl.nist.gov/div898/handbook.

112 DOE Pro XL. Version 3.0, Digital Computations, Inc. and Air Academy Asoociates, LLC; 1998; c1998-2001.

113 Nishihama, S. and Takayuki, H. K. I., A seperation and recovery process of gallium and indium from zinc refinery residues, Solvent Extraction for the 21st Century (Proceedings of ISEC' 99), M. Cox, M. Hidalgo, and M. Valiente, eds. London: Society of Chemical Industry, 1999. p.723-8.

114 Benedetto, J. S., Tamourgl, E. B., and Mingote, R. M., Indium recovery from industrial zinc residues, Solvent Extraction for the 21st Century (Proceedings of ISEC' 99), M. Cox, M. Hidalgo, and M. Valiente, eds. London: Society of Chemical Industry, 1999. p.711-16.

115 Nishihama, S., Hirai, T., and Komasawa, I., Separation and recovery of gallium and indium from simulated zinc refinery residue by liquid-liquid extraction, Industrial &

Engineering Chemistry Research, 38(3), 1999, p.1032-1039.

116 Dutrizac, J. E., An overview of iron precipitation in hydrometallurgy, Crystallization and Precipitation, G. L. Strathdee, M. O. Klein, and L. A. Melis, eds. Oxford, UK: Pergamon Press, 1987. p.259-83.

117 Filippou, D., Innovative hydrometallurgical processes for the primary processing of zinc, Mineral Processing and Extractive Metallurgy Review, 25(3), 2004, p.205-252.

118 von Plessen, H., Sodium sulfates, Ullmann's Encyclopedia of Industrial Chemistry, A24, 6th ed. New York, NY: Wiley Interscience, 2002.

119 Leber, A., Procedure for the production of sulfuric acid from sodium sulfate and hydrogen chloride, DE868742, Feb. 26, 1952.

120 Vodolazov, L. I., Stepanova, L. M., Laskorin, B. P., and Gol'tyakova, R. I., Ion-exchange conversion of mineral salts. I. Conversion of sodium sulfate to solutions of sulfuric acid and sodium nitrate, Issled. Obl. Neorg. Tekhnol., 1972, p.274-9.

121 Inogamov, U. A., Tadzhiev, S. M., and Rustamova, M. N., Ion exchange synthesis of substances during processing of sulfate salts, Doklady Akademii Nauk USSR, (7), 1975, p.29-30.

122 Sokolova, N. P. and Erlikhman, E. I., Sodium(+)-hydrogen(+) ion-exchange system in sulfate solutions, Izvestiya Sibirskogo Otdeleniya Akademii Nauk SSSR, Seriya Khimicheskikh Nauk, (5), 1973, p.18-25.

123 Grafton, R. W., Treatment of Glauber salt with ion-exchange resins, GB801527, Sept. 17, 1958.

124 Thieme, C., Sodium carbonates, Ullmann's Encyclopedia of Industrial Chemistry, A24, 6th ed. New York, NY: Wiley Interscience, 2006.

125 Pal, S. K. and Sharma, M. M., Solvay type processes: absorption of carbon dioxide in ammoniated aqueous and non-aqueous solutions of sodium nitrate, calcium nitrate, and potassium chloride, Industrial & Engineering Chemistry Process Design and Development, 22(1), 1983, p.76-9.

126 Shibano, T., The corrosion of lead anode in zinc sulfate solution. V. The effect of chloride, Nippon Kogyo Kaishi, 78(199-204), 1962.

127 Orlandini, B. and Schmittroth, W., Removing fluorine from zinc concentrates and manganese dioxide, US3494841, Feb. 10, 1970.

128 Chen, T. T. and Dutrizac, J. E., Mineralogical characterization of anode slimes - 9. The reaction of Kidd Creek anode slimes with various lixiviants, Canadian Metallurgical Quarterly, 32(4), 1993, p.267-79.

129 Kaddouri, A. H., Leaching with acetic acid for recovery of lead and salt values from galena-type ores, or from spent lead-acid storage batteries, WO2001021846, Mar. 29, 2001.

130 Moure, W. B. Jr. and Etsell, T. H., Method and apparatus for recovery of lead from batteries, US5211818, May 18, 1993.

131 Ruhrberg, Martin. ICSG Information Circular - End of Life Vehicles (ELV) - ICSG/IC/13 [Web Page]. 2004 May; Accessed June 27, 2006. Available at: http://www.icsg.org/News/Infocirculars/ICSGInfoCircularELV.pdf.

132 Li, C. L. and Tsai, M. S., Mechanism of spinel ferrite dust formation in electric arc furnace steelmaking, ISIJ International, 33(2), 1993, p.284-90.

133 Xia, D. K. and Pickles, C. A., Extraction of nonferrous metals from electric arc furnace dust, Waste Processing and Recycling in Mineral and Metallurgical Industries III, S. R. Rao, ed. Montreal, Que: Canadian Institute of Mining, Metallurgy and Petroleum, 1998. p.221-245.

134 Hagni, A. M., Demars, C., and Hagni, R. D., Mineralogy of electric arc furnace (EAF) dusts., EPD Congress 91, D. R. Gaskell, ed. Warrendale, Pa: Minerals, Metals & Materials Society, 1991. p.801-9.

135 Hagni, A. M., Demars, C., and Hagni, R. D., Mineralogy of electric are furnace (EAF) dusts, Process Mineralogy XI : Characterization of Metallurgical and Recyclable Products, D. M. Hausen, ed. Warrendale, Pa: Minerals, Metals & Materials Society, 1991. p.57-66.

136 Hagni, A. M., Hagni, R. D., and Demars, C., Mineralogical characteristics of electric arc furnace dusts, JOM, 43(4), 1991, p.28-30.

137 Chen, T. T., Dutrizac, J. E., and Owens, D. R., Mineralogical characterization of EAF dusts from plain carbon steel and stainless steel operations, Waste Processing and Recycling in Mineral and Metallurgical Industries III, S. R. Rao, ed. Montreal, Que: Canadian Institute of Mining, Metallurgy and Petroleum, 1998. p.511-525.

138 Sofilic, T., Rastovcan-Mioc, A., Cerjan-Stefanovic, S., Novosel-Radovic, V., and Jenko, M., Characterization of steel mill electric-arc furnace dust, Journal of Hazardous Materials, 109(1-3), 2004, p.59-70.

139 Liebman, M., The current status of electric arc furnace dust recycling in North America, International Symposium on Recycling of Metals and Engineered Materials, 4th, D. L. Stewart Jr., J. C. Daley, and R. L. Stephens, eds. Warrendale, Pa: Minerals, Metals & Materials Society, 2000. p.237-250.

140 Zunkel, A. D., Recovering zinc and lead from electric arc furnace dust: a technology status report, International Symposium on Recycling of Metals and Engineered Materials, 4th, D. L. Stewart Jr., J. C. Daley, and R. L. Stephens, eds.

Warrendale, Pa: Minerals, Metals & Materials Society, 2000. p.227-236.

141 Zunkel, A. D., Electric arc furnace dust management: a review of technologies, Iron and Steel Engineer, 74(3), 1997, p.33-38.

142 Mager, K., Meurer, U., Garcia-Egocheaga, B., Goicoechea, N., Rutten, J., Saage, W., and Simonetti, F., Recovery of zinc oxide from secondary raw materials: new developments of the Waelz process, International Symposium on Recycling of Metals and Engineered Materials, 4th, D. L. Stewart Jr., J. C. Daley, and R. L. Stephens, eds. Warrendale, Pa: Minerals, Metals & Materials Society, 2000. p.329-344.

143 Nakazawa, S., Azakami, T., and Yazawa, A., Chemistry of pyrometallurgical processing of EAF dust, Waste Processing and Recycling in Mineral and Metallurgical Industries III, S. R. Rao, ed. Montreal, Que: Canadian Institute of Mining, Metallurgy and Petroleum, 1998. p.497-510.

144 Funahashi, T., Kaikake, A., and Sugiura, T., Recent development of Waelz kiln process for EAF dust treatment at Sumitomo Shisaka Works, EPD Congress 1998, B. Mishra, ed. Warrendale, Pa: Minerals, Metals & Materials Society, 1998. p.487-496.

145 Garcia-Carcedo, F., Ayala, J. N., Goicoechea, N., Allain, E., Hernandez, A., Ruiz-Ayucar, G. E., Danobeitia, I., and Cornejo, N., Production of an ultra-pure fraction of ZnO by the recycling of EAF dust, EPD Congress 2000, P. R. Taylor, ed. Warrendale, Pa: Minerals, Metals & Materials Society, 2000. p.293-310.

146 Menad N, Ayala J N, Garcia-Carcedo Fernando, Ruiz-Ayucar E, and Hernandez A, Study of the presence of fluorine in the recycled fractions during carbothermal treatment of EAF dust, Waste Management (New York, N.Y.), 23(6), 2003, p.483-91.

147 Thomas, S. S. and Clifton, E. D., Economic evaluation of the HTR process for treating EAF dust, Electric Furnace Conference Proceedings, 45, 1988, p.413-419.

148 James, S. E. and Bounds, C. O., Recycling lead and cadmium, as well as zinc, from EAF dust, Lead-Zinc '90, T. S. Mackey and R. D. Prengaman, eds. Warrendale, PA: TMS - Minerals, Metals & Materials Society, 1990. p.477-95.

149 B.U.S. Group AB. Portrait - B.U.S. Group AB [Web Page]. Accessed Aug. 4, 2005. Available at: http://www.busgroup.se/en/portrait.html.

150 Morris, A. E., O'Keefe, T. J., Cole, E. R., and Neumeier, L. A., Treatment options for carbon steel electric-arc furnace dust, Electric Furnace Conference Proceedings, 43, 1986, p.167-82.

151 Zunkel, A. D., EAF dust as an electrolytic zinc resource, Recycling of Metals and Engineered Materials, 3rd, P. B. Queneau and R. D. Peterson, eds. Warrendale, Pa:

Minerals, Metals & Materials Society, 1995. p.579-87.

152 Cernak, E. C. and Maselli, A. J., Reclamation of valuable metals from hazardous waste, International Symposium on Recycling of Metals and Engineered Materials, 4th, Stewart Jr., D. L. D. J. C. , and R. L. Stephens, eds. Warrendale, Pa: Minerals, Metals & Materials Society, 2000. p.251-259.

153 Ye, G., Characterization and removal of halogens in the EAF dust and zinc oxide fume obtained from thermal treatment of EAF dust, International Symposium on Recycling of Metals and Engineered Materials, 4th, D. L. Stewart Jr., J. C. Daley, and R. L. Stephens, eds. Warrendale, Pa: Minerals, Metals & Materials Society, 2000. p.271-280.

154 Xia, D. K. and Pickles, C. A., Caustic roasting and leaching of electric arc furnace dust, Canadian Metallurgical Quarterly, 38(3), 1999, p.175-186.

155 Zhao, Y. and Stanforth, R., Extraction of zinc from zinc ferrites by fusion with caustic soda, Minerals Engineering, 13(13), 2000, p.1417-21.

156 Morsi, M. B., Nasr, M. M., Abdalla, F. H. A., and El-Tawil, S. Z., Soda ash roasting of electric-arc steelmaking dust (E.A.S.D), Transactions of the Indian Institute of Metals, 51(4), 1998, p.193-200.

157 Lynn, J. D., Jablonski, C. E., and Egan, W. D., Process for chemical stabilization of heavy metal bearing dusts and sludges, US 4911757, Mar. 27, 1990.

158 Environmental Protection Agency. Hazardous waste management system; identification and listing [Web Page]. 1995 Jan 5; Accessed Feb. 2, 2006. Available at: http://www.epa.gov/fedrgstr/EPA-WASTE/1995/January/Day-05/pr-113.html.

159 Ballmer, Greg. Super Detox Brochure [Web Page]. Accessed Feb. 3, 2006. Available at: http://www.envirosafeservices.com/images/K061Flyer1.pdf.

160 Vinals, J., Balart, M. J., and Roca, A., Inertization of pyrite cinders and co-inertization with electric arc furnace flue dusts by pyroconsolidation at solid state, Waste Management (Amsterdam, Netherlands), 22(7), 2002, p.773-782.

161 D'Souza, N., Kozinski, J. A., and Szpunar, J. A., EAF stainless-steel dust: characteristics and potential metal immobilization through thermal treatment, Waste Processing and Recycling in Mineral and Metallurgical Industries III, S. R. Rao, ed. Montreal, Que: Canadian Institute of Mining, Metallurgy and Petroleum, 1998. p.247-258.

162 Aota, J., Morin, L., Mikhail, S. A., Chen, T. T., and Liang, D. T., Immobilization of hazardous elements in EAF dust by vitrification process, Waste Processing and Recycling in Mineral and Metallurgical Industries II, S. R. Rao, ed. Montreal, Que: Canadian Institute of Mining, Metallurgy and Petroleum, 1995. p.335-49.

163 Ionescu, D., Meadowcroft, T. R., and Barr, P. V., High-iron content glasses - an alternative in the use of electric arc furnace dust, Waste Processing and Recycling in Mineral and Metallurgical Industries II, S. R. Rao, ed. Montreal, Que: Canadian Institute of Mining, Metallurgy and Petroleum, 1995. p.351-60.

164 Zunkel, A. D. and Schmitt, R. J., Review of electric arc furnace dust treatment processes and environmental regulations, Electric Furnace Conference Proceedings, 53, 1996, p.147-158.

165 Mantovani, M. C. and Takano, C., The strength and the high temperature behaviors of self-reducing pellets containing EAF dust, ISIJ International, 40(3), 2000, p.224-230.

166 McCrea, J. and Pickles, C. A., Agglomeration and recycling of electric arc furnace dust, Electric Furnace Conference Proceedings, 53, 1996, p.159-170.

167 Sandstroem, A., Yang, Q., Menad, N., and Lindblom, Bo., EAF dust processing with a combination of hydro- and pyrometallurgical techniques, EPD Congress 2003, M. E. Schlesinger, ed. Warrendale, Pa: Minerals, Metals & Materials Society, 2003. p.377-388.

168 Eschenfelder, A. H., Ionic valences in manganese-iron spinels, Journal of Applied Physics, 29, 1958, p.378-80.

169 Esmaelii, A., Mesdaghinia, A., and Vazirinejad, R., Chromium (III) removal and recovery from tannery wastewater by precipitation process, Americal Journal of Applied Sciences, 2(10), 2005, p.1471-73.

170 Xue, Tao (txue@inco.com). RE: FW: request for research samples. E-mail to: Preston Holloway (prestonh@ualberta.ca). 2005 May 12.

171 Kuck, P. H., Nickel, Mineral Commodity Summaries 2006, Washington, DC: United States Department of the Interior, 2006, p. 116-117.

172 Edelstein, D. L., Copper, Mineral Commodity Summaries 2006, Washington, DC: United States Department of the Interior, 2006, p. 56-57.

173 Yin, Z. B., Caba, E., Barron, L., Belin, D., Morris, W., Vosika, M., and Bartlett, R., Copper extraction from smelter flue dust by lime-roast/ammoniacal heap leaching, Residues and Effluents : Processing and Environmental Considerations : Proceedings of an International Symposium Sponsored by Extraction and Process Division of TMS and the Iron and Steel Society at the 1992 TMS Annual Meeting, San Diego, California, USA, March 1-5,1992, 1992, p.255-67.

174 Haver, F. P. and Wong, M. M., Making copper without pollution, Mining Engineering, 6, 1972, p.53-58.

175 Haver, F. P. and Wong, M. M., Lime roast-leach method for treating chalcopyrite concentrates, United States Department of the Interior Report of Investigations, RI 8006, 1975, p.17 pp.

176 Bartlett, R. W. and Haung, H. H., The lime-concentrate-pellet roast process for treating copper sulfide concentrates, JOM, 12, 1973, p.28-34.

177 Bartlett, R. W. and Haung, H. H., Pollution-free process for treating copper sulfide flotation concentrates and recovering copper , US 3,915,689, Oct. 28, 1975.

178 Bartlett, R. W. and Haung, H. H., Fluidized bed roasting of lime copper concentrate pellets, Metallurgical Transactions B: Process Metallurgy, 7B(3), 1976, p.489-90.

179 Pentz, R. D., Tunley, T. H., Marran, J. L., and Murphy, T. G., A study of copper recovery by lime roasting and leaching, Report - National Institute for Metallurgy (South Africa), 1772, 1975, p.28 pp.

180 Duyvensteyn, W. P. C. and Lastra, M. R., Roasting of powdered sulfide ores in fluidized mixture with lime for removal of sulfur and arsenic oxide vapors, South African ZA 9206237, Mar. 3, 1993.

181 Som, P. K. and Choudhury, S. K. R., Lime - roast -leach technique for treating chalcopyrite concentrates, Transactions of the Indian Institute of Metals, 35(6), 1982, p.578-82.

182 Shen, Y. and He, L., Reliability of technology for recovery of gold from refractory ores by baking with lime for fixation of sulfur and arsenic, Youse Jinshu, Yelian Bufen, (5), 1999, p.31-35.

183 Riveros Urzua, G., Roasting of copper-iron sulfides without the emission of sulfur dioxide, Minerales, 47(199), 1992, p.59-70.

184 Terry, B. S., Riveros, G., Sanchez, M., and Jeffes, J. H. E., Lime-concentrate process for roasting of copper-bearing sulfides - Part 1: analysis of optimum roasting conditions, Transactions of the Institution of Mining and Metallurgy, Section C: Mineral Processing and Extractive Metallurgy, 103(Sept.-Dec.), 1994, p.C193-C200.

185 Terry, B. S., Riveros, G., and Jeffes, J. H. E., Lime-concentrate process for roasting of copper-bearing sulfides - Part 3: mechanisms of roasting reactions, Transactions of the Institution of Mining and Metallurgy, Section C: Mineral Processing and Extractive Metallurgy, 103(Sept.-Dec.), 1994, p.C210-C216.

186 Terry, B. S., Riveros, G., and Jeffes, J. H. E., Lime-concentrate process for roasting of copper-bearing sulfides - Part 2: effect of sulfide:lime ratio, air flow rate, pellet size and porosity on reaction kinetics, Transactions of the Institution of Mining and Metallurgy, Section C: Mineral Processing and Extractive Metallurgy, 103(Sept.-Dec.), 1994, p.C201-C209.

187 Riveros, G., Marin, T., and Puga, C., Lime-concentrate roasting studies - effect of activated limestone, Minerals Engineering, 17(3), 2004, p.469-71.

188 Terry, B. S., Sanchez, M. A., and Ulloa, A. G., Calcium oxide as a reagent for the capture of arsenic emissions during the roasting of enargite (Cu_3AsS_4), Extraction and Processing for the Treatment and Minimization of Wastes,1994: Proceedings of an International Symposium, 1994, p.201-15.

189 Hagni, A. M., Hagni, R. D., and Taylor, P. R., Process mineralogy of roasted pyrite and arsenopyrite, JOM, 4, 1992, p.36-38.

190 Hagni, A. M., Hagni, R. D., and Taylor, P. R., Mineralogical and textural characterization of lime roasted pyrite and arsenopyrite for gold leaching, EPD Congress 1993, J. P. Hager, ed. Warrendale, Pa: Minerals, Metals & Materials Society, 1993. p.393-401.

191 Agar, G. E., Gold and silver recovery method, US 5074909, Dec. 24, 1991.

192 Nyavor, K. and Egiebor, N. O., Controlling SO_2 emissions in the roasting of gold concentrates, JOM, 12, 1991, p.32-34.

193 Nyavor, K. and Egiebor, N. O., Arsenic and sulfur emission control in the pretreatment of a secondary refractory gold concentrate by lime agglomeration roast, Waste Processing and Recycling in Mineral and Metallurgical Industries II, S. R. Rao, ed. Montreal, Que: Canadian Institute of Mining, Metallurgy and Petroleum, 1995. p.75-83.

194 Qiu, M., Ou, Q., Jiang, Q., Du, J., and Wei, C., Application of industrial waste in fixing-roasting of a refractory gold concentrate, Kuangchan Zonghe Liyong, (1), 2004, p.40-44.

195 Zeng, Z., Liang, J., and Liu, J., Pretreatment in arsenic-fixing roasting of refractory gold ore, Kuangye Gongcheng, 17(3), 1997, p.39-42.

196 Liu, J., Chi, R., Zeng, Z., Liang, J., and Xu, Z., Selective arsenic-fixing roast of refractory gold concentrate, Metallurgical and Materials Transactions B: Process Metallurgy and Materials Processing Science, 31B(6), 2000, p.1163-1168.

197 Taylor, P. R. and Yin, Z. B., Soda ash roasting of As-Sb-precious metal concentrates, Transactions of Society for Mining, Metallurgy, and Exploration, Inc., (294), 1994, p.163-9.

198 Taylor, P. R. and Yin, Z. B., Soda ash roasting of arsenic-antimony-precious metal concentrates, Minerals & Metallurgical Processing, 10(4), 1993, p.163-9.

199 Wu, G., New technology of removal of arsenic from arsenic containing gold concentrates, Huang Jin, 19(7), 1998, p.38-9.

200 Zhang, G., Wu, X., Sheng, G., and Qiu, D., Sulfur-fixation roasting of refractory gold concentrate with magnesium salt, Huang Jin, 20(8), 1999, p.33-36.

201 Luganov, V. A., Plakhin, G. A., Luganov, A. V., and Gorbatenko, G. V., Oxidizing roasting of arsenic gold bearing concentrates with the soda presence, Randol Gold Forum '96, N. McPherson Nilles, ed. Golden, CO: Randol International, 1996. p.253-256.

202 Luganov, V. A., Sajin, E. N., Li, H., and Guo, B., Oxidizing roasting of carbon-bearing arsenic-gold concentrates in presence of sodium carbonate, Zhongguo Youse Jinshu Xuebao, 9(2), 1999, p.398-402.

203 Dundua, R. G. and Dobrokhotov, G. N., Roasting and leaching of arsenopyrite ores and concentrates, SU 1477760, May 7, 1989.

204 Xue, G., Improvement of recovery rates of gold, silver and copper by roast-cyanidation, Huang Jin, 23(5), 2002, p.26-28.

205 Fernandez, R. R., Le Vier, K. M., Hannaford, A. L., and Ramadorai, G., Oxidation roasting of gold ores containing arsenic and sulfides, US 5123956, Apr. 12, 1991.

206 Hannaford, A. L., Le Vier, M. K., Fernandez, R. R., Ramadorai, G., Fitting, A., Samant, G., Peinemann, B., Bandel, G., and Kofalck, H., Process for treating ore having recoverable metal values including arsenic containing components, US 6248301.

207 Hannaford, A. L., Le Vier, M. K., Fernandez, R. R., Ramadorai, G., Fitting, A., Samant, G., Peinemann, B., Bandel, G., and Kofalck, H., Process for treating ore having recoverable metal values including arsenic containing components, US 6482373.

208 Makhmetov, M. Zh., Effect of sodium and calcium compounds on selenium recovery degree from copper electrolyte sludges, Kompleksnoe Ispol'Zovanie Mineral'Nogo Syr'Ya, (4), 1985, p.44-7.

209 Tishchenko, A. A. and Smirnov, V. I., Thermodynamics and experimental investigation of the formation reactions of sodium selenite and sodium selenate by sintering copper selenide with soda ash, Doklady Akademii Nauk SSSR, (145), 1962, p.863-6.

210 Hoffmann, J. E., Recovering selenium and tellurium from copper refinery slimes, JOM, 41(7), 1989, p.33-8.

211 Fester, G. A., Sodium arsenate from nickel arsenides, Revista Facultad De Ingenieria Quimica, (25), 1956, p.143-51.

212 Zhu, C. and Kou, J., A new technology for normal atmosphere dearsenifying of speiss, Youse Jinshu, Yelian Bufen, (1), 2002, p.15-17.

213 Omarova, F. M., Poprukailo, N. N., and Makhmetov, M. Zh., Enthalpies of the formation of sodium orthoarsenate and iron arsenate dihydrate, Deposited Document, VINITI 5357-80, 1980, p.8 pp.

214 Sharipova, Z. M., Kasenov, B. K., and Bukharitsyn, V. O., Heat capacity and thermodynamic functions of sodium arsenates at 223-700 K, Zhurnal Fizicheskoi Khimii, 65(5), 1991, p.1408-10.

215 Kasenov, B. K. and Mustafin, E. S., Heat capacity and thermodynamic functions of iron(III) orthoarsenate in the range 298.15-673 K, Kompleksnoe Ispol'Zovanie Mineral'Nogo Syr'Ya, (1), 1994, p.83-4.

216 Adams, M. and Johnson, G., Advances in nickel sulfide process development, Alta 2001 Nickel/Cobalt-7 Technical Proceedings. Melbourne, Australia: ALTA Metallurgical Services, 2005.

217 Jones, D. and Moore, R., The application of the CESL process to nickel laterites, Alta 2001 Nickel/Cobalt-7 Technical Proceedings. Melbourne, Australia: ALTA Metallurgical Services, 2005.

218 Gabb, P. J. and Davies, A. L., The industrial separation of copper and arsenic as sulfides, JOM, 51(9), 1999, p.18-19.

219 Beard, H. C. and Cuninghame, J. G., Radiochemistry of arsenic, Nuclear Science Series (National Academy of Sciences and National Research Council), No. 3002, United States Atomic Energy Commision, 1965.

220 Mirza, A. H., Tahija, D., Chen, K., and Haung, H. H., Formation and stability studies of iron-arsenic and copper-arsenic compounds from copper electrorefining sludge, Arsenic metallurgy: fundamentals and applications, R. G. Reddy, J. L. Hendrix, and P. B. Queneau, eds. Warrendale, PA: TMS, 1987. p.37-58.

221 Robins, Robert G. Some chemical aspects relating to arsenic remedial technologies [Web Page]. 2001; Accessed July 21, 2006. Available at: http://www.epa.gov/ttbnrmrl/ArsenicPres/78.pdf.

222 Twidwell, L. G., McCloskey, J., Lee, M. G., and Saran, J., Arsenic removal from mine and process waters by lime/phosphate precipitation, Arsenic Metallurgy, R. G. Reddy and V. Ramachandran, eds. Warrendale, PA: TMS, 2005. p.71-86.

223 Twidwell, L. G., McCloskey, J., Lee, M. G., and Saran, J., Arsenic removal from mine and process waters by lime/phosphate precipitation: pilot scale demonstration, Arsenic Metallurgy, R. G. Reddy and V. Ramachandran, eds. Warrendale, PA: TMS, 2005. p.87-100.

224 Huang, H. P., Shi, Y., Li, W., and Chang, S. G., Dual alkali approaches for the capture and separation of CO_2, Energy & Fuels, 15(2), 2001, p.263-268.

Appendix

Exraction Calculations

Generally, extractions were calculated by two different methods, using the chemical analyses from the solid and solution samples obtained from this testwork. Sample extraction calculations are given below.

$$\%\,Retained\ in\ Solids = \frac{(Roasted\ Waste\ Analysis,\ \%)(Roasted\ Waste\ Weight,\ g)}{(Feed\ \ Analysis,\ \%)(Feed\ \ Weight,\ g)}\ x100$$

$$Extraction\ (Solids\ \ Basis) = 100 - \frac{(Residue\ Analysis,\ \%)(Residue\ Weight,\ g)}{(Feed\ \ Analysis,\ \%)(Feed\ \ Weight,\ g)}\ x100$$

$$Extraction\ (Solution\ \ Basis) = \frac{(Solution\ Analysis,\ mg\,/\,L)(Solution\ Volume,\ mL)}{(Feed\ \ Analysis,\ \%)(Feed\ \ Weight,\ g)}\ x100$$

In general, solution analyses were used to calculate extractions where the extractions were less than 50% and solids analyses were used to calculate extractions of greater than 50%. Weights of samples taken for analysis were recorded and the feed weight was corrected to compensate for the removal of these samples.

For the Inco copper residue, element deportments were calculated using solution analyses for the extraction during water leaching and with solids analyses for the overall extraction after water and acid leaching.